

National Water Infrastructure Adaptation Assessment

Part II, Smart Urban Design (SUD) and Application Case Studies



(Intentionally left blank)

National Water Infrastructure Adaptation Assessment: Part II, Smart Urban Design (SUD) and Application in Case Studies

Y. Jeffrey Yang¹, Heng Wei², Xinhao Wang³, Steven Buchberger², Marissa S. Liang⁴
Ni-bin Chang⁵, Britta Bierwagen⁶, Susan Julius⁶, Zhiwei Li⁷, Dominic L. Boccelli²,
Robert M. Clark⁸, Hou Liu², and Jill Neal¹

- (1) U.S. EPA, ORD, Center for Environmental Solutions and Emergency Response, Water Infrastructure Division, Cincinnati, OH 45268
- (2) University of Cincinnati, College of Engineering and Applied Science, Cincinnati, OH 45221
- (3) University of Cincinnati, School of Planning, Cincinnati, OH 45221
- (4) U.S. EPA, ORD, Center for Public Health and Environmental Assessment, ORISE participant, Cincinnati, OH 45268
- (5) University of Central Florida, Department of Civil, Environmental, and Construction Engineering, Orlando, FL 32816
- (6) U.S. EPA, ORD, Center for Public Health and Environmental Assessment, Washington, DC 20460
- (7) Carbon Sequestration Technologies, LLC., Pittsburgh, PA 15241
- (8) Environmental and Health Consultant, Cincinnati, OH 45268

DISCLAIMER

The U.S. Environmental Protection Agency, through its Office of Research and Development, conducted, funded, and managed the research described herein. The report, *National Water Infrastructure Adaptation Assessment: Part II, Smart Urban Design (SUD) and Application Case Studies*, EPA/600/R-20/165, has been subjected to the Agency's peer and administrative review and has been approved for external publication. Any opinions expressed in this paper are those of the authors and do not necessarily reflect the views of the Agency; therefore, no official endorsement should be inferred. Any mention of trade names or commercial products does not constitute endorsement or recommendation for use.

FOREWORD

The U.S. Environmental Protection Agency (EPA) is charged by Congress with protecting the Nation's land, air, and water resources. Under a mandate of national environmental laws, the Agency strives to formulate and implement actions leading to a compatible balance between human activities and the ability of natural systems to support and nurture life. To meet this mandate, EPA's research program is providing data and technical support for solving environmental problems today and building a science knowledge base necessary to manage our ecological resources wisely, understand how pollutants affect our health, and prevent or reduce environmental risks in the future.

The Center for Environmental Solutions and Emergency Response (CESER) within the Office of Research and Development (ORD) conducts applied, stakeholder-driven research and provides responsive technical support to help solve the Nation's environmental challenges. The Center's research focuses on innovative approaches to address environmental challenges associated with the built environment. We develop technologies and decision-support tools to help safeguard public water systems and groundwater, guide sustainable materials management, remediate sites from traditional contamination sources and emerging environmental stressors, and address potential threats from terrorism and natural disasters. CESER collaborates with both public and private sector partners to foster technologies that improve the effectiveness and reduce the cost of compliance, while anticipating emerging problems. We provide technical support to EPA regions and programs, states, tribal nations, and federal partners, and serve as the interagency liaison for EPA in homeland security research and technology. The Center is a leader in providing scientific solutions to protect human health and the environment.

This publication has been produced as part of the EPA ORD's Air-Energy (A-E) research program. The research report is published and made available by ORD to assist the user community and to link researchers with their clients.

Gregory Sayles, Ph.D.
Director, Center for Environmental Solutions and
Emergency Response

PREFACE

Water is essential to life. Uneven distribution of population and water resources in the world results in more than 1.1 billion people with a lack of access to clean drinking water and 2.6 billion people deprived of adequate water sanitation. Today fresh water is being consumed at an alarming rate, almost doubling every 20 years. Global changes further exacerbate this already stressed situation. It can be said that water availability is not only a problem for developing countries, but one facing developed nations that are saddled with aging water infrastructure. Pressed by challenges, however, civilizations always have found innovative solutions to meet water resource needs and adapt to evolving social and environmental conditions. This spirit of adaptation continues to date and will continue.

Today, one of the most complex challenges facing our nation revolves around water supply sustainability, often framed in the name of water-environment-energy nexus. The challenge is acute considering occurring and future changes in land use and hydroclimatic conditions and, thus, requires a holistic water management approach. For the purpose, interdisciplinary research and development to supplement and improve water management and engineering practice are often the first steps of the effort.

The national adaptation assessment reports synthesize the results of multidisciplinary research and development in the past 8 years. This report presents an assessment of our nation's water resource infrastructure, characterizes hydroclimatic provinces, and future hydroclimatic and land use conditions. It further introduces planning and engineering means to develop the quantitative scientific basis for adapting water infrastructure and, in general, for urban development. The systematic adaptation approach is structured at multiple levels from integrated watershed management to urban-scale planning and individual water system engineering.

In considering water infrastructure adaptation needs, a suite of tools ranging from those in master planning and systems engineering to those in watershed modeling and drinking water plant simulations has been developed or adopted. These adaptation techniques for different levels of planning and engineering are described in this report and accompanying publications and are illustrated by case studies. The focus is to develop actionable science and engineering bases for adapting to the likely future environmental stressors at local scales and, by doing so, to support water resource managers and technical stakeholders who face the technical complexity. Although this report provides a wealth of technical data and information, it only marks the beginning of a long march toward the goal of the sustainable water resource and resilient infrastructure in a time of accelerating global changes.

ACKNOWLEDGMENTS

The U.S. Environmental Protection Agency (EPA), through its Office of Research and Development (ORD), funded, managed, and conducted the intramural and extramural research described herein. The research was a part of the ORD Air and Energy (A-E) research program. It was implemented by the EPA Water Resources Adaptation Program in ORD's Water Systems Division by Pegasus Technical Services, Inc., through EPA Contract EP-C-05-056, and Cadmus, Inc., through EPA Contract EP-C-06-100.

Programmatic guidance from ORD's former Aging Water Infrastructure Program is acknowledged. Special thanks are due to Jeff Peterson, Karen Metchis, Elizabeth Corr, Robert Cantilli (now with ORD), Rachael Novak, Elana Goldstein, and Curt Baranowski of the EPA Office of Water for their efforts to bring together experts and practitioners from around the country and for their involvement in this research. Additionally, the EPA Office of Air and Radiation Climate Division and the Office of Transportation Air Quality were engaged with interests in this research through the A-E research program.

The project team would like to acknowledge numerous technical staff and participants from EPA and contracting research organizations. This investigation of both a wide breadth and a substantial depth was accomplished only with their participation and contribution, including the administrative and contract support from Dr. Michael Moeykens, Michelle Latham, Steve Harmon, and Stephen Wright. Finally, technical data and collaboration efforts by the Manatee County [Florida] Water Department, the Greater Cincinnati Water Works, the Las Vegas Valley Water District, and local governments on the Massachusetts coast are acknowledged.

The national adaptation assessment reports were a result of continuing research efforts over the past several years. These reports initially were prepared in 2011 and reviewed by individuals inside and outside of EPA. Per review comments, additional technical contents were added with new research, especially in the areas of adaptation tools and methods. This development led to rewriting and reorganization of the entire reports. In the process, three rounds of internal and external peer reviews were conducted. After these peer reviews, Part I of the national water infrastructure assessment report was published in 2015. This current Part II report also has been subjected to administrative review and is now approved for publication.

The EPA project team includes Y. Jeffrey Yang (ORD/ Center for Environmental Solutions and Emergency Response [CESER]), Jill Neal (CESER), Chelsea Neal (former CESER ORISE participant, now with Department of Energy's Sandia National Laboratories), Marissa Liang (ORD/Center for Public Health and Environmental Assessment [CPHEA] ORISE participant), Britta Bierwagen (CPHEA), Susan Julius (CPHEA), and Jeri Weiss (EPA Region 1), among many others involved in the past several years. Principal research participants from contracting organizations are listed below.

University of Cincinnati:

Dr. Steven Buchberger, P.E.; Dr. Zhiwei Li (now with Carbon Capture Scientific, LLC.); Dr. Heng Wei; Dr. Xinhao Wang; the late Dr. Timothy C. Keener, P.E.; Dr. Dominic L. Boccelli (now at the University of Arizona); Dr. Hou Liu; Dr. Zhuo Yao (now at the State of California Air Resources Board); Ting Zuo; Dr. Yu Sun (now at the University of North Georgia); Amy Burgess; Heng Yang; Jie He; Patcha Huntra; Dr. Pamela Heckle, P.E. (now at American Red Cross); Dr. Thushara Ranatunga (now at the Houston-Galveston Area Council, Texas)

Consultants:

Dr. Robert M. Clark, Dr. Walter Grayman, P.E.

University of Central Florida:

Dr. Ni-Bin Chang, P.E.; Dr. Ammarin Makkeasorn; Dr. Sanez Imen; Lee Mullon

Pegasus Technical Services:

Dr. Karen Koran

Cadmus, Inc.:

Chi Ho Sham (now at Eastern Research Group), Jaime Rooke, Brent Ranalli, Laurie Potter, Laura Blake, Julie Blue, Donna Jensen, Patricia Hertzler

The following reviewers are acknowledged for peer reviews of this report and its previous versions.

Dr. Weiwei Mo, University of New Hampshire
Dr. Frederick Bloetscher, Florida Atlantic University
Dr. James Goodrich, ORD/National Homeland Security Research Center, EPA
Karen Kleier Schrantz, NRMRL
Dr. Mark Rodgers, NRMRL
Dr. Vahid Alavian, World Bank
Mr. Jeff Adams, ORD
Dr. Nancy Beller-Simms, National Oceanic and Atmospheric Administration
Dr. E.P.H. Best, ORD
Dr. Pratim Biswas, P.E, Washington University
Dr. Levi Brekke, Bureau of Reclamation
Mr. Mao Fang, P.E., Las Vegas Valley Water District
Mr. Gary Hudiburgh, EPA Office of Water, American Indian Environmental Office
Dr. Timothy C. Keener, P.E., University of Cincinnati
Dr. Paul Kirshen, University of New Hampshire
Dr. Julie King, U.S. Geological Survey
Dr. Thomas Johnson, ORD
Mr. Craig Patterson, P.E., ORD
Dr. Joo-Youp Lee, University of Cincinnati
Dr. Steven McCutcheon, P.E., D.WRE, ORD
Mr. Ken Moraff, EPA Region 1
Ms. Angela Restivo, EPA Region 6
Dr. Neil Stiber, EPA Office of Science Advisor

Mr. Michael J. Wallis, East Bay Municipal Utility District, CA
Dr. Xinhao Wang, University of Cincinnati
Cadmus, Inc.: Glen Boyd, Dr. Rudd Coffey, Laura Dufresne, Charles A. Hernick,
Ken Klewicki, Dr. Jonathan Koplos, William M. Jones, Frank Letkiewicz,
Richard Kro, Vanessa M. Leiby, Jeff Maxted, G. Tracy Mehan III, Tom
Mulcahy, Karen Sklenar, Mary Ellen Tuccillo
Dr. Audrey Levine, formally at the National Science Foundation

ABSTRACT

This report, *National Water Infrastructure Adaptation Assessment: Part II, Smart Urban Design (SUD) and Case Studies*, is a part of the research effort led by the EPA Office of Research and Development (ORD) Water Systems Division. The multiyear research, organized by ORD's Air and Energy (A-E) research program, has generated data, models, and methods to assess the water infrastructure vulnerability and develop sustainable planning and designs for urban infrastructure. The research results are summarized in separate EPA reports.

The first report, published in 2015, contains a preliminary regulatory and technical analysis of the U.S. water infrastructure and its relationship to hydroclimatic and socioeconomic changes. This second report presents SUD tools and methods for urban planning and infrastructure adaptation design. The report and its content aim to assist water practitioners and urban planners in developing resilient water supply systems and water management programs. The tools and methods also help users with an understanding of the interconnectedness among urban growth, transportation, and water systems. In sequence, the report first outlines adaptation objectives and the SUD framework. Next, it evaluates the unique environmental properties associated with urban growth and describes current planning practices that facilitate such growth. In Sections 3.0 through 7.0, the core SUD components in urban planning and water system engineering are described with case studies for illustration. In Section 8.0, the SUD applications in coastal areas are presented to illustrate adaptation consideration and approaches against complex and interconnected hydroclimatic impacts.

Water infrastructure adaptation may take place at three different levels: (1) urban-wide planning and adaptation, (2) system-scale water master planning, and (3) local-scale adaptive engineering and design of infrastructure components. The urban-wide adaptive planning relies on integrated analysis and scenario-based simulation of future land use, socioeconomics, and transportation and water infrastructure. The aim is to improve urban efficiency and achieve adaptation co-benefits in economics and systems resilience. At the system scale, SUD adaptation tools enable systems evaluation (e.g., trade-off analysis) for master planning options. At the local scale, the newly developed SUD tools and methods enable users to model, evaluate, and optimize water treatment, distribution, storage, and energy conservation. Together with monitoring and forecasting techniques to be described in other assessment documents, these SUD methods and tools form a suite of adaptation techniques designed for water infrastructure planning and system improvement.

The SUD adaptation methods were examined in case studies in the U.S. inland and coastal regions. These applications include studies of urban infrastructure and water systems in Cincinnati, Ohio; Manatee County, Florida; Las Vegas Valley Water District, Nevada; and Mattapoisett, Massachusetts. They are presented to highlight the adaptation considerations and the use of SUD tools and methods.

Table of Contents

DISCLAIMER	i
FOREWORD	ii
PREFACE	iii
ACKNOWLEDGMENTS	iv
ABSTRACT	vii
Definitions and Abbreviations	xviii
Part Two: Smart Urban Design (SUD) and Application Case Studies	1
1. Sustainable Development of Urban Water Systems	1
1.1. Adaptation considerations	2
1.1.1. Defining adaptation objective	3
1.1.2. Understanding urban adaptation constraints	6
1.1.3. Revising or redefining planning and engineering focus	10
1.1.4. Selecting adaptation evaluation matrix	13
1.2. Three levels of water infrastructure adaptation	15
1.3. Smart Urban Design (SUD) for systems analysis	15
1.3.1. Integrated Watershed Modeling (IWM)	15
1.3.2. Adaptive Urban Planning and Engineering Tool (AUP&ET)	20
1.3.3. SmartWater for water supply	22
1.3.4. Source-to-tap water supply in a systems approach	24
2. Adaptive Urban Planning in Urban Scales	24
2.1. Physical infrastructure and urban forms in current practice	25
2.1.1. Land use encouraging urban sprawl	26
2.1.2. Transportation and energy performance	28
2.1.3. Water planning and engineering	29
2.2. Transformation toward smart growth	30
2.3. Monitoring and re-evaluation	31
3. SUD Methods and Tool in Adaptive Urban Planning	32
3.1. AUP&ET principles and utilities	33
3.1.1. Land use projection – CA-Markov model and ICLUS	33
3.1.2. Calibration and validation of the land use simulation model	35
3.1.3. AIR-SUSTAIN system for transportation simulation	36
3.1.4. The linkage to water infrastructure simulations	38
3.2. The AIR-SUSTAIN simulation tool for transportation	38
3.2.1. Basic functions and interfaces of AIR-SUSTAIN	39

3.2.2.	Travel demand forecasting – VISUM.....	41
3.2.3.	Assistance in traffic congestion identification.....	42
3.2.4.	Microscopic simulation using VISSIM	43
3.2.5.	Emission estimation using MOVES	43
4.	Adaptive Urban Planning in SUD Case Studies	45
4.1	Urban form and urban infrastructure	46
4.1.1.	Urban form and land use patterns	46
4.1.2.	Transportation and traffic distribution.....	48
4.1.3.	Urban form and air quality.....	50
4.1.4.	Thermal inversion and mixing height.....	53
4.1.5.	Urban and exurban differences	54
4.1.6.	Urban form effects on urban heat island and air quality.....	55
4.2.	Adaptive urban planning modeling and analysis in Cincinnati	64
4.2.1	Three development scenarios.....	64
4.2.2	Transportation and emission analysis using AIR-SUSTAIN tool	65
4.3	Adaptation analysis for water master planning in Manatee County, Florida	75
4.3.1	Water supply assessment	76
4.3.2	Expansion scenario analysis	82
4.3.3.	Quantitative modeling and systems analysis	85
4.3.4.	Adaptation analysis results on cost and carbon/energy footprint	89
5.	System-Scale Adaptation for Existing Urban Water Infrastructure.....	93
5.1.	Basic considerations in adaptation engineering.....	95
5.1.1.	Adaptation engineering for water infrastructure.....	95
5.1.2.	Adaptation attributes of three types of water infrastructure	97
5.1.3.	The capacity reserve concept and climate resilience	99
5.1.4.	CR and engineering practice.....	101
5.2.	Water infrastructure capacity reserve and resilience	102
5.2.1.	Stormwater infrastructure functions and design tolerances	102
5.2.2.	Drinking water infrastructure functions and design tolerances	107
5.2.3.	Wastewater infrastructure functions and design tolerances.....	111
5.3.	Water infrastructure vulnerability analysis for adaptation.....	115
5.3.1.	The resilience assessment and two approaches	115
5.3.2.	Water resilience evaluation and resilience tool – CREAT	117
5.3.3.	From vulnerability analysis to adaptation engineering.....	120
6.	SUD Methods and Tools for Drinking Water Treatment.....	120
6.1.	Principle, models and algorithms in WTP-cam	121
6.1.1.	Conventional treatment unit processes	121

6.1.2.	Customization of GAC unit process	122
6.1.3.	Adaptation cost and economics	124
6.1.4.	Other unit processes for adaptation.....	126
6.2.	Adaptation Analysis using WTP-cam.....	126
6.2.1.	Treatment process and compliance targets	126
6.2.2.	Monte Carlo methods in modeling source water quality	128
6.2.3.	Advanced unit process and adaptation cost	132
6.3.	GCWW Richard Miller Treatment Plant case study using WTP-cam	133
6.3.1.	Miller water treatment plant operation and performance	134
6.3.2.	WTP-cam simulation of hydroclimatic change impacts.....	137
6.3.3.	Engineering analysis for water treatment adaptation.....	143
7.	Adaptation Engineering for Drinking Water Distribution	146
7.1.	Water age and water quality changes in distribution: The need for adaptation.....	147
7.1.1.	EPANET-based risk assessment on DBP formation	147
7.1.2.	Water age variations, modeling and adaptive control.....	150
7.2.	In-network water treatment as adaptation measure	152
7.3.	Water conservation, storage and reuse through adaptive planning.....	155
8.	SUD Applications in Coastal Regions: Water Infrastructure and Emergency Planning ..	155
8.1.	Water infrastructure vulnerability in coastal regions.....	155
8.2.	Wastewater vulnerability and adaptation in storm surge.....	159
8.3.	Emergency evacuation and water supplies	160
9.	Summary and Recommendations	162
10.	References	165
Appendix A AIR-SUSTAIN Program Input and Output Structures		184
Appendix B Water Treatment Plant – Climate Adaptation Model (WTP-cam) User’s Manual		248

List of Tables

Table 2-1	Adaptation attributes for common objectives	14
Table 2-2	General advantage and challenges of three-level adaptation actions.....	16
Table 2-3	Selected urban functions impacted by hydroclimatic conditions	25
Table 2-4	Four daily periods of traffic compositions on the highway in Cincinnati, OH.....	49
Table 2-5	Locations and traffic flow in 2009 for selected locations in the Cincinnati road network	52
Table 2-6	Statistics of daily temperature measurements at NQAAS Station 17-061-00040	53
Table 2-7	Temperature differences between the reference station and other stations abstracted from the >10-year daily temperature measurements	59
Table 2-8	Trip generation results in the number of trips per day by the target year 2030	72
Table 2-9	Trip distribution results for the number of trips per day originated from and attracted to centers	72
Table 2-10	Average queue length, average wait time, total delay, and average delay during morning peak hours (7:00 ~9:00 am).....	73
Table 2-11	Water demand in 2006 and projections for wholesale customers in annual average.	78
Table 2-12	Water demand projections for retail and significant users in annual average	78
Table 2-13	Twenty alternatives for water supply expansion in the county master planning..	79
Table 2-14	Maximum water credit and unit cost of the twenty water supply alternatives	82
Table 2-15	Life cycle analysis of carbon footprint for the twenty water supply alternatives	84
Table 2-16	Optimal solutions of the multi-objective model	90
Table 2-17	The Pareto optimal expansion strategies (n = 1).....	90
Table 2-18	The Pareto optimal expansion strategies for the best and worst cases (n = 1).....	91
Table 2-19	Water infrastructure design and engineering domains, and their attributes.....	103
Table 2-20	Important engineering attributes for stormwater infrastructure adaptation	105
Table 2-21	Important engineering attributes and likely vulnerability in drinking water treatment and distribution systems for community water supplies.....	109
Table 2-22	Important engineering attributes and potential vulnerability of wastewater infrastructure	112
Table 2-23	Types and approaches of eight water utilities in climate vulnerability assessment	116
Table 2-24	GAC contactor cost estimate parameters	124

Table 2-25	GAC reactivation cost	125
Table 2-26	Illustration of calculating running annual average for finished water TOC	128
Table 2-27	Options for Monte Carlo analysis.....	131
Table 2-28	Miller WTP unit process design parameters.....	134
Table 2-29	Inflow and chemical feed levels for the Miller WTP	135
Table 2-30	Statistics of full-scale field measurements.....	135
Table 2-31	Source water inputs for the Miller water treatment plant in 1998 (Baseline).....	138
Table 2-32	Correlation matrix for source water quality parameters (for Ohio River from July 1997 to December 1998).....	140
Table 2-33	Projected raw water quality parameters for the Miller WTP in 2050.....	141
Table 2-34	Comparison of sampled and modeled water quality results	142
Table 2-35	Selected hydrological impacts and adaptation variables in coastal area.....	157
Table 2-36	SLOSH modeling parameters for storm surge modeling at Mattapoisett, MA. .	159
Table 2-37	Population affected for evacuation under four categories of hurricane	161

List of Figures

Figure 2-1	Schematic process diagram of iterative monitoring-adaptation framework for water infrastructure adaptation	3
Figure 2-2	Typical spatial relationships of water infrastructure in an urban environment with illustration of infrastructure adaptation scales and general process	4
Figure 2-3	Schematic diagram showing three major types of urban forms and their typical properties.....	7
Figure 2-4	General process of the current urban master planning and its relations to transportation and water infrastructure engineering.	8
Figure 2-5	Three major types of urban sprawl expanding the urban footprints into exurban areas	10
Figure 2-6	General process of adaptive urban planning and engineering.	12
Figure 2-7	Schematic diagram of the Smart Urban Design (SUD) structure for scenario-based urban development planning and engineering.	17
Figure 2-8a	Process flow diagram of the Integrated Water Management (IWM) modeling for watershed simulations.....	18
Figure 2-8b	Process flow diagram of the Integrated Water Management (IWM) modeling for urban catchment using EPA’s National Stormwater Calculator (U.S. EPA, 2014).	19
Figure 2-9	Process flow diagram of the scenario-based Adaptive Urban Planning and Engineering Tool (AUP&ET) for urban planning and engineering	21
Figure 2-10	Schematic diagram of conceptual modeling framework for WTP3.0 as a major SUD element.....	22
Figure 2-11	Schematic diagram of water supply and major system variables	23
Figure 2-12	Urban expansion and urban form transformation for Atlanta (upper) and Phoenix (lower) metropolitan regions between 1970 and 1992.	27
Figure 2-13	Transportation efficiency (annual delay, travel index, excess fuel use, and annual cost) in year 2007 as a function of urban population in the U.S. urban centers...	28
Figure 2-14	Simulation block diagram for CA-Markov based urban land projections	34
Figure 2-15	AIR-SUSTAIN modeling framework for transportation analysis of efficiency and carbon dioxide emission in urban infrastructure adaptation	37
Figure 2-16	AIR-SUSTAIN graphic interface for scenario modeling and analysis.....	39
Figure 2-17	The Results Comparison module interface in the AIR-SUSTAIN tool.....	40
Figure 2-18	General relationship between model precision and data requirements in traffic modeling	44

Figure 2-19	Modeling framework for emission estimation using both the macroscale VISUM and microscopic VISSUM traffic simulation models	45
Figure 2-20	Major transportation traffic routes and the urban physical footprints of the Cincinnati metropolitan region	47
Figure 2-21	Different land use patterns in areas among the 12 EPA's NAAQS monitoring stations	48
Figure 2-22	A schematic diagram of three-dimensional model for the urban form, traffic and atmospheric structure in the Cincinnati metropolitan region	49
Figure 2-23	Truck and passenger car traffic volume distribution in the Cincinnati metropolitan region.	51
Figure 2-24	Representative temperature profiles showing the boundary inversion and capping inversion	54
Figure 2-25	Temporal L_R and H_{inv} variations showing diurnal thermal inversion in the urban boundary layer in October 2011	55
Figure 2-26	T_{min} , ΔT , and $PM_{2.5}$ variations with time at NAAQS monitoring station 061-0040.	56
Figure 2-27	Temporal change of ambient temperature T_{min} and ΔT at station 061-0040 in the Cincinnati urban core	57
Figure 2-28	T_{min} at 17-061-0040 station is linearly correlated with those of other stations in the year 2005 measurements	58
Figure 2-29	Spatial variations of temperature difference for mean and maximum T_{avg} and $PM_{2.5}$ in cross section O-O'	60
Figure 2-30	Co-variation of minutely average wind speed at the I-75 site with the lapse rate in the boundary layer during the roadside black carbon dispersion experiments	61
Figure 2-31	Schematic diagram showing major types of microclimate conditions in the surface roughness layer (SRL) equivalent to the urban canopy layer (UCL)	63
Figure 2-32	The base-year distribution maps for the Cincinnati metropolitan area in 2009: A) population; B) household; and C) employment	65
Figure 2-33	Three development scenarios for the Cincinnati metropolitan area in the target year 2030.....	66
Figure 2-34	Setup of a new scenario in AIR-SUSTAIN	67
Figure 2-35	Program interface for A) importing the Base Year data; B) assigning population change; and C) assigning employment changes at TAZ levels	67
Figure 2-36	Simulation module of demographic analysis for a development scenario.	68
Figure 2-37	Transportation congestion areas identified for typical peak-hour traffic for 2009 in Hamilton County, showing concentrations along I-71, I-75, I-275N, and Ronald Reagan Highway.....	69

Figure 2-38	Population changes by 2030 for the three developmental scenarios (S1, S2, and S3 in the inserts) in comparison to the distribution of base year 2010 (background) ...	70
Figure 2-39	Changes in number of household by 2030 for the three developmental scenarios (S1, S2, and S3 in the inserts) in comparison to the distribution of base year 2010 (background).....	71
Figure 2-40	Employment changes by 2030 for the three developmental scenarios (S1, S2, and S3 in the inserts) in comparison to the distribution of base year 2010 (background).....	71
Figure 2-41	Simulated peak hour (7:00-9:00 am) traffic volume distribution over the Cincinnati road network for the base year (2010) and under three development scenarios in the target year (2030).....	73
Figure 2-42	Comparison of three development scenarios (S1, S2, and S3) in peak hour (7:00-9:00) vehicular CO ₂ emission and energy (fuel) consumption.....	74
Figure 2-43	Location of the Manatee County water supply system along the upper Manatee River in Florida	76
Figure 2-44	Locations of WTP, ASR, well fields (ECWF-1, MPWF), and the twenty potential water supply alternatives A1-A20.	77
Figure 2-45	The life-cycle system analysis flow diagram for determining carbon footprint in water infrastructure expansion alternatives.	83
Figure 2-46	Pareto solution fronts for the best compromised solutions to meet the projected future water demand (base case) and the demand with 10% uncertainties (best case and worst case).....	92
Figure 2-47	Suggested optimal facility expansion strategies in each of five-year periods based on the optimization modeling of water infrastructure expansion options for Manatee County, Florida	94
Figure 2-48	Assessment-adaptation process for water infrastructure planning and engineering.	96
Figure 2-49	Process schematic diagrams for typical centralized drinking water, wastewater, and stormwater infrastructure in an urban watershed.	98
Figure 2-50	Four types of infrastructure vulnerability under the threat of external impact event (e.g., storm surge).	99
Figure 2-51	Maximum percentage increase ($\Delta Q\%$) in hydraulic capacity of stormwater conveyance using commercial concrete pipes of discrete nominal diameters (D)	106
Figure 2-52	BOD removal efficiency of a wastewater activated aeration tank as a function of flow, BOD mass loading, and aeration capacity.....	113

Figure 2-53	Relative magnitude of infrastructure <i>CR</i> installed in current engineering practice (left) in comparison with the relative precipitation change (solid bar) and uncertainty (pattern and solid line with whisker) by 2060.	114
Figure 2-54	The process of climate vulnerability analysis using the EPA tool CREAT	118
Figure 2-55	Unit process, inputs and outputs in model simulation of WTP2.0 adopted in WTP-cam program	122
Figure 2-56	Cost curve for annual cost of GAC unit, indicating the cost associated with a given GAC reactivation period for the Miller WTP in Cincinnati.	125
Figure 2-57	Schematic diagram for (A) treatment unit process at the GCWW Miller water treatment plant, and (B) WTP-cam program flow in the example simulation....	126
Figure 2-58	Original input data for the example process train at the Miller WTP.....	127
Figure 2-59	Program logic sequences in Monte Carlo simulation of future source water quality variations using the correlation matrix method	129
Figure 2-60	Graphic user interface for inputs in Monte Carlo simulations of future water qualities.	130
Figure 2-61	Manual input window for influent water quality statistics	132
Figure 2-62	Temporal variations of influent and blended effluent TOC in the GAC unit	136
Figure 2-63	Temporal variations of inflow, mass inflow and active number of GAC contactors	136
Figure 2-64	Temporal variations of active contactors and blended effluent TOC concentration	137
Figure 2-65	Time series of plant inflow and EBCT variations	137
Figure 2-66	Normal probability plots for source water pH (107 samples) and TOC (93 samples) for Ohio River from the ICR database (July 1997-December 1998)...	138
Figure 2-67	Modeled treatment performance of the Miller WTP in baseline (1998) and future (2050) scenarios.	144
Figure 2-68	Accumulative probability of net annual adaptation cost for the source water change scenario in year 2050.....	145
Figure 2-69	Schematic diagram showing the simultaneously occurring chlorine reactions in bulk and wall demands, and mass exchange between the bulk water and pipe wall.	149
Figure 2-70	Water demand and computed <i>Re</i> variations in a two-week period for a single home, 31 and 114 homes of a pipe dead-end section, showing significant differences between the APAD model and the generalized water demand pattern.	151
Figure 2-71	Probability distribution and corresponding CDF of simulated water age for the network	152

Figure 2-72	Schematic views of in-network aeration in the LVVWD water distribution network to remove volatile THM from drinking water in the alpha tank reservoir	153
Figure 2-73	EPANET simulation of flow and THM distribution in the Western Hill portion of the LVVWD water distribution system.	154
Figure 2-74	Schematic illustration of long-term climate and short-term meteorological and disruptive storm surge events in a typical coastal zone... ..	156
Figure 2-75	Schematic diagram showing wave action and storm surge height as a function of storm surge, tidal cycle, and sea level rise.....	158
Figure 2-76	Location of the water infrastructure at the Town of Mattapoisett aside of the Mattapoisett Harbor... ..	160
Figure 2-77	A cartoon illustration of SLOSH modeling results on likely inundation risk for the wastewater transfer station at Mattapoisett, MA	161
Figure 2-78	Hourly traffic map in the Mattapoisett region after evacuation order activated at noon time.. ..	162

ABBREVIATIONS AND NOTATIONS

Definitions and Abbreviations

AADT	annual average daily traffic
AERMOD	American Meteorological Society and U.S. Environmental Protection Agency Regulatory Model
AIR-SUSTAIN	Air Impact Relating Scenario-Based Urban Setting and Transportation Asset in Network
APAD	all-pipe and all-demand
ASR	aquifer storage and recovery
AUP&ET	Adaptive Urban Planning and Engineering Tool
AwwaRF	former name of Water Research Foundation
BASINS	U.S. Environmental Protection Agency's Better Assessment Science Integrating Point and Non-Point Sources model
BOD	biological oxygen demand
CA-Markov	cellular automata-Markov
CAL3QHC	CALINE3-based monoxide model with queuing and hot spot calculations and with a traffic model to calculate delays and queues
CBD	central business district
CDF	cumulative density function
CR	capacity reserve
CREAT	Climate Resilience Evaluation and Awareness Tool
CRWU	Climate Ready Water Utilities
CSO	combined sewer overflow
CSS	combined sewer system
CWA	Clean Water Act
D/DBP	disinfectant/disinfection by-product
DALR	dry adiabatic lapse rate
DBP	disinfection by-product
DOC	dissolved organ carbon
EBMUD	East Bay Municipal Utility District
GAC	elemental carbon in air emission
ECWF-1	East County Wellfield I
EPA	U.S. Environmental Protection Agency
FHWA	Federal Highway Administration
GAC	granular activated carbon
GCWW	Greater Cincinnati Water Works
GHG	greenhouse gas
GIS	geographical information system
GUI	graphical user interface
HAAs	haloacetic acids (nine individual species and the total of five (HAA ₅), six (HAA ₆) and nine (HAA ₉) species)

HDVC	hourly demand variation curve
HSPF	Hydrological Simulation Program – Fortran
ICLUS	U.S. Environmental Protection Agency’s Integrated Climate and Land Use Scenarios
ICR	information collection rule
IDF	precipitation intensity-duration-frequency
IPCC	United Nation’s Intergovernmental Panel on Climate Change
IWM	integrated watershed modeling
LANDSAT	land remote-sensing satellite (system)
LCA	life cycle analysis
LID	low-impact development
LVVWD	Las Vegas Valley Water District
MARS	Manatee [County, Florida] Agricultural Reuse Supply
MCE	multiple criteria evaluation
MCL	maximum contaminant level
MCUD	Manatee County Utility Department
MS4s	Municipal separate storm sewer systems
MEOW	Maximum Envelope of Water
MGD	million gallons per day
MIA	most impacted area
MODIS	moderate resolution imaging spectroradiometer (for satellite)
MOM	Maximum of MEOW (Maximum Envelope of Water)
MOVES	U.S. Environmental Protection Agency’s Motor Vehicle Emission Simulator model
MPWF	Mosaic Phosphate Wellfield
MSX	EPANET-Multi Species Extension
NAAQS	U.S. Environmental Protection Agency’s National Ambient Air Quality Standards
NHSA	North Hudson Sewerage Authority
NOAA	National Oceanic and Atmospheric Administration
NOM	natural organic matter
NPDES	National Pollutant Discharge Elimination System
NRMRL	U.S. Environmental Protection Agency’s National Risk Management Research Laboratory
NTU	nephelometric turbidity unit
NYCDEP	New York City Department of Environmental Protection
O&M	operation and maintenance
OC	organic carbon in air emission
OKI	Ohio-Kentucky-Indiana Regional Council of Governments
ORD	U.S. Environmental Protection Agency’s Office of Research and Development
OTAQ	U.S. Environmental Protection Agency’s Office of Transportation Air Quality
PR/MRWSA	Peace River Manasota Regional Water Supply Authority
PVC	polyvinyl chloride
RSSCT	rapid small-scale column test

SAWS	San Antonio Water System
SBL	stable boundary layer
SCMs	Stormwater control measures
SDWA	Safe Drinking Water Act
SLOSH	Sea, Lake, and Overland Surges from Hurricanes
SRES	Special Report on Emissions Scenarios
SUD	Smart Urban Design
SWAT	Soil and Water Assessment Tool
SWFWMD	Southwest Florida Water Management District
SWMM	U.S. Environmental Protection Agency's Stormwater Management Model
TAZ	traffic analysis zone
TDF	travel demand forecasting
THM	trihalomethane
TOC	total organic carbon
TTHM	sum of four individual species of trihalomethanes
UHI	urban heat island
USGS	U.S. Geological Survey
UVA	ultraviolet absorbance at 254 nm
VISSIM	a microscopic traffic model after "Verkehr In Städten - SIMulationsmodell"
VISUM	a macroscopic traffic model after "Verkehr In Städten - SIMulationsmodell"
VSP	vehicle specific power
WASP	Water Quality Analysis Program
WEAP	Water Evaluation and Planning
WTP	water treatment plant
WTP-cam	water treatment-climate adaptation model
WUP	water use permit

Notation and Symbols in Equations

α	level of significance
η_{BOD}	biological oxygen demand (BOD) removal rate
\mathcal{E}_t	a vector of independent, normally distributed random variables with mean zero and variance one
θ	hydraulic residence time
θ_c	biomass cell age in aeration tank
ϑ	defined by $\vartheta = (1 + k_d \theta_c) / \theta_c$
μ_0	average of water quality for the baseline scenario
μ_1	average of water quality for the future scenario in 2050
ρ	correlation coefficient
σ_0	standard deviation of water quality for baseline scenario
σ_1	standard deviation of water quality for future scenario in 2050
$\sigma_{Q_{ij}}$	standard deviation of Q_{ijk}

$\sigma_{Q_{2ij}}$	standard deviation of Q_{2ijk}
Ψ	defined by $\Psi = X/Y_0$
c_0	initial BOD concentration
D	GAC reactivation period
D_0	a known correlation matrix for the nine raw water quality parameters
$EBCT$	empty bed contact time
i	sequence number of pixels of a quantitative component
j	sequence number of time period
k_d	BOD degradation constant
m_0	mass loading
Q	flow rate
TOC_{eff}	effluent TOC concentration from GAC processing
TOC_{in}	input TOC concentration to GAC unit
$USRT$	process design or operating variable
V	aeration tank volume
w	weighing factor
X	microorganism concentration in the aeration tank in milligrams per liter; and TOC increment over the compliance criterion, 2 mg/L
y	capital of operation and maintenance cost for GAC processing
Y	maximum yield coefficient in mg/mg for an aeration tank; and net annual cost of GAC processing
z_t	vector of nine raw water quality parameters used in water treatment plant -climate adaptation model (WTP/WTP-cam) modeling

Part Two: Smart Urban Design (SUD) and Application Case Studies

The national adaptation report Part I (U.S. EPA, 2015a) described multiple environmental and economic stressors facing our nation's water infrastructure. It further discussed the adaptation need for improving infrastructure resilience and sustainability. This Part II report investigates the relationship through scenario-based adaptation among the factors of hydroclimatic and land use changes, urban growth, population shifts, transportation, energy, air and water pollution, and water management. These factors can be shown to interact at the watershed, urban, and system-specific scales. For example, urban development may lead to the occurrence of an urban heat island (UHI), which increases energy use and water consumption, but may reduce overall energy needs when smart growth policies are devised. Low-density development leads to a lesser UHI effect but higher energy use in transportation, adding to air pollution. Development can alter rainfall and runoff characteristics, which, subsequently, can impact water quality and water supplies. The water quality and quantity changes may require water plant processes to be altered, potentially increasing energy needs. Poorly planned patterns in urban development also affect water demand distribution and sewer system operations with respect to water age and quality, sanitary and storm sewer pipe network, and, hence, power usage. These examples show that water infrastructure sustainability is a multidimensional issue intrinsically related to watershed management, urban development pathways, and individual water system engineering.

This Part II report presents the Smart Urban Design (SUD) tools and methods, their principles for urban planning and infrastructure adaptation design. SUD development in this research aims to define the interconnectivity and to assist water practitioners and urban planners in developing more resilient and efficient water infrastructure. In sequence, the report first outlines adaptation objectives and the SUD framework at three spatial scales. Next, it describes unique environmental properties associated with urban growth and current planning practices that facilitate such growth. In Sections 3.0 through 7.0, the core SUD components in urban planning and water system engineering are described. Case studies are presented to provide further insight into the function and utility of SUD tools and methods. For SUD application in coastal areas, Section 8.0 briefly illustrates the complex factors of the hydroclimatic impacts in adaptation planning. The summary and recommendations are presented in Section 9.0.

1. Sustainable Development of Urban Water Systems

Given that practitioners and water managers are risk-averse, a properly defined design basis for hydrological impacts from climate and land use changes is the first and fundamental step. How to develop the design basis can affect directly the infrastructure management objectives in years to come. Because much of this infrastructure will remain in place for 50 to 100 years, there is significant uncertainty on how it relates to planning today and on the potential for stranded capacity in the future, which is costly to tax and ratepayers. Failure to provide adequate infrastructure has serious economic and social consequences. Similarly, the uncertainty resulting from the capacity excess or deficit creates significant concern for local officials charged with infrastructure management. Providing methods and tools to help reduce these uncertainties and, thus, assist technical managers to construct a more resilient future is the focus of this research report.

1.1. Adaptation considerations

The projections of future hydroclimatic and land use conditions have uncertainties. Often the degree of uncertainty can be too large for widely used planning and engineering practices without undue economic cost in urban development. Inflexible water infrastructure is capital-intensive, and the water industry is risk-averse. Incorporating uncertainty into the planning and design process is essential. The adaptation process defined by this report is intended to manage the uncertainties of the hydrological and land use projections (Figure 2-1). It aims to reduce the uncertainty to the degree appropriate for infrastructure projects. The process incorporates a step of reevaluating the adaptation design and objectives for the ability of further adaptation to the changing circumstances. This adaptive practice is pertinent when significant hydroclimatic impacts are realized in a local watershed.

Because of the uncertainty in future projections, water managers need to manage the risk from inadequate, poorly planned, or delayed adaptation efforts. The consequences of inadequate adaptation and adaptation limitations have been described in the literature (e.g., Felgenhauer and Bruin, 2009; Felgenhauer and Webster, 2013). For this consideration, SUD tools and methods are developed in systems approach with the aim to maximize adaptation co-benefits of the long-life and capital-intensive water infrastructure investment by minimizing contributions to global impacts (e.g., reduced emissions), providing for added economic efficiency (e.g., improved transportation and water service), protecting public and private infrastructure investments, and minimizing the need for future costly infrastructure retrofitting and even reconstruction.

Hydrological responses to climate and land use changes are realized over long durations, while short-term disruptive meteorological events or climate impacts of large magnitudes can be explicit and quantifiable. Examples of disruptive events include storm surge, urban flooding, and salt water intrusion, all of which commonly are found in coastal areas. For these explicit impacts, actionable technical information is usually available for the design and implementation of adaptation actions. This scenario is marked as step 1 in Figure 2-1. For long-term hydrological impacts, model simulations of land use and future climate frequently are used to project hydrological conditions in a local watershed where the water infrastructure is located. These projections often have a substantial degree of uncertainty. Corresponding adaptation actions are marked as the Tier-I in Figure 2-1. The integrated model simulation and monitoring framework to quantify the combined hydrological effects of future climate, land use, and population changes will be presented in subsequent publications.

Processes A and B in Figure 2-1 involve real-time or near real-time monitoring and data analysis as tools to validate and further refine climate and land use projections. This approach can decrease the uncertainty in future projections. The land use and climate modeling updates, marked as actions a and b in Figure 2-1, may improve the projections for less uncertainty. Then the outputs and subsequent integrated hydrological modeling may help develop the technical basis for adaptation planning and engineering design. This step is marked as step 2 in Figure 2-1. In case the results have large certainty for engineering design and adaptation evaluation, the iterative process continues in steps 3 and 4. For this objective-oriented monitoring-to-adaptation process, the tools for integrated hydrological modeling and the near real-time monitoring are available. Examples include the framework using MODIS and LANDSAT satellite imagery (e.g., Chang et al., 2006, 2014a,b), the integrated hydrological modeling of climate and land use changes in a local watershed (e.g., Tong et al., 2012).

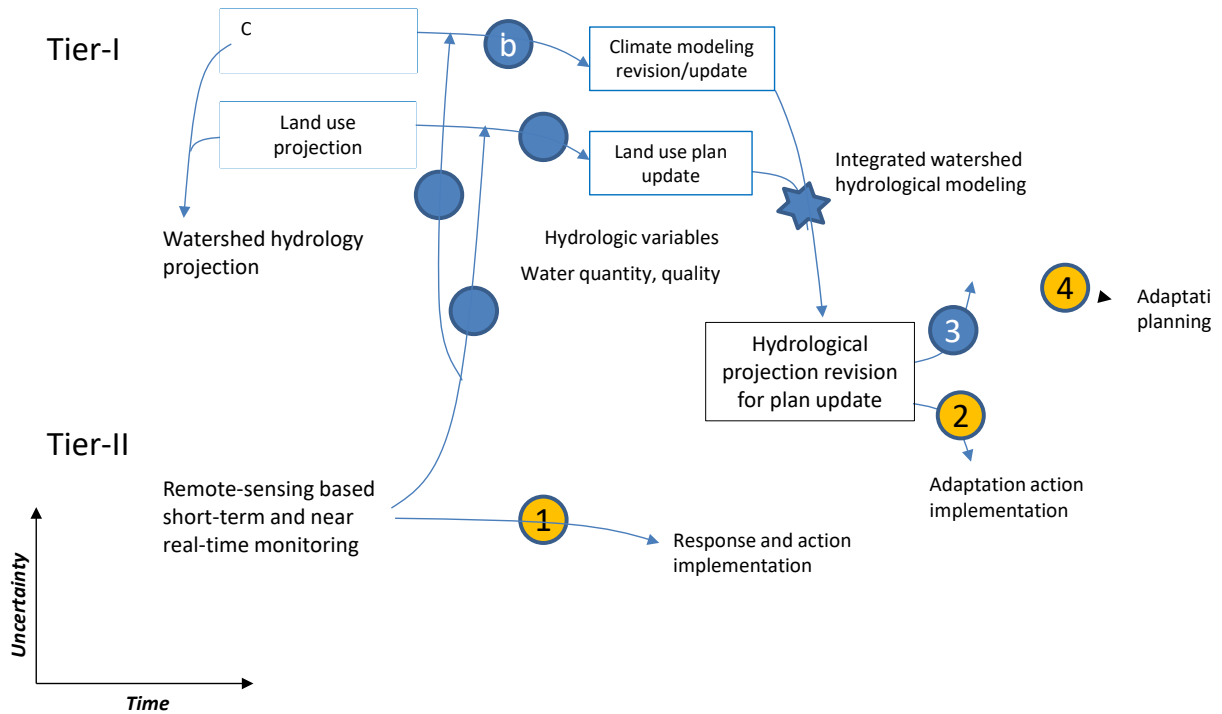


Figure 2-1 Schematic process diagram of iterative monitoring-adaptation framework for water infrastructure adaptation. Symbols show steps in design basis development for processes A/a and B/b (see text for details).

Water infrastructure and transportation infrastructure are two fundamental elements in urban developments that provide vital urban services and support economic activities. Several considerations in framing the infrastructure adaptation are important, including objective definition; constraint assessment; adaptation feasibility analysis; adaptation option comparison; and, finally, adaptation effectiveness evaluation. These considerations are specific to the physical boundary of the service area or projected service area under consideration (Figure 2-2), whether the adaptation is on the scale of a watershed, urban water systems, or unit operations (e.g., distribution pipe network). The adaptation effectiveness evaluation yields data and results to compare with the urban development objectives. When necessary, the stakeholders and local managers may take further urban adaptation actions, and even adjust the development goals and objectives. This systematic approach can serve as a venue to better communicate the adaptation options and their trade-offs to stakeholders.

1.1.1. Defining adaptation objective

Water infrastructure adaptation to future hydroclimatic and land use conditions is effective when taken in the context of sustainable urban and socio-economic development, a central objective for many stakeholders. This emphasis agrees with the objective “downscaling” concept described by Brown et al. (2012). Although specific goals of adaptation may vary among

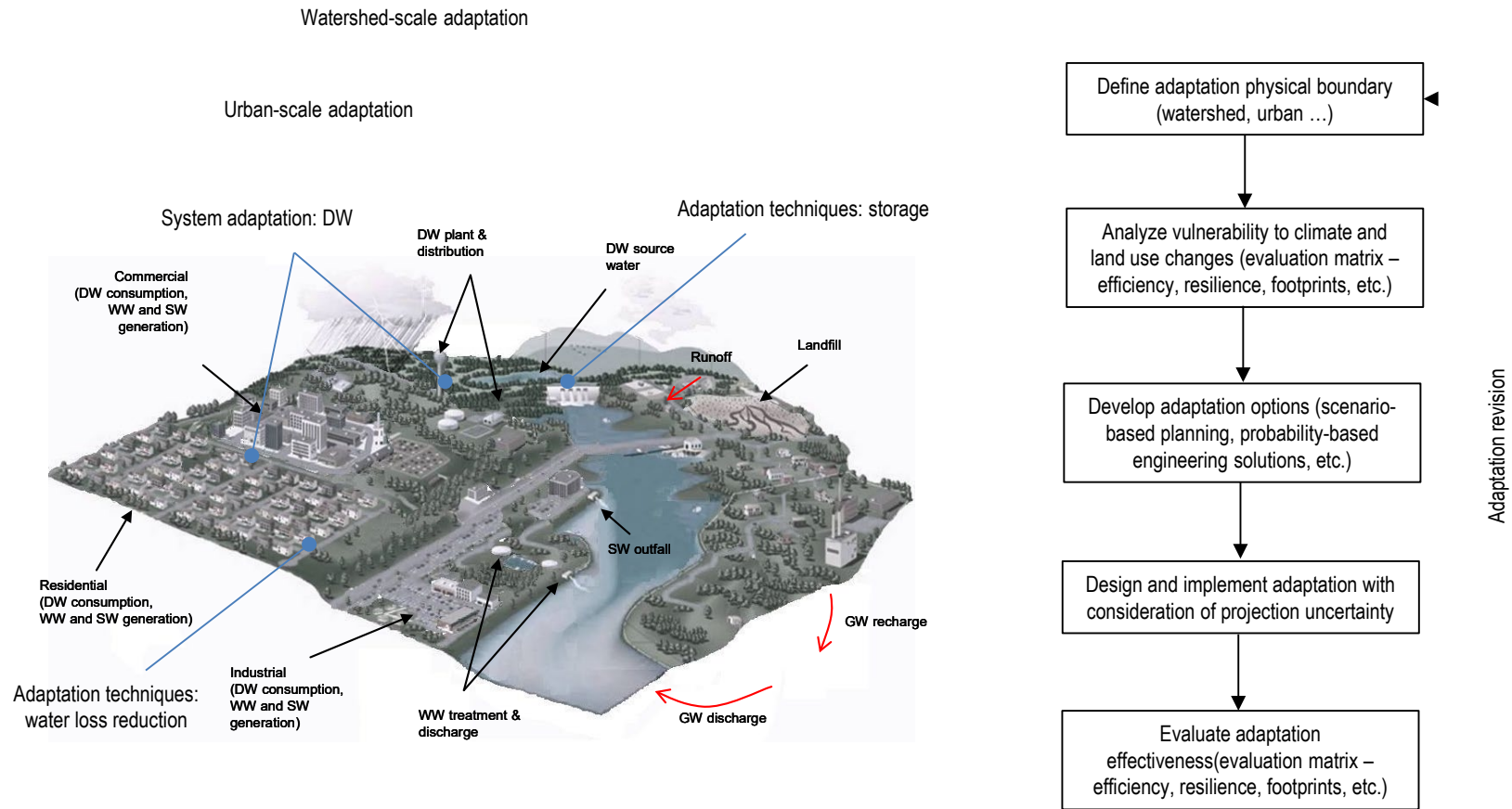


Figure 2-2 Typical spatial relationships of water infrastructure in an urban environment with illustration of infrastructure adaptation scales and general process. (SW – stormwater, DW – drinking water, GW – groundwater, WW – wastewater)

stakeholders and local conditions, an overreaching and commonly shared objective can be described as follows:

- To enhance water infrastructure resilience. The ultimate purpose is to provide uninterrupted water supply and wastewater services and to provide stormwater management and urban drainage for a projected socioeconomic growth under both current and future climate conditions.
- To increase the technical ability to comply with the existing regulations and help the implementation of urban development policies. The environmental regulations related to hydrological impacts were reviewed in the National Water Infrastructure Adaptation Assessment Part I (U.S. EPA, 2015a). For example, the case studies in Sections 6.0 and 7.0 show examples of adaptation actions against the projected increase of total organic carbon (TOC) content in source water, the increase of water age in underutilized sections of the drinking water distribution network, and, consequently, the increase in disinfection by-product (DBP) formation in the water supply. Such a combination of natural and developmental factors can be a prominent concern for water managers.
- To achieve the co-benefits of water infrastructure adaptation in environmental resilience and sustainable urban growth. Water infrastructure construction and operation consume a significant amount of energy and yield air emissions, water pollution, and negative ecological impacts. Thus, the co-benefit in optimized transportation and water infrastructure development and operation should be and can be maximized through systematic analysis. This is important in the view of urban growth and future energy needs (Yang and Goodrich, 2014; Yang, 2010; Dodder, 2014; Dodder et al., 2011).
- To minimize the systems' adaptation cost

There is a need to analyze water and transportation infrastructure together; both infrastructure types are the traditional and fundamental focus of urban planning and development. Transportation and water infrastructure are planned for a given urban development. In turn, they also induce and can facilitate further expansion and shifting of population and economic activities as the urban area grows. In addition to the traditional water management functions, attention has been galvanized recently on water availability on the supply side and water footprints on the consumption side. For water infrastructure, these fundamental concepts can be expressed as water reuse or reclamation; water storage; water loss prevention; water conservation; and, more importantly, water-energy nexus (PNNL, 2012; Yang and Goodrich, 2014, and references therein).

One important attribute in adaptation is the time horizon for infrastructure planning and urban development in general. In many parts of the United States, rapid urbanization and newly improved or constructed infrastructure services are projected to concurrently occur with significant changes in hydroclimatic conditions. Globally at the beginning of this decade, urban centers only occupied about 2% of land area on Earth but accounted for 70% of global energy consumption and air emissions (e.g., Parshall et al., 2010; ADB, 2012; IEA, 2013a,b). The urban population is projected to increase further, from 3.4 billion in 2009 to 6.3 billion by 2050 (IPCC, 2014). In the future, the urban change likely will lead to an even greater contribution to global energy, water, and food consumption, as well as air emissions. Adaptation action is necessary to improve sustainability to meet the needs of projected urban growth.

Because of the higher population density in urban centers, emission intensity, and water consumption rates on a per capita basis are mostly lower than national averages (Dodman, 2009; ADB, 2012). Therefore, the shifting of energy and water consumption into high-density urban centers creates the location-specific socioeconomic dynamics that adaptation needs to address. The conditions in the U.S. are similar. In this urbanization trend, adaptation offers opportunities to reduce per capita emissions and water consumption, enabling meaningful changes in global energy consumption growth (Dodman, 2009). Urban infrastructure development and redevelopment have significant potentials to recognize these co-benefits (Yang and Goodrich, 2014). Further decreases in per capita emissions and water intensity are possible, depending on the design and implementation of urban planning and adaptation actions that are both effective and economically viable.

Effective infrastructure adaptation can be achieved in a systems approach. Many urban sustainability issues and assessment matrices are described in relevant U.S. Environmental Protection Agency (EPA) publications (e.g., U.S. EPA, 2007b,c; 2009b; 2012a). For example, high-density developments, mixed-use zoning, walkable communities, and green development all are specific sustainability measures. These measures have the potential to eliminate unnecessary urban sprawl, thereby effectively adapting water and transportation infrastructure to a changing environment. Such developments all are focused on urban performance and efficiency in the form of energy and water footprints and their combination with economic benefits (e.g., Chang et al., 2012; Yao et al., 2014). These considerations will be discussed further in Sections 2.0 through 4.0.

1.1.2. Understanding urban adaptation constraints

The National Water Infrastructure Adaptation Assessment Part I (U.S. EPA, 2015a) described the vast water infrastructure built in the nation over the past century, and discussed the stressors on these water infrastructure systems (e.g., aging infrastructure, increasing demand) and the implications of their ability to be adaptable to future changes while complying with regulations. In the past, a significant national investment has been made to create this vast physical urban infrastructure. Now it is being made continuously to improve the infrastructure's reliability, resilience, and service. Thus, the physical footprints, planning guidelines, and existing engineering practices, all define the premise on which the constraints must be understood and managed for adaptation.

In urban development, water infrastructure is associated spatially with transportation infrastructure: highways, roads, and mass transit. Both types of urban infrastructure form the structural building blocks of urban communities. The resulting "urban form" defines the social structure, population, and business distribution, and it is reinforced by local zoning laws and ordinances. Common types of urban forms are monocentric, polycentric, and the combination of two (Figure 2-3). Each of the urban forms defines how urban population and economic activity are distributed in space. This reinforcing mechanism results in the so-called infrastructure "locked-in condition" that limits the optimization potential in water infrastructure and other urban systems. Consequently, change to how urban systems are planned is necessary. This requires the ability to overcome the physical as well as socioeconomic barriers associated with these locked-in infrastructure systems.

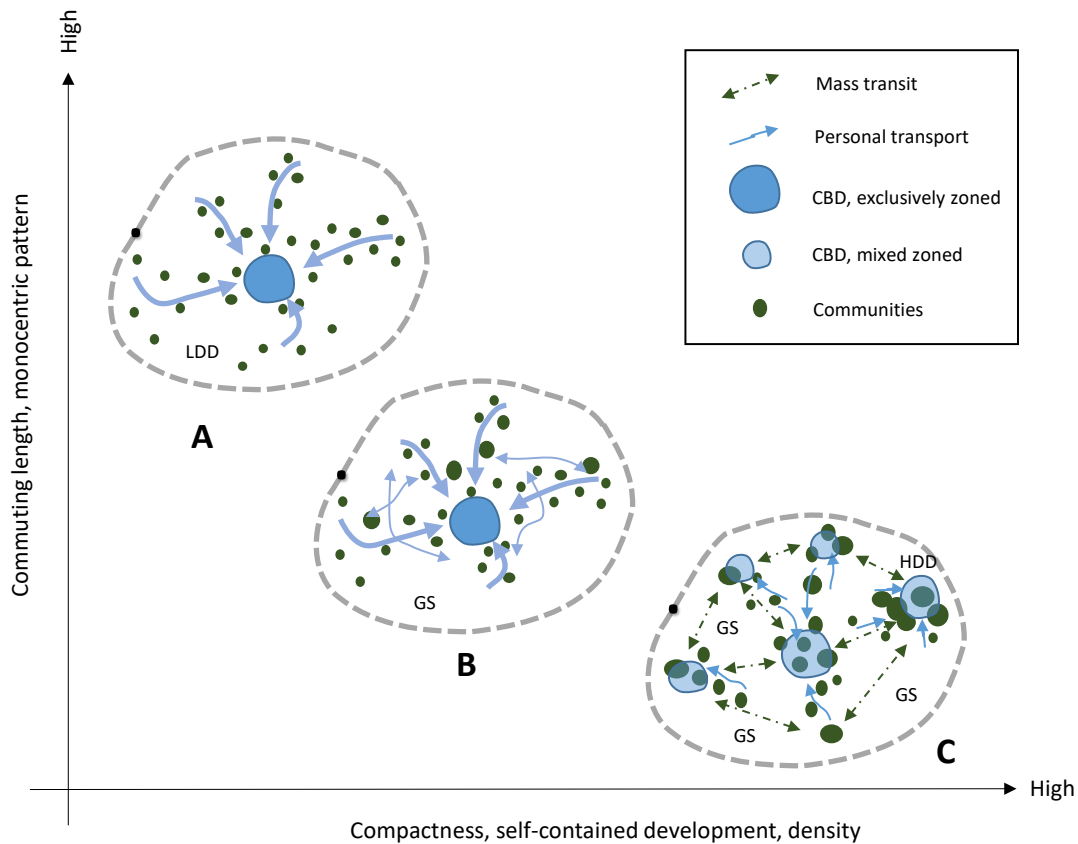


Figure 2-3 Schematic diagram showing three major types of urban forms and their typical properties: A – monocentric, B – mixed development with high reliance on personal transport, and C – polycentric developments with mass transit. (GS – green space; LDD – low-density development area; HDD – high-density development area; and CBD – central business district).

The current urban development is oriented toward protecting public health and meeting service demands, while being limited by economic considerations. The development mode has resulted in an unprecedented urban sprawl that expands the urban footprint into exurban areas. Figure 2-4 shows the process in the current practice of urban infrastructure planning and engineering. It starts with stakeholder engagement to determine urban socioeconomic goals, the projected or anticipated growth factors, and other socio-physical conditions. The subsequent master urban planning guides the type and spatial distribution of urban land use, economic activities, residential distribution, and environmental assets, including water resources, parks, green space, and preservation of environmentally sensitive areas. The guidelines can be implemented and enforced using the zoning ordinances and other local regulations. This traditional practice in urban planning leads to a final urban form, in which population and urban activities are distributed in the monocentric, polycentric forms, and variations between these two end-members (Figure 2-3).

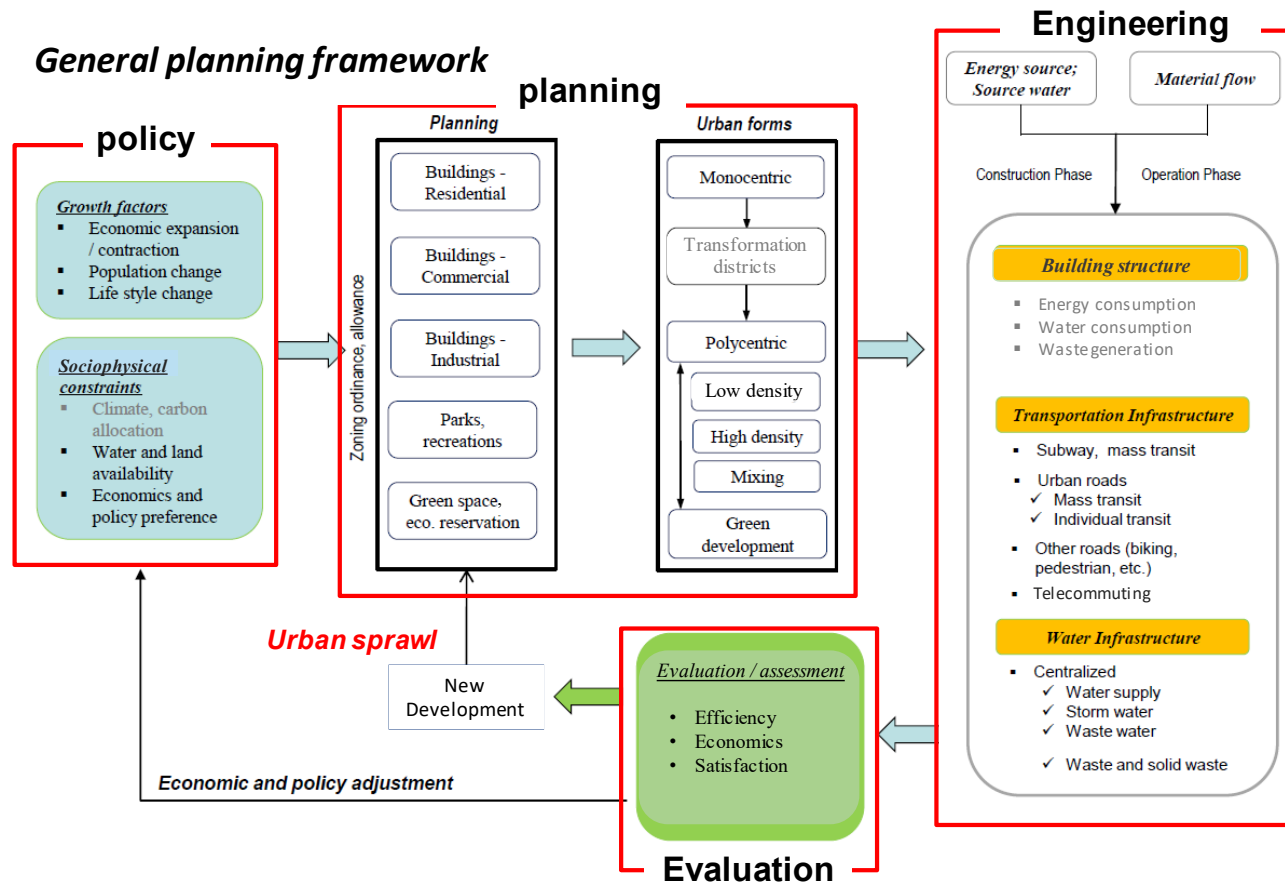


Figure 2-4 General process of the current urban master planning and its relations to transportation and water infrastructure engineering. Less emphasis on urban form transformation and the evaluation criteria often results in urban sprawl. The element in gray text in Planning step is not applicable; those in the engineering step are not discussed in this report.

To the extent to which a specific urban form depends on topography and natural environments, planning policies play a significant role. They either reinforce the monocentric form or change it to a multicenter polycentric configuration. As shown in Figure 2-4, each of these urban forms has distinct composition and configuration of land use patterns; population distribution; and, thus, different characteristics of transportation and water infrastructure. The subsequent phase of infrastructure planning and design follows various guidelines and economic considerations. For example, the Department of Transportation has published a series of guidelines on transportation mobility and infrastructure improvements (e.g., FHWA, 2002, 2012). The EPA's Office of Transportation Air Quality (OTAQ) has issued guidelines on the emissions criteria, fuel standards, and transportation-vehicle technologies that affect urban air quality (e.g., U.S. EPA, 2015a, 2011). Other technical models and tools are used widely to evaluate and simulate the transportation needs, travel demand simulation (e.g., VISUM, VISSIM), and air quality analysis (e.g., MOVES, AERMOD, CAL3QHC). These topics related to urban adaptation will be discussed further in Section 3.0.

Water infrastructure is one principal element of urban infrastructure supporting and shaping the urban form. The water services start with potable water supplies in distributing drinking water to customers, followed by the collection and management of sewage and stormwater to protect public health and property. Generally, master plans are developed for a given set of land use and economic projections with the purpose to satisfy the current and future water supply and water sanitation expectations. Many municipalities follow a well-defined process in developing planning objectives and determining planning variables. Planning and engineering tools are widely available, including EPANET and its commercial derivatives (e.g., WaterCAD, H2Omap) for drinking water supply, EPA's Stormwater Management Model (SWMM) and related stormwater packages for stormwater management and urban drainage, and engineering software platforms (e.g., SewerGems, H2Omap/Sewer, HydraSewer). Overall, most municipalities pay attention to the operation and management of existing infrastructure, which is aging across the U.S. Some communities have expended efforts focusing on component optimization, system improvement, and capacity expansion, but system-wide re-planning and redesign rarely happen. These focus areas, for example, are identified in the nationwide assessment (see Section 7.0 of U.S. EPA, 2015a).

Overall, the current practice promotes the expansion of the existing water system infrastructure and its physical footprints. In the master planning process, municipalities and stakeholders periodically assess urban infrastructure performance after construction and a period of operation (Figure 2-4). This step aims to compare infrastructure performance against the intent of the original master plans or new urban growth objectives. The performance evaluation serves as a basis for master planning revision and modifications of existing urban infrastructure. This master plan revision occurs periodically; a revision frequency every 5 to 10 years is common in practice. Many county or municipal master planning time horizons are 5 to 30 years, depending on the infrastructure types. The exact planning timeframe has more to do with the uncertainty than with other factors; generally, public officials are reluctant to invest too far ahead, particularly when the future is uncertain. A side effect of this current planning and engineering process is the continuous urban sprawl into the exurban areas, as opposed to reevaluating the underlying framework of urban systems (Figure 2-4). Flanders et al. (2014) described this type of urban sprawl in an EPA internal report and further analyzed its implications on urban infrastructure development.

Radial sprawl, ribbon sprawl, and leapfrog sprawl, as shown schematically in Figure 2-5, are the three common types of urban sprawl. In terms of water infrastructure, general planning and engineering consists of three major steps: (1) land use and economic projection, (2) analysis of spatial population distribution, and (3) projection of water demand and wastewater generation in a planning timeframe. The economy of scale for operations favors a centralized water supply system, which results from the initial monocentric urban form. The result is the single water, wastewater, and stormwater management network, if the hydrographic conditions permit, as commonly found in most U.S. cities.

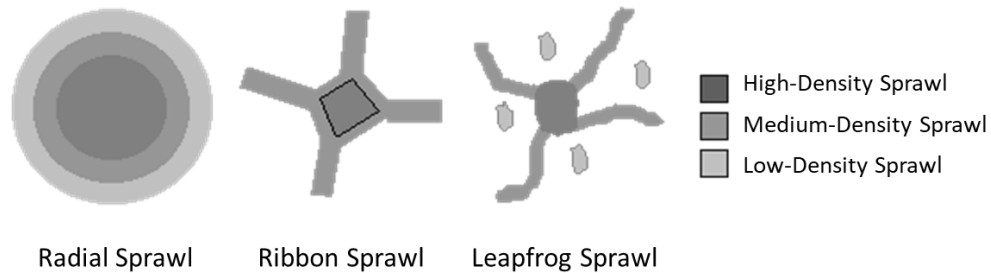


Figure 2-5 Three major types of urban sprawl expanding the urban footprints into exurban areas. Reproduced from Sudhira et al. (2005).

In principle, a centralized water supply system delivers water from a central treatment plant through a vast distribution network at a lower treatment cost than a decentralized system. But it may do so at the expense of increased energy consumption and greater risk of water quality changes in downstream use areas. The same trade-off between the economy of scale and energy expense occurs for sewer systems that collect wastewater from individual users and carry it to a central location for treatment before discharge. Municipal separate storm sewer systems (MS4s) drain an urban area and discharge overland runoff, often untreated, into local water bodies. This arrangement is the most energy-efficient service within a monocentrically distributed population.

Compounding the current planning and engineering practice is that all design guidelines are based on the assumed climate stationarity. This assumption and implication on water infrastructure were described in the adaptation report Part I (U.S. EPA, 2015a) and in the early EPA’s adaptation conference proceeding (U.S. EPA, 2009c). The stationarity issue is embedded in planning guidelines and engineering codes but needs to be assessed; for example, the recently revised American Society of Civil Engineers’ code of ethics includes language on the need to “*comply with the principles of sustainable development in the performance of their professional duties.*”

1.1.3. *Revising or redefining planning and engineering focus*

There is a critical need for a significant national investment to improve and renovate the nation’s water infrastructure. This new investment will provide a rare opportunity to reevaluate the current urban development framework and, if needed, to break up the current urban sprawl cycle and reorient the growth pathways toward sustainability (Yang and Goodrich, 2014). Among many technical pathways, the master planning and revision process presents the most practical opportunity to reduce unnecessary urban expansion and increase urban efficiency. This

point in the process also enables initiating and developing effective water infrastructure adaptation to future hydroclimatic changes, in addition to the traditional land use considerations.

The urban planning process to incorporate global changes is schematically illustrated in Figure 2-6. The revised process, called adaptive urban planning, contains two sets of adjustments to overcome deficiencies of the current practice that are identified in performance evaluation.

The first pathway revolves around the urban and infrastructure adaptation through adaptively realigning of the urban layouts and basic functions. These preplanned and adaptive actions induce changes to urban forms for better sustainability attributes. Through adaptive planning, for example, transformation districts and corresponding infrastructure (e.g., smart transportation, water supply systems) may be able to induce existing urban transformation into multicenter high-density configurations and to avoid low-density development to the extent possible (Figure 2-6). The transformation district concept stems from spatial continuity in urban development and stipulates that an urban initiative can attract additional development radiating from the original location or district; some are called transformation corridors. A handy example is the development of the I-270 technology corridor in the Washington, DC, metropolitan region. Many large cities, such as Philadelphia, PA; Glynn County, GA; and Ludwigsburg, Germany, have transformation districts in their master planning, largely for sustainability consideration.

The principles, along with an example of urban transformation, will be illustrated in Section 4.1 by analyzing the potential development scenarios for the Cincinnati metropolitan area. In general, such scenario-based analysis in urban adaptation is important to compare the cost and benefits among developed adaptation alternatives. The results provide a technical basis to inform decision makers on the limitation of physical adaptation approaches and the likelihood of success for water and other urban infrastructure systems. The results also can help understand the feasibility and limitation of adaptation compared with other options, such as an infrastructure rebuild (Felgenhauer and Webster, 2013). In the analysis, the future hydroclimatic and land use changes need to be first assessed.

The second pathway is to change or adjust the urban developmental objectives or local land use regulations (Figure 2-6). Using the measured urban sustainability and performance attributes, developmental objectives can be adjusted in a way to change or modify the growth against the hydrological and socio-physical constraints (i.e., the basic planning variables). The process and its attributes such as environmental justice, capital flows, centralized versus decentralized management, have been discussed in the literature (Small and Song, 1994; Ewing, 2008; Heikkila et al., 1989; U.S. EPA, 2006, 2007b; Baynes, 2009; Ostrom, 2010).

Adaptation option evaluation and analysis depend on how the impacts of future hydroclimatic and land use changes are projected and defined at the scale of interest. Also relevant is the relative magnitude between the projected future changes and those originally assumed in the existing master planning. This important hydrological evaluation includes several key elements, including those below.

- The degree of hydroclimatic change that affects the precipitation intensity-duration-frequency (IDF) relationship in the watershed of interest. Because of its impacts on the infrastructure's hydrological design basis, the long-term hydrological effects deserve

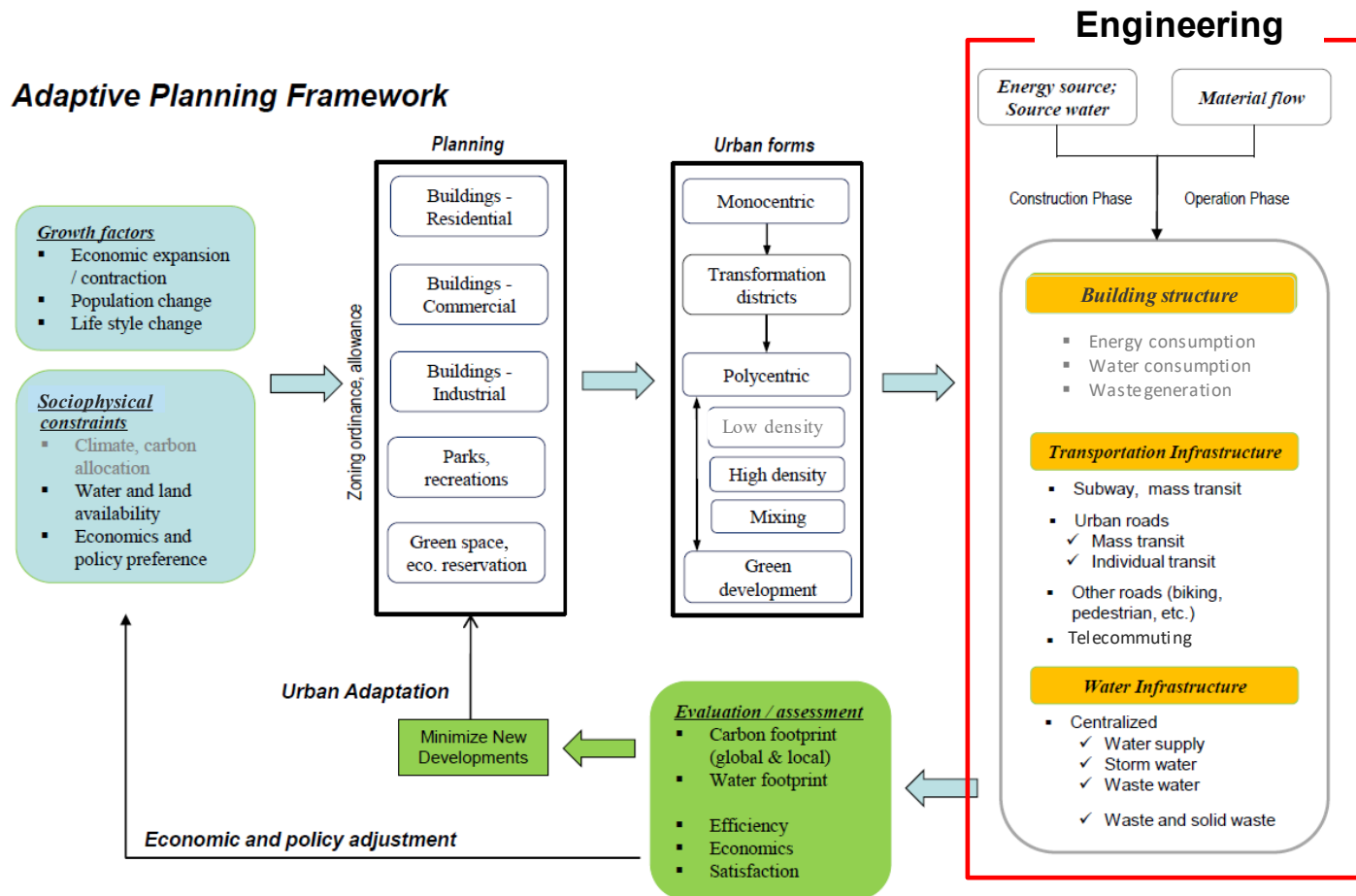


Figure 2-6 General process of adaptive urban planning and engineering. Compared to traditional master planning in Figure 2-4, adaptive planning promotes economic and policy adjustment on urban development goals and urban adaptation for high-density, polycentric form through transformation and proper transportation and water infrastructure adjustment. The element in gray text in the planning step is not applicable; those in the engineering step are not discussed in this report.

careful reevaluation (Mailhot et al., 2007). The relevance of this important hydrological impact has been extensively discussed in the literature (e.g., Wilby, 2007; Beck, 2005; Semadeni-Davies et al., 2008; Ashley et al., 2007; Pielke et al., 2007).

- The degree of infrastructure capacity reserve in the current planning and engineering practices; for example, the safety factors used in a design basis. A quantitative evaluation of the capacity reserve (see Section 5.2 later) helps identify the vulnerability under future conditions. The evaluation results can inform decision makers on the need for local economic and developmental policy adjustments (see U.S. EPA, 2015a). This type of “bottom-up” assessment is facilitated by the Climate Resilience Evaluation and Awareness Tool (CREAT) available from the U.S. EPA’s Office of Water¹. It is generally accepted that the precipitation and temperature changes in the future can directly affect hydrological and water quality engineering. The impact can be exacerbated through a complex interaction among hydrology, land use, and population growth in an urban catchment. Furthermore, atmospheric feedback of land use change can be significant to the urban microclimate, as described in Section 4.1. The effect on mass conservation and energy momentum in the planetary boundary layer is known to create precipitation variations in local and regional scales (Adegoke et al., 2007; Pielke et al., 2007), and in changes of soil erosion and soil moisture (O’Neal et al., 2005; Miller et al., 2007). For simplicity, this type of feedback-loop interaction is often neglected in adaptation analysis. All these factors can affect the capacity reserve needed for successful infrastructure adaptation.
- The adaptation co-benefits in energy efficiency when developing and evaluating the adaptation options. These co-benefits are often neglected currently in the evaluation of urban infrastructure performance, causing a major unrealized benefit to remain unassessed. However, this co-benefit concept deserves attention in adaptive urban planning as shown in Figure 2-6.

1.1.4. Selecting adaptation evaluation matrix

In adaptive urban planning, the urban performance evaluation and assessment step (see Figure 2-6) requires a selection of the appropriate evaluation matrix. The matrix may include criteria that address hydrologic adaptation impacts, describe the dependence between water and carbon footprints, and consider the time of adaptation in terms of capital flow and adaptation limitations in trade-off analysis. Some attributes in adaptation evaluation are listed in Table 2-1.

The adaptation co-benefits in energy and air emissions are an important and basic attribute in urban infrastructure adaptation (Yang and Goodrich, 2014). Water infrastructure contains significant energy footprints, yielding significant air emissions both during construction and thereafter operations. Water infrastructure operation is often the largest energy user in most communities. To evaluate the co-benefits and tradeoffs, one method relies on conjugate water and energy/carbon footprints (PNNL, 2012; Yang, 2010). These two sustainability indices unlock the dependence between energy usage and water availability, and therefore can provide a useful criterion to find compromised solutions in the adaptation option analysis. For example, adaptation solutions to address water availability in water-stressed regions often include water

¹ <http://water.epa.gov/infrastructure/watersecurity/climate/creat.cfm>

Table 2-1 Adaptation attributes for common objectives

Attribute	Objective
1. Adaptive urban planning	
Urban form	Sustainable land use and resilient infrastructure
Urban sprawl index	Reducing exurban development
Population density	Achieving compact development
Housing density	Achieving compact development
Transforming district	Transitioning to polycentric form
Zoning	Land use change for planned developments
2. Urban transportation	
Traffic delay	Increasing transportation efficiency
Trip generation	Promoting walkable community and mass transit
Fuel consumption	Reducing fuel use in urban activities
Emissions	Increasing mitigation co-benefit
3. Urban water systems	
Water availability	Adequate supply to meet demand
Water quality	Compliance to SDWA and CWA regulations
Energy use	Reducing energy cost in managing water systems
Energy and emission	Reducing life-cycle emission and improving overall energy efficiency for the mitigation co-benefit
Resilience	Ability to provide service function under natural and man-made emergency and disruptive events

reclamation, reuse of treated wastewater for non-portable and even potable purposes, desalination, and water storage (Oron et al., 2007; Yang et al., 2007, 2010). These adaptation options have high energy intensities and generate air emissions when producing the new “virgin water.” Similarly, compromised solutions between energy/carbon footprint and economic cost are relevant to water infrastructure planning (Chang et al., 2012). For illustration, the case study on water infrastructure expansion alternatives in Manatee County, Florida is described in Section 4.2.

Evaluation matrix selection is always objective-dependent. Some commonly investigated pairs include water and energy/carbon footprints, water availability and cost analysis, and water footprints (see Table 2-1). Defining the evaluation matrix is often the first step in the adaptation process that can affect adaptation pathways and outcomes (Figure 2-6), and often involves the

extensive engagement of the public and stakeholders. Therefore, the evaluation matrix may be highly location-specific and should be clearly described in the performance evaluation.

1.2. Three levels of water infrastructure adaptation

Physical adaptation to urban infrastructure can take place at three levels on a spatial scale (Figure 2-2). Referring to Figure 2-6, adaptation may also occur at the different stages of the planning-engineering-evaluation process, such as in the planning phase or the engineering of specific adaptation measures against specific hydroclimatic impacts (e.g., floods and chronic droughts). As the adaptation level changes from systems adaptation (e.g., storage, water conservation, and water loss prevention) to urban-scale or watershed-scale adaptation, the complexity increases for the systems analysis, and thus for adaptation planning and engineering design. The remainder of this report describes the technical approach for adaptation in these three levels and illustrates the considerations in selected case studies.

1.3. Smart Urban Design (SUD) for systems analysis

Water infrastructure adaptation in the watershed scale, the urban scale, and the water system scale has own advantages and challenges (Table 2-2). To quantify specific adaptation actions, one integrated modeling tool “Smart Urban Design (SUD)” has been developed from this research. It consists of scenario-based modeling tools integrated as a platform to assist the design of adaptation actions (Figure 2-7). The main SUD components are described below.

1.3.1 Integrated Watershed Modeling (IWM)

The IWM tool is built upon the EPA’s Better Assessment Science Integrating Point and Non-Point Sources (BASINS) program (U.S. EPA, 2019) with further integration of a land use model under the future global conditions (Figure 2-8a,b).

The EPA’s Integrated Climate and Land Use Scenarios (ICLUS) is a land use model that provides an explicit projection of population, housing, and land use under future climate scenarios. Future climate is specified in the four Intergovernmental Panel on Climate Change’s (IPCC) Special Report on Emissions Scenarios (SRES) scenarios. At present, the ICLUS projections are made at the county-scale spatial resolution through the year 2100. This development scenario tool is based on a pair of models: a demographic model for population projection and a spatial allocation model to distribute the projected county population into housing units at a 1-ha (1-hectare) pixel resolution. Population allocation from a county scale to census tract resolution is technically challenging, because of the model assumptions for the present, near-term and distant economic growth. For example, the spatially explicit regional growth model (SERGoM) is used in population allocation to generate the projections at a spatiotemporal resolution of 10 years and one (1) hectare. The associated uncertainty with low-resolution population projection may be excessive for infrastructure planning. This potential risk has not been assessed fully at the time of this reporting. More details on the methodology can be found in U.S. EPA (2009b, 2010b). Projections covering the contiguous U.S. can be accessed at <https://www.epa.gov/ICLUS/ICLUS-downloads#tab-1>.

Table 2-2 General advantages and challenges of three-level adaptation actions

Adaptation Level	Methods/Tools	Advantages	Challenges
<i>Integrated Watershed Management</i>	IWM, ICLUS, CA-Markov, HSPF, SWAT	<ul style="list-style-type: none"> • Ability to protect source water quality and assure water availability • High implementation feasibility through the CWA and SDWA regulatory framework 	<ul style="list-style-type: none"> • Data requirements for watershed process analysis • Land use planning and action often difficult to implement • Close interactions of land use and urban catchment hydrology
<i>Adaptive Urban planning</i>	AUP&ET SWMM, VISUM, MOVES	<ul style="list-style-type: none"> • Large emission mitigation potential • Changes amendable to urban development goals • Increasing urban resilience • Potential to accommodate multiple objectives (e.g., economic development) 	<ul style="list-style-type: none"> • Complex, requiring integrated planning • The transformation required in urban development • Cost and time for capital investment payoff • Public acceptance
<i>Infrastructure Systems Adaptation</i>	WTP-cam, EPANET, SWMM, SWC	<ul style="list-style-type: none"> • Taken as a part of capital improvement • Well-defined actions for decision making • Increasing infrastructure capacity for specific needs • Independent for quick actions at a relatively small capital cost 	<ul style="list-style-type: none"> • Difficult to resolve urban-wide performance issues • Limited adaptation potentials after years of improvement • Difficult to resolve urban-wide performance issues

Urban land use changes are dynamic and often difficult to model. They occur at a spatial resolution much finer than the county level resolution used in ICLUS. For this reason, the cellular-automaton Markov (CA-Markov) land use model can be used available in the IWM module (Figure 2-8a,b). The CA-Markov method for land use projection combines the stochastic probability of future evolution that builds on the current situation (namely, the statistical state), and the geographic association with current and projected land use. The latter is captured using the cellular automaton modeling that depicts the probability of spatial association in state changes. In combination, the CA-Markov modeling can estimate probable land changes in spatial aggregation using the geographical information system (GIS) modeling capabilities (see Tong et al., 2012; Sun et al., 2013). Nevertheless, population and land use projections in planning scenarios are the most difficult and least quantifiable for urban areas, especially as they may relate to large-scale hydroclimatic impacts like sea level rise that will alter the current landform.

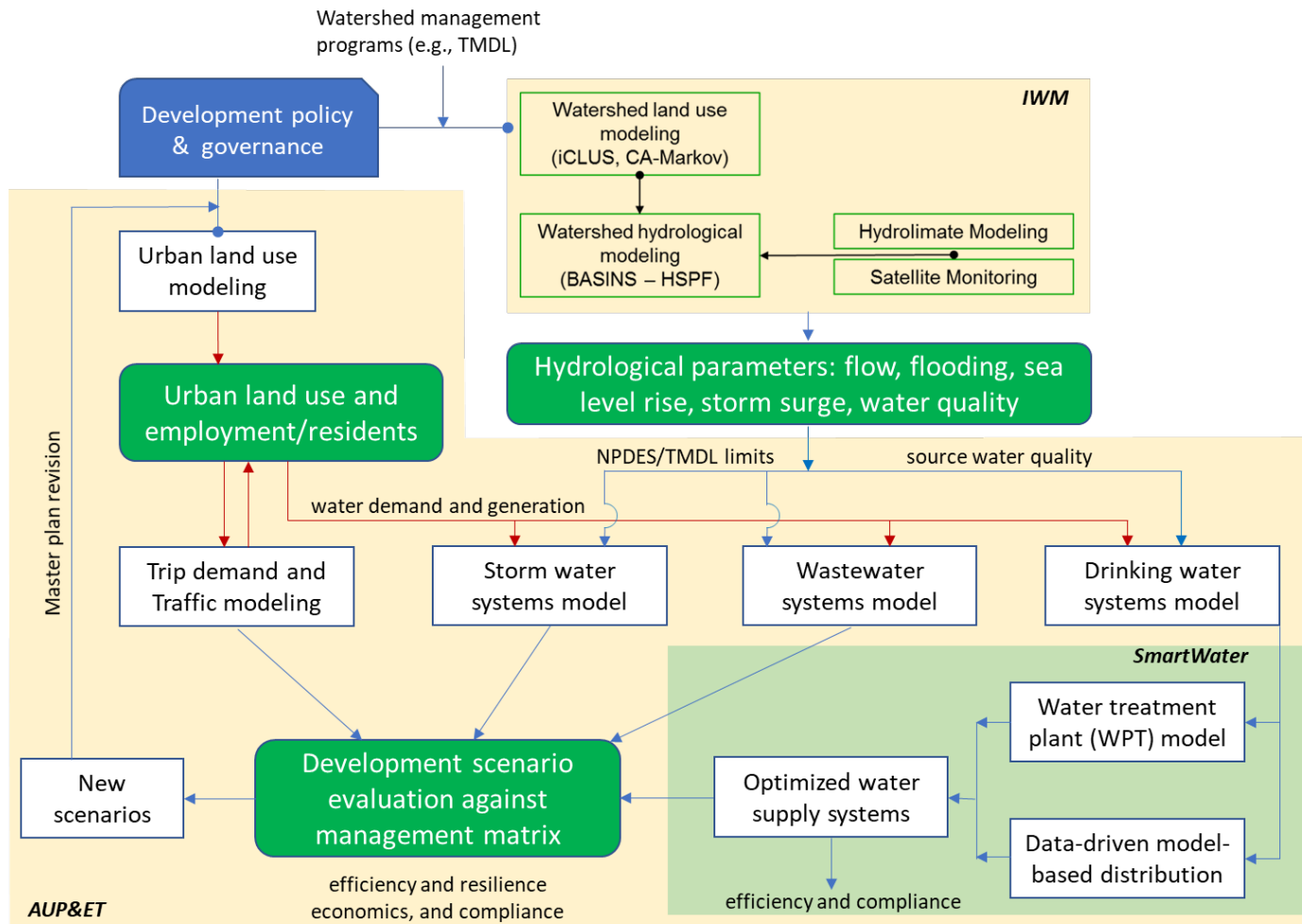


Figure 2-7 Schematic diagram of the Smart Urban Design (SUD) structure for scenario-based urban development planning and engineering. Program linkage between the three major modules of IWM – integrated watershed management models for hydrological changes, SmartWater – water supply engineering design tool, and AUP&ET – adaptive urban planning & engineering tool for scenario analysis. Colors indicate different blocks in the integrated simulation process.

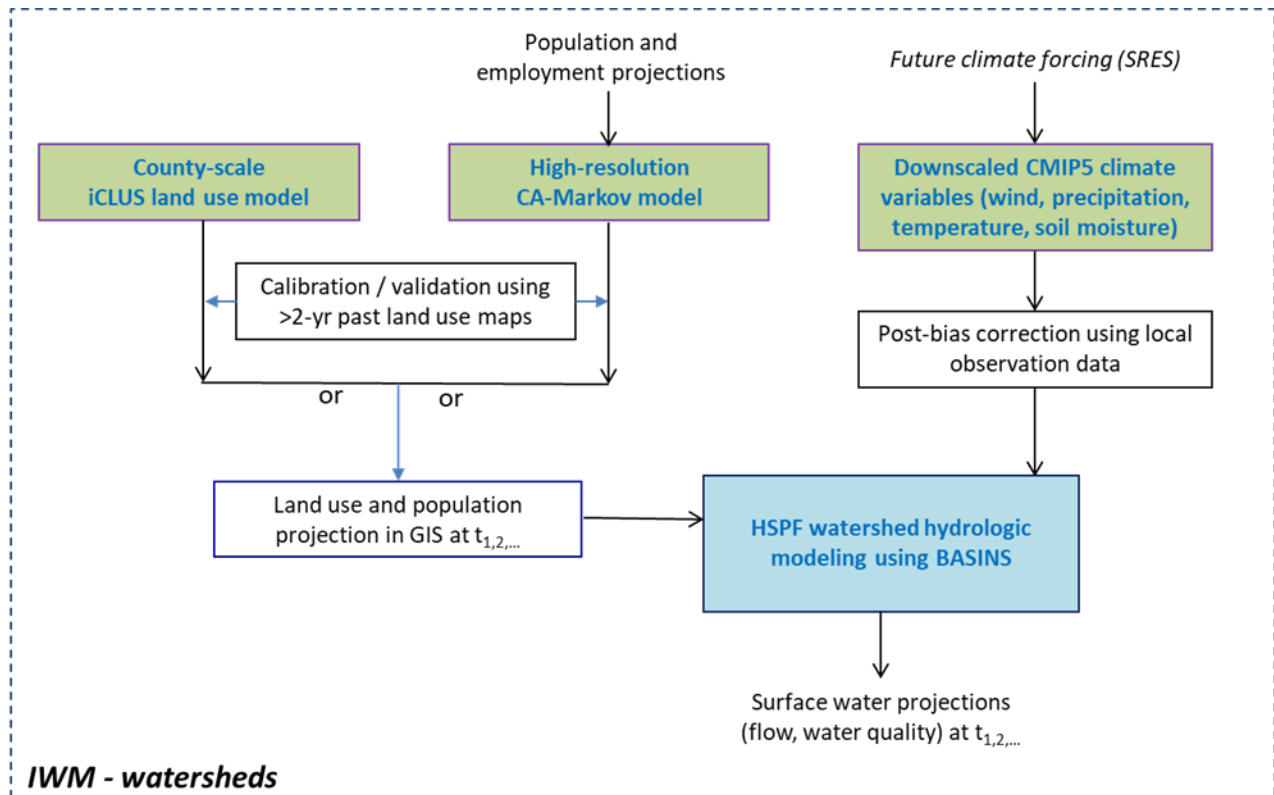


Figure 2-8a Process flow diagram of the Integrated Water Management (IWM) modeling for watershed simulations. It consists of the climate-influenced hydrological model HSPF and land use models either by ICLUS or high-resolution CA-Markov modeling. The program resides in the EPA's BASINS framework. Colors indicate different blocks in the integrated simulation process.

The problem is confounded for projections requiring high spatial resolutions, like in the census tract levels. In addition, disruptive development decisions and events can make model projections less accurate and not useful. These factors can lead to conditions inconsistent with the spatial continuum assumptions embedded in the semi-empirical CA-Markov method. This potential problem can result in erroneous model projections, a limitation that cannot be underestimated.

Figure 2-8a shows a general modeling framework for suburban and rural watersheds. For urban catchments experiencing significant changes, the modeling framework is shown in Figure 2-8b. In Figure 2-8a, the hydrological parameters (e.g., streamflow and water quality) are modeled for future time frames of interest (e.g., t_1 , t_2 , etc.) using EPA's BASINS program. BASINS for assessment of water quality and flow variations in watershed runoff and surface streams is documented in U.S. EPA (2013b) and application studies (Tong et al., 2012; Sun et al., 2013). The newly released BASINS4.1 is a comprehensive platform, providing a choice of multiple hydrological simulation engines. Available models include Hydrological Simulation Program – Fortran (HSPF), the Soil and Water Assessment Tool (SWAT), the EPA's Stormwater Management Model (SWMM), Generalized Watershed Loading Function model extension (GWLFE) MapShed, and the simple watershed model Pollutant Loading Estimator (PLOAD), as well as two instream water quality models AQUATOX and the Water Quality Analysis Program (WASP).

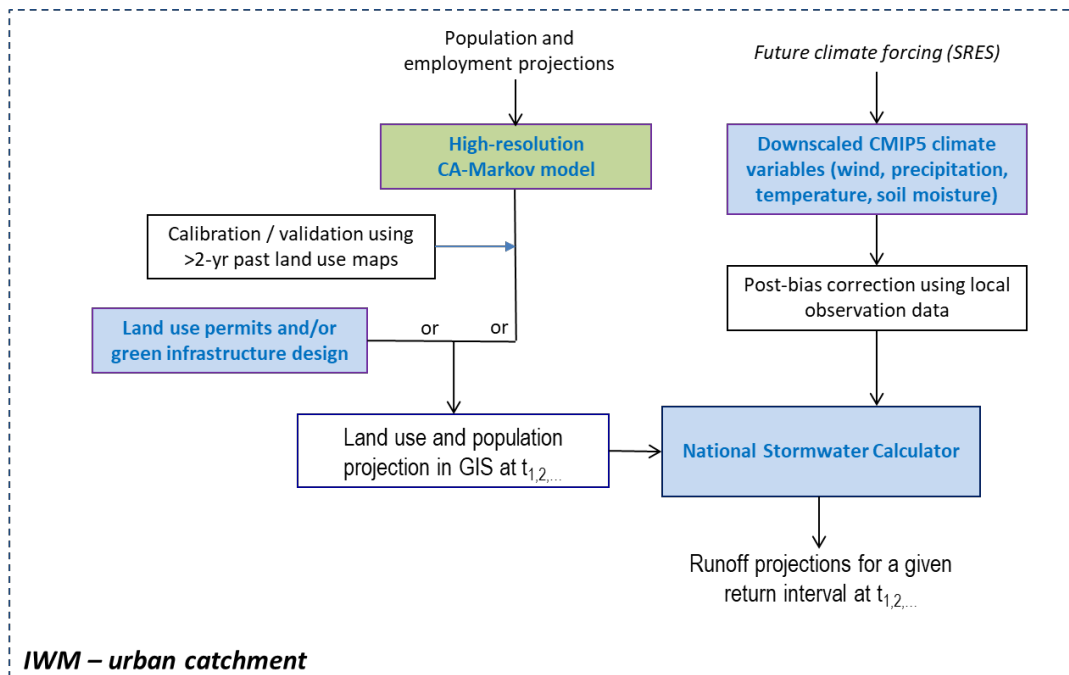


Figure 2-8b Process flow diagram of the integrated watershed management (IWM) modeling for urban catchment using EPA’s National Stormwater Calculator (U.S. EPA, 2014). Modeling functions in the light blue box exist in the National Stormwater Calculator. Colors indicate different blocks in the integrated simulation process.

There are some generalities with model inputs for the IWM tool. The parameters for hydrological and land use are of greatest interest. First, land use projections can be made for the desired future period, using past land use in digital format for model calibration and validation. Additional land use constraints, including nature preservations, water bodies, historical preservations, are specified as model constraints in the GIS land use simulation. Examples can be found in Sun et al. (2013). Separate anticipated population changes can be directly downloaded from the ICLUS model outputs. When higher spatial resolution than the county-scale projection is needed, population change is often available from master plans created by local governments. The model outputs of land use types and population distributions are the inputs for subsequent BASINS hydrological modeling (Figure 2-8a).

Future climate parameters (i.e., precipitation, temperature, dew point, wind) are another set of input parameters for hydrological modeling in BASINS. The IWM module obtains these parameters from climate models. The model projections used in IWM are further revised for post-bias corrections using the techniques from Liang and Julius (2017) and Yang et al. (2017). The projected precipitation for given return intervals is used as one HSPF parameter in BASINS simulation. Furthermore, the urban catchment is smaller in size than a rural watershed but may contain more dynamic changes in land use and land cover, and built infrastructure. For urban application, EPA’s National Stormwater Calculator (U.S. EPA, 2014) is the main simulation engine (Figure 2-8b); it is a simplified model based on EPA’s SWMM on a GIS platform. The Stormwater Calculator accepts future land use either by green infrastructure design (e.g., detention and retention ponds, swales, and other catchment areas) or directly from CA-Markov

modeling of land use at census tract resolutions. The land use modeling techniques are described in Tong et al. (2012), Sun et al. (2013), and Fu et al. (2018).

Precipitation is the other important modeling input for IWM-urban catchment. For this purpose, downscaled climate modeling outputs may not be suitable for infrastructure design or planning because of their coarse spatial resolution and large projection uncertainty. One principal reason is that microclimate in urban centers can significantly differ from the regional climate of natural land cover. One example is the UHI effect often discussed in the literature. The unique nature of the urban microclimate is discussed in a case study described in Section 4.1.

For both watershed and urban catchment areas, the IWM helps project key hydrological parameters at a future time for subsequent analysis in the Adaptive Urban Planning and Engineering Tool (AUP&ET) discussed next. These projections include:

- Unit hydrographs for storms of a given return interval. Both peak flow and time of concentration are specified. Often these parameters are given for specific storm return intervals.
- Stream base flow. The model outputs can be analyzed for changes in stream base flow under the future land use and climate conditions. Application examples can be found in Johnson et al. (2015) and U.S. EPA (2013b).
- Surface water quality parameters such as total nitrogen, total phosphorus, turbidity, and organic pollutants (e.g., Tong et al., 2012).

1.3.2 Adaptive Urban Planning and Engineering Tool (AUP&ET)

The schematic diagram in Figure 2-9 shows major modeling components and data flows for the scenario-based Adaptive Urban Planning and Engineering Tool (AUP&ET). The tool considers urban development scenarios for transportation, water supply, wastewater, and stormwater systems. These infrastructure systems are the controlling factors over the basic urban form, employment and economic activity, and population distributions. The scenario-based feature in model simulation allows one to develop alternative development scenarios.

Urban infrastructure has a large physical footprint. The existing infrastructure systems are capital-intensive and difficult to change once built. The nature of the infrastructure precludes the potential to perform real-world experiments for optimal planning and design solutions. Thus AUP&ET takes the technical approach in a scenario-based computer simulation. The tool relies on two major inputs. First, the development objectives are defined, for which a set of development options can be created for a given physical and environmental setting. Second, for water infrastructure adaptation, water availability and hydrological parameters of surface streams (e.g., peak and base flows, water quality) are basic variables for quantification in developing the urban scenarios (Figure 2-9). Each urban scenario yields quantitative outputs of the future land use and urban parameters, including urban form, community functions such as parks, transportation, water sanitation, and supply services. These model variables are then incorporated into the land use modeling and imported into GIS for spatial analysis (Figure 2-9).

Perrone et al. (2011) analyzed the roles of transportation and water infrastructure in determining the physical form and efficiency of urban systems. Flander et al. (2014) further investigated the attributes and inter-dependency of the infrastructure. Here in AUP&ET, the inter-dependence and interactions are modeled for environmental attributes on an urban scale in

development scenarios. An application example will be described in Section 4.1. Potential analysis outcomes may include:

- Population distribution for specified development goals;
- Daily and peak traffic flow at road link levels;
- Urban-wide emissions, and traffic congestion identification;
- Drinking water supply needs and their spatial variations;
- Stormwater and wastewater generation rates and spatial variations;
- Energy consumption and cost comparisons in the transportation and water sector.

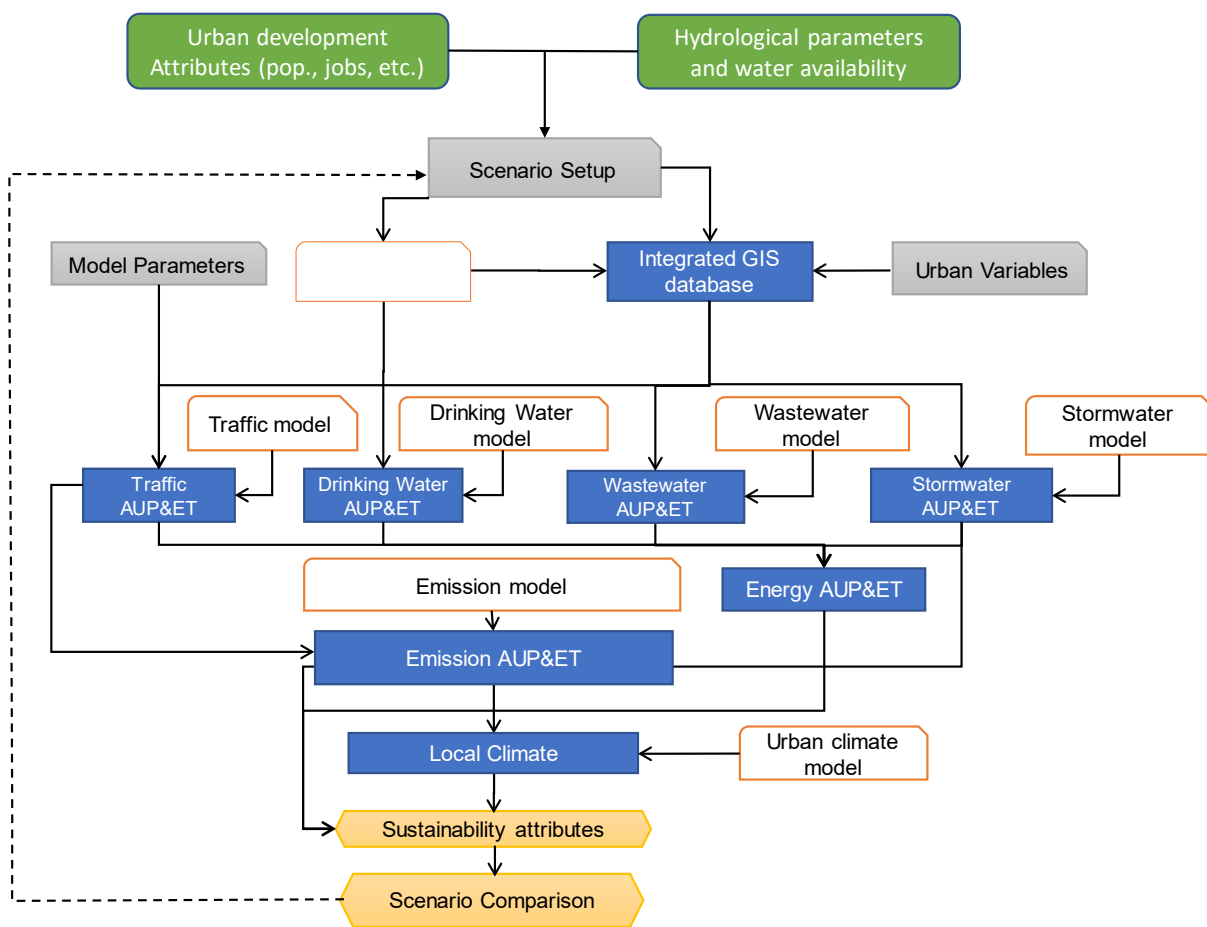


Figure 2-9 Process flow diagram of the scenario-based Adaptive Urban Planning and Engineering Tool (AUP&ET) for urban planning and engineering. Each of the four program modules – traffic, drinking water, wastewater and stormwater, is discussed separately in Sections 3.1 and 5.0. Colors indicate major elements in the integrated simulation process.

1.3.3 SmartWater for water supply

Within AUP&ET, one engineering tool is the SmartWater module for water treatment and distribution. Different from the other planning-centric AUP&ET modules, the SmartWater tool is developed for system engineering, evaluation, and detailed unit process analysis in adaptation. It consists of an updated Water Treatment Plant (WTP) model for water treatment process engineering, and a sensor-based data-driven EPANET engine for water distribution (Figure 2-10).

SmartWater’s WTP3.0 consists of two separate modules that are linked by an overall graphic user interface (GUI) (Figure 2-10). WTP2.0/2.2, originally developed in 1994 and updated in 2004 (U.S. EPA, 2005), was intended for the national evaluation of water treatment plant performance to support the promulgation of the Safe Drinking Water Act (SDWA) DBP Stage II regulations. In the SUD, the water treatment plant – climate adaptation model (WTP-cam) is developed from WTP2.2 for plant-specific adaptation analysis. Its application in a case study at the Greater Cincinnati Water Works (GCWW) Richard Miller Water Treatment Plant (“Miller WTP”) is described later in Section 6.3.

The SmartWater module in SUD treats the two processes (water treatment, and distribution) as a single system (Figure 2-11). This approach aligns well with U.S. water utilities starting to align water treatment and distribution operations under the same management, or to

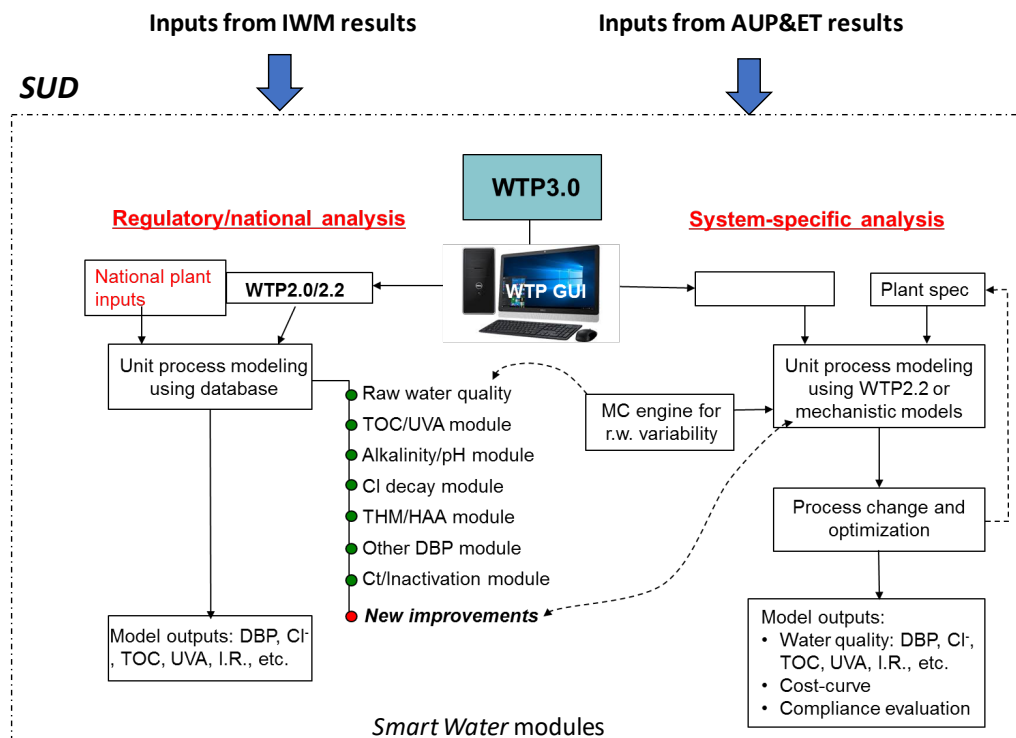


Figure 2-10 Schematic diagram of conceptual modeling framework for WTP3.0 as a major SUD element. It consists of the system-specific analysis using WTP-cam (Water treatment plant – Climate Adaptation Model) and the regional analysis in WTP2.0/2.2.

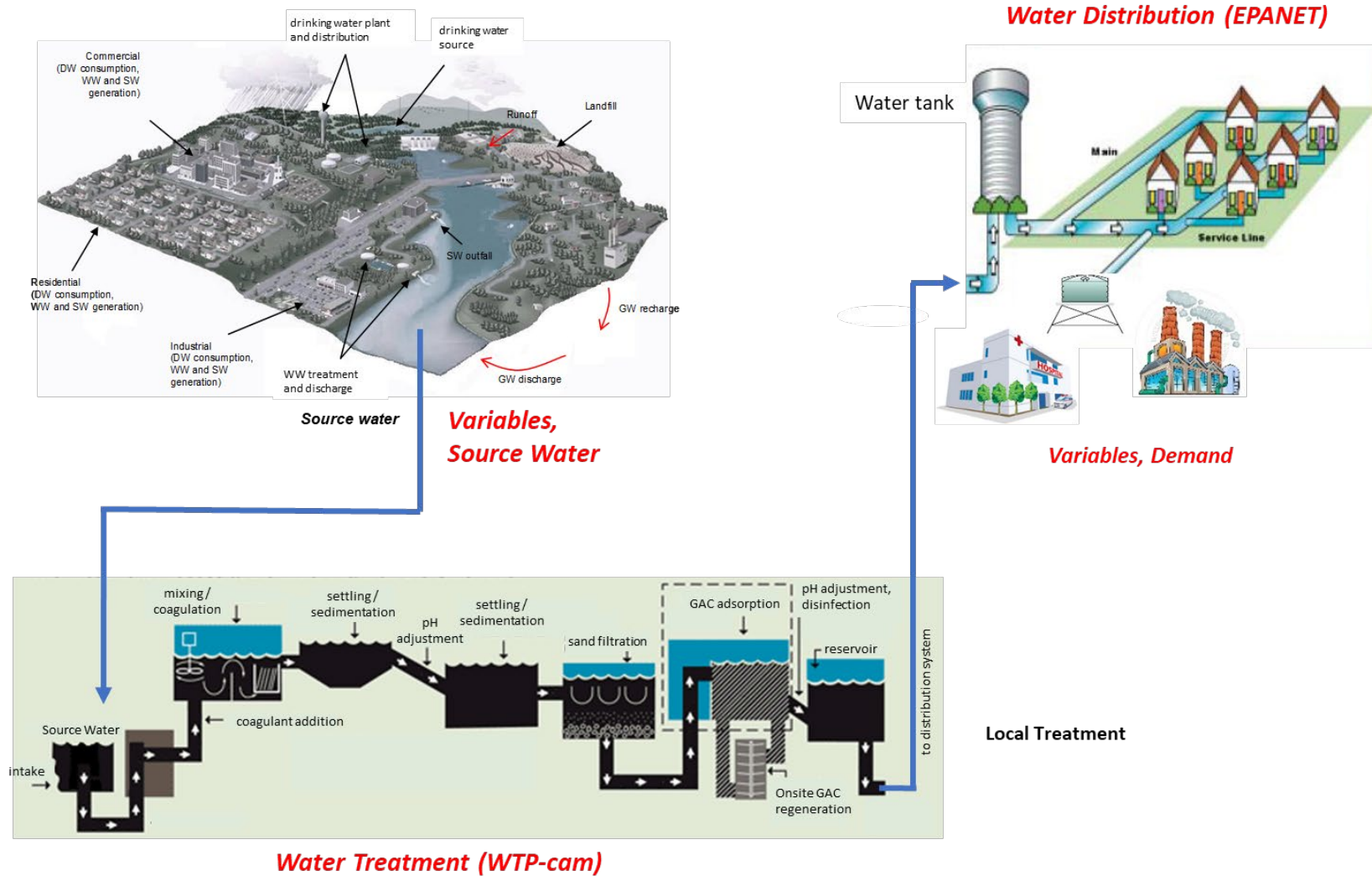


Figure 2-11 Schematic diagram of water supply and major system variables. Water treatment and distribution are the two engineered systems to meet variations in source water quality and water demand. The consideration of disinfection by-products (DBPs) is cited for specific management and technical considerations. Other abbreviations: DW – drinking water; GAC – granular activated carbon; SW – stormwater; and WW – wastewater.

link those distributors with water producers in real-time data exchange. As shown in Figure 2-11, this integrated approach allows one to manage and optimize the treatment and distribution infrastructure in a timely manner to address changes in source water quality and to meet changing water demands. This communication exchange has become feasible because of recent technical advances in sensor-based monitoring, real-time data communication, and algorithm-assisted system operation. More technical details will be presented in Section 6.0.

1.3.4. Source-to-tap water supply in a systems approach

The SUD methodology takes a systems approach toward efficient and resilient water infrastructure. In current engineering practice, line process diagrams in infrastructure analysis usually describe a water system and unit processes with simplistic consideration of the spatial interactions with other urban components and surrounding watersheds. This traditional approach is convenient in technical analysis. However, it may discount interactions between the highly-dense socioeconomic activities and an ever-changing urban environment.

Taking water supply as an example, the “source-to-tap” systems approach (Figure 2-11) is the basis of SUD. Currently, the SUD tool only has surface water as the source water in drinking water production; modules for groundwater and reclaimed water will be considered for addition at a later time. The rest of this Part II report discusses the four basic steps in the systems approach, its tools, methods, and application examples:

- IWM and analysis for water quantity and quality variations in watersheds;
- AUP&ET modeling and analysis for urban development scenarios. The objective is to define the water demand and its spatiotemporal variations at present and in the future. Energy and economic efficiency of the urban scenarios for decision making also is analyzed;
- SmartWater modeling and analysis to optimize water supply efficiency. First, the system capacity and capacity reserve are defined for the water supply objectives and service resilience against future hydroclimatic impacts. Second, for changing source water or water demand, the potential system alteration/expansion/addition is evaluated;
- Upon evaluation of the infrastructure performance, a new round of system evaluations may take place. The results are used to evaluate the necessary adaptation for improving infrastructure’s resilience and sustainability. This iterative re-evaluation and adaptation process, as commonly practiced in periodic master planning, is shown in Figure 2-7.

2. Adaptive Urban Planning in Urban Scales

In the recent fifth IPCC climate assessment report (IPCC, 2014), the 3rd Work Group investigated mitigation and adaptation in the urban environment. They concluded that urban form transformation has, by far, the single largest potential to achieve meaningful carbon emission reductions and urban efficiency improvement. Many publications (e.g., U.S. EPA, 2006, 2009b, 2012a, 2013a, and references therein) identified several common planning options including infill, inner-city redevelopment, mixed land use, and employment centers. These measures can introduce urban transformation to more desired and sustainable configurations.

These smart growth practices and transformation measures have been applied in U.S. cities (U.S. EPA, 2007b, 2013a). They are designed to slow down urban sprawl and achieve adaptation-mitigation co-benefits, but often require changes in metropolitan transportation and water services. Other urban forms alternative to the traditional monocentric configuration may offer a smaller urban physical footprint with a higher population and housing density. However, this change is accompanied with more complicated transportation and water infrastructure, and thus greater difficulties with planning on how to incorporate existing infrastructure assets. To overcome these planning and engineering challenges, new approaches are essential for smart growth through urban form transformation. Attention in this report is given to the planning methods and tools for transportation and water infrastructure.

Because of the high population density and integrated urban infrastructure, urban centers also are vulnerable to natural and man-made disruptions including significant hydroclimatic changes in the future. Three major categories of impacts on urban functions are listed in Table 2-3.

Table 2-3 Selected urban functions impacted by hydroclimatic conditions

Hydroclimate Factors	Urban Functions
Long-term drought and large swings in precipitation variation	<ul style="list-style-type: none"> • Water supply, landscape, local agriculture • Wastewater and stormwater NPDES discharge to streams • Urban heat island effects and heat spells on population health • Example: U.S. Southwest, Southeast, Rocky Mountains
Heavy downpour, disruptive climate/meteorological events (e.g., tornados damaging winds, etc.)	<ul style="list-style-type: none"> • Transportation management and roads operations • Urban flooding and water service systems operation • Water pollution management from nonpoint source • Inundated sewer systems resulting in sewer overflows and property damage
Storm surge and sea level rise	<ul style="list-style-type: none"> • Disruption to water supplies; changes to hydraulic gradients affecting stormwater drainage and wastewater collection • Disruption to transportation systems • Inundations of roads and pipe systems

Note: CSO - combined sewer overflow

2.1 Physical infrastructure and urban forms in current practice

The monocentric urban formation is common in the U.S., where the urban population is distributed around a single central business district (CBD) of concentrated economic activities. In this urban form, automobile-based mobility is a precondition to facilitate the urban-suburban-

exurban arrangement (Theobald, 2005). The typical geometry of the urban form is schematically shown in Figure 2-5. Examples include numerous, mostly middle-to-large sized, urban centers such as Las Vegas, Cincinnati, Houston, and most urban centers of the Northeast and the Midwest.

As a city grows into a very large metropolitan center, the population becomes more dispersed and the monocentric form evolves into a polycentric arrangement of connected satellite cities. This urban form is now characteristic of very large metropolitan regions, such as New York City, Washington DC, San Francisco, and Los Angeles. The urban form transformation, and its implications to the CBD formation, population distribution, and transportation service, have been investigated in literature (e.g., Gordon et al., 1986; Small and Song, 1994; Heikkila et al., 1989; Larson et al., 2012, Garcia-López, 2012, and Zhou et al., 2013). The nature and process of the transformation have significant implications for the feasibility of developing and implementing adaptation options.

Polycentric urban form is marked by a multi-center urban configuration; for example, in the leapfrog sprawl of Figure 2-5. The transition toward a polycentric form may take different pathways. Continuous urban expansion toward a more dispersed polycentric form is a persistent trend leading to unplanned uncontrolled urban sprawl. On the contrary, the transition can permit high-density development, less personal travel, better use of mass transit and green space. This requires a different configuration for fixed urban infrastructure assets. As population and urban activities are redistributed, water infrastructure is accordingly transitioned in space for a new set of operational requirements to meet new water service and management needs. The three typical urban expansion configurations in Figure 2-5 are all linked to the transportation routes and other infrastructure services, forming the mode of radial, ribbon and leapfrog sprawl (Sudhira et al., 2005). For these different urban forms, the trade-off is under debate on urban efficiency and infrastructure sustainability ranging from resource allocation and urban ecology to engineering and operations.

Urban-developmental effects on water infrastructure have been widely recognized. For example, the centralized operation and management in water services have allowed for better control of water pollution and management toward meeting water regulations. It benefits from the economy-of-scale. However, negative environmental consequences are found in energy use and thus potentially higher indirect emissions, barriers to resource recovery, excessive water age in distribution systems, and vulnerability to the impact of natural and man-made incidences. The alternative form of urban development promotes more decentralized water systems. As urban transforms into polycentric form, the centralized water system may become decentralized, and the urban water cycle may become more localized (Hering et al., 2013; Luthy, 2013). This can result in better service to localized, high-density population centers. However, the required infrastructure transformation can be a difficult technical and engineering challenge. It requires coordinated urban planning among land use, transportation, and water services.

2.1.1. Land use encouraging urban sprawl

The three types of sprawl modes (Figure 2-5) can be easily found in the historical developments of U.S. cities. In Figure 2-12, the old urban centers of Atlanta and Phoenix expanded radially toward exurban at a rapid rate in merely 22 years from 1970 to 1992. The older urban centers, such as DeKalb County in Atlanta, further evolved into spatially continuous

high-density development. Smaller development centers in exurban perimeters in 1970 were later expanded in size, linking to the major urban centers through fill-in development. This leapfrog pattern is very common; for example, in the Norcross, Marietta, and Douglas communities in the Atlanta metropolitan area, and in the communities of Sun City, Mesa, and Chandler in the greater Phoenix area (Figure 2-12). Furthermore, the ribbon sprawl (Figure 2-5) can be observed along transportation roads, forming linear spreading of urbanized lands. This development pattern is obvious along the roads of regular shapes around the Luke Air Force Base west of Phoenix (see 1992 map in Figure 2-12).

Urban population and land use are difficult to project. Future population and land use are a function of urban economic conditions, political motives, and development initiatives; the last can introduce sudden changes in spatial continuity of land use patterns, and thus poses a modeling challenge in mathematic formulations. As an approximation, the CA-Markov simulation in GIS can be used with model boundary conditions representing urban land development restrictions. Wei et al. (2012, 2017), Tong et al. (2012), and Sun et al. (2013)

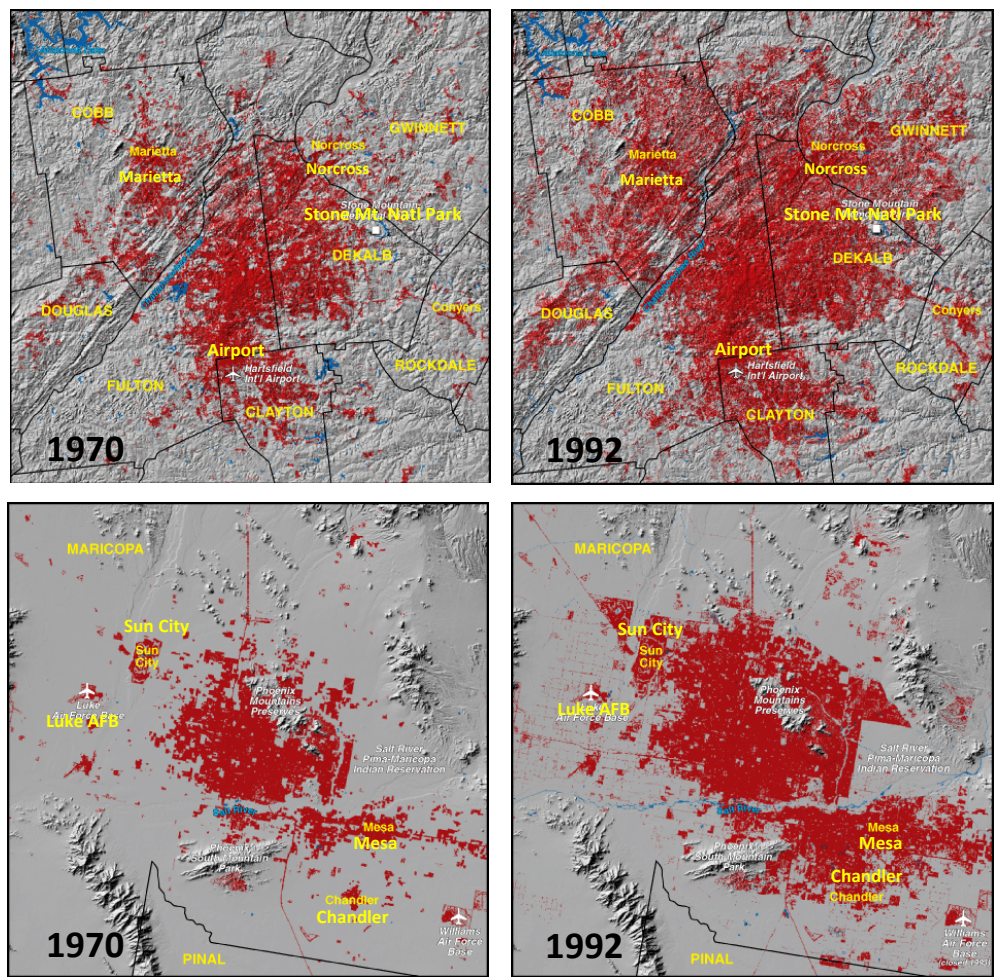


Figure 2-12 Urban expansion and urban form transformation for Atlanta (upper) and Phoenix (lower) metropolitan regions between 1970 and 1992. Red color indicates developed urban land use. Imagines obtained and modified from Auch et al. (2004).

successfully projected future land use changes in the urban communities, suburban watersheds of the Cincinnati and Las Vegas metropolitans. Their modeling methodologies incorporate population and land use variables as a GIS model filter in the CA-Markov simulations. The ICLUS tool and projections (U.S. EPA, 2010b) is an alternative to project future housing density and land use categories. See associated discussions in Section 1.3.1.

2.1.2. Transportation and energy performance

The concept of urbanization along transportation routes is shared by most U.S. cities. Such urban expansion, facilitated by current urban planning practices, has a set of characteristic physical layouts for water and transportation infrastructure, which in turn defines urban functions and affects infrastructure efficiency and adaptability.

Figure 2-13 shows the evolutionary trajectory of transportation efficiency as the U.S. cities grow from medium to very large metropolitan areas. Plotted statistical data were obtained from the Department of Transportation annual urban mobility reports prepared by the University of Texas (Schrank and Lomax, 2009). In these plots, the efficiency variables (annual delay,

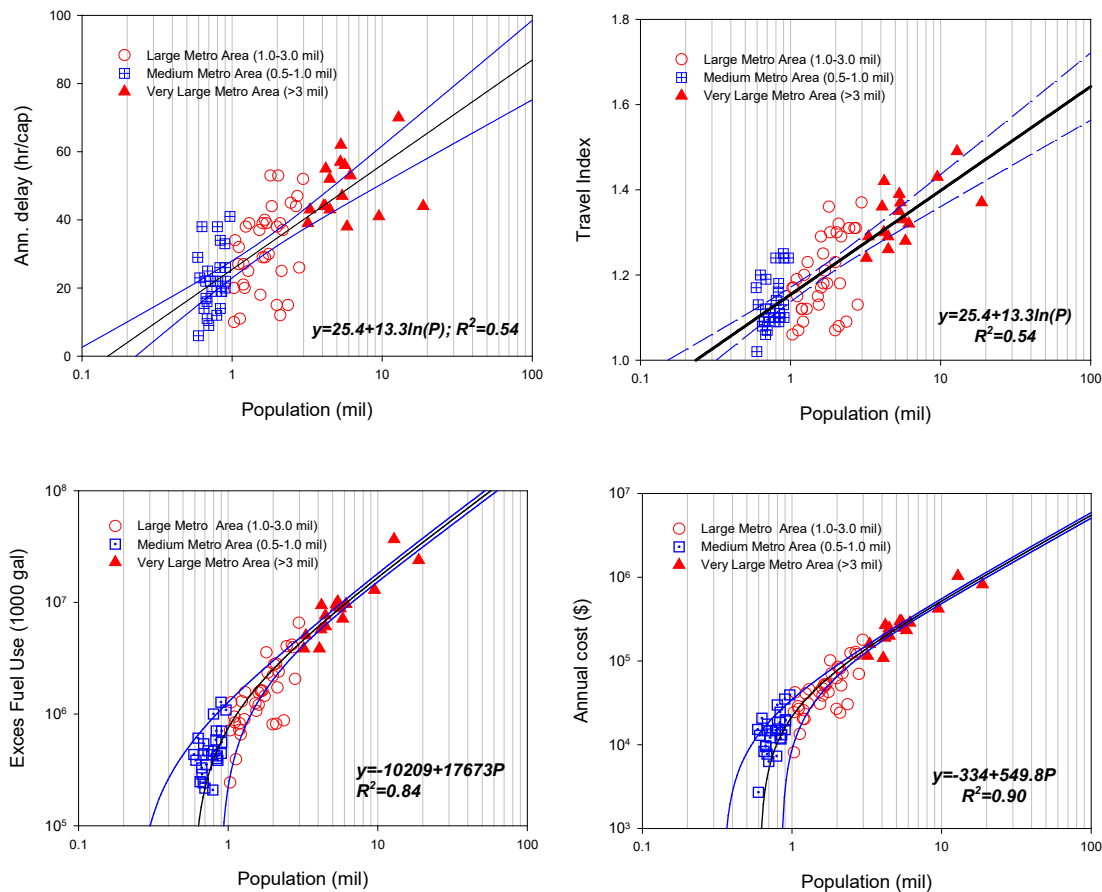


Figure 2-13 Transportation efficiency (annual delay, travel index, excess fuel use, and annual cost) in year 2007 as a function of urban population in the U.S. urban centers. Data from the 2009 urban mobility report (Schrank and Lomax, 2009). The blue dash lines are 95% upper and lower bounds of the regression of all data.

excess fuel usage, travel index, and annual cost) in 2007 are all based on a comparison between peak hour traffic and free flow conditions in principal freeway and arterials. Travel index is a ratio between time used in peak hour versus free flow at 60 and 35 miles per hour (mph) on the freeway and arterials, respectively. The excess fuel usage is defined as fuel wasted at vehicles moving at a slower speed than at free flow conditions. These measures quantify the consequences of urban traffic, indicative of urban transportation efficiency.

The transportation efficiency is correlated to urban population size (Figure 2-13). The correlation is the strongest ($R^2=0.84$) on the excess fuel use. The correlation slope indicates the change in transportation performance (e.g., delay or excess fuel use) as the population grows and urban sprawls. The excess fuel use and cost curves indicate that as cities grow into very large metropolitan centers, the slope becomes smaller and nearly a constant. For cities of population <3 million, they tend to plot to the left side of the regression line indicating greater excess fuel consumption (Figure 2-13). Efficiency appears to be attributable to the effect of mass transport and high-density development in large cities (Schrank and Lomax, 2009). The similarities and differences reveal the underlying principles that govern the efficiency of urban transportation systems.

In all cases, the limitation in infrastructure adaptation under the current decades-long urban planning practice is important. More meaningful improvement may come from the change in urban form from the traditional monocentric to polycentric urban arrangements. Transformation districts and adaptive planning are critical elements in the process (see Figure 2-6). Such change is conceptually illustrated in Figure 2-5. How to facilitate the urban form transformation for improved urban efficiency is a challenge to urban planners and infrastructure engineers. An example of this transition has been examined in a detailed mechanistic study of the transportation system in the Cincinnati metropolitan area. The results are described in the subsequent sections to illustrate the likely benefits from urban form transformation using computer simulation of adaptation planning scenarios.

2.1.3. Water planning and engineering

Water infrastructure planning and design follow the guidelines in urban development master plans, and further details the needed assets and management required to provide water services (see Figure 2-4 and 2-6). In general, the water infrastructure is scoped mostly during or after transportation planning according to master plans or development policies.

In expansion, an urban form evolves and, sometimes, develops into polycentric configurations. The transportation structure reinforces the changes. Such infrastructure-facilitated change can alter the spatial distribution of population and economic activity, and in return generates new water service needs. Often passively, the water service is compelled to adapt and expand to meet the new water service demands (Figure 2-4). It is not uncommon that the legacy of the centralized water system configuration remains intact even after cities are transformed into a polycentric formation. Practical examples are numerous, such as the vast centralized water service infrastructure in Cincinnati, Detroit, Cleveland, Los Angeles, and New York City.

Existing water systems are mostly monocentric in the U.S.: centralized water treatment and water distribution, centralized wastewater collection and discharge treatment, and, to a lesser extent, centralized stormwater systems (mainly gravity-driven) with discharges to available

waterways. Specific engineering of the water supply and water sanitation infrastructure is described later in Section 5.0. Additionally, current water infrastructure planning and design are often focused on component optimization, system improvement, and capacity expansion. This tendency in development has the following notable attributes:

- Water infrastructure, most of which is buried, is planned and designed to meet water and wastewater demands as defined in urban master plans. Once designed and built, the water infrastructure and their functions create a “locked-in” condition whereby the infrastructure framework can be difficult to change or modify in the future.
- For the most part, the treatment plants characteristic of centralized water and wastewater systems are located away from urban centers. This was done to protect water supplies from pollution by discharging treated wastewater downstream of the population to limit the potential for waterborne disease. In addition, few people desire to live in the vicinity of these plants. Compounding the issue, many older city centers have lost population and industry to the extent to which having excess capacity to “sell.” This current practice in the development cycle results in a natural tendency to expand distribution and collection pipe networks into the new areas of development because of relatively small capital cost and leverage over the utilization efficiency of the centralized system. However, this sprawling expansion occurs at the price of a potential increase in energy usage and a decrease in environmental qualities. There is a limit to this expansion before the basic system configuration and operational parameters require changes, often at a substantial economic cost.
- Water infrastructure has as its primary service function to ensure compliance with applicable SDWA and Clean Water Act (CWA) regulations. “Secondary” requirements include providing adequate capacity and reliability to meet the urban service needs, providing fire service, and controlling rates through managing capital and operational costs. The system efficiency, energy consumption, and emissions are often lesser priorities in master planning (U.S. EPA, 2015a).
- Although subject to the master development plans, urban water infrastructure is often engineered independently from transportation infrastructure. The two may become decoupled and uncoordinated. As a result, water infrastructure may not be adequate to meet the service needs when transportation infrastructure and associated land use induce further spatial shifts in population and business activities (Flanders et al., 2014). This nature in planning may not only create conflicts with construction and service timing for the two types of urban infrastructure, but also add greater complexity when changes and adaptation become necessary to support new urban functionalities in the future.

2.2 Transformation toward smart growth

Smart urban growth aims to achieve low-carbon and energy-efficient service-reliable development through adaptive planning. Urban transformation is one approach to change the existing urban form to a configuration of high urban density, walkable communities, and livable environments (U.S. EPA, 2013a). This smart growth concept is now being incorporated by many municipalities. In the national trends, smart growth often entails techniques such as infill, green planning, and high-density residential developments, which has been increasingly applied throughout the U.S. (U.S. EPA, 2013a, 2009b). Infill development and mixed transportation

mode are demonstrated to improve system efficiencies and reduce transportation emissions. A series of EPA reports have been published on smart growth applied to residential development and its pertinent transportation and water infrastructure (e.g., U.S. EPA, 2006, 2009b, 2011, 2013a, and 2012a).

Transformation districts as a smart growth measure (Figure 2-6) can induce a transition from a monocentric to a polycentric urban form that has higher efficiency. These districts are planned with degrees of flexibility to evolve into polycentric, high-density, walkable communities with ready access to mass transit. The planning process rests on the ability to modify infrastructure to accommodate urban growth and population increase with the minimum environmental impacts. For this purpose, the transformation districts are the necessary links for the natural evolution toward very large polycentric urban centers. For example, multi-mode transportation systems and multiple water supply or wastewater management districts are common examples for very large urban centers. These urban features are characteristic of smart urban growth principles. They can be initiated by adaptive urban planning as a part of the long-term master planning process.

The transition from monocentric to polycentric forms, when realized in practice, has significant implications for water infrastructure planning, engineering, and operation. In the polycentric urban development, highly urbanized centers of impermeable surfaces are scattered among and surrounded by undeveloped natural or low-impact developments (See Figure 2-6 and related discussions in Section 1.1.3). Smart urban development, through measures such as compact neighborhood design and the use of infill and green infrastructure, can reduce water demand, improve water availability and water quality, and provide reliable water services at a reduced cost (U.S. EPA, 2006). The use of green infrastructure is emphasized in the management of combined sewer overflows (CSO) for many cities in the U.S. Midwest, East, and Northeast. With adaptive planning, several possibilities are potentially achievable through the design and implementation of a polycentric urban form. For example, the polycentric distribution of urban populations and activities may allow for developing the decentralized or satellite systems for water supply and wastewater management. Decentralized water management shortens the urban water cycle, by increasing water recycling and onsite water infiltration, thus making it possible to increase wastewater reclamation, nutrient recovery, and potential energy harvesting (see Luthy, 2013; Lee et al., 2013). In addition, the high-density housing development in the multiple centers yields a smaller carbon footprint per capita (ADB, 2012), and may facilitate the development of mass transit systems to connect the new urban centers. Examples include Washington DC, San Francisco, and New York City. The resulting higher urban efficiency and lower carbon footprint per capita in these urban centers can be observed from Figure 2-13 in Section 2.1.2.

2.3. Monitoring and re-evaluation

Adaptive planning helps examine viable urban development options against a set of adaptation objectives. Such analysis aims to evaluate the capacity and efficiency of existing transportation and water infrastructure, identify future improvement options, and compare their benefits against a set of planning objectives, mostly through model simulations. Major planning activities may include:

- Population and land use planning and future projections
- Transportation analysis and planning, including air quality analysis

- Water infrastructure analysis and planning to either assist or limit transportation development in urban development scenarios

Adaptive urban planning can be readily incorporated in the conventional master planning process. The current urban planning (Figure 2-4) evaluates water and transportation infrastructure conditions, and defines infrastructure improvements, mostly by increments, between two adjacent master planning periods. Often the transportation and water infrastructure development are uncoordinated, producing a condition that could potentially hamper future water service optimization. To avoid this undesired consequence, adaptive planning uses an iterative process and integrates the planning, engineering, outcome assessment, and re-planning through scenario simulations (see Figure 2-6). It first evaluates urban efficiency against the evaluation criteria, such as energy consumption, urban efficiency, and compliances. Then it gradually, and systematically shifts the development paradigm toward those favoring smart growth.

The change in the development path by adaptation takes place at two endpoints. At one end, the adaptation weighs into the readjustment of developmental goals, local water, and land use policies. This adjustment varies among locations and individual cities, because of potentially different constraints in local environmental and socioeconomic conditions. At the other end, adaptive planning is focused on urban form and infrastructure itself. Urban growth is adaptively planned to change the paradigm from urban sprawl to the high-density, low-carbon, and high-efficiency urban form (Figure 2-6). One example of such adaptive planning is to expand wastewater management service through a combination of gray and green water infrastructure, often in decentralized management, for increased water harvesting and overland runoff reduction. This report does not cover the adaptation approach through adjustment of the development goals, but instead focuses on adaptive planning for physical systems.

In addition to the mandatory environmental standards, water and energy/carbon footprints are two indices of urban efficiency that can be used in evaluating urban adaptations. The two non-parameterized orthogonal indices can be used to quantify the water and energy tradeoffs at a systems scale. This evaluation matrix can be used to compare developmental options. Published studies are mostly based on simple water or energy usage and for analysis of a single industry or single service sectors such as a municipal drinking water supply or a transportation system. Nevertheless, these previous studies provided insight into the water-energy interactions in energy production (Cooley et al., 2011; Rothausen and Conway, 2011; Zhou et al., 2013; Azadi et al., 2013; Dodder, 2014; Dodder et al., 2011; Webster et al., 2013; Chang et al., 2012; and Ibrahim et al., 2008) and in urban planning and operation (Perrone et al., 2011; Hering et al., 2013; Yang et al., 2013; Wang et al., 2013; Kenworthy, 2006; Novotny, 2013; Lee et al., 2013). More attention is now made toward both indices (water and energy/carbon footprints) and their relative importance for a given system, infrastructure asset or industrial sector; for example, to the planning of energy biomass and hydropower production in the water-stressed U.S. west (PNNL, 2012; Yang and Goodrich, 2014).

3. SUD Methods and Tool in Adaptive Urban Planning

Much of the discussion to this point has been focused on the water sector and how the change in urban form might impact it. The limited discussion has concerned the fact that in urban planning, energy usage and air emissions are intimately related to the construction and operation of water infrastructure. This interrelationship can be dissected in many ways. For example, as

noted in Section 1.1 (especially 1.1.2), transportation and water infrastructure are closely related to the urban form and the potential development mode. In return, an urban form defines population and economic activities, and thus can significantly affect the energy use of water supply in both infrastructure construction and operation.

The other principle effect of urban development is found in spatiotemporal variations of water demand, because of the demand distribution and the unique UHI effect. The concept of the UHI is that urban gray infrastructure (such as pavements, buildings, and concrete structures) creates a greater amount of reflective heat than undeveloped vegetated areas. Hence as an area develops, the man-made gray structure absorbs and emits heat in a day cycle, causing higher ambient temperature and stagnant air flow in urban centers especially during night time. The degree of UHI effect and temperature variation depends on land use and land covers, local topography, and ultimately the urban form. Such conclusions were made by several studies on a detailed thermal mapping of the UHI effects (e.g., Liu et al., 2012; Buyadi et al., 2013; Weng et al., 2004). In later Section 4.1, a case study in the Cincinnati metropolitan region shows how the urban form, defined by highways and roads, can lead to the occurrence of UHI, its magnitude and spatial distributions. Overall, the urban form has an impact on traffic emission, ambient air quality, the distribution of population and business activities, water demand, and water services. These combined effects are the basis for adaptive urban planning.

3.1 AUP&ET principles and utilities

The adaptive urban planning and engineering tool (AUP&ET) is developed to assist the analysis of urban development options. This integrated simulation tool is intended for planners to simulate urban transportation performance (e.g., travel delay, air emission) in adaptation scenarios. The integrated modeling framework for AUP&ET is shown in Figure 2-9. Overall, the AUP&ET tool consists of three major modules: land use projection, urban-scale transportation modeling, and water infrastructure modeling. In this framework, the urban variables refer to physical attributes such as topography, environmental conditions, and natural resources. The urban developmental goals and growth factors, along with the impacts of climate variations, are collectively represented in the scenario attributes. Future developmental and environmental conditions can be defined in terms of the probabilistic occurrence.

In this section, the AUP&ET module for transportation infrastructure, its simulation methods, functionality, and applications in the Cincinnati metropolitan area, are described.

3.1.1. Land use projection – CA-Markov model and ICLUS

Land use projection is one of the primary bases for scenario-based planning (Figure 2-9). In subsequent publications, methods and examples of future land use projections will be discussed in detail for rural, suburban, and urban watersheds. As discussed in Section 1.3.1., the ICLUS land use database can be used when the analysis is based on county-level spatial resolutions. Many urban adaptive planning exercises, however, require land use and employment projections in finer spatial resolutions, typically at census block levels. Thus, the CA-Markov modeling technique is incorporated as the default in the AUP&ET module.

A land use model predicts target year land use according to the base year data (land use, demographic, and socioeconomic factors) and develops viable land use scenarios involving demographic and socioeconomic changes anticipated for the target year. In a CA-Markov

analysis, the CA model is combined with Markov Chain analysis, incorporating the Multiple Criteria Evaluation (MCE). The Markov model is based on the formation of the Markov random process for the prediction and optimal control theory (Jiang et al., 2009). The calculation is a multifaceted cross-tabulation between a pair of land use images from two times of different historical observations. Future change probabilities are derived from observed change patterns (Eastman, 2009). Markov modeling predicts each land use transition area for a future year using the transition probability derived from two different historical land use data sets (Sang et al., 2011; Eastman, 2009).

Geographic proximity, also known as spatial autocorrelation, assumes that adjacent areas tend to be similar in land use in a gradual land use change. In a natural environment, similar soil characteristics, terrain, weather, and vegetation are usually found within a defined region. The impacts of all these factors are evaluated according to the factor’s relative importance or weights (Rao, 2005). MCE as a multi-attribute decision-making tool is incorporated in CA-Markov modeling to provide land suitability analysis with the support of GIS (Fu et al., 2018). Overall, the CA-Markov model allocates land use under the objective that was produced by Markov Chain analysis according to terrestrial suitability produced by MCE. It takes original land use and its neighborhood land suitability into consideration (Feng et al., 2011; Eastman, 2009). These basic principles and applications can be found in land use projection literature (Tong et al., 2012; Sun et al., 2013; U.S. EPA, 2010b, and references therein).

Figure 2-14 shows a framework of urban land use projection used in the AUP&ET. There are three properties essential to calculate the transition probability: (1) past trends, (2) geographic proximity, and (3) spatial dependency.

Past trends are land use changes observed during a previous period. They can be measured by comparing land uses in the initial year and the base year. The elements of

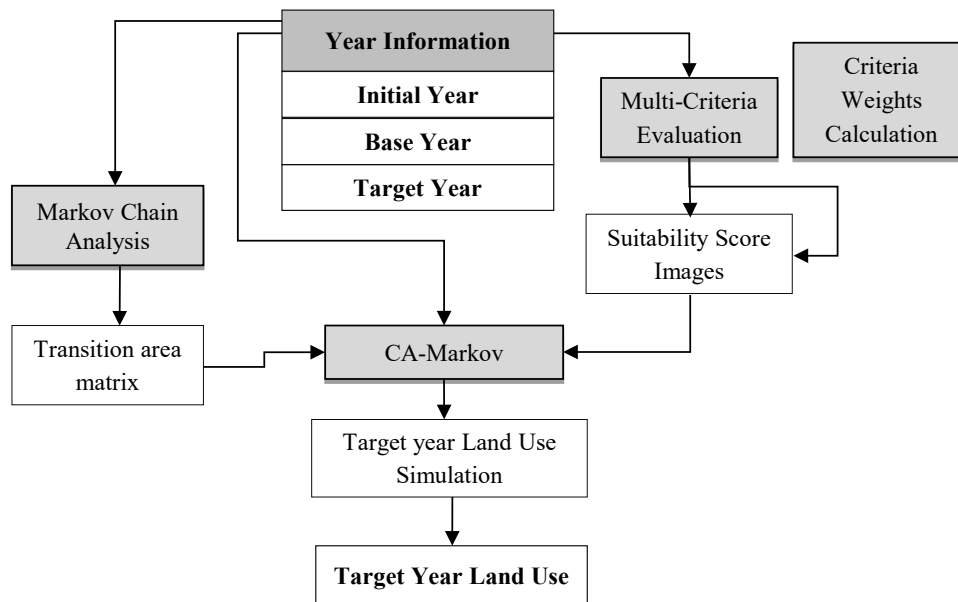


Figure 2-14 Simulation block diagram for CA-Markov based urban land projections.

multicriteria evaluation using different criteria weights are converted numerically into a sustainability score (Figure 2-14) that can be analyzed spatially. Furthermore, geographic proximity and local developmental drivers are necessary considerations in any land use analysis. For example, population density and land value are similar within a defined geographic unit (i.e. neighborhoods, cities), but significantly differ among such units. Spatial dependency may restrict or promote future land use changes. Although spatial dependency factors may vary by location and types of land use, they are derived from four major categories: (1) population density, (2) accessibility, (3) administrative restrictions, and (4) physical limitations.

The land use projection in AUP&ET consists of three major steps (Figure 2-14) and uses four major modules in AUP&ET: (1) Markov Chain Analysis, (2) Criteria Weights Calculation, (3) Multi-Criteria Evaluation, and (4) CA-Markov simulation. In CA-Markov modeling, the base year land use image is taken as the model input from which changes are projected. The modeling further considers transition area objective, as produced by Markov analysis, and a collection of suitability images that express the suitability of a pixel for each of the land use types from MCE criteria. Then the modeling begins with an iterative process of reallocating land use until it meets the area totals predicted by the Markov analysis. The modeling process and underlying principles are as follows (Eastman, 2009).

- The total number of iterations is based on the number of time steps, namely the projection time frame. For example, if the projection is for 10 years into the future, the time steps might be chosen to complete the model simulation in 10 steps. The time step is chosen to strike a balance between model precision and computation time. It also needs to be appropriate for the rate of urban development in the past and, potentially, in the future.
- Every land use type in model iteration typically will lose some of its lands to one or more of the other classes. It may also gain land area from others. For each modeling iteration, claimant classes select the land from the host according to the suitability map for that class.
- The CA component arises, in part, from the iterative process of land allocation. It also results, in part, from a filtering stage with each iteration that reduces the possibility of unsuitable changes. The net result of this iterative process is that the land use changes occur in response to the growth in the areas of high suitability spatially proximate to existing areas.

3.1.2. Calibration and validation of the land use simulation model

Model calibration is important for the projection of urban land use because of its dynamic evolution with time. Calibration aims at obtaining values of the transition rule parameters that enable the most accurate reproduction of the past evolution in land uses. There are two traditional methods to calibrate CA-based models: (1) methods based on trial and error, and (2) methods based on statistical techniques.

The first category does not require a set of strict mathematical formulas. It assesses the results obtained from alternative combinations of parameter values (Ward et al., 2000) and the sequential multistage optimization by an automated exploration of combinations of parameters (Silva and Clarke, 2002). For the second category, the most frequent statistical method is logistic regression that provides the weights of the variables involved. However, the statistical equations

might not reflect the actual relationships or explain the underlying mechanisms (Santé et al., 2012). The first method is used in the case study in Cincinnati (see Section 4.2).

The general validation method consists of the visual comparison of model results and observed data in a historical period/point of time. The method usually is complemented by quantitative methods that evaluate overall accuracy. For the accuracy measurement, the most frequent metrics in increasing order of complexity are (i) ratio of simulated to the real number of cells (or clusters) for given land use, (ii) overall accuracy measured by the percentage of correctly classified pixels, (iii) regression analysis between simulation results and real data, and (iv) a coincidence matrix and the Kappa index (Santé et al., 2012, and references therein). Because the method based on trial and error is applied in the calibration process, overall accuracy and the Kappa index are popular measurements in comparing simulated land use with reference land use. Therefore, the overall accuracy and the Kappa index were adopted for land use calibration and validation in the AUP&ET simulations.

3.1.3. AIR-SUSTAIN system for transportation simulation

The other major AUP&ET component is for urban transportation planning in adaptation (Figure 2-9). This scenario-based adaptive planning has basic objectives for high transportation efficiency and reduced air emission, energy usage, and carbon footprints under the current and future land use scenarios. The land use types and spatial relations are the basis for defining the population, employment, and urban activity distributions in transportation modeling (see Section 3.1.1 above).

The scenario analysis for transportation planning is hosted within a newly developed simulation tool, “Air Impact Relating Scenario-Based Urban Setting and Transportation Asset in Network” or AIR-SUSTAIN (Yao et al., 2014). Figure 2-15 shows the program’s architectural structure. The current version consists of three application modules: (1) scenario development, (2) regional level analysis, and (3) project-level analysis. The scenario development module is built upon the base-year land use, demographic and socioeconomic factors, and transportation infrastructure data. It further considers the assumed changes in the demographic and socioeconomic factors for a target year. The target year land use is projected by the CA-Markov land use model. For regional level analysis at county-resolution, the ICLUS model (U.S. EPA, 2010b) also can be used. Land use projections are described in the preceding subsection.

In general sequence, the AIR-SUSTAIN’s regional level analysis can be used to assess the impacts of a growth scenario on transportation system performance at urban scales (Figure 2-15). Here the traffic projection results are used to assist in identifying the *traffic congestion area* of the road links, where the transportation efficiency deteriorates in traffic flow and CO₂ emission. It is noted here that the traffic congestion analysis in Figure 2-15 is different from the EPA’s regulatory conformity *hot-spot* analysis.

Once the traffic-congested areas are identified, a project-level analysis can be conducted to identify the most appropriate traffic control measures and other engineering solutions (Figure 2-15). The analysis is centered on options to improve transportation performance and reduce on-road traffic emissions. Together, technical results on transportation performance at both the regional level and project levels enable users to quantify environmental benefits in an urban

planning scenario. Again, the tool and models are not designed for regulatory compliance analysis. For the latter, EPA’s transportation conformity regulation (40CFR Part 93)² applies.

The AIR-SUSTAIN modeling and analysis start with the computation of target-year demographic and socioeconomic distributions based on projected land use. The modeling basis and techniques were described in preceding Sections 3.1.1 and 3.1.2. Using the user-specified growth rates, a linkage model in AIR-SUSTAIN populates the spatial distribution of the future land use changes within an urban area of analysis. The linkage model projection includes future population, employment, university enrollment, and high school enrollment in each traffic analysis zone (TAZ) in a target year. The principal variables in the regional-level analysis for travel demand forecasting include employment, student enrollment, etc. Subsequently, traffic emissions based on the travel demand forecasting (TDF) outputs are estimated using the EPA program MOVES. Section 3.2 further describes data flows and model simulation using the AIR-

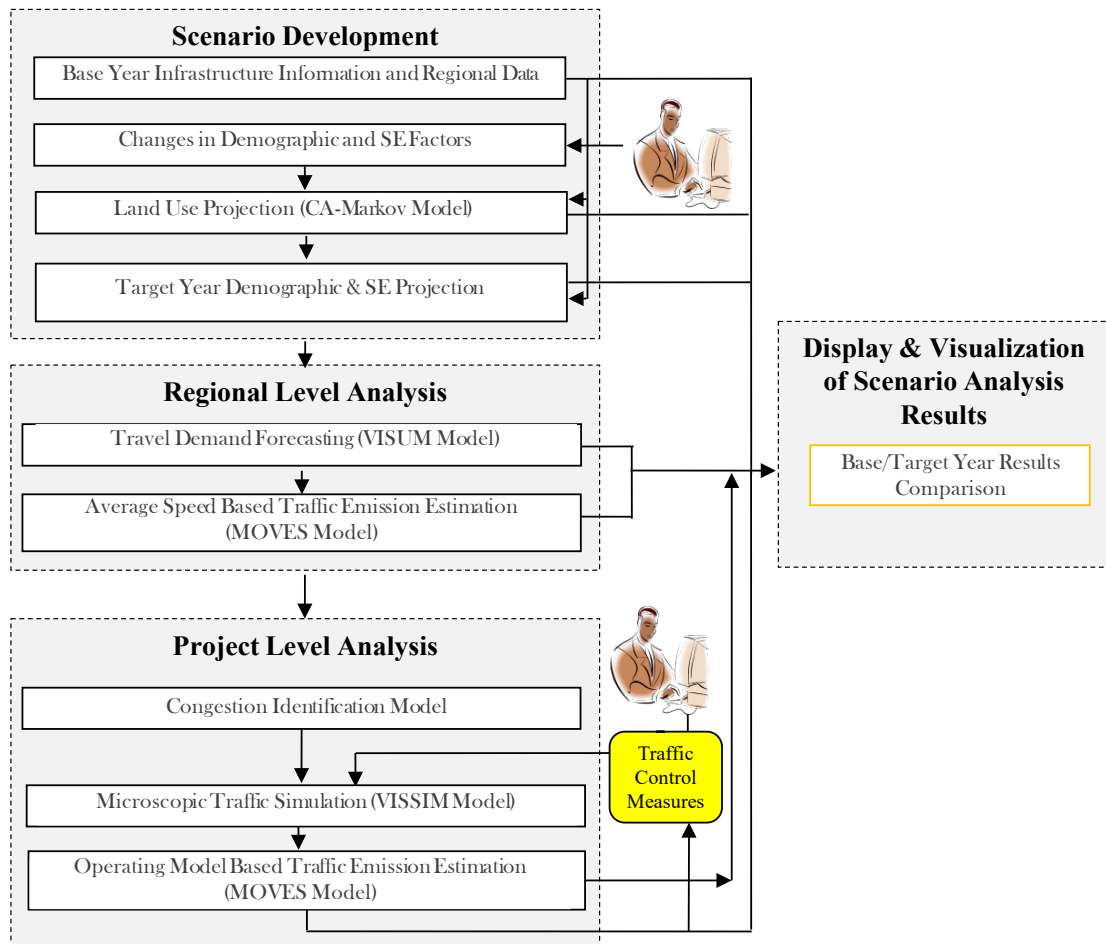


Figure 2-15 AIR-SUSTAIN modeling framework for transportation analysis of efficiency and carbon dioxide emission in urban infrastructure adaptation. Abbreviation: SE – socioeconomic

² EPA has guidance for transportation conformity available on its web site: <https://www.epa.gov/state-and-local-transportation/current-law-regulations-and-guidance-state-and-local-transportation>.

SUSTAIN tool. Section 4.1 presents a real-world case study in the Cincinnati metropolitan region for illustration.

3.1.4. *The linkage to water infrastructure simulations*

The adaptive planning framework within SUD also contains water infrastructure modules for drinking water supply, wastewater and stormwater management (see Figure 2-9). Because water infrastructure normally follows the population and land use changes, its planning and design are assumed to be sequential after transportation infrastructure evaluation.

3.2 The AIR-SUSTAIN simulation tool for transportation

Following the SUD overview in Section 3.1, this section details the functions of the transportation simulation tool AIR-SUSTAIN. AIR-SUSTAIN is a software interface developed in this research to integrate land use projection, traffic simulations and optimization. The purpose is to evaluate development scenarios of land use and transportation by modeling and analyzing CO₂ emissions over a transportation network, fuel usage, and transportation performance in terms of excess travel time, traffic congestion, etc. The tool utilizes a GIS platform to provide the urban-wide spatial information on model projections of land use, employment, residential development, travel demand, and automobile-based travel conditions. Other environmental performance criteria in the modeling include fuel consumption and total carbon emissions.

AIR-SUSTAIN software contains functions in data flows and linkages among the model components (Figure 2-15). In Appendix A, details of the program structure and model input and output are described. Major modeling components include those below:

- Linkage model. The linkage model combines the land use model output, the target year population and employment projections, and base year population and employment data. This prepares the target year population and employment for each TAZ as the model inputs for traffic simulation.
- Travel demand forecasting (TDF) model using VISUM software. VISUM is comprehensive flexible software widely used worldwide for metropolitan, regional, state, and national planning applications. The TDF model simulates the link (i.e., roadway segment) traffic volume and speed. Simulation results then are used as inputs for the traffic-related emission estimation in AIR-SUSTAIN.
- Microscopic traffic simulation model using VISSIM software. The commercial traffic analysis software enables the analysis of traffic measures designed to improve traffic capacity. It also is used with AIR-SUSTAIN to evaluate engineering options to reduce carbon and pollutant emissions.
- Automobile vehicular emissions calculation using EPA's regulatory model MOVES³ (U.S. EPA, 2010a; 2015c) for different scenarios of urban-wide transportation or specific traffic measures in adaptation.

³ <https://www.epa.gov/moves/latest-version-motor-vehicle-emission-simulator-moves>

3.2.1. Basic functions and interfaces of AIR-SUSTAIN

The AIR-SUSTAIN software interface integrates transportation and land use models for scenario analysis. The use of scenario-based planning analysis helps assess sensitive interactions among travel demand, the impact of transportation activities on-road emissions, and urban development policies. The quantitative analysis is executed in the AIR-SUSTAIN software through interfaces embedded in a GIS environment (Figure 2-16). The main functions and interfaces of the AIR-SUSTAIN include Scenario Information Specification, Scenario Development, Regional Level Analysis, Project Level Analysis, and Results Comparison.

▪ Scenario Development

Scenario development for transportation adaptation is set by importing base year data and developing demographic and socioeconomic attributes of a scenario. The base year demographic and socioeconomic data are imported with the feature class *TAZ*. The target year demographic and socioeconomic data are contained in the feature class *TargetYearTAZ* of the computer program (its format is shown in Appendix A's Tables A1-1 to 1-4). It is computed based on the assumed demographic and socioeconomic changes, target year land use projection, and base year demographic and socioeconomic data.

Among those datasets, the demographic and socioeconomic changes are projected, and often assumed, for a future scenario. They depend on urban development policies or objectives. This group of data is specified by the user through the functions in the *Scenario Development* software module. The target year land use data are projected by the land use model embedded in the AIR-SUSTAIN model. The data inputs, specification of demographic and socioeconomic factors, and model execution are implemented in the Scenario Development module.

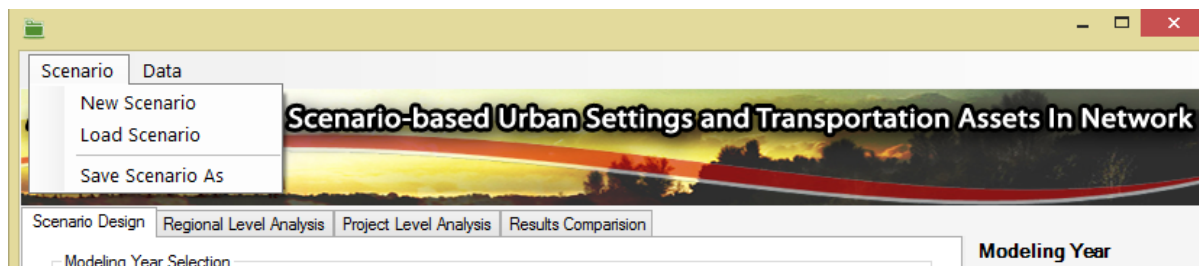


Figure 2-16. AIR-SUSTAIN graphic interface for scenario modeling and analysis.

▪ Regional Level Analysis

The Regional Level Analysis module is used to estimate travel demand and on-road emissions for the base and target year in a project area. It should be noted that this traffic analysis is different from the regional emissions analysis done for transportation conformity. Overall, AIR-SUSTAIN's Regional Level Analysis consists of two major elements: (1) Travel Demand Forecasting, and (2) Emission Estimation. When performing the regional level analysis, a TDF model first simulates trips on roadway links for the entire area of concern based on demographic and social-economic data, as well as transportation infrastructure, such as road network, parks, water bodies, TAZs, etc. Subsequently, the forecasted traffic data are used to generate inputs for traffic emissions modeling to estimate vehicle emissions for each road link.

In the emission analysis, CO₂ equivalent ($CO_{2,T}$), criteria pollutants, and energy consumption are estimated by using the EPA's MOVES model (U.S. EPA, 2010a; 2015c).

- **Project Level Analysis**

In the Project Level Analysis, the traffic congestion links are identified from the regional level analysis results. As aforementioned, the traffic congestion analysis is different from assessing whether a project needs a transportation conformity hot-spot analysis. The microscopic traffic simulation model VISSUM is used to estimate the traffic flow operations on the congestion links under alternative traffic control measures. The assumed traffic control measures then can be assessed in terms of traffic operation performance and their influence on the on-road traffic emission rates. Emission rates for each congestion link are calculated using the MOVES model in the project-level analysis module.

- **Results Comparison**

After performing the scenario design, regional level analysis, and project level analysis, the AIR-SUSTAIN simulation outputs from the base year and target year can be compared and visualized in ArcGIS by the Results Comparison tab (Figure 2-17). In the subsequent sections, the AIR-SUSTAIN tool is described on its data structure; model linkage; travel demand; traffic

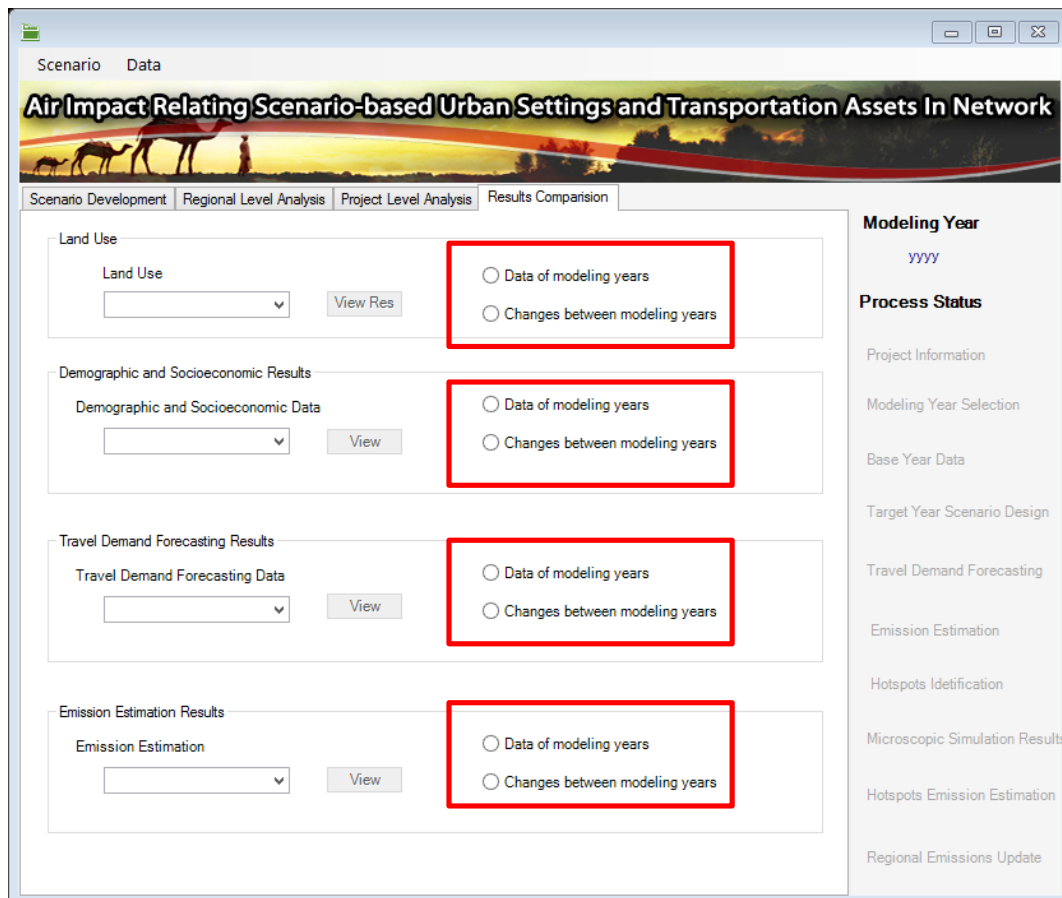


Figure 2-17 The Results Comparison module interface in the AIR-SUSTAIN tool.

congestion identification; the microscopic simulation of adaptation options; and, lastly, the emissions and energy consumption estimation.

3.2.2. Travel demand forecasting – VISUM

Travel demand forecasting (TDF) is essential in the traffic analysis that links transportation to land use and socioeconomic factors at a regional level. In the AIR-SUSTAIN tool, the TDF model is used to forecast travel demand for the base year and target year. This projection is primarily dependent on the settings of land use based on the socioeconomic datasets. TDF model outputs include the link (i.e., roadway segment) traffic volume and speed, which further can be used as inputs for the traffic-related emission estimation.

3.2.2.1. Modeling

Travel demand analysis was first developed in the late 1950s for highway planning using a four-step model. This model, using the conventional trip-based approach, is a primary tool for modeling future travel demand and performance of a regional transportation system. The AIR-SUSTAIN tool adopts this traditional four-step model for the travel demand forecasting. The demand forecasting involves these four basic steps:

- Trip generation. This is the process in estimating the number of person-trips that will begin from or end in each TAZ within the region on a typical day. The traditional trip-based approach considers each trip as the unit of analysis. When an individual makes a series of trips, each trip is treated as a separate, independent travel event (McNally, 1996, 2007).
- Trip distribution. This modeling process allocates the trips generated in one zone to other zones.
- Mode split. It estimates modal percentages of the travel according to the time and cost characteristics of various competing modes based on demographic and socioeconomic characteristics of the urban residents.
- Traffic assignment. This last step in travel demand forecasting assigns trips to the transportation network.

Notably, the four-step models rely on *average* transportation behavior between and within traffic zones. More sophisticated activity-based models attempt to represent focus groups of populations. This approach considers underlying travel behavior (Jones et al., 1990), and thus explicitly recognizes and addresses the limitations of the conventional trip-based approach. The model analysis is shifted from rough aggregates to the level of the individual traveler (Zmud et al., 2014). This recent development makes it possible to incorporate detailed demographic data.

However, considering the data needs in modeling, the current VISUM software in AIR-SUSTAIN is based on the four-step model approach. The same approach is used in other traffic modeling packages such as Cube and TransCAD.

3.2.2.2. Model calibration and validation

Model calibration and validation are fundamental to travel demand forecasting. Model calibration and validation data may include:

- reliable estimates of base-year TAZ household characteristics and employment information,
- an accurate representation of the base year highway (and transit, if any) network, and
- a reliable base-year travel survey or monitored traffic data based on main permanent stations.

Model calibration and validation can proceed after the model parameters are estimated in the AIR-SUSTAIN simulation. Model calibration enables model parameters to be adjusted until the predicted travel matches the surveyed travel (e.g., origin-destination [O-D] survey data) across the region for the base year. The model calibration assumes that these calibrated parameters will remain constant over time (Pedersen and Sandahl, 1982). Furthermore, model validation tests the model predictability of the future. In many areas, traffic counts commonly are used for model validation. Validation requires comparing the TDF model predictions on specific roadways with the traffic counts data (e.g., Annual Average Daily Traffic [AADT]) that occurred on the same roadways in a validation period.

TDF calibration and validation is based on the Mean Absolute Percentage Error (MAPE) in Eq. 2.2. In the travel demand model, parameters, such as the utility functions' parameters and network capacity are adjusted to calibrate the model.

$$MAPE = \frac{1}{T} \sum_{t=1}^T \left| \frac{M_{abs}(t) - M_{sim}(t)}{M_{abs}(t)} \right| \quad (2.2)$$

where $M_{abs(t)}$ and $M_{sim(t)}$ are the field measured time-series values and the simulated time-series values during a period of time t respectively. In the AIR-SUSTAIN, MAPE is calculated for the measured and simulated traffic count and model volume. The MAPE ranges for total error by functional classification (the type of road) are set by FHWA (1990):

Freeway	<7%
Expressway	<10%
Arterial	<15%
Collector	<25%
Frontage/Ramps	<25%

3.2.3. Assistance in traffic congestion identification

AIR-SUSTAIN in the SUD tools has the technical capability in analyzing traffic conditions and identifying traffic congestion areas for given land use and urban developmental scenario. It uses MOVES2014 (EPA, 2015c, 2010a) to calculate pollutant emission for the identified traffic congestion areas in need of traffic management in adaptation. This analysis provides technical data such as link traffic volume, speed, and emission estimate. The traffic congestion analysis in AIR-SUSTAIN is not equivalent to and not applicable to regulatory analysis for transportation conformity.

Using AIR-SUSTAIN, the locations of traffic congestion in future urban development options can be identified from the land use and traffic simulations. Theoretical basis and application examples of traffic and air emission modeling are given in this section and later in

Section 4.2. Details of the modeling program steps are also provided in Appendix A. In summary, the AIR-SUSTAIN simulation program identifies all corridors for the traffic congestion area analysis according to the regional-level analysis results. Their link information is saved in the database and marked in ArcGIS for the microscopic analysis in the subsequent modeling step.

3.2.4. *Microscopic simulation using VISSIM*

The AIR-SUSTAIN simulation identifies links of traffic congestion and high emission rates based on the regional-level analysis results. Identified locations can be further modeled using VISSIM software for evaluating traffic measures on highway corridors, local arterial roads, and other road segments. VISSIM was developed at the University of Karlsruhe in Germany and is distributed by PTV Transworld AG for microscopic simulation at a higher spatial resolution. The model enables analysis of the traffic flow by modeling each entity (car, train, or person) within a traffic stream and of the interaction between drivers (Barceló et al., 2005). This modeling capability makes it possible to simulate the traffic control and management systems at all levels, from traffic control platform to individual traffic controllers (Gettman and Head, 2003). This type of analysis facilitates urban adaptation planning and engineering down to a local project level. The current version of the AIR-SUSTAIN tool has this microscopic simulation capability added by emission calculations using EPA's MOVES software. Appendix A provides the details of principles and modeling steps, including input data structure, scenario determination, model calibration and validation. Both high-resolution traffic results and evaluation results can be input values in MySQL and Geodatabase available in AIR-SUSTAIN. Possible simulation results include the following:

- high-resolution traffic condition at the link, including second-by-second speed and acceleration. Such results can be used as the inputs for emission calculation, for example, using MOVES at the project level.
- evaluation results on average speed, delay, and queue length of each link. This modeling output can be used to compare the differences and effectiveness of possible transportation control measures.

3.2.5. *Emission estimation using MOVES*

AIR-SUSTAIN incorporates EPA's MOVES2014 as the energy and emission analysis tool. In 2010, the MOVES model and software were released by the U.S. EPA (U.S. EPA., 2010a) for estimating air pollution emissions from on-road mobile sources. U.S. EPA (2015c) released the updated MOVES2014 program. At the time of development, the AIR-SUSTAIN based on MOVES2014 uses traffic data from the regional level and project-level simulations to estimate the emissions factors. This model integration makes it possible for users to evaluate air quality, carbon emission, and energy consumption for competing for urban adaptation scenarios.

In emission calculation, vehicle activity inputs can be defined at three levels of data requirement and precision: (1) average speed, (2) drive cycle, and (3) operating mode distribution. Each is associated with different levels of model accuracy (Figure 2-18). Average speed is a basic parameter in traffic operation. It is calculated from AIR-SUSTAIN's TDF model. Using the average speed as the traffic input, MOVES modeling in AIR-SUSTAIN selects the operating mode distribution based on vehicle characteristics. On the other hand, the second

option Drive Cycle is a second-by-second description of vehicle activity over time. Such data are usually collected by using a GPS-equipped probe car. It is assumed that every on-road vehicle is following the same trajectory of the probe car. This option can better represent the traffic operation than average speed but requires extensive data collection.

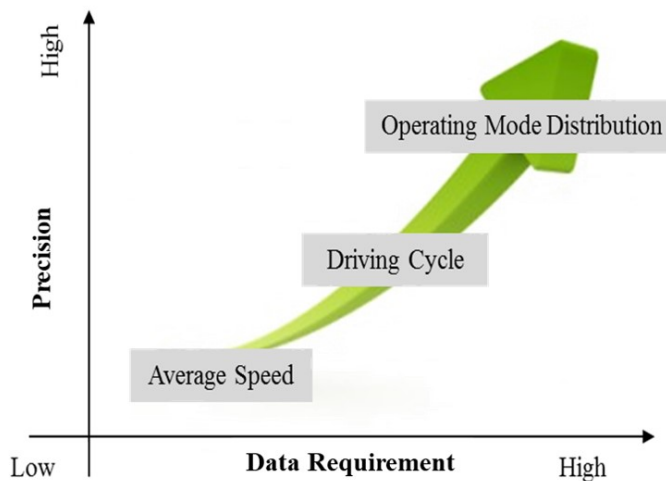


Figure 2-18 General relationship between model precision and data requirements in traffic modeling.

At the highest level, the operating mode distribution method takes a different approach. It

assumes a fraction of vehicle operation mode bins based on its instantaneous operating mode distribution that is determined by vehicle specific power (VSP) and speed. This method describes the entire vehicle population’s operation in the study area and provides the highest individual vehicle level in data resolution. It is worth noting that the MOVES program internally converts all the average speed and drive cycle inputs into the operating mode distribution for the use of the MOVES emission rate database.

A general comparison of the relative model accuracy and data requirement for the three methods are schematically illustrated in Figure 2-18. Considering traffic data availability in general applications, the AIR-SUSTAIN tool uses the average speed option for regional level analysis and the operating mode distribution for project-level analysis. This technical approach is illustrated schematically in Figure 2-19. Traffic inputs for the regional level analysis are extracted from TDF model outputs. In addition to the average speed, other traffic inputs include link traffic volume and vehicle composition. Traffic inputs for the project-level analysis are generated by the microscopic simulation model. They consist of traffic volumes, link average speed, operating mode distribution, and vehicle composition. Details of model inputs, governing equations, and model simulations for traffic flow, vehicle compositions, and operating modes are contained in Appendix A.

Commonly used parameters for model inputs include emission source type, road type, vehicle age distribution, and operating mode:

Emission Source Type

The source type in MOVES is a combination of vehicle type and how the vehicle is used. For example, long-haul and short-haul trucks tend to be very similar in size and design, but the way they are used defines their source use type in the emission category. Table A2-5 in Appendix A shows the source types, descriptions, and their equivalents as defined by the Highway Performance Monitoring System (HPMS).

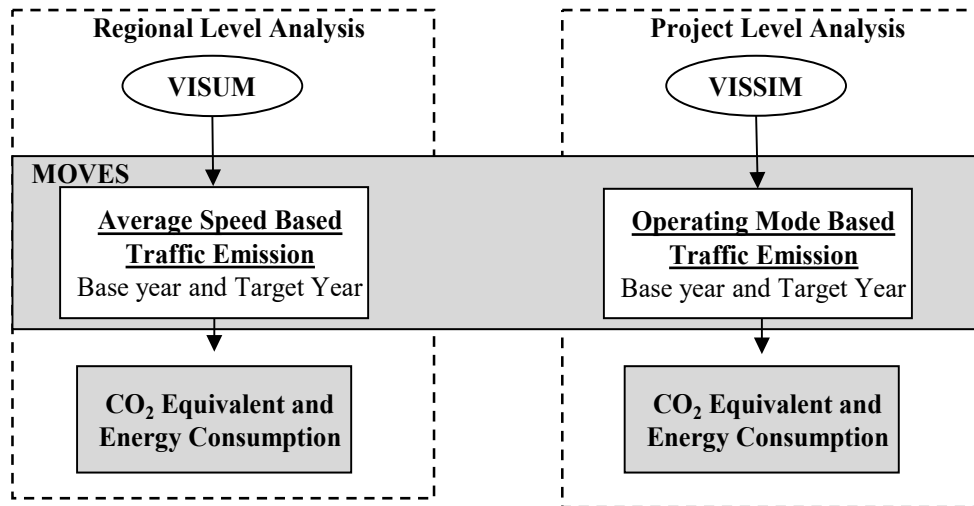


Figure 2-19 Modeling framework for emission estimation using both the macroscale VISUM and microscopic VISSUM traffic simulation models.

Road Type

The list of Road Types is contained in the MOVES database. The default database has Road Types that represent urban and rural driving on roads with restricted and unrestricted vehicle access. Restricted access road types usually are used to model freeways and interstates; ramps are considered part of restricted access road types. In the modeling program, the Ramp Fraction tab of the County Data Manager only will become available if an unrestricted road type (i.e. 2 or 4) is selected. Table A2-6 in Appendix A shows the MOVES road type.

Vehicle Age Distribution

The MOVES model uses vehicle age information, groups the vehicle-specific power (VSP) for light-duty vehicles and the scaled tractive power for heavy-duty vehicles into the age groups. Table A2-7 in Appendix A shows the age categories used in the MOVES model.

Operating Mode

The operating mode bins are predefined in the MOVES model, as shown in Table A2-8 in Appendix A. Each operating mode, categorized by vehicle source type, road type, and vehicle age group, is assigned an emission rate that is determined previously in the MOVES database.

4. Adaptive Urban Planning in SUD Case Studies

Urban-scale adaptation, as described in Section 2.0, aims to develop sustainable infrastructure under current and future hydroclimatic and land use conditions. Adaptation co-benefits can be achieved simultaneously for increased water infrastructure resilience and emission reduction. The two benefits do not conflict with each other but are achievable through

adaptive planning in urban infrastructure development. The sequence for such planning analysis is shown in Figure 2-6. To illustrate urban adaptation and considerations, two SUD application case studies in Cincinnati, Ohio, and Manatee County, Florida, are described in Section 4.0. The case studies are drawn from the existing publications of this research (Liang and Keener, 2015; Liang et al., 2013; Yao et al., 2014; Wang et al., 2013; Yang et al., 2013; Chang et al., 2012).

The case study in Cincinnati shows the relationships among land use, population, transportation under the present urban form, and possible future adaptation scenarios in development. The scenarios are compared using urban efficiency parameters, including fuel and energy consumption, emission and air quality, the UHI effects, and commuting times. In the second case study, this type of scenario analysis for water systems is showcased in master planning for Manatee County.

4.1 Urban form and urban infrastructure

4.1.1. Urban form and land use patterns

Cincinnati metropolitan area hosts approximately 2.1 million people in 15 counties over 7350 km² of land on the banks of the Ohio River (Figure 2-20). Traffic patterns in the region are characteristic of a monocentric urban framework centered on downtown Cincinnati. Rolling hills with limited topographic relief follow the Ohio River and the NNE-SSW oriented Mill Creek. The surrounding suburban area is dominated by flat to moderately hilly farm lands and forests to the east and south. Valleys along the Ohio River and the Mill Creek are about 100 m lower in elevation.

The north-south trending, narrow high-density urbanized zone with heavy surface pavement was delineated from a U.S. Geological Survey urban land use map and by interpretation of a Google® satellite map dated 2013. The high-density zone is shown in Figure 2-20; O-O' marks its long axis. Inside the zone, the land use and cover are characterized by a large fraction of surface pavements and roofs (Figure 2-21a,b). Small patches of green lands and lawns are interspersed among the man-made structures. Besides the continuous large area of the heavily urbanized Mill Creek corridor, two small areas of high-density development appear in the Western Hills area west of I-75, and in the Blue Ash-Mason area along I-71. These small and isolated patches of high-density development are surrounded by residential development of single houses and forest reserves.

Beyond the high-density urbanized urban center is a mixed zone of dispersed low-density developments characteristic of detached residential houses and commercial areas separated by lawns and tree zones. Typical development pattern is shown in Figures 2-21c,d. Figure 2-22 schematically shows the spatial transition from the high-density urban core, to the mixed zone and, ultimately, to the exurban farm lands. In recent decades, urban development in the Cincinnati metropolitan area has been concentrated in several areas or transformation districts leading to the direction of a polycentric urban form.

- Significant urban development has occurred in the West Chester area and the Mason area along north I-75 and north I-71, respectively. Substantial development also has been seen in northern Kentucky along these two interstate highways. These developments sprouted from the significant establishment of commercial activities, introducing satellite urban centers through the process of ribbon and leapfrog sprawl in Figure 2-5.

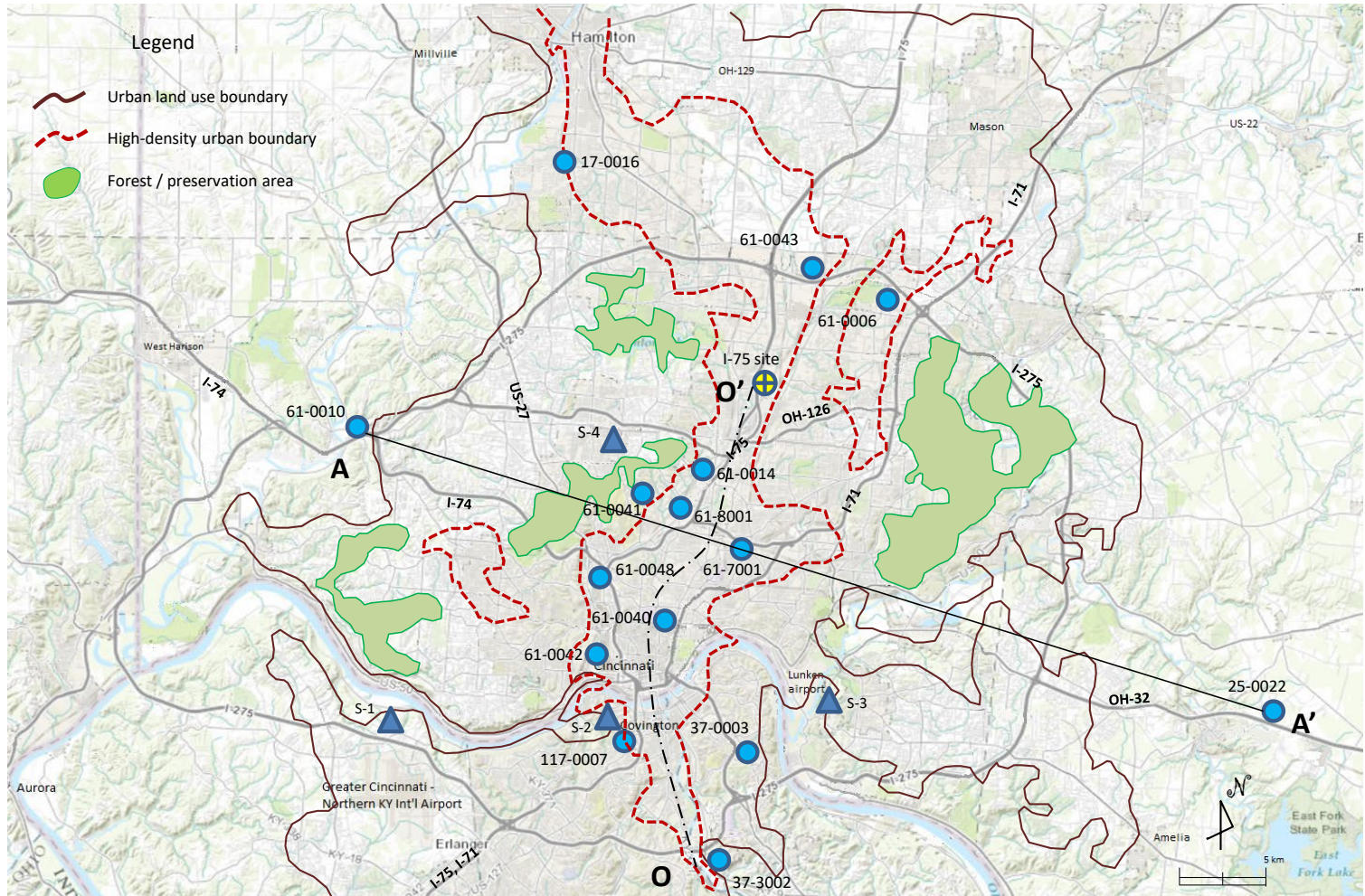


Figure 2-20 Major transportation traffic routes and the urban physical footprints of the Cincinnati metropolitan region. Also shown are the locations of four radio sounding locations (S-1 to S-4) and 15 EPA's NAAQS air quality monitoring stations in filled blue circles. The I-75 site location refers to the study area by Liang et al. (2013). Urban footprint and high-density pavement areas are delineated from the 2007 USGS land use maps. Modified from Liang and Keener (2015).

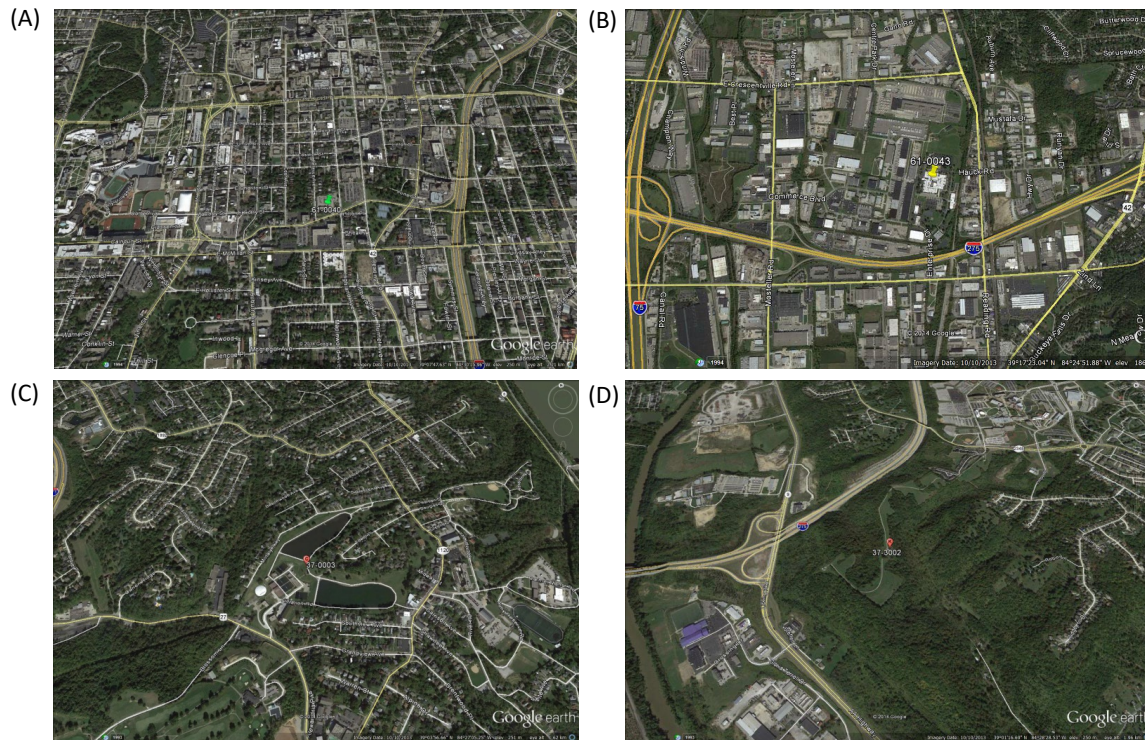


Figure 2-21 Different land use patterns in areas among the 12 EPA's NAAQS monitoring stations. (A) high-density urban core of residual/commercial area at NAAQS station 061-0040; (B) urban core of industrial/commercial area at station 061-0043; (C) low-density residual area at station 037-0003; (D) greenness in urban perimeter at station 037-3002. Each photo's long side is ~2.0 km. Maps obtained from GoogleMap™. From Liang and Keener (2015).

- Cincinnati downtown has been redeveloped over the past decades, with the increasing development of high-density residential communities. The recent development of a street car system solidifies the current development further into a walkable urban center.

The city's preference on infill development along I-75 and I-71, and continued development in the northern Kentucky region, have led to significant transformation of the commercial activities in the region. These developments further lead to a formation of the polycentric form with implications in both transportation and water management.

In the following subsections, the urban form and the land use and cover types are investigated for their relations to the urban climate, transportation demands, and the unique atmospheric structure above the urban center. The most important property is the UHI formation shown in ambient temperature (T_a) and thermal inversion in the urban boundary layer (Figure 2-22). These unique environmental phenomena affect air quality as well as water consumption and hydrology. Thus they are the constraints in urban adaptation.

4.1.2. *Transportation and traffic distribution*

Current transportation in the Cincinnati metropolitan area mostly relies on automobiles. The limited bus-based mass transit and the recently constructed street car system that started operation in 2016, provide mass transportation mostly limited in the downtown area. The major

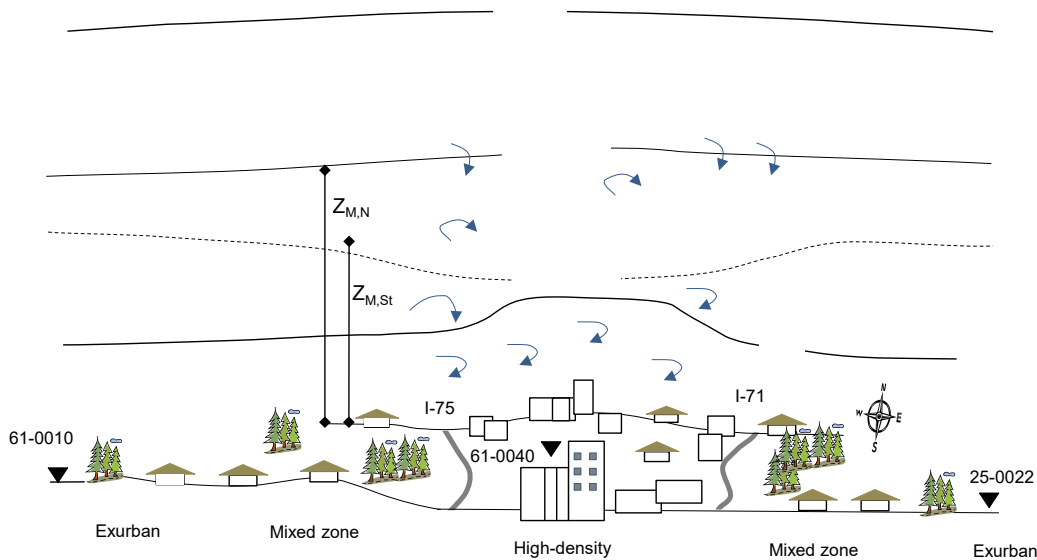


Figure 2-22 A schematic diagram of three-dimensional model for the urban form, traffic and atmospheric structure in the Cincinnati metropolitan region. T_a – ambient temperature; ABL – Atmospheric boundary layer; UBL – urban boundary layer; subscripts N and St for neutral and very stable atmosphere, respectively, and Z is height. NAAQS stations are indicated for their relative locations. From Liang (2014).

road network in the metropolitan region consists of interstate freeways and arterials (I-71, I-75, I-74, and I-275), collectors (SR-126, SR-129), and local roads. The road network connects north-south high-density industrial-commercial zone to low-density residential and commercial districts in the urban perimeters and exurban areas. The high-density zone is extended along the Mill Creek valley with the automobile as the primary transportation means. The Ohio-Kentucky-Indiana Regional Council of Governments (OKI) collected the 2009 traffic data and provided traffic counts and composition of 20 traffic stations for this research.

Analysis of the year-2009 traffic data indicates strong diurnal and spatial variations of daily traffic counts and traffic composition at interstate freeways and arterials (I-71, I-75, I-74, and I-275), collectors (SR-126, SR-129) and local roads. The traffic is generalized into the five time periods of different traffic compositions in Table 2-4. Similar traffic diurnal variability

Table 2-4 Four daily periods of traffic compositions on the highway in Cincinnati, OH*

Period	Time	Traffic Composition
Night period	11 pm – 6 am	Diesel truck dominant
Morning rushing hours	6 am – 8 am	Gasoline car dominant
Daytime period	8 am – 3 pm	Mixture
Afternoon rushing hours	3 pm – 5 pm	Gasoline car dominant
Evening period	5 pm – 11 pm	Increasing diesel truck

Note: * - from Liang (2014).

and spatial distributions were reproduced by Yao et al. (2014) in a detailed area-wide trip generation and traffic volume modeling. For the analysis, hourly traffic profiles during weekdays were constructed for each of the stations.

Figure 2-23 shows the year-2009 averaged traffic volume for passenger cars in automobile class C1-C3, diesel trucks including single-unit trucks (C4-C7) and multi-unit trucks (C8-C13) on the highways and local roads. Average weekly traffic compositions for selected major monitoring stations are listed in Table 2-5. The highest traffic volume and large variations occurred along I-71 and I-75. The average and standard deviation of weekday total traffic volumes were 69485 ± 26590 vehicles/day (N=13 stations), 34770 ± 14180 vehicles /day (N=3 stations), and 43452 ± 22661 vehicles /day (N=3 stations), for the interstate freeways, collectors, and local roads, respectively. The level of service is consistent with the field traffic measurements Liang et al. (2013) reported for October 2010 during the I-75 black carbon dispersion studies.

In the Cincinnati area, most multi-unit truck traffic is concentrated along the interstate highways. Traffic volume was 8159 ± 4339 vehicles/day or approximately 10 times more than in the collector and local roads. Truck volume above 13300 vehicles /day was measured at north I-75 serving the industries and in I-75/I-71 after merger leaving Ohio into northern Kentucky of mixed land use in perimeter and exurban. Representative land use examples are shown in Figure 2-21.

4.1.3. Urban form and air quality

The transportation system described above, and current centralized water services facilitate the formation of the present monocentric urban form in Cincinnati. The environmental impacts of this urban planning are shown by ambient air quality variations through the metropolitan region. From Liang (2014), the spatial correlation between air quality and the urban form is evident:

- by the analysis of the decade-long measurements of PM_{2.5} for 13 U.S. EPA National Ambient Air Quality Standards (NAAQS) monitoring stations, and
- by quantitative modeling of black carbon dispersion experiment for 10 days (October 6 to October 15, 2010) at the roadside of northern highway I-75.

The locations of the 10-day experimental study and the 15 NAAQS stations over different land use types are shown in Figure 2-20. Station 17-061-0040 is in the high-density urbanized zone at the center of the Cincinnati metropolitan area. It is used as the reference station for analysis of spatial relationships among UHI effects, ambient air temperature and air quality variations. The statistics of 10.5 years of ambient temperature and PM_{2.5} measurements at the reference station 17-061-0040 is given in Table 2-6. The yearly temperature and PM_{2.5} means have a range of standard deviation. Frequency distribution of PM_{2.5} concentration measurements are asymmetric, with a bias toward small concentrations (Kurtosis =2.21 and Skewness>1; see Table 2-6). In general, yearly minimum and maximum occurred in the winter and summer season, respectively.

Despite the large seasonal variations, the daily temperatures and PM_{2.5} concentrations are highly correlated among the 15 NAAQS stations. The correlations using Eq.2.1 were obtained for four temperature parameters (daily maximum, daily minimum, daily average, and diurnal

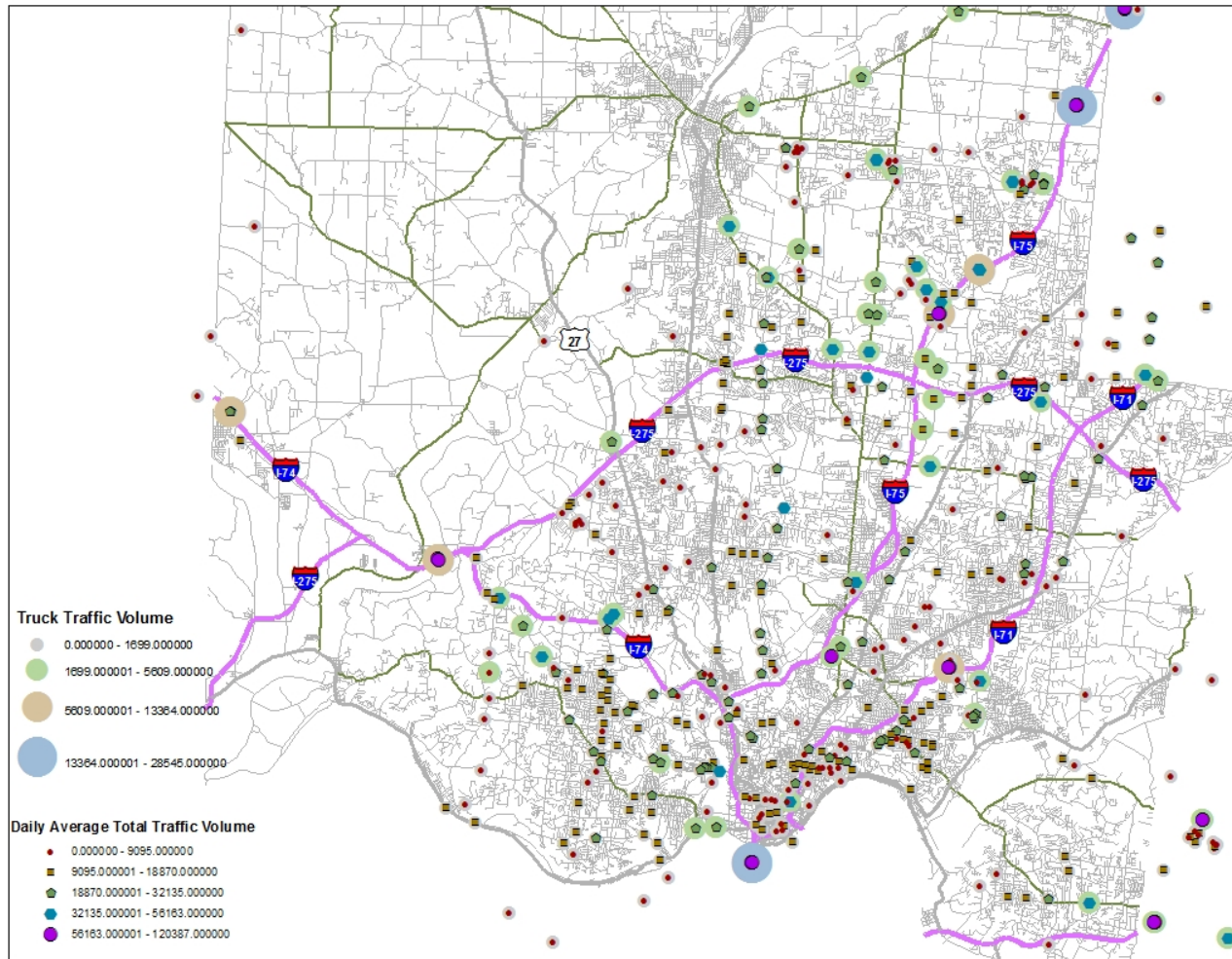


Figure 2-23

Truck and passenger car traffic volume distribution in the Cincinnati metropolitan region. Heavy truck traffic concentrated in I-75, I-74 and the confluence of I-75/I-71 leading to Kentucky in the south. Relatively, I-71 has greater car traffic. From Liang (2014).

Table 2-5 Locations and traffic flow in 2009 for selected locations in the Cincinnati road network (From Liang, 2014).

OKI Station	Traffic Roads		Average Weekday Traffic**				Location
	Target	Cross-by	Auto	SU Truck	MU Truck	Total	
HAM3343	I-71 (E)	Kennedy Ave	96907	6371	6791	110039	1
WAR0422	I-71 (E)	SR-48	25164	3376	9989	38528	2
WAR0509	I-71 (E)	SR-123	32617	3833	9048	45498	3
WAR0471	I-75 (N)	Central Ave	62956	11445	13943	88344	4
WAR0548	I-75 (N)	SR-63	54975	7265	11432	73671	5
BUT0475	I-75 (S)	Kyles Station Rd	61260	5878	11664	78802	6
BUT0670	I-75 (S)	Union Center Blvd	53124	4347	6245	63715	7
BUT0701	I-75(S)	Cincinnati-Dayton Rd	47391	2996	5776	56164	8
KEN0458	I-71/75(S)	Fifth St	91842	12444	16101	120386	9
HAM2246	I-74-275(W)	I-74	62234	4797	5303	72334	10
CLE0180	I-275(N)	SR-32	66355	2885	1964	71204	11
CLE0211	I-275(S)	SR-125	54706	2412	1868	58987	12
HAM3383	I-74(W)	New Haven Rd	18106	1576	5948	25631	13
HAM0970	SR-126(W)	I-75	51627	2386	580	54593	14
BUT0437	SR-129(W)	SR-747	32603	1901	876	35380	15
BUT0842	SR-129(W)	SR-4 Bypass	22117	1204	469	23790	16
BUT0479	SR-129(W)	I-75	23310	1237	771	25318	17
HAM2022	Norwood Lateral (E)	I-75	63692	4099	1510	69301	18
HAM3818	Lebanon Rd (US-42) (S)	Cottingham Dr	25565	1110	331	27006	19
HAM3408	Winton Rd (S)	Fleming Rd	32653	1115	279	34048	20

Note: * - Data from OKI.

** - Vehicle types following ODOT: Auto - 4-axial passenger cars; SU Truck - Single unit truck; and MU truck - multi-unit truck.

Table 2-6 Statistics of daily temperature measurements at NQAAS Station 17-061-00040

Statistics	T _{AVG} (°C)	T _{MIN} (°C)	T _{MAX} (°C)	ΔT (°C)	PM _{2.5} (mg/m ³)
Mean	14.22	9.20	20.09	10.88	13.89
Standard Deviation	10.17	9.66	11.14	3.83	7.27
Kurtosis	-0.91	-0.84	-0.90	-0.51	2.21
Skewness	-0.35	-0.32	-0.35	-0.03	1.25
Minimum	-15.2	-20.4	-10.2	1.1	1.2
Maximum	34.3	27.4	42.1	22.8	52.1
Count	1661	1458	1458	1457	1717

Note: Raw data from the EPA NAAQS monitoring network.

temperature range) and PM_{2.5} concentrations. Compared to the reference station 17-061-0040 (C_{ref}), temperature and PM_{2.5} measurement data of other stations (C_i) are correlated by:

$$C_i = \alpha_i C_{ref} + \epsilon_i \quad (2.1)$$

The obtained slope (α_i) and intercept (ϵ_i) are statistically significant (see Liang, 2014) with a large correlation coefficient ($R^2 \sim 0.99$). Departure from 1:1 relationship indicates atmospheric differences among stations rather than measurement errors.

4.1.4. Thermal inversion and mixing height

Liang and Keener (2015) analyzed atmospheric sounding data from NOAA/NESDIS⁴, and constructed atmospheric temperature profiles using the method by Ma et al. (1999). Two satellites, GOES-8 and GOES-9, equipped with filter wheel radiometers, collected radiance measurements from the on-board thermal infrared channels, while allowing retrieval of the atmospheric temperature and moisture profiles. The data were retrieved at a 10-km spatial grid and in hourly intervals for sounding data locations S-1 to S-4 in Figure 2-20.

Figure 2-24 shows a typical diurnal atmospheric profile in the Cincinnati metropolitan region. The tropopause layer separates the turbulent troposphere from the temperature-inverted laminar stratosphere above. A nocturnal temperature inversion is evident in the lapse rate⁵ in the near-ground urban boundary layer. At this location (39°14'43", -84°26'46"), thermal inversion reached its maximum in the early morning, followed by inversion destruction and then the recovery to normal lapse rate as a slightly stable boundary layer (SBL) in the early afternoon. The daytime lapse rate returned to a level of neutral stability close to the dry adiabatic lapse rate (DALR) at 9.8 °C/km (Figure 2-24). The nocturnal temperature inversion was then re-established by the late evening. This diurnal variation is evident for all four radio-sounding locations S-1 to S-4. From the temperature profiles, the lapse rate (L_h) and mixing height (Z_{inv}) were determined for each day.

⁴ <http://www.star.nesdis.noaa.gov/smcd/opdb/goes/soundings/skewt23L/html/skewhome.html>

⁵ Lapse rate is defined as the gradient of temperature change per unit distance from ground surface.

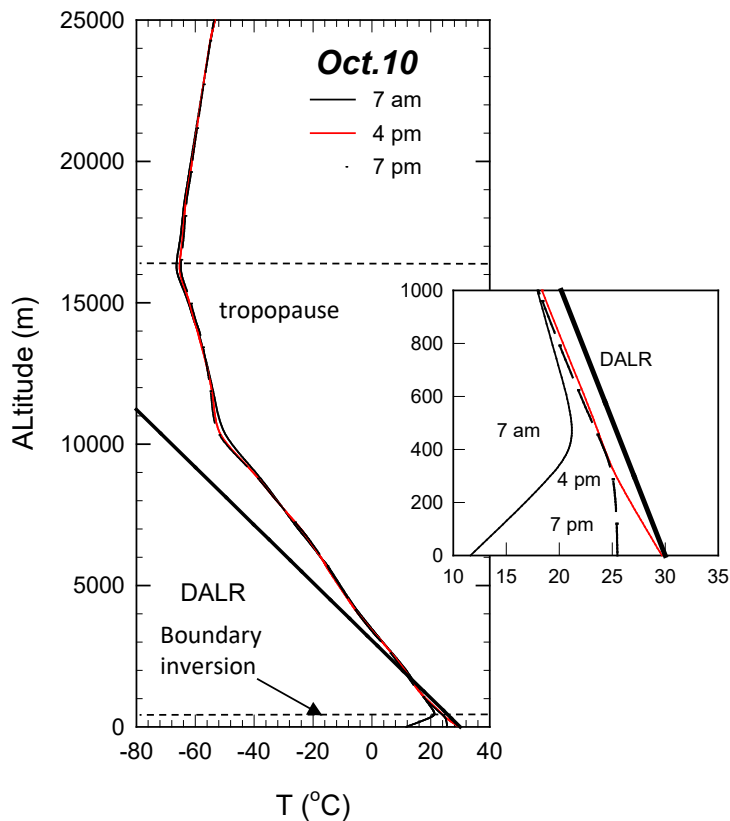


Figure 2-24 Representative temperature profiles showing the boundary inversion and capping inversion, Temperature data were obtained from NOAA for the northern Cincinnati site. Altitude 0 is set at surface elevation. DALR is the atmospheric dry adiabatic lapse rate. From Liang and Keener (2015).

The determined L_h and Z_{inv} values in a 10-day period of October 2010 are shown in Figure 2-25. Clearly, a sequential occurrence of nocturnal thermal inversion with the strongest phase in the days of October 7-12. Changes in temperature gradients in altitude became gradual in the tropopause. Returning of lapse rate in the daytime to a level of neutral stability close to neutral DALR of $9.8\text{ }^\circ\text{C}/\text{km}$ is found across the observation period. The near-surface boundary layer above the urban canopy marks the extent to which thermal and mechanical mixing occurs. A maximum inversion strength with a lapse rate of $-29.2\text{ }^\circ\text{C}/\text{km}$ occurred at 4 am on October 9 for the near-surface boundary layer thickness of 421-607 m.

4.1.5. Urban and exurban differences

Thermal inversion development in the region had similar overall diurnal L_h and Z_{inv} variability. However, a small difference exists between the Lunken airport station and others (Figure 2-25). The measured inverse lapse rates are lower at Lunken airport compared to the other locations inside of the high-density urbanized area. The smaller profile slope reflects weaker inversion strength in the peak inversion phase. Liang (2014) further showed the difference was persistent based on linear correlations of L_h values at different locations.

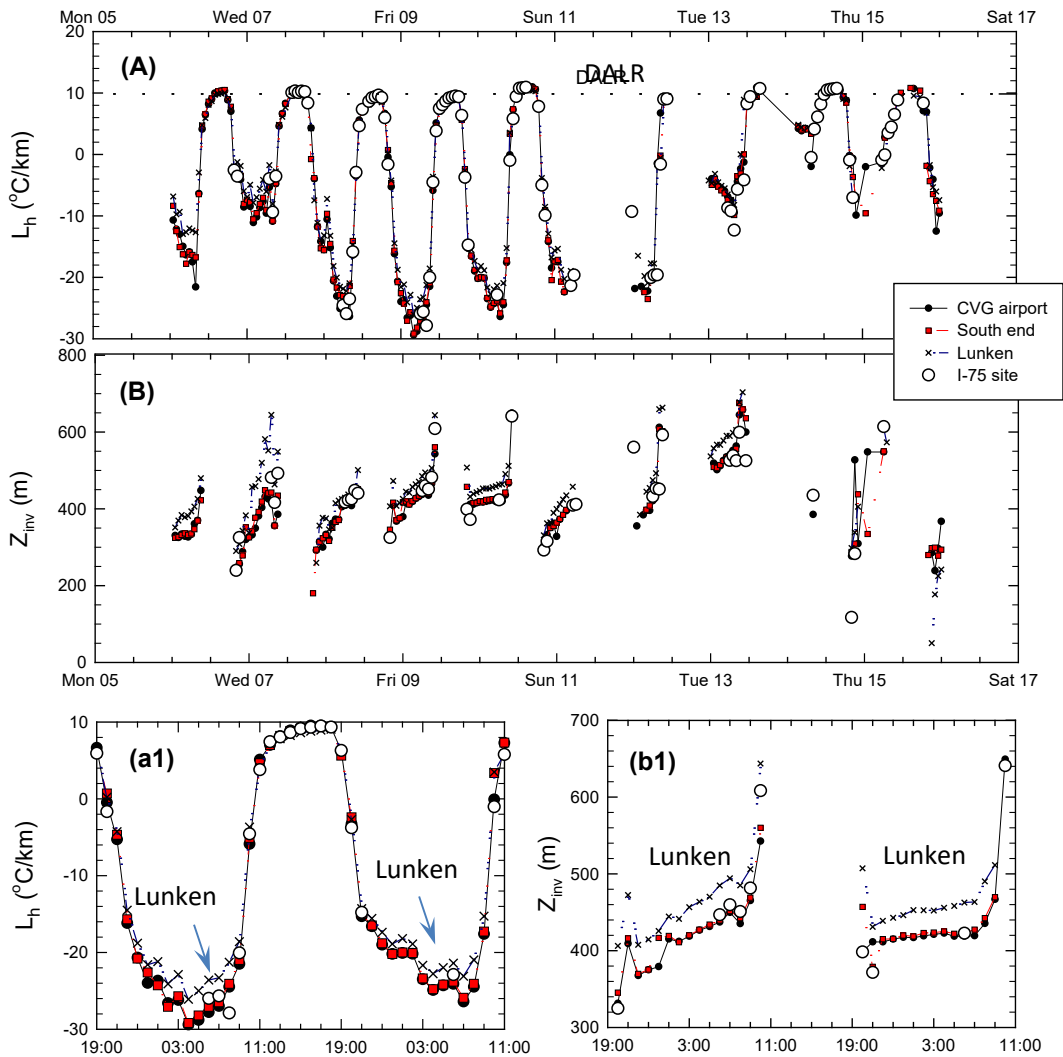


Figure 2-25 Temporal L_R and H_{inv} variations showing diurnal thermal inversion in the urban boundary layer in October 2011. The inserts (a1) and (b1) show the observed difference of hourly variation among the sounding sites in the period of October 9-10. From Liang (2014).

4.1.6. Urban form effects on urban heat island and air quality

4.1.6.1 Long-term changes in the urban center

The unique structure of urban boundary layer is considered responsible for causing UHI formation and related air quality deterioration (Rotach et al., 2005; Liang et al., 2013; Trompeter et al., 2013; Wang et al., 2012). This relationship is found from analysis of the long-term ambient temperature and $PM_{2.5}$ concentration data from 1999 to 2013 when all stations of the Cincinnati metropolitan area are compared to the reference station 17-061-0040 in the urban core.

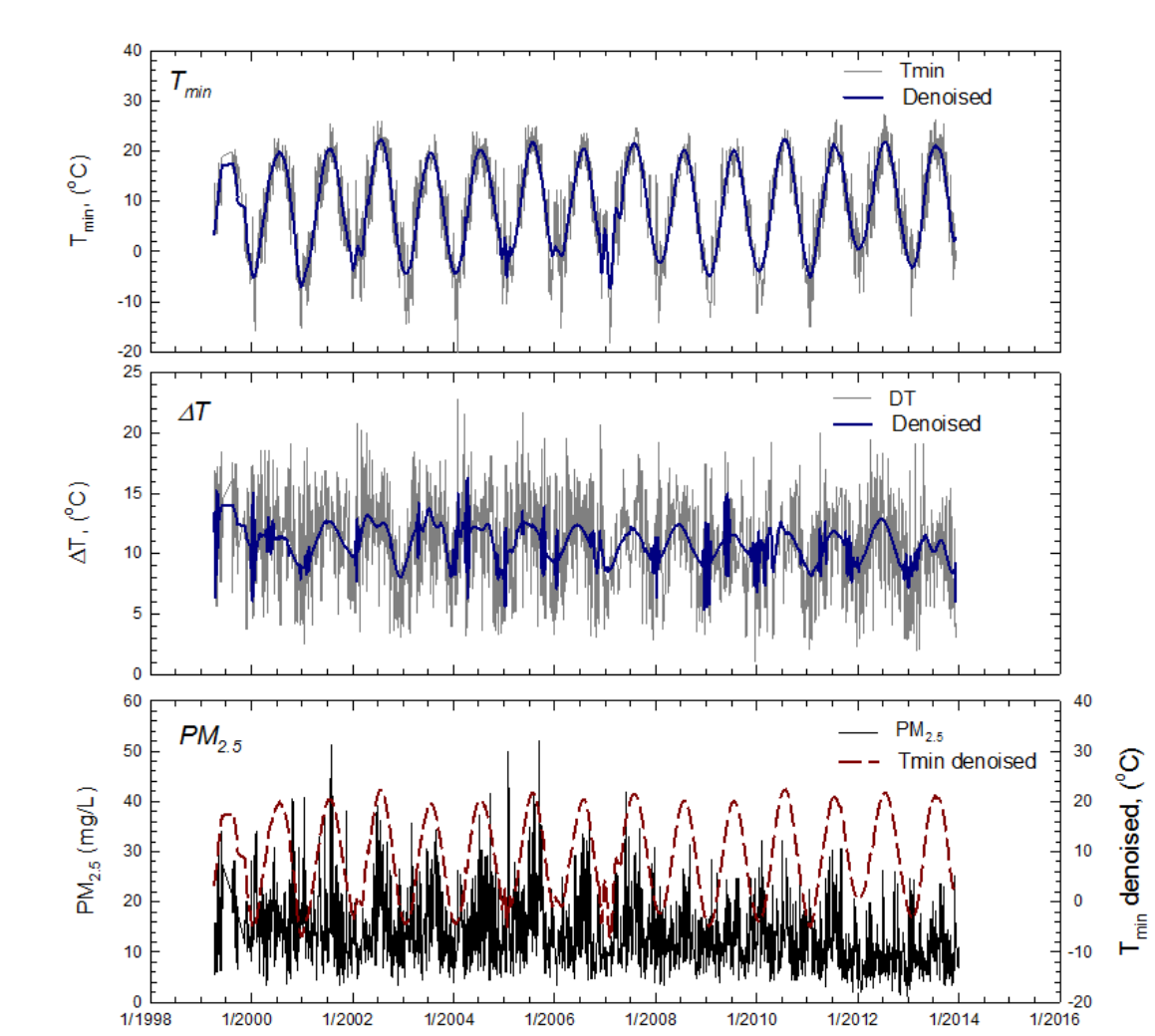


Figure 2-26 T_{min} , ΔT , and $PM_{2.5}$ variations with time at NAAQS monitoring station 061-0040. After wavelet denoise, the seasonal variations are shown in heavy lines. From Liang and Keener (2015).

The 1457 daily measurements at the reference station show no statistically significant change over time for daily T_{max} and T_{avg} . However, long-term changes in T_{min} and ΔT can be convincingly identified beyond the noise of seasonal variations using the so-called continued wavelet transformation techniques. At a data noise threshold $db=0.80$, wavelet-denoising (Torreice and Compo, 1998; Farge, 1992) of the T_{min} and ΔT data captured nearly 80% of the variation in Figure 2-26. Wavelet-transformed T_{min} and ΔT maxima occurred in May-June of each year, and the minima in the winter period. The seasonal cyclic variation is evident.

These temperature highs and lows after denoise show an increase of ~ 1.6 and ~ 2.1 °C over 10 years, respectively, by linear regression (Figure 2-27). These long-term changes correspond to night-time maximum and minimum temperature, respectively, in the summer and winter seasons. Because of the increase in night-time temperature, diurnal temperature range ΔT

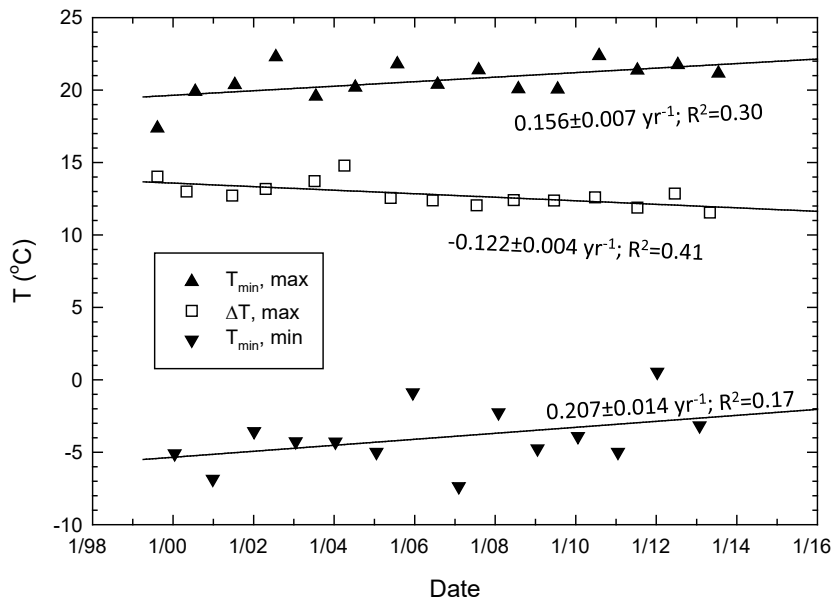


Figure 2-27 Temporal change of ambient temperature T_{min} and ΔT at station 061-0040 in the Cincinnati urban core. The regression slopes are statistically significant with $p < 0.0001$. Adopted from Liang (2014).

decreased by 1.2 °C over a decade (Figure 2-27). These long-term changes are consistent with the other publications on urban microclimate (Wang et al., 2012; Braganza et al., 2004).

4.1.6.2 Urban-wide co-variations in temperature and $PM_{2.5}$

- *Ambient temperature*

The UHI effect across the region is shown by ambient temperature measurements. Ambient temperatures measurements each year are correlated among stations, and the slope of the correlation quantitatively is determined according to Eq.2.1. An example is shown in Figure 2-28 between the reference station 17-061-0040 at the urban core and other stations. The average square coefficient of correlation (R^2) for the 91 to 116 station-year correlations is >0.993 (0.941-0.999). Because the data covers a 10.4-year long period and for all seasons, the strong linear correlation indicates an effective and time-persistent urban-scale heat flux and air circulation above the canopy layer.

Based on the correlation, temperature difference T' between a location and the reference station in the urban core is calculated for the decade-long measurements. The results are presented in Table 2-7. Apparently, the calculated T' values are spatially correlated with the delineated urban land use. Quantifiable and statistically significant UHI effects coincide with high-density urbanized zones. In cross-section A-A' (see location in Figure 2-20), ambient temperatures above the canopy layer are consistently higher inside the high-density zone than in the surrounding suburb and exurban areas (Figure 2-29). For three stations outside of the zone, annual mean T'_{avg} and the largest T'_{avg} in summer are lower by 0.89 ± 0.14 °C and 1.55 ± 0.30 °C,

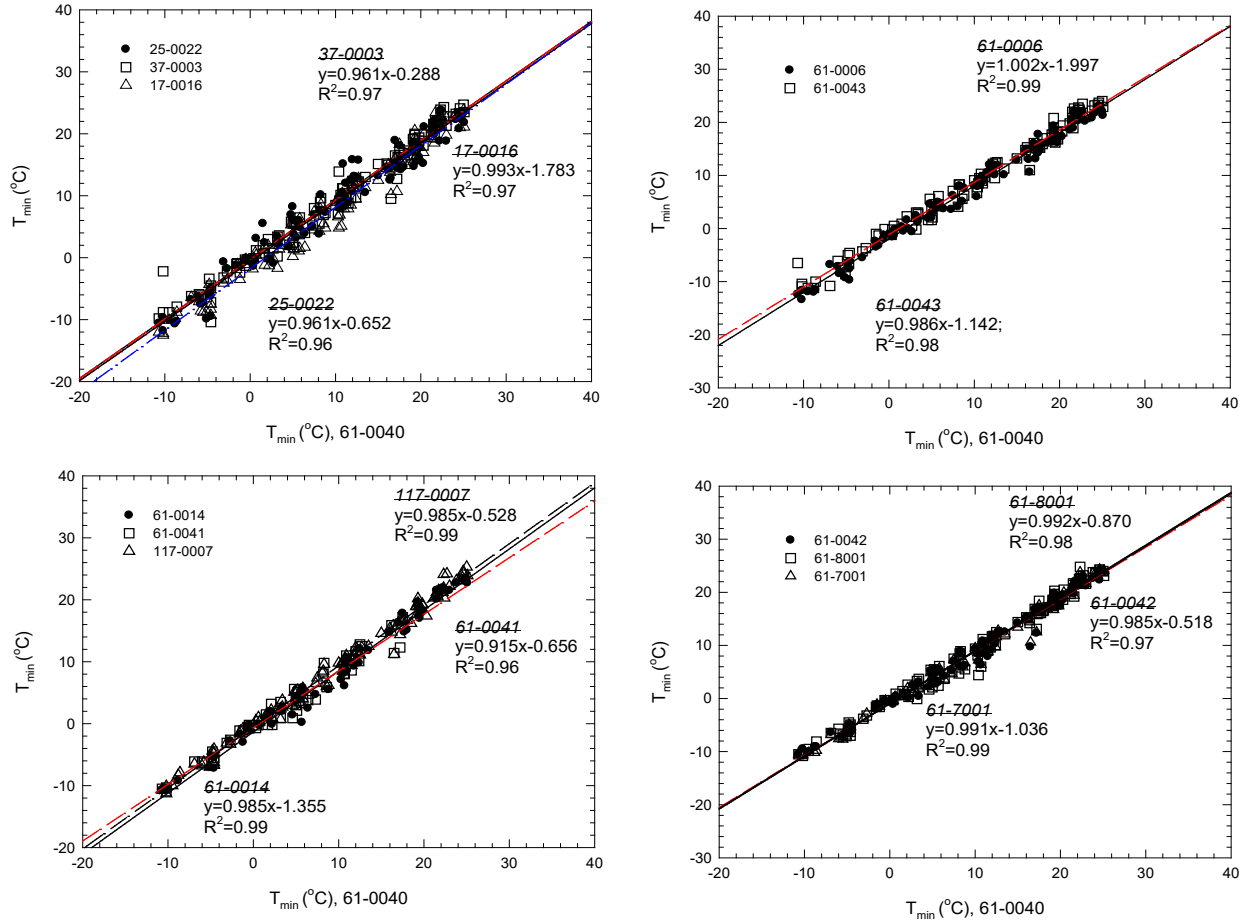


Figure 2-28 T_{min} at 17-61-0040 station is linearly correlated with those of other stations in the year 2005 measurements. Modified from Liang and Keener (2015).

respectively. The largest $\Delta T'$ also occurred in summer when highest night-time $T_{min}=27.4$ °C and highest day-time $T_{max}=42.1$ °C were measured in the 17-61-0040 station. The average $\Delta T'_{min}$ and $\Delta T'_{max}$ were -1.69 °C and -1.71 °C.

In contrast, temperatures are relatively uniform inside of the high-density zone. The mean T'_{avg} is $-0.09(\pm 0.27)$ °C. The annual mean T'_{avg} increases slightly from its southern tip at station 037-3002 toward station 061-0040 in the urban core.

- $PM_{2.5}$ variability

Like ambient temperature, the observed $PM_{2.5}$ concentrations are linearly correlated between the reference station 39-061-0040 and all other stations (Liang, 2014). The correlation is persistent for all years of measurements at the sampling height above the canopy layer. This correlation covers all $PM_{2.5}$ concentration range [1.2 - 52.1 mg/m^3 ($\bar{m}=13.89$, $N=1717$)]. See Table 2-6.

Table 2-7 Temperature differences between the reference station and other stations abstracted from the >10-year daily temperature measurements (From Liang, 2014).

Station	Annual Mean			Winter			Summer		
	T _{AVG} (°C) 14.22	T _{min} (°C) 9.30	T _{max} (°C) 20.09	T _{AVG} (°C) -15.20	T _{min} (°C) -20.40	T _{max} (°C) -10.20	T _{AVG} (°C) 34.3	T _{min} (°C) 27.4	T _{max} (°C) 42.1
39-061-0006	-0.79 ± 0.45	-1.82 ± 0.20	-1.52 ± 0.19	-1.17 ± 0.93	-2.50 ± 0.65	-1.19 ± 0.87	-0.53 ± 0.82	-1.40 ± 0.72	-1.76 ± 0.96
39-061-0010*	-1.05 ± 0.22	NA	NA	-0.67 ± 0.74	NA	NA	-1.31 ± 0.78	NA	NA
21-037-3002#	-0.58 ± 0.48	-1.18 ± 0.82	-0.34 ± 0.54	0.06 ± 0.90	-1.15 ± 1.06	0.64 ± 1.11	-1.03 ± 0.91	-1.19 ± 1.07	-1.05 ± 1.09
21-117-0007	-0.25 ± 0.38	-0.33 ± 0.42	-0.58 ± 0.54	0.08 ± 0.47	-0.33 ± 0.63	0.48 ± 0.75	-0.48 ± 0.74	-0.32 ± 0.91	-1.34 ± 0.99
39-025-0022*	-0.82 ± 0.65	-1.40 ± 0.51	-0.37 ± 0.36	0.11 ± 0.85	-0.50 ± 1.05	0.80 ± 1.65	-1.46 ± 0.86	-1.95 ± 0.19	-1.22 ± 0.57
39-017-0016	0.39 ± 0.54	0.91 ± 0.64	-0.61 ± 0.87	-0.16 ± 0.88	0.22 ± 1.27	-0.90 ± 0.86	0.77 ± 0.60	1.33 ± 0.81	-0.40 ± 1.02
39-061-0014	-0.28 ± 0.58	-0.69 ± 0.65	0.02 ± 0.69	0.17 ± 0.87	0.16 ± 1.34	1.13 ± 2.19	-0.58 ± 0.77	-1.21 ± 0.74	-0.78 ± 0.94
39-061-8001	-0.05 ± 0.31	-0.31 ± 0.43	-0.18 ± 0.51	0.18 ± 0.61	-0.12 ± 0.53	0.51 ± 0.46	-0.21 ± 0.64	-0.43 ± 0.69	-0.68 ± 0.75
39-061-7001	-0.22 ± 0.52	-0.39 ± 0.41	-0.36 ± 0.70	0.29 ± 0.71	0.25 ± 0.86	1.54 ± 3.29	-0.57 ± 0.77	-0.78 ± 0.49	-1.73 ± 1.55
39-061-0041#	-0.48 ± 0.38	-1.04 ± 0.41	-0.38 ± 0.41	0.38 ± 0.46	-0.24 ± 0.84	0.41 ± 0.49	-1.07 ± 0.80	-1.52 ± 1.12	-0.95 ± 0.63
39-061-0043	-0.36 ± 0.42	-0.60 ± 0.46	-0.14 ± 0.58	0.05 ± 0.69	-0.32 ± 0.91	0.26 ± 0.62	-0.63 ± 0.65	-0.77 ± 0.65	-0.43 ± 0.82
21-037-0003*	-0.79 ± 0.93	-0.86 ± 1.08	-0.77 ± 0.60	0.81 ± 0.71	0.08 ± 0.82	1.20 ± 0.53	-1.88 ± 1.18	-1.43 ± 1.36	-2.20 ± 0.92
39-061-0042	0.11 ± 0.57	-0.03 ± 0.71	-0.11 ± 0.79	0.84 ± 0.88	0.95 ± 1.49	0.98 ± 0.76	-0.39 ± 0.79	-0.63 ± 0.70	-0.90 ± 0.94

Note: * Stations are outside of the high-density urban area.

Stations are outside but near the high-density urban area.

NA - Data not available.

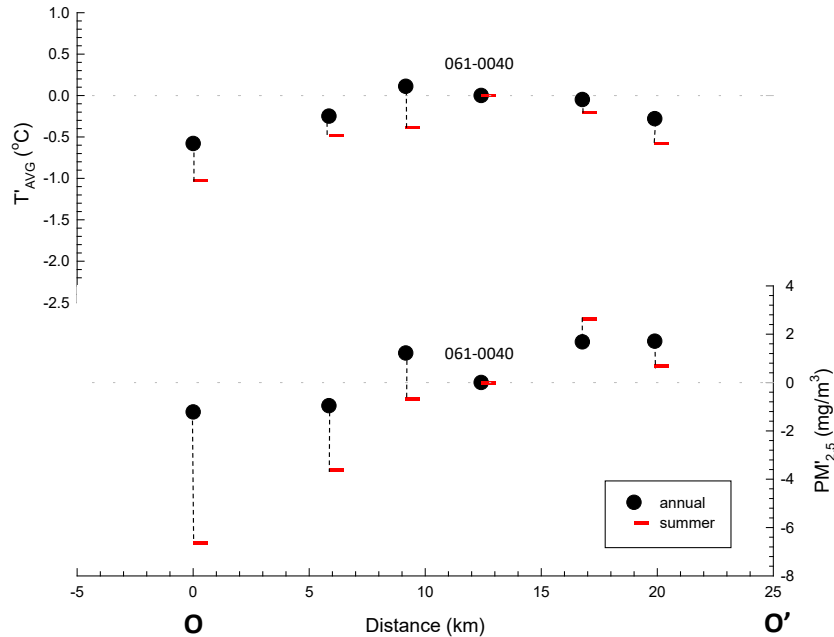


Figure 2-29 Spatial variations of temperature difference for mean and maximum T_{avg} and $PM_{2.5}$ in cross section O-O'. The profile starting point a is station 037-3002 at southern tip of the high-density zone. See Figure 2-20 for the cross-section locations. From Liang (2014).

The high degree of linear correlation among the stations is significant for the long duration of monitoring. The correlation coefficient (R^2) for the 130 station-year correlations ranges 0.53-0.99 with an average of 0.92. Nearly 92% of $PM_{2.5}$ variability can be explained by the urban-wide correlations. Similar conclusions on area-wide $PM_{2.5}$ variations were made by Martuzevicius et al. (2005) using hourly monitoring data, instead of daily, of the 13 NAAQS network stations in the Cincinnati area

In summary, the intra-station correlations both in temperature and $PM_{2.5}$ strongly suggest atmospheric mixing and mass communication at the station's sampling height. The UHI effect is evident at the urban core along with the air quality variations.

4.1.6.3. Thermal inversion and wind conditions

The frequent and high-strength thermal inversion in the Cincinnati metropolitan area is linked to the weakened wind field and deteriorating air qualities. Liang et al. (2013) reported onsite measurements of black carbon, $PM_{2.5}$, and other air pollutants in a field study at the I-75 highway. The study was in the high-density urbanized zone of northern Cincinnati (see Figure 2-20 for location). Their results clearly showed the weak to stagnant wind conditions in early morning hours, associated high black carbon concentrations near roads, and a high ratio of organic carbon (OC) over elemental carbon (EC).

The co-variation between field-observed wind speed and the determined temperature lapse rate (L_h) is shown in Figure 2-30. Here L_h values quantitatively measure the inversion strength; the SBL, weak SBL, and very weak SBL are defined as $L_h = 5$ to -15 , 5 - 10 °C/km, and

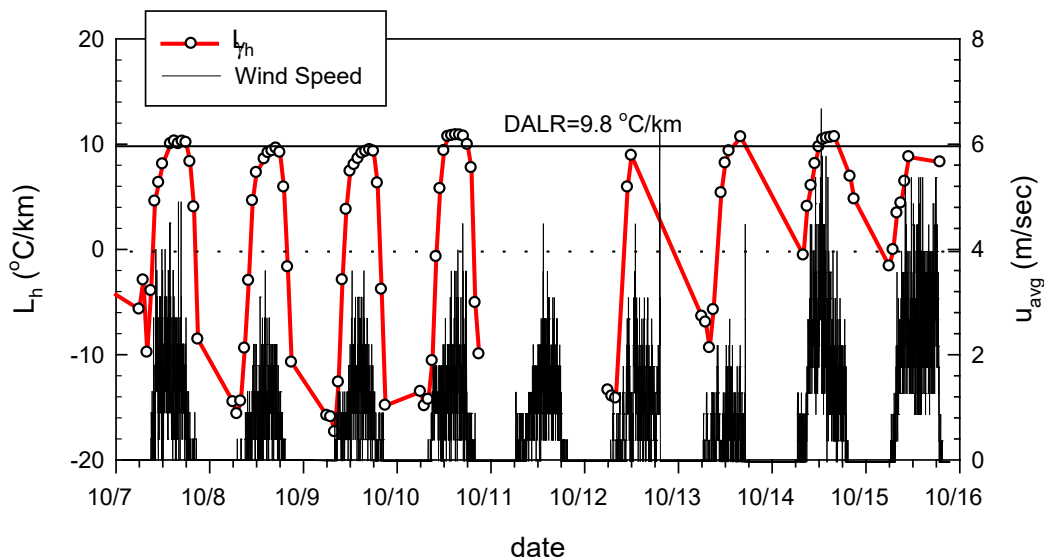


Figure 2-30 Co-variation of minutely average wind speed at the I-75 site with the lapse rate in the boundary layer during the roadside black carbon dispersion experiments. U_{avg} is the hourly average wind speed. From Liang (2014).

$<15\text{ }^{\circ}\text{C}/\text{km}$, respectively. Clearly, the weak SBL on October 14-15 corresponds to the highest wind speed at 1.47-2.6 m/s measured in the field study of Liang et al. (2013). The high winds and convection led to low OC and EC concentrations, and a low OC/EC ratio around 1.272.

The very weak SBL with $L_h < -15\text{ }^{\circ}\text{C}/\text{km}$ was pronounced at the beginning of the period, notably in the early morning of October 7-13 before 8:28-9:10 am (Figure 2-30). The lapse rate L_h was $< -10\text{ }^{\circ}\text{C}/\text{km}$, and the inversion reached a maximum strength at $-29.2\text{ }^{\circ}\text{C}/\text{km}$ at 4 am on October 9. Strong thermal inversion in this phase was non-stationary and induced downward thermal flux due to radiative urban cooling (Martilli, 2002; Uno et al., 1988, 1989; Iziomon et al., 2003). As a result, a near-surface non-Gaussian transport mechanism such as meandering (Cooper et al., 2006; Guzman-Torres et al., 2009) could have happened for which the similarity theory cannot be applied (Uno et al., 1989). This relationship among black carbon (and other pollutants) concentrations, weak wind speed and the thermal inversion has been observed in numerous field studies worldwide (Trompeter et al., 2013; Uno et al., 1988; Guzman-Torres et al., 2009; Kumar et al., 2012).

4.1.6.4. UHI formation and spatial variations

The weak wind condition and weak atmospheric circulation in the urban area occurred under a condition of high nighttime temperature or larger degrees of UHI effects. Understanding of this urban-scale phenomenon helps develop urban adaptation measures.

The hilly topography in Cincinnati metropolitan area has a small relief $< \sim 50\text{m}$ except for along the Ohio River banks and Mill Creek valley (see Figure 2-20). Such a general geographic feature may permit the occurrence of thermal inversion that Clarke (1969) proposed for the Mill Creek valley west of the Cincinnati downtown. Similar topography-induced inversion was reported in later studies, notably by Fernando (2010) suggesting that the thermal and gravity-

induced upslope and downslope airflow is needed to produce nocturnal inversion in complex terrain. For areas with a gentler topographic slope like the Cincinnati metropolitan area, other possible mechanisms are likely. One possible mechanism may involve UHI-induced thermal flux and horizontal air movement. Upward sensible heat flux and air aloof from the warmer urban interior can induce movement of colder air masses from surrounding rural areas, leading to evening urban breeze, colder air at the ground surface, and hence the concurrence of UHI and thermal inversion (Rotach et al., 2005; Rendón et al., 2014; Hidalgo et al., 2010). Temperature condition for this UHI formation was observed in the higher night-time temperature T'_{min} , in the high-density urban zone (see Table 2-7).

The UHI effect and temperature variations are not uniform across the Cincinnati metropolitan area. They depend on land use and land covers, and ultimately, the urban form. Similar conclusions were made by several recent studies using detailed thermal mapping of the UHI effects (e.g., Liu et al., 2012; Buyadi et al., 2013). As shown in this case study, the high-density urbanized zone is associated with an increase of ambient daily temperature by 0.89-1.55 °C. Night-time temperature increase is larger at ~1.7 °C. The increase closely follows the high-density zone boundary in cross-section A-A'. The N-S trending high-density zone of varying width is found to have a varying degree of UHI effects (Figure 2-29 and Table 2-7). The temperature increase is the largest in the Cincinnati downtown area, around stations 37-061-0040 and 37-061-0042. The UHI effect reduces in the north, where the high-density zone narrows, and nearly disappears in the southern tip at station 21-037-3002.

The variation trend and its association with land use types are further corroborated by a negligible small temperature increase found outside of the high-density zone in residential areas. Three stations in the perimeters of Cincinnati metropolitan area show a smaller daily average T'_{avg} than in the high-density zone. Similarly, the station 37-061-0006 is located in a small and isolated high-density urban area along I-71 (Figure 2-20). Calculated T'_{avg} values are close to that of three exurban stations. Not coincidentally, these residential areas are characteristic of detached single houses with large trees, large yards, and acres of natural area in between (Figure 2-22). This type of suburban region with less UHI effect was common for over 38 U.S. urban centers that Imhoff et al. (2010) studied using LANDSAT satellite imagery data.

UHI effects measured in this study are much smaller than one derived using the empirical formulation of Oke (1976 and references therein). Based on the formula, the Cincinnati metropolitan area of ~2.1 million population would yield a 4.91 °C temperature increase. The majority of the Cincinnati area is typical of the medium to low-density suburban areas in the new classification Oke (2006) proposed for urban climate zone. The urban form, the use of green space, and the elongated narrow shape of the high-density zone may be contributing factors for the observed smaller UHI effect.

4.1.6.5. *Adaptation and potential effects*

Urban-scale UHI occurrence affects both air pollutant transport and water demand. The planning of the high-density urbanized area and green spaces affect UHI occurrence and atmospheric circulation in the boundary layer. The studies in the Cincinnati metropolitan area indicate the potential of adaptation co-benefits in the following two areas.

- *Air pollutant transport*

The Cincinnati case study shows that the urban form and its physical structure configurations can affect urban microclimate and, thus, the air pollutant transport. Figure 2-31 illustrates three typical types of canopy layer settings that can affect near-ground pollutant distribution. These include the open-field setting at the highway I-75 site (Liang et al., 2013), the street canyons among the low- and high-rise buildings of the urban interior, and lastly, residential areas with significant tree canopy effects. Among the three types, highway roads in open fields are most common in the Cincinnati metropolitan area. Both the UHI and PM_{2.5} levels are a function of the canopy, transportation infrastructure, vehicle numbers, and emission rates.

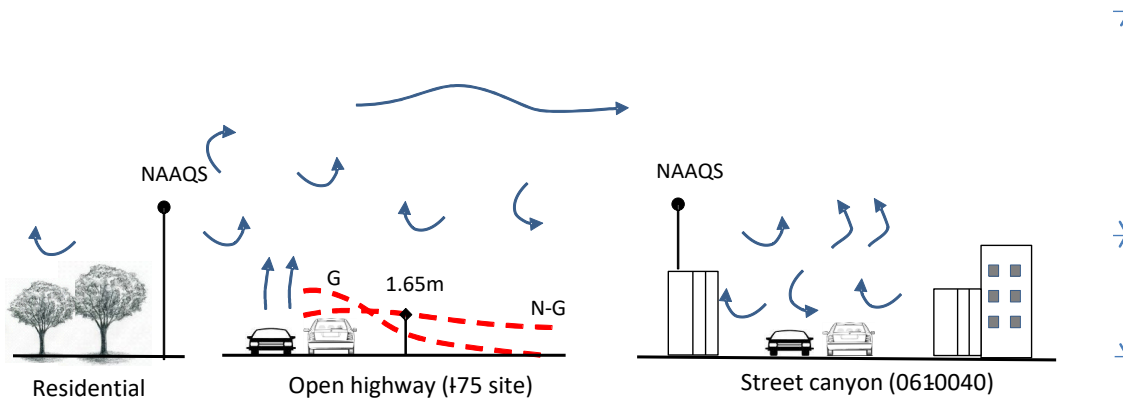


Figure 2-31 Schematic diagram showing major types of microclimate conditions in the surface roughness layer (SRL) equivalent to the urban canopy layer (UCL). The NAAQS stations above the UCL are affected by urban boundary layer (UBL) circulations. Other symbols: G – Gaussian dispersion, NG – Non-Gaussian dispersion. Modified from Liang and Keener (2015).

U.S. EPA has published guidelines on quantitative modeling and assessments for these urban settings (U.S. EPA, 2017b, 2004b). Numerous literature also elucidated adaptation actions that have the potential to mitigate the negative consequence in air pollution, for example, the use of tree barriers along traffic routes (e.g., Baldauf et al., 2008). Urban adaptation can likely be planned to affect and even modify the microclimate settings, including those in Figure 2-31, and their locations and spatial distribution.

- *The UHI and controlling factors*

The Cincinnati case study shows interrelationships among urban form, air quality, UHI formation, and population distributions. The high-density urbanized zone along the I-75 highway and the Mill Creek has many properties of UHI effects: night-time temperature increased by ~1.7 °C compared to exurban areas, a long-term night temperature increased by 2.0 °C per decade, and a higher PM_{2.5} concentration occurred above the urban canopy layer. The UHI formation and thermal inversions are attributed to high concentrations of air pollutants near ground levels. The UHI occurrence can increase water consumption, altering water demand variations in space and seasons. Although the exact impact is not quantified in the case study, it is generally understood that the higher daily temperature, smaller diurnal temperature ΔT , weak winds can produce changes in evapotranspiration rate for lawns and vegetation and lead to greater water

consumption per capita. This association has been described in the literature (e.g., Guhathakurta and Gober, 2007).

Major factors affecting the UHI effects include spatial continuity of high-density areas with altered ground surface (e.g., concrete pavements), size and locations of green space, forest and native land coverage, non-continuous multiple urban centers, even tree canopy barrier that helps modify the interactions between the urban canopy and the overlying urban boundary layer. On this basis, subsequent Section 4.2 outlines how adaptive urban planning could be made for future development scenarios.

4.2. Adaptive urban planning modeling and analysis in Cincinnati

The Cincinnati metropolitan area follows development trajectories of many very large U.S. metropolitan regions. Notable development actions include downtown revitalization, infill developments, the Ohio River bank development, and a series of land use policies to improve the urban efficiency including transportation and initiatives like the street car system. These development initiatives have changed the population and urban activity distribution. The change, when coordinated in planning, could lead to reduce the UHI occurrence and to positively affect water and transportation infrastructure planning and operation.

4.2.1 Three development scenarios

The scenario-based adaptive planning was conducted for the Cincinnati metropolitan area to assess development options. It was focused on land use changes and their downstream effects on transportation performance and benefits in carbon emissions. Parts of the research have been published in Wei et al. (2017, 2012) and Yao et al. (2014). Through this example, the step-by-step process is illustrated for using AUP&ET tools.

Figure 2-32 shows the distribution of base-year population, household, and employment in the metropolitan area in 2010. It is noted that the classic monocentric urban form is starting to evolve into multi-centers of employment, with the population and households scattered and distributed across the region. Transformation districts in Mason north of the city, Norwood, and Downtown are further reshaping the population distribution along the north-south trending I-71 and I-75 corridors along with changes in the employment distribution.

To explore the potential future developmental scenarios, three options were analyzed using AIR-SUSTAIN for Hamilton County, Ohio. The year 2010 was chosen as the base year, and the year 2030 was set as the target year. The three developmental scenarios were analyzed using the AIR-SUSTAIN tool on transportation first; the results can be used later for water infrastructure planning and adaptation. The three scenarios are:

- Scenario 1 (S1) is referred to the single-center development pattern. The single center is taken to occur in the Downtown and Uptown Cincinnati areas, as shown in Figure 2-33a.
- Scenario 2 (S2) is referred to the multiple-center development pattern. Two-center development is assumed in this scenario; one in the Downtown Cincinnati and the other in Mason area in the northern Hamilton County and southern Warren County. The development case is shown in Figure 2-33b.
- Scenario 3 (S3) adopts the same development pattern as S2. However, it differs by having two Rapid Bus Transit lines connecting these two centers, as shown in Figure 2-33c.

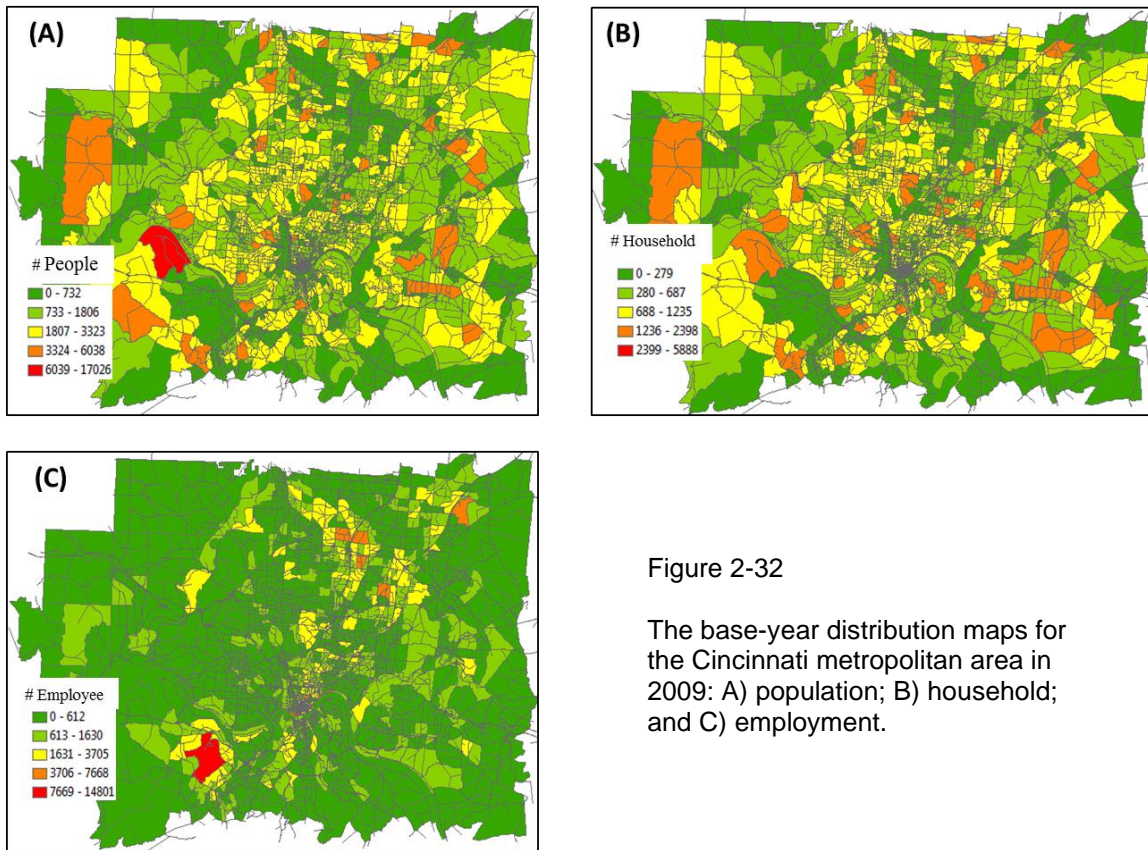


Figure 2-32

The base-year distribution maps for the Cincinnati metropolitan area in 2009: A) population; B) household; and C) employment.

Generally, this type of planning and engineering analysis requires stakeholder engagement, economic analysis, and engineering evaluation. The analysis presented here is simplified and intended to show how the AIR-SUSTAIN tool can be used in scenario-based adaptive planning.

4.2.2 Transportation and emission analysis using AIR-SUSTAIN tool

4.2.2.1 The modeling processes

All three competing scenarios assume the same 15% increase of population and employment to occur from the base year to the target year 2030. The population and employment increases are allocated and distributed around the activity center(s). The process for a scenario analysis was developed through 19 steps in the analysis from a new scenario setup (Figure 2-34), regional and project level traffic analysis, to emissions modeling using MOVES to obtain the final simulation results. Details of these simulation steps are contained in Appendix A. Important modeling steps are discussed below.

After setting up the adaptive planning project, a new scenario was created and saved with an AIR-SUSTAIN database in MySQL and ArcGIS. Figure 2-35 shows a graphic user interface for the project scenario setup. The subsequent Steps 2-4 specify the existing TAZ, road network,

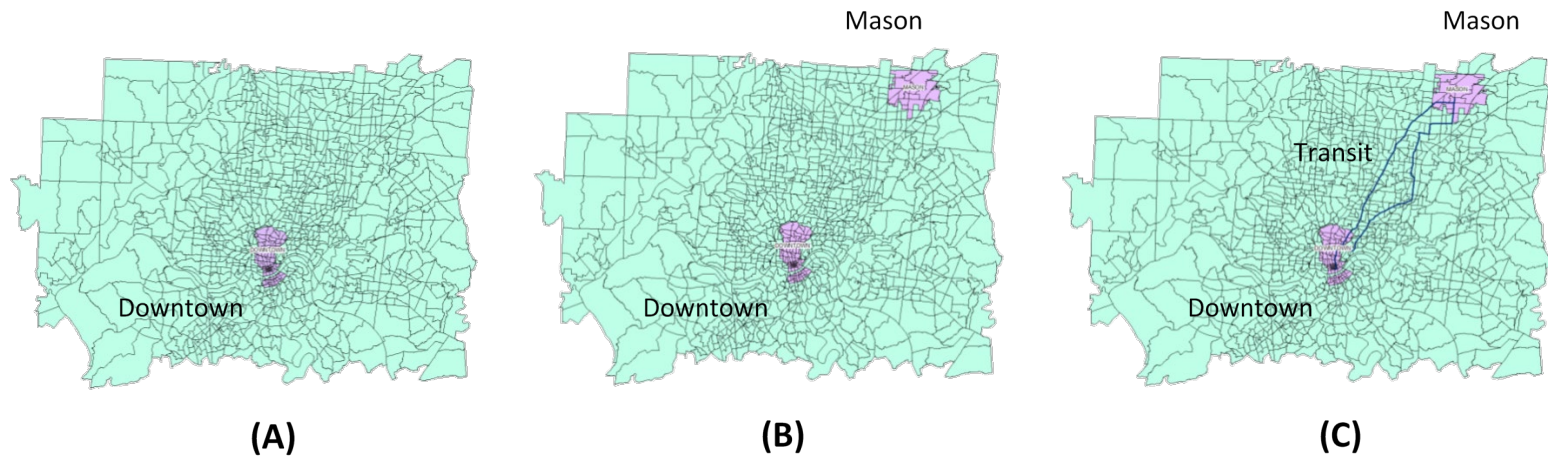


Figure 2-33 Three development scenarios for the Cincinnati metropolitan area in the target year 2030. A) monocentric development around the downtown; B) two-center configuration in downtown and Mason area; and C) two-center configuration with mass transit between the centers.

and boundaries of the activity centers in adaptive urban planning. Activity centers or incentive districts function as the transformation districts (see Figure 2-6) important to urban adaptation, and, by design, they introduce changes to the urban form and associated changes in population and urban activities. These projected changes define the technical basis for transportation and water infrastructure adaptations. In the modeling, the tool has the capability of specifying the changes in population and employment from the base year at the TAZ level. Population Change and Employment Change in the program were specified for regions inside and outside of the incentive boundaries separately (Figure 2-35).

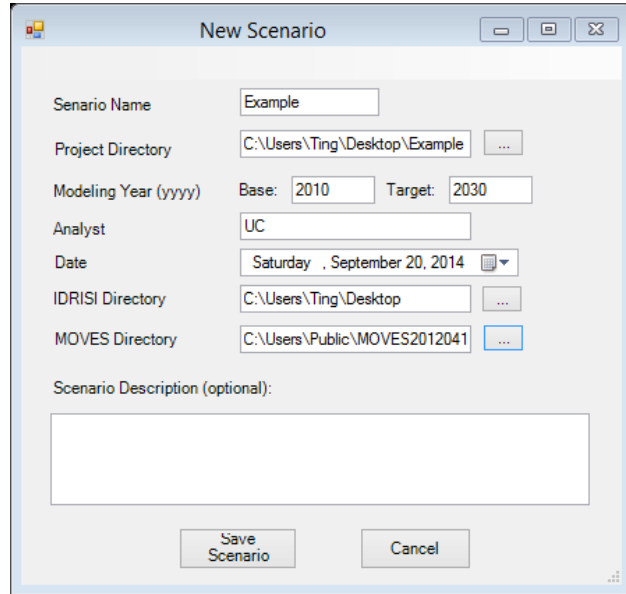
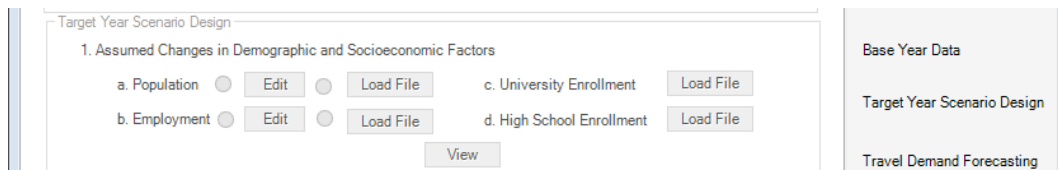
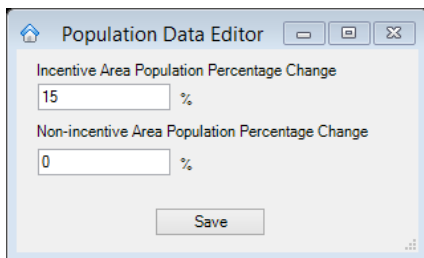


Figure 2-34 Setup of a new scenario in AIR-SUSTAIN

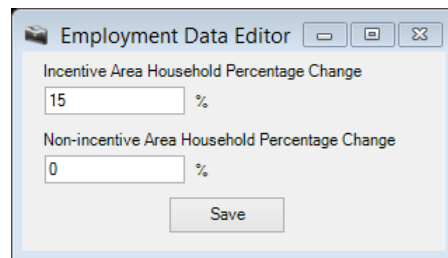
Land use for the base year and the target year is generated from modeling in another AUP&ET module. Urban land use projection is implemented using the CA-Markov method or in combination with the ICLUS available in AUP&ET (see Figure 2-14 and Section 1.3.1 for details). In the AIR-SUSTAIN, the land use projection maps are used as a GIS layer for trip generation modeling and forecasting. See Appendix A and Wei et al. (2017) for more details.



(A)



(B)



(C)

Figure 2-35 Program interface for A) importing the Base Year data; B) assigning population change; and C) assigning employment changes at TAZ levels.

One potential option for using the adaptive urban planning is to specify the maximum population density in the transformation districts. Such planning measures can potentially transform a monocentric urban form into a polycentric configuration (see Figure 2-6). Examples of high-density development and urban transformations can be found in the literature (U.S. EPA, 2007b, 2013a; Oh et al., 2005; Gim, 2012; and Sukkoo, 2007).

For illustration, Figure 2-36 shows an example of setting up the scenario-based population and demographic simulations. By defining the *Maximum Population Density* in the incentive area, i.e., 15,000 (person/mile²), the target year demographic and socioeconomic data are generated by using the linkage model according to the base year data and the specified demographic and socioeconomic changes. Alternatively, one can input the population density projected in other population-based land use models such as ICLUS (U.S. EPA, 2010b). After completing a demographic projection for a developmental scenario, the adaptive planning process continues in several consecutive steps shown below to help understand the adaptation attributes:

- Projecting the future trip generation or the “travel need” in a future time (Steps 7-10). This analysis is based on scenarios of growth policies in anticipation of future economic status and the conditions specified at the beginning of an urban planning cycle (Figure 2-6).

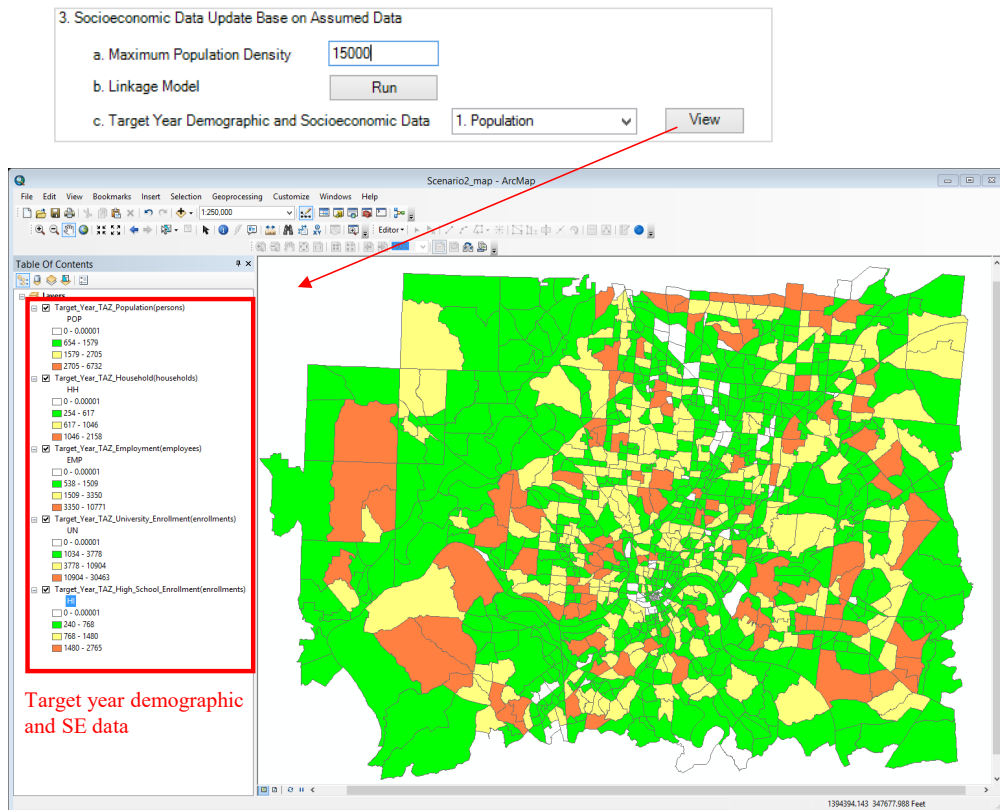


Figure 2-36 Simulation module of demographic analysis for a development scenario. High population density is specified for analysis of urban adaptation options.

- Analyzing the transportation impacts on air emissions (Steps in 11-13). These simulations yield technical information on traffic vehicle-to-capacity ratio (V/C), locations of traffic congestion areas, and also allow users to explore potential planning or engineering solutions in adaptation. An example of the congestion analysis in the Cincinnati metropolitan area is shown in Figure 2-37.
- Developing traffic management solutions and evaluation of adaptation limits relying on traffic management and improvement of the existing transportation network. Normally this adaptation analysis (Steps 15-16) relies on the analysis of infrastructure optimization using the microscopic simulation model VISSUM.
- Evaluating environmental and economic consequences for urban planning scenarios (Steps 17-19). In these final steps, the adaptive urban planning is evaluated using quantitative analysis of carbon emission emissions, transportation performance (traffic delay, fuel consumption, etc.), and economics of adaptive measures.

In the step-by-step analysis, transportation performance is reviewed and evaluated against the master planning or adaptation objectives. The selected developmental scenario is then examined further in the analysis of the infrastructure adaptation for water supply, wastewater, and stormwater management. See the AUP&ET process diagram in Figure 2-9.

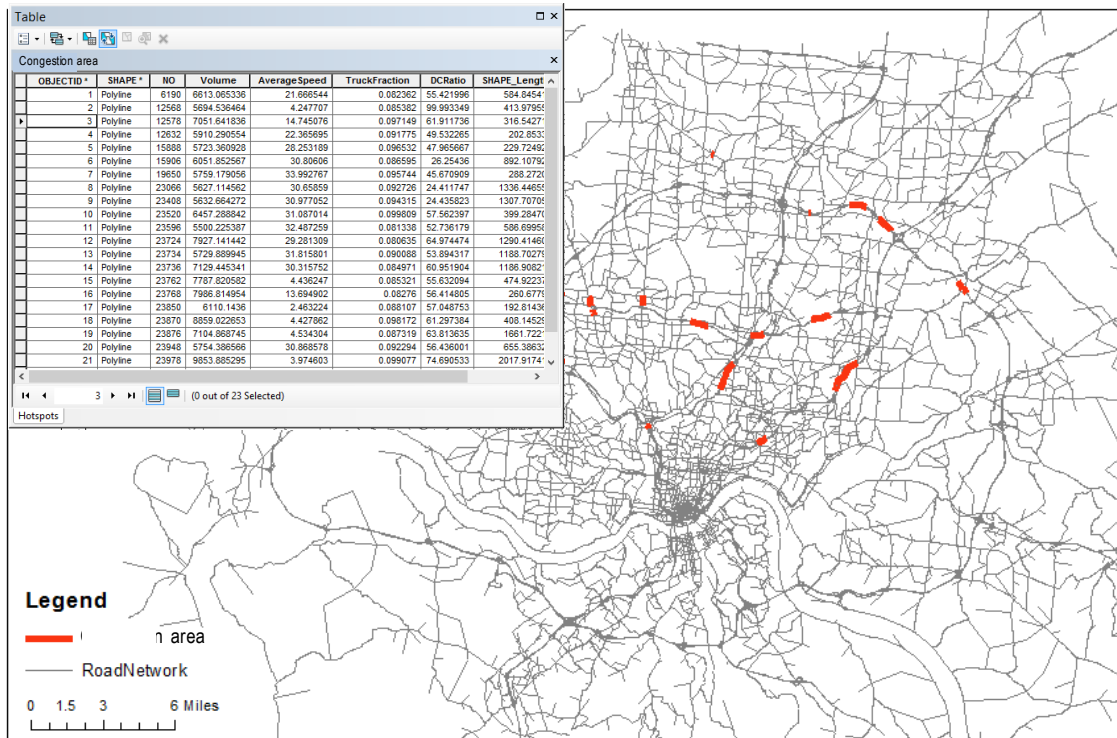


Figure 2-37 Traffic congestion areas identified for typical peak-hour traffic for 2009 in Hamilton County, showing concentrations along I-71, I-75, I-275N, and Ronald Reagan Highway. Annual traffic data from Ohio-Kentucky-Indiana Council of Governments.

4.2.2.2 Comparison of future developmental scenarios

The scenario analysis for the Cincinnati metropolitan area yields a quantitative basis to compare and evaluate the three development scenarios for the target year 2030.

1) Demographic and socioeconomic changes

The changes in population, household, and employment from 2010 base year to 2030 target year are shown in Figures 2-38, 2-39, and 2-40, respectively. The result shows that future population distribution is significantly dependent upon the developmental scenario. In the S1 scenario, all anticipated population growth is allocated in the downtown area. Such an increase is most likely to occur throughout downtown, particularly in the Over-the-Rhine area to the north. In comparison, the changes in downtown are less prominent in S2 and S3 scenarios, because of significant change in the Mason-West Chester region along the northern I-75 and I-71 highways and their connectors (Figure 2-38).

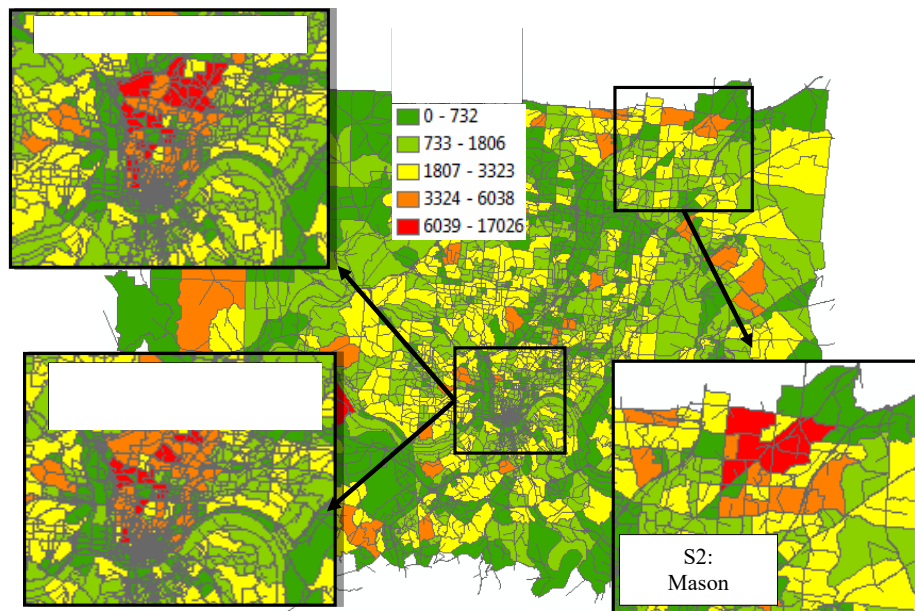


Figure 2-38 Population changes by 2030 for the three developmental scenarios (S1, S2, and S3 in the inserts) in comparison to the distribution of base year 2010 (background). Land boundaries indicate census blocks.

Future household numbers in 2030 would experience similar changes as the population (Figure 2-39). The household number is projected for the largest increase in the number of small downtown TAZs, where only a moderate-high rate of population increase is anticipated. This disparity is found to be related to the smaller households in the downtown area. The intercity re-development initiatives by the City of Cincinnati may have facilitated these changing trends.

Figure 2-40 shows the employment changes at the TAZs level. The change shows a large increase in northern Cincinnati (West Chester – Springdale – Mason area), the downtown (Ohio River bank, and university hospital area), and in northern Kentucky. These projected increases

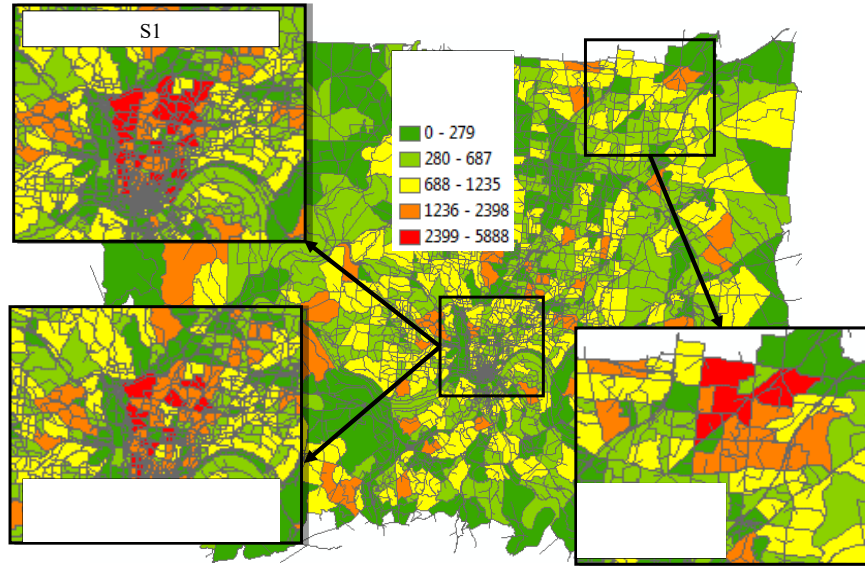


Figure 2-39 Changes in number of household by 2030 for the three developmental scenarios (S1, S2, and S3 in the inserts) in comparison to the distribution of base year 2010 (background). Land boundaries indicate census blocks.

are considered reasonable based on the current developmental trends; for example, there are projected increases of employment in the Ohio River bank area that has been redeveloped in the past two decades and continues to experience relocation of business operations into the area – an example is the recently relocated GE business operation headquarter. In S2 and S3

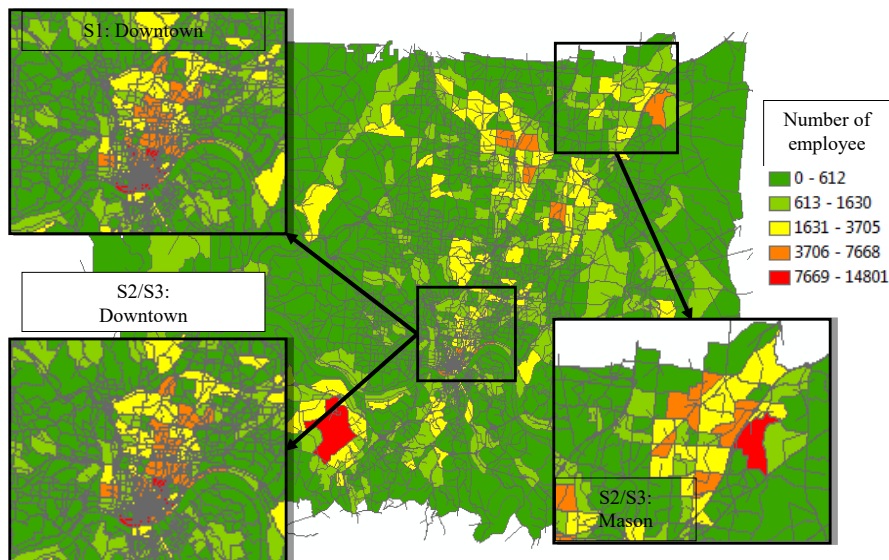


Figure 2-40 Employment changes by 2030 for the three developmental scenarios (S1, S2, and S3 in the inserts) in comparison to the distribution of base year 2010 (background). Land boundaries indicate census blocks.

developmental scenarios, a large increase in employment is predicted in the Mason area in the northeast (Figure 2-40).

Table 2-8 Trip generation results in the number of trips per day by the target year 2030

Daily Trips-	Base Year	S1	S2/S3
HBO	2,237,609	2,795,451	2,802,678
HBSC&HBU	66,635	93,287	93,553
HBW	1,127,146	1,347,873	1,359,091
NHB	1,541,498	1,794,372	1,780,907
Total Trips	4,972,888	6,030,983	6,036,229

Note: HBO – home-based-other trips; HBW – home-based-work trips; NHB – nonhome-based trips; HBSC – home-based school trips; HBU – home-based university trips

2) Travel demand forecasting results

The travel demand forecasting results are illustrated by trip generation (Table 2-8) and trip distribution (Table 2-9) for the three scenarios. Based on the AIR-SUSTAIN modeling results, there would be a ~20% increase in trip generation from the base year (2010) to the target year (2030). This increase is largely due to the targeted population increase of 15% and related business activities. The daily trip generation would be around 6 million for the S1 and S2/S3 scenarios. Furthermore, the model projection shows the nature of the trips would change. Comparing the two sets of scenarios, the multi-center configuration in S2/S3 favors home-based work trips (HBW) with trips within the home TAZs. In contrast, the monocentric S1 scenario has a greater number of non-home-based (NHB) trips (Table 2-8).

Table 2-9 Trip distribution results for the number of trips per day originated from and attracted to centers*

Daily Trips	Base Year	S1	S2/S3
Intracenter	181,232	398,746	422,073
External	432,667	425,816	435,525
Total	613,899	824,562	857,598

*Note: Centers are future incentive areas as shown in Figure 2-33.

Table 2-10 summarizes traffic performance for the three developmental scenarios simulated for the year 2030. Average queue length and wait time would increase because no expansion of the transportation network was assumed for the modeling period (2010-2030). This assumption was used to evaluate the potential capacity reserve of the current roadways. The analysis results allow one to evaluate the maximum potential of existing network utilization, namely the threshold, when adapted through traffic management tools. For the same queue length, the S3 scenario with mass transit between two future centers would decrease the average

Table 2-10 Average queue length, average wait time, total delay, and average delay during Morning Peak Hours (7:00 ~9:00 am)

Scenario	Base Year	S1	S2	S3
Average queue length (vehicle per link)	9	12	12	12
Average wait time (minute per link)	2.03	2.87	2.56	2.08
Total Delay (vehicle·hour)	113,456.4	205,121.3	179,796.6	153,018.4
Average Delay (minute per vehicle)	10.8	16.1	14.1	12.0

Note: Link refers to model road segment in model space.

time by 27.5% or $2.87 - 2.08 = 0.79$ min/link. The average total delay would be reduced from 16.1 to 12.0 min/vehicle or by 25.4% (Table 2-10).

The traffic improvement by using mass transit in the two-center configuration is graphically shown in the peak-hour (7:00-9:00 am) traffic volume distribution over the metropolitan’s road network (Figure 2-41). Compared to the current condition, the 2030 peak-

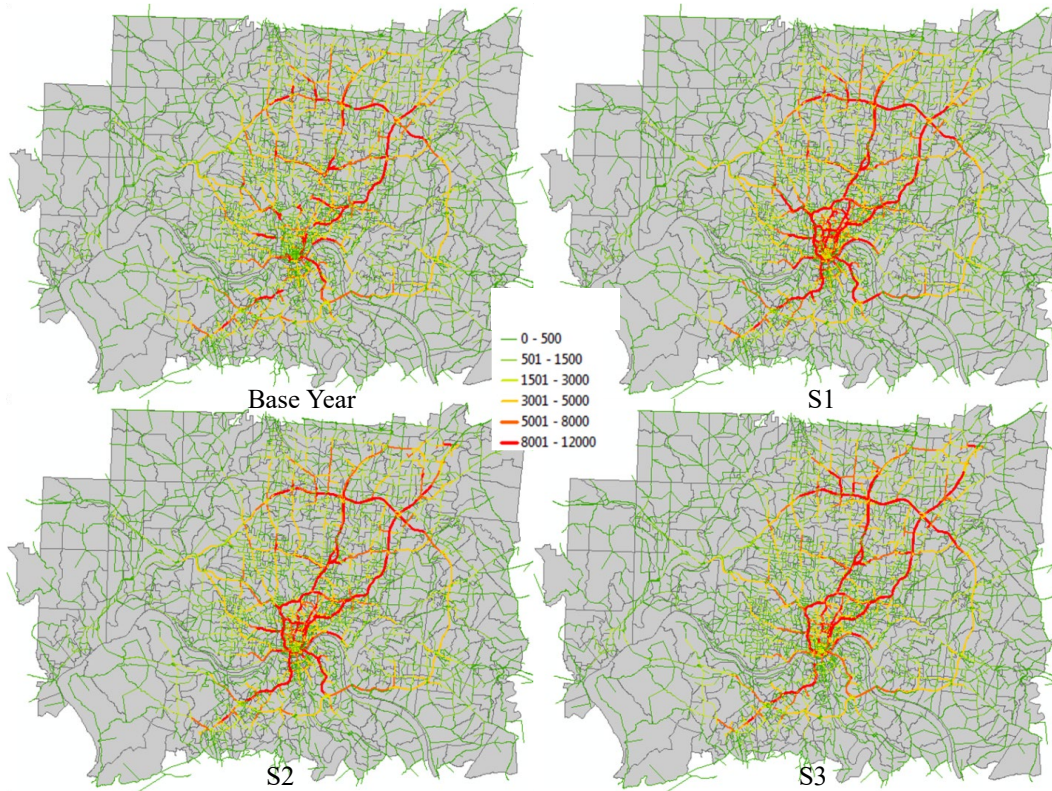


Figure 2-41 Simulated peak hour (7:00-9:00 am) traffic volume distribution over the Cincinnati road network for the base year (2010) and under three development scenarios in the target year (2030).

hour traffic pattern is characterized by increased traffic along the I-75 and I-71 highways. The traffic around the Cincinnati downtown area (I-71, I-75, I-562, and connectors) would become increasingly heavy in S1 of the concentrated downtown development. The condition would improve for the two-center configuration particularly with the help of the mass transit development in the S3 scenario.

3) Energy and emission reduction as adaptation co-benefits

Computer-simulated city-wide CO₂ emissions and energy consumption (per day) from the transportation sector are shown in Figure 2-42. They are compared among the development scenarios. From 2010 to 2030, the S1 developmental scenario is projected to have the largest increase in CO₂ emissions and energy or gallons of fuel consumed. These two variables (energy/fuel and emissions) are internally related to each other. The CO₂ emissions would increase by 13.6%. This degree of increase is comparable to and slightly less than a 17.5% increase in the trip generation (see Table 2-10), mostly due to the higher population density and employment in the downtown area. The improvement is attributed to the use of the smart development approach in favor of high-density residential and “walkable” communities.

The largest and most significant improvement in CO₂ emission reduction and the energy consumption is predicted for the S3 development scenario with two centers and mass transit. The emissions are 15.6% less compared to that in the S1 scenario that continues the monocentric development (Figure 2-42). Transportation efficiency would also increase in the multi-center configuration. The average traffic delay per person is calculated to be 25% less than in the S1 scenario, and only slightly higher than the base year in 2010 while at over 17.5% increase in travel demand (see Table 2-10).

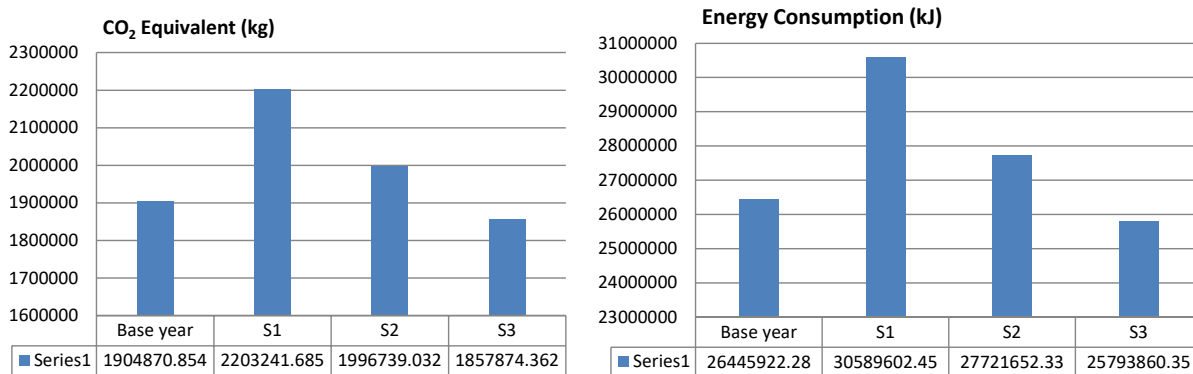


Figure 2-42 Comparison of three development scenarios (S1, S2, and S3) in peak hour (7:00-9:00) vehicular CO₂ emission and energy (fuel) consumption.

4.2.2.3 Implications on adaptation co-benefits

The case study in the Cincinnati metropolitan area illustrates the utility of an integrated analysis tool AIR-SUSTAIN in AUP&ET for the analysis of urban-scale development scenarios. The interactions among travel demand from population and land use change, demographic and

socioeconomic distributions, as well as the transportation activities and their on-road emissions can be quantified in model simulation to assess the effects of urban infrastructure adaptation policies.

The scenario-based analysis reveals the co-benefit of urban adaptation and highlights critical elements of adaptive planning through transportation optimization. Even with no large road network expansion, multi-center urban transformation is projected to reduce emissions and, at the same time, improve urban efficiency. Transportation measures such as mass transit can facilitate the urban form transformation from the current monocentric form to polycentric development.

It should be noted, however, the urban-scale adaptation case study in Cincinnati is a first-order analysis in urban planning. The model simulation only considered land use and transportation with assumptions for simplification given the data availability. For example, the CO₂ emission calculation assumes average speed under normal driving conditions in adaptation scenarios. The model simulation did not differentiate light passenger trucks (source type 31) from passenger cars (source type 21) in emission calculation. The MOVES engine in AIR-SUSTAIN has the capability of performing detailed emission analysis. For this extended capability, please refer to MOVES user's manual and related technical references (U.S. EPA, 2010a; 2015e; 2017b).

Another important element in adaptive urban planning is water infrastructure and service functions. After transportation planning, subsequent analysis of water infrastructure adaptation may lead to further refinement of the developmental scenarios. See the adaptive process in Figure 2-6. In the next Section 4.3, a case study in Florida is used to illustrate the use of adaptation in master planning to evaluate and optimize planning options for county/urban-scale water supply expansion.

4.3 Adaptation analysis for water master planning in Manatee County, Florida

The case study on master planning for water infrastructure expansion was conducted in 2009-2011 for Manatee County in Florida (Figure 2-43). The research results have been published in Chang et al. (2012).

The large growth in population, tourism, and economic development occurred in the past two decades preceding this study. This trend was expected to continue in the future. The combination of increasing water demand, climate-related chronic droughts, and depletion of the Upper Floridian Aquifer as the main source water was the central concern to local water resource managers who were tasked to provide adequate and sustainable water supplies for the future.

In response to the chronic drought conditions, the Southwest Florida Water Management District (SWFWMD) designated the entire western portion of Manatee County as the Most Impacted Area (MIA) and managed it as a part of the Eastern Tampa Bay Water Use Caution Area. In May 2008, the Manatee County Board of County Commissioners adopted the Water Supply Facilities Work Plan (Master Plan hereafter) that describes alternative capital improvement options for water resource development. The long-term strategies are documented in the county's development master plan.

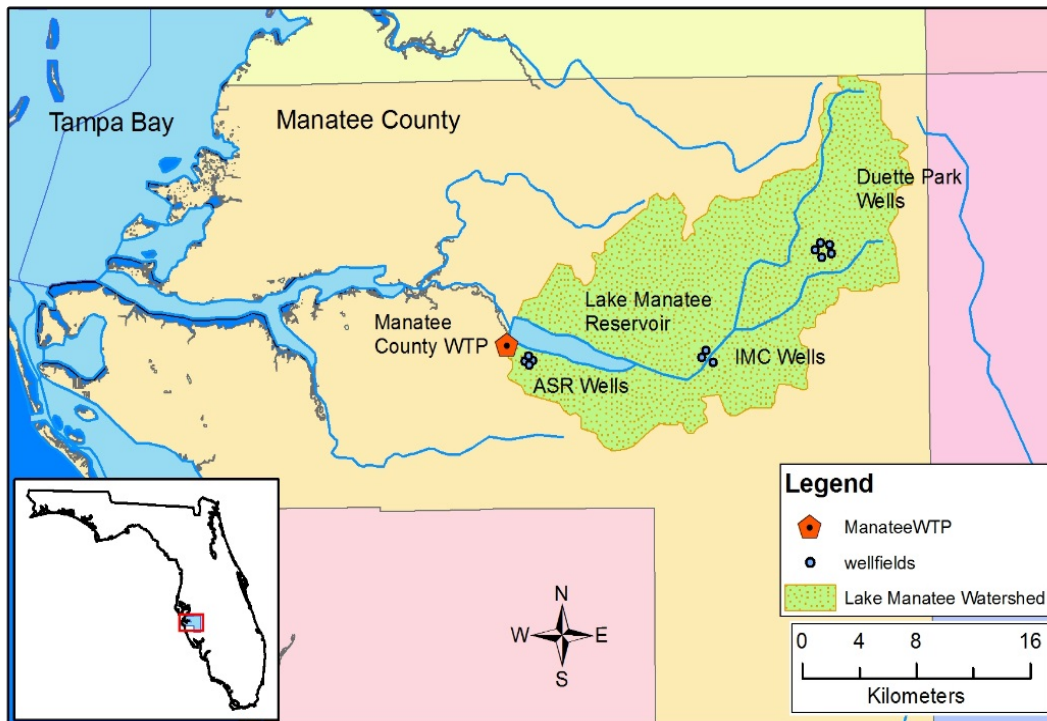


Figure 2-43 Location of the Manatee County water supply system along the upper Manatee River in Florida. From Chang et al. (2012).

The adaptation study documented here was designed to analyze the Master Plan options for water supply expansion and to identify the most feasible and effective adaptation solutions. Life-cycle analysis (LCA) approach was used to analyze carbon emissions, energy consumption, and cost/cash flows. The study systematically considered each phase of planning, design, construction, and operation for the existing and planned new water infrastructure facilities. The focus was to find alternatives that reduce CO₂ emissions and at the same time, achieve socioeconomic objectives. Details of the analysis can be found in Chang et al. (2012). By implementation of the Master Plan and other adaptation measures, the county successfully provided uninterrupted water supply in recent years, even during the severe drought of 2017⁶.

4.3.1 Water supply assessment

4.3.1.1 Water supplies

Water supply for the county is sourced from surface water and groundwater in the area. Surface water from Lake Manatee, a man-made reservoir on the Manatee River, provided an average of 132,111 m³d⁻¹ (34.9 million gallons per day). The permit for withdrawal was governed by permits issued by the Southwest Florida Water Management District according to Florida water law (Chapter 373 FS).

⁶ <http://www.bradenton.com/news/local/article145043929.html>

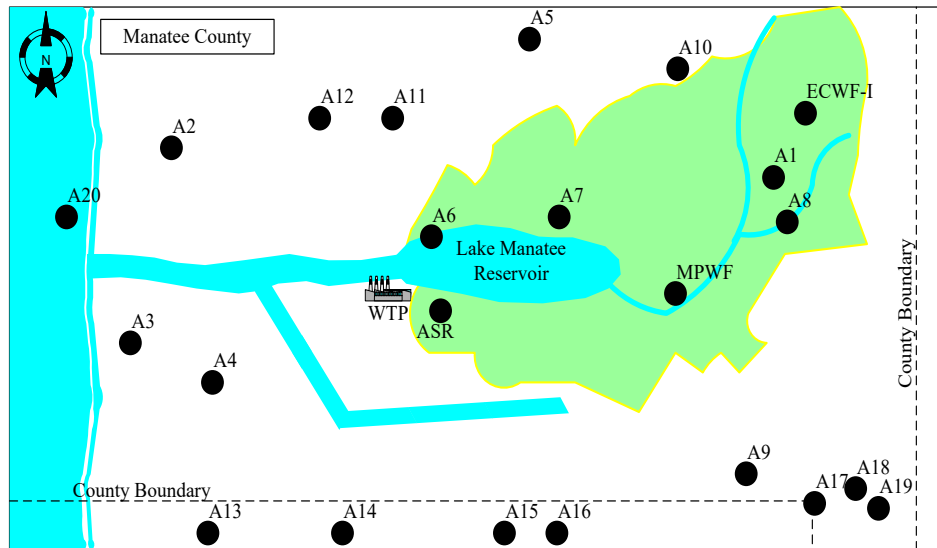


Figure 2-44 Locations of WTP, ASR, well fields (ECWF-1, MPWF), and the twenty potential water supply alternatives A1-A20. Not drawn to scale. From Chang et al. (2012).

Groundwater for water treatment was derived from two local wellfields: East County Wellfield I (ECWF-1) and the Mosaic Phosphate Wellfield (MPWF). Their relative locations are schematically shown in Figure 2-44. The ECWF-1 wellfield was permitted for average annual withdrawals at $60,514 \text{ m}^3\text{d}^{-1}$ (16.0 million gallons per day), while MPWF was permitted for $7,419 \text{ m}^3\text{d}^{-1}$ (2.0 million gallons per day). The Lake Manatee Water Treatment Plant (WTP) located in the southwest of the Lake Manatee was the only WTP in the Manatee County, providing all potable water supplies from the Manatee County Utility Department (MCUD). The treatment plant had a maximum operating capacity of $317,975 \text{ m}^3\text{d}^{-1}$ (or 84 million gallons per day); $204,412 \text{ m}^3\text{d}^{-1}$ (or 54 million gallons per day) was for surface water treatment and $113,562 \text{ m}^3\text{d}^{-1}$ (or 30 million gallons per day) was for groundwater treatment.

A total of six (6) aquifer storage and recovery (ASR) wells were located next to the Lake Manatee WTP. The ASR wells were used to store treated potable water in the Floridian Aquifer and for withdrawal to augment water supply during the drought season. These ASR wells had been in operation since 1986. This operation was permitted to provide up to $11,356,235 \text{ m}^3$ (3 billion gallons) of storage with a combined capacity of $37,854 \text{ m}^3\text{d}^{-1}$ (10 million gallons per day).

Figure 2-44 schematically shows the locations of water supply system components, including Lake Manatee WTP, the ASR wells, Lake Manatee surface water system, and the two groundwater wellfields. Manatee County also connected three (3) regional wastewater treatment plants to a 32-mile regional distribution system called Manatee Agricultural Reuse Supply (MARS) for customers to use reclaimed wastewater for agricultural irrigation. The use of reclaimed water saved groundwater from the Florida Aquifer that would otherwise be used for irrigation. The saved credits from reduced groundwater use became the net benefits that could be used as future potable water sources.

4.3.1.2 Water demand

MCUD provided water to retail customers, significant users, and wholesale customers. Retail customers distributed in both incorporated (e.g., administrative) areas and unincorporated areas of the County. Significant users refer to those with demands over 94,635 m³d⁻¹ (or 25,000 gallons per day). In 2006, this category of customers accounted for approximately 8782 m³d⁻¹ (or 2.3 million gallons per day). Wholesale customers included the cities of Bradenton, Palmetto, Longboat Key, and some regions in Sarasota County south of the Manatee County. Detailed water demand for wholesale customers is listed in Table 2-11. Reserve capacities available to the wholesale users remained constant over time as defined in the fixed water supply agreements.

Table 2-11 Water demand in 2006 and projections for wholesale customers in annual average (Board of County Commissioners, 2008)

Wholesale Customers	Water Demand (cubic meters per day)					
	2006	2010	2015	2020	2025	2030
City of Bradenton	1892.7	1892.7	1892.7	1892.7	1892.7	1892.7
City of Palmetto	7570.8	7570.8	9463.5	10,409.9	11,356.2	12,113.3
Town of Longboat Key	9463.5	9463.5	9463.5	9463.5	9463.5	9463.5
Sarasota County	37,854.1	30,283.3	22,712.5	18,927.1	NA	NA

Note: NA – Not available

Future water demands for retail customers and significant users were generally unknown because of the uncertainty in socio-economic development. Detailed population projections using historical population trends (Board of County Commissioners, 2008) were used as the basis to calculate future water supply needs. A constant water usage rate per capita, according to the Master Plan, was assumed for the period of analysis. The water usage per capita in the MCUD service area was set by permitting and planning. The total municipal water demand estimated for MCUD corresponding to the population growth is listed in Table 2-12.

Table 2-12 Water demand projections for retail and significant users in annual average (Board of County Commissioners, 2008)

Customers	Water Demand (cubic meters per day)					
	2006	2010	2015	2020	2025	2030
Retail customers	115,455.1	115,303.6	132,186.6	149,864.5	168,299.4	187,605.0
Significant users	8,782.2	14,346.7	16,466.5	18,662.1	20,933.3	23,356.0

The historical data show an average daily demand of 181,018 m³ (or 47.8 million gallons) in 2006. The demand total included 115,455 m³d⁻¹ (or 30.5 million gallons per day) for domestic water usage, 65,563 m³d⁻¹ (or 17.3 million gallons per day) for wholesale customers and significant users. With the projected population growth, annual average potable water demand would increase to 234,317 m³d⁻¹ (or 61.9 million gallons per day) by 2030 as specified in the Master Plan (Board County Commissioners, 2008). MCUD had an annual average of the permitted water supply of 200,059 m³d⁻¹ or 52.9 million gallons per day in 2009. According to

the Master Plan, a total of 34,447 m³d⁻¹ (or 9.1 million gallons per day) of additional water supply would be required by the year 2030.

4.3.1.3 Future water supply alternatives

MCUD identified twenty potential water supply alternatives to meet the increased water demands in the future. The master planning called for a combination of surface water and groundwater source expansion options. They are grouped into five categories: groundwater options, surface water options, water permit transfer options, regional water options, and other options. Table 2-13 lists the twenty competing water supply alternatives. Groundwater options included building new wellfields in various locations of Manatee County. By operating the MARS system with less groundwater for irrigation, MCUD could increase the permitted groundwater pumping for potable water supply. Overall, the MARS projects consist of four phases: MARS-I, MARS-II, MARS-III, and MARS-IV; MARS-I and MARS-II projects had been implemented as of 2012 (Chang et al., 2012).

Table 2-13 Twenty alternatives for water supply expansion in the county master planning

Alternative	No.	Brief Description
Groundwater Options		
MARS-I	1	This option is to supply new groundwater by developing a new wellfield in the central Duette Park area near the existing ECWF-1.
MARS-II	2	This option is to supply new groundwater by developing a new wellfield in the Erle Road Tank site.
MARS-III	3	These options are to supply new groundwater by developing a new wellfield. The location of the new wellfield has not yet been decided.
MARS-IV	4	
Surface Water Options		
Lake Parrish Reservoir	5	This option is to divert more surface water from the Little Manatee River into the existing Lake Parrish Reservoir located in the northern part of Manatee County as a cooling pond for a power plant. The increased water storage in the Lake Parrish Reservoir is used for irrigation to obtain well credits. Improvements in the existing systems include upgrading diversion pumps, distribution pumping, and piping facilities.
Dredging of Lake Manatee	6	This option is to increase the storage of the Lake Manatee Reservoir to increase the surface water annual yield from Lake Manatee. The capital investment includes the creation and maintenance of a new reservoir and dam, wetlands mitigation costs, and water transmission and treatment at the existing water treatment plant. This alternative may or may not be funded by the Southwest Florida Water Management District (SWFWMD).

Alternative	No.	Brief Description
Gilley Creek Reservoir	7	This option is to build a new reservoir upstream of Lake Manatee at the Gilley Creek location to yield more annual surface water. This alternative may or may not be funded by SWFWMD.
North and East Fork Reservoir	8	This option is to create an upstream impoundment at the North and East Fork locations to increase storage and yield available at the Lake Manatee intake. The capital investment includes the creation and maintenance of a new reservoir and dam, wetlands mitigation costs, and water transmission and treatment at the existing water treatment plant. This alternative may or may not be funded by SWFWMD.
Tatum Reservoir – Lake Manatee WTP	9	This option is to develop a reservoir to store surface water diverted from the Myakka River located in the southeastern portion of Manatee County. The stored surface water from the Tatum Reservoir is used for irrigation purposes so that the water credits that originally are used for irrigation can be transferred for potable water supply. The facilities to be built include an impoundment structure and distribution pumping and piping.
Transferred Water Use Permit Options		
Well Credit from Current Reuse Customers	10	This option is to renegotiate with the current reclaimed water customers for increased reclaimed water flows in the new agreement term. The cost associated with this alternative is for pumping to and treatment at the existing water treatment plant.
Developer-Provided Water Use Permits (WUP) Transfer	11	This option is to implement a management option that will require new farmland developers to obtain the previous landowner's water use permit as a part of a land purchase. In this way, the Manatee County Utility Department (MCUD) can take off the burden of increasing the water supply to the new potable water demand of new developers.
Direct Purchase of WUP	12	This option is to buy water use permits from permittees who are discontinuing farming operations instead of making new developers purchase the water use permit. This alternative conflicts with option No.11; Manatee County wishes to forego the option if option No.11 can be implemented.
Regional Water Options		
Peace River Water Treatment Facility Expansion	13	This option is to improve the existing Peace River water treatment facility in Desoto County by the construction of a new 6.0-billion gal reservoir and expansion of the water treatment facility's production capacity from 12- to 24- and, finally, to 48-million gal/day.
Shell Creek Restoration	14	This option is based on improvements on the existing Shell Creek water system by restoration and enhancement of natural water storage areas. This alternative is for potable water supply to the City of Punta Gorda and the region. An environmental benefit is identified for this alternative because of the restoration of natural conditions.
Dona Bay/Cow Pen Slough Restoration (Option A)	15	This option is to build a new surface water supply system located within Sarasota County. Dona Bay Option A is a two-phase project. The first phase is to build a new reservoir and a new water treatment

Alternative	No.	Brief Description
		plant at the Dona Bay site, and the second phase is to expand the size and capacity of the reservoir and the water treatment plant.
Dona Bay/Cow Pen Slough Restoration (Option B)	16	This option is to build a new surface water supply system located within Sarasota County. Dona Bay Option B is a single-phase project. This alternative conflicts with option No.15.
Flatford Swamp Restoration	17	This option is to build a new water supply system at the Flatford Swamp area located in the southeastern portion of Manatee County. The water source comes from the excess irrigation runoff in Flatford Swamp that causes widespread tree mortality. This alternative conflicts with options No.18 and No.19.
Other Options		
Flatford Swamp – Stored and Treated at Tatum Reservoir	18	This option is to pump the surplus water stored in the Flatford Swamp, which is located in the southeastern portion of Manatee County immediately north of Myakka City to the Tatum Reservoir for storage and to build a new water treatment plant to treat the water to potable water standards at the Tatum Reservoir site. This alternative conflicts with options No.9, No.17, and No.19. This alternative may or may not be funded by SWFWMD.
Flatford Swamp supplemented with Diversion from the Myakka River – Stored and Treated at Tatum Reservoir	19	This option is similar to option no. 18. The difference is that this option will divert seasonal surface water from the Myakka River to supplement the Flatford Swamp irrigation runoff. Diversion structure, pumping facilities, and additional capacity of the new water treatment plant will be needed. This alternative conflicts with option No.9, No.17, and No.18. This alternative may or may not be funded by SWFWMD.
Seawater Desalination	20	This option is to treat seawater to potable water standards. New seawater desalination facilities at the Port Manatee site need to be built. High operation and maintenance costs may be experienced. However, potential price reduction equipment and funding from SWFWMD may make this alternative a competitive one.

Surface water options refer to those alternatives that involve new or expansion of existing reservoirs, by which additional surface water could be diverted from rivers into the reservoirs during the wet season. Some of the surface water could be used for irrigation purposes without treatment at Manatee WTP. This amount was then counted as groundwater credits for MARS-I expansion. The expansion timing for MARS-III and IV were unknown. Groundwater credits could be reserved for the MARS-I expansion when replaced with surface water sources. Water permit transfer options were possible where a water use permit holder no longer needed the water or where reclaimed water became available.

Regional water supply is another option. The Peace River Manasota Regional Water Supply Authority (PR/MRWSA) intended to integrate and improve water resource management in Charlotte County, DeSoto County, Manatee County, and Sarasota County in order to provide the region with an adequate, reliable, and sustainable water supply into the future. Starting in 2014, the PR/MRWSA had begun providing water to Manatee County. Other water options considered in the master planning process included seawater desalination and swamp restoration at the Flatford Swamp in southeastern Manatee County. The Flatford Swamp received a

significant amount of irrigation runoff. Reducing the irrigation runoff flow into the swamp was predicted to help re-establish hardwood trees in the swamp and reduce environmental impact. Seawater desalination involved building a seawater treatment plant at the Tampa Bay.

Figure 2-44 schematically illustrates the relative locations of all twenty potential water supply alternatives. Among them, locations of alternatives #10, #11, and #12 are shown only for illustration; these three alternatives require no physical facilities. Some of the twenty alternatives may be eligible for SWFWMD funding, thus decreasing the county’s capital investment and, thereby, the unit cost of potable water. It was noted, however, that the SWFWMD funding was not guaranteed even when all required criteria were met. In the comparative analysis, the highest (conservative) unit cost was used for the alternative following the common practice of engineering feasibility analysis.

Table 2-14 summarizes the maximal water credit and unit cost for each of the 20 water supply alternatives. The maximum water credit was defined as the maximum permitted water withdrawal. Unit cost was calculated as the present value for a cubic meter in U.S. dollars based on the 2007 value. It includes the amortization of the estimated initial capital investments and the operation and maintenance (O&M) costs.

4.3.2 Expansion scenario analysis

Most decision-making systems nowadays rely on a single attribute; for example, economic cost or water supply capacity. Traditional decision-making mostly relies on the outcome of a cost and benefit analysis in the context of single-objective optimization, which was of particular interest to both water supply (Urbaniak, 1988; Slowinski et al., 1985) and wastewater treatment (Ong and Adams, 1990).

Table 2-14 Maximum water credit and unit cost of the twenty water supply alternatives*

	1	2	3	4	5	6	7	8	9	10
Max Water Credit	8.21	11.36	7.57	18.93	15.52	44.29	34.83	40.13	17.79	17.03
Unit Cost (dollars per cubic meter)	0.34	0.53	0.31	0.50	0.51	1.09	0.67	0.74	1.08	0.50
	11	12	13	14	15	16	17	18	19	20
Max Water Credit	0†	0†	45.42	75.71	75.71	75.71	56.78	30.28	43.15	37.85
Unit Cost (dollars per cubic meter)	0.53	0.60	0.30	0.51	0.76	0.62	0.72	0.61	0.55	1.07

Notes: *Adopted from the 2008 Manatee County Water Supply Facilities Work Plan (Board of County Commissioners, 2008)

†The maximum (max) water credits for alternative #10 and #11 are not available and the value of zero was assigned as the default. The maximum water credit is 1000 m³/day.

However, the cost-saving alone does not reflect all sustainability attributes in evaluating the adequacy of competing for water supply expansion options. In the case study of Manatee County’s water expansion, a decision-making framework included both carbon footprint and economic cost, in addition to the management objective of adequate water supplies. Two

approaches in a systems evaluation are common in finding the global optimal solution among competing alternatives. One is a top-down modeling assessment; the other is bottom-up threshold analysis. Optimization models for the top-down water supply system planning have been developed to address multiple planning goals (Harrington and Gidley, 1985; Yamout and El-fadel, 2005). Various analysis techniques are long available including nonlinear programming models (Mulvihill and Dracup, 1974) and multicriteria decision analyses (Slowinski et al., 1985).

The framework was based on the LCA method for comparative alternative evaluation. The purpose was to select the best expansion options. LCA is a well-established and standardized method of analysis for cost comparisons and can be applied to evaluate and reduce possible environmental impacts as a part of sustainability analysis. For example, some LCA investigations use greenhouse gas (GHG) emissions in form of carbon footprint, as one of the evaluation categories to evaluate multiple technical solutions or alternatives for municipal wastewater treatment systems (Tillman et al., 1998; Dennison et al., 1998; Lundin et al., 2000; Peters and Lundie, 2001) and in water supply assessment (Voivontas et al., 2003; Lundie et al., 2004).

Evaluation of the expansion alternatives in Manatee County followed the LCA principles in an analysis of the cost and life-cycle GHG emissions. Based on these determined parameters, a multi-objective optimization scheme was developed to identify the global optimal planning solutions (Chang et al., 2012).

4.3.2.1. Carbon footprint estimates

The carbon footprint is a sum of CO₂ equivalents in all phases of each expansion alternative. The time duration for this analysis was twenty years (from 2011 to 2030) during which the construction, production, use, and recycle phases were analyzed sequentially as shown in Figure 2-45. The systems analysis diagram shows material and energy flows, where each

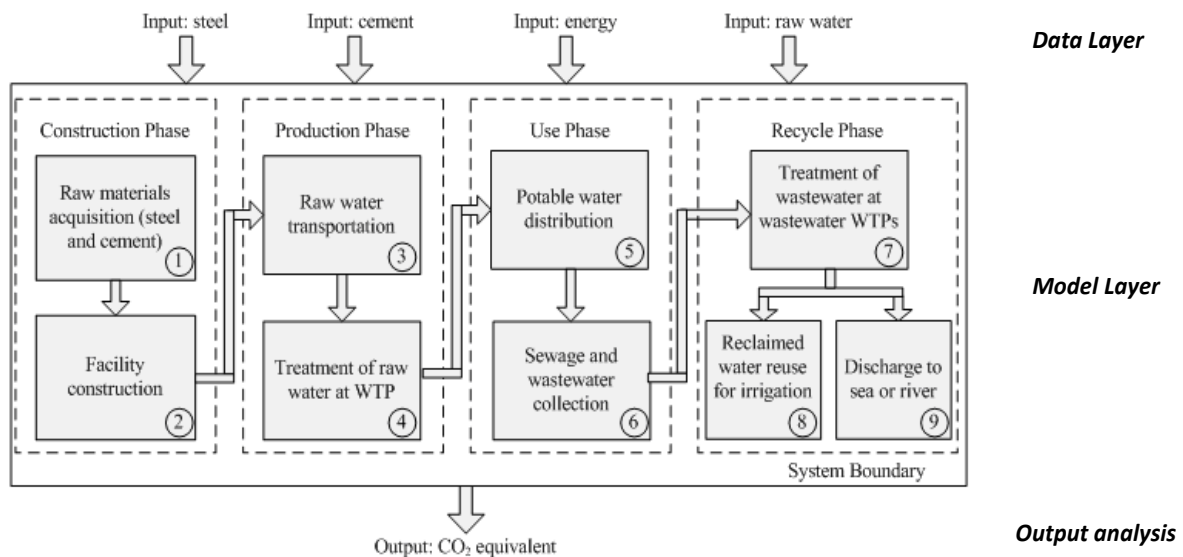


Figure 2-45 The life-cycle system analysis flow diagram for determining carbon footprint in water infrastructure expansion alternatives. Process is divided into three layers. Adopted from Chang et al. (2012).

block represents material stocks and is connected by arrows to surrounding blocks indicating critical material flows. Materials, or raw water in this analysis, are extracted at the beginning of a life cycle, pass through intermediate phases, and finally return to the environment at the end of the life cycle. In this LCA analysis, the end-of-life phase of water facilities is not included because water facilities usually have a service life far beyond the analysis period.

Chang et al. (2012) analyzed the carbon footprint for all twenty water supply alternatives. Their results were used in this LCA analysis. The emissions in construction and operation phases were calculated in the 20-year period. The total CO₂ equivalent emission in a 20-year period was the sum of CO₂ equivalent emissions for construction and operations. As shown in Figure 2-45, the construction phase includes the processes ① and ②. When a potential water supply alternative was selected and implemented, the CO₂ equivalent emissions were determined for both facility construction and operation. The operation phase included the processes ③, ④, ⑤, ⑥, ⑦, ⑧, and ⑨.

The LCA analysis results are listed in Table 2-15. The CO₂ equivalent emissions were proportional to the amount of water supplied, but the total energy usage in the water infrastructure life-cycle computation varied significantly among the expansion options (Table 2-15).

Table 2-15. Life cycle analysis of carbon footprint for the twenty water supply alternatives (modified from Chang et al., 2012)

Alternative		CO ₂ equivalent emissions in constructional phase Process ① + ② (kilograms)	CO ₂ equivalent emissions in operational phase. Process ③+④+⑤+⑥+⑦+⑧+⑨ (kilograms per cubic meter)
Groundwater	1	1.96×10 ¹⁰	2.35
	2	2.85×10 ¹⁰	2.68
	3	2.08×10 ¹⁰	2.48
	4	4.11×10 ¹⁰	2.87
Surface water	5	3.40×10 ¹⁰	2.71
	6	1.88×10 ¹⁰	1.16
	7	2.67×10 ¹⁰	1.99
	8	8.91×10 ¹⁰	3.75
	9	4.63×10 ¹⁰	3.13
Water use permit transfer*	10	Negligible*	1.16
	11	Negligible*	1.16
	12	Negligible*	1.16
Regional water	13	1.81×10 ¹¹	5.89
	14	2.72×10 ¹¹	6.85
	15	1.07×10 ¹¹	3.35

Alternative		CO ₂ equivalent emissions in constructional phase Process ① + ② (kilograms)	CO ₂ equivalent emissions in operational phase. Process ③+④+⑤+⑥+⑦+⑧+⑨ (kilograms per cubic meter)
	16	1.07×10 ¹¹	3.35
	17	6.56×10 ¹⁰	2.71
Others	18	4.88×10 ¹⁰	2.71
	19	5.75×10 ¹⁰	2.71
	20	6.28×10 ¹⁰	3.28

*Water permit transfer is simply an administrative action with almost no obvious carbon footprint relative to other options.

4.3.2.2. Multi-objective evaluation

A multi-objective mixed integer programming modeling was conducted to assess these multi-stage expansion strategies based upon the LCA and cost evaluation results. The analysis of future water supply scenarios covered a 20-year timeframe from 2011 to 2030. The trade-off analysis for a compromised solution was based on two objectives. One was to minimize the total system costs required for the water supply expansion. The other was to minimize the total GHG emissions expressed as CO₂ equivalent, reflecting overall energy consumptions. Both objectives were applied through modeling to screen and order the relevant water supply alternatives.

Simulations using a compromise programming model yielded the best Pareto frontier solutions for the alternative expansion options. The model computation was a function of the total number of planning periods in the multi-stage framework of infrastructure planning, construction, operation, and disposal (or decommission) (see Figure 2-45). The time interval was, generally, location-specific depending on local decision-making objectives. More stages and greater implementation details lead to more decision variables and parameters that require greater computation time. For this illustration, a 5-year time span was assumed for the construction phase in the case-study decision analysis. The 5-year duration is generally in agreement with the capital expenditure process.

4.3.3. Quantitative modeling and systems analysis

In quantitative analysis, the multi-stage planning horizon was divided into four time periods with each having a 5-year time span. Decisions in each period of expansion to meet the growing water demand were evaluated in a trade-off analysis between the two objectives. The Multi-objective and Multistage Mixed Integer Programming model used in the Manatee County evaluation is described below.

Objective Functions

Two governing objective functions were implemented for each 5-year interval. The carbon emission equivalent (CO_{2,eq}) was calculated using the LCA procedures in Figure 2-45. Monetary values of cost were discounted to the year 2007. According to Chang et al. (2012),

Objective function 1:

$$\text{Minimize } Z_1 = \text{total CO}_{2,\text{eq}} \text{ emissions (unit: g)} = \sum_{i=1}^{20} (1000A_{i1}CO_{2,\text{eoi}} \times 1825 + Y_{i1}CO_{2,\text{eci}}) + \sum_{t=2}^4 \sum_{i=1}^{20} [1000A_{it}CO_{2,\text{eci}} \times 1825 + (Y_{it} - Y_{i(t-1)})CO_{2,\text{eci}}]$$

Objective function 2: Minimize $Z_2 = \text{total cost (unit: \$)} =$

$$\sum_{i=1}^{20} (1000A_{i1}C_i \times 1825 + Y_{i1}F_i) + \sum_{t=2}^4 \sum_{i=1}^{20} [1000A_{it}C_i \times 1825 + (Y_{it} - Y_{i(t-1)})F_i]$$

where Y_{it} is 1 if the alternative i is implemented in and after time stage t ; otherwise $Y_{it} = 0$, $i = 1, 2, \dots, 20$; $t = 1, 2, 3, 4$ for the period of 5-year implementation interval. $CO_{2,\text{eci}}$ is the amount of $CO_{2,\text{eq}}$ emission in the construction phase of alternative i in unit of g, and $CO_{2,\text{eoi}}$ is the amount of $CO_{2,\text{eq}}$ in the operational phase of alternative i in unit of $g \text{ m}^{-3}$, $i = 1, 2, \dots, 20$. A_{it} is actual water withdrawn ($10^3 \text{ m}^3 \text{ d}^{-1}$) from alternative i ($i = 1, 2, \dots, 20$), and $t = 1, 2, 3, 4$. C_i is unit water cost of the alternative solution i in $\$ \text{ m}^{-3}$ ($i = 1, 2, \dots, 20$). F_i is the fixed capital investment for the alternative solution i ($i = 1, 2, \dots, 20$).

Model Constraint Setting

Constraint setting in the compromise programming model included definitional constraints, water demand constraints, capacity limitation constraints, availability constraints, sequencing constraints, mutually exclusive constraints, irreversible constraints, screening constraints, and non-negative and binary constraints. These constraints provided different functionalities in an intertwined solution space that narrowed down the dynamic selection and ranking according to streamlined logic described by the coupled objective functions and constraints over the planning time horizon.

Seven model constraints below defined both the current maximum water supply and the projected water demand in the unit of $10^3 \text{ m}^3/\text{day}$ in each time period:

$$S = 200.04 \text{ } 10^3 \text{ m}^3 \text{ d}^{-1} \quad (2.3)$$

$$D_1 = 192.19 \text{ } 10^3 \text{ m}^3 \text{ d}^{-1} \quad (2.4)$$

$$D_2 = 209.14 \text{ } 10^3 \text{ m}^3 \text{ d}^{-1} \quad (2.5)$$

$$D_3 = 211.83 \text{ } 10^3 \text{ m}^3 \text{ d}^{-1} \quad (2.6)$$

$$D_4 = 234.43 \text{ } 10^3 \text{ m}^3 \text{ d}^{-1} \quad (2.7)$$

$$F_i = 0.001 \text{ \$} \quad (2.8)$$

$$G = \text{a large dumb number (e.g., 9999999)} \quad (2.9)$$

where S is the limit in current water supply upper; D_t is water demand in time period t ($= 1, 2, 3, 4$); F_i is the virtual fixed-cost, an artificially assigned small number relative to all cost parameters to support screening logic in the cost-effectiveness objective and associated constraints. The use of dumb number G in programming is to assure computing stability for the If-Then logic screening in constraints by Eqs.(2.10)-(2.12) below. The settings of F_i and G also help avoid the selection of an alternative with no additional water supply over the planning horizon:

- The constraints between demand (D) and supply (S) were applied to the entire 20-year period in the modeling space:

$$\sum_{i=1}^{20} A_{it} \geq D_t - S \quad \text{for all } t \quad (2.10)$$

- The water amount supplied by each future water source could not exceed its predetermined supply limit due to water rights:

$$A_{it} \leq A_i^{max} Y_{it} \quad \text{for all } t \text{ and all } i \quad (2.11)$$

in which A_i^{max} is the maximum water credit ($10^3\text{m}^3\text{d}^{-1}$) for A_i , $i = 1, 2, \dots, 20$.

- Only MARS-I and MARS-II were available in the time period 1 and the rest of future water supply alternatives were available only after time period 1:

$$Y_{it} = \begin{cases} 1 & i = 1, 2 \\ 0 & i = 3, 4, \dots, 20 \end{cases} \quad (2.12)$$

Construction sequencing constraints

This set of constraints assured that the MARS-II project was not be implemented until the completion of the MARS-I project according to the County's infrastructure expansion work plan. Similarly, the MARS-II project implementation could only occur before the MARS-III project. This forward-looking sequence applies to MARS-III project that might be implemented ahead of the MRAS-IV project. Mathematically,

$$\begin{aligned} Y_{1t} &\geq Y_{2t} \\ Y_{2t} &\geq Y_{3t} \\ Y_{3t} &\geq Y_{4t} \end{aligned} \quad \text{for all } t \quad (2.13)$$

Mutually exclusive constraints:

Some future water supply alternatives were mutually exclusive according to the county's original work plan. This set of constraints assured that only one of the exclusive future water supply alternatives could be implemented in any time period. For example, Alternatives 11 and 12 are mutually exclusive because the water use permit allocation is either transferred from developers to the county or otherwise acquired by Manatee County through other means. An example was to exchange the county's reclaimed water for groundwater currently used for agricultural irrigation. The MARS-III project conflicts with the other regional water supply alternatives because any one of the regional water supply sources or implementation completion of the MARS projects could provide adequate water supply (Board of County Commissioners, 2008). Alternatives 15 and 16 are mutually exclusive because both alternatives intended to use the same water supply sources but in different implementation schedules. Similarly, Alternatives 17, 18, and 19 are mutually exclusive because all three alternatives rely on Flatford Swamp as the water source. The three alternatives differ because of assumptions on the construction of a new WTP as a part of the regional water supply option. Alternatives 9, 18, and 19 are mutually exclusive because all three were related to a new reservoir site at Tatum. The difference is

whether the new reservoir site would be used to store water pumped from the Myakka River or the Flatford Swamp.

The construction sequences and mutually exclusive constraints were mathematically expressed in modeling. Eqs.2.19-2.22 define the need for MARS-I implementation before considering relevant Alternatives #5, #9, #10, and #11, because of the constraints from sequential water credit transfer. These constraints are as follows:

$$Y_{11t} + Y_{12t} \leq 1 \quad \text{for all } t \quad (2.14)$$

$$Y_{3t} + Y_{13t} + Y_{14t} + Y_{15t} + Y_{16t} + Y_{17t} \leq 1 \quad \text{for all } t \quad (2.15)$$

$$Y_{15t} + Y_{16t} \leq 1 \quad \text{for all } t \quad (2.16)$$

$$Y_{17t} + Y_{18t} + Y_{19t} \leq 1 \quad \text{for all } t \quad (2.17)$$

$$Y_{9t} + Y_{18t} + Y_{19t} \leq 1 \quad \text{for all } t \quad (2.18)$$

$$Y_{5t} \leq Y_{1t} \quad \text{for all } t \quad (2.19)$$

$$Y_{9t} \leq Y_{1t} \quad \text{for all } t \quad (2.20)$$

$$Y_{10t} \leq Y_{1t} \quad \text{for all } t \quad (2.21)$$

$$Y_{11t} \leq Y_{1t} \quad \text{for all } t \quad (2.22)$$

Irreversible constraints:

This set of constraints assured that the implemented water supply alternatives in one time period were available in and after that time period.

$$Y_{it} \leq Y_{i(t+1)} \quad i = 1, 2, \dots, 20, t = 1, 2, 3 \quad (2.23)$$

Screening constraints:

This set of constraints defined sequence by which alternatives for meeting water demands would be considered. A new water supply alternative was screened when the maximum capacity of the current water supply in a given time period became incapable of meeting the projected water demand for the next time period; otherwise, there was no need in planning to implement a new water supply alternative. In Eqs. 2.24-2.26, the formulation would allow n number of water supply alternatives to be included in each time period for capacity expansion; n is a positive integer. For $n=1$, the model would only pick up one alternative at a time for ranking in sequence. The number of alternatives to be selected at one time is 1, 2, or 3.

$$\sum_{i=1}^{20} Y_{i1} A_i^{\max} - (D_2 - S) < GY_1 \quad (2.24)$$

$$\sum_{i=1}^{20} Y_{i2} - \sum_{i=1}^{20} Y_{i1} \leq n(1 - Y_1)$$

$$\sum_{i=1}^{20} Y_{i2} A_i^{\max} - (D_3 - S) < GY_2 \quad (2.25)$$

$$\sum_{i=1}^{20} Y_{i3} - \sum_{i=1}^{20} Y_{i2} \leq n(1 - Y_2)$$

$$\sum_{i=1}^{20} Y_{i3} A_i^{\max} - (D_3 - S) < GY_3 \quad (2.26)$$

$$\sum_{i=1}^{20} Y_{i4} - \sum_{i=1}^{20} Y_{i3} \leq n(1 - Y_3)$$

where Y_1 , Y_2 , and Y_3 are binary integer variables for screening multiple alternatives associated with different scenarios in the optimization context.

Non-negative and binary constraints:

This set of constraints assured that the amount of water assigned to each water supply alternative was non-negative and the binary decision variables were dichotomous.

$$A_{i,t} > 0 \quad (2.27)$$

$$Y_{i,t} = 0, 1 \quad i = 1, 2, \dots, 20, t = 1, 2, 3, 4 \quad (2.28)$$

$$Y_1, Y_2, Y_3 = 0, 1 \quad (2.29)$$

4.3.4. Adaptation analysis results on cost and carbon/energy footprint

4.3.4.1. Carbon/energy footprint and cost optimization

Optimal solutions were identified using the multi-objective model simulation by solving each of the individual objective equations sequentially. The solution (shown in Table 2-16) was considered optimal when each objective is optimized individually and achieved as a whole. One caveat is that the ideal solution may not be feasible or practical because the objectives may be competing, even conflicting in the decision space. In this type of application, the “Pareto Optima” solution set is commonly used. The solution optimization can be found in the Pareto Optima frontier in the solution space of the compromise programming model. Alternatively, the compromised solution can also be obtained by applying the distance-based metrics defined in a compromise programming model (Zeleny, 1973).

The solution space for the Manatee County case study is two-dimensional as defined by the two objective functions. The x -axis was selected for CO₂ equivalent emissions (Z_1) and the y -axis for total system cost (Z_2). In all cases, a Pareto Optimal solution in global optimization space represents the best alternative that may perform better for both objectives. For the exclusive optimization decision ($n = 1$), five sets of solutions are found in Table 2-17. Solution #1 is the

GHG-effective solution; Solution #5 is the most cost-effective; and the other three are compromised solutions. For alternative management decisions at $n=2$ and $n=3$, the Pareto Optimal solutions were found and described in Chang et al. (2012).

Table 2-16 Optimal solutions of the multi-objective model

	Minimize Z_1 (kg)	Minimize Z_2 (\$million)
$n = 1$	1.15×10^{11}	223
$n = 2$	7.55×10^{10}	172
$n = 3$	7.54×10^{10}	172

Note: n is the number of alternatives allowed in one set of ideal solutions.

A sensitivity testing for the optimal solution was conducted at assumed 10% uncertainty in the estimates of future water demand change at all four stages. For water managers, future prediction is the basis for decision making and often contains uncertainty. The sensitivity analysis results are shown in Table 2-18. The best case is that future water demand is 10% less than the prediction or $0.9D_i$; conversely, the future water demand of more than 10% than predicted or $1.1D_i$ is the worst-case scenario in planning, requiring attention in further analysis.

Table 2-17 The Pareto optimal expansion strategies ($n = 1$)

Solution Number	Z_1 (kg)	Z_2 (\$million)	Expansion Strategies			
			Period 1	Period 2	Period 3	Period 4
1	1.15×10^{11}	313	1, 2	17	-	6
2	1.42×10^{11}	295	1, 2	17	-	7
3	<i>1.56×10^{11}</i>	260	1, 2	16	-	10
4	2.14×10^{11}	258	1, 2	16	-	19
5	3.22×10^{11}	223	1, 2	14	-	10

Note: Best compromised solution #3 is in bold and italic.

For $n = 1$, the Pareto Optimal solution sets were examined for the best case $0.9D_i$ ($D_1 = 172.97$, $D_2 = 188.23$, $D_3 = 190.65$, and $D_4 = 210.99$) and the worst case of $1.1D_i$ ($D_1 = 211.41$, $D_2 = 230.05$, $D_3 = 233.01$, and $D_4 = 257.87$). Solutions marked by “-” or “+” represents 10% lower or higher water demand than the predicted level in the Master Plan, respectively. The results indicate robust analysis conclusion insensitive to 10% uncertainty in water demand projection, as the Pareto Optimal frontier remains unchanged in shape.

4.3.4.2. Optimal expansion solutions and construction sequence

Water supply system expansion normally takes place in phases considering water service needs and economic factors such as capital flow and construction cost. The preceding analysis for the Manatee County water infrastructure expansion showed multiple compromised solutions in the trade-off between the overall system’s cost and life-cycle carbon footprints. In engineering practice, master planning of water infrastructure improvement often considers other factors such

as land availability, engineering feasibility, capital expenditure, and cash flow, among the others. For these reasons, one can further assess the best options in the Manatee County case study, which offer the optimal management options. Such an assessment is discussed below.

Table 2-18 The Pareto optimal expansion strategies for the best and worst cases ($n = 1$)

Solution Number	Z_1 (kilograms)	Z_2 (\$million)	Optimal Expansion Strategies			
			Period 1	Period 2	Period 3	Period 4
1-	4.87×10^{10}	2.77	1, 2	6	-	10
2-	7.54×10^{10}	193	1, 2	7	10	6
3-	9.63×10^{10}	185	1, 2	7	10	3
4-	<i>1.06×10^{11}</i>	<i>172</i>	<i>1, 2</i>	<i>19</i>	-	<i>10</i>
5-	2.31×10^{11}	111	1, 2	13	-	10
1+	1.57×10^{11}	347	1, 2	16	10	6
2+	1.84×10^{11}	339	1, 2	16	10	7
3+	1.91×10^{11}	335	1, 2	16	10	5
4+	<i>2.14×10^{11}</i>	<i>333</i>	<i>1, 2</i>	<i>16</i>	<i>10</i>	<i>19</i>
5+	3.23×10^{11}	303	1, 2	14	10	6
6+	3.50×10^{11}	296	1, 2	14	10	7
7+	3.57×10^{11}	293	1, 2	14	10	5

Note: Best compromised solutions 4- and 4+ are in bold italics. From Chang et al. (2012).

Best Compromised Solution

The optimal solutions represent the best combination of systems' cost and carbon footprints for the projected future water demand at the 10% uncertainty bounds. To find the best compromised solutions for all three sets of future water demands, the two objective functions are normalized for Z_1 and Z_2 in the same scale between 0 and 1. The normalized objective functions (NZ_1 and NZ_2) are given by:

$$NZ_1 = \frac{Z_1 - Z_1^{\min}}{Z_1^{\max} - Z_1^{\min}} \quad (2.30)$$

$$NZ_2 = \frac{Z_2 - Z_2^{\min}}{Z_2^{\max} - Z_2^{\min}} \quad (2.31)$$

The normalized solution space for optimal water infrastructure solutions is shown in Figure 2-46. By the normalization, the best solution can be found by the distance to an imaginable solution of zero cost and zero carbon emission or the origin (0,0) in Figure 2-46. A

widely accepted definition of such distance is based on Minkowski's L_a metrics (Zeleny, 1973), where $1 \leq a \leq \infty$.

$$L_a = \left[\sum_{i=1}^2 w_i (NZ_i)^a \right]^{1/a} \quad (2.32)$$

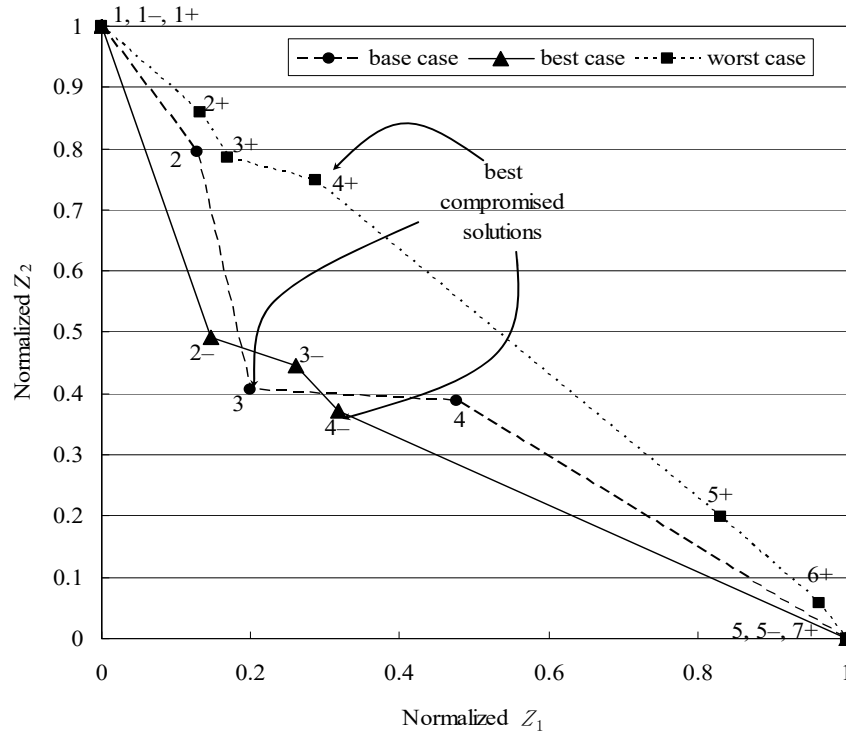


Figure 2-46 Pareto solution fronts for the best compromised solutions to meet the projected future water demand (base case) and the demand with 10% uncertainties (best case and worst case). From Chang et al. (2012).

For water managers, $a = 1$ means equal weighing for both objectives; $a = 2$ implies a weighted geometric distance between the solution (NZ_1, NZ_2) to the ideal solution $(0, 0)$; and $a = \infty$ implies minimization of the maximum NZ_i when L_a is to be minimized. The parameters in the Manatee County case study were set at $a = 2$ and $w_1 = w_2 = 1$, for an illustration. Using these assumptions, the best compromised solutions are:

- For the projected water demand, the best compromised solution #3 would cost \$2 million or 0.8% more than the next less expensive option. The $CO_{2,eq}$ emissions would decrease by 27.1%.
- For the best case with lower future water demand, the best solution #4+ would cost more by 55% or \$61 million than the next less expensive option. It would result in a 54% reduction in $CO_{2,eq}$ emissions.
- For the worst case of 10% higher future water demand, the best solution #4- would increase the cost by \$30 million or 9.9% more than the next less expensive option. The carbon emissions reduction would be 33.9%.

Decision support in master planning

It is noteworthy that the Pareto front is not continuous because practical water engineering solutions are discrete. The trade-offs of the best discrete alternatives, as described above and in Tables 2-20 and 2-21, present a quantitative basis for managers to use for decision-making. The co-benefits and compromise among emission reduction, cost saving, and engineering feasibility are obvious when adaptive planning is considered for water infrastructure expansion.

Based on the optimization results, Figure 2-47 shows the optimal facility expansion strategies for each of the five-year implementation periods. Both the cost and carbon emissions are considered with the following conclusions:

- In the base case and the best case, the current water supply would be self-sufficient in the first five-year period. The modeling results indicate that if water demand is higher than the forecast, extra water resources would be needed. Then the MARS-I and MARS-II projects could provide sufficient water supplies to meet the demand until 2025.
- According to Chang et al. (2012), the need for and the nature of optimal expansion strategies in this time-period are sensitive to the forecasted water demand. The regional water option offers larger water supply capacity and, at relatively lower unit costs, than other alternatives. It could be needed in the worst case. In the best case, however, regional water supply options could be avoided due to their relatively larger carbon footprints due to the long-distance water transfer. Other alternatives available within the Manatee County could provide better performance to satisfy both objectives, and therefore could be used as a contingency.
- Water demand is anticipated to increase further starting from 2026. The modeling results indicate a variety of expansion strategies available for selection. In all cases, the water use permit alternative (e.g. alternative #10) would be always preferred due to its zero-carbon footprint, or energy neutral, and low unit cost. Not coincidentally it was considered as a priority in the county's master planning.
- For the worst case in future water demand, MARS-I and MARS-II would be still the most desirable alternatives by 2016 (Figure 2-47). Regional supply alternatives would be cost-effective compared to other alternatives except for the MARS projects. They may not represent the most favorable solution in carbon emissions, because of necessary facility expansion/construction and long-distance water transfer. Instead, Dona Bay/Cow Pen Slough Restoration Option B (alternative #16) could be selected as a compromised solution. It has the lowest carbon emission impacts among all the regional alternatives.

Worth noting, there are several limitations in this analysis. These include uncertainties surrounding water pricing, a discount of the potential to receive SWFWMD funding, and thus arbitrarily higher unit costs, among the others. Their impacts on the determined optimal solutions were not evaluated.

5. System-Scale Adaptation for Existing Urban Water Infrastructure

As shown in Figure 2-6, urban planning is one major element in infrastructure adaptation. Urban-scale adaptive planning of water and transportation infrastructure has the potential to generate adaptation co-benefits and improve the urban performance and resilience against the

impact of hydroclimatic and land use changes. Examples of co-benefit potential were examined in preceding Section 4.0. The next step is adaptation at local system-scales. This critical adaptation step is focused on specific water systems and infrastructure components (Figure 2-2) in the engineering steps (construction and operation) after master planning (Figure 2-6).

One key element of system-scale adaptation is to define the limit of adaptation actions. Felgenhauer and Webster (2013) defined the adaptation limit as the point beyond which adaptation's economic return is diminished and a paradigm shift is necessary. To determine this threshold, engineering assessments with an accurate technical basis are necessary to evaluate adaptation potentials and their feasibility. When necessary, additional rounds of planning-engineering-adaptation may be conducted in periodic planning revisions.

Here in Section 5.0, these topics and basic considerations for adaptation are detailed in terms of the system-scale engineering approach. The concept of the capacity reserve (*CR*) (Yang, 2016; Levine et al., 2016) is introduced in the analysis of the threshold to define adaptation engineering needs and limitations. Other contents are withdrawn from publications of this research (Yang and Goodrich, 2014; Yang, 2010, 2016). In the subsequent Sections 6.0 and 7.0, case studies will be used to illustrate the engineering approach for *CR* improvement in drinking water treatment and distribution. Associated adaptation tools will be described.

5.1. Basic considerations in adaptation engineering

5.1.1. Adaptation engineering for water infrastructure

Engineering design and implementation for adaptation of existing infrastructure can be broken down into stages of (1) system assessment of adaptation feasibility, (2) adaptation design and implementation, and (3) effectiveness monitoring and adaptation update. These adaptation elements are schematically shown in Figure 2-48 in the context of existing water planning and engineering processes.

The first step is to understand the capacity of existing water infrastructure and its resilience against the impacts of projected hydroclimatic and land use changes. The process, marked as Stage “1” in Figure 2-48, follows the traditional water infrastructure planning. Before the step is the quantification of projected global changes to assess the needed improvement or renovation of existing infrastructure (see Stage “0” in Figure 2-48). The capacity assessment of the existing structure is commonly known as the “bottom-up” approach. The purpose is to evaluate the design capacity and remaining capacity reserve of water infrastructure and then determine the threshold beyond which the water infrastructure service would be compromised. An example of this “bottom-up” approach is taken by the EPA’s Climate Resilience Evaluation and Assessment Tool (CREAT)⁷. In Section 5.3.2, the CREAT tool and its applications will be discussed.

Adaptation engineering takes place in Stage “2” (Figure 2-48). This second stage is focused on the improvement of the system’s *CR* by adapting and improving the existing water infrastructure. New infrastructure or system revitalization often requires a substantial initial capital investment. Thus, common management practice is to first improve the resilience of existing infrastructure through capacity improvement before new capital projects for new

⁷ <http://water.epa.gov/infrastructure/watersecurity/climate/creat.cfm>

infrastructure or systems. This management consideration is also shared in urban transportation infrastructure management. Nevertheless, as described in Sections 3.0 and 4.0, scenario analysis for transportation and water infrastructure offers a practical means to identify the most cost-effective options; mostly by capacity improvement rather than new construction.

By considering climate as a variable, the adaptive planning and engineering approach deviates from the traditional water infrastructure practice (Figure 2-48). Hydroclimatic variables important to water infrastructure services include the rate of precipitation change, changes in watershed hydrologic variables such as runoff properties, and water quality changes. Precipitation IDF, and ambient and water temperature are the most fundamental hydrologic parameters. All of them are currently assumed to be constant in hydrological design (Figure 2-48); for example, in the Atlas-14 IDF design charts (Bonnin et al., 2006, 2011). Small rates of change and hydrological uncertainties can be managed by using engineering safety factors, a traditional way to manage engineering uncertainty.

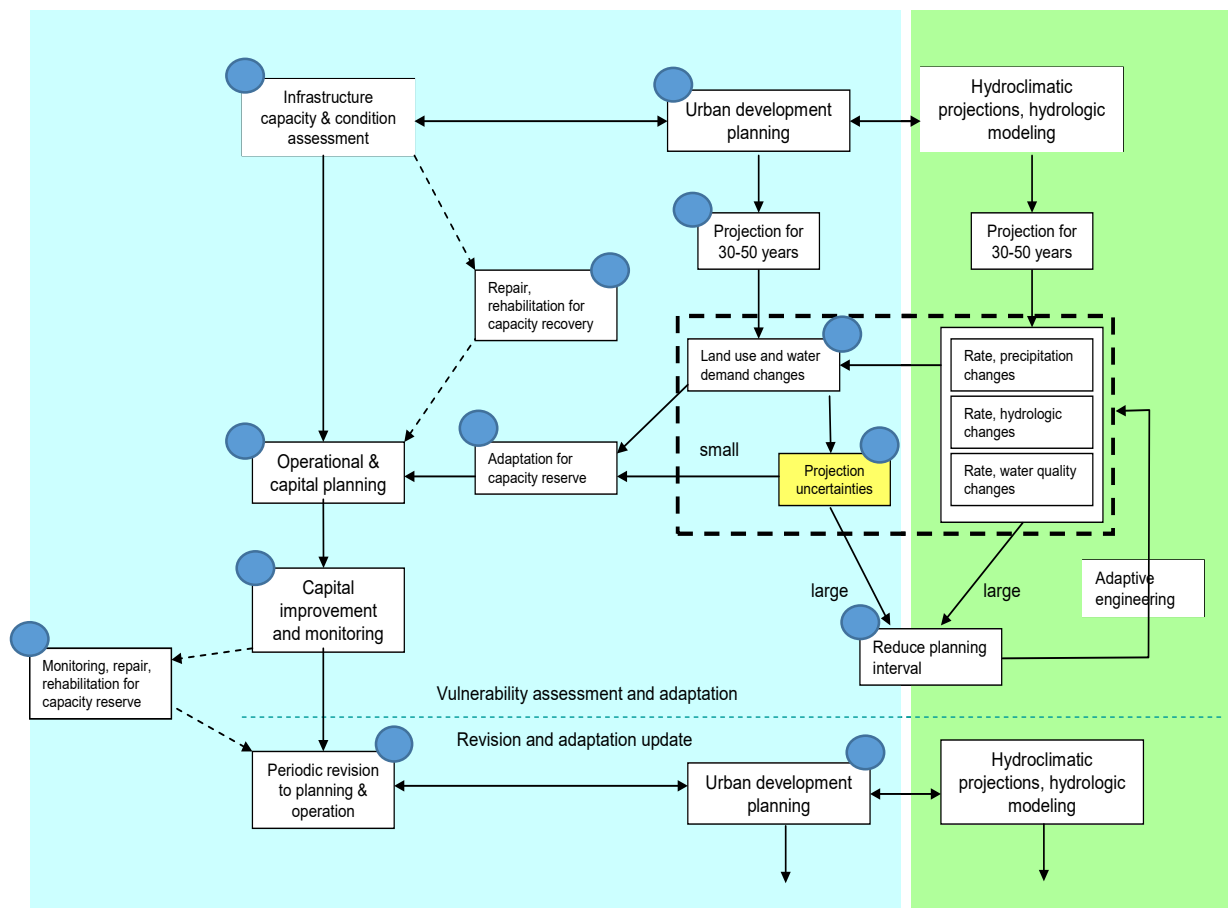


Figure 2-48 Assessment-adaptation process for water infrastructure planning and engineering. The box in dashed line contains the elements of climate and land use projections in infrastructure master planning. Arrows indicate process direction. Numbered labels indicate the stages of engineering analysis (See text for explanation).

Planning time horizons, normally as long as 30-50 years, is comparable to the time in which change in hydroclimatic conditions may materialize. Potential implications to water infrastructure and water programs were discussed in U.S.EPA (2015a). A large rate in hydroclimatic changes may invalidate the current design basis for existing infrastructure, prompting the development of a proper design basis for adaptation (Yang and Goodrich, 2014; Yang et al., 2017). However, the current model projections of future climate and land use often have substantial degrees of uncertainty (Miller and Yates, 2006; IPCC, 2014, 2007) due to error promulgation from multiple sources (Hosseinzadehtalaei et al., 2017). The risk of projection uncertainty is also compounded by other decision factors such as capital investment. Because the uncertainty is likely to decrease time, flexibility in infrastructure design and program implementation is important to properly manage the climate uncertainties (Fletcher et al., 2017). One approach is the iterative adaptive approach outlined earlier in Figure 2-1. For water infrastructure, this iterative process and associated adaptation strategy are detailed in Figure 2-48 for water systems engineering. This approach can lead to better management of climate risk and adaptation economics. Case studies are provided for illustration in subsequent Section 6.0-7.0.

5.1.2. Adaptation attributes of three types of water infrastructure

Existing water infrastructure has a large physical footprint that is difficult to change, without large capital investment. Over the past century, water infrastructure was designed and constructed mostly underground for anticipated population growth and land use changes to meet the water needs, while climate and precipitation regimes were assumed to be stationary (see Figure 2-48). The properties of this infrastructure and its urban service functions, developed under the stationarity assumption, can severely limit adaptation approaches and engineering options.

Three principal types of water infrastructure are prevalent in the U.S.: wastewater collection and treatment, drinking water treatment and distribution, stormwater collection and management (Figure 2-49). While the service function varies geographically and differs among types of water infrastructure, general engineering and management principles follow a triple bottom line of management objectives: protection of public health, safety and welfare; system reliability; and engineering economics. In this specific context, the drinking water treatment and distribution in the U.S. are designed to meet regulatory compliance with drinking water quality standards and to provide an uninterrupted water supply. Centralized wastewater systems serve to collect wastewater from individual users, transfer it to a location for treatment and subsequent discharge into a water body under a regulatory permit while minimizing public health risks and exposure. Onsite small wastewater systems and decentralized wastewater management are the alternative systems serving small communities and individual households (U.S. EPA, 2002); they are not discussed here because, by their very nature, they are not used generally in dense urban communities. Additionally, stormwater infrastructure has been constructed on a massive scale to provide drainage, sanitation, and flood control in an urban catchment area, primarily to protect public infrastructure and private property. In the U.S. Northeast and the Great Lakes region, stormwater and wastewater networks often share the same pipe networks in a combined sewer system (CSS). Combined sewer overflows (CSOs) occur during high-intensity precipitation, causing untreated or partially treated wastewater to be by-passed of the treatment plants for discharge at CSO outfalls. The result is pollution in the receiving water bodies (U.S. EPA, 2001, 2008, 2009a; Weinstein, 2009; Capodaglio, 2004).

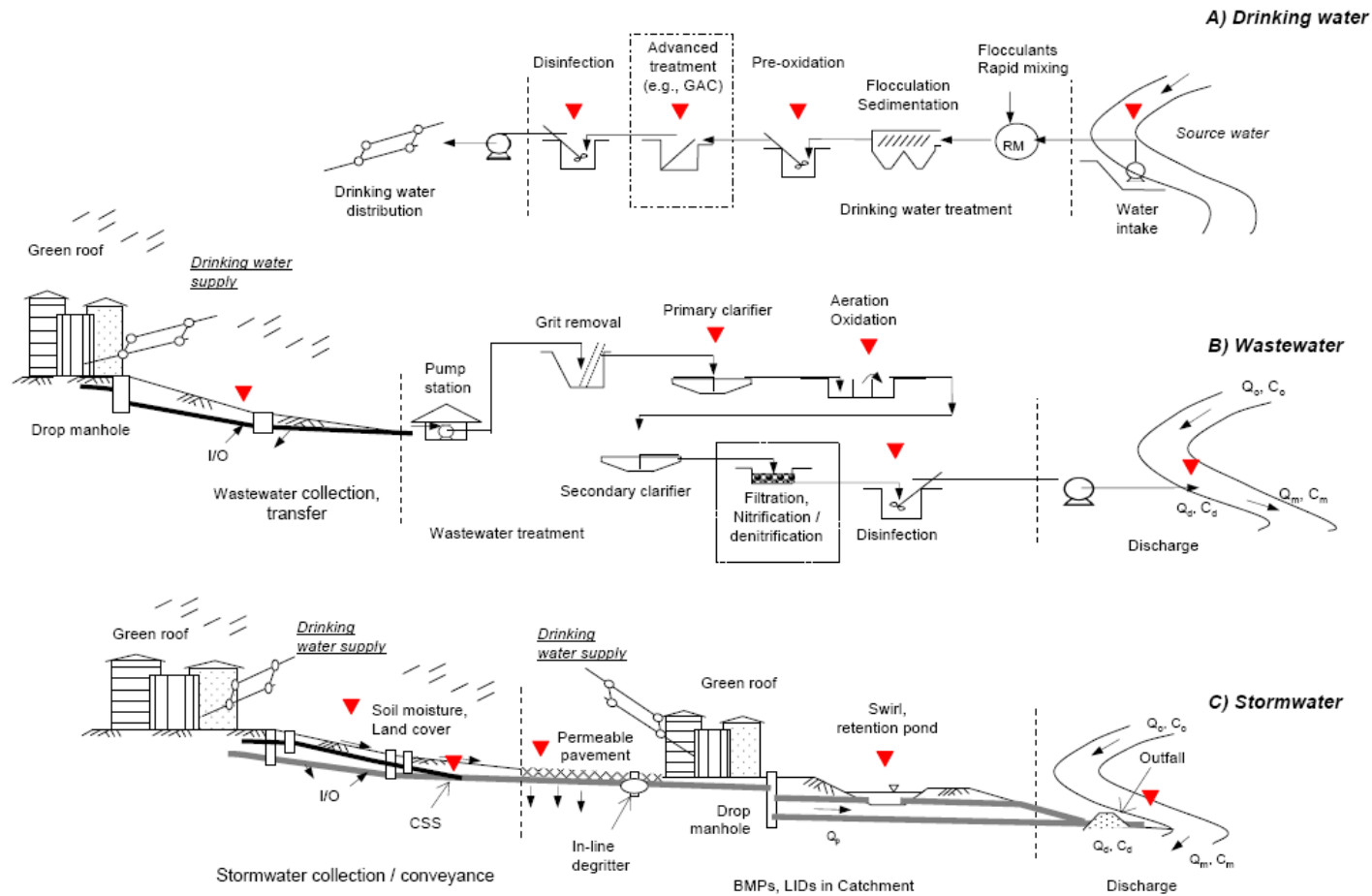


Figure 2-49 Process schematic diagrams for typical centralized drinking water, wastewater, and stormwater infrastructure in an urban watershed. Combined sewer system (CSS), stormwater, and wastewater treatment effluent discharges (Q_d, C_d) are regulated for stream flow (Q_o) and pollutant concentration before and after the discharge point (C_o and C_m). Solid arrow indicates water flow directions. I/O is water inflow and outflow in the buried pipes through infiltration and exfiltration. Solid triangle indicates a process unit potentially vulnerable to future precipitation and hydroclimatic changes. From Yang (2016).

In the urban water cycle of water-wastewater-stormwater, extreme precipitation impacts on surface urban watersheds can potentially make several infrastructure components vulnerable to failure, i.e., unable to provide desired service functions. These vulnerable locations are marked in Figure 2-49. The nature of the vulnerability is explained in Tables 2-22 and 2-23. Further technical discussions for each are presented subsequently in the aspect of infrastructure *CR*.

5.1.3. The capacity reserve concept and climate resilience

The sustainability of water infrastructure is shown in its resilience and adaptability to a changing environment. Resilience is defined here as the ability for a system to recover its physical state and service functions after an external impact (Milman and Short, 2008; McDaniels et al., 2008). Capacity reserve (*CR*) is an important physical attribute that quantifies the resilience as discussed extensively in sustainability science literature (Tillman et al., 2005, 1998; Dominguez and Gujer, 2006; Yang, 2016). Some (e.g., Oh et al., 2005; Chen et al., 2008) have discussed *CR* in the context of urban carrying capacity.

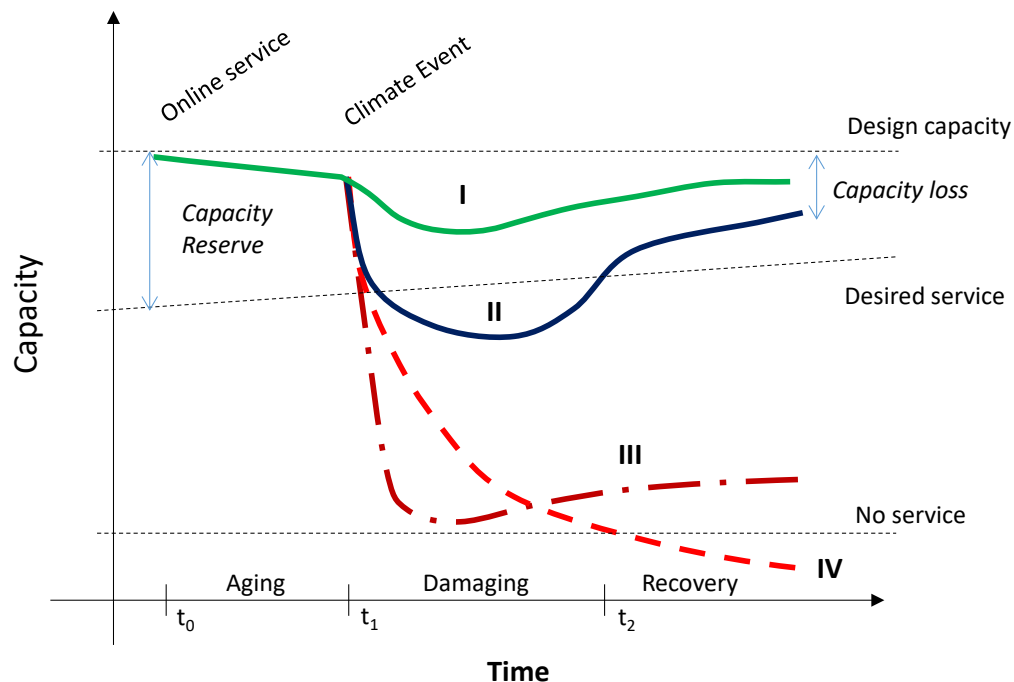


Figure 2-50 Four types of infrastructure vulnerability under the threat of external impact event (e.g., storm surge). In all cases, capacity reserve is the capacity difference between the minimum service required and the design capacity. See text for more explanations. From Yang (2016) and Levine et al. (2016).

The *CR* concept has long been used in civil, structural and process engineering, referring to extra capacity or flexibility for assurance of desired structural integrity or performance (e.g., Tillman et al., 2005; Matos et al., 2013). A commonly used term is the margin of safety or safety factor in design. The system resilience in *CR* is measured by the ability of a water system to provide a service level above the desired level of service. In engineering, one ultimate goal is to balance *CR*, the risk of failure, and adaptation cost. Note that the risk of failure of water

infrastructure is the overarching concern. This is why significant redundancy or *CR* is often built into these systems. Similar social, environmental, and economic objectives, known as the “triple-bottom-line,” apply to hydroclimatic adaptation in general (Cromwell III et al., 2007).

Figure 2-50 schematically shows the *CR* concept and its relationship with infrastructure resilience. The installed *CR* is a parameter to quantitatively measure the vulnerability threshold from which the ecological system resilience concept of Marshall and Toffel (2005) is modified for infrastructure adaptation analysis. For capital-intensive water infrastructure, at the core of adaptation is the ability to increase its resilience for unanticipated changes and to build-in adequate flexibility for control of the uncertainty-related risk. This capacity is shown for the scenario I and II upon an external impact from hydroclimatic or other environmental changes (Figure 3-51). Scenario II represents the temporary vulnerability of the infrastructure “out-of-service” below the desired capacity. This condition in urban water supply and sanitation happened in an increasing frequency in the past decade; examples include the impacts of the 2012 Hurricane Sandy in New York City and the adjacent coastal states, the droughts in Florida during the 2000s, flooding in Houston in 2017 from Hurricane Harvey, and the ongoing droughts and wildfires in California. After such hydroclimatic disruptions, some urban water infrastructure may not recover to the original design capacity. The difference is capacity loss (Figure 2-50), requiring management attention.

In contrast, the Types III and IV changes in infrastructure service are not fully recoverable (Figure 2-50). The impact at t_1 results in permanent impairment of the infrastructure service functions, while Type IV leads to the failure of water services, a condition that water managers strive to avoid. In both cases, the infrastructure service functions are significantly impaired in their ability to provide the desired service. A service recovery requires capital investment for rebuilding at a significant cost or a paradigm shift to avoid future recurrence of such service disruptions. Examples of these potential scenarios include the damage by coastal hurricanes, storm surge, sea level rise and periodic inundation (Comfort, 2006; Turnipseed et al., 2007; Gesch, 2005; Wing et al., 2002), impacts from water pollution resulting from a climate event (e.g., Wing et al., 2002; Cann et al., 2013), as well as preventative measures taken for adaptation and mitigation (e.g., Rosenzweig et al., 2007). In the 2012 Hurricane Sandy, boil water advisories were issued to a large number of customers and local health agencies, during and after the disruptive event⁸.

Significant functional damage to water infrastructure in Type III and IV situations needs attention in “no-regret” adaptation. It requires adaptation planning because of the long-lasting effects. While conventional rebuilding and reconstruction are often effective measures, long-term sustainability has been discussed to avoid repeated system failures. Examples of adaptation include water supply and sanitation paradigm changes (Gleick, 2000; Pahl-Wostl, 2007), urban system re-planning, and avoidance of disaster areas (Bull-Kamanga, et al., 2003; Godschalk, 2003; Comfort, 2006), and coordination with urban-scale or region-scale water management. In urban-scale adaptive planning, the urban resiliency is analyzed through a systematic analysis of land use, population distribution, in which water infrastructure improvement can be made in conjunction with transportation infrastructure. Examples of these adaptive planning were discussed in preceding sections 2.0 and 3.0.

⁸ <https://www.health.ny.gov/environmental/emergency/weather/hurricane/>

One further complication in the systems analysis is the evolving nature of urban management objectives. The required service capacity $f(t)$ often varies with time. The $f(t)$ increases with urban population and economic activities while decreasing as water conservation takes place. This places a challenge on adaptation engineering. When the CR limit is exceeded, the water structure functions are compromised (Figure 2-50) with partial or complete loss of service capacity (Type III and IV). Then the central question is how to take necessary and proactive adaptation measures and to minimize or avoid the hydroclimatic impacts that lead to Type II, III, and IV changes. This subject is discussed below.

5.1.4. *CR and engineering practice*

Engineering practices use different approaches to define and use CR for various water infrastructure. More details will be provided in Section 5.2. In current engineering practice, accurate determination of the design variables is emphasized to minimize the uncertainty and ensures adequate system capacity at a reasonable cost for a margin of safety or safety factor. By doing so water managers can minimize the excess capacity that could later become stranded (unused) capacity for economic considerations, or on the opposite side avoid the lack of capacity for intended services. For many water managers, engineering such systems commonly assumes stationarity whereby the climate and hydrological design parameters can be specified with appreciable degrees of “perceived” certainty, for which CR is then often defined as a constant. Progressive refinement of design basis and engineering objective is widely used to minimize uncertainty and thus the system costs.

This traditional engineering practice is challenged for non-stationary climate and hydrological variables. Because failure is so judiciously avoided, excess capacity is common in the water industry, in the form of redundant systems. The large uncertainties in consideration of a non-stationary climate would ensure excessive, if not prohibitive, capital and operational cost. The alternative approach is to use adaptive engineering, by which the modification of water infrastructure CR is planned, but not installed until the uncertainty is adequately reduced. One pre-requisite for this adaptive approach is the general modeling-monitoring framework shown in Figure 2-1 and, specifically, for water system engineering in Figure 2-48.

Several widely used engineering practices have a potential for the adaptive engineering, such as modular design and phased construction (Girard and Mortimer, 2006; Chung et al., 2009), decentralized water supply, wastewater and stormwater management (Weinstein, 2009; Gikas and Tchobanoglous, 2009), as well as model-driven water reservoir operations for river flow management under changing hydroclimatic conditions. For existing water infrastructure, adaptation potential can be pre-installed during retrofitting, realignment, and expansion of existing infrastructure assets, process optimization, as well as operational changes. All of these adaptation techniques may require substantial physical asset alteration which may be reasonably managed as a part of the renovation and replacement of aging infrastructure. The consideration of the adaptation can be necessary under the following three conditions:

- The infrastructure planning horizon is long, for which future precipitation, land use, and population changes are not precisely determined. Only by using this timeline can one evaluate whether the rate of hydroclimatic change is too small to be “tangible” for adaptation, or too excessive for the infrastructure to adapt at a reasonable cost. In this report, the adaptation need analysis is set for the next 30-50 years;

- The rate of precipitation change is larger than assumed in the original engineering design, or the rate is comparable to those of the other two non-stationary variables – population and land use changes;
- Large uncertainty in precipitation projection is translated and further propagated into infrastructure engineering parameters, affecting the *CR* determination. The uncertainty is also time-dependent, decreasing over time as the climate (precipitation) projection improves.

Similarity and differences among the three engineering approaches are summarized in Table 2-19. The engineering methods and techniques are different in improving the infrastructure *CR* and performance of the existing water infrastructure. They are further described below for each of the three major water infrastructure types.

5.2. Water infrastructure capacity reserve and resilience

5.2.1. Stormwater infrastructure functions and design tolerances

Stormwater, drinking water, and wastewater infrastructure in an urban catchment are schematically shown in Figure 2-49. Stormwater infrastructure manages overland runoff and channel flows. Its major components, service functions, and likely vulnerability to precipitation change are listed in Table 2-20. In a nonstationary climate, future runoff time-flow (t - Q) variations can significantly differ from that of the original engineering basis. This difference affects the designed hydraulic conveyance capacity of a built stormwater network. The difference can also adversely affect the hydraulic and water quality design functions of low-impact-development (LID) and stormwater control measures (SCMs)⁹ in urban stormwater management.

5.2.1.1. Realized hydraulic capacity reserve

Carrying capacity and hydraulic profiles of a stormwater network are designed to limit the nominal pipe flow to a range of 0.6-4.6 m/sec. This design criterion is intended to prevent excessive sedimentation in the conveyance pipes or erosive damage to the pipe and receiving water bodies. For a fixed topography, the runoff t - Q profile in a stormwater pipe depends on the precipitation intensity, pre-storm soil moisture content, vegetation cover, and land-use patterns. Among these factors, precipitation intensity and soil moisture are climate-dependent. Design precipitation intensity at a given return interval (e.g., 10-year design storm) is commonly determined from categorized IDF charts such as NOAA precipitation Atlas 14 (Bonin et al., 2006, 2011), National Weather Bureau Technical Paper 40 (Hershfield, 1961), and the SCS 24-hour rainfall curves (Guo and Hargadin, 2009). These current methods are all based on assumed precipitation stationarity.

Hydraulic *CR* of a stormwater pipe is realized from two primary sources. Because of the stochastic hydrologic process and the uncertainties in hydrologic parameters, a large empirical safety factor around 1.5–2.0 is often used in hydraulic design. For example, Schaad et al. (2009) described an approach of using large safety factors in hydraulic engineering of a holistically managed stormwater system. The other primary source of hydraulic *CR* comes from the fact that stormwater pipes are available only at fixed nominal diameters, and that a minimum diameter

⁹ <https://www.nap.edu/catalog/12465/urban-stormwater-management-in-the-united-states>

Table 2-19. Water infrastructure design and engineering domains, and their attributes.

	Deterministic Engineering Domain (1)		Adaptation Engineering Domain (2)		Re-design & Re-construction Domain (3)	
	Attribute	Potential action*	Attribute	Potential action*	Attribute	Potential action*
<u>New Infrastructure</u>						
Hydraulic capacity	Specific value	Process adjustment and retrofitting; No large-scale asset modification; Go to Domain (2) or (3) in severe CR limitation	Range; capacity adaptively installed	Assessment-adaptation-monitoring for optimal cost-benefit balance; Go to Option (3) for severe CR limitation	Specific value	Optimization, retrofitting; Management and objective re-evaluation
Engineering flexibility	Limited in quantity. Realized at construction		Flexible timing for extra capacity installation			
Water quality capacity**	Specified value		Range; capacity adaptively installed			
Engineering flexibility	Limited in quantity. Realized at construction		Flexible timing for extra capacity installation			
<u>Techniques and examples</u>						
Stormwater infrastructure	Hydraulic design using runoff rational methods for facilities (e.g., retention ponds and storm sewer)	Satellite retention facilities; Slice gate automation; Go to Domain (2) or (3) in severe CR limitation	Structure, stormwater control design for non-stationary precipitations; Module design, phased installation; System monitoring and forecasting	Adaptive capacity installation; Go to Domain (3) for severe CR limitation	New infrastructure network with or without use of existing assets	Optimization, retrofitting; Management and objective re-evaluation.
Wastewater infrastructure	Ten-State design standards, other design protocols	Process automation; Flow detention facility; Go to Domain (2) or (3) in severe CR limitation.	Module design, phased installation; Decentralized wastewater system; Onsite wastewater reuse; System monitoring and forecasting.	Adaptive capacity installation; Go to Domain (3) for severe CR limitation	New designs and use of revolutionary technologies and concepts	
Drinking water infrastructure	Unit process and system modeling and specifications (e.g., disinfection chamber)	Disinfectant, dosage change; Go to Domain (2) or (3) in severe CR limitation	System optimization, retrofitting; Module design, phased installation; System monitoring and forecasting.	Network expansion; Adaptive capacity installation; Go to Domain (3) for severe CR limitation	New designs and use of revolutionary technologies	
References	ASCE (2004), Lin (2001), USEPA (1994; 2002a; 2008), Salvato et al. (2008), engineering codes and guidelines		Carter and Jackson (2007); Chung et al. (2009); Semadeni-Davies et al. (2008); Gikas and Tchobanoglous, (2009); Oron et al., (2007), Gupta and Shrivastava (2006), and USEPA (2009b)		Chang et al., 2006; Neuman (2009); Neuman and Smith (2010).	

Table 2-19 continued.

	Deterministic Engineering Domain (1)		Adaptation Engineering Domain (2)		Re-design & Re-construction Domain (3)	
	Attribute	Potential action*	Attribute	Potential action*	Attribute	Potential action*
<u>Existing Infrastructure</u>						
Hydraulic capacity	Fixed	Infrastructure optimization, retrofitting; Go to Domain (2) or (3) for severe CR limitation	Range of values	Iterative assessment-adaptation-monitoring for optimal cost-benefit ratio; Go to Domain (3) for severe CR limitation	Specific value	Optimization, retrofitting; Management and objective re-evaluation
Engineering flexibility	Limited, and deteriorated after construction		Large, adaptively installed		Large CR expansion after re-construction	
Water quality capacity**	Fixed		Range of values		Specified value	
Engineering flexibility	Limited and deteriorated after construction		Large, adaptively installed		Large CR expansion after re-construction	
<u>Techniques and examples</u>						
Stormwater infrastructure	Operation and maintenance	CSO division adjustment; Go to Domain (2) or (3) for CR expansion	Urban SCMs including GI designed for non-stationary precipitation; Structure retrofitting; Recursive monitoring-adaptation-assessment	Adaptive CR installation (new infrastructure); Go to Domain (3) for severe CR limitation	New infrastructure network with or without use of existing assets	Optimization, retrofitting; Management and objective re-evaluation.
Wastewater infrastructure		Operational adjustment for CR increase; Process optimization without large asset change; Go to Domain (2) or (3) for severe CR limitation	Model-based system design and upgrading; Adaptive system retrofitting and improvement; Recursive monitoring-adaptation-assessment	Adaptive CR installation (new infrastructure); Go to Domain (3) for severe CR limitation	Application of new and revolutionary technologies	
Drinking water infrastructure		Operational adjustment for CR increase; Process optimization without large asset change; Go to Domain (2) or (3) for severe CR limitation	System optimization; Process retrofitting without large asset alteration; Recursive monitoring-adaptation-assessment	Adaptive CR installation; Network expansion; Go to Domain (3) for severe CR limitation.	Application of new and revolutionary technology; New infrastructure expansion for CR	
References		ASCE/AWWA (2004), USEPA (2004), engineering codes and guidelines	Chung et al. (2009), Gikas and Tchobanoglous (2009), Montalto et al. (2007); and Donofrio et al. (2009).		Chang et al., 2006; Neuman (2009); Neuman and Smith (2010).	

Note: * - Potential actions at the upper limits of infrastructure CR and flexibility.
 ** - Refers to the capacity of a water infrastructure in maintaining performance on specific water quality criteria.

Table 2-20. Important engineering attributes for stormwater infrastructure adaptation

Unit Operation	Function	Major Design Criteria*		Vulnerability **			Adaptation	
		Physical	Chemical, biological	Physical damage	Hydraulic Function	Water Quality Function	Function	Example
<u>Stormwater collection</u>								
Stormwater collection	Stormwater runoff collection in urban area for reliable drainage and sanitation	Drain inlet spacing <183 m; Manhole spacing: 122-183 m (varied with pipe diameter); 25-year design storm (varied)	Prevent methane and sewer gas generation; Remove oil and grease, debris and large objects.	Likely medium	Likely high	Likely low	Stormwater ponding, urban flooding, and drainage management.	Stormwater inlet design for non-stationary precipitation.
Stormwater gravity drain and conveyance	Stormwater transfer by pipe network to discharge locations or retention facilities	I/O design limit in per day -km-cm; Flow velocity: 0.6-4.6 m/s for gravity sewer	Prevent methane and sewer gas generation	Likely medium	Likely high	Likely low	Infiltration / exfiltration (I/O) management; Pipe flow velocity control	Pipe repair, I/O management; Drop manhole alignment for new Q-t profiles; In-line degritter for debris
<u>Stormwater control measures #</u>								
Hydraulic retention	Increased water retention in urban catchment basin for reduced peak flows	Varies, based on assumed precipitation stationarity		Varied	Likely high	Varied	Increased retention function for non-stationary precipitation	Detention pond, stormwater swirl, and permeable pavements
Stormwater treatment ponds and bioretention facilities	Enhanced water quality improvement within an urban catchment		Performance design for target pollutant removal.	Varied	Varied	Likely high	Enhanced water quality improvement within an urban catchment	Distributed stormwater retention and treatment ponds
Groundwater recharge or evapotranspiration	Diverting water from the urban catchment and channel flows			Varied	Likely low	Likely low	Reduced stormwater channel flow and discharge	Permeable pavement, green roof, recharge sewer.
Stormwater reclamation	Reclamation and reuse of stormwater diverted from channel flows		Contaminant prevention for source water in reclamation	Varied	Likely high	Likely high	Collection and treatment of stormwater for beneficial reuse	Cisterns, rain barrels, rain gardens
<u>CSS and CSO control</u>								
Stormwater diversion	Prevent hydraulic overloading of wastewater treatment plant in high-intensity precipitations	Flow rate and water level for diversion valves in CSS; Water level control in CSO retention facilities.		Likely low	Likely high	Likely high	Reduce CSO impacts to both wastewater treatment plants and discharge receiving water	System engineering of retention and CSO treatment facilities; Extreme precipitation forecasting and emergency responses.
Discharge at stormwater outfalls	Stormwater discharge into a water body under a NPDES permit	Flow rate and discharge velocity	Varied in water quality parameters	Likely low	Likely medium	Likely medium	Reduce discharge impacts on receiving water in erosion, temperature, turbidity, nutrients and other pollutants.	Discharge swirl and detention; Sensor-based monitoring-controlled discharge

Note: * Summarized from civil engineering manuals and U.S. engineering codes and guidelines. These design criteria are for general guidance.

** - Qualitative rating for anticipated major changes in precipitation and hydrology, excluding the extreme meteorological events.

- Stormwater control measures are organized in the four groups by primary functions.

(typically 15 inches) is often required. This means that the hydraulic carrying capacity (Q_2) of installed pipe with a diameter (d_2) can be greater than the design peak flows (Q_1) for a pipe diameter (d_{min}). The maximum increase for the installed carrying capacity $\left(\frac{Q_2 - Q_1}{Q_1}\right)$ is:

$$\frac{Q_2 - Q_1}{Q_1} = \left(\frac{d_{min}}{d_2}\right)^{\frac{2}{3}} - 1 \quad (2.33)$$

For storm pipe mains larger than 0.60 m (24 in) in diameter, this engineering practice potentially offers a hydraulic CR of 31% on average while satisfying the design criteria on pipe flow velocity. This design consideration is shown in Figure 2-51. In this simple envelope calculation, $\Delta Q\%$ is calculated using Eq.2.33 for pipes at a hydraulic slope (S) of 0.2% and 0.5%. Pipe flow velocity (V) in a range of 0.6-4.6 m/sec by engineering standards, is calculated using Manning's equation. The maximum capacity increase is approximately 60% for lateral pipes of diameter <0.61 m (24-in). Therefore, combining with a safety factor of 1.5-2.0, the pipe engineering practice could have installed a maximum hydraulic capacity up to 230% of the design value.

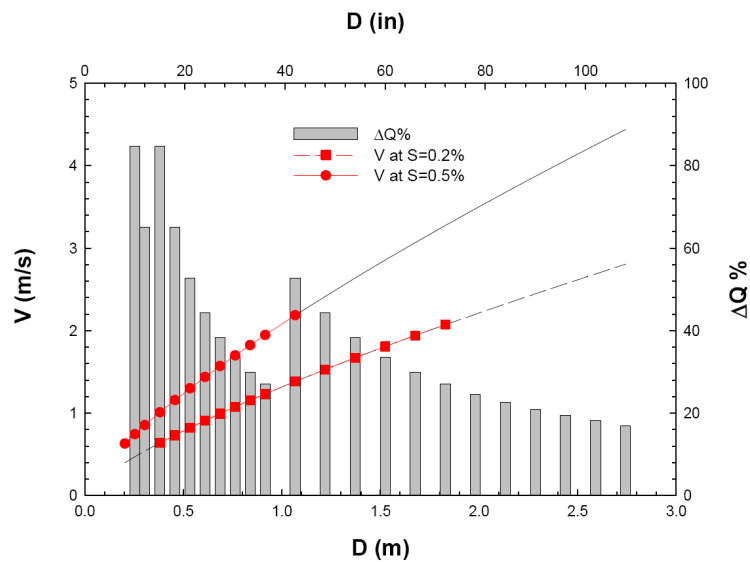


Figure 2-51 Maximum percentage increase ($\Delta Q\%$) in hydraulic capacity of stormwater conveyance using commercial concrete pipes of discrete nominal diameters (D). Eq. 2.33 is used for the calculations.

Of course, one reason for doing this is that the stormwater pipes often contain sand and other material building up on the bottom since the flows are often not continuous. The pipe sedimentation reduces the capacity of the pipe and this the available CR.

5.2.1.2. Water quality limitations

Climate-driven water quality changes can significantly limit the infrastructure CR in stormwater adaptation. Studies (e.g., Horowitz, 2009; Whitehead et al., 2009; Yang et al., 2002) have linked the intensity of peak runoff to the increased turbidity, and higher metals, chemical, and dissolved organic carbon loading in urban streams. Peak pipe flow and high discharge velocities are also found to be responsible for soil erosion, water quality change, and ecological deterioration at stormwater outfalls and their immediate downstream segments (see McCorquodale, 2007; Novotny and Witte, 1997). These hydrologic and water quality changes

can be attenuated or amplified within an urban catchment of higher paved ground surfaces (Table 2-20).

Combined sewer overflow (CSO) events during intense precipitation in many U.S. communities are a major factor limiting infrastructure *CR* otherwise available for adaptation. Stormwater runoff and untreated, but diluted, sewage are diverted for discharge when stormwater flows exceed the hydraulic capacity of the wastewater treatment plants and available retention facilities. The peak flow, on the other hand, is a function of the precipitation duration and intensity, catchment basin hydrograph, and the groundwater infiltration rate into the pipes (Black and Endreny, 2006; Lai, 2008; and Diaz-Fierros et al., 2002). More intense precipitation events projected as future climate conditions will likely yield greater peak flows and more frequent CSO events unless efforts are undertaken to separate flows (U.S. EPA, 2009a, 1994; Capodaglio, 2004; Alp and Melching, 2009). The EPA 20-watershed study (U.S. EPA, 2013b) showed significant hydrological flow modifications across the U.S. that can worsen the CSO occurrence (Johnson et al., 2015).

Land use and the degree of impervious surface in the urban watersheds can amplify hydrological responses to future climate-related precipitation changes, often in the form of increasing peak flows and runoff. On the other side, stormwater control measures including the LIDs are used for enhanced stormwater retention and reduced peak runoff. They are often engineered assuming precipitation stationarity (e.g., Lai, 2008; Montalto et al., 2007; U.S. EPA, 2004a; Marsalek and Chocat, 2002; Dietz, 2007; Carter and Jackson, 2007; and Gilroy and McCuen, 2009). Thus, the stormwater control measures are vulnerable under a non-stationary climate (Table 2-20). For example, Semadeni-Davies et al. (2008) and Sun et al. (2016) suggested the need to consider climate and precipitation changes in stormwater structure designs.

The U.S. EPA's National Stormwater Calculator estimates and evaluates SCMs applicability in reducing stormwater runoff (U.S. EPA, 2014). While the tool includes precipitation projections under future climate scenarios, a comprehensive nationwide evaluation has not been completed. With this data not yet available, the maximum *CR* of 230% of the design value was taken as the upper limit for stormwater infrastructure.

5.2.2. Drinking water infrastructure functions and design tolerances

5.2.2.1. Engineering resilience in a distribution network

Community water systems in the U.S. provided water supplies to over 292 million people in 2008. Engineering attributes of major community water system components and their potential vulnerability to precipitation changes are shown in Table 2-21. Drinking water distribution following the treatment (Figure 2-49) is engineered to meet water demand for both domestic consumption and firefighting throughout a service area. Long-term water demand variations, a prime engineering factor in water distribution design and operation, are linked to demographic and land use changes, urban microclimate, and the transformation of water-intensive industries (Levin et al., 2002; Pires, 2003; Hummel and Lux, 2006). Such water demand changes are commonly captured in urban development master plans and regional economic development projections (see Figure 2-48) that may have intrinsically included hydraulic capacity reserve adequate for adaptation.

Water quality changes within a distribution system have been extensively studied. However, little is known about the water quality change in pipes under future climate and

hydrological conditions. In a study of climate adaptation for a large U.S. Midwest utility, Li et al. (2009, 2014) and Clark et al. (2009) reported that an increased total organic carbon (TOC) level in (surface) source waters under future climate scenarios could lead to higher TOC concentrations in produced water and subsequently greater disinfection by-product (DBP) formation even at levels in violation of the U.S. drinking water standards. This type of potential water quality effect can significantly reduce the available infrastructure *CR*, making adaptation necessary. In Table 2-20, a variety of adaptation options are listed for changes in unit process, such as enhanced TOC removal using GAC or chemical flocculation (e.g., Järvinen et al., 1991; Crozes et al., 1995; Li et al., 2009; and Clark et al., 2009), water age reduction and chlorine addition optimization for DBP control (Carrico and Singer, 2009; Prasad et al., 2004; Boccelli et al., 2003). In addition, higher surface water and associated drinking water temperatures likely in future climate will change the disinfection kinetics, DBP formation rates, and biological stability in a distribution system. These areas of indirect hydroclimatic impacts are worthy of further investigations.

5.2.2.2. *Realized capacity reserve in drinking water treatment*

Water intake and water treatment are vulnerable to the direct impacts of precipitation changes (Table 2-21). Detailed modeling-monitoring studies have shown the degree of these impacts in surface water bodies of different sizes across the U.S. (e.g., U.S. EPA, 2013b; Chang et al., 2006, 2014a,b; Neil et al., 2019; Imen et al., 2016). The impacts vary among watersheds, different types of land use and land cover, as well as the nature of precipitation and temperature changes. A resilient water treatment process is required to accommodate these source water variations and to provide finished drinking water in compliance with the SDWA regulations.

As shown in Figure 2-49, a typical surface water treatment process in the U.S. consists of pre-oxidation, rapid mixing, flocculation and sedimentation, granular filtration, advanced treatment if necessary [e.g., GAC filtration, membrane separation], and finally disinfection in clear wells before distribution to consumers. In the design of these treatment process units, a simple empirical safety factor of 1.2-1.5 is often used; some larger values are possible. For example, Kim and Bae (2007) proposed a safety factor of 2.0 in the hydraulic design of a baffled GAC contactor for odor control. More advanced probability-based methods are now developed for systematic reliability- cost tradeoff evaluation. Boccelli et al. (2007) described process optimization guided by a cost-performance ratio to determine safety factors in the flow rate design of an infiltration-based surface water treatment plant. Gupta and Shrivastava (2006) introduced a water treatment design method using Monte-Carlo simulation to quantify performance uncertainties in suspended solids removal. Li et al. (2009) developed a Monte Carlo methodology to simulate the cost-probability relationship in GAC contactor process modification.

While these advanced design methods better quantify the capacity and cost cumulative density function (CDF) curves, they often require extensive input data and computation. Instead, the traditional safety factor method is widely used in field engineering of the deterministic domain. This practice alone yields a maximum treatment capacity at 150% of the design value to permit redundancy when units are out of service. For impacts exceeding the *CR* limits, adaptation is needed to increase infrastructure *CR*, mostly through treatment plant retrofitting, process modification, change of unit operations, or installation of a new process (Table 2-21).

An engineering adaptation example is given by Li et al. (2014; 2009) and Clark et al. (2009). These investigations led to the development of the adaptation engineering model “Water

Table 2-21. Important engineering attributes and likely vulnerability in drinking water treatment and distribution systems for community water supplies.

Unit Operation	Function	Major Design Criteria*		Vulnerability **			Adaptation	
		Physical	Chemical, biological	Physical	Hydraulic Function	Water Quality Function	Function	Example
Source water protection								
Source water intake	Protect source water quality at water intake Assure water availability for drinking water production	Water level at water intake	Minimize daily and seasonal water quality variations;	Likely	Likely	Likely	Adaptive change of intake elevation and location;	Multi-elevation intake aprons
		Intake security against physical damage	Minimize biological growth at intake (e.g., mussel).	High	Medium	Medium	Physical damage protections	Enhanced structure supports
Drinking water treatment								
Rapid mixing	Rapid dispersion of coagulants in water	<1 min retention time		Likely Low	Likely Low	Likely Low		
Coagulation & Flocculation	TOC and particulate removal	15-20 min and 18-25 min residence time for high-energy and low-energy flocculation.	Varied dosage among coagulants: alum, chlorine, polymer, and potassium permanganate	Likely Low	Likely Low	Likely High	Inflow TOC variations monitoring and chemical dosing control.	Sensor-based TOC monitoring and process adaptive control
Clarification	Remove settleable solids after flocculation. Alternative unit processing by membrane and particulate filtrations	32.6-48.9 m ³ /d/m ² for turbidity removal 20.4-32.6 m ³ /d/m ² for algae removal		Likely Low	Likely Medium	Likely Medium	Reduce high-turbidity effect on downstream units; Remove excessive algae present in raw water.	Process monitoring and control; Unit process optimization
Dissolved air floatation (DFA)	Remove solids and odor with ascending fine bubbles	10-12 m/h air flow; 5-10% recycle flow.	Follow coagulation / flocculation unit process	Likely Low	Likely Low	Likely Low	Adjust particle surface charge for enhanced DFA	Unit process optimization
High rate filtration	Remove various constituents, including turbidity, coliform, color, taste, metals, and toxic chemicals	hydraulic loading: 83 L/m ² min (rapid sand) Backwash monitoring and operation.		Likely Low	Likely Medium	Likely Medium	Reduce shock loading of high turbidity; Optimize backwash scheduling, operation.	Process monitoring and control
Oxidation and disinfection	Biological inactivation and oxidation of organic matters		Disinfectant concentration limit: 1.0 mg/L Cl ⁻ ; Contact time	Likely Low	Likely Low	Likely High	Reduce TOC concentration and variations; Unit process optimization.	Retrofitting for higher contact efficiency; Change of oxidants.
Ion exchange	Cation or anion exchange to remove nitrate, Fe, Mn, and hardness	Service flow rate: <668 L/m ³ for N ² removal; Backwash rate: 81-122 L/m ² for N ² removal		Likely Low	Likely Low	Likely Medium	Remove excess turbidity in pretreatment; Process unit arrangement, optimization, retrofitting.	Process adjustment; Enhanced water pretreatment; Process monitoring
Membrane filtration	Remove organic and inorganic contaminants by using membranes	Hydraulic loading rate; Temperature; Suspended solids.	Inflow pH range; Membrane anti-degradation; Biological growth.	Likely Low	Likely Low	Likely Low	Pretreatment to remove excessive turbidity; Backwash operations.	Pretreatment with coarse membrane filter; Back-wash automation
GAC adsorption	Absorb chemicals onto absorbent media	10-12 m/h loading; Bed depth and volume.	Regeneration time; DOC, odor, and other contaminant removal.	Likely Low	Likely Low	Likely High	Increase GAC adsorption efficiency and prevent break-through	Adjust GAC regeneration cycle; Operation optimization.

Table 2-21 continued.

Major Operation Unit	Function	Design Criteria*		Vulnerability **			Adaptive Engineering and Management	
		Physical	Chemical, biological	Physical	Hydraulic Function	Water Quality Function	Functions	Example
Treatment process	Overall specification of each process unit for treatment objectives	Process flow rate; Flow variations.	Drinking water treatment guidelines Drinking water quality standards.	Likely Low	Likely Medium	Likely High	Increase treatment capacity reserve for new source water variations and water demand changes	Process optimization, retrofitting, or change and expansion
<u>Drinking water distribution</u>								
Water demand	Spatial and temporal demand variation affect network operation and water age	Not applicable	Not applicable	Not Applicable	Likely High	Likely High	Water demand management under high temperature and heat stress of future climate	Water pricing, lawn irrigation timing and management
Pipe network	A network of pipes in different diameters and materials to deliver water from treatment plant to consumer's tap	Pressure management: 413 kpa (241-689 kpa) Flow velocity: 1.2-1.8 m/s in mains.	Corrosion protection; Water age management; Water quality standard compliance at user's tap.	Likely High	Likely Low	Likely High	Prevent pipe corrosion and leaks under future climate; Water quality management;	In-network water treatment such as chlorine addition and THM stripping.

Note: * Summarized from ASCE/AWWA (2004), Lin (2001), Salvato et al. (2008).

** - Qualitative rating given for major changes in precipitation and hydrology, excluding the extreme meteorological events.

Treatment Plant – Climate Adaptation Model” or WTP-cam. The model and its application at the Greater Cincinnati Water Work’s Miller WTP will be described in Section 6.0.

5.2.3. Wastewater infrastructure functions and design tolerances

5.2.3.1. Realized capacity reserve in hydraulic loading

Important engineering functions and physical attributes for wastewater infrastructure are shown in Table 2-22. A general wastewater treatment process in the U.S. includes physiochemical pretreatment, biological oxidation of macronutrients (primarily biological oxygen demand [BOD], N and P), possible filtration to reduce suspended solids, optional tertiary treatment (N and P removal), and finally effluent disinfection before discharge (see Figure 2-49). Hydraulic loading capacity is often specified for future wastewater generation within a service area and to account for groundwater infiltration into wastewater collection pipes (Lai, 2008; Lin, 2001). These variables are lumped into a single parameter – wastewater generation rate per capita in engineering designs [e.g., 1900-4550 lpd/person (500-1200 gpd/person)]. In addition, an empirical safety factor of 1.2-4 is used to accommodate unexpected hydraulic variations (peak flows). Values up to 4.0 are justified for special engineering conditions, such as complex hydrogeological regions, aged water collection networks with extensive infiltration and exfiltration, very small service areas, or service areas of the large variation in wastewater generation rates.

5.2.3.2. Realized capacity reserve in biological systems

Space-demanding aerobic and anaerobic biological treatment is often a limiting unit process that determines available *CR* at a wastewater treatment plant. Most wastewater plants have significant *CR* to permit unit operations to be taken out of service for maintenance due to the corrosive environment in which they operate. Since the early study of Kincannon and Gaudy (1966), biological wastewater treatment is known for its sensitivity to both hydraulic and contaminant shock loading (Jing et al., 2009; Chen et al., 2008), leading to treatment process upset (Ray and Peters, 2008; Capodaglio, 2004) and performance deterioration (O’Reilly et al., 2009). Other causes for reduced treatment capacity include aging treatment equipment and wastewater infrastructure, poor process control, and operational inefficiencies.

Here the limitation and vulnerability are illustrated in the design or retrofitting of an aeration tank, a principal unit in the activated sludge wastewater treatment process. BOD removal rate (η_{BOD}) in an aeration basin/clarifier combination, or the ratio of tank influent (C_o) and effluent (C) is a function of flow rate (Q), tank volume (V), BOD oxidation rate (K_d), biomass cell age (θ_c), microorganism concentration in the tank (X), waste rate, and maximum yield coefficient (Y). Following Lin (2001), the removal rate can be written as:

$$\eta_{BOD} = \frac{c_o - c}{c_o} = \frac{\theta_c X V}{(1 + k_d \theta_c) Y c_o} \frac{1}{Q} \quad (2.34)$$

An increase in wastewater flow rate reduces hydraulic retention time and decreases the BOD removal rate (Figure 2-52). This likely occurrence under future climate conditions may occur due to more frequent hydraulic overloading responding to the increased variability of

Table 2-22. Important engineering attributes and potential vulnerability of wastewater infrastructure

Major Operation Unit	Function	Major Design Criteria*		Vulnerability**			Adaptation	
		Physical	Chemical, biological	Physical	Hydraulic Function	Water Quality Function	Function	Example
Wastewater collection								
Wastewater collection	Wastewater collection from all users in a service area	WW yield: 0.38 m ³ /person-day; Flow velocity: 0.6-4.6 m/s; Flow rate: 1.5 m ³ /person-day (laterals and branches)	Sulfur and methane gases generation	Likely High	Likely High	Likely Low	Pipe I/O flow management; Wastewater reuse and separation.	Pipe leak detection; Dual pipe system; Onsite wastewater treatment
Wastewater pumping and conveyance	Wastewater transfer to a central location(s) for treatment	I/O rate: < 0.45 m ³ /day-km-cm; Flow: 0.95 m ³ /ca-day (main); Flow velocity: 0.6-4.6 m/s	Sulfur and methane sewer gas management; Fire hazard prevention.	Likely High	Likely High	Likely Low	I/O management; Flow velocity & abrasive damage control.	Pipe leak detection Drop manholes; In-line degritter
Wastewater treatment								
Preliminary treatment (screening, degritting)	Solids and debris removal in headworks	Screen debris removal: >5.1-cm Flow (grit chamber): ~0.328 m/s; Aerated grit chamber: 2-5 min residence time	Not applicable	Likely Low	Likely Low	Likely Low		
Primary treatment - Sedimentation tank	Removal of settleable solids and 25-35% BOD	Peak flow <0.71 lps/m ² ; Maximum weir load: 2.16 lps/m; Water depth: >2.1m.	Target removal rates: BOD: 20-40%, TSS: 35-65%; Settleable biosolids: 50-75%.	Likely Low	Likely Medium	Likely Medium	Flow equalization facilities to smooth flow variations; Process monitoring	Monitoring and increased maintenance
Secondary treatment - Trickling filters	Biological treatment to remove BOD and macronutrients	Filter depth: 1.5 - 3.0 m; Hydraulic loading: 0.012 - 0.047 lps/m ² , or 0.047- 0.47 lps/m ² (high rate).	Normal: 0.08 - 0.40 kg BOD/m ³ -day; High-rate: 0.48 - 1.44 kg BOD/m ³ -day.	Likely Low	Likely High	Likely High	Process control for resilience in shock loading Process flow stabilization	Trickling filter retrofitting; Change recirculation ratios; Process monitoring and control for weir loading.
Secondary treatment - Activated sludge process	High efficiency of BOD and nutrient removal	Weir loading: 1.44 lps/m; Hydraulic loading: 0.47-0.57 lps/m ² 0.38 lps/m ² with nitrification	Maximum BOD loading: 0.24-0.64 kg/day/m ³ ; Aeration rate: 93.5-125 m ³ oxygen / kg BOD	Likely Low	Likely High	Likely High	Process control for resilience in shock loading Increase treatment capacity reserve.	Modify cell age and sludge return rate; Improve aeration efficiency; Increase aeration capacity.
Secondary and final clarifier	Settleable biosolid removal	Surface settling rate: 50-62 lps/m ²	Not applicable	Likely Low	Likely Low	Likely Low	Enhance biomass setting	Operational adjustment
Nitrogen removal	Successive nitrification and denitrification	Varies. See U.S. EPA (2009b).	Varies. See U.S. EPA (2009b).	Likely Low	Likely Low	Likely High		
Chlorination	Treatment effluent disinfection	> 15 min contact time in chlorination contact basin	<200 fecal coliform / 100 ml	Likely Low	Likely Low	Likely Low		
Treatment process	Overall specifications of each process unit for treatment objectives	Process flow rate; Flow rate variance.	Surface water quality standards for discharge control	Likely Low	Likely Medium	Likely High	Increase treatment capacity reserve to against source water variations and water demand changes	Process optimization, retrofitting, or change and expansion
Wastewater effluent discharge								
Treatment effluent discharge	Treatment effluent discharge under a permit	Varies depending on discharge regulations	Varies depending on discharge regulations	Likely Low	Likely Medium	Likely High	Discharge limits sensitive to the impacts on receiving streams; Compliance to discharge limits.	Adjust treatment process for likely to-be-revised discharge limits.

Note: * Summarized from "10-state" wastewater treatment standards and Lin (2001). These design criteria are for general guidance.

** - Qualitative rating given for major changes in precipitation and hydrology, excluding the extreme meteorological events.

I/O - wastewater inflow and outflow by infiltration and exfiltration; WW - wastewater.

precipitation. An increase in the flow is a likely sign of such overloads. These events are responsible for the treatment process upsets and discharge violations (e.g., Tafuri and Selvakumar, 2002). Efforts to split combined systems and seal the piping at the surface are appropriate adaptation measures to address this problem. Other potential adaptation actions are listed in Table 2-22.

Capacity reserve in biological treatment is recognized by using an empirical design safety factor of commonly 1.2–1.3, and by modifying unit operations without large physical asset alteration (Table 2-22). In addition, the treatment *CR* is also made available through the optimization of the biological process. One operational adjustment, for example, is to increase the capacity by changing biomass cell age, aeration rate and efficiency. When cell residence age and aeration rates are adjusted for higher aeration capacity $\left(\frac{V}{\Psi g}\right)$ from 2.27 to 2.83, the BOD removal rate is increased theoretically by 56.9%, or $A_1 \rightarrow A_2$ and $B_1 \rightarrow B_2$ (Figure 2-52).

For a treatment plant of 100 m³/day design capacity, a 166% increase in flow rate can potentially decrease the BOD removal rate from 75.5% to 45.5%. This decrease from A_0 to A_1 is illustrated in Figure 2-52. Similarly, treatment efficiency decreases from A_0 to B_1 as a result of increased BOD concentration and mass loading into a plant. An increase in flow and BOD mass loading reduces the BOD removal rate from starting position A_0 to A_1 and B_1 , respectively. In process adaptation, aeration capacity adjustment from 2.27 to 2.83 can partially recover the lost performance, or B_1 to B_2 and from A_1 to A_2 in Figure 2-52. Labels 30, 50, and 70 mg/L are plant inflow BOD concentrations. This is a partial recovery of the capacity loss due to the future increase in flow rate and BOD mass loading. These are many engineering measures currently available in the market to make these aeration changes.

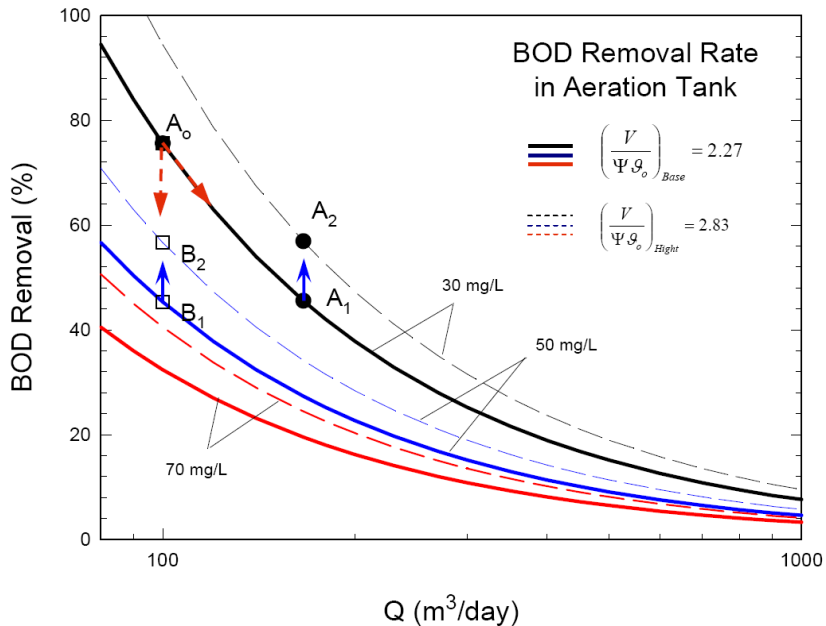


Figure 2-52 BOD removal efficiency of a wastewater activated aeration tank as a function of flow, BOD mass loading, and aeration capacity.

By a combination of using design safety factors and operational adjustments, the total realized *CR* could reach 30-80% of the design value in an activated sludge process. In *CR* evaluation, however, one should also consider performance deterioration over time for aging wastewater treatment facilities. This portion of the treatment *CR* is recoverable by process monitoring, control and adjustment, or by using advanced engineering techniques such as fuzzy logic control (e.g., Müller et al., 1997; Peng et al., 2007). The analysis here assumes that the performance reduction is minimized through process adjustment and optimization. Thus, the realized *CR* of 30-80% design value is considered as a reasonable estimate.

5.2.3.3. The *CR* efficacy in current system design

Based on the analysis in Sections 5.2.1.-5.2.3., Figure 2-53 schematically shows a general range of percent *CR* installed in the current infrastructure engineering. The adaptation need can be seen by comparing the installed *CR* against the rates of precipitation change in the contiguous U.S. The change in precipitation can result in changes in watershed hydrology, including both stream flow and water quality. It is assumed that the rate of precipitation change in the next 50 years is proportionally translated into hydraulic design parameters (e.g., runoff).

In the integrated watershed simulation of future climate and land use change, the investigations over three watersheds in Ohio and Nevada (Tong et al., 2012; Sun et al., 2013; Fu et al., 2018) showed similar degrees of change in stream flow and water quality. For example, in the Little Miami River watershed, 20% precipitation increase or decrease in 2050 would result in a 43.83% increase and 53.08% decrease in stream flow, respectively. The total phosphorus

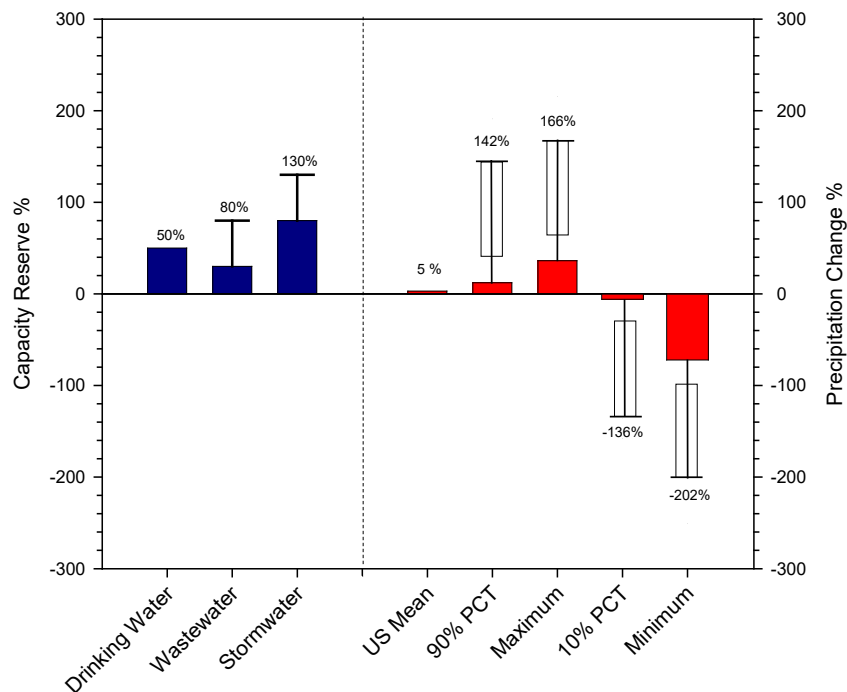


Figure 2-53 Relative magnitude of infrastructure *CR* installed in current engineering practice (left) in comparison with the relative precipitation change (solid bar) and its uncertainty (pattern and solid line with whisker) by 2060. PCT – percentile. From Yang (2016).

increases in both cases by 21.35% and 6.73%. Total nitrogen concentrations change by a smaller amount <11.55% and 3.97% respectively. Thus, the hydroclimatic impacts on watershed hydrology would likely be in the same order of magnitude as precipitation changes. This generalization is also reported by numerous climate model simulations.

On the national average, the precipitation change is notably smaller almost by an order of magnitude in some places (Rajagopalan and Lall, 1998; and IPCC, 2014). In a nationwide analysis, this research analyzed the likely precipitation changes recorded in long-term historical measurements. The average and range for approximately 1100 weather stations in the U.S. are shown in Figure 2-53. Along with the average (U.S. Mean) are 90% and 10% percentiles, the maximum and minimum, and their associated uncertainties. In comparison, the infrastructure *CR* installed by current engineering practice is a magnitude of order larger than the national average rate of 5% for precipitation changes in the next 50 years (Figure 2-53).

However, the change of extremes with the projection uncertainties far exceeds the *CR*% in current practice. Therefore, the adaptation is very likely needed in places with extreme precipitations. This relatively simple evaluation has two noteworthy implications:

- As a national average, the future precipitation changes of ~5% by 2060 can likely be managed by the installed *CR* in existing infrastructure. This generalized conclusion supports the current engineering practice that has been applied worldwide for decades. However, the national average cannot represent all local conditions because of uneven changes across geographic areas (IPCC, 2007; Rajagopalan and Lall, 1989; and this study).
- The second implication is important to adaptation at the local watershed levels. Climate stations with precipitation increase in the 90% percentile are spatially clustered in many areas such as the eastern Texas-Oklahoma region. For areas in Arizona and New Mexico, precipitation decrease in the <10% percentile is compounded by the high rate of population growth. The combined effect makes water availability the dominant adaptation factor for these regions. Thus, the degree of these vulnerabilities is a focus of infrastructure assessments in the location-specific analysis. There are “bottom-up” analysis tools available, one of which will be described subsequently in Section 5.3.2.

5.3. Water infrastructure vulnerability analysis for adaptation

5.3.1. *The resilience assessment and two approaches*

In a bottom-up approach, the climate vulnerability of water infrastructure is assessed to determine the *CR* threshold. Below the threshold, the water infrastructure service function is impaired either in the short- or long-term. The result is a basis to determine infrastructure resilience against specific impacts of hydroclimatic and land use changes.

The U.S. water utilities have taken both top-down and bottom-up approaches in the threshold analyses (e.g., Miller and Yates, 2006; Freas et al., 2008; Stratus Consulting and MWH Global, 2009). Most utility water managers who are engaged in climate vulnerability analysis have a strong technical understanding of their water systems, including local hydrology, historical operating conditions, and standard operational practices, but have little access to climate model projections tailored to their specific regions. Interestingly, the U.S. EPA conducted a review of 50 water utilities nation-wide in 2010 on their analysis methodology.

Among them, eight utilities had conducted their climate vulnerability analysis, and only two followed the bottom-up approach (Table 2-23).

Table 2-23 Types and approaches of eight water utilities in climate vulnerability assessment*.

Utility	Service Provided			Vulnerability Assessment
	Type	Population	State	
East Bay Municipal Utility District (EBMUD)	Water, Wastewater	1.3 million	CA	Bottom-up
City of Boulder Utilities Division	Water, Wastewater	113,000	CO	Top-down
Denver Water	Water	1.3 million	CO	Top-down
Massachusetts Water Resources Authority	Water, Wastewater	2.2 million	MA	Top-down
New York City Department of Environmental Protection (NYCDEP)	Water, Wastewater	9.2 million	NY	Top-down
Portland Water Bureau	Water	860,000	OR	Top-down
San Antonio Water System (SAWS)	Water, Wastewater	1 million	TX	Bottom-up
Seattle Public Utilities	Water	1.35 million	WA	Top-down

Note: * - according to a U.S. EPA 2010 study (see U.S. EPA, 2015a)

The bottom-up approach generally includes a component to quantify the likely vulnerability and identify the most vulnerable critical assets in the water systems. For example, the East Bay Municipal Utility District (EBMUD), a water and wastewater utility in the Greater Oakland, CA area, used an approach adopted from the AwwaRF (now the Water Research Foundation) publication “*Climate Change and Water Resources: A Primer for Municipal Water Providers*” (Miller and Yates, 2006). The EBMUD analysis consists of several steps:

- Identify the vulnerability of potential portfolio components (e.g., new reservoirs, expanded reservoir storage, increased conservation, conjunctive use, water reclamation, desalination, inter-basin transfers) and screen those components for technical, environmental, and economic feasibility in adaptation;
- Develop alternate portfolios of multiple components that could meet projected demands (e.g., increased conservation and conjunctive use, or water reclamation and inter-basin transfers).
- Conduct a preliminary portfolio analysis using a combination of the Water Evaluation and Planning (WEAP) system model and the district’s EBMUDsim model – known

collectively as the “W-E model.” Portfolios that performed poorly under current hydrological conditions were eliminated. The remaining portfolios were subjected to detailed analyses under anticipated climate conditions using the W-E model.

- Identify portfolios with adaptation potentials and use sensitivity analysis to evaluate critical vulnerabilities and ways to address the vulnerabilities.

The San Antonio Water System (SAWS) in western Texas, serving a population similar in size to EBMUD, also used a bottom-up approach. This threshold approach identifies system components that are dependent on the status of climate variables (precipitation, temperature, etc.) and the overall system risk under the future hydroclimatic conditions. The preliminary risk assessment is also based on the professional judgment of experts who know the system and the planning area (see U.S. EPA, 2015a, and reference therein). The qualitative or semi-quantitative analysis consisted of:

- identifying the climate variables of importance and exploring the sensitivity of SAWS to these variables;
- determining water system responses to a range of potential future climate conditions;
- assessing the vulnerability of SAWS to hydroclimatic impacts;
- assessing system performance according to the uncertainty associated with hydroclimatic factors driving SAWS vulnerability;
- evaluating overall system risk and identifying areas in need of further analysis.

5.3.2. *Water resilience evaluation and resilience tool – CREAT*

A systematic examination is considered a necessary process in evaluating the threshold for adaptation. While many utilities take various approaches according to their own needs, a systematic process for vulnerability analysis has emerged from the U.S. EPA’s Climate Ready Water Utilities (CRWU) program¹⁰. The program conducted case studies and vulnerability analysis at participating facilities. These actions led to the establishment of an adaptive response framework (U.S. EPA, 2012b), and the publication of Climate Resilience Evaluation and Awareness Tool (CREAT) Version 2.0.

CREAT is a software tool that guides users through a series of investigative steps (Figure 2-54). CREAT Version 3.0 is the most recent software available. As a stand-alone risk assessment product, CREAT allows users to assess potential impacts of future climate on their utility and to evaluate adaptation options to address those impacts. It follows a structured approach with the threat analysis leading to the adaptation actions. Major features are:

- A library of drinking water and wastewater utility assets (e.g., water resources, treatment plants, reservoirs, distribution system components, pump stations) for one-by-one evaluation of hydroclimatic impacts
- A list of hydroclimatic impacts (e.g., sea-level rise, precipitation changes, reduced snow pack) covering a broad range of future conditions that potentially affect water utilities

¹⁰ <http://water.epa.gov/infrastructure/watersecurity/climate/index.cfm>

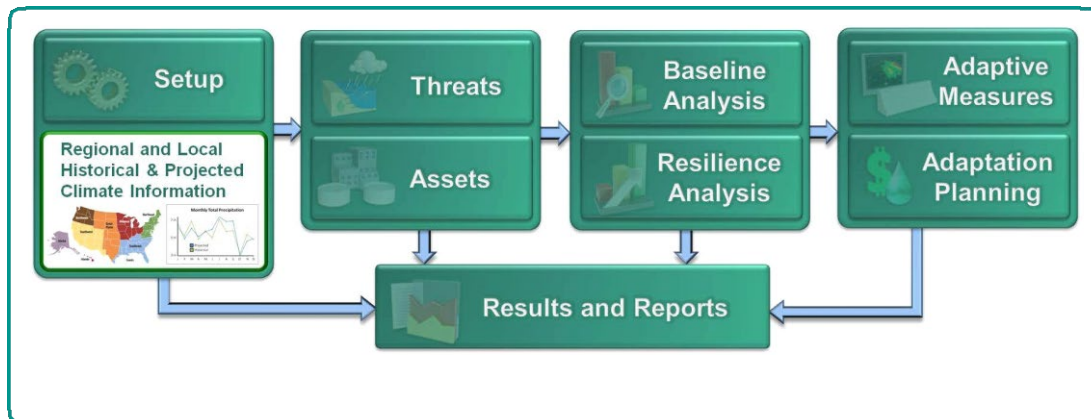


Figure 2-54 The process of climate change vulnerability analysis using the EPA tool CREAT. Adopted from EPA CRWU website.

- Adaptation suggestions that can be implemented to adapt to the hydroclimatic impacts that can be customized by the user
- A series of risk-reduction cost reports that will allow the user to evaluate various adaptation options

Water sector utility owners and operators can use information about their utility in CREAT to identify climate and hydrological threats, assess potential consequences, and evaluate adaptation options. This approach allows utilities to assess impacts and identify the thresholds where asset or mission failure could occur. Users can also consider existing climate science data to evaluate the plausibility of climate-related impacts and how soon these impacts may affect the utility. CREAT has been applied to many case studies in the contiguous U.S. A few examples of the case studies conducted by the EPA CRWU program include:

New York City Department of Environmental Protection (NYCDEP)

In 2010-2011, a CREAT pilot study was conducted for the NYCDEP water and wastewater systems. The pilot site is located in Corona, New York. Through the study, CREAT was used to assist utilities in making risk management and planning decisions, and to identify areas of potential refinement for the tool before it is finalized for broader use in the water sector. Climate information embedded in CREAT was used to assess the risk and likelihood of climate threats. Through a desk-top exercise and technical data analysis using CREAT, the vulnerability to future hydroclimatic conditions, particularly sea level rise and storm surge, was identified for the district’s water and wastewater assets. In fact, the water and wastewater transfer facilities in low-lying areas identified by CREAT later experienced operational difficulties during Hurricane Sandy in October 2012.

New York/New Jersey Harbor

One of the first CREAT pilot tests was conducted in conjunction with The New York/New Jersey (NY/NJ) Harbor Estuary Program and the North Hudson Sewerage Authority

(NHTSA). The receiving waters for the NHTSA system are part of the NY/NJ Harbor Estuary ecosystem providing critical habitat, recreation and transportation services. The NHTSA system includes 107 miles of combined sewers, 17 combined sewer overflow (CSO) regulators, 11 CSO outfalls, and 6 pump stations. This system serves many communities and is fed by a system of rivers draining five states and flowing through several metropolitan areas. It also serves as an important habitat for over 300 species of migratory birds, spawning ground for several species of fish, and provides recreation and transportation services. In the pilot study, the CREAT tool was used to identify potential future impacts for water utilities and helps the utilities catalog potential actions in adaptation planning. The exercise fostered dialogue among stakeholders that share a common interest in climate resilience.

Manteo and Columbia, North Carolina

Another CREAT pilot testing was conducted with a workgroup comprised of town officials and water managers from Manteo and Columbia, North Carolina, as well as representatives from the Albemarle-Pamlico National Estuary Partnership. The towns of Manteo and Columbia are located in the Albemarle-Pamlico watershed with Manteo along the coast and Columbia on the banks of the Scuppernon River, 40 miles inland to the west. Both towns have suffered damage to natural resources and water-sector infrastructure from heavy precipitation events along with coastal and inland storm surge. A major goal of this exercise was to determine how CREAT can best provide a framework and tool for small communities.

Morro Bay, California

The CREAT pilot study was located on the west coast with representatives from the Morro Bay National Estuary Program, Los Osos Water Purveyors, and contractors. The aim was to identify strategies for the Los Osos Groundwater Basin Management Plan. The Los Osos aquifer system only has one freshwater input and no inter-basin transfers, and thus is very sensitive to nitrate pollution from septic systems, overdraft, and hydroclimatic impacts on precipitation. Morro Bay is located along the central coast of California. Two communities in the area only provide limited wastewater and stormwater infrastructure serving approximately 25,000 residents. Through the desk-top studies, the U.S. Geological Survey's SEAWAT model was added to assess potential changes in groundwater quality due to salt water intrusion and changes in recharge dynamics.

The Ohio River basin case study

The Great Miami River watershed is located in southwestern Ohio and drains an area of 5,300 square miles including portions of fifteen Ohio counties. Principal tributaries to the Great Miami River (170.3 miles in length) include the Stillwater River, the Mad River, and Loramic Creek. The watershed has a population of 1.5 million people and more than 75% of the population resides in the urban areas surrounding Dayton, Cincinnati, Hamilton, and Troy. Approximately 83% of the land within the watershed is used for agriculture, primarily row-crop production of corn, soybeans, and wheat. Typical livestock includes swine, cattle, and poultry. Residential, commercial, and industrial lands account for approximately 12% of land use in the watershed, with the remaining area consisting of forests (4%) and water bodies or wetlands (1%).

Major industries located in the watershed produce automobile parts, chemicals, household goods, paper products, and processed foods and beverages. CREAT was tested for a medium-sized utility (serving approximately 20,000 people) located in the Great Miami River watershed. The results indicate the vulnerability over turbidity and water quality deterioration in flood and related events.

5.3.3. From vulnerability analysis to adaptation engineering

The vulnerability analysis on a water system, combined with climate information derived from the watershed-scale modeling-monitoring framework (Figure 2-1), can provide actionable data to support adaptation engineering. This process is represented by Steps 1, 2, or 4 in Figure 2-1 leading to adaptation design and implementation. In the CREAT process (Figure 2-54), the vulnerability assessment is followed by adaptation planning.

An effective adaptation action may take place in watershed-scale or urban-scale for fundamental changes of an urban system. It can also occur in system scale, aiming to improve the infrastructure's resilience and service functions under future climate and land use conditions. These three levels of adaptation were shown in Figure 2-2 and described in Section 1.2. In the subsequent sections 6.0-8.0, specific adaptation engineering tools and engineering methods for water systems are described with illustrations of case studies:

- Water treatment plant – climate adaptation model (WTP-cam) developed for adaptation analysis of water treatment plants;
- Water distribution adaptation methods to quantify and analyze the risk of elevated disinfection by-products (DBPs) in the distribution system;
- Surface water management to tackle the climate-induced increase of surface runoff in stormwater systems;
- Managed aquifer recharge and water reuse in adaptation to climate-induced water availability problems.

6. SUD Methods and Tools for Drinking Water Treatment

For existing drinking water treatment plants, adaptation engineering involves the probability-based projection of the future source water changes as well as the adaptive engineering of unit processes to accommodate the change. This section describes one major SUD component – the EPA WTP-cam (Water Treatment Plant-Climate Adaptation Model) computer program, and its application for water supply system adaptation at the GCWW Richard Miller Treatment Plant. The description is focused on new features including Monte Carlo analysis, customization of the granular activated carbon (GAC) unit process, and GAC adaptation cost analysis. Much of the content is drawn from publications from this research (Clark et al., 2002, 2009; Li et al., 2009, 2012, 2014; and Levine et al. 2016).

The WTP-cam version 1.0 is based on the climate adaptation models published by Li et al. (2009; 2014) and Clark et al. (2009). The computer program was developed from the Water Treatment Plant (WTP) model that was originally proposed by the U.S. EPA for support of drinking water disinfection rule promulgation (U.S. EPA, 2005). The original WTP model was designed for single case runs with deterministic solutions. In other words, when model inputs are

defined, the model outputs will be a single value for modeled water parameters. More details on the WTP program can be found in Appendix B.

Given the uncertainties in defining hydroclimatic impacts on source water, the WTP model was upgraded to accept stochastic inputs from source water quality through a Monte Carlo simulation. The latest model was renamed to be WTP-cam. WTP-cam also includes features to examine the performance and associated cost of incremental adaptation to the treatment process in response to changing source water quality. At present, the model is only applicable to surface water sources subject to the climate and land use changes. Major features include the ability to:

- Predict natural organic matter (NOM), disinfectant residuals, and DBP concentrations.
- Predict the impact of the water treatment process on water quality parameters affecting disinfectant residual decay and DBP formation.
- Assist utilities in evaluating the possible effects of source water variation and treatment process operations on DBP formation.
- Simulate the impact of uncertainties in raw water qualities through Monte Carlo analysis.
- Design treatment process adaptation and estimate adaptation cost.
- Assist regulatory programs in evaluating adaptation design or new requirements.

6.1. Principle, models and algorithms in WTP-cam

6.1.1. Conventional treatment unit processes

For conventional treatment processes, WTP-cam version 1.0 uses the statistical regression equations in the existing WTP2.0 program. The latter utilizes empirical correlations intended to predict central tendencies in NOM removal, disinfection, and DBP formation for conventional water treatment and GAC adsorption. The user manual in Appendix B (U.S. EPA, 2005) and references therein provide details of these linear regression equations and data used for the unit process analysis. The empirical correlations were established from regressions of water plant treatment data from usually consist of independent variables and empirical constants. Such results are informational to national and regulatory analysis (see Figure 2-10). However, the modeling results may not be accurate predictions for a specific water plant.

Figure 2-55 schematically shows unit processes of a conventional water treatment plant, modeling data needs, and outputs in WTP2.0 as adopted in WTP-cam. The original WTP model uses empirical algorithms to predict TOC and UVA removal, disinfectant chlorine decay, and DBP formation. Underlying modeling algorithms were established from the regression analysis of observed water plant data in the EPA's Information Collection Rule (ICR) database (see Appendix B). For the coagulation-flocculation-filtration unit process, the TOC removal rate (Δ_{TOC}) and UVA removal rate (Δ_{UVA}) in alum ad ferric-based coagulation were derived from ICR data of 39 and 21 plants, respectively. The removal rate is a linear combination of raw water quality ($SUVA_{raw}, TOC_{raw}$) and operating parameters (pH, and coagulant dose):

$$\Delta_{TOC} = f(pH, SUVA_{raw}, TOC_{raw}, dose)$$

A similar relationship is also found for the softening process. Differently, the GAC performance in TOC removal is based on a semi-empirical model on TOC breakthrough in GAC

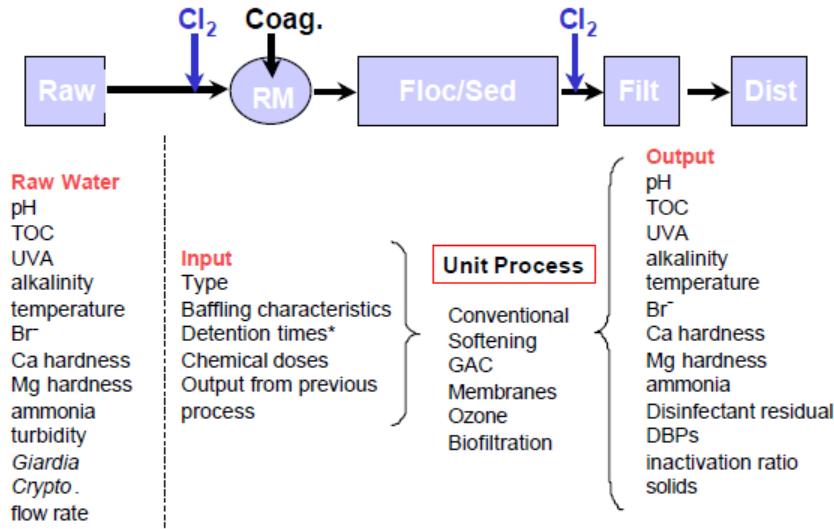


Figure 2-55 Unit process, inputs and outputs in model simulation of WTP2.0 adopted in WTP-cam program.

columns. The TOC breakthrough curve for a single GAC contactor is given by the classic logistic function (U.S. EPA, 2005),

$$f(t) = \frac{TOC_{eff}}{TOC_{in}} = \frac{a}{1 + be^{-d \cdot t}} \quad (2.35)$$

where, $f(t)$ is TOC fraction remaining; TOC_{in} and TOC_{eff} are TOC influent and effluent concentrations at the GAC unit, respectively; t is GAC service time; a , b and d are model parameters estimated by statistical regression. The model constants a , b and d are mostly a function of influent TOC, pH, and empty bed contact time (EBCT). Based on statistical regression, these parameters can be estimated by (U.S. EPA, 2005),

$$a = 0.682 \quad (2.36)$$

$$b = 0.167pH^2 - 0.808pH + 19.086 \quad (2.37)$$

$$d = TOC_{in} [pH(-0.0000058 \cdot EBCT^2 + 0.000111EBCT + 0.00125) + 0.0001444 \cdot EBCT^2 + 0.005486EBCT + 0.06005] \quad (2.38)$$

6.1.2. Customization of GAC unit process

For TOC removal, the use and customization of the GAC unit process is a viable technical approach for many U.S. water plants (Levine et al., 2016; Clark et al., 2009; Li et al., 2014, 2012). In WTP-cam, the GAC unit process is modeled with a new feature to estimate parameters a , b and d in Eqs.2.36-2.38. The new model parameterization relies on a non-linear regression method for a given plant instead of the statistical values. This improvement allows

one to customize site-specific conditions in estimating the model parameters. Either TOC treatment monitoring data or long-duration bench-scale studies can be used (Li et al., 2014). The model when calibrated aims to examine the treatment effects of different raw water sources, GAC size, pretreatment configuration, and bed depth/empty bed contact time (EBCT).

Total organic carbon removal in GAC is often characterized using TOC breakthrough experiments using GAC column experiments. This testing is normally conducted when changing GAC suppliers or in pretreatment configurations. Roberts and Summers (1982) also found that complete removal of TOC by GAC cannot be achieved under common water treatment conditions. An immediate, partial breakthrough of TOC, can be observed even with virgin GAC, indicating that a portion of the influent TOC is not amenable to removal by GAC treatment.

Roberts and Summers (1982) observed that the GAC effluent TOC is always lower than the influent level, even if the GAC reactor is saturated with organics. This degree of removal under the steady-state is attributed to biodegradation (U.S. EPA, 1996) in a way similar to the biofiltration process (Levine et al., 2016). The ratio of TOC concentration between effluent and influent, called “fraction remaining,” generally ranges from 0.1 to 0.5 during the early stages of operation. The ratio depends on the compositions of organic constituents in water and the EBCT/bed depth of a GAC contactor. For steady-state removal, the fraction remaining varies from 0.6 to 0.9 with service times from 3,000 to 14,000 bed volumes.

To obtain site-specific model parameters for design a pilot-plant or full-scale study of GAC adsorption processes is often required, which is both time-consuming and expensive. Instead, rapid small-scale column tests (RSSCT) (Crittenden et al. 1991; Zachman and Summers 2010) are widely used as a substitute. The RSSCT method is based on mass transfer models to scale down a full-size GAC contactor. The hydraulic and kinetic similarity is assured by properly selecting the GAC particle size, hydraulic loading, and EBCT of the small contactor. For this purpose, U.S. EPA (1996, 2000) described the standardized guidelines for GAC treatment studies to obtain high-quality TOC breakthrough data in RSSCT.

WTP-cam provides a new feature to custom-parameterize a , b and d in Eq.2.35 for specific water plant operations. For accurate modeling, the model uses a non-linear regression method of site-specific TOC treatment data when collected. When training data are not available, one can opt to choose default statistical values. In WTP-cam, plant-specific parameterization is based on the modified Gauss-Newton method to estimate the model parameters a , b and d . The procedure (Li et al., 2009 and Clark et al., 2009) relies on the non-linear regression function through the least square analysis. This modeling technique was developed and validated using the ICR treatment database for 63 treatment studies nationwide (U.S. EPA, 2000), including 44 RSSCT studies, 18 pilot studies, and 1 full-scale study. For a given plant, the training historical dataset is analyzed in WTP-cam using the fitting objective function below:

$$\text{Min } Q(a,b,d) = \sum_{k=1}^n (y_k - f(t_k; a,b,d))^2 \quad (2.39)$$

where, $f(t; a,b,d) = \frac{a}{1 + be^{-dt}}$ in Eq.2.35; a , b and d are the model parameters to be estimated; $A = t_k$ and y_k are the known field values, representing GAC service time and TOC fraction remaining respectively; n is a known number of field samples.

6.1.3. Adaptation cost and economics

The economic analysis of adaptation can be estimated for engineering options. For treatment adaptation, WTP-cam allows estimating the costs to the changes in GAC process design or operation. In general, the GAC process cost includes the cost for GAC contactor cost, initial GAC cost in setup, annual GAC make-up cost, and GAC reactivation cost. The initial GAC cost is a one-time charge for GAC required to fill the contactor, equal to the product of the total volume of contactors, the density and unit cost of virgin GAC. The annual GAC make-up cost is the yearly cost of GAC lost due to reactivation. It is the product of the GAC loss rate in reactivation, GAC reactivation rate, and virgin GAC cost. The GAC contactor cost can be estimated from the cost model by Adams and Clark (1988):

$$y = a + b(USRT)^c d^z \quad (2.40)$$

where y is the capital, operational or maintenance cost; $USRT$ is the process design or operating variable that is the total surface area of the GAC filter for contactors (total hearth area for GAC reactivation) or the total effective volume of the GAC unit for capital cost; a , b , c and d are empirical parameters determined from nonlinear regression analysis, and z is either 0 or 1 for adjusting the cost functions for a given range of $USRT$ values.

The costs in Adam and Clark (1988) are based on the year-1983 dollar value. In WTP-cam model computation, all costs are converted to the year 2009 dollar using the Producers Price Index (US BLS, 2008). The same method can be used for other years of interest; revision to other benchmark years will be made later. The contactor cost can be further categorized by the costs of capital, process energy, building energy, maintenance material, and operational and maintenance (O&M) labor. The computational parameters are listed in Table 2-24. GAC reactivation cost is the other variable estimated using a similar algorithm (Eq.2.40). The model parameters are different and are listed in Table 2-25.

Table 2-24 GAC contactor cost estimate parameters

Type of Cost	Capital	Process energy	Building energy	Maintenance Material	O&M Labor
USRT	volume	area	area	area	area
a	93700	0	15150	540	1160
b	1999.1	12	350	23.6	0.3
c	0.712	1	0.916	0.753	1.068
d	0.958	1	1	1	1.152
z	1	1	1	1	1
Unit cost	Construction Cost 1.3y	0.08 \$/kwh (in 2009)	0.08 \$/kwh (in 2009)	--	9 \$/hr (in 1983)
Ratio of 2009 to 1983 cost	2009ENR/1983ENR= R=2.16	--	--	2009PPI/1983 PPI = 2.56	2009 PPI/1983 PPI = 2.56

Table 2-25 GAC reactivation cost

Type of Cost	Capital	Process energy	Building energy	Maintenance Material	O&M Labor	Natural Gas
USRT	area	area	area	area	area	area
a	144000	354600	12250	0	2920	648400
b	198300.4	6387	312.1	4456.6	282	287714.9
c	0.434	0.755	0.649	0.401	0.7	0.899
d	1	1	1	1	1	1
z	1	1	1	1	1	1
Unit cost	Construction Cost 1.3y	0.08 \$/kwh (in 2009)	0.08 \$/kwh (in 2009)	--	9 \$/hr (in 1983)	\$0.0035 /scf (in 1983)
Ratio of 2009/1983 cost	2009ENR/1983ENR = R = 2.16	--	--	2009PPI/1983 PPI = 2.56	2009PPI/1983 PPI = 2.56	2009PPI/1983 PPI = 2.56

WTP-cam also introduces annualized cost in economic analysis. In a capital recovery analysis, for example, a 20-year return period and a 5% annual interest rate can be assigned to construct a cost curve that illustrates the total annual cost of the GAC system in adaptation options in different GAC service time or reactivation period. For illustration, Figure 2-56 shows an example cost curve developed for the GCWW’s Miller WTP. The Miller WTP has 12 down-flow gravity GAC contactors and two multi-hearth furnaces for onsite reactivation. Each of the Miller WTP contactors

has a volume of 595 m³ and a surface area of 181 m². The overall GAC loss rate through the system is about 8%. The carbon loading rate is 482 kg/day of GAC per square meter of the hearth area. This cost curve is the basis for GAC adaptation analysis at the treatment plant. Details of this adaptation case study will be described later in Section 6.3.

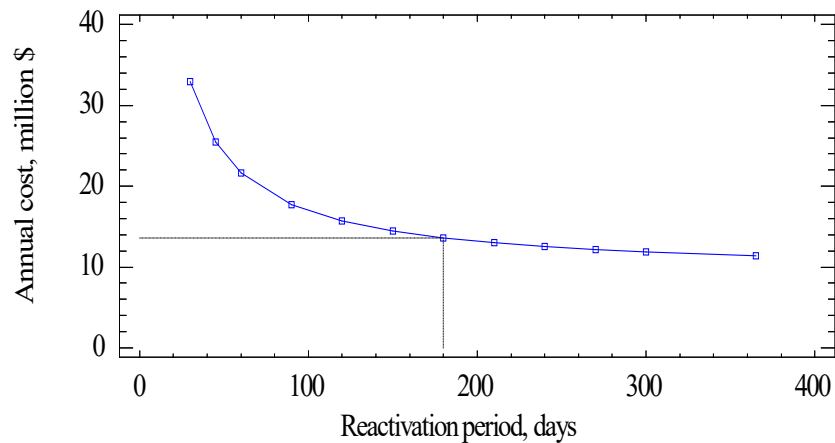


Figure 2-56 Cost curve for annual cost of GAC unit, indicating the cost associated with a given GAC reactivation period for the Miller water treatment plant in Cincinnati.

6.1.4. Other unit processes for adaptation

Other unit processes in advanced water treatment are applicable for adaptation to the changes in source water quality. Examples include membrane and advanced oxidation for removal of emerging and trace contaminants such as endocrine-disrupting compounds, algae toxins, herbicide, and pesticides, etc. Such advanced tertiary processes will be added to WTP-cam in the future.

6.2. Adaptation Analysis using WTP-cam

A WTP-cam simulation can proceed in the following sequential steps: (1) source water quality definition, (2) product water quality projection, (3) model validation, and (4) result analysis and visualization. Appendix B provides program illustrations and instructions for the WTP-cam simulation. The program is Windows-based running in a Windows 8 or newer operating system.

6.2.1. Treatment process and compliance targets

6.2.1.1. Treatment processes in simulation

In a WTP-cam simulation, the first step is to develop a physical model of a treatment plant for examination. Figure 2-57 shows an example for the GCWW Miller WTP. Raw water from the Ohio River is pumped into two large equalization basins at the plant. Then the water

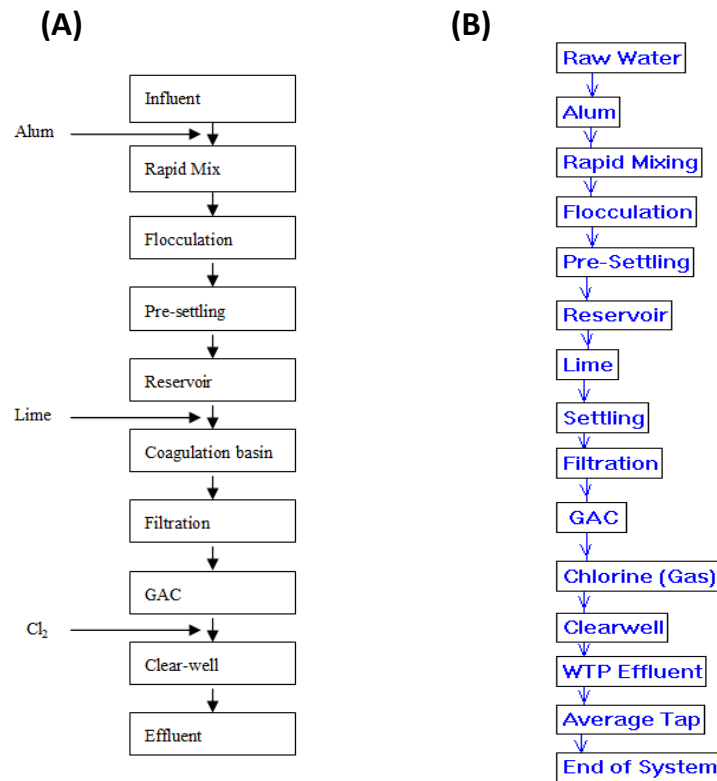


Figure 2-57 Schematic diagram for (A) treatment unit process at the GCWW Miller water treatment plant, and (B) WTP-cam program flow in the example simulation.

compliance criterion for TOC is <2.0 mg/L calculated quarterly as a running annual average. Other regulatory targets or treatment objectives are not considered in WTP-cam version 1.

In a WTP-cam simulation, four computed running averages are calculated; one for each quarter of a year. The running annual average is defined as the arithmetic average of TOC concentrations at a current season and previous three seasons based on the U.S. EPA disinfectant/disinfection by-product (D/DBP) regulations. For example, the running annual average for TOC is calculated for the GAC treatment effluent of the GCWW’s Richard Miller Treatment Plant (Table 2-26).

The means, variances, and cross-correlations of raw water parameters vary with seasonal changes in most cases. Thus, four sets of input parameters for raw water qualities need to be prepared as modeling inputs, for which four simulations are conducted each year responding to the four seasons (Table 2-26). The TOC concentration is recomputed for each season as the running average.

Table 2-26 Illustration of calculating the running annual average for finished water TOC

Year	Season	TOC concentration	Running annual average
2009	Spring	1.3	--
	Summer	1.7	--
	Autumn	2.2	--
	Winter	1.7	1.7
2010	Spring	1.2	1.7
	Summer	1.4	1.6
	Autumn	2.4	1.7
	Winter	1.5	1.6

6.2.2. Monte Carlo methods in modeling source water quality

6.2.2.1. Incorporation of hydroclimate uncertainties

Several source water quality changes, such as increasing levels of turbidity, nutrients, blue algae, and biological contaminants, can affect the removal of TOC and other contaminants in water treatment. A newly developed modeling-monitoring platform in Figure 2-1 utilizes near real-time (daily) high-resolution satellite monitoring to provide real-time water quality information in assisting water plant operations (Imen et al., 2016). Now many water quality parameters relevant to drinking water treatment can be quantitatively monitored, including major nutrients, turbidity, TOC, chlorophyll-a, and microcystin (Chang et al., 2014a,b). Furthermore, the modeling-monitoring platform integrates climate and land use models to project future changes of major water quality parameters such as TOC, total phosphorous, total nitrogen, and turbidity. If the change is significant, these water quality projections are needed for design basis development in water infrastructure adaptation. However, future water quality projections often contain large uncertainties. Even with the use of the integrated modeling-monitoring techniques,

the full range of water quality parameters of necessary accuracy for engineering planning and design may not be readily available. Water managers in charge of water adaptation will likely face the uncertainty challenge in the foreseeable future.

In this context, Li et al. (2014, 2012) proposed the use of Monte Carlo analysis as a practical tool to characterize the range of future water quality changes. In this approach, Monte Carlo analysis is used to obtain sample solutions by repeating a simulation process for problems involving random variables of known probability distributions. The correlations among water quality parameters are assumed to remain for the future period of interest in order to establish the water quality parameters such as TOC and turbidity for WTP-cam simulation. This Monte Carlo simulation to account for climate-related hydrological uncertainty is a new feature not previously available in WTP v2.0.

Figure 2-59 shows the key steps of the Monte Carlo analysis in WTP-cam simulation; new inputs are marked in bold. Three key considerations in the Monte Carlo analysis are: (1) the Quarterly Running Average, (2) Preservation of the correlation among parameters, and (3) Pollutant removal targets. The

Quarterly Running Average parameter is specially designed for the regulation consideration over TOC concentrations. TOC ≤ 2.0 mg/L in finished water, calculated quarterly as a running annual average, is an important compliance criterion according to the EPA disinfectant/disinfection

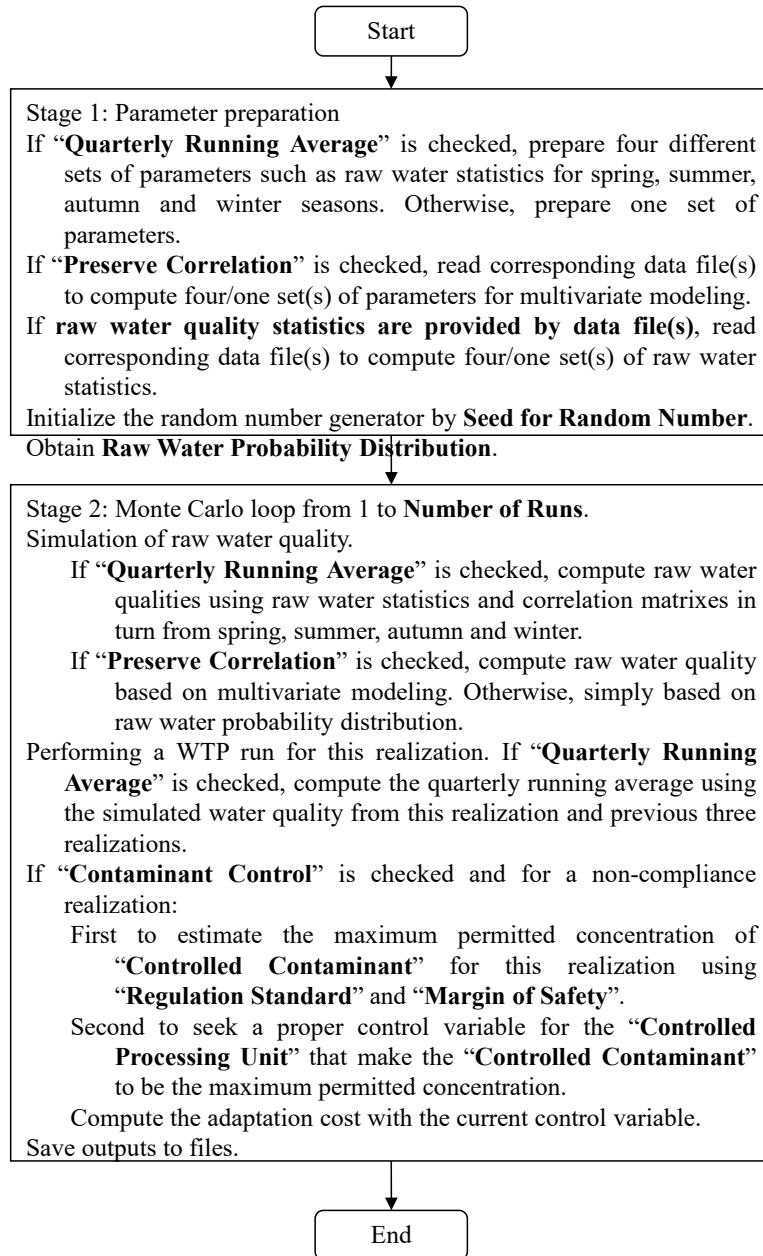


Figure 2-59 Program logic sequences in Monte Carlo simulation of future source water quality variations using the correlation matrix method (from Li et al., 2014).

byproduct (D/DBP) rule. Furthermore, WTP-cam applies four quarterly statistics to represent annual seasonal variations. See the preceding Section 6.1.1.

The modeling option for “Preserve Correlation” is designed to preserve the joint correlation among raw water quality parameters when simulating stochastic raw water quality variables. In the presence of cross-correlation, concentrations of correlated reactants vary simultaneously in the source water. This assumed cross-correlation among raw water quality parameters can affect the calculation of DBP formation during water treatment and distribution. A first-order multivariate seasonal autoregressive model (Bras and Rodriguez-Iturbe, 1984) was used in the WTP-cam. This seasonal model preserves all seasonal means and variance of water quality parameters, all cross-correlations among all water quality parameters, and lag-one correlations between adjacent seasons and between all water quality parameters. Section 6.2 describes the theoretical basis for the applied multivariate analysis.

The Pollutant Option in the modeling is designed to modify the design and operation of the current processing train when a non-compliance realization is detected in simulation. For example, when a TOC non-compliance in finished water occurs, the WTP-cam program can be used to design operation modification by increasing the frequency of GAC regeneration. Such an adaptation measure aims to bring the TOC excursion within acceptable limits. The inputs for this option are made for a given contaminant, regulation standard, margin of safety, and unit processes in a treatment plant. For the WTP-cam version 1, the engineering option has been developed for TOC control in the GAC treatment process.

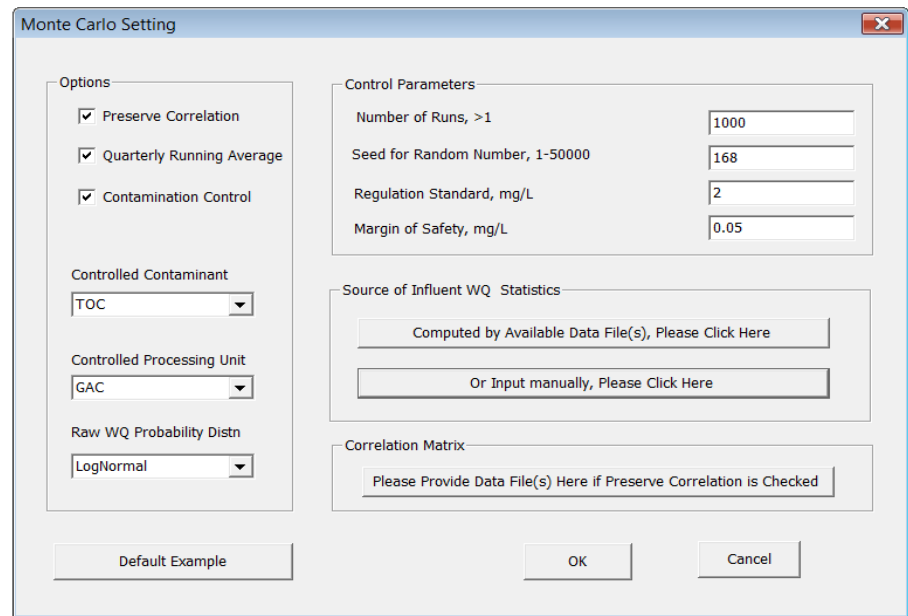


Figure 2-60 Graphic user interface for inputs in Monte Carlo simulations of future water qualities.

6.2.2.2. Inputs for Monte Carlo Setting

The input parameters for Monte Carlo analysis may be divided into three groups: analysis options, control parameters, and the source of influent water quality statistics/correlation. Figure 2-60 shows a graphic user interface (GUI) for these inputs in the example process train of Figure 2-57.

Analysis options: the options are designed to govern the flow of Monte Carlo simulation. Table 2-27 lists the name of the option, range of available values, and description of the option.

Control parameters: there are four control parameters used in the Monte Carlo simulation:

- Number of Runs – a user-defined integer to specify the number of runs required.
- Seed for Random Number – a positive number to initialize the random number generator in the program. The Monte Carlo simulation can be repeated using the same random number seed.
- Regulation standard – a value representing the compliance standard for the controlled contaminant selected in **Options**.
- Margin of Safety – refers to the difference between the compliance standard and the real controlled concentration that provides extra reliability for compliance. The margin of safety is usually set within 1-10% of the regulation standard.

Table 2-27 Options for Monte Carlo analysis

Control	Range of value	Description
Preserve Correlation	TRUE/FALSE	Multivariate analysis will be used to simulate stochastic raw water quality if TRUE (checked).
Quarterly Running Average	TRUE/FALSE	Simulation will be based on four seasons of variation if TRUE.
System Adaptation	TRUE/FALSE	Loading adaptation program for the non-compliance realizations if TRUE.
Controlled Contaminant	TOC/None	Determining the contaminant to be controlled by adaptation.
Controlled Unit Process	GAC/None	Determining the unit process that can be adapted for controlled contaminant.
Raw Water Probability Distribution	Normal/Lognormal	Determining the probability distribution for all raw water quality parameters

6.2.2.3. Source of influent water quality statistics/correlation

Influent water quality statistics are essential to generate raw water quality parameters for the input of each simulation. Two methods provided by WTP-cam are available to obtain these parameters. The first is to simulate source water quality using the correlation matrix (see Section 6.2 for details). The second method is to input these parameters manually through the manual input function. Four dialogue windows appear one at a time for the four seasons if Quarterly Running Average is checked. Figure 2-61 shows an example of a manual input window for the Spring in the example process train at the Miller WTP in the Cincinnati case study. These datasets are saved in separate files for retrieval and simulation. See Appendix B for program details.

To project future water quality, it is assumed that the covariations among water quality parameters in the Ohio River source water will remain. This assumption allows one to compute all other important parameters from a target TOC level, which are modeling parameters in WTP-cam simulations. The joint correlations among raw water quality parameters are preserved when computing the stochastic raw water quality in the future. This statistics-based seasonable multivariate analysis was conducted through Monte Carlo simulations. Detailed principles and mathematical relations are contained in Section B4.1.1 of Appendix B.

Raw Water Quality Statistics Input Window

Time Horizon: Spring

Parameter	Average	Standard Deviation
pH, -	7.7	0.17
Alkalinity, mg/L	55.5	18.2
Turbidity, NTU	43.4	38.0
Calcium Hardness, mg/L	63.5	23.3
Total Hardness, mg/L	110.4	18.4
TOC, mg/L	2.3	0.6
UVA, 1/cm	0.12	0.06
Bromide, mg/L	0.03	0.01
Ammonia, mg/L	0.29	0.41
Temperature, Celsius	12.4	0
Flow Rate, MGD	108.4	0

OK Cancel

Figure 2-61 Manual input window for influent water quality statistics.

In summary, the first-order multivariate seasonal autoregressive model AR(1) (Bras and Rodriguez-Iturbe, 1984; Salas et al., 1980) was adopted in the WTP-cam algorithm for the model simulation. For each season of a year, water quality measurements are Log-transformed in WTP-cam simulation into variables x'_i and y'_i . These two variables become normally distributed with means m_{x_i} and m_{y_i} , standard deviations S_{x_i} and S_{y_i} , and the correlation coefficient among them. The sample means, standard deviations and correlation coefficients of the transformed variables x'_i and y'_i are calculated. These parameters are then used to build the necessary auto-covariance and cross-covariance matrices (see Appendix B, Section B4.1.1.). The final results are projected water quality value and its associated range in the probability distribution. This analysis follows the following steps:

- Define a domain of possible inputs.
- Generate inputs randomly from the domain using a specified probability distribution.
- Perform a deterministic computation using the inputs.
- Aggregate the results of the individual computations into the final result.

6.2.3. Advanced unit process and adaptation cost

Adaptation analysis using WTP-cam is conducted after a noncompliance event is identified. Adaptation refers to necessary changes in the design and/or operation of the current

water treatment train or unit process. At this time, the adaptation module is fully developed for TOC treatment in GAC adsorption. Adaptation for other treatment unit processes has not yet been programmed into the WTP-cam software.

The margin of safety is an option in adaptation analysis using WTP-cam. The margin of safety refers to the difference between the compliance cut-off point and the calculated concentration. For example, if the margin of safety is 0.1mg/L, the controlled TOC concentration will be 1.9 mg/L. The simulated running annual average of TOC concentration should be <1.9 mg/L in engineering analysis.

When a TOC noncompliance event is identified, one effective adaptation technique is to reduce the GAC service time through treatment process adjustment (Li et al., 2014). In the WTP-cam simulation, the appropriate GAC service time is calculated and the process control is adjusted to ensure TOC <1.9 mg/L. The computation procedure is as follows:

- Reducing current GAC service time by one day.
- Using the new service time to re-compute the TOC concentration for each of four seasons without change to the other operating conditions in each season.
- Calculating the new running annual average of TOC.
- Comparing the new calculated TOC to the controlled concentration of 1.9 mg/L. The new service time is adopted if new TOC is less than 1.9 mg/L; otherwise, repeat computation from the first step until the solution is found.

Treatment adaptation by modifying the GAC process can reduce the likely future risk of TOC noncompliance. Such potential options are further evaluated in WTP-cam on adaptation cost and treatment effectiveness. Apparently, a reduced GAC reactivation period and operational adjustment may increase energy consumption a major item in the primary adaptation cost. The cost for GAC replacement and reactor optimization can be estimated using the equations and procedures described in the preceding section 6.1.3. An example of such engineering and economic analysis is described next.

6.3. GCWW Richard Miller Treatment Plant case study using WTP-cam

GCWW provides drinking water at ~5.26 m³/s or 120 million gallons per day (MGD) to ~ 235,000 customer accounts through 5,100 km of water mains. Built in 1907, the GCWW's Miller WTP treats surface water from the Ohio River and provides 88% of the drinking water supply to the customers at a maximum summer capacity of 9.65 m³/s (220 MGD). In this adaptation case study, the WTP-cam tool was used in the simulation to assess the likely hydroclimatic changes in the future on drinking water treatment at the Miller WTP. The investigation results have been published by Li et al. (2014, 2012) and others. The technical questions for adaptation study include:

- How the climate-related risk to drinking water standard violations can be assessed?
- What adaptation limit or climate impact threshold can be established?
- What is the probable cost associated with the adaptation scenarios?

6.3.1. Miller water treatment plant operation and performance

6.3.1.1. Treatment process and modeling

Figure 2-57 in Section 6.2.1 shows the treatment process at the Miller WTP. Raw water is taken from the Ohio River. At the time of the investigation, the treatment process consisted of coagulation, sedimentation, biologically active rapid sand filtration, GAC adsorption, and water disinfection. A new UV disinfection facility started operation shortly after this adaptation analysis. It replaced the conventional chlorination. All data acquired before the UV unit operation are used in this analysis based on chlorine disinfection (see Figure 2-57). The intent was to examine the conventional use of chlorination as the basis for the adaptation analysis.

TOC and turbidity are the subjects of the adaptation study. These DBP-formation precursors or potential indicators are removed by the conventional coagulation, sedimentation, biologically active rapid sand filtration, and GAC adsorption at the plant. The Miller WTP design parameters are listed in Table 2-28. In the table, T₁₀ value is the hydraulic retention time required for the effluent tracer concentration to reach 10% of the inflow tracer concentration. It is normally determined in a step-dose conservative tracer test of the treatment unit.

The plant performance and treatment efficiency of each unit process were evaluated using the U.S. EPA's ICR database. The database was designed to obtain water quality, water treatment, and occurrence information needed for the development of Safe Drinking Water Act regulations. ICR data include detailed information on plant design, treatment processes, and operations for all large public water utilities in the U.S., each serving a population >100,000. The data collection covered an 18-month monitoring period from July 1997 through December 1998. The ICR database also provides water quality measurements at various sampling locations along the water treatment train and in a water distribution system.

For the Miller WTP, specific data utilized for the treatment simulation cover three sampling periods: sample period 10 (April 1998), sample period 13 (July 1998), and sample period 16 (October 1998). Raw water inflow rate and chemical feed doses during each period are listed in Table 2-29. Based on the information provided by GCWW, the GAC reactivation during these periods was set at 8 months for the winter-spring season and as 4 months for the summer-early autumn season.

Table 2-28 Miller WTP unit process design parameters

Unit Process	Volume, m ³	T ₁₀ , min
Rapid mixing	32	2
Flocculation basin	7343	14
Pre-settling	8441	14
Reservoir settling	1411805	1,728
Coagulation basin	98410	144
Filtration	9352	4
GAC Contactors	9311	--
Clear-well	107116	77

Note: -- data not available.

Data source: U.S. EPA ICR database.

6.3.1.2. GAC absorption and TOC removal

Table 2-30 shows statistics of the performance parameters for the GAC unit based on weekly samples for the 76-month period from January 2004 to April 2010. The data includes the influent and blended effluent TOC concentrations, the number of active GAC contactors, the plant inflow rates, and the GAC reactor empty bed contact time (EBCT). Influent TOC concentrations follow an annual cycle with seasonal extremes ranging from 1.01 mg/L (March 24, 2004) to 2.76 mg/L (September 22, 2004). Blended effluent TOC varied from 0.26 mg/L (July 13, 2005) to 1.44 mg/L (November 1, 2006); all concentrations were below the compliance standard of 2.00 mg/L.

Table 2-29 Inflow and chemical feed levels for the Miller WTP

Parameter	Sampling period		
	10	13	16
Inflow rate, m ³ /s	4.41	5.27	5.76
Alum at RM, mg/L	0.87	1.82	0.87
Lime at COAG, mg/L	6.73	7.92	4.62
Chlorine at CLR, mg/L	1.26	1.56	1.46

Note: RM-rapid mixing; COAG-coagulation basin; CLR-clearwell.

Data source: U.S. EPA ICR database.

The GAC plant flow rates averaged 5.26 m³/s (120 MGD), ranging from 3.26 m³/s (74 MGD) on December 27, 2006 to 7.61 m³/s (174 MGD) on September 5, 2007. Among the 12 available GAC contactors, 6 to 11 contactors were in operation at any given time. GCWW's operational strategy for the GAC process demands that GAC contactors be brought on-line, reactivated, and taken off-line in a staggered sequence. This operation aimed to balance a variety of operational goals including total trihalomethane (TTHM) reduction, water production, furnace operation schedules, GAC storage, and the effective removal of Spring pesticide runoff in the source water. To meet these operational goals, the monthly average EBCT was set consistently around 17 minutes

Table 2-30 Statistics of full-scale field measurements

Field Measurements (units)	Average	Standard Deviation	Coefficient of Variation	Minimum	Maximum	Sample Size
Influent TOC, (mg/L)	1.72	0.36	0.21	1.01	2.76	289 ^a
Blended effluent TOC, (mg/L)	0.85	0.26	0.31	0.26	1.44	289 ^a
Number of active GAC contactors	9	1.22	0.14	6	11	289 ^a
EBCT, (minute)	17.1	0.8	0.05	12.1	24.4	279 ^b
Plant water inflows, (m ³ /s)	5.26	0.81	0.15	3.26	7.61	279 ^b
Plant TOC mass inflow, (g/s)	9.17	2.57	0.28	4.72	16.6	279 ^b

Note: ^a 2296-day sample period from Jan 7, 2004 to April 21, 2010 (one sample every 7.94 days)

^b 2184-day sample period from Jan 7, 2004 to Dec 30, 2009 (one sample every 7.83 days)

Figure 2-62 shows the temporal pattern of influent TOC and blended effluent TOC concentrations at the GAC unit process during the 76-month sampling period. Seasonal changes of influent TOC to the GAC reactor are evident. Higher concentration always occurred in the second half of the year compared to the first half, and this seasonal variability is consistent with TOC levels in the Ohio River.

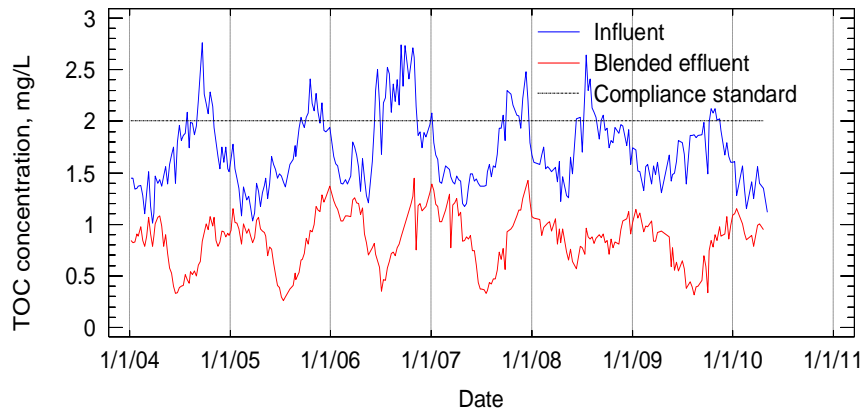


Figure 2-62 Temporal variations of influent and blended effluent TOC in the GAC unit.

Influent TOC concentrations and blended effluent TOC concentrations are not significantly correlated with each other (Figure 2-62). Pearson product-moment correlation coefficient R is only 0.08. However, as shown in Figure 2-63, the number of active GAC contactors is highly correlated with plant inflow ($R=0.75$) and mass inflow ($R=0.65$). Due to increased water demands during warm weather, summer months had higher plant inflow rates than winter months, and, hence, more GAC contactors were active in the summer time. The number of active GAC contactors is negatively correlated to the blended effluent TOC concentration ($R=-0.69$). See Figure 2-64. This indicates that TOC in the finished water is controlled mainly by the number of GAC contactors in service, not TOC concentration entering the treatment unit. This result strongly shows the effectiveness of GAC operation in TOC removal.

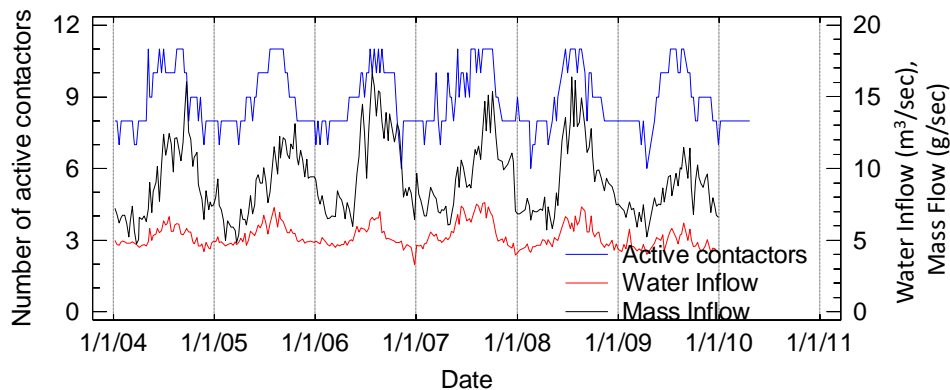


Figure 2-63 Temporal variations of inflow, mass inflow and active number of GAC contactors.

Figure 2-65 compares temporal variations in EBCT and plant inflow. While the plant inflow rate displayed pronounced seasonality, the overall average EBCT across the bank of

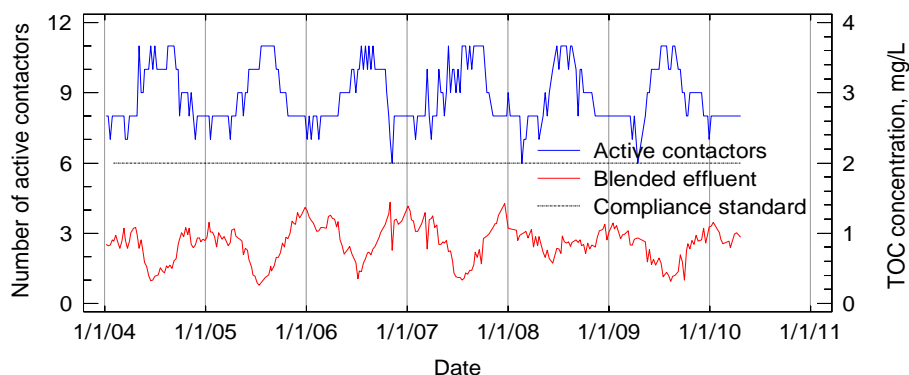


Figure 2-64 Temporal variations of active contactors and blended effluent TOC concentration.

active GAC contactors was relatively stable. This quasi-steady EBCT is achieved in operation successfully by adjusting the number of active GAC contactors to meet GCWW’s operational goals including the offsetting of the seasonal inflow variations.

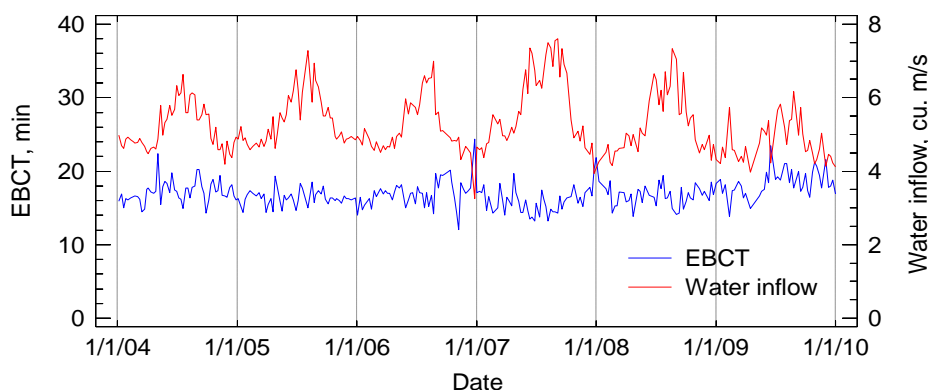


Figure 2-65 Time series of plant inflow and EBCT variations.

6.3.2. WTP-cam simulation of hydroclimatic change impacts

6.3.2.1 Simulation and model assumptions

The changes in hydroclimatic conditions and land use may impact source water quality and thus affect water plant operations and drinking water quality at the tap. Extreme variations and associated uncertainties in source water are primary design parameters in adaptation engineering. To characterize the impact, future source water variability is calculated using the Monte Carlo simulation methods described in preceding Section 6.2.1.1.

In the Monte Carlo simulation, all source water quality parameters were assumed to be log-normally distributed. This assumption is verified in Figure 2-66 for pH and TOC using ICR data of the Ohio River collected at the Miller WTP intake. The log-normal probability distribution reasonably describes the variability except for a small bias in the lower 5% probability for TOC. In the Monte Carlo simulation, the number of runs is an important criterion in reliability analysis. Therefore, numerical tests were made to determine the minimum number of runs needed to yield a constant mean, standard deviation, and skewness using a quarterly

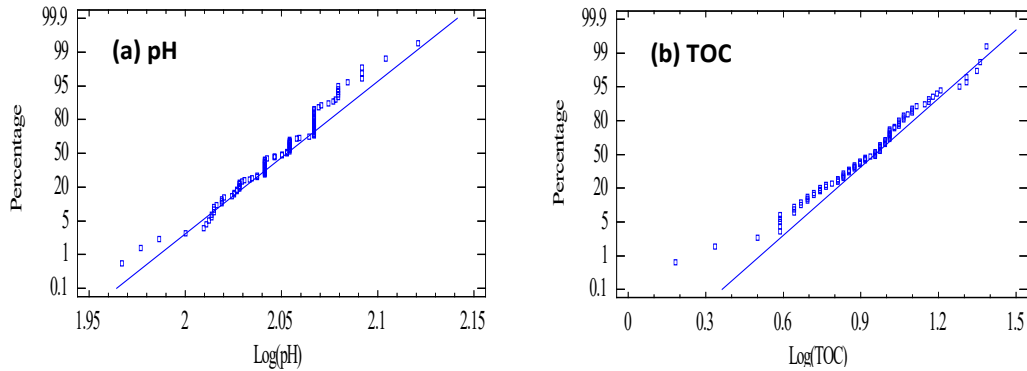


Figure 2-66 Normal probability plots for source water pH (107 samples) and TOC (93 samples) for Ohio River from the ICR database (July 1997-December 1998).

running annual average of TOC in the finished water. The mean and standard deviation become a stable constant after 500 and 2,000 runs, respectively; the skewness becomes constant after 5,000 runs. Therefore, 5,000 runs were chosen for all Monte Carlo simulations.

Another assumption is that the confounding effects of population growth can be neglected for plant flow rates. This simplification allows identification of the climate-induced water quality changes impacting water treatment performance. The design and operation conditions for the Miller WTP under future scenarios were initially kept unchanged from the baseline period. In addition, it was assumed that the coefficients of variation for all water quality parameters in 2050 would remain the same as those for the baseline data. This similarity is guided by the ratios of σ_o/μ_o in Table 2-31.

Table 2-31 Source water inputs for the Miller water treatment plant in 1998 (Baseline)

Parameter	Unit	Spring		Summer		Autumn		Winter	
		μ_o	σ_o	μ_o	σ_o	μ_o	σ_o	μ_o	σ_o
pH	--	7.7	0.17	7.7	0.20	7.8	0.22	7.8	0.18
Alkalinity	mg/L	55.5	18.2	77.2	21.7	81.4	21.0	62.3	23.1
Turbidity	NTU	43.4	38.0	26.9	36.9	8.5	7.6	41.5	64.7
Ca hardness	mg/L	63.5	23.3	76.2	31.6	87.1	35.6	74.2	33.7
Total hardness	mg/L	110.4	18.6	140.3	26.1	161.3	31.1	133	36.5
TOC	mg/L	2.3	0.6	2.9	0.6	2.6	0.3	2.5	0.6
UVA	cm ⁻¹	0.12	0.06	0.11	0.06	0.08	0.02	0.09	0.05
Bromide	mg/L	0.03	0.01	0.05	0.02	0.10	0.04	0.07	0.04
NH ₃ _N	mg/L	0.29	0.41	0.20	0.11	0.18	0.10	0.18	0.10
Temperature	°C	12.4	NA	25.7	NA	20.8	NA	9.8	NA
Flow	m ³ /s	4.75	NA	5.01	NA	5.75	NA	5.30	NA

Note: μ_o is average and σ_o is standard deviation in the year of 1998; NA – not applicable.

6.3.2.2 *Source water characterization*

Surface water quality at the plant intake from the Ohio River varies significantly in response to upstream hydrological changes and watershed management. Factors affecting the water quality variation include upstream watershed management, river spills from ships, and the hydroclimatic factors such as seasonal and long-term precipitation changes.

Baseline Condition in 1998

Water quality variability in the river is characterized for a period July 1997 to December 1998 using water quality data from the ICR database. Averages and standard deviations for the baseline period are shown in Table 2-31. Because the SDWA TOC regulation requires reporting of quarterly running annual average, the raw water quality at the plant is divided into spring (March to May), summer (June to August), autumn (September to November) and winter (December to February). The source water quality exhibited a statistically significant difference among the seasons.

Joint Correlation of Source Water Quality Parameters

For the lognormal distribution (see Figure 2-65), a Monte Carlo simulation was used in modeling source water quality parameters. The basis for the modeling, such as the joint correlation, was described in preceding section 6.2.1. Monte Carlo simulations after 5000 runs established correlations among the 9 water quality parameters for the Ohio River water. The numbers in italics (Table 2-32) illustrate that more than half of the pairs of source water quality parameters are statistically correlated; their correlation coefficient is >0.2 and the p-value is <0.1 .

6.3.2.3 *Projecting raw water quality in 2050*

To assess future source water quality, the 1998 baseline data was modified to project possible water quality scenarios in the Ohio River in 2050. The 2050 water quality projection considered the following aspects of anticipated changes.

- TOC, Alkalinity, and Total Hardness

Skjelkvale et al. (2005) studied the regional trend of surface water chemistry and acidification for 12 geographic regions in Europe and North America from 1990 to 2001. As one of the 12 regions, the Appalachian Plateau includes the upstream reaches of the Ohio River. Therefore, the regional trends in their study for alkalinity, total hardness, and dissolved organic carbon (DOC) were adopted to estimate these parameters for the period 1998 to 2050. The trends for alkalinity, total hardness, and DOC are equivalent to a change by +0.036, -0.22, and +0.03 mg/L per year, respectively. Because DOC is usually the main component of TOC, the trend for TOC is assumed the same as that for DOC.

- Ammonia

The most important sources of ammonia are from decomposed plant and animal matter, fertilizer, sewage, and industrial effluents. Whitehead et al. (2006) investigated the hydroclimatic impacts on ammonia in the River Kennet of the U.K. for the period from 1961 to 2100. A 25% increase in ammonia from 1998 to 2050 can be assumed based on their study. It is believed that

Table 2-32 Correlation matrix for source water quality parameters (for Ohio River from July 1997 to December 1998)

Parameter	Statistics	Alkalinity	Turbidity	Ca hardness	Total hardness	TOC	UVA	Bromide	NH ₃ _N
pH	ρ	0.63	-0.11	0.04	0.43	0.36	0.11	-0.02	-0.02
	p-value	0.00	0.27	0.67	0.00	0.00	0.32	0.87	0.83
Alkalinity	ρ	1	-0.15	0.06	0.80	0.63	0.25	0.26	-0.08
	p-value		0.13	0.51	0.00	0.00	0.02	0.02	0.45
Turbidity	ρ		1	-0.15	-0.27	0.32	0.54	-0.38	0.32
	p-value			0.11	0.01	0.00	0.00	0.00	0.00
Ca hardness	ρ			1	0.25	0.02	-0.29	0.20	-0.17
	p-value				0.01	0.85	0.01	0.06	0.14
Total hardness	ρ				1	0.36	0.10	0.59	-0.26
	p-value					0.00	0.35	0.00	0.02
TOC	ρ					1	0.65	-0.04	0.18
	p-value						0.00	0.71	0.13
UVA	ρ						1	-0.42	0.29
	p-value							0.00	0.02
Bromide	ρ							1	-0.12
	p-value								0.31

the 25% increase in ammonia is reasonable for the source water quality in this study, but the effect of ammonia on TOC in finished water is negligible (see later discussion).

- Bromides, UVA, pH, Turbidity, and Calcium Hardness

Bromides occur naturally in both surface and groundwater but are particularly high in areas of saline intrusion. Cromwell III et al. (2007) pointed out that sea level rise in future climate would increase bromide levels in coastal regions. However, there is presently no evidence to indicate changes of bromide levels in inland regions because of future climate conditions. This finding was assumed to apply to the Miller WTP in 2050.

Similarly, there is no evidence found yet to quantify changes on the levels of water quality parameters UVA, pH, turbidity, and calcium hardness under future climate conditions, these parameters in 2050 were assumed the same as the 1998 baseline values.

- Temperature

Cromwell III et al. (2007) predicted increases in surface water temperatures ranging from 1.1 to 6.6°C from 1990 to 2100. The average water temperature in 2050 is estimated to be 2°C higher than the baseline values for all seasons during the 52-year period.

The analysis above generates an estimate of the key parameters for the 2050 raw water quality. Furthermore, the changes are translated to the other water quality parameters using the correlation matrix in Table 2-32. This empirical statistical analysis leads to a proposed source water quality in the Ohio River intake in 2050. The result is shown in Table 2-33.

Table 2-33 Projected raw water quality parameters for the Miller WTP in 2050

Parameter	Unit	Spring		Summer		Autumn		Winter	
		μ_1	σ_1	μ_1	σ_1	μ_1	σ_1	μ_1	σ_1
pH	--	7.7	0.17	7.7	0.20	7.8	0.22	7.8	0.18
Alkalinity	mg/L	57.3	18.9	79.1	22.1	83.3	21.7	64.1	23.7
Turbidity	NTU	43.4	38.0	26.9	36.9	8.5	7.6	41.5	64.7
Ca Hardness	mg/L	63.5	23.3	76.2	31.6	87.1	35.6	74.2	33.7
Total Hardness	mg/L	98.8	16.8	128.9	24.5	149.9	28.5	121.5	32.8
TOC	mg/L	3.8	1.0	4.4	0.9	4.1	0.5	4.1	0.9
UVA	cm ⁻¹	0.12	0.06	0.11	0.06	0.08	0.02	0.09	0.05
Bromide	mg/L	0.03	0.01	0.05	0.02	0.10	0.04	0.07	0.04
NH ₃ _N	mg/L	0.36	0.50	0.25	0.13	0.23	0.13	0.23	0.13
Temperature	°C	14.4	--	27.7	--	22.8	--	11.8	--
Flow	m ³ /s	4.75	--	5.01	--	5.75	--	5.30	--

Note: μ_1 is average and σ_1 is standard deviation in 2050; -- Not applicable.

6.3.2.4 WTP-cam model calibration and validation

Before applications to treatment process modeling were performed, the WTP-cam for the Miller WTP was calibrated and validated using input data extracted from the ICR database.

Model calibration and validation were based on sample period 10 (April 1998), sample period 13 (July 1998), and sample period 16 (October 1998). Plant operation data for the three periods were described in detail in preceding Section 6.3.1.

Results from the WTP-cam simulation for the field data of validation periods are shown in Table 2-34. Reasonable agreements for most water quality parameters are achieved including pH, alkalinity, total hardness, TOC, free chlorine residual, and TTHMs. The measured and simulated TOC concentrations were in good agreement in the finished water:

- The relative projection error is <10% for bulk water parameters pH, alkalinity, and total hardness. The error was $8.4\pm 8.3\%$ in the coagulation basin and filters, $7.5\pm 7.4\%$ for the GAC units and finished water, and $1.5\pm 5.0\%$ in the distribution system. These uncertainty assessments include all the data analyzed without excluding the period-13 data that are statistically different from the others of the calibration periods. Excluding period 13 data, the projection errors are only a half.
- For the sampling periods 10 and 16, model-simulated TOC concentrations were projected higher than measured concentrations by $26.2\pm 2.7\%$ in the coagulation basin and filters, but very close at the GAC units and finished water. The model estimates are >50% than the measured for the sampling period 13 when TOC concentrations were low (Table 2-34).
- The ICR data showed that UVA was removed by coagulation and GAC in the Miller WTP, while the WTP-cam predicted most UVA removal by GAC. The simulated UVA agreed well in the finished water for sampling period 10.
- Excellent agreement was achieved between the simulated and the sampled chlorine residuals in the finished water.

Table 2-34 Comparison of sampled and modeled water quality results

Water quality parameter	Sampling period	Data type	Influent	Coag. Basin	Filtration	GAC	Finished water	AVG1*	AVG3**
pH [--]	10	Sampled	7.7	8.7	8.6	8.0	8.5	8.6	8.6
		Modeled	7.7	9.4	9.4	9.4	9.1	9.1	9.1
	13	Sampled	7.6	7.9	7.8	7.8	8.2	8.4	8.5
		Modeled	7.6	9.2	9.2	9.2	8.9	9.0	9.0
	16	Sampled	7.7	8.3	8.1	8.0	8.4	8.3	8.6
		Modeled	7.7	8.8	8.8	8.8	8.2	8.2	8.2
Alkalinity [mg/L]	10	Sampled	56	59	58	58	58	60	60
		Modeled	56	64	64	64	62	62	62
	13	Sampled	63	56	59	58	57	64	68
		Modeled	63	72	72	72	69	69	70
	16	Sampled	75	77	80	77	81	81	82
		Modeled	75	81	81	81	78	78	78
Total Hardness [mg/L]	10	Sampled	113	128	120	119	120	121	115
		Modeled	113	122	122	122	122	122	122
	13	Sampled	98	106	107	108	106	115	120
		Modeled	98	109	109	109	109	109	109
	16	Sampled	164	162	166	164	169	164	165
		Modeled	164	170	170	170	170	170	170

Table 2-34 cont'd

Water quality parameter	Sampling period	Data type	Influent	Coag. Basin	Filtration	GAC	Finished water	AVG1*	AVG3**
TOC [mg/L]	10	Sampled	1.8	1.5	1.4	1.0	1.0	--	--
		Modeled	1.8	1.8	1.8	0.8	0.8	0.8	0.8
	13	Sampled	3.6	2.55	2.2	--	0.51	--	--
		Modeled	3.6	3.6	3.6	1.3	1.3	1.3	1.3
	16	Sampled	2.3	1.9	1.7	--	0.54	--	--
		Modeled	2.3	2.3	2.3	0.6	0.6	0.6	0.6
UVA [cm ⁻¹]	10	Sampled	0.069	0.028	0.024	0.012	0.010	--	--
		Modeled	0.069	0.061	0.061	0.009	0.006	0.006	0.006
	13	Sampled	0.178	0.068	0.054	--	--	--	--
		Modeled	0.178	0.151	0.151	0.018	0.013	0.013	0.013
	16	Sampled	0.075	--	--	--	--	--	--
		Modeled	0.075	0.067	0.067	0.004	0.003	0.003	0.003
Free chlorine residual [mg/L]	10	Sampled	--	--	--	--	1.0	0.9	0.7
		Modeled	0.0	0.0	0.0	0.0	1.0	0.7	0.5
	13	Sampled	--	--	--	--	1.2	0.8	0.7
		Modeled	0.0	0.0	0.0	0.0	1.2	0.7	0.5
	16	Sampled	--	--	--	--	1.3	1.0	0.7
		Modeled	0.0	0.0	0.0	0.0	1.2	1.0	0.9
TTHMs [µg/L]	10	Sampled	--	--	--	--	11.9	23.7	28.8
		Modeled	0.0	0.0	0.0	0.0	9	16	22
	13	Sampled	--	--	--	--	8.1	30.9	47.8
		Modeled	0.0	0.0	0.0	0.0	20	37	53
	16	Sampled	--	--	--	--	8.5	29.6	46.5
		Modeled	0.0	0.0	0.0	0.0	8	16	23

Note: *AVG1 refers to average retention time 1 day. **AVG3 refers to the maximum retention time, 3 days. --: data not available.

6.3.3. Engineering analysis for water treatment adaptation

6.3.3.1. Adaptation feasibility evaluation

Tables 2-31 and 2-33 list the source water quality at the plant water intake in the 1998 base year and the 2050 target year, respectively. For these projected source water changes, the adaptation feasibility of the treatment plant was evaluated using the calibrated and validated WTP-cam model. In this evaluation, the plant treatment processes were assumed to remain unchanged. However, adaptation took place by modifying the GAC treatment operations because GAC was projected to be the most effective process for TOC removal (see Section 6.3.1.2).

Figure 2-67 compares the TOC and TTHM results between the baseline and the future scenarios. The cumulative density function (CDF) was defined by adding the probability of simulated TOC or TTHM concentrations in the finished water. The CDF curves displayed the vulnerability of potential exceedance of the drinking water standards when the treatment processes and GAC operation remain unchanged. Under the baseline conditions, the Miller WTP meets the TOC compliance criteria of 2.0 mg/L (see Figure 2-67a). Under future climate conditions, however, the source water would likely have higher TOC concentrations and different water chemistry. 2765 of the 5000 Monte Carlo runs in the WTP-cam simulations show TOC concentration >2 mg/L in finished water. This result indicates a 55% probability of violating the TOC compliance criterion under the same TOC and TTHM regulation limits. If the

TTHM maximum contaminant level (MCL) became more stringent in future, greater risk of a violation would be higher: if the TTHM MCL decreased to 60 $\mu\text{g/L}$ or 40 $\mu\text{g/L}$, the risk of an MCL violation would increase to 4% or 36% under the future scenario, respectively.

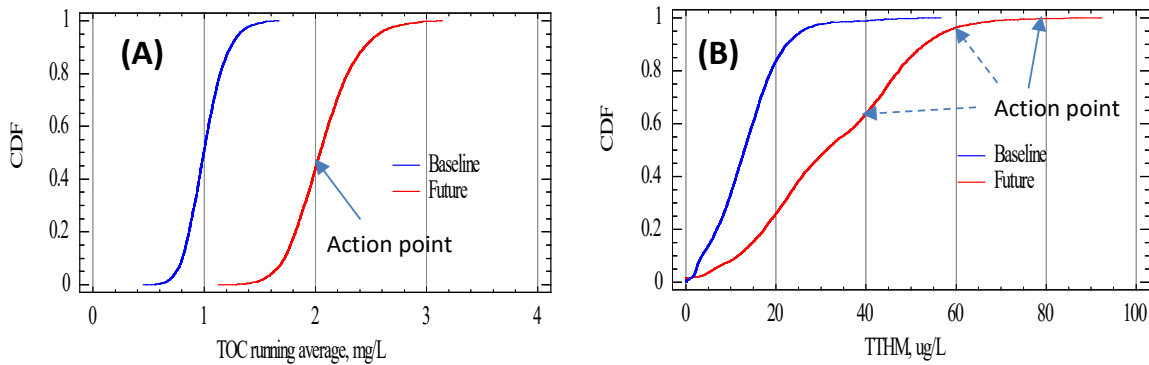


Figure 2-67 Modeled treatment performance of the Miller WTP in baseline (1998) and future (2050) scenarios. (A) TOC running average at finished water; (b) TTHM after 3 days residence in distribution system. Results based on 5000 Monte Carlo simulations.

Li et al. (2014) analyzed these model projections and discussed potential engineering options in the system-scale adaptation. They noted two potential engineering options for current plant configuration and operation:

- One option is to replace the chlorination system with the newly deployed UV disinfection treatment unit in the plant. After UV disinfection, chlorination takes place in the clear well before the product water is distributed at the Miller WTP. Compared to solely relying on chlorination, the modified process using UV disinfection can significantly reduce DBP generation in the treatment and the subsequent distribution. When re-chlorination is required to satisfy the contact time (CT) rule for biological control, the DBP formation may still become a technical challenge when TOC is not adequately removed during water treatment. Boccelli et al. (2003) proposed a mathematical model to analyze the re-chlorination effects.
- The engineering feasibility also depends on the water age in the distribution system. The GCWW water distribution system is a single network that supplies water to the population in a monocentric urban form. As described in Section 4.2, the Cincinnati metropolitan area started to evolve toward a multi-center configuration with increased expansion in the northern portion of the city. How to manage the water age and system efficiency is a central subject in a detailed adaptation feasibility analysis involving both the GCWW treatment and the distribution system. Currently, for assurance of contact time rule compliance in the distribution system, the post-UV product water is disinfected using chlorination at clear well at a reduced level.
- Another option is to optimize the Miller WTP operation by the configuration of the GAC adsorption process for the current and future climate conditions. This option requires no significant capital investment, representing a practical and attractive adaptation solution. Two variables are important to the adaptation feasibility analysis. One is the adaptation threshold of the current system beyond which new GAC contactors or other treatment

units are required. The second is energy consumption in the GAC regeneration and its CO₂ emission in the life-cycle analysis.

6.3.3.2. Adaptation economics in TOC treatment

Currently, the Miller WTP has a total of 12 downflow gravity contactors and two multi-hearth furnaces for onsite reactivation. Each of the contactors has a volume of 595 m³ and a surface area of 181 m². The overall GAC loss rate through the system is 7-8%. According to the past operational data, the carbon loading rate is 482 kg/day of GAC per square meter of the hearth area in GAC reactivation.

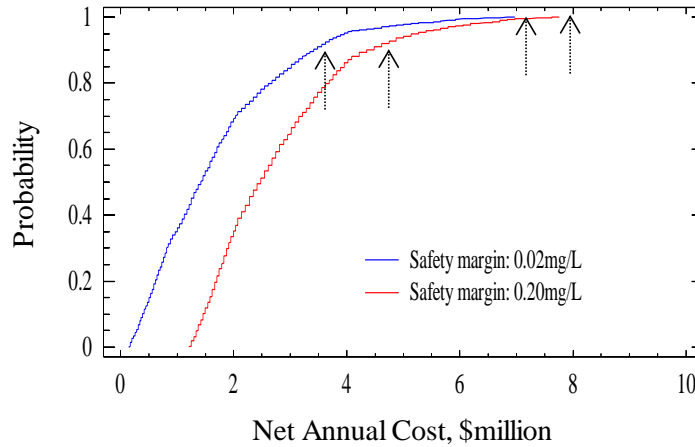


Figure 2-68 Accumulative probability of net annual adaptation cost for the source water change scenario in year 2050. The energy cost can be readily converted into CO₂ emissions.

A capital recovery analysis assumes a return period of 20 years with an interest rate of 5%. The resulting cost curve between the reactivation period and the annualized cost is shown previously in Figure 2-56. The annual cost of the GAC system is expected to decrease with increasing reactivation period. For a reactivation period shorter than 90 days, the annual cost increases rapidly at a shorter reactivation period. The implication of this reactivation period threshold is obvious in adaptation economics.

The net annual adaptation cost is defined as the difference between annual cost calculated using the cost curve in Figure 2-56 and the base annual cost at the current operation. The annual cost for the current operation was \$13.6 million for an average GAC reactivation period of 180 days at the plant. Based on the cost calculation outlined in Section 6.1.3, the cost at a given level of TOC removal – namely, a probability of meeting the compliance level of 2 mg/L can be calculated. The results are shown in Figure 2-68. The net annual cost to control TOC <2.0 mg/L in the 2050 climate scenario would decrease to \$7.0 million for a 0.02 mg/L safety margin or \$7.8 million for a 0.20 mg/L safety margin. If the plant performance criterion allows a 10% risk for TOC above the 2.0 mg/L limit or a 0.9 compliance probability, the net annual cost would further reduce to \$3.4 million for a 0.02 mg/L safety margin and \$4.4 million for 0.20mg/L safety margin (Figure 2-68).

6.3.3.3. Implication for engineering practice

The adaptation case study at the Miller WTP shows an example of the quantitative analysis that examines engineering approaches in system-scale adaptation. The results show the system’s adaptability to offset source water changes projected for the year 2050. The adaptation reliability is quantified by evaluating and comparing the ability to achieve regulatory compliance, adaptation economics, and climate co-benefits in energy reductions.

Quantitative engineering analysis using WTP-cam allows one to project the likely future changes in source water quality and engineering options in a successful adaptation. It is important to note, however, that several assumptions were built into the analysis. These assumptions include: (1) the correlation matrix among water quality parameters used in WTP-cam modeling is assumed to remain unchanged through time; (2) compliance criteria in SDWA regulations such as DBP standards in drinking water remain unchanged in the future; and (3) the current treatment technologies in the removal of TOC are effective and remain deployed. One can observe from these assumptions that such adaptation analysis depends on location-specific conditions, anticipated future technological and regulatory environments.

7. Adaptation Engineering for Drinking Water Distribution

Water quality management in drinking water distribution networks is another important area in system-scale infrastructure adaptation to address the changes with climate and land use conditions. Efficient and adaptive water distribution (this Section 7.0) and treatment (Section 6.0) are the two essential components of the SmartWater system (Figure 2-7).

Drinking water quality at consumers' tap depends on both the water demand management over a service area and the control of water quality variations in the treatment and the distribution itself. This relationship is schematically shown in Figure 2-11. The changes in climate and land use have produced and likely will continue to produce impacts to surface water quality. Some examples include long-term hydrological changes, short-term disruption of meteorological extremes, seasonal variations of water quality parameters (e.g., TOC, turbidity), as well as the occurrence of eutrophication conditions (e.g., high temperature and nutrients) with the prevalent presence of *chlorophyll-a* and cyanobacteria. These types of source water changes are pertinent challenges to the planning and operation of a water treatment plant and distribution system. Despite the multi-barrier approach utilized to protect public health in the U.S., perturbations or changes in source water may affect the performance of the conventional drinking water treatment plant.

Water demand variation, both in space and time, is the primary factor affecting drinking water quality in the municipal water supply (Figure 2-11). Water demand is a function of urban development, urban adaptation, asset management, and socioeconomic factors. These factors are often dependent upon a collection of urban management and policies, rather than a simple technical issue on the distribution network itself. For example, the urban adaptation facilitated by land use planning and transportation infrastructure can significantly affect the spatial distribution of population and business activities, and thus result in substantial changes in the location of water demands.

Municipal development goals play an important role. Many water utilities are now focusing on two water conservation measures (see U.S. EPA, 2015a). One is water conservation through the reduction of water loss or non-revenue water in the water distribution pipelines to customers' taps. This measure is a part of the water utility asset management described extensively in the literature and U.S. EPA reports (e.g., Barlett et al., 2017; EPA, 2007c). Because of the aging water infrastructure, a nation-wide average rate of water loss is around 18-20%. Some utilities with old water pipes and complex pressure zones to manage may experience water loss as high as 50% in some distribution network segments. The other measure relies on water use reduction on the per capita basis through market and management actions. Some U.S.

water utilities in water-poor regions are actively developing management and economic incentives to encourage water-saving practices, such as artificial lawns. It is noted that this option may bring other implications. For example, strict per capita goals may impact water utility revenue and thus have a negative response in limiting the ability of commercial development and job growth.

For water distribution, the SmartWater system for adaptation leverages technological advances in sensor-based model-driven system controls. Drinking water distribution modeling and system control based on the EPANET hydraulic model of Rossman (2002) and extensions (Uber et al., 2004; Shang et al., 2008) are widely used. Water quality control in distribution systems has been also investigated extensively since the 1990s. A wide range of technical data, models, and management methodologies are now available (e.g., Rossman, 2002; Uber et al., 2004; Shang et al., 2008; Boulos et al., 2006; Mays, 1999; and references therein). However, these existing advances are mostly without consideration of changes in future climate-dependent demand and urban conditions.

When considering the impacts of climate and land use changes, a confluence of factors can all affect the water quality management in a distribution system. To reduce the water quality deterioration in distribution is the focus of adaptation. Important factors include high TOC in source water and potentially in the finished water of a treatment plant, rising water temperatures, higher ground temperatures surrounding buried water pipes, as well as changes in the reactivity of organic matter under future climate. There are several U.S. EPA guidelines on water distribution systems; those practices will be not repeated in this report. Instead, the report here is focused on adaptation methods and tools in three areas below:

- modeling DBP concentrations in water supply for vulnerability assessment;
- in-network water treatment to manage DBPs formed in the distribution system; and
- modeling of the water demand changes for developmental scenario analysis.

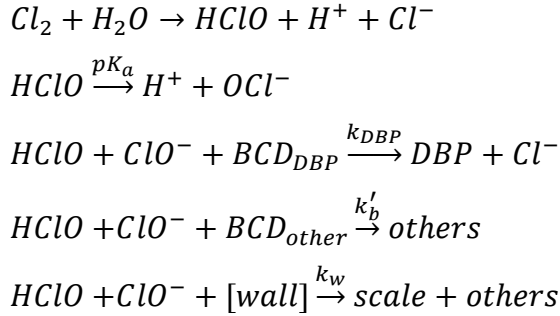
7.1. Water age and water quality changes in distribution: The need for adaptation

Disinfection by-product (DBP) formation during drinking water distribution is an inevitable outcome due to reactions between residual disinfectants and DBP-formation precursors in the organic matter. The well-known water quality impacts are regulated under the SDWA contact time rule/DBP Stage-II rules (see U.S. EPA, 2015a). The need for adaptation in water distribution can be assessed through compliance monitoring that is often guided by EPANET-based simulation of residual chlorine and DBP concentrations. This section is based on recent publications by Zhao et al. (2018a, 2018b, 2017) and others cited therein.

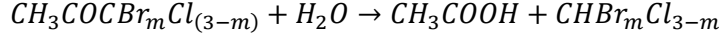
7.1.1. EPANET-based risk assessment on DBP formation

Model simulation has been widely practiced for the water distribution system since its inception in the late 1980s. Chlorine as an oxidant in drinking water reacts with TOC to form DBPs, including the regulated trihalomethanes (THMs) and haloacetic acids (HAAs). At the same time, chlorine is also simultaneously transferred to pipe walls and consumed in reactions with pipe wall materials and biofilms. In the simplest terms, total free chlorine [Cl] – the sum of hypochlorous acid [$HClO$] and hypochlorite ion [ClO^-] in a flowing pipe, reacts with natural organic matters [NOM_{DBP}](e.g., humic and fulvic acids) in the bulk water demand [BCD] to

form DBPs. A fraction of $[Cl]$ also reacts with other bulk demand $[BCD']$ without DBP formation. Bulk water demand consists of organic materials and other chlorine reactants and those forming from a detachment of biofilms and pipe scales in water distribution. Chlorine also reacts with pipe wall materials and attached biofilm, with both terms lumped together as the wall demand. Generally, the multi-component chlorine reactions can be written as:



DBPs, represented by trihalomethane (THM) compounds – trichloromethane, bromodichloromethane, dibromochloromethane, tribromomethane, collectively as total THMs (TTHMs), form during chlorination through stepwise NOM-oxidation and hydrolysis as illustrated below. Using the model compound propanone CH_3COCH_3 and m as the Br molar fraction:



The simultaneously occurring processes in a flowing water pipe are schematically shown in Figure 2-69. Analytical solutions for the chlorine transport and DBP formation have been published (e.g., Biswas et al., 1993; Rossman, 2002; and Clark, 1998). Clark and Haught (2005) developed a mass transfer limited chlorine model and compared it with others in Rossman et al. (1994) and Biswas et al. (1993). Clark et al. (2010) further analyzed the competing chemical reactions in the modeling of chlorine decay and DBP formation. In the center of discussion are the water quality models of Clark (1998) and other subsequent publications (e.g., Clark and Sivaganesan, 2002; Boccelli et al., 2003). These models stipulate that in second-order kinetics, the DBP concentration increase from an initial condition ($C_B - C_{B,0}$) is proportional to the decay of chlorine concentration ($C_{A,0} - C_A$) by the proportion constant T' in the distribution pipe:

$$C_B = C_{B,0} + T'(C_{A,0} - C_A) \quad (2.41)$$

$$T' = \frac{k_D}{k_w + k'_b} \quad (2.42)$$

The proportion constant T' is simply a ratio of DBP formation kinetic rate (k_D) over the total chlorine decay ($k_E = k_w + k'_b$); k_w and k'_b are the reaction rates for wall demand and bulk demand, respectively. In this research, the analytic solution of Clark (1998) was further refined based on kinetic theory and comparative experiments conducted at the U.S. EPA Test and Evaluation Facility. The study led to the proposal of new analytical models in Eqs.2.43-2.44, respectively, for chlorine decay and DBP formation (Zhao et al., 2018a; Yang et al., 2008). The

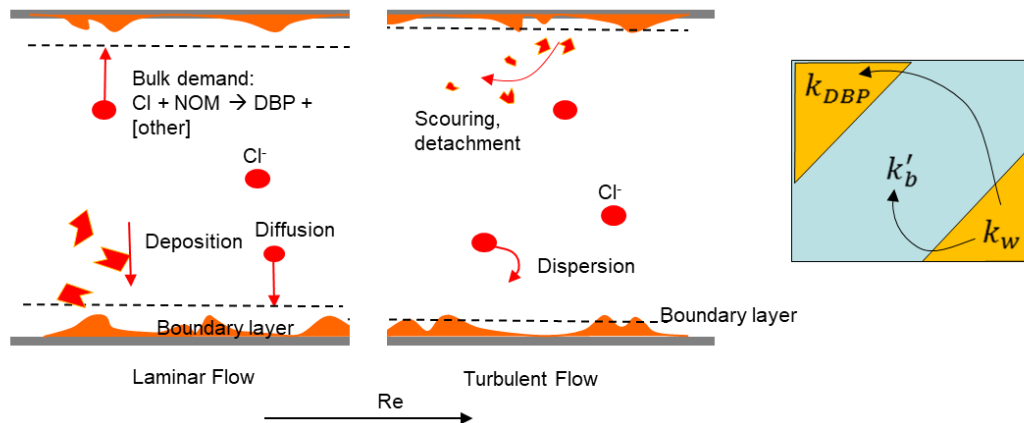


Figure 2-69 Schematic diagram showing the simultaneously occurring chlorine reactions in bulk and wall demands, and mass exchange between the bulk water and pipe wall. Implications on reaction kinetics for bulk decay (k'_b), DBP formation (k_D), and wall decay (k_w) are shown on the right. From Zhao et al., (2018a).

DBP analytical equation can be simplified to Eq.2.45 under common conditions in water distribution when DBP-forming fractions in the bulk demand are very small or $\theta \sim 0$:

$$\frac{\Delta C_B}{C_{A,0}} \cong \frac{k_{DBP} \left(1 - \frac{C_A}{C_{A,0}}\right)}{(k'_b + k_w)} C_{E,0} - \frac{k_{DBP} \theta \cdot C_{A,0}}{2(k'_b + k_w)} \left(1 - \frac{C_A}{C_{A,0}}\right)^2 \quad (2.43)$$

$$C_A = \frac{C_{A,0}}{\left(1 + \frac{\theta}{\gamma} C_{A,0}\right) e^{k_E t} - \frac{\theta}{\gamma} C_{A,0}} \quad (2.44)$$

$$\Delta C_B \approx Y \cdot C_{A,0} - \frac{k_D}{(k'_b + k_w)} \cdot C_A \quad (2.45)$$

The DBP formation in distribution systems depends on not only initial chlorine concentration but more importantly, the reactivity of DBP-forming precursors and their reactivity. This is expressed as the kinetic ratio $\frac{k_D}{k_w + k'_b}$ in Eq.2.45, and θ in Eq.2.43. The models will be further reviewed and incorporated into the EPANET for the SUD's SmartWater module. First, the simultaneous occurrence of chlorine decay and THM formation depends on the kinetic ratio $\frac{k_D}{k_w + k'_b}$ that, in turn, is a function of pipe flow hydrodynamics. Several common water quality parameters, including total organic carbon (TOC), residual chlorine, UV256, water pH, and temperature, have been used to estimate the THM formation potential (Clark and Sivaganesan, 2002). As shown in Eqs. 2.43-2.45, the non-DBP forming bulk demand and the

wall demand compete for the finite chlorine residual in water and thus affect the THM formation potential in competitive reaction.

Second, NOM properties and specifically the chlorine-reaction fraction are the controlling variables in competitive reactions. Removal of reactive NOM fractions in treatment is the effective approach to decrease θ , T and Y in order to simultaneously maintain the required chlorine residual level and reduce the THM formation potential. For aged NOM with small θ , such as GAC-treated tap water, the hydrodynamic effects on k_E and $\frac{k_D}{(k'_b + k_w)}$ cannot be neglected. The reaction competition from flow-dependent wall demand becomes comparable with THM-forming and other bulk demand.

Finally, the kinetic constants and the time to reach a pseudo-steady state are all related to pipe flow hydrodynamics. Many parts of a distribution network may have water ages exceeding 24 hours, with re-chlorination possibly necessary to compensate for the excessive loss of chlorine residuals for biological control. Re-chlorination, however, will further increase the DBP levels (Boccelli et al., 2003) even to the extent of violating drinking water standards. Therefore, it is of fundamental importance to reduce water age through adaptive engineering measures, such as through tank operations and better monitoring water demand in real-time throughout a distribution network, and perhaps structurally by changing the routing of water, pipe sizes, and other network configurations. The need for adaptation to water demand and water age management is described next.

7.1.2. Water age variations, modeling and adaptive control

Water age varies significantly in a distribution network. An extended water age (t) in Eqs.2.44-2.45 can result in low residual disinfectant levels and elevated DBP concentrations, a phenomenon that has been widely documented. One central adaptation objective is to assess the vulnerability and to plan and design corresponding adaptation measures.

For vulnerability analysis, this research recently completed real-time water demand measurements over 25% of the network nodes for 2 months for an independent distribution segment in Cincinnati, Ohio. Subsequently, a hydraulic and water age simulation was conducted using the EPANET model (Zhao et al., 2017). The $\sim 38.6 \text{ km}^2$ network serves 8,485 buildings, consisting of 4,843 pipes, two elevated water tanks, four booster pumps, three control valves, and one water reservoir for water supply. In the network, the north and south supply areas supplied by the two elevated tanks contain numerous local pipe loops many in “H” configurations and dead-end branches of < 8 -in diameter. The study results clearly showed large water age variations that can be monitored and analyzed using all-pipe and all demand (APAD) techniques (Zhao et al., 2018b). In comparison, the hourly demand variation curve (HDVC) modeling widely used currently is incapable of assessing the water age variability. Two conclusions are particularly noteworthy with implications to the water age assessment and management:

- The pulse nature of water demand is prevalent among individual water users throughout the network. In the one-week 68-hr period, measured pulse demand in most network nodes is zero for approximately 70% of the time (Figure 2-70). In the analysis, the time-discontinuity in water demand starts to disappear at the level of 31-home demand

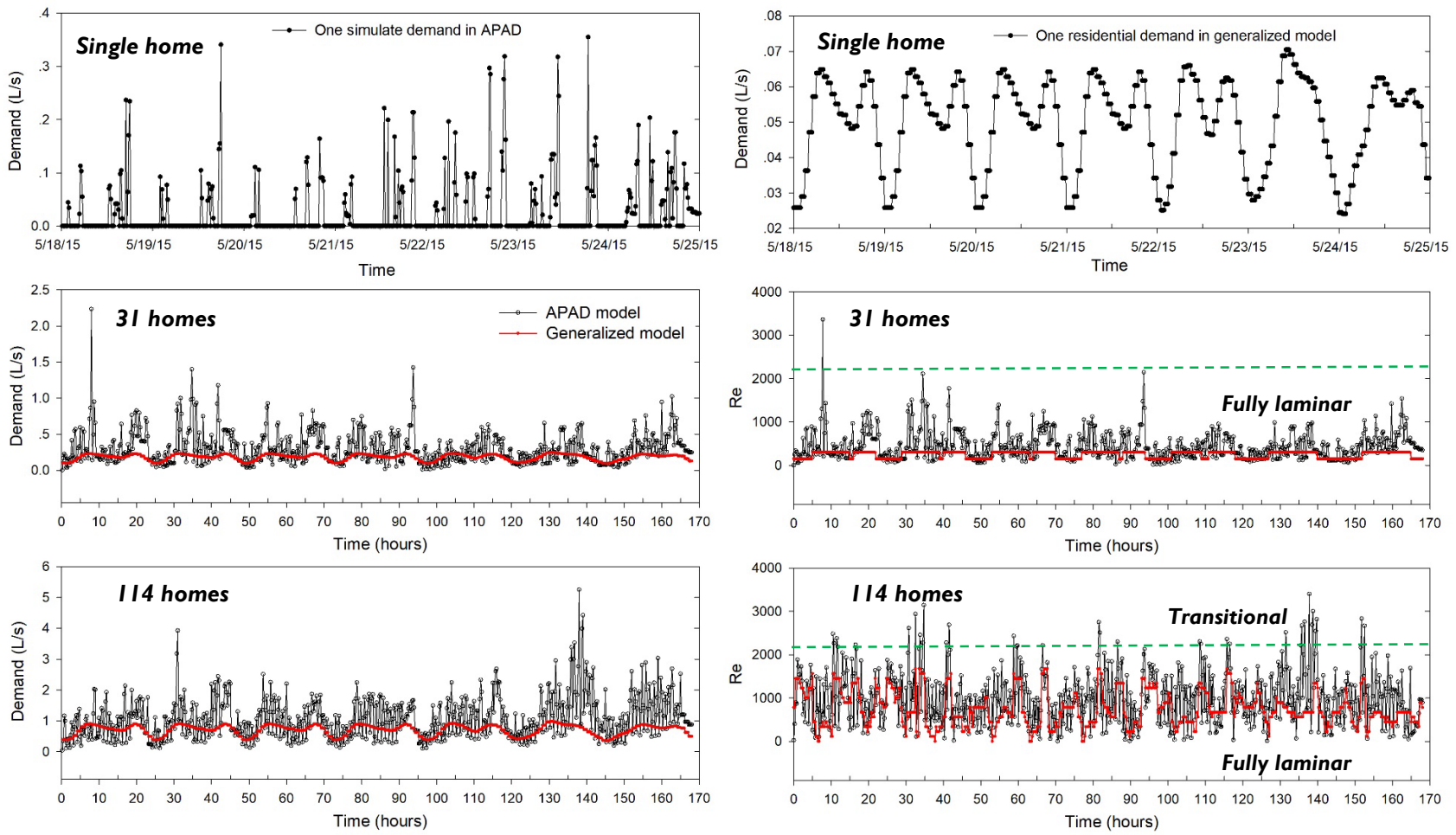


Figure 2-70 Water demand and computed Re variations in a two-week period for a single home, 31 and 114 homes of a pipe dead-end section, showing significant differences between the APAD model and the generalized water demand pattern. From Zhao et al. (2018b).

aggregation. It is replaced by time-continuous variation patterns for a block of 114 homes (Figure 2-70).

- There is a large range of water ages among all network nodes (Figure 2-71). Simulated water ages during the two-week validation period average at 35.8 and 34.6 hours given by the APAD and HDVC models, respectively. Both demand models yield a large spread of simulated water ages from <15 hours near the pump stations to over 180 hours in dead-end branches.
- In all cases, the large spreads in water age and their spatial association with the network configurations (Zhao et al., 2018b) point to the need for network optimization and adaptations. Some adaptation measures that were discussed in the literature include reconfiguration of local pipe loops, synchronized tank operations, re-chlorination, and in-network water treatment. The latter is one major technical approach as described in the next Section 7.2.

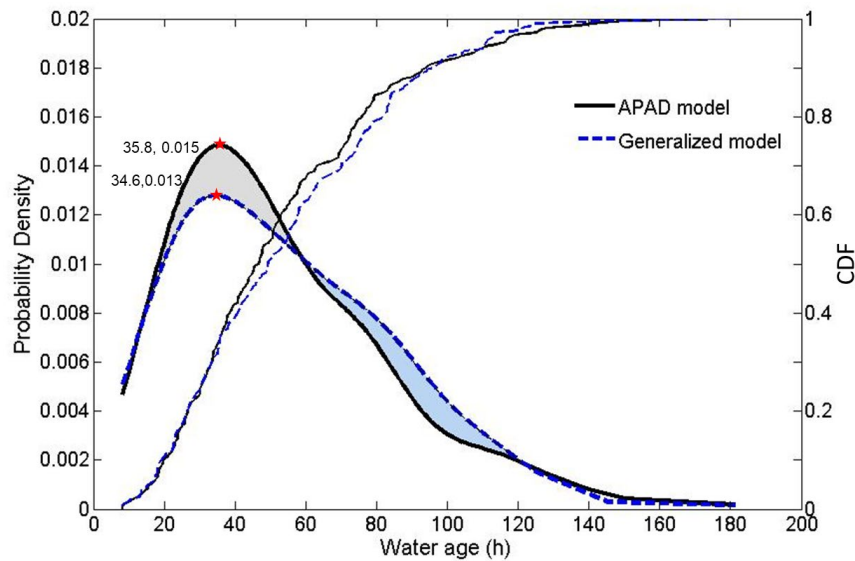


Figure 2-71 Probability distribution and corresponding CDF of simulated water age for the network. From Zhao et al. (2018b, 2017).

7.2. In-network water treatment as adaptation measure

Except for TOC removal in water treatment plants, other adaptation approaches for effective THM management rely on water quality management in finished water distribution as the last barrier to protect human health. Water quality management in distribution is not new. Decades of research and practical engineering have produced a suite of distribution system models (e.g., EPANET, EPANET-MSX, etc.¹¹) and technological innovations in the in-network water treatment. For the latter, examples can be found in re-chlorination, in-network GAC absorption, and aeration.

¹¹ <http://www.epa.gov/nrmrl/wswrd/dw/epanet.html>

Unique for source water changes is the focus of adaptation measures on extreme conditions giving arise from climate and land use changes. These changes are not considered in traditional water supply engineering. For example, some water supply systems have experienced a rapid decrease in water demand due to socioeconomic changes or the loss of major employment centers, resulting in an oversized distribution system. The hydroclimatic changes also can generate conditions resulting in high TOC concentrations in source water and finished water, as well as leading to warm water temperatures in pipelines. Higher water temperature, high-concentration of reactive NOMs in water will likely make DBP control a necessary but difficult task. It will concurrently increase biofilm formation. For these impacts, the in-network aeration and GAC treatment during distribution have been investigated to remove THM and other volatile contaminants.

In-network aeration

The use of aeration to remove volatile organic compounds, including THMs, relies on the principles of air-liquid two-film mass transport. In water distribution networks, the air stripping process is commonly used by retrofitting the existing water storage tanks and in-ground reservoirs. Such an application was being tested and investigated at the Las Vegas Valley Water District (LVVWD). Figure 2-72 shows a schematic illustration of the aeration system constructed at the Alphas twin tank storage basins.

In the EPA-LVVWD joint research, one retrofitted water aeration system in the LVVWD alpha tank was investigated. The system consisted of low-profile fine bubblers, air manifold, and tank mixer (Figure 2-72). The mixer and other media (e.g., plastic cubicle) were used to improve the stripping efficiency of fine bubblers. However, because of the limited water depth above the bubbler, these types of aeration systems tend to have low stripping efficiencies or use high air-to-water ratio for greater removal rates; for the latter, the improvement is at the expense of energy consumption, a major consideration in adaptation design.

McDonnell (2012) investigated the mechanisms and modeling of in-network aeration for THM removal. The investigation included experimental testing of the THM stripping in an

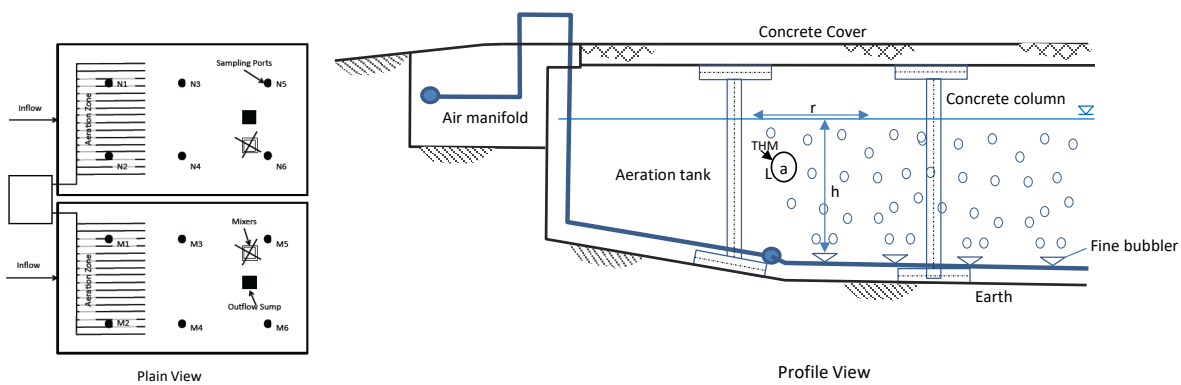


Figure 2-72 Schematic views of in-network aeration in the LVVWD water distribution network to remove volatile THM from drinking water in the alpha tank reservoir. Illustration after actual tank-retrofitted aeration system: left – plain view of air sparging pipes lines and tank mixers (M1-M6, and N1-N6); right – profile view showing air bubble plume geometry and the two-film transport mechanisms. h – effective water depth; r – diameter of air bubble plume.

experimental water column, and mass transport modeling of field testing in the LVVWD's tank Alpha. The results led to the development of a THM stripping model as a program extension for the EPANET Multi Species Extension (MSX) v.1.2.0 (Shang et al., 2008). The effect of in-network aeration on water quality was further modeled using EPANET and the extension.

The aeration in the Alpha tank has significant effects on THM concentrations in the network. As shown in Figure 2-73a, pressure zone 2 receives 75% of its water from the Alpha Tank during an average day. In response, pressure zone two received the greatest reduction in average total THM concentration. The TTHM removed in nearly half of the nodes is 90 mg/L (Figure 2-73b). This is expected since pressure zone two is heavily influenced by the Alpha tank. Water quality network modeling using EPANET 2.0 for the study is provided in McDonnell (2012).

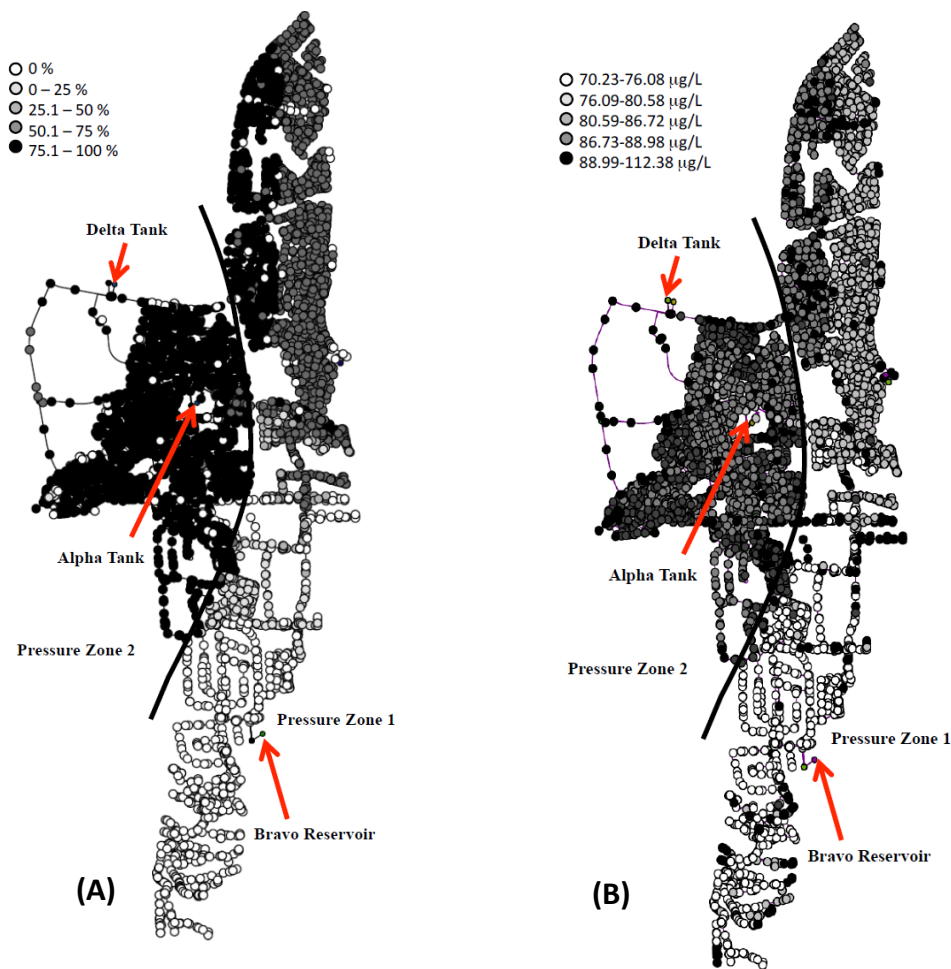


Figure 2-73 EPANET simulation of flow and THM distribution in the Western Hill portion of the LVVWD water distribution system. (A). fractions of water from Alpha Tank; (B). distribution of THM reduction after aeration at normal air flow rate of 2 standard cubic feet per second in the Alpha Tank. Adopted from McDonnell (2012).

GAC treatment and other post-formation treatment processes

GAC and other absorbents (e.g., zeolite) have been used in the removal of DBP compounds from drinking water; this technology has also been applied at the point-of-use and point-of-entry (Stubbart, 2004) as a part of the small systems¹². The adsorption logistic models for TOC simulation were presented in Sections 6.2-6.3. Similarly, GAC has been used to remove THMs, whereas it is less effective for mono and dihaloacetic acids (Tung et al., 2006). In addition, membrane filtration such as reverse osmosis and nanofiltration (Kimura et al., 2003; Uyak et al., 2008) have been tested and studied for removal of THM species from drinking water.

7.3. Water conservation, storage and reuse through adaptive planning

Water availability and water shortage are other characteristic impacts of the hydroclimatic and land use change. Water conservation, storage and reuse of reclaimed water are valuable practices in adaptation for many water-stressed regions. Examples can be found in Las Vegas and other cities in the U.S. southwest and southern California. Even in water-rich regions, water conservation is often a technique for the reduction in water and energy usage. These adaptation techniques to relieve hydroclimatic impacts are described in Ranatunga et al. (2014), Wang et al. (2013), Neil et al. (2012, 2014), Yang and Restivo (2010). Details of these adaptation techniques are contained in U.S. EPA (2017a, 2015b).

8. SUD Applications in Coastal Regions: Water Infrastructure and Emergency Planning

Existing data and research results show that changes in precipitation patterns and overland runoff hydrographs will almost certainly impact the drainage capacity, stormwater control measures, LID, and green infrastructure, as well as stormwater discharges, including the long-standing CSO challenges facing many U.S. cities (U.S. EPA, 2013b; Johnson et al., 2015). Coupled with land use changes, the vulnerability of these infrastructure assets cannot be underestimated. Some specific analysis is shown in Tables 2-23 and 2-25. Impacts on unit processes are illustrated in Figure 2-49 of Section 5.2.2.2. Specific adaptive engineering solutions are location-specific, mostly related to changes in precipitation, runoff, disruptive storms such as hurricanes, storm surge, and sea level rise.

In this section, vulnerability and adaptation analysis for the stormwater and wastewater infrastructure in coastal regions are briefly discussed. A full analysis of the coastal water resources and water infrastructure will be published separately, where case studies along the Atlantic coast and the Gulf of Mexico will be examined.

8.1. Water infrastructure vulnerability in coastal regions

The U.S. coastal zone hosts over 80% of the population, vast built infrastructure, over 90% economic outputs, and invaluable ecological resources. Nearly 39% U.S. population in 2010 lives within 50 miles (~90 km) of coastal lines¹³. In the low-lying Atlantic coast and the Gulf coast, the built and future infrastructure and sensitive environmental assets are vulnerable to extreme meteorological events such as Hurricane Sandy. Tropical cyclones, hurricanes, and

¹² http://www.mae.gov.nl.ca/waterres/reports/cwws/BMPs_for_Control_of_DBPs_Apr_13_2009.pdf

¹³ <http://oceanservice.noaa.gov/facts/population.html>

storm surges have demonstrated the potential to compromise structural integrity and service functions of critical aboveground assets by wind damage, flooding, and the change of surface water and groundwater hydrology. The impacts and destruction of “soft” environmental assets such as coastal marshes and wetlands cannot be neglected either.

Figure 2-74 schematically shows three principal types of short-term disruptive and long-term hydroclimatic threats to the coastal infrastructure. Near the coast, sea level rise changes the hydraulic gradient for communities in low lying areas. For example, according to the City’s Department of Environmental Protection, the City of New York has experienced the sea level rise effects on drainage systems and wastewater pump stations in the low-lying Queens district. Storm surge, particularly those associated with hurricanes, are shown to repeatedly result in severe inundation of the coastal areas. The combined effect of sea level rise and storm surge is even more disruptive. To above-ground infrastructure, wind damage associated with hurricanes

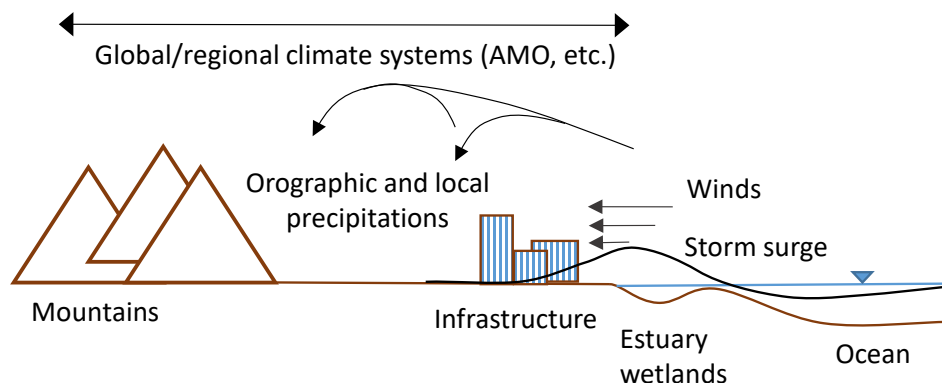


Figure 2-74 Schematic illustration of long-term climate and short-term meteorological and disruptive storm surge events in a typical coastal zone.

can be disruptive. The electric grid damage and supply disruption are particularly important to the water infrastructure services, during and after the events.

In the inland region away from the coastline, the coastal mountains and other geophysical features induce strong atmospheric interactions with global/regional climate systems such as Atlantic Meridian Oscillation. This atmospheric interaction can introduce localized moisture circulations such as orographic precipitations and rain shadows (e.g., McKenny et al., 2006; Konrad II, 1997; Wallis et al., 2007; Changnon, 2006). These localized rainfall anomalies and changes in the future climate may not be captured in conventional hydrological design guidelines such as NOAA’s Atlas-14 precipitation design tables.

Table 2-35 lists major hydrological impacts and adaptation design variables for water infrastructure and other environmental assets. These engineering considerations of intense precipitation, wind speed, and storm surge include a revision to engineering parameters for wind (average speed, gust speed, and direction), precipitation (duration, depth, and intensity), and inundation level (depth and duration). Specifically:

- Design precipitation (duration, depth, and intensity). Urban infrastructure systems or components are planned and designed to assure adequate hydraulic capacities providing

Table 2-35 Selected hydrological impacts and adaptation variables in coastal area.

	Design Precipitation	Design Wind*	Design Inundation*
<u>Infrastructure assets</u>			
Roadways	Movement of vehicles Runoff management Pavement damage	Damage to light fixtures and signs	Pavement damage Base damage Damage to structures/bridges
Water supply	- Source water quality, - Equipment flooding	- Damage to power supply - Physical damage to structures	- Flooding and inundation - Salt water intrusion
Stormwater and wastewater facilities	- Runoff management; - Hydraulic capacity of structures (e.g., pipe, culvert, sluice gate) - Stormwater quality and discharge - Flooding	- Damage to power supply - Physical damage to structures	- Flooding and inundation
Solid and hazardous waste facilities	- Flooding - Cover design - Groundwater level and control	- Cover design - Dust dispersion and control - Disruptive wind damage	- Flooding and inundation
<u>Environmental assets</u>			
Estuary wetlands	- Nutrient flux - Changing hydraulics of flows	- Disruptive wind damage	- Flooding and inundation
Riverine	- Base flow and drought - Nutrient flux and flora ecohealth - Peak flow and erosion	- Disruptive wind damage	- Flooding and inundation

Note: * Refer to wind and inundation in coastal shores are related to cyclones and storm surge.

desired water services. The design basis is often in the form of a design storm such as 10-year 24-hour precipitation. Application examples include culvert sizing in road construction, pipe sizing and grading for drainage of urban runoff, and retention pond design for stormwater management (Table 2-35). Note roadways are not exempt from this type of damage to the pavement and electrical fixtures.

- Design wind (average speed, gust speed, and direction). Design values for average wind and gust wind vary among engineering conventions and often are specific to the design objective and its risk category. For example, the 25-year, 50-year, and 100-year wind speeds are used in determining the minimum strength load requirements for Occupancy Category I, II, and III infrastructure, respectively (ASCE, 2014; Simiu, 2011; Cook et al. 2011). The U.S. EPA specification requires a temporary landfill cover to be designed against a gust wind speed of 2 m/s (Table 2-35).
- Design inundation (depth and duration). In coastal areas, the inundation level is the sum of flooding and wave action or surge. The surge actions increase the flooding level and spatial extent, and the surge-related inundation is temporary. Acute hydraulic impacts recede after the disruptive storm surge event. The schematic in Figure 2-75 shows the concept of water action and storm surge height during a hurricane event. Thus, both inundation depth and duration are two primary design parameters (Table 2-35). Road bases and pavement may be permanently damaged by inundation.

How to plan and manage these valuable assets under the current and future conditions are essential to coastal risk assessment and management. For this purpose, the SUD methods and tools are designed to analyze the hydrological and transportation impacts in coastal hydroclimatic events. Detailed analysis and technical basis for these tools will be presented in subsequent publications. Here in this report, the case study at the town of Mattapoisett in the

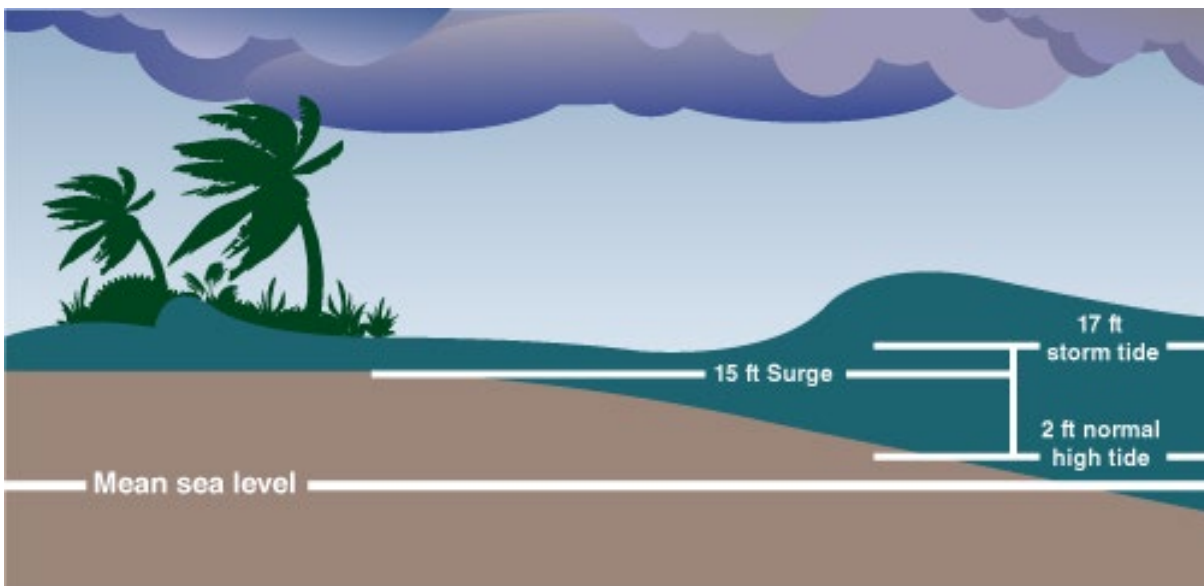


Figure 2-75 Schematic diagram showing wave action and storm surge height as a function of storm surge, tidal cycle, and sea level rise. Numbers are for illustrative purpose. From NOAA website (<https://www.nhc.noaa.gov/surge/>).

Massachusetts southeast coast is described to show how SUD is used to develop the technical basis for wastewater adaptation and emergency evacuation planning

8.2. Wastewater vulnerability and adaptation in storm surge

Mattapoisett is a small fishing town at the shore of Mattapoisett Harbor. Wastewater from the residence and commercial entities is collected by a network of gravity sewer pipes and then pumped to a regional wastewater plant using a transfer pump station at the side of the harbor (Figure 2-76). One objective for the risk assessment was to quantify inundation and its impacts on wastewater system operations.

In this analysis, the NOAA’s Sea, Lake, and Overland Surges from Hurricanes (SLOSH) model was used to simulate the storm surge height under specific local conditions including topography, Mattapoisett Harbor bathymetry, likely storm tracks in the Mattapoisett area, and atmospheric profiles at the origin of storm surge in the open sea. Table 2-36 shows the ranges of major variables, yielding a total of 432 model runs. The modeling results yield estimates of water depth, wind speed, and direction at a point of 50×200 m spatial grids. For each geographic location, the projected water depth for all model runs form an envelope of inundation depth estimates. The Maximum Envelope of Water (MEOW) provides the worst-case basin snapshot for a particular storm category, forward speed, trajectory, and initial tide level, incorporating uncertainty in the forecasted landfall locations. The Maximum of MEOW (MOM), on the other hand, provides the worst-case snapshot for a particular storm category under "perfect" storm conditions described by a combination of forwarding speed, trajectory, and initial tide level. In practice, MEOW can be used for planning while MOM would be for emergency planning and evacuation.

Table 2-36 SLOSH modeling parameters for storm surge modeling at Mattapoisett, MA

Parameters	Values	No. of Variations
Landfall location	1 (Hurricane Bob)	1
Pressure (mb)	40, 60, 80	3
Radius of maximum wind (mile)	25, 40, 55	3
Forward wind speed (mph)	30, 45, 60	3
Track direction (degree)	NNW, N, NNE, NE	4
Sea level rise (ft)	0, 1, 2, 4	4
Total Number of Model Runs		432

The location-specific SLOSH modeling was calibrated against the inundation extent of historical Hurricane Bob in August 1991. During Hurricane Bob, storm surge pushed salt water over the salt-lock dam into the Mattapoisett River northwest of the town. The overtopping resulted in salt water intrusion into the river, and consequently into the unconfined aquifer and impacted groundwater at the Fairhaven Tubular well field immediately north of the dam. The aquifer is source water for the regional drinking water treatment plant, approximately 3.5 miles southwest of the town. Using the calibrated model, the inundation map based on MEOW results for a Category-4 hurricane is constructed (Figure 2-76). Major findings are:

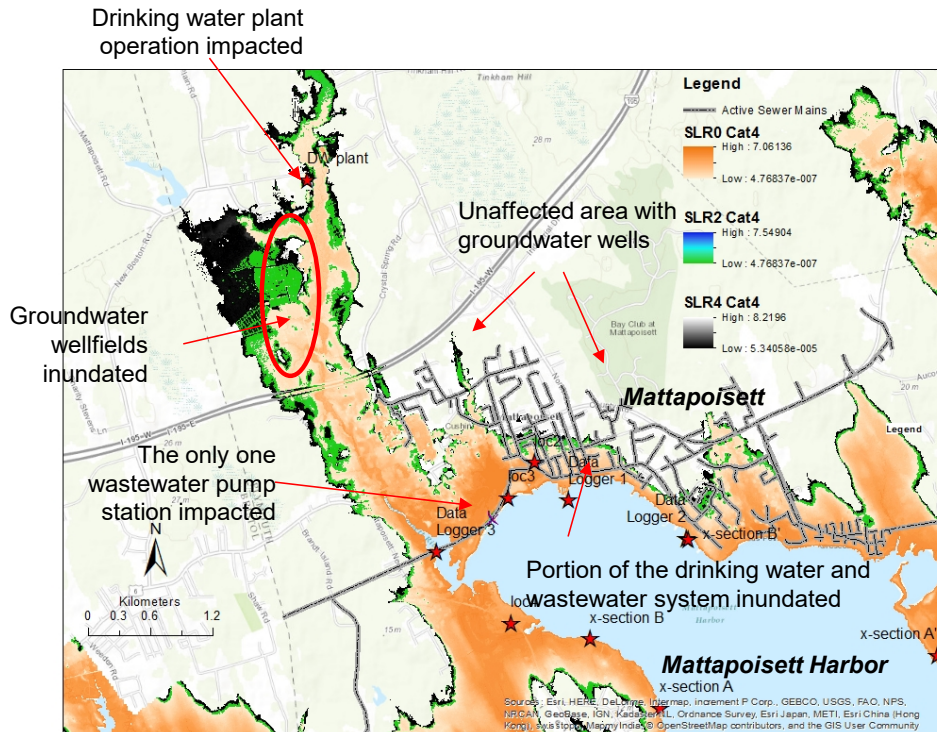


Figure 2-76 Location of the water infrastructure at the Town of Mattapoissett aside of the Mattapoissett Harbor.

- The vulnerable areas of Mattapoissett (the southeastern region) that are inundated by storm surge remain approximately the same under the different hurricane and sea level rise scenarios. This is due to the topographic slope towards the harbor. Storm surge and rate of inundation from a Category 4 hurricane at the current sea level could result in inundation depths over 13.4 feet in some locations in Town. The maximum inundation depth can be reached within 5 hours of the time of landfall.
- The wastewater pump station at Eel Pond in the southwestern corner of the town is also at significant risk. The pump station could be submerged under a Category 2 hurricane or above. In a Category 3 hurricane and at the current sea level, the SLOSH simulation shows 5.8 feet water depth at the Eel Pond (Figure 2-77). The water depth would increase to over 13 feet under a Category 4 hurricane.
- Such inundation and physical damage can make the critical wastewater transfer station at Eel Pond inoperable. Currently, the wastewater transfer station has no backup. Loss of service could affect the town's residents after the hurricane during the recovery phase.

8.3. Emergency evacuation and water supplies

The AIR-SUSTAIN module of the SUD system was further applied to assess the traffic conditions during hurricane evacuations, likely evacuee migration paths and bottled water supply at shelters. In this simulation, SLOSH-model generated inundation maps were used as inputs to the AIR-SUSTAIN module to estimate the inundated area, affected population, and potential evacuation routes under four categories of hurricanes (Table 2-37). The population and

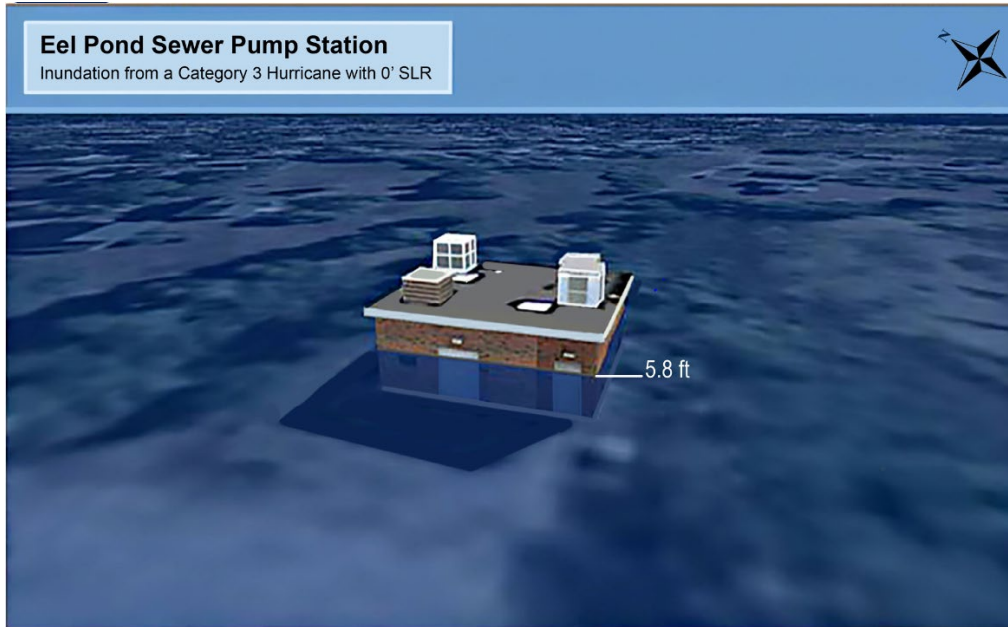


Figure 2-77 A cartoon illustration of SLOSH modeling results on likely inundation risk for the wastewater transfer station at Mattapoisett, MA.

households are based on the 2010 population census data. Overall, there would be over 2200 people and over 1500 households likely in the estimated evacuation area when a Category 4 hurricane landed directly in Mattapoisett Harbor.

Traffic simulation using AIR-SUSTAIN considers evacuees and the traffic flow from the two large cities to the west: New Bedford and Fairhaven. It is further assumed that 80% of the evacuees elect to travel to family and friends outside of the inundation zone, while the other

Table 2-37 Population affected for evacuation under four categories of hurricane

Sea Level Rise (ft)	Hurricane Category 1			Hurricane Category 2		
	Traffic analysis zones	Affected Population	Affected Household	Traffic analysis zones	Affected Population	Affected Household
SLR 0	121	15,995	8,429	136	28,117	14,589
SLR 1	122	16,086	8,487	136	28,235	14,675
SLR 2	122	16,196	8,561	136	28,335	14,735
SLR 4	122	16,380	8,677	136	28,514	14,845
Sea Level Rise (ft)	Hurricane Category 3			Hurricane Category 4		
	Traffic analysis zones	Affected Population	Affected Household	Traffic analysis zones	Affected Population	Affected Household
SLR 0	144	39,325	20,150	183	78,030	39,323
SLR 1	144	39,488	20,269	183	78,159	38,395
SLR 2	144	39,563	20,313	183	78,276	38,461
SLR 4	144	39,749	20,422	184	78,754	38,731

20% of the population travels to public shelters. In Mattapoisett, the interstate highway I-195 and Main Street were determined to be the main evacuation routes according to the Mattapoisett transportation and police departments.

Under these assumptions, the total clearance time from the affected area is estimated for three cases of the emergency evacuation activation: slow (8 hours), moderate (6 hours), and fast (4 hours). Adding about approximately 1 hour and 20 minutes of transportation, the total time for complete clearance of the inundation area (emergency activation plus transportation) ranges from 5 hr 14 min to 9 hr 18 min (Figure 2-78). Main traffic delays were projected to occur on I-195 north of Mattapoisett due to emergency traffic from the west. Most of the traffic congestion would occur on I-195 as the main regional evacuation route. For the fast 4-hr evacuation activation starting at noon, the hourly traffic maps are shown in Figure 2-78. Route traffic management is necessary to ensure a fast and smooth evacuation ending at 8 pm (Figure 2-78).

Emergency water supply would be required for evacuees in public shelters or friends/families. Because the Mattapoisett drinking water treatment plant is likely to be adversely affected under a Category 4 hurricane, water sources for emergency supply need to be arranged in emergency preparedness planning.

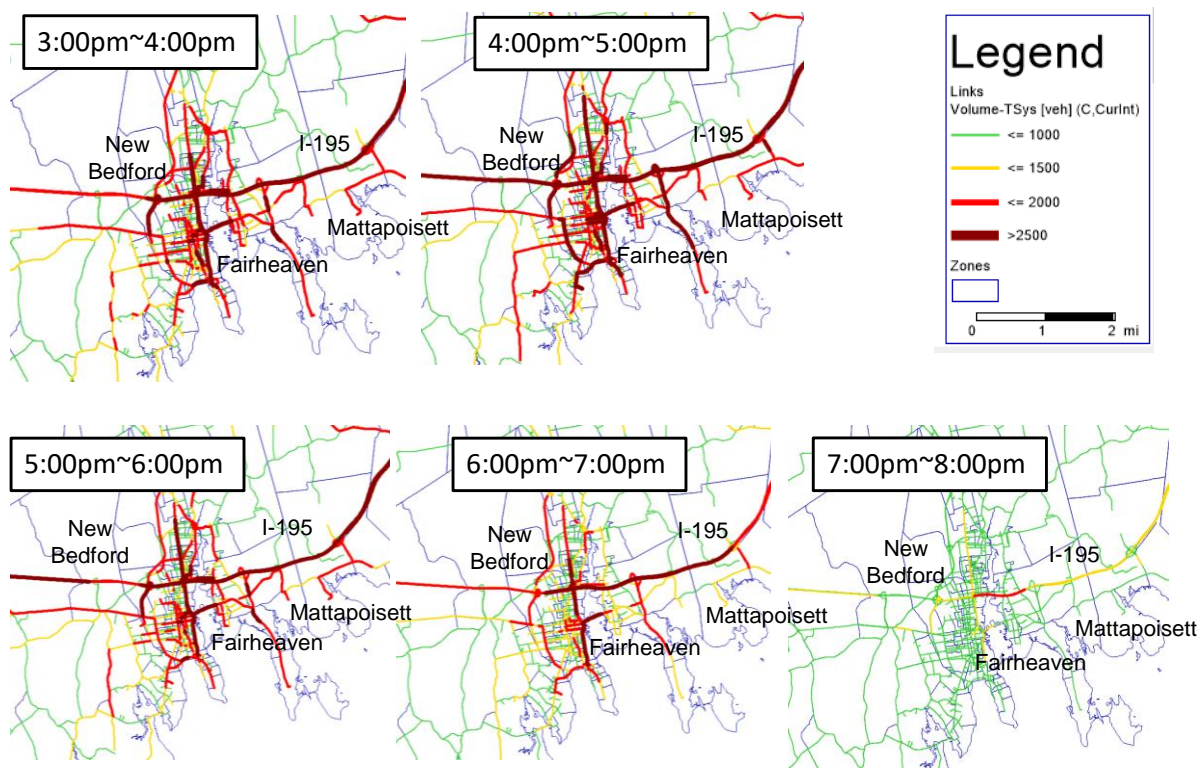


Figure 2-78 Hourly traffic map in the Mattapoisett region after evacuation order activated at noon time.

9. Summary and Recommendations

This Part II infrastructure adaptation report describes methods, techniques, and case studies for adapting water infrastructure to and improving its resilience against the projected

impacts of hydroclimatic and land use changes. The focus is to establish actionable science for adaptation planning and engineering at local scales.

As a part of this investigation, the relationship between climate, land use, transportation, energy, pollution, and water management were shown to intersect. Urban development can lead to a substantial UHI formation, which increases energy use. Urban sprawl leads to less heat island effects, but higher use for energy in transportation, both urban residents and material flows including water, thus adding to pollution. Development can alter rainfall and runoff characteristics, which have subsequent impacts on water supplies and water quality. The latter changes can challenge water plant operations, requiring process engineering adaptation. This can result in increasing energy needs. Urban development patterns also impact water distribution and sewer collection. Ultimately to address the sustainability of our communities, this EPA Office of Research and Development research has analyzed the inter-connectedness and developed systematic adaptation strategy and tools to better inform decision-makers for informed decisions. Such guided decision-making can help to find optimal investments to protect their economy, property, social systems, and infrastructure in anticipation of future conditions.

Water infrastructure adaptation can be planned and evaluated in three different levels: adaptation at the watershed scale, urban scale, and water system scale. This spatial boundary helps define the adaptation objectives that often require inputs with stakeholder involvement and identifies the adaptation parameters to investigate in planning and engineering design. Adaptation at the three-scale levels share the same iterative adaptation process (see Figure 2-2). Following defining the adaptation objective and adaptation physical boundary, the adaptation process begins with analyzing the water infrastructure vulnerability to the concurrent and future changes of hydroclimatic and land use conditions. This analysis is conducted in the context of urban developments. This first step is followed by technical and engineering analysis to define specific adaptation planning and engineering options. Upon design and implementation with consideration of the future change uncertainties, the last phase is centered on adaptation effectiveness monitoring and evaluation. For the iterative process, the monitoring-evaluation results lend a basis to revise the adaptation planning and, if necessary, urban development policies and management objectives. This proposed adaptation framework is readily adopted into the current urban planning practice. Figures 2-4 and 2-6 show the current practice and adaptive urban planning, respectively.

To support the water infrastructure adaptation in three spatial scales, the developed Smart Urban Design (SUD) methods and tools are described in this report with case studies for illustration. At the watershed scale, the adaptation aims to protect source water quality. The developed integrated watershed modeling tools and methods inside of SUD can be used to project water quality in response to future climate and land use management options. On the urban scale, the SUD provides an integrated analysis of land use, transportation, and water infrastructure in scenario-based simulations that quantify basic urban functions and efficiency in transportation and water services. Specific evaluation metrics are defined to evaluate the urban development options, including air quality, water resources and utilization, and transportation access for a given urban development scenario. In the local system scale, SmartWater models and simulation tools were developed to provide specific engineering analysis of water system vulnerability and engineering options to adapt. Through case studies covering different climate regimes in the U.S. Midwest, Southwest, and coastal areas, the following major findings were made:

- It is clear from the studies across the country that water infrastructure and, to a larger extent, urban adaptation can be effective in improving infrastructure resilience, and importantly, can offer potential climate-economic-compliance co-benefits. To achieve these outcomes, the adaptation must be planned and designed in a systems approach considering interactions among urban systems.
- Scenario-based adaptive monitoring and planning are essential to urban and water infrastructure adaptation. As described earlier, the large physical footprints and inflexible infrastructure assets have created a “locked-in” condition for which alteration and changes to the infrastructure can often be cost-prohibitive and difficult to overcome social and political barriers. Model-aided computer simulation, when conducted appropriately, can provide managers the tool to examine urban-scale adaptive planning, water infrastructure master planning, water treatment adaptation, as well as engineering options to improve water system services. The results can provide an effective venue for water professionals to communicate to stakeholders involved.
- Urban environments present one of the important potential areas for adaptation and mitigation of hydroclimatic change impacts (IPCC, 2014; Yang and Goodrich, 2014). This potential is evident in the case studies described in this report. For example, a multi-center transformation of the Cincinnati metropolitan area calls for a mix of automobile and mass transit framework that can reduce fuel consumption and air emission by 15.6% and average traffic delay by 25% in 2030. A large degree of carbon/energy reduction can be also achieved by selecting optimal water infrastructure expansion actions in Manatee County, Florida when adaptation is incorporated in the master planning.
- Water supply adaptation is effective when water treatment and distribution are considered together through systems investigation. Only by this approach, future changes can be grouped into those affecting source water quality and water demand. Then, the systems analysis using the SmartWater tools can identify the most effective and economic engineering solutions to adapt the water system for better compliance at a reasonable cost. A practical example in the GCWW’s Richard Miller Treatment Plant shows the feasibility by changing and optimizing GAC reactor operations under future source water conditions.
- Coastal areas host multiple dimensions of long-term hydroclimatic impacts and short-term meteorological disruptions in the narrow coastal zone. As a result, integrated modeling and qualitative analysis are often necessary to develop options for long-term adaptation options and emergency preparation plans against disruptive events like storm surges.

The central question for many urban managers and decision-makers is as what Timmerman and White (1997) described, namely, how the urban growth can be planned adaptively to reduce the negative impacts of urban metabolism and ensure sustainable growth. This question is especially important at this stage because of the nation’s impending strategic investment in infrastructure. For this purpose, SUD methods and tools need to be developed beyond the initial stage with applications in different climate and socioeconomic settings.

10. References

- Adams, J.Q., and R.M. Clark (1988). Development of cost equations for GAC treatment systems. *J. Environ Engineering*, 114(3): 672-688.
- Adegoke, J.O., R. Pielke Sr., and A.M. Carleton (2007). Observational and modeling studies of the impacts of agriculture-related land use change on planetary boundary layer processes in the central U.S. *Agricultural and Forest Meteorology*, 142:203-215.
- Alp, E., and C.S. Melching (2009). Evaluation of the duration of storm effects on in-stream water quality. *J. Water Resour. Plng. & Mgmt.*, 135(2):107-116.
- ASCE/AWWA (2004). *Water Treatment Plant Design*, 4th edition. E.E. Baruth (ed.), McGraw-Hill, 896p.
- ASCE (2014). Minimum design loads for buildings and other structures, *Standard ASCE/SEI 7-10*. ASCE, Reston, VA.
- Ashley, R., J. Blanksby, A. Cashman, L. Jack, G. Wright, J. Packman, L. Fewtrell, T. Poole, and C. Maksimovic (2007). Adaptable urban drainage: Addressing change in intensity, occurrence and uncertainty of stormwater (AUDACIOUS). *Built Environment*, 33(1):70-84.
- Asian Developmental Bank (ADB) (2012). *Green Cities*. M. Lindfield, F. Steinberg (eds.), Manila, Philippines, adbpub@adb.org, 412p.
- Auch, R., J. Taylor, and W. Acevedo (2004). Urban growth in American Cities. *USGS Circular 1252*, 52p.
- Azadi P, O.R. Inderwildi, R. Farnood, and D.A. King (2013). Liquid fuels, hydrogen and chemicals from lignin: A critical review. *Renewable and Sustainable Energy Review*, 21:506-523.
- Baldauf, R., E. Thoma, A. Khlystov, V. Isakov, G. Bowker, T. Long, and R. Snowe (2008). Impacts of noise barriers on near-road air quality. *Atmospheric Environment*, 42: 7502-7507.
- Barceló, J., E. Codina, and J. Casas (2005). Microscopic traffic simulation: A tool for the design, analysis and evaluation of intelligent transport systems. *J. Intelligent and Robotic Systems*, 41(2-3):173-203.
- Bartlett, S., H. Cisneros, G. Heartwell, K. McAndrew, A. Warnock, M. Nellenbach, M., S. Kline, A. Winkler, and J. Varn (2017). *Understanding America's water and wastewater challenges*. Bipartisan Policy Center, Washington, DC., 28p.
- Baynes, T.M. (2009). Complexity in urban development and management: Historical overview and opportunities. *J. Industrial Ecology*, 13(2): 214-227.
- Beck, M.B. (2005). Vulnerability of water quality in intensively developing urban watersheds. *Environmental Modelling and Software*, 20:381-400.
- Biswas, P., C. Lu, and R.M. Clark (1993). A model for chlorine concentration decay in drinking water distribution pipes. *Water Research*, 27(12): 1715-1724.

- Black, J., and T. Endreny (2006). Increasing stormwater outfall duration, magnitude, and volume through combined sewer separation. *J. Hydrol. Engrg.*, 11(5):472-481.
- Board of County Commissioners (2008). *Manatee County Water Supply Facilities Work Plan*, Manatee County Administrative Center Commission Office Commission, Bradenton, FL.
- Boccelli, D.L., M.E. Tryby, J.G. Uber, and R.S. Summers (2003). A reactive species model for chlorine decay and THM formation under rechlorination conditions. *Water Research*, 37: 2654-2666.
- Boccelli, D.L., M.J. Small, and U.M. Diwekar (2007). Drinking water treatment plant design incorporating variability and uncertainty. *J. Envir. Engrg.* 133(3):303-312.
- Bonnin, G., D. Martin, T. Parzybok, B. Lin, D. Riley, and M. Yekta (2006). Precipitation Frequency Atlas of the United States. *NOAA Atlas 14*, Volume 2, Version 3.0, National Weather Service, Silver Spring, MD.
- Bonnin, G.M., D. Martin, B. Lin, T. Parzybok, M. Yekta, and D. Riley (2011). Precipitation-frequency Atlas of the United States, *NOAA Atlas 14*, Volume 1-9. National Weather Service, Silver Spring, D.
- Boulos, P.F., K.E. Landsey, and B.W. Karney (2006). *Comprehensive Water Distribution Systems Analysis Handbook for Engineers and Planners*. MWH SOFT, Pasadena, CA.
- Braganza, K., D.J. Karoly, and J.M. Arblaster (2004). Diurnal temperature range as an index of global climate change during the twentieth century. *Geophysical Research Letters*, 31(13): L13217,
- Bras, R.L., and I. Rodriguez-Iturbe (1984). *Random Functions and Hydrology*. Addison-Wesley Publishing Company.
- Brown, C., Y. Ghile, M. Laverty, and K. Li (2012). Decision scaling: Linking bottom-up vulnerability analysis with climate projections in the water sector. *Water Resources Research*, 48: W09537.
- Bull-Kamanga, L., K. Diagne, A. Lavell, E. Leon, F. Lerise, H. MacGregor, A. Maskrey, M. Meshack, M. Pelling, H. Reid, D. Satterthwaite, J. Songsore, K. Westgate, and A. Yitambe (2003). From everyday hazards to disasters: The accumulation of risk in urban areas. *Environment & Urbanization*, 15(1): 193-203.
- Buyadi, S.N.A., W.M.N.W. Mohd, and A. Misni (2013). Green spaces growth impact on the urban microclimate. *Procedia-Social and Behavioral Sciences*, 105: 547-557.
- Cann, K.F., D.R. Thomas, R.L. Salmon, A.P. Wyn-Jones, and D. Kay (2013). Extreme water-related weather events and waterborne diseases. *Epidemiol. Infect.*, 141: 671-686.
- Capodaglio, A.G. (2004). Improving sewage treatment plant performance in wet weather. *NATO Science Series: IV: Earth and Environmental Sciences*, 43: 175-185.
- Carrico, B., and P.C. Singer (2009). Impact of booster chlorination on chlorine decay and THM production: Simulated analysis. *J. Envir. Engrg.* 135(10): 928-935.
- Carter, T., and C.R. Jackson (2007). Vegetated roofs for stormwater management at multiple spatial scales. *Landscape and Urban Planning*, 80: 84-94.

- Chang, H.-J., R. Hargrove, Y.-X. Long, and D.J. Osborne (2006). Reconstruction after the 2004 tsunami: ecological and cultural considerations from case studies. *Landscape Ecol Eng*, 2: 41-51.
- Chang, N.-B., C. Qi, and Y.J. Yang (2012). Optimal expansion of a drinking water infrastructure system with respect to carbon footprint, cost-effectiveness and water demand. *J Environ Management*, 110: 194-206.
- Chang, N.-B., B.W. Vannah, Y.J. Yang, and M. Elovitz (2014a). Integrated data fusion and mining techniques for monitoring total organic carbon concentrations in a lake. *International Journal of Remote Sensing*, 35:3: 1064-1093.
- Chang, N.-B., B. Vannah, and Y.J. Yang (2014b). Comparative sensor fusion between hyperspectral and multispectral satellite sensors for monitoring microcystin distribution in Lake Erie. *IEEE J. Selected Topics in Appl. Earth Observation & Remote Sensing*, 7(6): 2426-2442.
- Changnon, D. (2006). Regional and temporal variations in heavy precipitation in South Carolina. *Int'l J. Climatology*, 14(2): 165-177.
- Chen, Y., J.J. Cheng, and K.S. Creamer (2008). Inhibition of anaerobic digestion process: A review. *Bioresource Technology*, 99: 4044-4064.
- Chung, G., K. Lansey, and G. Bayraksan (2009). Reliable water supply system design under uncertainty. *Environmental Modelling & Software*, 24: 449-462.
- Clark, R. M. (1998). Chlorine demand and TTHM formation kinetics: a second order model, *Journal of Environmental Engineering*, 124(1): 16-24.
- Clark, R.M, and M. Sivaganesan (2002). Predicting chlorine residuals in drinking water: second order model, *J. Water Resour. Plng. and Mgmt.*, 128(2): 152-160.
- Clark, R.M., and R.C. Haught (2005). Characterizing pipe wall demand: Implications for water quality modeling. *J. Water Resour. Plng. and Mgmt.*, 131(3): 208-217.
- Clark, R.M., Z. Li, S.G. Buchberger, and Y.J. Yang (2009). Evaluating the effects of climate change on the operation, design and cost of water treatment. *WQTC 09*, Seattle, WA.
- Clark, R.M., Y.J. Yang, C. Impellitteri, R.C. Haught, D. Schupp, S. Panguluri, and E.R. Krishnan (2010). Controlling disinfectant residual losses in drinking water distribution systems: Results from experimental and modeling studies. *J. AWWA*. 102(4): 1-21.
- Clarke, J. F. (1969). Nocturnal urban boundary layer over Cincinnati, Ohio. *Mon. Weather Rev.*, 97(8): 582-589.
- Comfort, L.K. (2006). Cities at risk: Hurricane Katrina and the drowning of New Orleans. *Urban Affairs Review*, 41(4): 501-516.
- Cook, R., L. Griffins, P. Vickery, and E. Stafford (2011). ASCE 7-10 wind loads. *Proc. 2011 Structure Congress*, Las Vegas, NV.
- Cooley, H., J. Fulton, and P.H. Gleick (2011). *Water for Energy: Future Water Needs for Electricity in the Intermountain West*. Pacific Institute, ISBN 1-893790-36-3.

- Cooper, D., M. Leclerc, J. Archuleta, R. Coulter, W. Eichinger, C. Kao, and C. Nappo (2006). Mass exchange in the stable boundary layer by coherent structures. *Agricultural and Forest Meteorology*, 136(3): 114-131.
- Crittenden, J.C., P.S. Reddy, H. Arora, J. Trynoski, D.W. Hand, D.L. Perram, and R.S. Summers (1991). Predicting GAC performance with rapid small-scale column tests. *J. AWWA*, 83(1): 77-87.
- Cromwell, J. E. III, J.B. Smith, and R.S. Raucher (2007). No doubt about climate change and its implications for water suppliers. *J. AWWA*, 99(9): 112-117.
- Crozes, G., P. White, and M. Marshall (1995). Enhanced coagulation: Its effect on NOM removal and chemical costs. *J.AWWA*, 87(1): 78-89.
- Dennison, F.J., A. Azapagic, R. Clift, and J.S. Colbourne (1998). Assessing management options for wastewater treatment works in the context of life cycle assessment. *Water Science and Technology*, 38(11), 23-30.
- Diaz-Fierros, T.F., J. Puerta, J. Suarez, and F.D. Fierros (2002). Contaminant loads of CSOs at the wastewater treatment plant of a city in NW Spain. *Urban Water*, 4(3): 291-299.
- Dietz, M.E. (2007). Low impact development practices: A review of current research and recommendations for future directions. *Water, Air, & Soil Pollution*, 186: 351-363.
- Dodder, R., T. Felgenhauer, W. Yelverton, and C. King (2011). Water and greenhouse gas tradeoffs associated with a transition to a low carbon transportation system. In *ASME 2011 International Mechanical Engineering Congress and Exposition*, 2011, pp. 531-547.
- Dodder, R.S. (2014). A review of water use in the U.S. electric power sector: Insights from systems-level perspectives. *Current Opinion in Chemical Engineering*, 5: 7-14.
- Dodman, D. (2009). Blaming cities for climate change? An analysis of urban greenhouse gas emissions inventories. *Environ. Urbanization*, 21: 185-201.
- Dominguez, D., and W. Gujer (2006). Evolution of a wastewater treatment plant challenges traditional design concepts. *Water Research*, 40: 1389-1396.
- Eastman, J.R. (2009). *IDRISI Help System*. IDRISI Taiga. Worcester, MA, USA: Clark University.
- Ewing, R.,H. (2008). *Characteristics, causes, and effects of sprawl: A literature review*. In *Urban Ecology*, John M. Marzluff, Eric Shulenberger, Wilfried Endlicher, Marina Alberti, Gordon Bradley, Clare Ryan, Ute Simon, Craig ZumBrunnen (eds.), 519-535. Springer US.
- Farge, M. (1992). *Wavelet transformations and their applications to turbulence*. Annual Reviews, Inc.
- Federal Highway Administration (FHWA) (1990). *Calibration and Adjustment of System Planning Models*. Washington DC, FHWA.
- FHWA (2002). *An Introduction to Urban Travel Demand Forecasting - A Self Instructional Text*. Retrieved December 23, 2013, from U.S. Department of Transportation: <http://ntl.bts.gov/DOCS/UT.html>.

- FHWA (2012). *Project-level Conformity and Hot-spot Analysis*. Retrieved 10 1, 2014, http://www.fhwa.dot.gov/environment/air_quality/conformity/guide/guide09.cfm
- FHWA (2017). *Transportation conformity: A basic guide for state & local officials. FHWA-HEP-17-034*. 19p.
- Felgenhauer, T., and K.C. Bruin (2009). The optimal paths of climate change mitigation and adaptation under certainty and uncertainty. *Int'l J. Global Warming*, 1: 66-88.
- Felgenhauer, T., and M. Webster (2013). Modeling adaptation as a flow and stock decision with mitigation. *Climatic Change*, 122(4): 665-679.
- Feng, Y., M. Liu, Y. Liu, X. Tong, and S. Deng (2011). Modeling dynamic urban growth using cellular automata and particle swarm optimization rules. *Landscape and Urban Planning*, 102: 188-196.
- Fernando, H.J.S. (2010). Fluid dynamics of urban atmospheres in complex terrain. *Annual Review of Fluid Mechanics*, 42: 365-389.
- Flanders, F., J. Yang, R. Dodder, G. Furie, R. Baldauf, L. Bachle, A. Bostrom, L. Berry, C. Walters, J. Bare, T. Barzyk, R. Bruins, E. Cooter, F. DiCosmo, T. Eason, T. Fontaine, L. Jackson, N. Schumaker, and J. Weaver (2014). Synthesis paper on sustainable transportation. *EPA Program Briefing Paper*. 126p. RTP, NC.
- Fletcher, S.M., M. Miotti, J. Swaminathan, M.M. Klemun, K. Strzepek, and A. Siddiqi (2017). Water supply infrastructure planning: Decision-making framework to classify multiple uncertainties and evaluate flexible design. *J. Water Resour. Plng. and Mgmt.*, 143(10): p.04017061.
- Freas, K., B. Bailey, A. Munevar, and S. Butler (2008). Incorporating climate change in water planning. *J. AWWA*, 100: 6.
- Fu, X., X. Wang, and Y.J. Yang (2018). Deriving suitability factors for CA-Markov land use simulation model based on local historical data. *J. Environ Management*, 206: 10-19.
- Garcia-López, M.-À. (2012). Urban spatial structure, suburbanization and transportation in Barcelona. *J. Urban Economics*, 72 (2-3):176-190.
- Gesch, D. (2005). *Topography-based Analysis of Hurrican Katrina Inundation of New Orleans*. U.S. Geological Survey, Sioux Falls, SD.
- Gettman, D., and L. Head (2003). *Surrogate Safety Measures From Traffic Simulation Models*, Final Report. Federal Highway Administration.
- Gikas, P., and G. Tchobanoglous (2009). The role of satellite and decentralized strategies in water resources management. *J. Environ Management*, 90: 144-152.
- Gilroy, K.L., and R.H. McCuen (2009). Spatio-temporal effects of low impact development practices. *J. Hydrology*, 367: 228-236.
- Gim, T.T. (2012). A meta-analysis of the relationship between density and travel behavior. *Transportation*, 39(3): 491-519.
- Girard, M., and M. Mortimer (2006). *The Role of Standards in Adapting Canada's Infrastructure to The Impacts of Climate Change*. <http://www.csa.ca/climatechange>, Canadian Standards Association. 71p.

- Gleick, P.H. (2000). The changing water paradigm, a look at twenty-first century water resources management. *International Water Resources Association*, 25(1): 127-138.
- Godschalk, D. (2003). Urban hazard mitigation: Creating resilient cities. *Nat. Hazards Rev.*, 4(3): 136-143.
- Gordon, P., H.W. Richardson, and H.L. Wong (1986). The distribution of population and employment in a polycentric city: The case of Los Angeles. *Environment & Planning A* 18 (2): 161-173.
- Guhathakurta, S., and P. Gober (2007). The impact of the Phoenix urban heat island on residential water use. *J. Am. Plann. Assoc.*, 73(3): 317-329.
- Guo, J.C.Y., and K. Hargadin (2009). Conservative design rainfall distribution. *J. Hydrologic Engrg*, 14(5): 528-530.
- Gupta, A.K., and R.K. Shrivastava (2006). Uncertainty analysis of conventional water treatment plant design for suspended solids removal. *J. Envir. Engrg.*, 132(11): 1413-1421.
- Guzmán-Torres, D., A. Eiguren-Fernández, P. Cicero-Fernández, M. Maubert-Franco, A. Retama-Hernández, R. Ramos Villegas, and A.H. Miguel (2009). Effects of meteorology on diurnal and nocturnal levels of priority polycyclic aromatic hydrocarbons and elemental and organic carbon in PM₁₀ at a source and a receptor area in Mexico City. *Atmospheric Environment*, 43(17): 2693-2699.
- Harrington, J.J., and J.S. Gidley (1985). Variability of alternative decisions in a water resources planning problem. *Water Resources Research*, 21(12): 1831-1840.
- Heikkila, E., P. Gordon, J.I. Kim, R.B. Peiser, H.W. Richardson, and D. Dale-Johnson (1989). What happened to the CBD-distance gradient?: Land values in a policentric city. *Environment and Planning A*, 21(2): 221-232.
- Hering, J.G., T.D. Waite, R.G. Luthy, J.E. Dewes, and D.L. Sedlak (2013). A changing framework for urban water systems. *Environ. Sci. Technol.*, 47: 10721-10726.
- Hershfield, D.M. (1961). Rainfall frequency atlas of the United States for durations from 30 minutes to 24 hours and return periods from 1 to 100 years. *Weather Bureau, Technical Paper No.40.*, Washington, DC.
- Hidalgo, J., V. Masson, and L. Gimeno (2010). Scaling the daytime urban heat island and urban-breeze circulation. *J. Applied Meteorology and Climatology*, 49(5): 889-901.
- Horowitz, A.J. (2009). Monitoring suspended sediments and associated chemical constituents in urban environments: lessons from the city of Atlanta, Georgia, USA Water Quality Monitoring Program. *J. Soils & Sediments*, 9(4): 342-363.
- Hosseinzadehtalaei, P., H. Tabari, and P. Willems (2017). Uncertainty assessment for climate change impact on intense precipitation: how many model runs do we need? *International J. Climatology*, 37: 1105-1117.
- Hummel, D., A. and Lux (2006). Population decline and infrastructure: The case of the German water supply system. *Vienna Yearbook of Population Research*, 2007, pp. 167-191.
- Ibrahim, H, A. Ilinca, and J. Perron (2008). Energy storage systems – Characteristics and comparisons. *Renew. Sustain. Energy Rev.*, 12: 1221-1250.

- Imen, S., N.-B., Chang, Y.J. Yang, and A. Golchubian (2016). Developing a Model-based Drinking Water Decision Support System Featuring Remote Sensing and Fast Learning Techniques. *IEEE Systems Journal*, 99: 1-11.
- Imhoff, M.L., P. Zhang, R.E. Wolfe, and L. Bounoua (2010). Remote sensing of the urban heat island effect across biomes in the continental USA. *Remote Sensing of Environment*, 114(3): 504-513.
- Intergovernmental Panel on Climate Change (IPCC) (2007). *Climate change 2007: The Physical Science Basis*. Cambridge University Press.
- IPCC (2014). *Climate Change 2014: Mitigation of Climate Change*. Draft. 2014, <http://www.ipcc.ch/>.
- International Energy Agency (IEA) (2013a). *World Energy Outlook 2013*. www.iea.org. 9 rue de la Fédération 75739 Paris Cedex 15, France. 2013a, 232p.
- IEA (2013b). *Redrawing the energy-climate map*. www.iea.org. 9 rue de la Fédération 75739 Paris Cedex 15, France. 2013b, 126p.
- Iziomon, M.G., H. Mayer, and A. Matzarakis (2003). Downward atmospheric longwave irradiance under clear and cloudy skies: Measurement and parameterization. *J. Atmospheric and Solar-Terrestrial Physics*, 65(10): 1107-1116.
- Järvinen, A.V.O., M.T. Pelkonen, and T. Vartiainen (1991). *Upgrading the Removal of Humic Substances and Mutagen Precursors in Water Treatment*. In: *Humic Substances in the Aquatic and Terrestrial Environment*, B. Allard, H. Borén, A. Grimvall (eds.), Springer Berlin/Heidelberg, 225-231.
- Jiang, G., F. Zhang, and X. Kong (2009). Determining conversion direction of the rural residential land consolidation in Beijing mountainous areas. *Transactions of the CSAE*, 25(2): 214-221.
- Jing, C., Z. Ping, and Q. Mahmood (2009). Simultaneous sulfide and nitrate removal in anaerobic reactor under shock loading. *Bioresource Technology*, 100: 3010-3014.
- Johnson, T., J. Butcher, D. Deb, M. Faizullabhoj, P. Hummel, J. Kittle, S. McGinnis, L.O. Mearns, D. Nover, A. Parker, S. Sarkar, R. Srinivasan, P. Tuppad, M. Warren, C. Weaver, and J. Witt (2015). Modeling streamflow and water quality sensitivity to climate change and urban development in 20 U.S. watersheds. *J. AWRA*, 50(5): 1321-1341.
- Jones, P., F. Koppelman, and J. Orfueil (1990). *Activity Analysis: State-of-the-art and Future Directions. New Developments in Dynamic and Acticity-based Approaches to Travel Analysis* (pp. 34-55). Gower Publishing, Aldershot, England.
- Kenworthy, J.R. (2006). The eco-city: ten key transport and planning dimensions for sustainable city development. *Environment & Urbanization*, 18(1): 67-85.
- Kim, Y-I, and B.-U. Bae (2007). Design and evaluation of hydraulic baffled-channel PAC contactor for taste and odor removal from drinking water supplies. *Water Research*, 41: 2256-2264.
- Kimura, K., G.L. Amy, J.E. Drewes, and T. Herberer (2003). Rejection of organic micropollutants (disinfection by-products, endocrine disrupting compounds, and

- pharmaceutically active compounds) by NF/RO membranes. *J. Membrane Science*, 227: 113-121.
- Kincannon, D.F., and A.F. Gaudy Jr. (1966). Some effects of high salt concentrations on activated sludge. *J. Water Pollution Control Federation*, 38(7): 1148-1159.
- Konrad II, C.E. (1997). Synoptic-scale features associated with warm season heavy rainfall over the interior southeastern United States. *J. Climate*, 12: 557-571.
- Kumar, M.S., V.K. Anandan, T.N. Rao, and P.N. Reddy (2012). A climatological study of the nocturnal boundary layer over a complex-terrain station. *J. Applied Meteorology and Climatology*, 51(4): 813-825.
- Lai, F.-S. (2008). Review of sewer design criteria and RDII prediction methods. *EPA/600/R-08/010*, USEPA, Office of Research and Development, Cincinnati, OH.
- Larson, W., F. Liu and A. Yezer (2012). Energy footprint of the city: Effects of urban land use and transportation policies. *J. Urban Economics*, 72 (2-3): 147-159.
- Lee, E.J., C.S. Criddle, P. Bobel, and D.L. Freyberg (2013). Assessing the scale of resource recovery for centralized and satellite wastewater treatment. *Environ. Sci. Technol*, 47: 10762-10770.
- Levin, R.B., P.R. Epstein, T.E. Ford, W. Harrington, E. Olson, and E.G. Reichard (2002). U.S. drinking water challenges in the twenty-first century. *Environmental Health Perspectives*, 110 (S.1): 43-52.
- Levine, A.D., Y.J. Yang, and J.A. Goodrich (2016). Enhancing climate adaptation capacity for drinking water treatment facilities. *J. Water and Climate Change*. 7(3): 485-497.
- Li, Z., R. Clark, S. Buchberger, and Y.J. Yang (2009). Assessing the impact of climate change on drinking water treatment plant design and operation. *EWRI 2009*, Kansas City.
- Li, Z., R. Clark, S. Buchberger, and Y.J. Yang (2012). Evaluation of Logistic Model for GAC Performance in Water Treatment, *J. AWWA*, 104(9): E489-E500.
- Li, Z., R. Clark, S. Buchberger, and Y.J. Yang (2014). Evaluation of Climate Change Impact on Drinking Water Treatment Plant Operation. *J Environ Engrg.*, 140(9), Special Issue: Drinking Water Safety, Security, and Sustainability, A4014005.
- Liang, M. S., T.C. Keener, M.E. Birch, R. Baldauf, J. Neal, and Y.J. Yang (2013). Low-wind and other microclimatic factors in near-road black carbon variability: A case study and assessment implications. *Atmospheric Environment*, 80: 204-215.
- Liang, M. S. (2014). *Quantitative Analysis of Major Factors Affecting Black Carbon Transport and Concentrations in the Unique Atmospheric Structure of Urban Environment*. Ph.D. Dissertation, University of Cincinnati.
- Liang, M.S., and T.C. Keener, (2015). Atmospheric feedback of urban boundary layer with implications for climate adaptation. *Environ. Sci. Technol.*, 49(17): 10598-10606.
- Liang, M.S., and S. Julius, (2017). On the coastal topography and storm surge for infrastructure risk assessment and adaptation. *EWRI 2017*, Sacramento, CA.
- Lin, S.D. (2001). *Water and Wastewater Calculations Manual*. McGraw-Hill, New York. 854p.

- Liu, Y., G. Shintaro, D. Zhuang, and W. Kuang (2012). Urban surface heat fluxes infrared remote sensing inversion and their relationship with land use types. *J. Geographical Sciences*, 22(4): 699-715.
- Lundie, S., G.M. Peters, and P.C. Beavis (2004). Life cycle assessment for sustainable metropolitan water systems planning, *Environ. Sci. Technol.*, 38: 3465-3473.
- Lundin, M., M. Bengtsson, and S. Molander (2000). Life cycle assessment of wastewater systems: influence of system boundaries and scale on calculated environmental loads. *Environ. Sci. Technol*, 34: 180-186.
- Luthy, R.G. (2013). Design options for a more sustainable urban water environment. *Environ. Sci. Technol*, 47: 10719-10720.
- Ma, X.L., T.J. Schmit, and W.L. Smith (1999). A nonlinear physical retrieval algorithm – its application to the GEOS-8/9 sounder. *J. Appl. Meteorol.*, 38(5): 501-513.
- Mailhot, A., S. Duchesne, D. Caya, and G. Talbot (2007). Assessment of future change in intensity-duration-frequency (IDF) curves for southern Quebec using the Canadian Regional Climate Model (CRCM). *J. Hydrology*, 347: 197-210.
- Marsalek, J., and B. Chocat (2002). International report: Stormwater management. *Water Science and Technology*, 46(6-7): 1-17.
- Marshall, J.D., and M.W. Toffel (2005). Framing the elusive concept of sustainability: A sustainability hierarchy. *Environ. Sci. Technol*, 39(3): 673-682.
- Martilli, A. (2002). Numerical study of urban impact on boundary layer structure: Sensitivity to wind speed, urban morphology, and rural soil moisture. *J. Applied Meteorology*, 41(12): 1247-1266.
- Martuzevicius, D., J. Luo, T. Reponen, R. Shukla, A.L. Kelley, H.S. Clair, and S.A. Grinshpun (2005). Evaluation and optimization of an urban PM2.5 monitoring network. *J. Environ. Monit.*, 7(1): 67-77.
- Matos, J.C., I.B. Valente, P.J.S. Cruz, and L.C. Neves (2013). An advanced probabilistic updating algorithm for life-cycle analysis of civil structures. In: *Life-Cycle and Sustainability of Civil Infrastructure Systems*, Strauss, Frangopol, Bergmeister (eds.), Taylor & Francis Group, London, ISBN 978-0-415-62126-7.
- Mays, L.W. (1999). *Water Distribution Systems Handbook*. McGraw-Hill, New York.
- McCorquodale, JA. (2007). Storm-water jets and plumes in rivers and estuaries. *Canadian J. Civil Engineering*, 34(6): 691-702.
- McDaniels, T., S. Chang, D. Cole, J. Mikawo, and H. Longstaff (2008). Fostering resilience to extreme events within infrastructure systems: Characterizing decision contexts for mitigation and adaptation. *Global Environmental Change*, 18: 310-318.
- McDonnell, B.E. (2012). *Controlling Disinfection By-Products Within a Distribution System by Implementing Bubble Aeration within Storage Tanks*. Master Thesis, University of Cincinnati, 206p.

- McKenney, D.W., J.H. Pedla, P. Papadopol, and M.F. Hutchinson (2006). The development of 1901-2000 historical monthly climate models for Canada and the United States. *Agricultural and Forest Meteorology*, 138: 69-81.
- McNally, M. (1996). *An Activity-Based Microsimulation Model for Travel Demand Forecasting*. UC Irvine: Center for Activity Systems Analysis.
- McNally, M. (2007). *The Four Step Model*. D.A. Hensher (ed.) Elsevier Science, Oxford, UK.
- Miller, K. and D. Yates (2006). *Climate Change and Water Resources: A Primer for Municipal Water Providers*. Jointly sponsored by AWWA Research Foundation, Denver, CO, and University Corporation for Atmospheric Research, Boulder, CO. AWWA Research Foundation, American Water Works Association, and IWA Publishing.
- Miller, G.R., D.D. Baldocchi, B.E. La, and T. Meyers, (2007). An analysis of soil moisture dynamics using multi-year data from a network of micrometeorological observation sites. *Advances in Water Resources*, 30: 1065-1081.
- Milman, A., and A. Short (2008). Incorporating resilience into sustainability indicators: An example for the urban water sector. *Global Environmental Change*, 18: 758-767.
- Montalto, F., C. Behr, K. Alfredo, M. Wolf, M. Arye, and M. Walsh (2007). Rapid assessment of the cost-effectiveness of low impact development for CSO control. *Landscape and Urban Planning*, 82: 117-131.
- Müller, A., S. Marsili-Libelli, A. Aivasidis, T. Lloyd, S. Kroner, and C. Wandrey (1997). Fuzzy control of disturbances in a wastewater treatment process. *Water Research*, 31(12): 3157-3167.
- Mulvihill, M.E., and J.A. Dracup (1974). Optimal timing and sizing of a conjunctive urban water supply and waste water system with nonlinear programming. *Water Resources Research*, 10(2): 170-175.
- Neil, C.W., Y.J. Yang, and Y-S. Jun (2012). A critical review of the potential impact of managed aquifer recharge on mineral-water interactions responsible for arsenic mobilization in groundwater. *J. Environ. Monit.*, 4: 1772-1788.
- Neil, C.W., Y.J. Yang, D. Schupp, and Y-S. Jun (2014). Water chemistry impacts on arsenic mobilization from arsenopyrite dissolution and secondary mineral precipitation: Implication for managed aquifer recharge. *Environ. Sci. Technol.*, 48(8): 4395-4405.
- Neil, C.W., Y. Zhao, A. Zhao, J. Neal, M. Meyer, and Y.J. Yang (2019). Trihalomethane precursor reactivity changes in drinking water treatment unit processes during a storm event. *Water Supply*. doi.org/10.2166/ws.2019.089
- Novotny V. (2013). Water–energy nexus: retrofitting urban areas to achieve zero pollution. *Building. Research & Information*, 41(5): 589-604.
- Novotny, V., and J.W. Witte (1997). Ascertaining aquatic ecological risks of urban stormwater discharges. *Water Research*, 31(10): 2573-2585.
- Oh, K., Y. Jeong, D. Lee, W. Lee, and J. Choi (2005). Determining development density using the urban carrying capacity assessment system. *Landscape and Urban Planning*, 73(1): 1-5.

- Oke, T.R. (1976). The distinction between canopy and boundary-layer urban heat islands. *Atmosphere*, 14(4): 268-277.
- Oke, T.R. (2006). Initial guidance to obtain representative meteorological observations at urban sites. *World Meteorological Organization, TD-No.1250*, 47p.
- O’Neal, M.R., M.A. Nearing, R.C. Vining, J. Southworth, and R.A. Pfeifer (2005). Climate change impacts on soil erosion in Midwest United States with changes in crop management. *Catena*, 61: 165-184.
- Ong, S.L., and B.J. Adams (1990). Capacity expansion for regional wastewater systems. *Journal of Environmental Engineering*, 116(3): 542-560.
- O’Reilly, J., C. Lee, G. Collins, F. Chinali, T. Mahony, and V. O’Flaherty (2009). Quantitative and qualitative analysis of methanogenic communities in mesophilically and psychrophilically cultivated anaerobic granular biofilms. *Water Research*, 43: 3365-3374.
- Oron, G., L. Gillerman, A. Bick, Y. Mnaor, N. Buriakovsky, and J. Hagin (2007). Advanced low quality waters treatment for unrestricted use purposes: imminent challenges. *Desalination*, 213: 189-198.
- Ostrom, E. (2010). Beyond markets and states: Polycentric governance of complex economic systems. *American Economic Review*, 100(3): 641-672.
- Pacific Northwest National Laboratory (PNNL) (2012). Climate and energy-water-land system interactions – Technical report to the U.S. Department of Energy in support of the national climate assessment. *PNNL-21185*. <http://www.ntis.gov>.
- Pahl-Wostl, C. (2007). Transitions towards adaptive management of water facing climate and global change. *Water Resour Manage*, 21: 49-62.
- Parshall, L., K. Gurney, S.A. Hammer, D. Mendoza, Y. Zhou, and S. Geethakumar (2010). Modeling energy consumption and CO₂ emissions at the urban scale: Methodological challenges and insight from the United States. *Energy Policy*, 38: 4765-4782.
- Pedersen, N., and D. Sandahl (1982). Highway traffic data for urbanized area project planning and design. *NCHRP Report 255*. Transportation Research Board, Washington, DC.
- Peng, Y., W. Zeng, and S. Wang (2007). DO concentration as a fuzzy control parameter for organic substrate removal in SBR Processes. *Environmental Engineering Science*, 21(5): 606-616.
- Perrone, D., J. Murphy, and G.M. Hornberger (2011). Gaining perspective on the water-energy nexus at the community scale. *Environ. Sci. Technol.*, 45: 4228-4234.
- Peters, G.M., and S. Lundie (2001). Life-cycle assessment of biosolids processing options. *J. Industrial Ecology*, 5(2): 1088-1980.
- Pielke Sr., R.A., J.O. Adegoke, T.N. Chase, C.H. Marshall, T. Matsui, and D. Niyogi (2007). A new paradigm for assessing the role of agriculture in the climate system and in climate change. *Agricultural and Forest Meteorology*, 142: 234-254.
- Pires, M. (2003). Watershed protection for a world city: the case of New York. *Land Use Policy*, 21: 161-175.

- Prasad, T.D., G.A. Walters, and D.A. Savic (2004). Booster disinfection of water supply networks: Multiobjective approach. *J. Water Resour. Plng. and Mgmt.*, 130(5): 367-376.
- Rajagopalan, B., and U. Lall (1998). Interannual variability in western US precipitation. *J. Hydrology*, 210: 51-69.
- Ranatunga, T., S.T.Y. Tong, Y. Sun, J.Y. Yang (2014). A comprehensive approach to total water management: A case study of the Las Vegas wash watershed, Nevada. *Physical Geography*, 35(3): 220-244.
- Rao, K.D. (2005). Multi-criteria spatial decision analysis for forecasting urban water requirements: a case study of Dehradun city, India. *Landscape and Urban Planning*, 71: 163-174.
- Ray, S., and C.A. Peters (2008). Changes in microbiological metabolism under chemical stress. *Chemosphere*, 71: 474-483.
- Rendón, A.M., J.F. Salazar, C.A. Palacio, V. Wirth, and B. Brötz (2014). Effects of Urbanization on the Temperature Inversion Breakup in a Mountain Valley with Implications for Air Quality. *J. Applied Meteorology and Climatology*, 53(4): 840-858.
- Roberts, P.V., and R.S. Summers (1982). Granular Activated Carbon Performance for Organic Carbon Removal. *J. AWWA*, 74: 113-118.
- Rosenzweig, C., D.C. Major, K. Demong, C. Stantion, R. Horton, and M. Stults (2007). Managing climate change risks in New York City's water system: Assessment and adaptation planning. *Mitigation and adaptation Strategies for Global Change*, 12(8): 1391-1409.
- Rossman, L.A. (2002). *EPANET Version 2 Users Manual*, USEPA, Cincinnati, OH.
- Rossman, L.A., R.M. Clark, and W.M. Grayman (1994). Modeling chlorine residuals in drinking-water distribution systems. *J. Env. Engng.*, 120(4): 803-820.
- Rotach, M., W. Vogt, R. Bernhofer, C. Batchvarova, E. Christen, A. Clappier, B. Feddersen, S.-E. Gryning, G. Martucci, H. Mayer, V. Mitev, T.R. Oke, E. Parlow, H. Richner, and H. Roth (2005). BUBBLE—an urban boundary layer meteorology project. *Theoretical and Applied Climatology*, 81(3-4): 231-261.
- Rothausen, S.G.S.A., and D. Conway (2011). Greenhouse-gas emissions from energy use in the water sector. *Nature Climate Change*, 1: 210-218.
- Salas, J.D., J.W. Delleur, V. Yevjevich, and W.L. Lane (1980). *Applied Modeling of Hydrologic Time Series*. Water Resources Publications, Littleton, CO, pp. 484.
- Salvato, J.A., N.L. Nemerow, and F.J. Agardy (2008). *Environmental Engineering*, 8th edition. Wiley & Sons, New York. pp1544.
- Sang, L., C. Zhang, J. Yang, D. Zhu, and W. Yun (2011). Simulation of land use spatial pattern of towns and villages based on CA-Markov model. *Mathematical and Computer Modelling*, 54: 938-943.
- Santé, I.S., A.M. García, D. Miranda, and R. Crecente (2012). Cellular automata models for the simulation of real-world urban processes: A review and analysis. *Landscape and Urban Planning*, 96: 108-122.

- Schaad, D.E., J. Farley, and C. Haynes (2009). Design and routing of storm flows in an urbanized watershed without surface streams. *J. Hydrology*, 375(3-4): 334-344.
- Schrank, D., and T. Lomax (2009). *2009 Urban Mobility Report*. Reports by Texas Transportation Institute, The Texas A&M University.
- Semadeni-Davies, A., C. Hernebring, G. Svensson, and L.-G. Gustafsson (2008). The impacts of climate change and urbanization on drainage in Helsingborg, Sweden: Suburban stormwater. *J. Hydrology*, 350: 114-125.
- Shang, F., J. Uber, and L. Rossman (2008). EPANET Multi-species Extension Users Manual. *EPA/600/S-07/021*. Cincinnati, OH.
- Silva, E.A., and K.C. Clarke (2002). Calibration of the SLEUTH urban growth model for Lisbon and Porto, Portugal. *Comput. Environ. Urban Syst*, 26: 525-552.
- Simiu, E. (2011). *Design of Buildings for Wind: A Guide for ASCE 7-10 Standard Users and Designers of Special Structures*. Second edition. John Wiley & Sons, Inc., Hoboken, NJ.
- Skjelkvale, B.L., J.L. Stoddard, D.S. Jeffries, K. Torseth, T. Hogasen, J. Bowman, J. Mannio, D.T. Monteith (2005). Regional scale evidence for improvements in surface water chemistry 1990-2001. *Environ. Pollut.* 137: 165-176.
- Slowinski, R., A. Urbaniak, and J. Weglarz (1985). Multicriteria capacity expansion planning of a water supply and wastewater treatment system. *International Journal of Modelling and Simulation*, 5(4): 124-127.
- Small, K.A., and S. Song (1994). Population and employment densities: Structure and change. *J. Urban Economics*, 36: 292-313.
- Stratus Consulting and MWH Global (2009). Implications of Climate Change for Adaptation by Wastewater and Stormwater Agencies. *Water Environment Research Foundation Report No. CC2R08*.
- Stubbart, J. (2004). How do we treat to prevent DBPs. *Opflow*, 30(9): 8-9.
- Sudhira, H.S., T.V. Ramachandra, A. Wytzisk, and C. Jeganathan (2005). *Framework for Integration of Agent-based and Cellular Automata Models for Dynamic Geospatial Simulations*. Bangalore: Indian Institute of Science, Centre for Ecological Sciences.
- Sukkoo, K. (2007). Changes in the nature of urban spatial structure in the United States, 1890-2000. *J. Regional Science*, 47(2): 273-287.
- Sun, Y., S.T.Y. Tong, M. Fang, and Y.J. Yang (2013). Exploring the effects of population growth on future land use change in the Las Vegas Wash Watershed: An integrated approach of geospatial modeling and analytics. *Environment, Development and Sustainability*, 15: 1495-1515.
- Sun, Y., S. Tong, and Y.J. Yang (2016). Modeling the cost-effectiveness of stormwater best management practices in an urban watershed in Las Vegas Valley. *Applied Geography*, 76: 49-61.
- Tafari, A.T., and A. Selvakumar (2002). Wastewater collection system infrastructure research needs in the USA. *Urban Water*, 4(1): 21-29.

- Theobald, D.M. (2005). Landscape patterns of exurban growth in the USA from 1980 to 2020. *Ecology and Society*, 10(1): 32. <https://www.jstor.org/stable/26267722>
- Tillman, A.M., H. Lundertroem, and M. Svingby (1998). Life cycle assessment of municipal waste water systems. *International Journal of LCA*, 3: 145-157.
- Tillman, D.E., T.A. Larsen, C. Pahl-Wostlm, and W. Gujer (2005). Simulating development strategies for water supply systems. *J. Hydroinformatics*, 7: 41-51.
- Timmerman, P., and R. White (1997). Megahydropolis: Coastal cities in the context of global environmental change. *Global Environmental Change*, 7(3): 205-234.
- Tong, S.T.Y, Sun, Y., and Y.J. Yang (2012). Generating a future land use change scenario with a modified population-coupled Markov Cellular Automata Model. *J. Environmental Informatics*, 19(2): 108-119.
- Torrence, C., and G.P. Compo (1998). *A Practical Guide to Wavelet Analysis*. Boulder, CO: American Meteorological Society.
- Trompeter, W.J., S.K. Grange, P.K. Davy, and T. Ancelet (2013). Vertical and temporal variations of black carbon in New Zealand urban areas during winter. *Atmospheric Environment*, 75: 179-187.
- Tung, H., R.F. Unz, and Y.F. Xie (2006). HAA removal by GAC adsorption. *J. AWWA*, 98(6): 107-112.
- Turnipseed, D.P., K. Van Wilson, J. Stoker, Jr., and D. Tyler (2007). Mapping hurricane Katrina peak storm surge in Alabama, Mississippi, and Louisiana. *37th Annual Mississippi Water Resources Conference*, Jackson, MS.
- Uber, J., F. Shang, and L. Rossman (2004). Extensions to EPANET for fate and transport of multiple interacting chemical or biological components. *Critical Transitions in Water and Environmental Resources Management*. doi: 10.1061/40737(2004)486.
- Uno, I., S. Wakamatsu, H. Ueda, and A. Nakamura (1988). An observational study of the structure of the nocturnal urban boundary layer. *Boundary-Layer Meteorology*, 45(1-2): 59-82.
- Uno, I., H. Ueda, and S. Wakamatsu (1989). Numerical modeling of the nocturnal urban boundary layer. *Boundary-Layer Meteorology*, 49(1-2): 77-98.
- Urbaniak, A. (1988). Multicriteria capacity expansion planning for an urban water system with random data. *Civil Engineering Systems*, 5: 129-136.
- U.S. BLS (Bureau of Labor Statistics) (2008). *BLS Handbook of Methods, Chapter 14 Producer Prices-Background*. http://www.bls.gov/opub/hom/homch14_a.htm.
- U.S. EPA (1994). Combined sewer overflow control policy. *Federal Register [FRL-4732-7]*, Part VII, April 19, 1994. 16p.
- U.S. EPA (1996). ICR manual for bench and pilot-scale treatment studies. *EPA/814/B-96/003*, Office of Water, Washington, DC.
- U.S. EPA (2000). ICR treatment study database, version 1.0. *EPA/815/C-00/003*, Office of Water, Washington, DC.

- U.S. EPA (2001). Report to Congress: Implementation and enforcement of the CSO control policy. *EPA/833/R-01/003*, Washington, DC.
- U.S. EPA (2002). Onsite wastewater treatment systems manual. *EPA/625/R-00/008*. Cincinnati, OH.
- U.S. EPA (2004a). Stormwater best management practice design guide: Volume 3 basin best management practices. *EPA/600/R-04/121B*.
- U.S. EPA (2004b). AERMOD description of model formulation. *EPA/454/R-03/004*, Research Triangle Park, NC. https://www3.epa.gov/scram001/7thconf/aermod/aermod_mfd.pdf.
- U.S. EPA (2005). Water Treatment Plant Model version 2.2 User's manual. Office of Ground Water and Drinking Water, U.S. EPA, Cincinnati, OH.
- U.S. EPA (2006). Growing toward more efficient water use: Linking development, infrastructure, and drinking water policies. *EPA/230/R-06/001*. Washington, DC.
- U.S. EPA (2007a). An approach for using load duration curves in the development of TMDLs. *EPA/841/B-07/006*, Washington DC., 68p.
- U.S. EPA (2007b). Moving toward sustainability. Retrieved July 12, 2011, from <http://water.epa.gov/infrastructure/sustain/index.cfm>.
- U.S. EPA (2007c). Aging water infrastructure research program: Addressing the challenge through innovation. *EPA/600/F-07/015*, Washington, DC.
- U.S. EPA (2008). A screening assessment of the potential impacts of climate change on combined sewer overflow (CSO) mitigation in the Great Lakes and New England regions. *EPA/600/R-07/033F*, Washington, DC, p.39.
- U.S. EPA (2009a). A Screening assessment of the potential impacts of climate change on combined sewer overflow (CSO) mitigation in the Great Lakes and New England regions (External Review Draft). *EPA/600/R-07/033A*, U.S. EPA, Washington, DC.
- U.S. EPA (2009b). Land-use scenarios: National-scale housing-density scenarios consistent with climate change storylines. *EPA/600/R-08/076F*, Washington, DC.
- U.S. EPA (2009c). Proceedings of the first national expert and stakeholder workshop on water infrastructure sustainability and adaptation to climate change. *EPA 600/R-09/010*. Cincinnati, OH
- U.S. EPA (2010a). Motor Vehicle Emission Simulator (MOVES); user guide for MOVES 2010a. *EPA/420/B-10/036*.
- U.S. EPA (2010b). Integrated climate and land-use scenarios (ICLUS) v1.3 User's manual: ArcGIS tools and datasets for modeling US housing density growth. *EPA/600/R-09/143F*. 19p.
- U.S. EPA (2011). Transportation control measures: An information document for developing and implementing emissions reduction programs. *EPA/430/R-09/040*. U.S. EPA.
- U.S. EPA (2012a). A framework for sustainability indicators at EPA. *EPA/600/R-12/687*. Cincinnati, OH.

- U.S. EPA (2012b). Adaptive response framework for drinking water and wastewater utilities. *EPA/817/F-12/009*, Office of Water. Washington, DC,
- U.S. EPA (2013a). Our built and natural environments. *EPA/231/K-13/001*. Washington, DC, 139p.
- U.S. EPA (2013b). Watershed modeling to assess the sensitivity of streamflow, nutrient, and sediment loads to potential climate change and urban development in 20 U.S. watersheds. *EPA/600/R-12/058F*, Washington, DC.
- U.S. EPA (2014). National stormwater calculator - Version 1.1 (Model). *EPA/600/C-13/106b*, Washington, DC.
- U.S. EPA (2015a). National water infrastructure adaptation assessment. Part I: Climate change adaptation readiness analysis. *EPA/600/R-15/141*. Cincinnati, OH
- U.S. EPA (2015b). The impact of traditional and alternative energy production on water resources: Assessment and adaptation studies. *EPA 600/R-14/272*. Cincinnati, OH
- U.S. EPA (2015c). MOVES2014a User Guide. EPA Office of Transportation and Air Quality. *EPA/420/B-15/095*. 264p.
- U.S. EPA (2015d). Transportation conformity guidance for quantitative hot-spot analyses in PM_{2.5} and PM₁₀ nonattainment and maintenance areas. *EPA/420/B-15/084*, Washington, DC, 152p.
- U.S. EPA (2015e). Using MOVES2014 in project-level carbon monoxide analyses. *EPA/420/B-15/028*, 51p.
- U.S. EPA (2017a). Decision support system for aquifer recharge (AR) and aquifer Recovery (ASR) planning, design, and evaluation: Principles and technical basis. *EPA/600/R-16/222*.
- U.S. EPA, (2017b). Appendix A to Appendix W of Part 51—Summaries of preferred air quality models. In *Revisions to the Guideline on Air Quality Models: Enhancements to the AERMOD Dispersion Modeling System and Incorporation of Approaches To Address Ozone and Fine Particulate Matter*. 40 CFR Part 51. Federal Register, 82, 10.
- U.S. EPA (2019). Better Assessment Science Integrating point & Non-point Sources - BASINS 4.5 User's Manual. RTP, NC. <https://www.epa.gov/sites/production/files/2019-03/documents/basins4.5scoremanual.2019.03.pdf>
- Uyak, V., K. Ozdemir, and I. Toro (2008). Seasonal variations of disinfection by-product precursors profile and their removal through surface water treatment plants. *Science of the Total Environment*, 390: 417-424.
- Voivontas, D., G. Arampatzis, E. Manoli, C. Karavitis, and D. Assimacopoulos (2003). Water supply modeling towards sustainable environmental management in small islands: the case of Paros, Greece. *Desalination*, 156: 127-135.
- Wallis, J.R., M.G. Schaefer, B.L. Barker, and G.H. Taylor (2007). Regional precipitation-frequency analysis and spatial mapping for 24-hour and 2-hour durations for Washington State. *Hydrol. Earth Syst. Sci.*, 11(a): 415-442.

- Wang, K., H. Ye, F. Chen, Y. Xiong, and C. Wang (2012). Urbanization effect on the diurnal temperature range: different roles under solar dimming and brightening. *J. Climate*, 25(3): 1022-1027.
- Wang X., A. Burguess, and Y.J. Yang (2013). A scenario-based water conservation planning support system (SB-WCPSS). *Stochastic Environmental Research and Risk Assessment*, 27(3): 629-641.
- Ward, D.P., A.T. Murray, and S.R. Phinn (2000). A stochastically constrained cellular model of urban growth. *Comput. Environ. Urban Syst*, 24, 539-558.
- Webster, M., P. Donohoo, and B. Palmintier (2013). Water-CO₂ trade-offs in electricity generation planning. *Nature Climate Change*, 3: 1029-1032.
- Wei, H., X. Wang, Z. Yao, H. Liu, S. Liang, and Y.J. Yang (2012). Framework for Integrating Traffic-Source Emission Estimates into Sustainability Analysis. *CICTP 2012*: 3612-3619. doi: 10.1061/9780784412442.364.
- Wei, H., T. Zuo, H. Liu, and Y.J. Yang (2017). Integrating land use and socioeconomic factors into scenario-based travel demand and carbon emission impact study. *Urban Rail Transit*, 3(1): 3-14. doi:10.1007/s40864-017-0056-2.
- Weinstein, N. (2009). Decentralized stormwater controls for urban retrofit and combined sewer overflow reduction, Phase 2. *WERF Report 03-SW-3A*. ISBN: 9781843393535.
- Weng, Q., D. Lu, and J. Schubring (2004). Estimation of land surface temperature–vegetation abundance relationship for urban heat island studies. *Remote sensing of Environment*, 89(4): 467-483.
- Whitehead, P.G., R.L. Wilby, D. Butterfield, and A.J. Wade (2006). Impacts of climate change on in-stream nitrogen in a lowland chalk stream: An appraisal of adaptation strategies. *Science of the Total Environment*, 365: 260-273.
- Whitehead, P.G., R.L. Wilby, R.W. Battarbee, M. Kernan, and A.J. Wade (2009). A review of the potential impacts of climate change on surface water quality. *Hydrological Sciences Journal/Journal des Sciences Hydrologiques*, 54(1): 101-123.
- Wilby, R.L. (2007). A review of climate change impacts on the built environment. *Built Environment*, 33(1): 31-45.
- Wing, S., S. Freedma, and L. Band (2002). The potential impact of flooding on confined animal feeding operations in Eastern North Carolina. *Environ. Health Persp.*, 110(4): 387-391.
- Yamout, G., and M. El-fadel (2005). An optimization approach for multi-sectoral water supply management in the Grater Beirut Area. *Water Resources Management*, 19: 791-812.
- Yang, Y.J., A. Hale, D. Chapman, and D. Keith (2002). Water quality and biological response to water aeration of glycol-contaminated streams in cold temperatures. Proc. of the Water Environment Federation, *Industrial Wastes 2002*, 962-978(17).
- Yang, Y.J., J.A. Goodrich, S.Y. Li, and R.C. Haught (2007). AST/R-based water reuse as a part of the total water solution for water-stressed regions: An overview of engineering practice and regulatory prospective. *EWRI 2007*, Tampa, FL.

- Yang, Y.J., C.A. Impellitteri, R.M. Clark, R. C. Haught, D.A. Schupp, S. Panguluri, and E.R. Krishnan (2008). Chlorine decay and DBP formation under different flow regions in PVC and ductile iron pipes: Preliminary results on the role of flow velocity and radial mass transfer. *EWRI 2008*, Atlanta, GA.
- Yang, Y.J. (2010). Re-define adaptation of water resource infrastructure to a non-stationary climate (Editorial). *J. Water Resour. Plng. & Mgmt.* 136(3): 297-298.
- Yang, Y.J., and A. Restivo (2010). ASR application in climate change adaptation: The need, issues and research focus. *Water & Energy in Changing Climate*, Ground Water Protection Council, Pittsburgh, PA. September 2010.
- Yang, Y.J., N.B. Chang, J. Neal, H. Wei, M.S. Liang, and T.C. Keener (2013). Water and carbon footprints for sustainability analysis of urban infrastructure. *EWRI 2013*, Cincinnati, OH.
- Yang Y.J., and J.A. Goodrich (2014). Toward quantitative analysis of water-energy-urban-climate nexus for urban adaptation planning. *Current Opinion in Chem Engrng*, 5: 22-28.
- Yang, Y.J. (2016). Adapting Water Infrastructure to Non-stationary Climate Changes. In: *Sustainable Water Management and Technologies*, D.H. Chen (ed.), Taylor & Francis/CRC Press.
- Yang, Y.J., M.S. Liang, Y. Zhao, and J. Neal (2017). Establishing design storm values from climate models in coastal regions: Challenges and opportunities. *EWRI 2017*, Sacramento, CA.
- Yao, Z., H. Wei, X. Wang, H. Liu, and J. Yang (2014). Scenario-based carbon footprint inventory tool for urban sustainable development decision support: The Cincinnati case study. *Transportation Research Board Annual Meeting 2014 Paper #14-3242*.
- Zachman, B.A., and R.S. Summers (2010). Modeling TOC breakthrough in granular activated carbon adsorbers. *J. Environmental Engineering*, 136(2): 204-210.
- Zeleny, M. (1973). Compromise programming. In: *Multiple Criteria Decision Making*, J.L. Cochrane, M. Zeleny (eds.), University of South Carolina Press, Columbia, SC, pp. 262-301.
- Zhao, Y., Y.J. Yang, Y. Lee, S. Panguluri, and Y. Shao (2017). Better water demand and Pipe description improve the distribution network modeling results. *EWRI 2017*, Sacramento, CA.
- Zhao, Y., Y.J. Yang, Y. Shao, J. Neal, and T. Zhang (2018a). The dependence of chlorine decay and DBP formation kinetics on pipe flow properties in drinking water distribution. *Water Research*, 141: 32-45.
- Zhao, Y., Y.J. Yang, Y. Shao, Y. Lee, and T. Zhang (2018b). Demand-driven spatiotemporal variations of flow hydraulics and water age by comparative modeling analysis of distribution network. *J. Wat. Resour. Plann. & Manag.*, 144(12): 04018074.
- Zhou, J., J. Lin, S. Cui, Q. Qiu, and Q. Zhao (2013). Exploring the relationship between urban transportation energy consumption and transition of settlement morphology: A case study on Xiamen Island, China. *Habitat International*, 37: 70-79.

Zmud, J.P., V.P. Barabba, M. Bradley, J.R. Kuzmyak, M. Zmud, and D. Orrell (2014). Strategic Issues Facing Transportation, Volume 6: The Effects of Socio-Demographic on Future Travel Demand. *TRB's National Cooperative Highway Research Program (NCHRP) Report 750*. Transportation Research Board, Washington, DC.

Appendix A

AIR-SUSTAIN Program Input and Output Structures

Table of Contents

List of Tables	186
List of Figures.....	187
List of Acronyms.....	188
A I.1 AIR-SUSTAIN Program and Operations.....	189
<i>A I.1.1</i> Program Interfaces	189
1. Scenario Information Specification.....	189
2. Regional Level Analysis.....	195
3. Project Level Analysis	197
4. Result Comparison	201
<i>A I.1.2</i> Inputs and outputs	202
A I.2 Database in AIR-SUSTAIN	213
<i>A I.2.1</i> Database Structure	213
<i>A I.2.2</i> MOVES Emission Lookup Tables.....	221
A I.3 Transportation Analysis Examples Using the AIR-SUSTAIN Tool	226

List of Tables

Table A1- 1 Sample of Population Change	194
Table A1- 2 Sample of Employment Change	194
Table A1- 3 Sample of University Enrollment Change.....	194
Table A1- 4 Sample of High School Enrollment Change.....	194
Table A1- 5 Inputs for the AIR-SUSTAIN.....	202
Table A1- 6 Outputs from the AIR-SUSTAIN.....	203
Table A1- 7 Inputs for the Scenario Development	204
Table A1- 8 Land Use Inputs.....	205
Table A1- 9 List of Outputs from the Scenario Development.....	206
Table A1- 10 Inputs for the Regional Level Analysis	207
Table A1- 11 Description of a VISUM File	209
Table A1- 12 Outputs from the Regional Level Analysis	210
Table A1- 13 Inputs for the Project Level Analysis	211
Table A1- 14 Outputs from the Project Level Analysis	212
Table A2- 1 Tables and fields of AIR-SUSTAIN Scenario Database.....	213
Table A2- 2 Tables and Items of the MOVES Input Database.....	215
Table A2- 3 Tables and Items of the MOVES Output Database.....	217
Table A2- 4 Geodatabase.....	218
Table A2- 5 The MOVES Source Types	221
Table A2- 6 The MOVES Road Type	221
Table A2- 7 MOVES Age Distribution Categories	222
Table A2- 8 MOVES Operating Modes	223
Table A3- 1 Sample of Population Change	228
Table A3- 2 Sample of Household Fraction and Trip Rate	232
Table A3- 3 Sample of Employment Fraction.....	232
Table A3- 4 Sample of Vehicle Composition.....	233
Table A3- 5 Sample of Age Distribution.....	234
Table A3- 6 Sample of Fuel Formulation.....	234
Table A3- 7 Sample of Fuel Supply	234
Table A3- 8 Sample of Meteorology	234
Table A3- 9 Sample of State and County	235
Table A3- 10 Sample of Selected Traffic Congestion Links for Corridor Level Impact Analysis	237
Table A3- 11 Vehicle Volume.....	239
Table A3- 12 Vehicle Type Class and Category	240
Table A3- 13 Car Following Behavior Parameters.....	240
Table A3- 14 Lane Change Parameters	240
Table A3- 15 Ramp metering design criteria of the Federal Highway Administration.....	241
Table A3- 16 Signal Control Parameters.....	241
Table A3- 17 VISSIM Calibration Final Parameter Values	241
Table A3- 18 VISSIM Validation Results	242
Table A3- 19 Microscopic Simulation Link ID (Sheet1)	243

Table A3- 20 Microscopic Simulation Link ID (Sheet2)	243
Table A3- 21 Microscopic Simulation Results (Sheet1)	244
Table A3- 22 Microscopic Simulation Results (Sheet2).....	244
Table A3- 23 An Example of Traffic Congestion link Emissions by Different Scenarios.....	245
Table A3- 24 Variable and parameter coding type in AIR-SUSTAIN program	246

List of Figures

Figure A1- 1 Scenario information.....	189
Figure A1- 2 Interface for (a) new scenario; (b) and load scenario.....	190
Figure A1- 3 “Save Scenario As” interface.....	191
Figure A1- 5 Load base year data.....	192
Figure A1- 4 Scenario development interface.....	192
Figure A1- 6 Assumed changes in demographic and socioeconomic factors.....	193
Figure A1- 7 Population and employment changes.....	193
Figure A1- 8 Land use projection.....	195
Figure A1- 9 Socioeconomic data update based on assumed changes.....	195
Figure A1- 10 Regional level analysis interface.....	196
Figure A1- 11 Travel demand forecasting panel.....	197
Figure A1- 12 Emission estimation panel.....	198
Figure A1- 13 Traffic congestion identification.....	198
Figure A1- 14 Project level analysis interface.....	199
Figure A1- 15 Microscopic simulation results import.....	200
Figure A1- 16 Traffic congestion area emission estimation.....	200
Figure A1- 17 Updating traffic congestion identification results to regional analysis.....	200
Figure A1- 18 Results comparison interface.....	201
Figure A3- 1 Import base year data in example.....	227
Figure A3- 2 Program interface for (A) importing the Base Year data; (B) assigning population change; and (C) assigning employment changes at TAZ levels.....	227
Figure A3- 3 Target year land use in example.....	228
Figure A3- 4 Target year land use in example.....	229
Figure A3- 5 VISUM demand set up.....	230
Figure A3- 6 Example of road network from the input function.....	230
Figure A3- 7 Example of VISUM matrix.....	231
Figure A3- 8 VISUM procedure set up.....	231
Figure A3- 9 Example of trip distribution result from VISUM (Trips between two centers)....	233
Figure A3- 10 Emission results displayed in ArcGIS.....	235
Figure A3- 11 Traffic congestion identification criteria.....	235
Figure A3- 12 Identified traffic congestion links in simulation.....	236
Figure A3- 13 VISSIM links over the base map.....	237
Figure A3- 14 Schematic for traffic congestion microscopic analysis.....	238
Figure A3- 15 An example of desired speed distribution for cars and trucks.....	239

List of Acronyms

ft	feet
GIS	geographic information system
SUD	Smart Urban Design
TDF	Travel Demand Forecasting

AIR-SUSTAIN is a major component of the Smart Urban Design (SUD) program. The principles and functionalities are described in the main report Sections 3.0-4.0. This Appendix describes program inputs, outputs, and major program interfaces for program use and project simulation.

A I.1 AIR-SUSTAIN Program and Operations

A I.1.1 Program Interfaces

The execution of each analysis function within the AIR-SUSTAIN is achieved through interfaces embedded in a geographic information system (GIS) environment. Main functions and interfaces of the AIR-SUSTAIN are:

- Scenario Information Specification
- Scenario Development
- Regional Level Analysis
- Project Level Analysis
- Results Comparison

1. Scenario Information Specification

The AIR-SUSTAIN provides a Scenario Information interface (Figure A1-1). Before performing a scenario analysis, the scenario information must be set up first either by creating a scenario (via the **New Scenario** button on the menu bar) or loading an existing scenario (via the **Load Scenario** button on the menu).

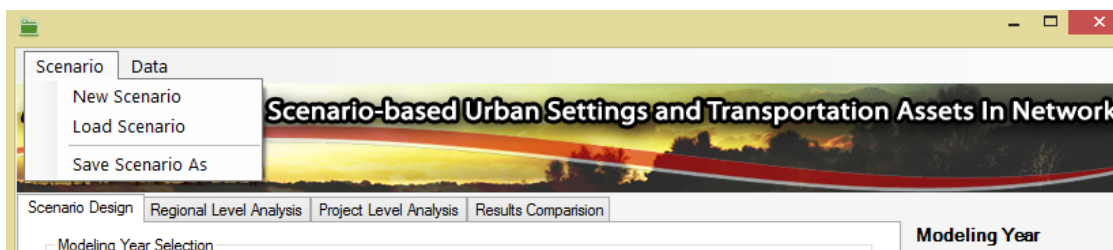


Figure A1- 1 Scenario information.

Scenario information in the **New Scenario** and **Load Scenario** windows (as shown in Figure A1-2) includes:

- 1) **Scenario Name** (required): the name of a scenario analysis specified by user
- 2) **Project Directory** (required): the route where user place the scenario folder
- 3) **Modeling Year** (required): Base Year and Target Year

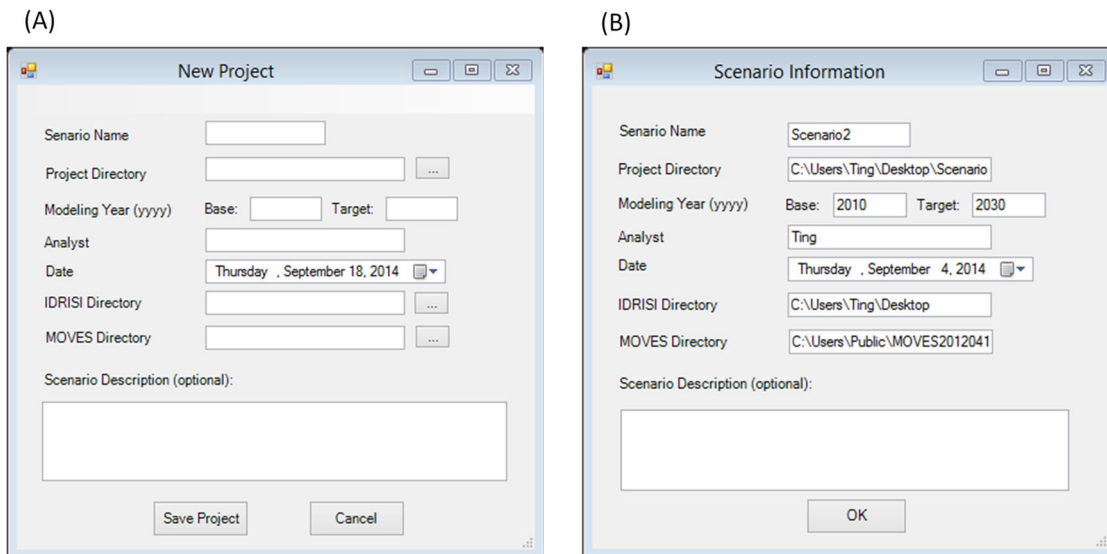


Figure A1- 2 Interface for (a) new scenario; (b) and load scenario.

- 4) **Analyst** (required)
- 5) **Date** (required)
- 6) **IDRISI Directory** (required): where IDRISI is installed;
- 7) **MOVES Directory** (required): where program MOVES is installed
- 8) **Scenario Description** (optional)

After setting up all required data, in the **New Scenario** tab, by clicking the **Save Project** button, a scenario folder and five MySQL databases are created. A scenario folder contains:

- GIS.gdb: a geodatabase store feature classes such as TAZ, road network, incentive boundary, and scenario analysis results
- IDRISI: a subfolder to store inputs and outputs for the land use projection
- MOVES: a subfolder to store inputs and outputs for the emission estimation
- VISSIM: a subfolder to store microscopic traffic simulation input and output files
- VISUM: a subfolder to store the TDF model inputs and outputs
- ScenarioName_map: an ArcGIS map file that contains input maps and analysis result maps

The MySQL database (see details later) includes:

- AIR-SUSTAIN_ScenarioName database, including: projectInfo, IDRISIIInfor, employmentGrowth, employmentTripRate, populationGrowth, householdTripRate,

increasePercentage, unversityEnrollment, HighSchoolEnrollment, baseYearResults, targetYearResults

- ScenarioName_In database: used as the MOVES input database in the regional level analysis
- ScenarioName_Out database: used as the MOVES output database in the regional level analysis
- ScenarioName_Project_In database: used as the MOVES input database in the project level analysis
- ScenarioName_Project_Out database: used as the MOVES output database in the project level analysis

If a scenario is created, the user can load the scenario information by clicking the **Load Scenario** on the menu bar. Afterwards, the scenario information is displayed in a pop-up window shown as Figure A1-2b.

The **Save Scenario As** (as shown as in Figure A1-3) window provides a function to save a new scenario based on current scenario data by specifying a new scenario name and a new scenario directory in the **SaveAsForm** window.

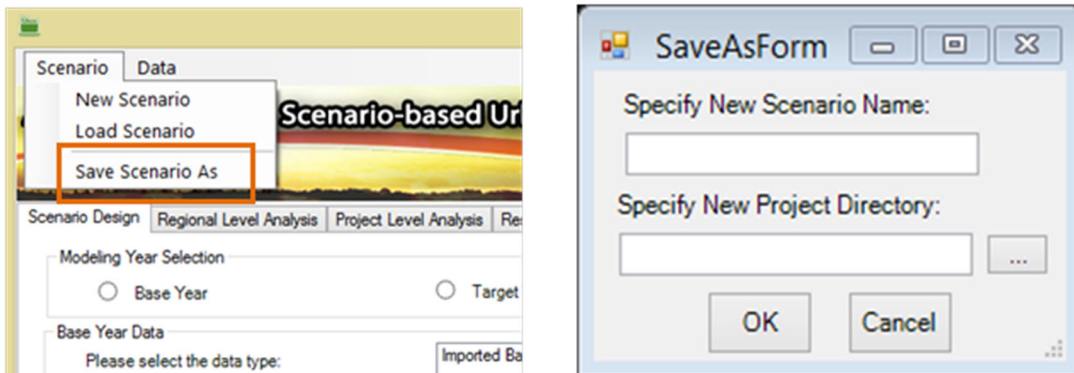


Figure A1- 3 “Save Scenario As” interface.

The **Scenario Development** tab (Figure A1-4) has three main panels: **Modeling Year Selection**, **Base Year Data**, and **Target Year Scenario Development**.

- The **Modeling Year Selection** panel is applied to select scenario analysis year by checking either the **Base Year** or **Target Year**.
- The **Base Year Data** panel provides the function (shown as Figure A1-5a) to import base year feature classes (i.e., *TAZ*, *RoadNetwork*, and *Incentiveboundary*). As illustrated by Figure A1-5, users can select the data type (i.e., *TAZ* shown as Figure A1-5b) from the dropdown list and import data by clicking the **Import** button (Figure A1-5c). The

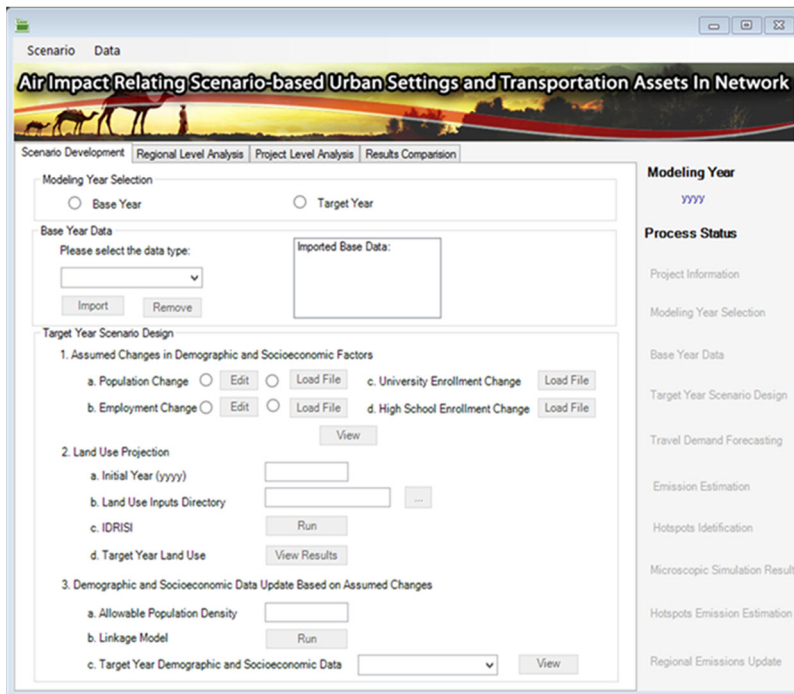


Figure A1- 4 Scenario development interface.

imported data will be listed in the right box (Figure A1-5d). Users can also remove the imported data by selecting the data name in the box and then clicking the **Remove** button in Figure A1-5c.

The **Target Year Scenario Design** panel provides functions to set up assumed changes in demographic and socioeconomic factors, including population change, employment change,

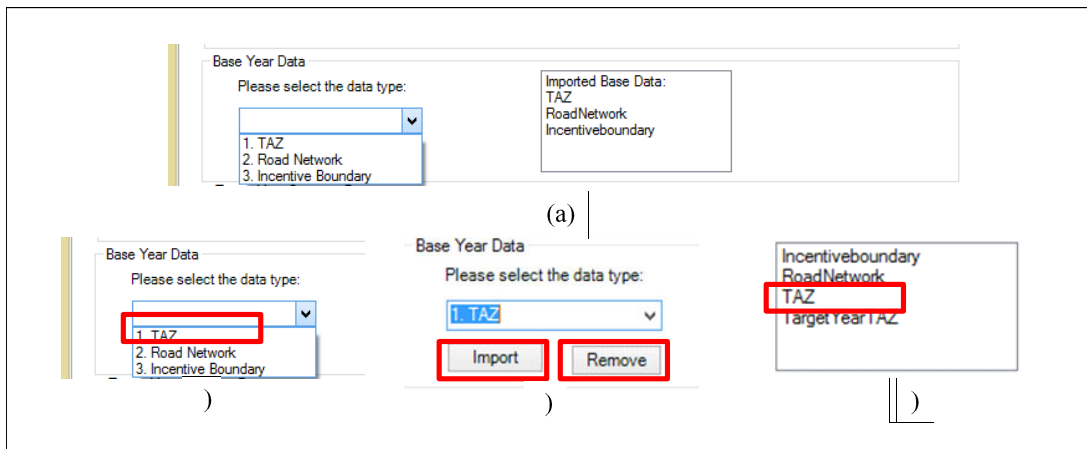


Figure A1- 5 Load base year data.

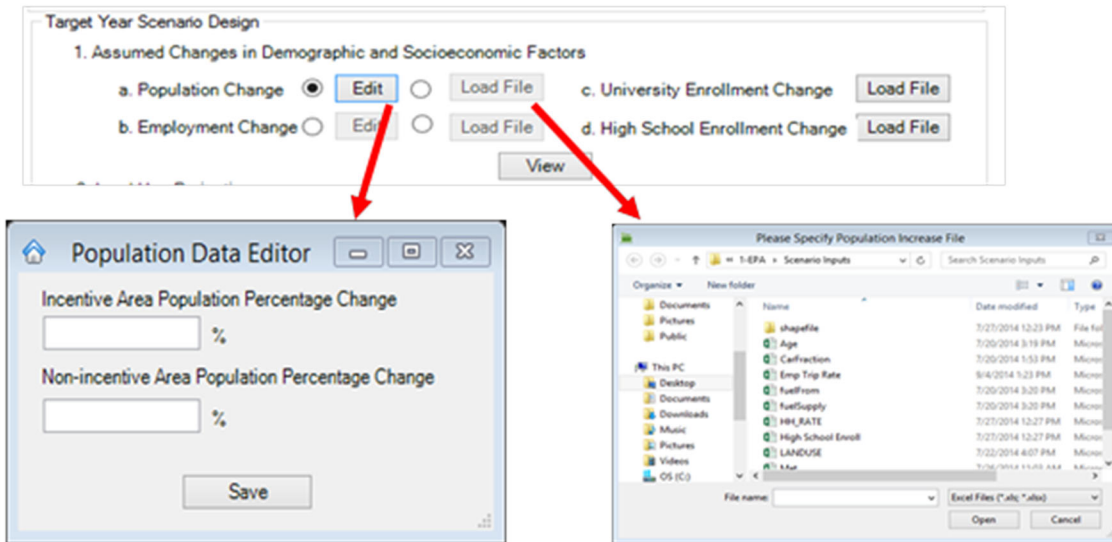


Figure A1- 6 Assumed changes in demographic and socioeconomic factors.

university enrollment change, and high school enrollment change. There are two ways to set up population change and employment change: (1) clicking the **Edit** button to set up the change percentages in incentive area and non-incentive area separately (left window of Figure A1-6), and (2) clicking the **Load File** button to import a Microsoft® Office Excel file including population change in each TAZ (right window of Figure A1-6). University enrollment change and high school enrollment change can be imported to AIR-SUSTAIN by clicking the **Load File** buttons at right side of item c and d (shown as Figure A1-7). The sample input files are shown in Figure A1-7 and Tables A1-1 through 1-4.

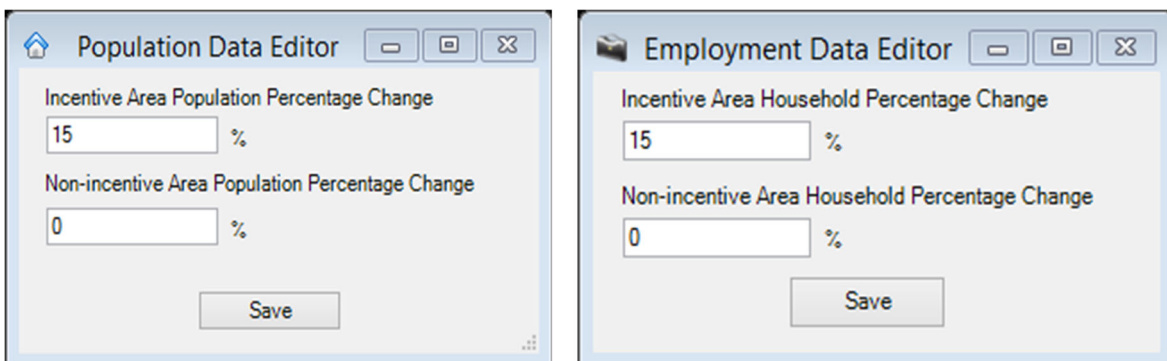


Figure A1- 7 Population and employment changes.

Table A1- 1 Sample of Population Change

TAZ	Population
330	156
338	191
318	268

Table A1- 2 Sample of Employment Change

TAZ	Employment
330	156
338	191
318	268

Table A1- 3 Sample of University Enrollment Change

TAZ	Enrollment	Name
330	156	Hebrew Union College
338	191	Institute of Technical Careers
318	268	God's Bible College

Table A1- 4 Sample of High School Enrollment Change

TAZ	Enrollment	Name
210	2556	Walnut Hills High School
244	613	Merry Middle School
251	584	Creative & Performing Arts High School

In the **Target Year Scenario Design** panel, target year land use is projected in the **Land Use Projection** (see Figure A1-8). Before performing land use projection, the **Initial Year** needs to be specified by the user. Other land use inputs are loaded by specifying the route of a folder that contains files listed in Table A1-4. Then by executing IDRISI, target year land use is projected, and land use projection results can be displayed in the ArcMap main window by clicking the **View Results** button.

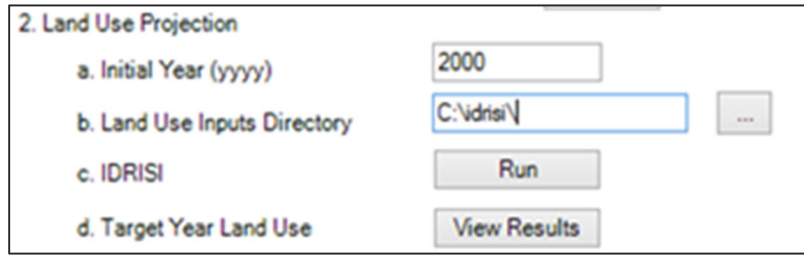


Figure A1- 8 Land use projection.

Figure A1-9 shows the **Socioeconomic Data Update Based on Assumed Data** panel. In the **Target Year Scenario Design**, target year demographic and socioeconomic data are generated by base year demographic and socioeconomic data, assumed changes in demographic and socioeconomic factors, base year land use, and target year land use by linkage model. Before running the linkage model, the allowable population density should be set up. The maximum population density is used as the maximum unit area population capacity in a TAZ. In this panel,

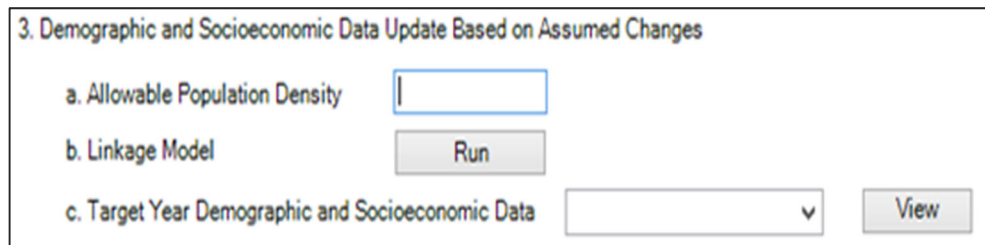


Figure A1- 9 Socioeconomic data update based on assumed changes.

target year socioeconomic data can be viewed by specifying the data type in the dropdown list and clicking the **View Results** button.

2. Regional Level Analysis

The Regional Level Analysis module is used to estimate the base and target year travel demand and on-road emissions for the study area. The **Travel Demand Forecasting** and **Emission Estimation** panels are highlighted by red boxes in Figure A1-10. When performing the regional level analysis, a TDF model first simulates trips on roadway links for the entire study area based on demographic and social economic data, as well as transportation

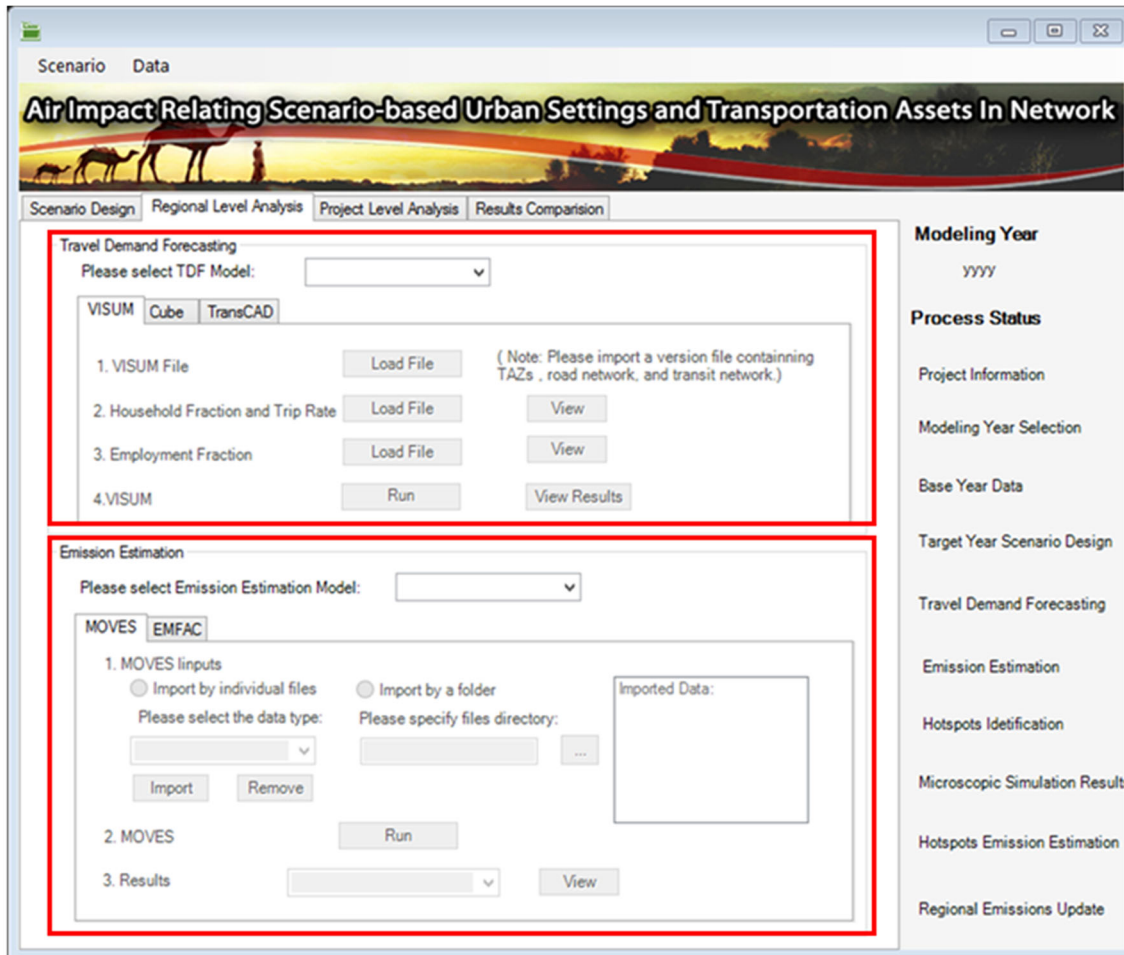


Figure A1- 10 Regional level analysis interface.

infrastructure, i.e., road network, TAZs. Afterwards, the forecasted traffic data are utilized to generate inputs for a traffic emission model, which is adopted to estimate road link based vehicle emissions. Particularly in the emission analysis, CO₂ equivalent and energy consumption for individual road links in the study area are estimated by the user selected emission model.

The **Travel Demand Forecasting** (TDF) panel has five components (Figure A1-11). In Component 1, the user needs to specify the TDF model. Among the popular TDF tools such as VISUM, Cube, and TransCAD, the current version of the AIR-SUSTAIN supports VISUM 13.0. Other models will be included in the software in the future. When the VISUM label is selected by the user, the VISUM panel is activated. In the VISUM model, a *VISUM file*, a *Household Fraction and Trip Rate*, and an *Employment Fraction* need to be loaded by Component 2, 3, 4 respectively (Figure A1-11). Component 5 provides functions to execute VISUM and view TDF results in VISUM.

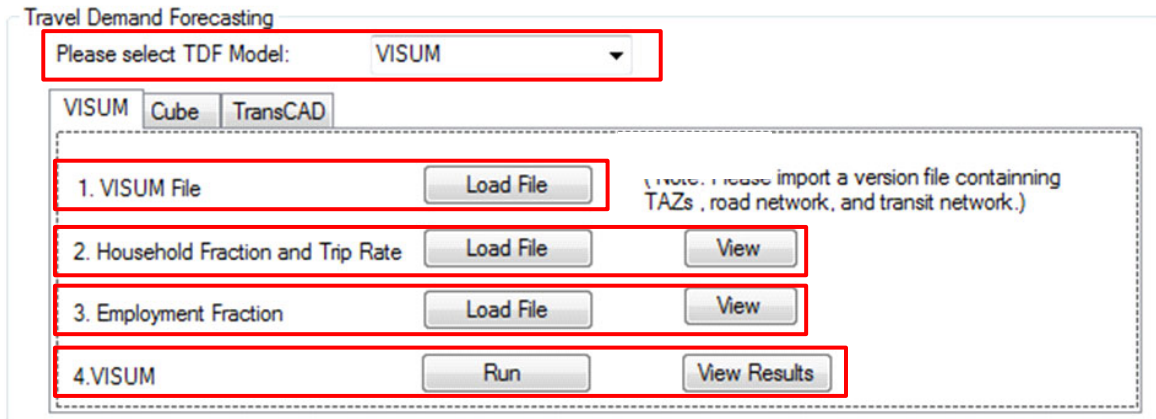


Figure A1- 11 Travel demand forecasting panel.

Figure A1-12 shows the **Emission Estimation** panel, which contains five components. Similar to travel demand forecasting, the user is allowed to specify the emission model in Component 1. For the current version of AIR-SUSTAIN, the regional level transportation emission estimation will be conducted by using the EPA’s MOVES model. The functions for supporting EMFAC model will be developed in the future. Two methods of loading MOVES inputs are provided in Component 2. When the **Import by individual files** is checked, MOVES input files can be imported individually. Alternatively, if the **Import by a folder** is checked, all files in the specified folder are imported as MOVES inputs. The steps in the two methods of loading MOVES inputs are:

- When **Import by individual files** is checked, the user should specify the input data type, (i.e., meteorology, age distribution, fuel formulation, fuel supply, and state and county), and import the corresponding file by clicking Import button. The imported file can be deleted by clicking the **Remove** button.
- When the **Import by a folder** is checked, the user only needs to specify the directory where all required files (listed in Table A1-1 and Table A1-4) are placed. The user needs to prepare each file in the folder according to specifications listed in Table A1-1.

Component 3 in Figure A2-12 is for displaying imported data. The user can select individual data files in Component 3 and click the **Remove** button to delete it. When all data files are imported, the user can run the MOVES by using Component 4. When MOVES simulation is finished, the user can visualize the results in Component 5.

3. Project Level Analysis

In the **Traffic Congestion Identification** panel (shown in Figure A1-13), the user can identify traffic congestion links by clicking **Run** button. This panel and function reside in the **Project Level Analysis** shown in Figure A1-14. Then the **Traffic Congestion Identification**

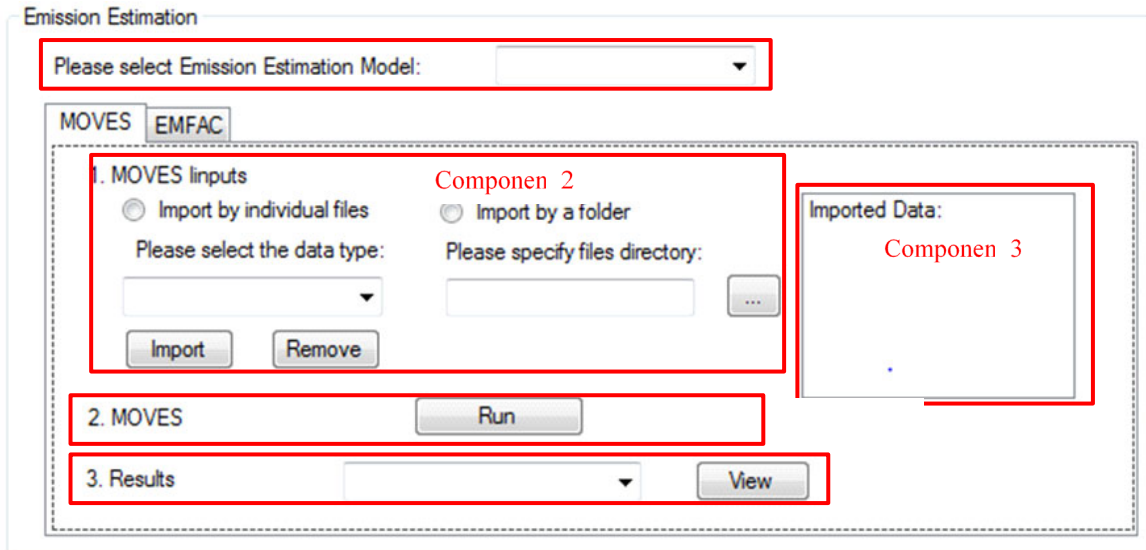


Figure A1- 12 Emission estimation panel.

window will be displayed. The window contains default and optional criteria for identifying congestion areas. Default criteria include the **Daily Link Volume** (equal to or larger than 125,000 passenger cars) and **Truck Fraction** (equal or larger than 8%). Optional criteria include the **Average speed**, **Delay**, **Queue length**, **D/C ratio**, **CO₂ equivalent**, and **Energy consumption**. In current version of the AIR-SUSTAIN system, only the default criteria are used. When criteria are set up, the traffic congestion link identification function is performed by clicking the **OK** button.

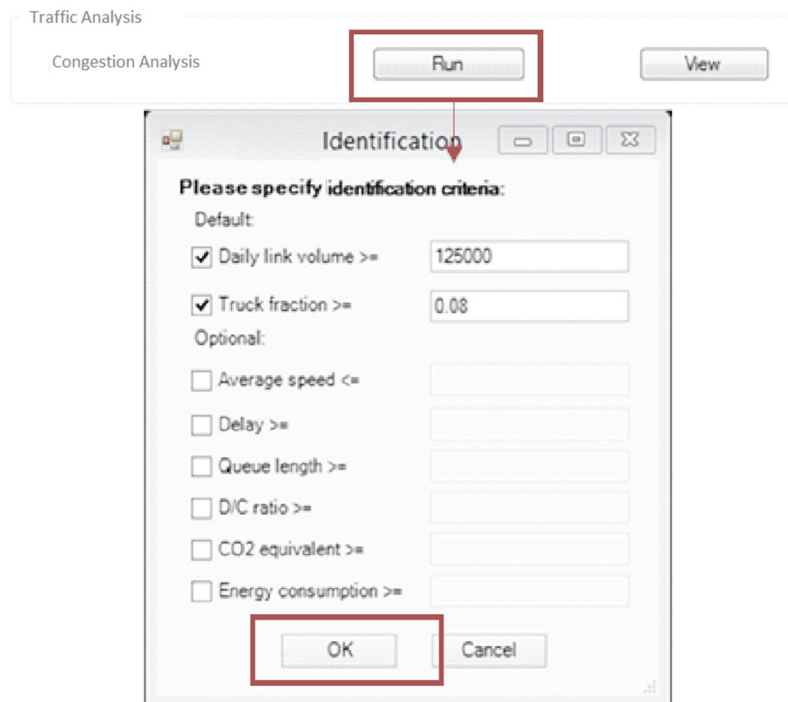


Figure A1- 13 Traffic Congestion identification.

In Component 1 of the **Microscopic Simulation Results Import** panel (as shown in Figure A1-15), the user needs to first import the **Microscopic Simulation Link ID** profile, which records a map between links in microscopic simulation network and links in VISUM. Then the micro-simulation results can be imported through Component 2. To this end, the user needs to set up names of traffic control measures in item *a* and load simulation results in item *b*. This process in Component 2 can be repeated if there are multiple files of simulations results to import. Imported files are listed on Component 3. A function of removing imported data is also provided in Component 4. Those simulation results by different traffic control measures can be compared and displayed by clicking the **View Results** button in Component 5.

With those imported results, emission estimate for traffic congestion area is recalculated by the emission estimation model, which is similar to the functions of emission estimation in the regional level analysis. The emission model can be directly executed without requiring users to import extra data. In fact, the traffic inputs of the emission model are automatically prepared based on the micro-simulation results and the non-traffic inputs are retrieved from regional analysis database. Figure A1-16 shows the panel of **Congested Area Emission Estimation**.

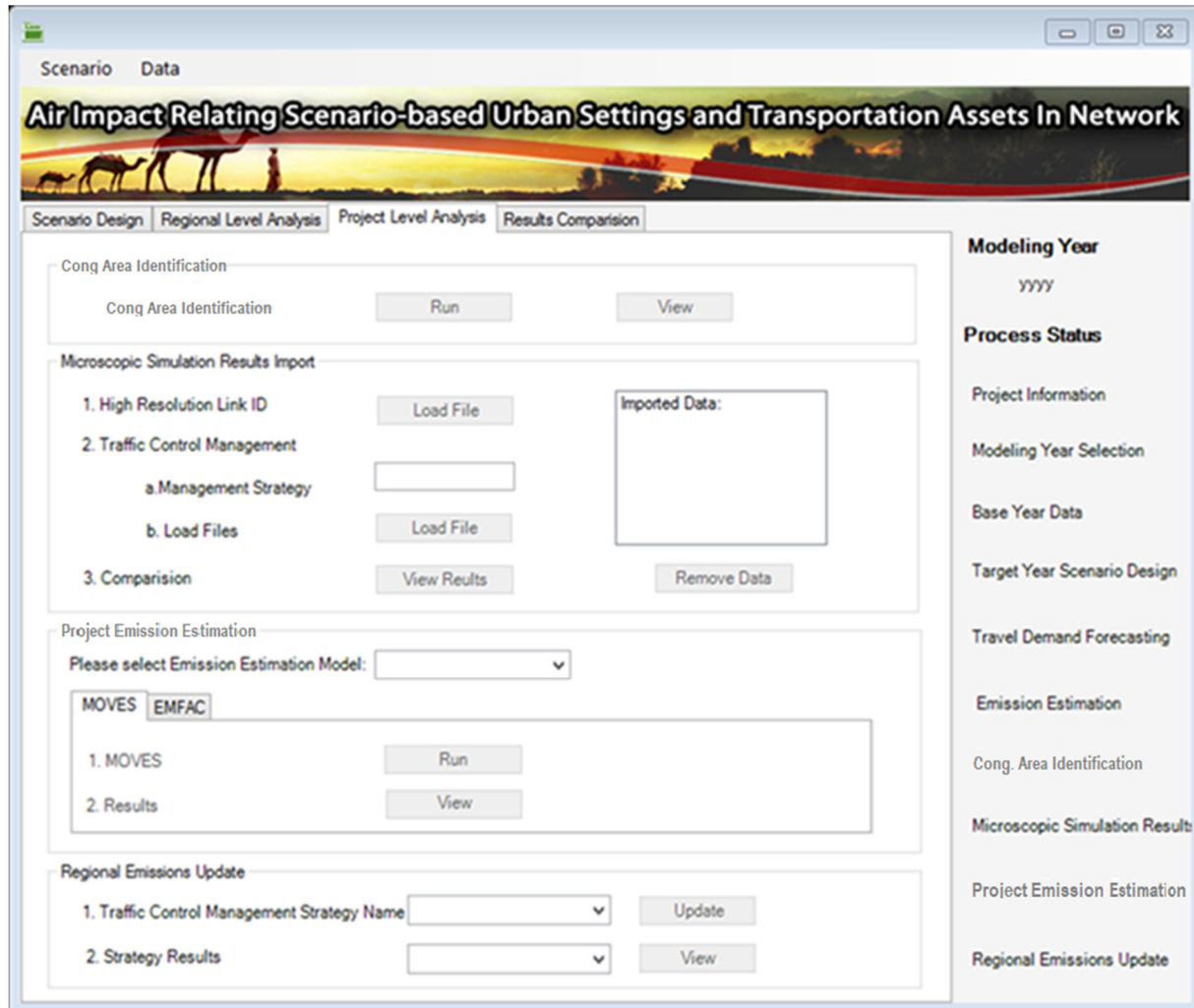


Figure A1- 14 Project level analysis interface.

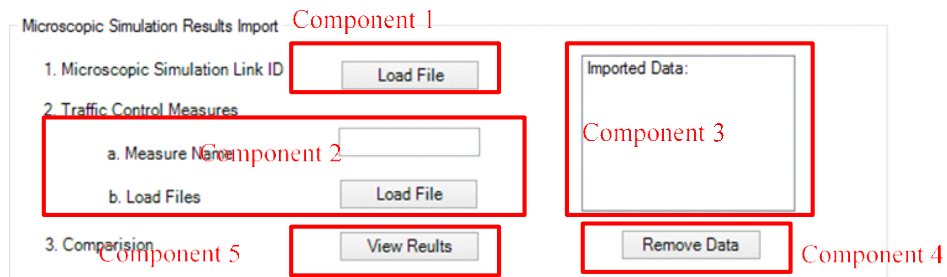


Figure A1- 15 Microscopic simulation results import.

The **Project Level Analysis** panel provides a function to feedback the effects of different traffic control measures to the regional level results database. This is achieved by updating traffic and emission results of the congestion links to corresponding regional links. Figure A1-17 shows the panel of this function. To perform this function, the emission results by which traffic control measures should be chosen first in the drop list of the **Traffic Control Measure Name**. Then the emission results are exported to the regional database by clicking on the Update button. The results can be displayed by clicking the **View** button after selecting the emission type in the drop list of the **Results**.

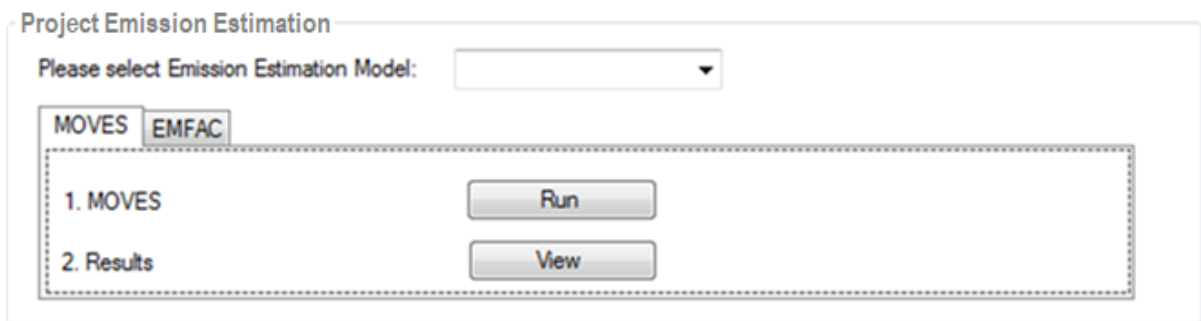


Figure A1- 16 Traffic congestion area emission estimation.



Figure A1- 167 Updating traffic congestion identification results for regional analysis.

4. Result Comparison

After performing the scenario design, regional level analysis, and project level analysis, results from the base year and target year can be compared and visualized in ArcGIS by the **Results Comparison** tab (Figure A1-18). Those visualized results include:

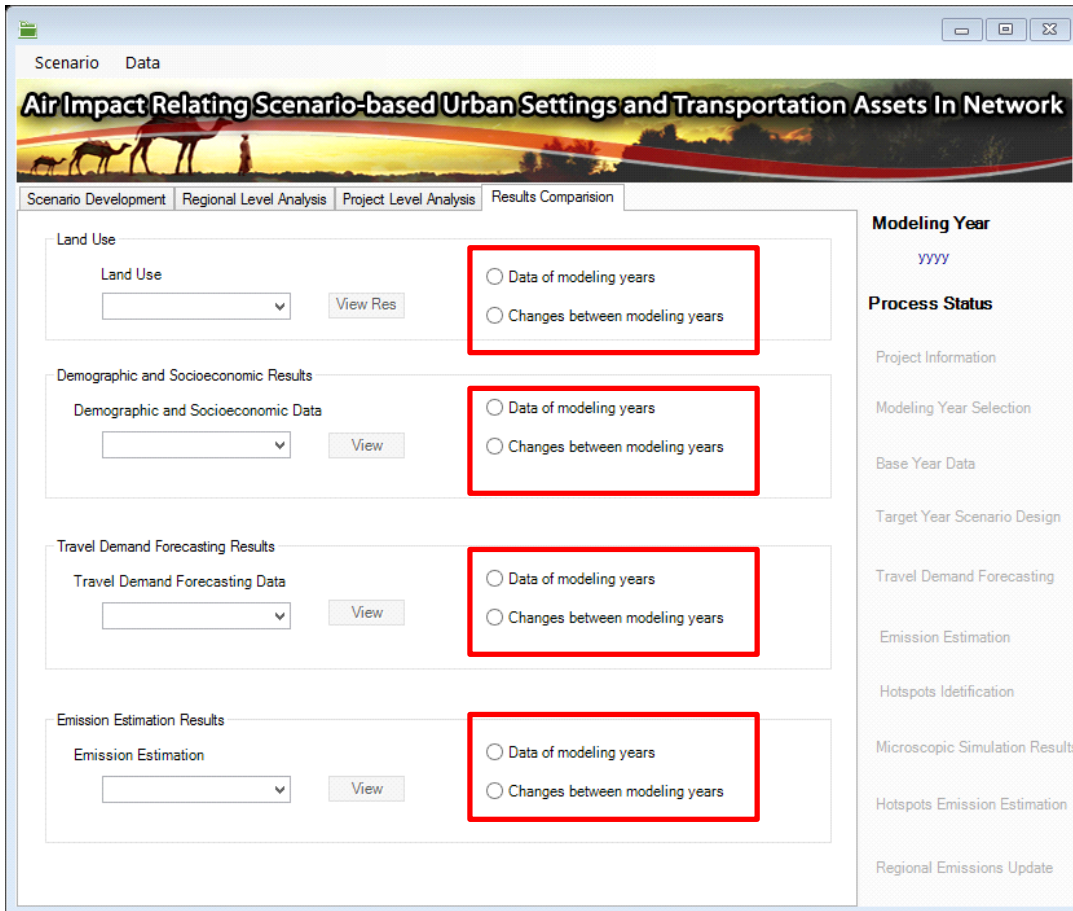


Figure A1- 17 Results comparison interface.

- Land Use, contains land use in the base year and target year
- Demographic and Socioeconomic Data, includes population, household, employment, university enrollment, high school enrollment
- Travel Demand Forecasting Results, views link traffic information including volume, average speed, D/C ratio, delay, and queue length
- Emission Estimation, includes CO₂ Equivalent and energy consumption

By clicking the **View Results** button in the **Land Use** panel, base year and target year land uses are displayed in ArcGIS. In the **Demographic and Socioeconomic Results** panel, demographic and socioeconomic data are displayed in ArcGIS by clicking the **View** button when either the **Data of modeling year** or **Changes between modeling years** is checked. The **Travel**

Demand Forecasting Results panel provides options to view the results of base year and target year or the difference between base year and target year by checking the **Data of modeling year** or **Changes between modeling years**. Similar functions are also provided in the **Emission Estimation Results** panel.

A1.1.2 Inputs and outputs

The summarized data items of the inputs and outputs for the AIR-SUSTAIN are listed in Tables A1-5 (inputs) and A1-6 (outputs).

Table A1- 5 Inputs for the AIR-SUSTAIN

Module	Function	Data Item	Format
Scenario Development	Base Year Data	TAZ	Feature Class
		RoadNetwork	Feature Class
		Incentiveboundary	Feature Class
	Assumed Changes in Demographic and Socioeconomic Factors	Population Change	Numbers or Excel
		Employment Change	Numbers or Excel
		University Enrollment Change	Excel
		High School Enrollment Change	Excel
Land Use Projection	Land Use Inputs Directory	Folder	
Regional Level Analysis	Travel Demand Forecasting	VISUM File	Version File
		Household Fraction and Trip Rate	Excel
		Employment Fraction	Excel
	Emission Estimation	Age Distribution	Excel
		Fuel Supply	Excel
		Fuel Formulation	Excel
		Meteorology	Excel
County and State	Excel		
Project Level Analysis	Microscopic Simulation Results Import	Microscopic Simulation Link ID	Excel
		Microscopic Simulation Results	Excel

Table A1- 6 Outputs from the AIR-SUSTAIN

Data Item	Description	Data Source	Format
Landuse_Target	Target year land use	Land use projection	Feature class
TargetYearTAZ	Target year population, household, employment, university enrollment, high school enrollment, residential area, employment area	Linkage model	Feature class
BaseTDF/ TargetTDF	Base/Target year travel demand forecasting results from trip generation, trip distribution, mode split, and traffic assignment	TDF	Version file
RoadNetwork	Base year traffic information including volume, average speed, D/C ratio, delay, and queue length	TDF	Feature class
	Target year traffic information including volume, average speed, D/C ratio delay, and queue length	TDF	Feature class
	Base year emission results including CO2 equivalent and energy consumption	Emission estimation	Feature class
	Target year emission results including CO ₂ equivalent and energy consumption	Emission estimation	Feature class
	Target year emission results including CO ₂ equivalent and energy consumption updated with project level emission results	Regional emission Update	Feature class
Congestion	Links meet Traffic congestion identification criteria	Traffic congestion identification	Feature class

Inputs and Outputs for the Scenario Development

Inputs for the scenario development are summarized in Table A1-7. Details of land use inputs are listed in Table A1-8. Outputs for the development are listed in Table A1-9.

Table A1- 7 Inputs for the Scenario Development

Date Item	Field	Description	Type
TAZ	TAZ	TAZ name, the format is TAZ_TAZ Number, i.e. TAZ_151	String
	TAZ_N	TAZ number	Integer
	TAZ_Order	The field to link TAZs in ArcGIS and TAZs in VISUM	Integer
	POP	Target year population	Integer
	HH	Target year household	Integer
	EMP	Target year employment	Integer
	HI	Target year high school enrollment	Integer
	UN	Target year university enrollment	Integer
	AREA_TYPE	1=CBD&Urban ; 2=suburban; 3= rural	Integer
	GEOCODE_Base_1	Base year residential area (ft ²)	Double
	GEOCODE_Base_2	Base year employment area (ft ²)	Double
	GEOCODE_Base_3	Base year institutional area (ft ²)	Double
	GEOCODE_Base_4	Base year undeveloped area (ft ²)	Double
	GEOCODE_Base_5	Base year other area (ft ²)	Double
	GEOCODE_1	Target year residential area (ft ²)	Double
	GEOCODE_2	Target year employment area (ft ²)	Double
	GEOCODE_3	Target year institutional area (ft ²)	Double
	GEOCODE_4	Target year undeveloped area (ft ²)	Double
GEOCODE_5	Target year other area (ft ²)	Double	
RoadNetwork	NO	Link number	Integer
	Length	Link length (mile)	Double
	t0	Free flow travel time (s)	Double
Incentiveboundary	Name	Incentive area name	String
	Shape_Area	Area (mile ²)	Double
Population Change	TAZ	TAZ number	Integer
	Population Change	Population change	Integer
Employment Change	TAZ	TAZ number	Integer
	Employment Change	Employment change	Integer
University Enrollment Change	TAZ	TAZ number	Integer
	University Enrollment Change	University enrollment change	Integer
	Name	University name(s)	String

Date Item	Field	Description	Type
High School Enrollment Change	TAZ	TAZ	Integer
	High School Change	High school enrollment change	Integer
	Name	High school name(s)	String
Land Use Inputs	See details in Table 3.4	See details in Table 3.4	N/A

ft, feet

Table A1- 8 Land Use Inputs

Name	Description	Format
21_natural_restrictions	Base year natural restricted areas	Raster
22_administrative_restrictions	Base year administrative restricted areas	Raster
231_residential_zoning	Residential zoning	Raster
234_employment_zoning	Employment zoning	Raster
30_incentive	User specified incentive layer	Raster
111_population_change	Suitability of Average Annual Percentage Change (AAPC) of population from initial year to base year	Table
112_employment_change	Suitability of Average Annual Percentage Change (AAPC) of employment from initial year to initial year	Table
113_median_income	Base year median income suitability	Table
114_distance_to_freeway	Base year Distance to Freeway exits suitability	Table
115_distance_to_transit	Base year walkable distance to transit stops suitability	Raster
116_VCratio	Base year D/C ratio suitability	Table
117_CarbonEmission	Base year carbon emission suitability	Table
118_slope	Slope suitability	Table
119_distance_to_employment	Base year distance to employment land suitability	Raster
120_distance_to_residential	Base year distance to residential land suitability	Raster
121_distance_to_vacant	Base year distance to vacant land suitability	Raster
01_ilu	Initial year land use	Raster
02_blu	Base year land use	Raster
Residential suitability image	Base year residential land use suitability score image	Raster
Employment suitability image	Base year employment land use suitability score image	Raster
Institution suitability image	Base year institution land use suitability image	Raster
Undeveloped suitability image	Base year undeveloped land use suitability score image	Raster
Others suitability image	Base year other land use suitability score image	Raster

Table A1- 9 List of Outputs from the Scenario Development

Name	Field	Description	Type
TargetYearTAZ	TAZ	TAZ name, the format is TAZ_TAZ Number, i.e. TAZ_151	String
	TAZ_N	TAZ number	Integer
	TAZ_Order	The field to link TAZs in ArcGIS and TAZs in VISUM	Integer
	POP	Target year population	Integer
	HH	Target year household	Integer
	EMP	Target year employment (employee)	Integer
	HI	Target year high school enrollment	Integer
	UN	Target year university enrollment	Integer
	AREA_TYPE	CBD&Urban or suburban or rural	Integer
	GEOCODE_Base_1	Base year residential area (ft ²)	Double
	GEOCODE_Base_2	Base year employment area (ft ²)	Double
	GEOCODE_Base_3	Base year institutional area (ft ²)	Double
	GEOCODE_Base_4	Base year undeveloped area (ft ²)	Double
	GEOCODE_Base_5	Base year other area (ft ²)	Double
	GEOCODE_1	Target year residential area (ft ²)	Double
	GEOCODE_2	Target year employment area (ft ²)	Double
GEOCODE_3	Target year institutional area (ft ²)	Double	
GEOCODE_4	Target year undeveloped area (ft ²)	Double	
GEOCODE_5	Target year other area (ft ²)	Double	
Landuse_Target	GEOCODE	Land use type, 1=residential, 2=employment, 3=institutional, 4=undeveloped, 5=other	Integer
	Shape_Area	Area (ft ²)	Double

ft - feet

1) Inputs and Outputs for the Regional Level Analysis

Inputs for the regional level analysis include the *Household Fraction and Trip Rate, Employment Fraction, VISUM File* for travel demand forecasting, *Age Distribution, Fuel Supply, Fuel Formulation, Meteorology, County and State* for emission estimation. Fields and data type

of those input files are listed in Table A1-10, and details about a VISUM file are provided in Table A1-11. Output files for the regional level analysis are listed in Table A1-12.

Table A1- 10 Inputs for the Regional Level Analysis

Name	Field	Description	Type
Household Fraction and Trip Rate	HH_ID	Household ID	Integer
	Fraction	The portion of households whose ID=HH_ID to the total number of households	Double
	HBO_Rate	The trip generation rate by trip purpose HBO	Double
	HBW_Rate	The trip generation rate by trip purpose HBW	Double
	HBSC_Rate	The trip generation rate by trip purpose HBSC	Double
	HBU_Rate	The trip generation rate by trip purpose HBU	Double
Employment Fraction	TAZ_N	TAZ number	Integer
	LEMP	The rate of low trip rate employment in TAZ_N	Double
	MEMP	The rate of medium trip rate employment in TAZ_N	Double
	HEMP	The rate of high trip rate employment in TAZ_N	Double
VISUM File	See details in Table 4-7	See details in Table 4-7	See details in Table 4-7
Age Distribution	SourceType	11=Motorcycle; 21= Passenger Car; 31= Passenger Truck; 32=Light Commercial Truck; 41=Intercity Bus; 42=Transit Bus; 43=School Bus; 51=Refuse Truck; 52=Single Unit Short-haul Truck; 53=Single Unit Long-haul Truck; 54 Motor Home; 61=Combination Short-haul Truck; 62=Combination Long-haul Truck	Integer
	YearID	Calendar year	Integer
	AgeID	Age	Integer
	AgeFraction	Distribution of AgeIDs	Double
	countyID	County	Integer

Name	Field	Description	Type
Fuel Supply	fuelYearID	Fuel year	Integer
	monthGroupID	Fuel month	Integer
	fuelFormulationID	Fuel formulation identification number. Must be greater than 100 and less than 25000	Integer
	marketShare	Market share	Double
	marketShareCV	Null	Double
Fuel Formulation	fuelFormulationID	Fuel formulation identification number. Must be greater than 100 and less than 25000	Integer
	fuelSubtypeID	Fuel Sub-type coding	Integer
	RVP	Reid vapor pressure in psi	Integer
	sulfurLevel	Fuel sulfur level in ppm Sulfur	Integer
	ETOHVolume	Ethanol Volume (% vol)	Double
	MTBEVolume	MTBE Volume (% vol)	Double
	ETBEVolume	ETBE Volume (% vol)	Double
	TAMEVolume	TAME Volume (% vol)	Double
	aromaticContent	Aromatic content (% wt)	Double
	olefinContent	Olefin content (% wt)	Double
	benzeneContent	Benzene content (% wt)	Double
	e200	Lower volatility percentage (%)	Integer
	e300	Upper volatility percentage (%)	Integer
	volToWtPercentOxy	Constant based on oxygenate type	Double
	BioDieselEsterVolume	BioDiesel Ester Volume (%)	Double
	CetaneIndex	NULL	NULL
	PAHContent	NULL	NULL
T50	Temperature (F) where 50% of the fuel is vapor	Integer	
T90	Temperature (F) where 90% of the fuel is vapor	Integer	
Meteorology	monthID	Calendar month	Integer
	zoneID	Zone	Integer
	hourID	Hour	Integer
	temperature	Temperature	Double
	relHumidity	Humidity	Double

Name	Field	Description	Type
County and State	State Name	State Name	Integer
	County Name	County Name	Integer

vol, volume; wt, weight

Table A1- 11 Description of a VISUM File

Data	Description	Format
TAZ	A shapefile of traffic analysis zones. Attributes which need to be created by users include TAZ_Num, HH_ID_1, HH_ID_2, HH_ID_3, HH_ID_4, HH, EMP, LEMP, MEMP, HEMP, HIEN, and UNEN.	Polygon
Road Network	A shapefile of street center lines. Attributes which need to be specified by users are Cap (capacity), V0 (free flow speed).	Line
Transit Network	A shapefile of transit lines and transit stops.	
Matrices	Matrices store number of trips, and travel times between TAZs	Table
Four Step Model Parameters	<p><i>a. Trip Generation</i></p> <p>The trip generation in VISUM is implemented by connecting the socioeconomic data to its corresponding trip production and attraction rates. Trip production rates and attraction rates including $NHBPRATE_{at(i)}^{mx}$, $LEMPRATE_i$, $MEMPRATE_i$, $HEMPRATE_i$, $HHRATE_i$, $URATE_i$, and $HRATE_i$ (in Eq. 3.17 and Eq. 3.18 in Section 3.3) are required.</p> <p><i>b. Trip Distribution</i></p> <p>The trip distribution in VISUM is implemented by assigning an appropriate distribution model in VISUM. An iterative procedure is employed to refine trip interchange estimates until convergence is met, i.e., the estimated zonal trip ends attracted to each zone closely match the desired zonal trip attractions calculated in the trip generation phase. To implement this, the parameter α in Eq. 3.19 needs to be set up, and k_{ij} is automatically estimated by balancing the trip generations and attractions.</p> <p><i>c. Mode Split</i></p> <p>The trip mode choice in VISUM is implemented by assigning an appropriate mode split model. The mode split model adapts the Logit utility function with parameters of β in Eq. 3.20.</p>	N/A

Data	Description	Format
	<p><i>d. Trip Assignment</i></p> <p>The equilibrium traffic assignment utilizes the Wardrop's first principle and breaks the OD demand matrix into the proportions per iteration step. The traffic assignment procedure is an iterative step where a proportion of traffic will be assigned in each iteration until convergence criteria meets.</p>	

Table A1- 12 Outputs from the Regional Level Analysis

Name	Field	Description	Type
TargetYearTAZ	TAZ	TAZ name, the format is TAZ_TAZ Number, i.e. TAZ_151	String
	TAZ_N	TAZ number	Integer
	TAZ_Order	The key field to link TAZs in ArcGIS and TAZs in VISUM	Integer
	POP	Target year population	Integer
	HH	Target year household	Integer
	EMP	Target year employment	Integer
	HI	Target year high school enrollment	Integer
	UN	Target year university enrollment	Integer
	AREA_TYPE	1=CBD&Urban; 2= suburban; 3= rural	Integer
	GEOCODE_Base_1	Base year residential area (ft ²)	Double
	GEOCODE_Base_2	Base year employment area (ft ²)	Double
	GEOCODE_Base_3	Base year institutional area (ft ²)	Double
	GEOCODE_Base_4	Base year undeveloped area (ft ²)	Double
	GEOCODE_Base_5	Base year other area (ft ²)	Double
	GEOCODE_1	Target year residential area (ft ²)	Double
	GEOCODE_2	Target year employment area (ft ²)	Double
	GEOCODE_3	Target year institutional area (ft ²)	Double
	GEOCODE_4	Target year undeveloped area (ft ²)	Double
	GEOCODE_5	Target year other area (ft ²)	Double
	GEOCODE	Land use type, 1=residential, 2=employment, 3=institutional, 4=undeveloped, 5=other	Double
Shape_Area	Area (ft ²)	Double	

Name	Field	Description	Type
RoadNetwork	Volume_Base/ Volume_Target	Base/ Target year volume (veh)	Double
	Speed_Base/ Speed_Target	Base/ Target year speed (mile/h)	Double
	DCRatio_Base/ DCRatio _Target	Base/ Target year demand/capacity ratio (%)	Double
	Delay_Base/ Delay_Target	Base/ Target year delay (min/veh/mile)	Double
	QueueLength_Base/ QueueLength_Target	Base/ Target year queue length (veh/mile)	Double
	CO2_Equivalent_Base/ CO2_Equivalent_Target	Base/ Target year CO2 equivalent (kg)	Double
	Energy_Consumption_Base/ Energy_Consumption _Target	Base/ Target year energy consumption (kJ)	Double
Vehicle Composition	LINKID	Link number	Integer
	Car fraction	The fraction of cars to the total number of vehicles on a link	Double

ft, feet; veh, vehicle

2) Inputs and Outputs for the Project Level Analysis

Details about inputs and outputs for the project level analysis are listed in Table A1-13 (inputs) and Table A1-14 (outputs).

Table A1- 13 Inputs for the Project Level Analysis

Name	Sheet	Field	Description	Type
Microscopic Simulation Links	Sheet1	GISLinkID	Link ID in RoadNetwork	Integer
	Sheet1	MicroscopicLinkID	Link ID in microscopic simulation	Integer
	Sheet2	GISLinkID	Link ID in RoadNetwork	Integer
	Sheet2	RoadType	(1=Off-Network; 2=Rural Restricted Access; 3=Rural Unrestricted Access; 4=Urban Restricted Access; 5=Urban Unrestricted Access)	Integer
	Sheet2	LinkLength	Link length (mile)	Double
	Sheet2	LinkGrade	Link grade	Double
		Sheet1	MicroscopicLinkID	Link ID in microscopic simulation
Sheet1		time (sim sec)	Time stamp	Integer

Microscopic Simulation Results VISUM File	Sheet1	Car #	Car number	Integer
	Sheet1	Car v	Car speed (mile/sec)	Double
	Sheet1	Car a	Car acceleration (mile/sec ²)	Double
	Sheet1	Truck #	Truck number	Integer
	Sheet1	Truck v	Truck speed (mile/sec)	Double
	Sheet1	Truck a	Truck acceleration (mile/sec ²)	Double
	Sheet2	MicroscopicLinkID	Link ID in microscopic simulation	Double
	Sheet2	AverageSpeed	Average speed (mile/h)	Double
	Sheet2	Delay	Delay (min/vehicle)	Double
	Sheet2	QueueLength	Queue length (vehicle)	Double

Veh, vehicle

Table A1- 14 Outputs from the Project Level Analysis

Name	Field	Description	Type
	TAZ	TAZ name, the format is TAZ_TAZ Number, i.e. TAZ_151	String
	TAZ_N	TAZ number	Integer
	TAZ_Order	The field to link TAZs in ArcGIS and TAZs in VISUM	Integer
	POP	Target year population	Integer
	HH	Target year household	Integer
	EMP	Target year employment	Integer
	HI	Target year high school enrollment	Integer
	UN	Target year university enrollment	Integer
	AREA_TYPE	1=CBD&Urban; 2= suburban; 3= rural	Integer
	GEOCODE_Base_1	Base year residential area (ft ²)	Double
	GEOCODE_Base_2	Base year employment area (ft ²)	Double
	GEOCODE_Base_3	Base year institutional area (ft ²)	Double
	GEOCODE_Base_4	Base year undeveloped area (ft ²)	Double
	GEOCODE_Base_5	Base year other area (ft ²)	Double
	GEOCODE_1	Target year residential area (ft ²)	Double
	GEOCODE_2	Target year employment area (ft ²)	Double
	GEOCODE_3	Target year institutional area (ft ²)	Double
	GEOCODE_4	Target year undeveloped area (ft ²)	Double
	GEOCODE_5	Target year other area (ft ²)	Double

Name	Field	Description	Type
Landuse_Target	GEOCODE	Land use type, 1=residential, 2=employment, 3=institutional, 4=undeveloped, 5=other	Integer
	Shape_Area	Area (ft ²)	Double
RoadNetwork	CO2_Equivalent_Updated	CO ₂ equivalent (kg)	Double
	Energy_Consumption_Updated	Energy consumption (kJ)	Double

ft, feet

A I.2 Database in AIR-SUSTAIN

A I.2.1 Database Structure

All model outputs and intermediate data are stored in five MySQL databases and an ArcGIS Geodatabase. The five MySQL databases are automatically generated for each AIR-SUSTAIN scenario. They are AIR-SUSTAIN scenario database, regional MOVES input database, regional MOVES output database, project-level MOVES input database, and project-level MOVES output database. The fields and data sources of data tables in the MySQL databases are listed in Table A2-1.

Table A2- 1 Tables and fields of AIR-SUSTAIN Scenario Database

Table Name	Fields	Data Source
projectInfo	scenarioID	Specified by the user in the AIR-SUSTAIN GUI
	baseYear	Specified by the user in the AIR
	targetYear	Specified by the user in the AIR
	analyst	Specified by the user in the AIR
	date	Specified by the user in the AIR
	projectDir	Specified by the user in the AIR
	idrisiDir	Specified by the user in the AIR
	movesDir	Specified by the user in the AIR
	projectDescription	Specified by the user in the AIR
Increase Percentage	PopIncrease	Specified by the user in the AIR
	EmplIncrease	Specified by the user in the AIR
PopulationGrowth	TAZ	Imported from Population Change
	Population	Imported from Population Change
EmploymentGrowth	TAZ	Imported from Employment Change
	Employment	Imported from Employment Change

Table Name	Fields	Data Source
UniversityEnrollment	TAZ	Imported from University Enrollment Change
	Enrollment	Imported from University Enrollment Change
	Name	Imported from University Enrollment Change
HighSchoolEnrollment	TAZ	Imported from High School Enrollment Change
	Enrollment	Imported from High School Enrollment Change
	Name	Imported from High School Enrollment Change
HouseholdTripRate	TAZ	Imported from Household Fraction and Trip Rate
	Fraction	Imported from Household Fraction and Trip Rate
	HBO	Imported from Household Fraction and Trip Rate
	HBW	Imported from Household Fraction and Trip Rate
	HBSC	Imported from Household Fraction and Trip Rate
	HBU	Imported from Household Fraction and Trip Rate
EmploymentTripRate	TAZ	Imported from Employment Fraction
	LowRate	Imported from Employment Fraction
	MediumRate	Imported from Employment Fraction
	HighRate	Imported from Employment Fraction
BaseYearResults	LinkID	Output from TDF
	Volume	Output from TDF
	FunctionClass	Output from TDF
	AvgSpeed	Output from TDF
	DCRatio	Output from TDF
	Delay	Output from TDF
	QueueLength	Output from TDF
	TruckFraction	Output from TDF
	CO2 Equivalent	Output from emission estimation
	EnergyConsumption	Output from emission estimation
BaseYearResults	LinkID	Outputted from TDF
	Volume	Outputted from TDF
	FunctionClass	Outputted from TDF (1=Off-Network; 2=Rural Restricted Access; 3=Rural Unrestricted Access; 4=Urban Restricted Access; 5=Urban Unrestricted Access)

Table Name	Fields	Data Source
	AvgSpeed	Output from TDF
	DCRatio	Output from TDF
	Delay	Output from TDF
	QueueLength	Output from TDF
	TruckFraction	Output from TDF
	CO2 Equivalent	Output from emission estimation
	EnergyConsumption	Output from emission estimation
IDIRSInfo	InitialYear	Specified by the user in AIR-SUSTAIN GUI
	Folderpath	Specified by the user in AIR-SUSTAIN GUI

TDF, Travel Demand Forecasting

The data tables for the regional and project-level MOVES inputs in the databases are the same. In addition, the data tables of regional and project-level MOVES outputs in the databases are also the same. The data tables and fields of MOVES input database are listed in Table A2-2. The data table and included items of the MOVES output database are illustrated in Table A2-3.

Table A2- 2 Tables and Items of the MOVES Input Database

Table Name	Items	Data Source
link	linkID	TDF
	countyID	Specified by the user
	zoneID	MOVES database
	roadTypeID	TDF
	linkLength	TDF based on geometry input
	linkVolume	TDF or microscopic simulation data source
	linkAvgSpeed	TDF or microscopic simulation data source
	linkDescription	N/A
	linkAvgGrade	Calculated by AIR-SUSTAIN based on geometry input
linksource-typehour	linkID	TDF
	sourceTypeID	TDF
	sourceTypeHourFraction	TDF or microscopic simulation data source
opmode-distribution	sourceTypeID	MOVES database
	hourDayID	TDF or micro-simulation data source
	linkID	TDF
	polProcessID	MOVES database

Table Name	Items	Data Source
	opModeID	MOVES database
	opModeFraction	Calculated by AIR-SUSTIAN based on traffic input
	opModeFractionCV	Null
	isUserInput	Null
County	countyID	From State and County
	stateID	From State and County
	CountyName	From State and County
	altitude	MOVES database
	GPAFract	MOVES database
	barometricPressure	MOVES database
	barometricPressureCV	Null
sourcetypeage-distribution	sourceTypeID	MOVES database
	yearID	Specified by user
	ageID	From Age Distribution
	ageFraction	Non-traffic input
state	stateID	From State and County
	stateName	From State and County
	stateAbbr	From State and County
year	yearID	From input base year or target year
	isBaseYear	Calculated by AIR-SUSTAIN based on traffic input
	fuelYearID	From file Fuel Supply
zone	zoneID	MOVES database
	countyID	From State and County
	startAllocFactor	1
	idleAllocFactor	1
	SHPAllocFactor	1
zone-monthhour	monthID	Specified by the user
	zoneID	MOVES database
	hourID	TDF
	temperature	From Meteorology
	temperatureCV	Null
	relHumidity	From Meteorology
	heatIndex	Null
	specificHumidity	Null
	relativeHumidityCV	Null
zoneroadtype	zoneID	MOVES database
	roadTypeID	TDF
	SHOAllocFactor	1
fuel-formulation	fuelFormulationID, fuelSubtypeID, RVP, sulfurLevel, ETOHVolume, MTBEVolume, TAMEVolume, aromaticContnet,	From Fuel Formulation

Table Name	Items	Data Source
	olefinContent, benzeneContent, e200, 2300, volToWtPercentOxy, BioDieselEsterVolume, CetaneIndex, PAHContent, T50, T90	
fuelsupply	countyID, fuelYearID, monthGroupID, fuelFormulationID, marketShare, marketShareCV	From Fuel Supply

Table A2- 3 Tables and Items of the MOVES Output Database

Table Name	Items	Description
activitytype	activityTypeID, activityType, activityTypeDesc,	This table lists the activity types that can be reported in the movesactivityoutput table and provides their activitytypeid (1= distance traveled; 2=source hours; 3= source hour idling; 4= source hours operating; 5= source hours parked; 6= population; 7= starts).
bundletracking	hostType, MOVESRunID, loopableClassName, workerVersion, workerComputerID, workerID, bundleNumber, isCleanUp, iterationID, processID, roadTypeID, linkID, zoneID, countyID, stateID, yearID, monthID, dayID, HourID, executionGranularity	This table contains information about data that is processed by the MOVES master and workers.
movesactivityoutput	MOVESRunID, iterationID, yearID, monthID, dayID, hourID, stateID, countyID, zoneID, linkID, sourceTypeID, fuelTypeID, modelYearID, roadTypeID, SCC	This table provides information on the vehicle activity generated and run.
moveserror	MOVESError, MOVESRunID, yearID, monthID, dayID, hourID, stateID, zoneID, linkID, pollutantID, processID, errorMessage	This table contains any error messages or diagnostic information that might be generated if the MOVES run is unsuccessful.
moveeventlog	EventRecordID, MOVESRunID, EventName, WhenStarted, WhenStoped, Durantion	This table stores diagnostic results.
movesoutput	MOVESRunID, iterationID, yearID, monthID, dayID, hourID, stateID, countyID, zoneID, linkID, pollutantID, processID, sourceTypeID, fuelTypeID, modelYearID, roadTypeID, SCC	This table contains the inventory emission results of the run disaggregated by parameters, such as Year, Month, etc.
movesrun	MOVESRunID, outputTimePeriod, timeUnits, distanceUnits, massUnits, energyUnits, runSpecFileName, runSpecDescription, runSpecFileDateTime, runDataTime, scale, minutesDuration, defaultDatabaseUsed, masterVersionDate, masterComputerID,	The table contains information about the date and time of the run, information about the run specifications, and the name of the units in which MOVES outputs are represented.

Table Name	Items	Description
	masterIDNumber, domain, domainCountyID, domainCountyName, domainDatabaseServer, domainDatabaseName, expectedDONEFiles, retrivedDONEFiles	
movestableused	MOVESRunID, databaseServer, databaseName, tableName, dataFileSize, dataFileModificationDate, tableUseSequence	This table stores a list of the tables used when executing MOVES.
movesworkerused	MOVESRunID, wokerversion, wokerComputerID, workerrID, bundleCount, failedBundleCount	This table contains information as to which copy of the MOVES Worker Program processed portions of the run.
rateperdistance	MOVESScenarioID, MOVESRunID, yearID, monthID, dayID, hourID, linkID, pollutantID, processID, sourceTypeID, SCC, fuelTypeID, modelYearID, riadTypeID, avgSpeedBinID, temperature, relHumidity, ratePerDistance	This table stores emissions as rates per distance with the units depending on those selected on run specification.
rateperprofile	MOVESScenarioID, MOVESRunID, temperatureProfile, yearID, dayID, hourID, pollutantID, processID, sourceTypeID, SCC, fuelTypeID, modelYearID, temperature, rateperVehicle	This table stores vapor venting emissions from parked vehicles as rates per vehicle.
ratepervehicle	MOVESScenarioID, MOVESRunID, yearID, dayID, hourID, pollutantID, processID, sourceTypeID, SCC, fuelTypeID, modelYearID, temperature, rateperVehicle	This table stores vapor venting emissions from starts and extended idle, and some evaporative emissions from parked vehicle as rates per vehicle.

All feature classes, including TAZ, TargetYearTAZ, RoadNetwork, Incentiveboundary, Congestion_Area, and Landuse_Target, are stored in a Geodatabase. The feature class names and items of each feature class are illustrated in Table A2-4.

Table A2- 4 Geodatabase

Feature class	Item	Source
TAZ	FID	Generated by ArcGIS automatically
	TAZ	Specified by the user
	TAZ_N	Specified by the user
	TAZ_Order	The key to link TAZs in feature class and TAZs in VISUM
	POP	Specified by the user
	HH	Specified by the user
	EMP	Specified by the user
	HI	Specified by the user
	UN	Specified by the user
AREA_TYPE	Specified by the user	

Feature class	Item	Source
	GEOCODE_1	Specified by the user
	GEOCODE_2	Specified by the user
	GEOCODE_3	Specified by the user
	GEOCODE_4	Specified by the user
	GEOCODE_5	Specified by the user
Incentiveboundary	FID	Generated by ArcGIS automatically
	Shape_Area	Generated by ArcGIS after the user specify the boundary
TargetYearTAZ	FID	Generated by ArcGIS automatically
	TAZ	Specified by the user
	TAZ_N	Specified by the user
	TAZ_Order	The key to link TAZs in feature class and VISUM
	POP	From linkage model
	HH	From linkage model
	EMP	From linkage model
	HI	From linkage model
	UN	From linkage model
	AREA_TYPE	From linkage model
	GEOCODE_1	From land use projection
	GEOCODE_2	From land use projection
	GEOCODE_3	From land use projection
	GEOCODE_4	From land use projection
	GEOCODE_5	From land use projection
Landuse_Target	FID	Generated by ArcGIS automatically
	GEOCODE	From survey data
	Shape_Area	From survey data
RoadNetwork	FID	Generated by ArcGIS automatically
	NO	Specified by users
	Length	Specified by the user
	Volume_Base	Output from TDF
	Speed_Base	Output from TDF
	DCRatio_Base	Output from TDF
	Delay_Base	Output from TDF
	QueueLength_Base	Output from TDF

Feature class	Item	Source
	CO2_Equivalent_Base	Output from emission estimation
	Energy_Consumption_Base	Output from emission estimation
	Volume_Target	Output from TDF
	Speed_Target	Output from TDF
	DCRatio_Target	Output from TDF
	Delay_Target	Output from TDF
	QueueLength_Target	Output from TDF
	CO2_Equivalent_Target	Output from emission estimation
	Energy_Consumption_Target	Output from emission estimation
	CO2_Equivalent_Update	Output from TDF
	Energy_Consumption_Update	Output from TDF
Congestion_Area	FID	Generated in ArGIS
	NO	From RoadNetwork
	Length	From RoadNetwork
	Volume_Base	From RoadNetwork
	Speed_Base	From RoadNetwork
	DCRatio_Base	From RoadNetwork
	Delay_Base	From RoadNetwork
	QueueLength_Base	From RoadNetwork
	CO2_Equivalent_Base	From RoadNetwork
	Energy_Consumption_Base	From RoadNetwork
	Volume_Target	From RoadNetwork
	Speed_Target	From RoadNetwork
	DCRatio_Target	From RoadNetwork
	Delay_Target	From RoadNetwork
	QueueLength_Target	From RoadNetwork
	CO2_Equivalent_Target	From RoadNetwork
	Energy_Consumption_Target	From RoadNetwork

TDF, Travel Demand Forecasting

A I.2.2 MOVES Emission Lookup Tables

The MOVES model incorporates similar regression-based equations for mean and variance model for braking/deceleration and uses similar approach of heavy-duty vehicles. The vehicle activity mix is determined by the emission source type, age group, road type and operating mode distribution. The lookup tables for emission source type, road type, and vehicle age distribution are presented in Table A2-5 to A2-8.

Emission Source Type

Table A2- 5 The MOVES Source Types

Source Type ID	Source Type Name	HPMS Vehicle Type ID	HPMS Vehicle Type Name
11	Motorcycle	10	Motorcycles
21	Passenger Car	20	Passenger Cars
31	Passenger Truck	30	Other 2 axle-4 tire vehicles
32	Light Commercial Truck	30	Other 2 axle-4 tire vehicles
41	Intercity Bus	40	Buses
42	Transit Bus	40	Buses
43	School Bus	40	Buses
51	Refuse Truck	50	Single Unit Trucks
52	Single Unit Short-haul Truck	50	Single Unit Trucks
53	Single Unit Long-haul Truck	50	Single Unit Trucks
54	Motor Home	50	Single Unit Trucks
61	Combination Short-haul Truck	60	Combination Trucks
62	Combination Long-haul Truck	60	Combination Trucks

Road Type

Table A2- 6 The MOVES Road Type

Road Type ID	Road Type Description
1	Off-Network
2	Rural Restricted Access
3	Rural Unrestricted Access

Road Type ID	Road Type Description
4	Urban Restricted Access
5	Urban Unrestricted Access

Vehicle Age Distribution

Table A2- 7 MOVES Age Distribution Categories

ageID	ageCategoryName	ageID	ageCategoryName
0	new	21	21 years old
1	one year old	22	22 years old
2	two years old	23	23 years old
3	three years old	24	24 years old
4	four years old	25	25 years old
5	five years old	26	26 years old
6	six years old	27	27 years old
7	seven years old	28	28 years old
8	eight years old	29	29 years old
9	nine years old	30	30 or more years old
10	ten years old		
11	eleven years old		
12	twelve years old		
13	13 years old		
14	14 years old		
15	15 years old		
16	16 years old		
17	17 years old		
18	18 years old		
19	19 years old		
20	20 years old		

Operating Mode

Table A2- 8 MOVES Operating Modes

opModel D	opModeName	VSP Lower	VSP Upper	Speed Lower	Speed Upper
0	Braking	0	0	0	0
1	Idling	0	0	-1	1
11	Low Speed Coasting; VSP < 0; 1 ≤ Speed < 25	0	0	1	25
12	Cruise/Acceleration; 0 ≤ VSP < 3; 1 ≤ Speed < 25	0	3	1	25
13	Cruise/Acceleration; 3 ≤ VSP < 6; 1 ≤ Speed < 25	3	6	1	25
14	Cruise/Acceleration; 6 ≤ VSP < 9; 1 ≤ Speed < 25	6	9	1	25
15	Cruise/Acceleration; 9 ≤ VSP < 12; 1 ≤ Speed < 25	9	12	1	25
16	Cruise/Acceleration; 12 ≤ VSP; 1 ≤ Speed < 25	12	0	1	25
21	Moderate Speed Coasting; VSP < 0; 25 ≤ Speed < 50	0	0	25	50
22	Cruise/Acceleration; 0 ≤ VSP < 3; 25 ≤ Speed < 50	0	3	25	50
23	Cruise/Acceleration; 3 ≤ VSP < 6; 25 ≤ Speed < 50	3	6	25	50
24	Cruise/Acceleration; 6 ≤ VSP < 9; 25 ≤ Speed < 50	6	9	25	50
25	Cruise/Acceleration; 9 ≤ VSP < 12; 25 ≤ Speed < 50	9	12	25	50
26	Cruise/Acceleration; 12 ≤ VSP; 25 ≤ Speed < 50	12	0	25	50
27	Cruise/Acceleration; 12 ≤ VSP < 18; 25 ≤ Speed < 50	12	18	25	50
28	Cruise/Acceleration; 18 ≤ VSP < 24; 25 ≤ Speed < 50	18	24	25	50
29	Cruise/Acceleration; 24 ≤ VSP < 30; 25 ≤ Speed < 50	24	30	25	50
30	Cruise/Acceleration; 30 ≤ VSP; 25 ≤ Speed < 50	30	0	25	50

opModel D	opModeName	VSP Lower	VSP Upper	Speed Lower	Speed Upper
33	Cruise/Acceleration; VSP < 6; 50 <= Speed	0	6	50	0
35	Cruise/Acceleration; 6 <= VSP < 12; 50 <= Speed	6	12	50	0
36	Cruise/Acceleration; 12 <= VSP; 50 <= Speed	12	0	50	0
37	Cruise/Acceleration; 12 <= VSP < 18; 50 <= Speed	12	18	50	0
38	Cruise/Acceleration; 18 <= VSP < 24; 50 <= Speed	18	24	50	0
39	Cruise/Acceleration; 24 <= VSP < 30; 50 <= Speed	24	30	50	0
40	Cruise/Acceleration; 30 <= VSP; 50 <= Speed	30	0	50	0
100	Starting (Used for all starts)	0	0	0	0
101	Soak Time < 6 minutes	0	0	0	0
102	6 minutes <= Soak Time < 30 minutes	0	0	0	0
103	30 minutes <= Soak Time < 60 minutes	0	0	0	0
104	60 minutes <= Soak Time < 90 minutes	0	0	0	0
105	90 minutes <= Soak Time < 120 minutes	0	0	0	0
106	120 minutes <= Soak Time < 360 minutes	0	0	0	0
107	360 minutes <= Soak Time < 720 minutes	0	0	0	0
108	720 minutes <= Soak Time	0	0	0	0
150	Hot Soaking	0	0	0	0
151	Cold Soaking	0	0	0	0
200	Extended Idling	0	0	0	0
201	Hotelling Diesel Aux	0	0	0	0
202	Hotelling Fuel Operated Heater	0	0	0	0
203	Hotelling Battery AC	0	0	0	0
204	Hotelling APU Off	0	0	0	0
300	All Running	0	0	0	0
301	running; speed < 2.5mph	0	0	0	2.5

opModel D	opModeName	VSP Lower	VSP Upper	Speed Lower	Speed Upper
302	running; 2.5mph <= speed < 7.5mph	0	0	2.5	7.5
303	running; 7.5mph <= speed < 12.5mph	0	0	7.5	12.5
304	running; 12.5mph <= speed < 17.5mph	0	0	12.5	17.5
305	running; 17.5mph <= speed < 22.5mph	0	0	17.5	22.5
306	running; 22.5mph <= speed < 27.5mph	0	0	22.5	27.5
307	running; 27.5mph <= speed < 32.5mph	0	0	27.5	32.5
308	running; 32.5mph <= speed < 37.5mph	0	0	32.5	37.5
309	running; 37.5mph <= speed < 42.5mph	0	0	37.5	42.5
310	running; 42.5mph <= speed < 47.5mph	0	0	42.5	47.5
311	running; 47.5mph <= speed < 52.5mph	0	0	47.5	52.5
312	running; 52.5mph <= speed < 57.5mph	0	0	52.5	57.5
313	running; 57.5mph <= speed < 62.5mph	0	0	57.5	62.5
314	running; 62.5mph <= speed < 67.5mph	0	0	62.5	67.5
315	running; 67.5mph <= speed < 72.5mph	0	0	67.5	72.5
316	running; 72.5mph <= speed	0	0	72.5	0
400	tirewear; idle	0	0	0	0
401	tirewear; speed < 2.5mph	0	0	0	2.5
402	tirewear; 2.5mph <= speed < 7.5mph	0	0	2.5	7.5
403	tirewear; 7.5mph <= speed < 12.5mph	0	0	7.5	12.5
404	tirewear; 12.5mph <= speed < 17.5mph	0	0	12.5	17.5
405	tirewear; 17.5mph <= speed < 22.5mph	0	0	17.5	22.5

opModel D	opModeName	VSP Lower	VSP Upper	Speed Lower	Speed Upper
406	tirewear; 22.5mph <= speed < 27.5mph	0	0	22.5	27.5
407	tirewear; 27.5mph <= speed < 32.5mph	0	0	27.5	32.5
408	tirewear; 32.5mph <= speed < 37.5mph	0	0	32.5	37.5
409	tirewear; 37.5mph <= speed < 42.5mph	0	0	37.5	42.5
410	tirewear; 42.5mph <= speed < 47.5mph	0	0	42.5	47.5
411	tirewear; 47.5mph <= speed < 52.5mph	0	0	47.5	52.5
412	tirewear; 52.5mph <= speed < 57.5mph	0	0	52.5	57.5
413	tirewear; 57.5mph <= speed < 62.5mph	0	0	57.5	62.5
414	tirewear; 62.5mph <= speed < 67.5mph	0	0	62.5	67.5
415	tirewear; 67.5mph <= speed < 72.5mph	0	0	67.5	72.5
416	tirewear; 72.5mph <= speed	0	0	72.5	0
500	Existing	0	0	0	0
501	brakewear; stopped	0	0	0	0

A I.3 Transportation Analysis Examples Using the AIR-SUSTAIN Tool

To evaluate the three competing scenarios for Cincinnati metropolitan area, a 15% increase of population and employment is assumed to occur from the base year 2010 to the target year 2030. All increase of population and employment is allocated and distributed around the center(s). The process for a scenario analysis is taken in Steps 1 through 18, as described below. Finally the analysis results of those three scenarios are compared at Step 19.

Step 1: Create a new scenario by clicking the **Scenario** button followed by clicking **New Scenario** button on the menu bar, and then, input the **Scenario Name** (e.g., “Example”) and other required information (as shown in Figure A3-1) in the **New Scenario** tab. Then, click on the **Save Scenario** button to save scenario files in the specified scenario folder, and create the AIR-SUSTAIN database in MySQL and ArcGIS. Then, go to step 2.

Step 2: Select the **Base Year** first, or the **Target Year** in the **Modeling Year** panel if the Base Year data is already created.

Step 3: Import three feature classes: *TAZ*, *RoadNetwork*, and *Incentiveboundary* in the **Base Year Data** panel. The data import panel and the sample feature classes are shown in Figure 3.44. If in Step 2, the **Base Year** is selected, go to step 7 to perform regional level analysis; if the **Target Year** is checked, go to step 4.

Step 4: Define the assumed **Population Change**, **Employment Change**, **University Enrollment Change** and **High School Enrollment Change** in **Assumed Changes in Demographic and Socioeconomic Factors** panel (as shown in Figure A3-2). *Population Change* and *Employment Change* can be specified within and without incentive boundaries separately. They can also be specified for individual TAZs and imported from Excel files as shown in Tables A3-1. Then, go to step 5.

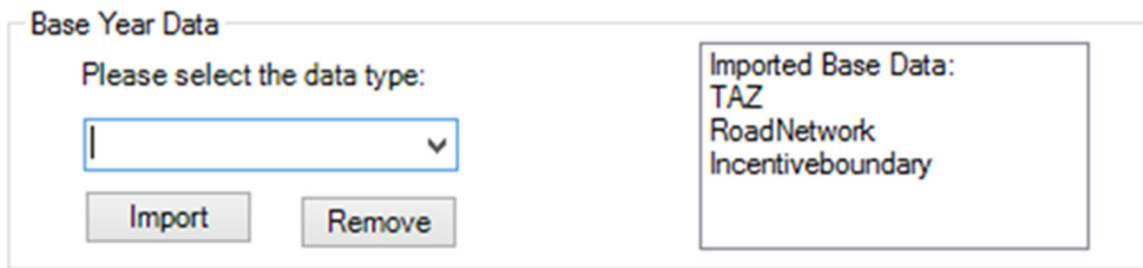
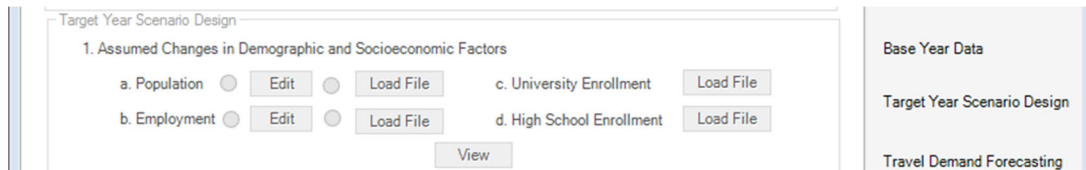
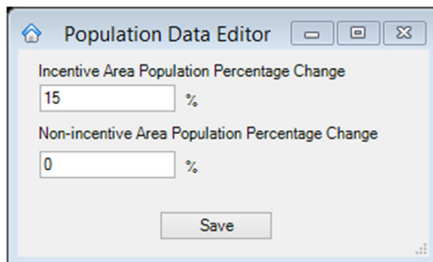


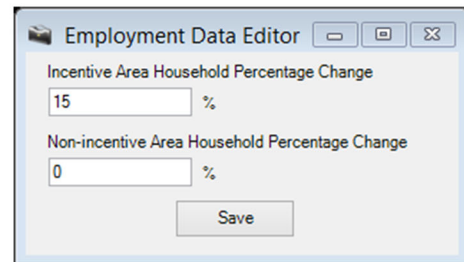
Figure A3- 1 Import base year data in example.



(A)



(B)



(C)

Figure A3- 2 Program interface for (A) importing the Base Year data; (B) assigning population change; and (C) assigning employment changes at TAZ levels.

Table A3- 1 Sample of Population Change

TAZ	Population
330	156
338	191
318	268
249	274
261	383
336	822
337	1249
349	3571
208	7980
332	36784

Step 5: Specify the **Initial Year**, i.e., 2000, and load *Land Use Inputs*, and then project the target year land use by clicking the **Run** button on the **Land Use Projection** panel. The target year land use (shown as Figure A3-3) can be visualized in ArcGIS by clicking **View Results** in the **Land Use Projection** panel. Go to Step 6.

Step 6: Set up the **Maximum Population Density** in the incentive area, i.e., 15000 (person/mile²), then generate target year demographic and socioeconomic data by the linkage model based on base year data and assumed demographic and socioeconomic changes. Results can be viewed by the user by selecting the corresponding data type and displaying it (as shown in Figure A3-4). Then, go to Step 7.

Step 7: Select a *TDF Model* (only VISUM is supported by the current version of AIR-SUSTAIN) and activate the **Travel Demand Forecasting** panel, then go to step 8.

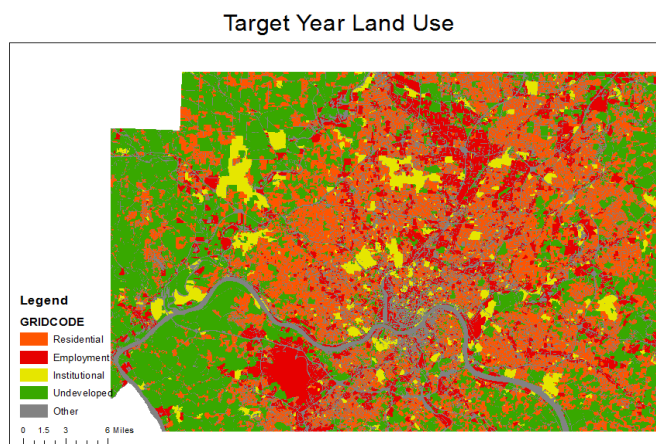


Figure A3- 3 Target year land use in example.

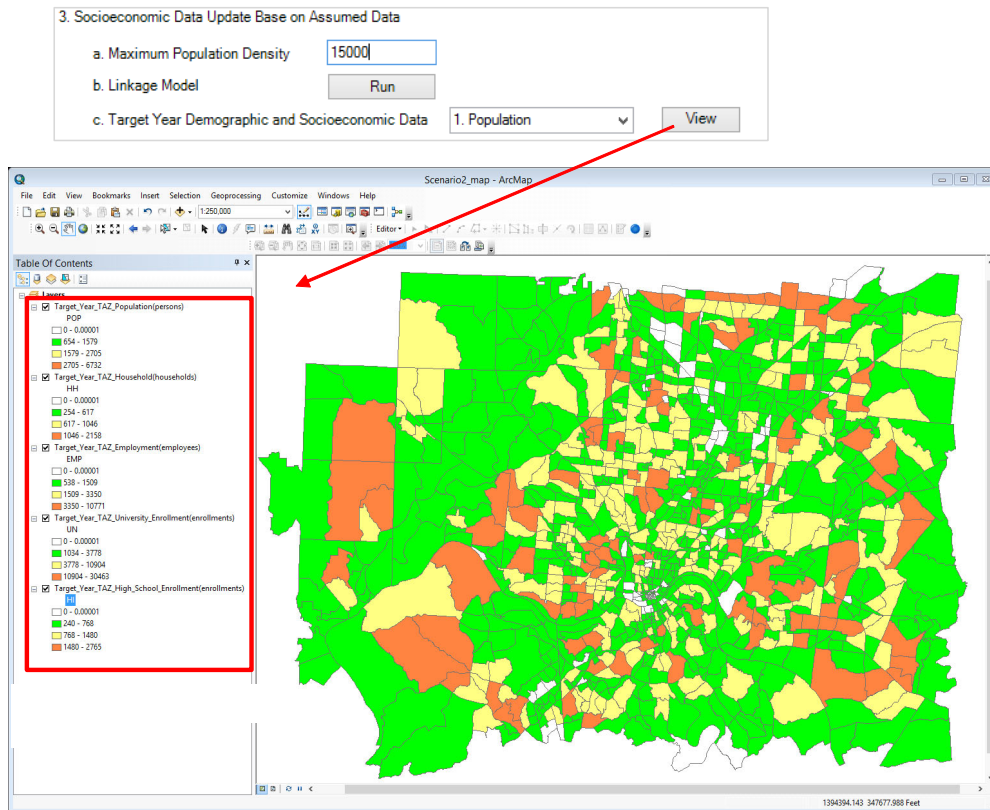


Figure A3- 4 Target year land use in example.

Step 8: Import a *VISUM File* containing TAZs, road network, and transit network, and four step model parameters (the steps in create a *VISUM file* are briefly introduced by Step 8.1 through 8.6, and details can be found in *VISUM user manual* (PTV *VISUM*, 2013)). When it is finished, go to step 9.

Step 8.1: Set up the travel demand model and travel demand segment in *VISUM* (shown as Figure A3-5). Go to step 8.2.

Step 8.2: Load TAZ and road network shapefiles, or draw them in *VISUM* directly (shown as Figure A3-6). For transit lines and stops, the user can only set them up manually in *VISUM*. Go to step 8.3.

Step 8.3: Generate connectors to connect TAZs with road network, then go to step 8.4.

Step 8.4: Create the required fields in zonelist and linklist in *VISUM* (see in Table 3.7 in Section 3.2), then go to step 8.5.

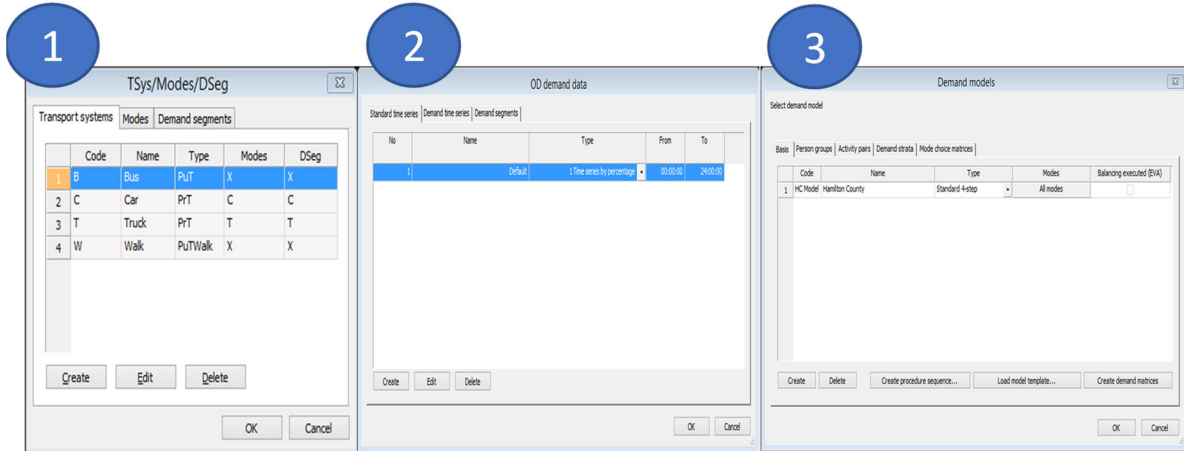


Figure A3- 5 VISUM demand set up.

Step 8.5: Build zone matrix (to store demand) and skim matrix (to store impedance) for each traffic mode (shown as Figure A3-7), then go to step 8.5.

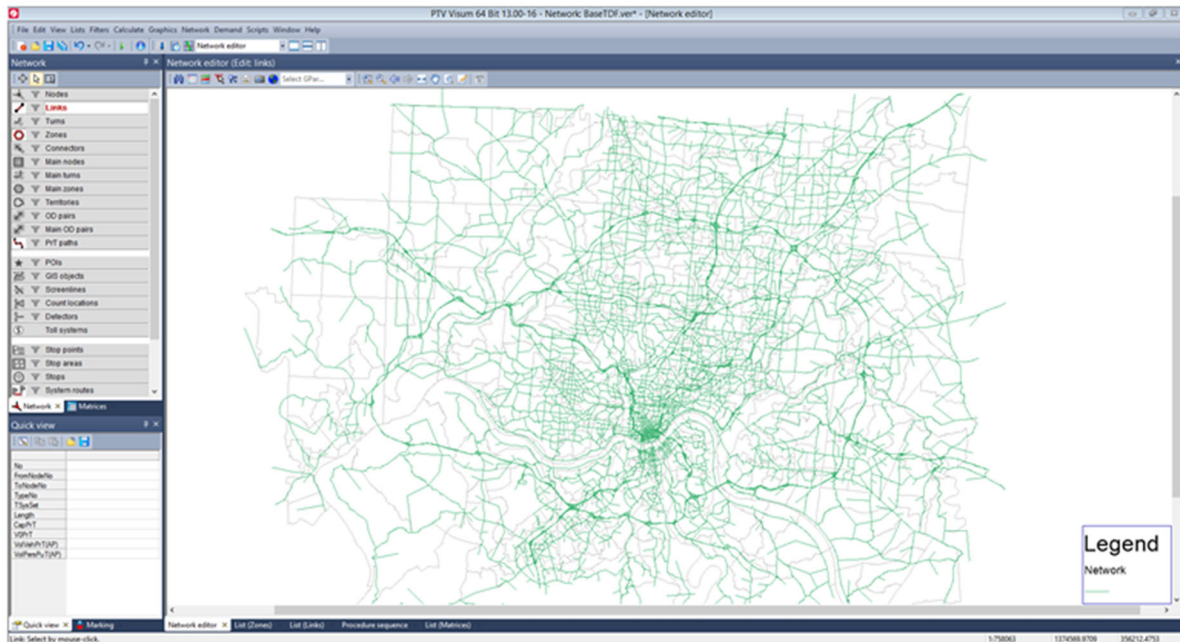


Figure A3- 6 Example of road network from the input function.

Step 8.6: Set up the calculation procedure, and parameters for each step (as shown in Figure A3-8), then stop.

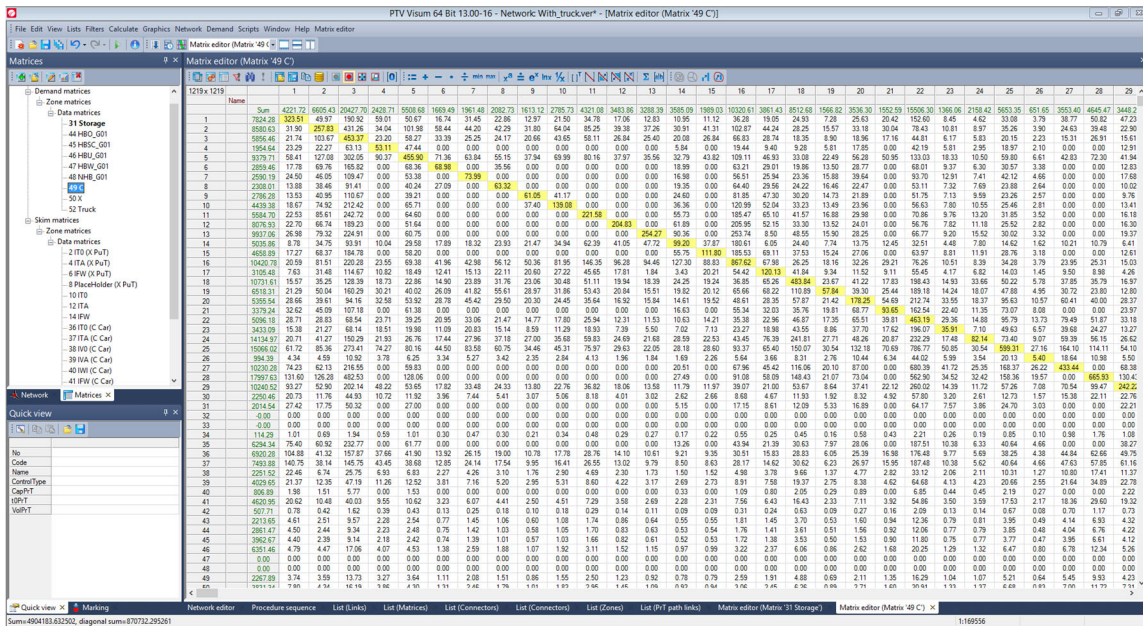


Figure A3- 7 Example of VISUM matrix.

Step 9: Import Household Fraction and Trip Rate (Excel file, as shown in Table A3-2), and Employment Fraction (Excel file, as shown in Table A3-3). Then go to Step 10.

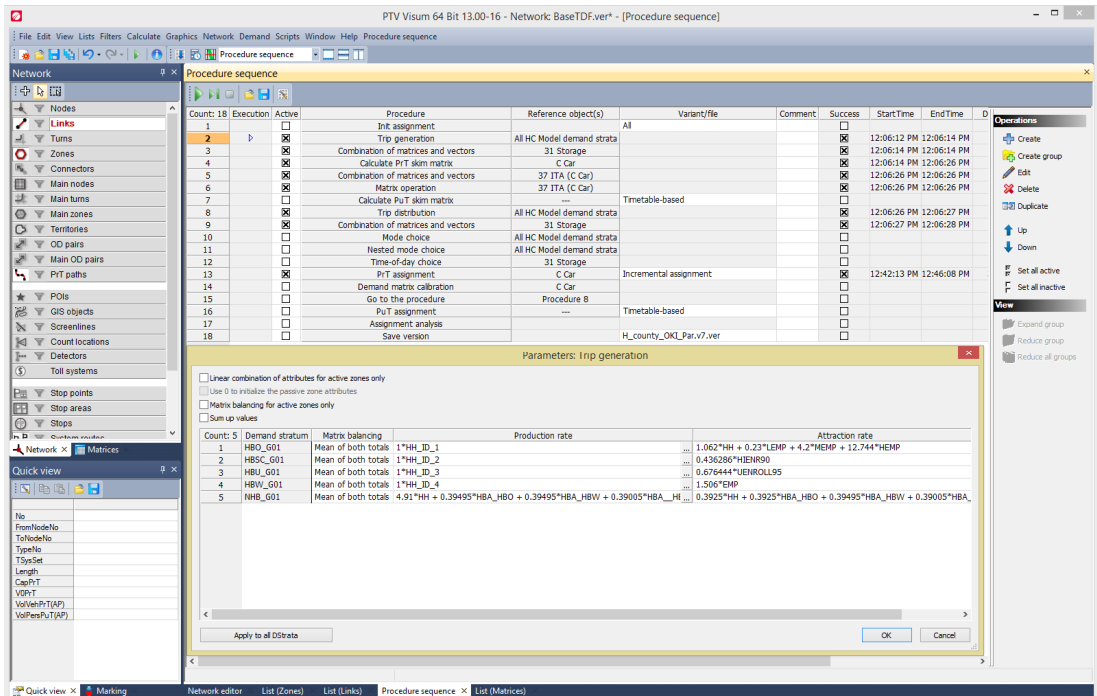


Figure A3- 8 VISUM procedure set up.

Table A3- 2 Sample of Household Fraction and Trip Rate

HH_ID	Fraction	HBO	HBSC	HBU	HBW
47	0.014699	0.0122	0.0122	0.0278	0.8797
48	0.009301	0.0122	0.0122	0.0278	0.8797
49	0.004951	0.0122	0.0122	0.0278	0.8797
50	0.002039	0.0122	0.0122	0.0278	0.8797
51	0.002277	0.0011	0.0011	0.0278	0.8797
52	0.197834	0.0011	0.0011	0.0278	0.8797
53	0.030421	0.0011	0.0011	0.0762	1.2348
54	0.007077	0.0011	0.0011	0.0762	1.2348
55	0.007276	0.0049	0.0049	0.0762	1.2348
56	0.008519	0.0049	0.0049	0.0762	1.2348
57	0.003471	0.0049	0.0049	0.0762	1.2348
58	0.019597	0.0049	0.0049	0.0762	1.2348

Table A3- 3 Sample of Employment Fraction

TAZ	Low Trip Rate Employment	Medium Trip Rate Employment	High Trip Rate Employment
151	0.18	0.55	0.27
162	0	0.94	0.06
163	0.13	0.37	0.5
156	0.06	0.44	0.5
155	0.03	0.67	0.29
161	0.14	0.79	0.07
159	0.36	0.49	0.16
160	0.01	0.86	0.13
165	0.14	0.5	0.37
164	0.05	0.42	0.53
168	0.15	0.52	0.34
170	0.04	0.66	0.3
171	0.06	0.74	0.2

Step 10: Run VISUM model, and go to Step 11 when VISUM model is finished. TDF outputs contain VISUM from four-step model, which can be viewed in VISUM (shown as

Figure A3-9), and vehicle composition (Excel file, as shown as Table A3-4), which will be used as an input for emission estimation.

Table A3- 4 Sample of Vehicle Composition

LinkID	Car Fraction
3	0.82
4	0.96
6	0.85
8	0.94
10	0.93
12	0.98
14	0.87
16	0.99

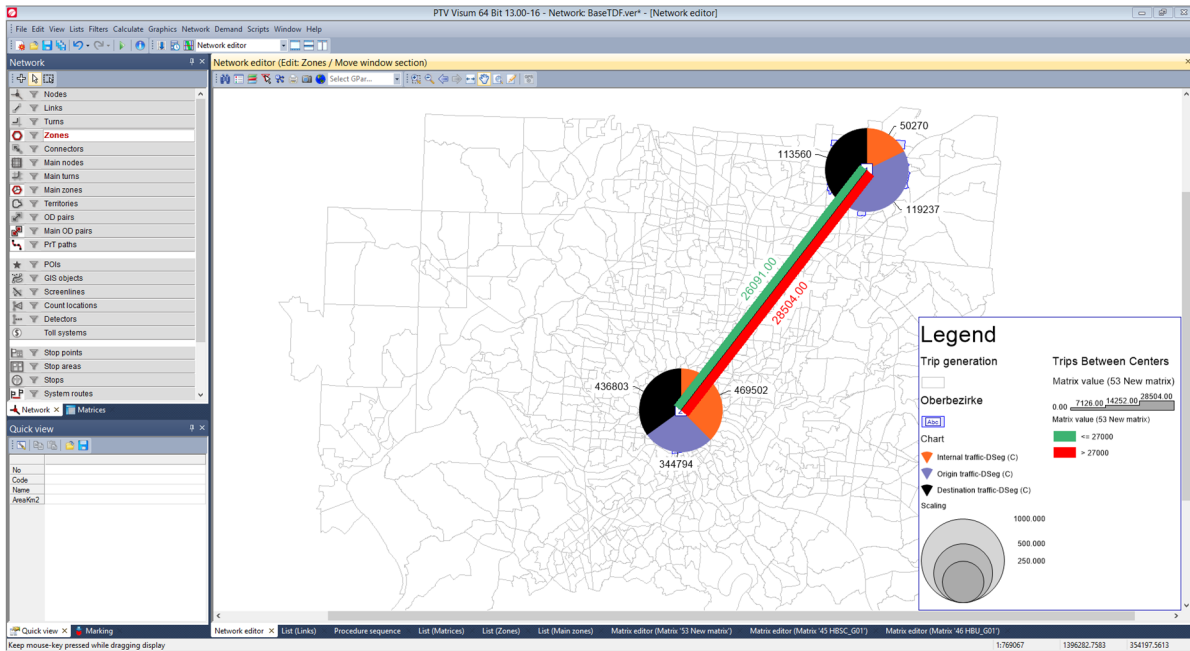


Figure A3- 9 Example of trip distribution result from VISUM (Trips between two centers).

Step 11: Select the **Emission Estimation Model**. In current version of the AIR-SUSTAIN, only MOVES is currently available. Go to step 12.

Step 12: Import MOVES Inputs including *Age Distribution* (Excel file), *Fuel Formulation* (Excel file), *Fuel Supply* (Excel file), *Meteorology* (Excel file), and *State and County* (Excel file). Samples of those files are shown in Tables A3-5 through A3-9. Then go to step 13.

Table A3- 5 Sample of Age Distribution

sourceTypeID	yearID	ageID	ageFraction
21	2000	0	0.0798
21	2000	1	0.0847
21	2000	2	0.0749
21	2000	3	0.0799
21	2000	4	0.0735
21	2000	5	0.0754

Table A3- 6 Sample of Fuel Formulation

fuelFormulationID	fuelSubtypeID	RVP	sulfurLevel	ETOHVolume	MTBEVolume	ETBEVolume	TAMEVolume	aromaticContent	olefinContent	benzeneContent	e200	e300	volToWtPBioDieselEsterVolume	CetaneIndex	PAHContent	T50	T90
10	10	0	0	0	0	0	0	0	0	0	0	0	0	0	0	0	219.345
97	10	6.6	150	0	11.7581	0	0	24	11	0.8	52	84	0	0	0	0	219.345
4979	10	6.7	22.71	0	11.7581	0	0	33.17	6.47	1.36	40.1	81.11	0	0	0	0	219.345
4980	10	6.7	22.71	0	11.7581	0	0	33.17	6.47	1.36	40.1	81.11	0	0	0	0	219.345
6807	10	6.7	22.71	0	0	0	0	33.17	6.47	1.36	40.1	81.11	0	0	0	0	219.345
6808	10	6.7	22.71	0	0	0	0	33.17	6.47	1.36	40.1	81.11	0	0	0	0	219.345
6879	10	6.7	50.71	0	0	0	0	21.56	8	0.71	40.42	85.08	0	0	0	0	219.345
4532	10	6.7	76.305	0	1.42319	0	0	32.085	7.635	1.08	39.8	80.705	0	0	0	0	219.345
6637	10	6.7	76.305	0	0	0	0	32.085	7.635	1.08	39.8	80.705	0	0	0	0	219.345
5022	10	6.7	92.29	0	0.609	0	0	25.43	12.51	1.04	45.21	80.89	0	0	0	0	219.345
5043	10	6.7	92.29	0	0.6885	0	0	24.91	12.54	1.04	46.25	80.95	0	0	0	0	219.345
6157	10	6.7	92.29	0	0	0	0.609	25.43	12.51	1.04	45.21	80.89	0	0	0	0	219.345
6170	10	6.7	92.29	0	0	0	0.6885	24.91	12.54	1.04	46.25	80.95	0	0	0	0	219.345
6819	10	6.7	92.29	0	0	0	0	25.43	12.51	1.04	45.21	80.89	0	0	0	0	219.345
4988	10	6.7	106.26	0	0.3314	0	0	25	11.18	1.25	49.87	82	0	0	0	0	219.345
6131	10	6.7	106.26	0	0	0	0.3314	25	11.18	1.25	49.87	82	0	0	0	0	219.345
4298	10	6.7	129.9	0	0.8	0	0	31	8.8	0.8	39.5	80.3	0	0	0	0	219.345
4537	10	6.7	131.505	0	2.64926	0	0	32.335	8.585	1.18	41.25	79.955	0	0	0	0	219.345
6642	10	6.7	131.505	0	0	0	0	32.335	8.585	1.18	41.25	79.955	0	0	0	0	219.345
4533	10	6.7	137.655	0	1.16693	0	0	31.035	8.335	1.08	42	80.855	0	0	0	0	219.345
6638	10	6.7	137.655	0	0	0	0	31.035	8.335	1.08	42	80.855	0	0	0	0	219.345
4538	10	6.7	142.41	0	2.11612	0	0	31.385	8.585	1.18	42.9	80.455	0	0	0	0	219.345
6643	10	6.7	142.41	0	0	0	0	31.385	8.585	1.18	42.9	80.455	0	0	0	0	219.345
6814	10	6.7	143.2	0	0	0	0	30.7	7.86	1.54	37.59	81.65	0	0	0	0	219.345
4685	10	6.7	165.945	0	1.46265	0	0	28.205	11.62	1.02	44.275	79.875	0	0	0	0	219.345
6669	10	6.7	165.945	0	0	0	0	28.205	11.62	1.02	44.275	79.875	0	0	0	0	219.345
4686	10	6.7	176.765	0	1.18842	0	0	27.255	11.62	1.02	45.975	80.375	0	0	0	0	219.345
6670	10	6.7	176.765	0	0	0	0	27.255	11.62	1.02	45.975	80.375	0	0	0	0	219.345

Table A3- 7 Sample of Fuel Supply

countyID	fuelYearID	monthGroupID	fuelFormulationID	marketShare	marketShareCV
39061	2010	7	9309	1	0
39061	2010	7	20011	1	0

Table A3- 8 Sample of Meteorology

monthID	zoneID	hourID	temperature	relHumidity
7	390610	10	63.93	41.42

Table A3- 9 Sample of State and County

State Name	County Name
Ohio	Hamilton

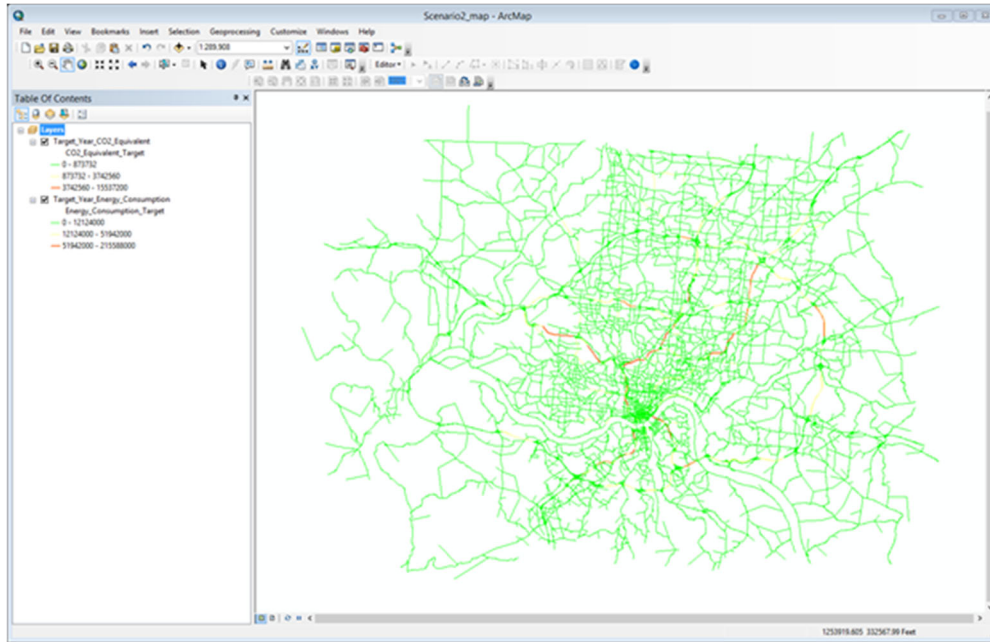


Figure A3- 10 Emission results displayed in ArcGIS.

Step 13: Run MOVES model. Sample result is shown by Figure A3-10. Then go to Step 14.

Step 14: Set up criteria in **Congestion Identification** window (Figure A3-11), and identify the traffic congestion links by clicking **OK** button (as shown in Figure A3-12). Then go to Step 15.

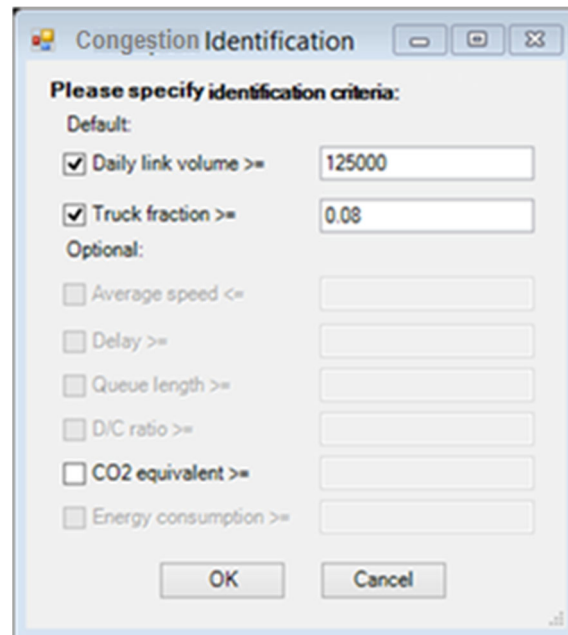


Figure A3- 11 Traffic congestion identification criteria.



Congestion Identification

Please specify identification criteria:

Default:

Daily link volume >= 125000

Truck fraction >= 0.08

Optional:

Average speed <=

Delay >=

Queue length >=

D/C ratio >=

CO2 equivalent >=

Energy consumption >=

OK Cancel

Table

OBJECTID*	SHAPE*	NO	Volume	AverageSpeed	TruckFraction	DCRatio	SHAPE_Lengt
1	Polyline	6190	6613.065336	21.666544	0.082362	55.421996	584.8454
2	Polyline	12568	5694.536464	4.247707	0.085382	99.993349	413.9795
3	Polyline	12578	7051.641836	14.745076	0.097149	61.911736	316.5427
4	Polyline	12632	5910.290554	22.365695	0.091775	49.532265	202.853
5	Polyline	15860	5723.305925	28.253189	0.096532	47.965667	229.7245
6	Polyline	15906	6051.852567	30.80606	0.086595	26.25436	892.1079
7	Polyline	19650	5759.179056	33.982767	0.095744	45.670909	288.272
8	Polyline	23066	5627.114562	30.65859	0.092726	24.411747	1336.4465
9	Polyline	23408	5632.664272	30.977052	0.094315	24.435823	1307.7070
10	Polyline	23520	6457.288842	31.087014	0.099809	57.562397	399.2847
11	Polyline	23596	5500.225387	32.487259	0.081338	52.736179	586.8995
12	Polyline	23724	7927.141442	29.281509	0.080835	64.974474	1290.4146
13	Polyline	23734	5729.889945	31.815601	0.090088	53.894317	1188.7027
14	Polyline	23736	7129.445341	30.315752	0.084971	60.951904	1186.9082
15	Polyline	23762	7787.826582	4.436247	0.085321	55.632094	474.9223
16	Polyline	23768	7986.814954	13.694902	0.08276	56.414805	260.677
17	Polyline	23850	6110.1436	2.463224	0.088107	57.048753	192.8143
18	Polyline	23870	8659.022653	4.427862	0.098172	61.297384	408.1452
19	Polyline	23876	7104.868745	4.534304	0.087319	63.813635	166.1722
20	Polyline	23948	5754.386566	30.868578	0.092294	56.436001	655.3863
21	Polyline	23978	9853.885295	3.974603	0.099077	74.690533	2017.9174

(0 out of 23 Selected)

Figure A3- 12 Identified traffic congestion links in simulation.

Step 15: Based on Congestion Identification results, select study road links and apply TCMs in the microscopic simulation model (note: this step is processed in the VISSIM model).

Step 15.1: Select the traffic links (an example is shown in Table A3-10) from the identified congestion areas (see Figure 3-12). Go to Step 15.2.

Table A3- 10 Sample of Selected Traffic congestion Links for Corridor Level Impact Analysis

LinkNO	Length (Mile)	Car Volume	Truck Volume
23540	0.477	5055	457
23523	0.385	5489	497
26830	0.316	5489	497
23876	0.991	6125	554
17830	0.193	435	39
16938	0.341	636	58



Figure A3- 13 VISSIM links over the base map.

Step 15.2: Load a base map to the VISSIM model. Then the VISSIM links are drawn on top of the base map. In this example, ramp metering is selected as a traffic control measure with the purpose of analyzing its impact on traffic congestion area and associated emissions. Selected traffic congestion road network is built up in the VISSIM environment as shown in Figure A3-13 (where the base map with VISSIM links is superimposed). Figure A3-14 shows the sketch of the congestion area

to be divided into six segments for scenario comparison. The segment in the red box is the study area, and red dash line illustrates the locations of data collection points for model calibration and validation.

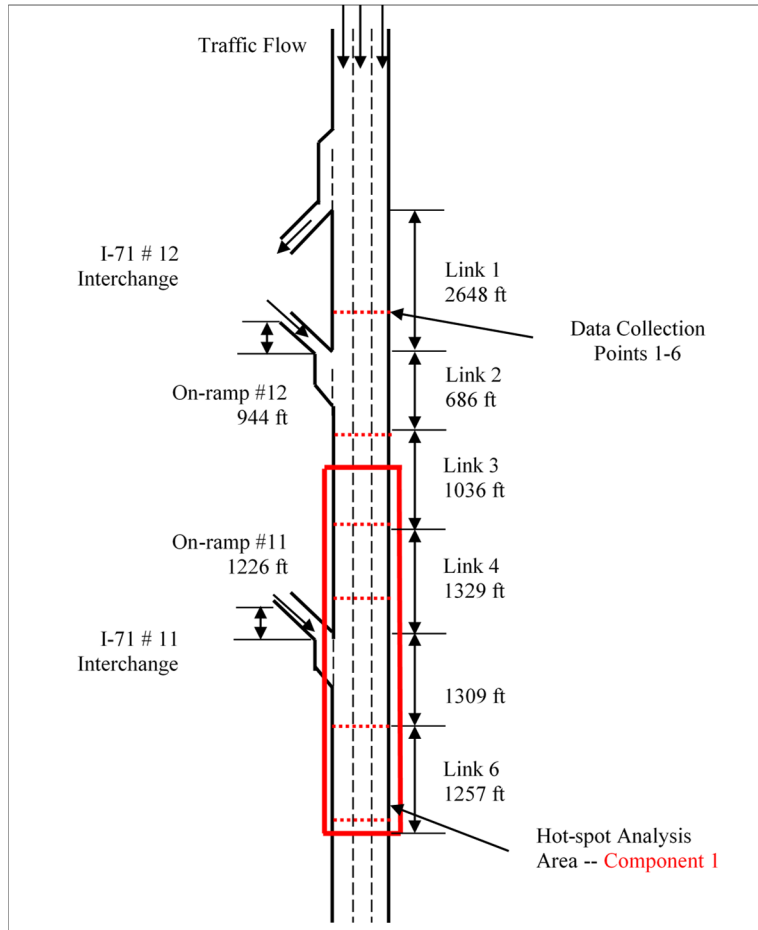


Figure A3- 14 Schematic for traffic congestion microscopic analysis.

Step 15.3: Prepare real vehicle volume input and truck percentage for microscopic simulation analysis. Table A3-11 shows a sample of the traffic volume and truck percentage for all links in the traffic congestion analysis corridor. Then go to Step 15.4.

Step 15.4: Set up the *Desired Speed Distribution*. They are used to model the changes of traffic flow speed within VISSIM network. The desired speed changes are determined based on the study site specifications and speed limits. An example is shown by Figure A3-15. Then go to Step 15.5.

Table A3- 11 Vehicle Volume

Link Number in VISSIM	Peak Hour Traffic Volume	Truck Percentage
1	4791	8%
2	5344	8%
3	5344	8%
4	5344	8%
5	6130	8%
6	6130	8%
On-ramp #12	553	8%
On-ramp #11	782	8%

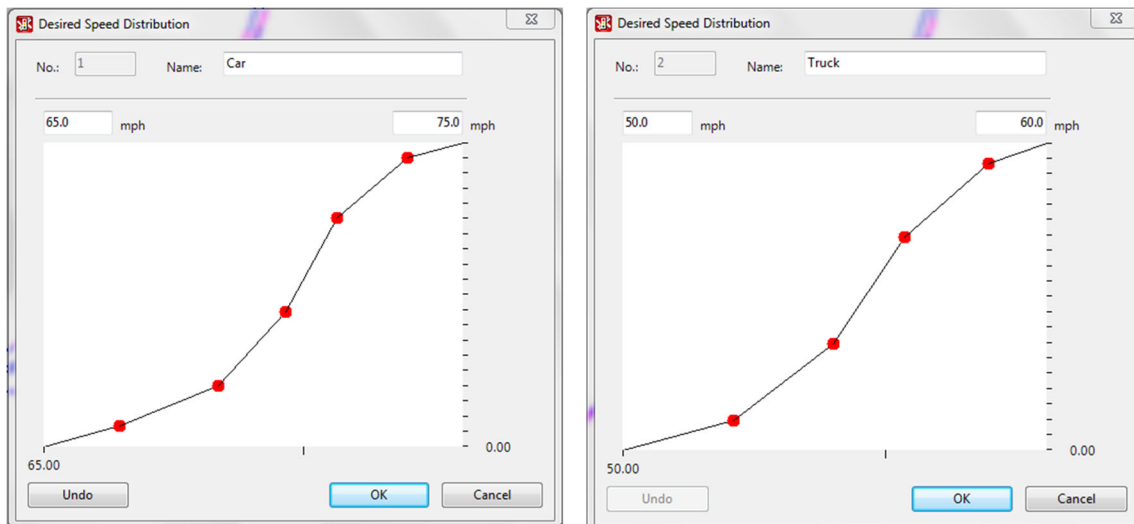


Figure A3- 15 An example of desired speed distribution for cars and trucks.

Step 15.5: Specify vehicle type, class, and category. Example is shown in Table A3-12. Then go to Step 15.6.

Table A3- 12 Vehicle Type Class and Category

No.	Name	Width (m)	Relative Flow	Desired Speed Range (mph)
100	Car	1.5	0.917	65, 75
200	HGV	2.5	0.083	50, 60

Step 15.6: Specify driving behavior. Car following and lane change are two main aspects of driving behavior. Tables A3-13 and A3-14 illustrate the car following and lane change parameters respectively in the VISSIM model for highway. Then go to Step 15.7.

Table A3- 13 Car Following Behavior Parameters

Parameters		Value	Unit
CC0	Standstill Distance	4.99	ft
CC1	Headway Time	0.91	s
CC2	'Following' Variation	13.12	ft
CC3	Threshold for Entering 'Following'	-8	-
CC4	Negative 'Following' Threshold	-0.35	-
CC5	Positive 'Following' Threshold	0.35	-
CC6	Speed Dependency of Oscillation	11.44	-
CC7	Oscillation Acceleration	0.82	ft/s ²
CC8	Standstill Acceleration	11.48	ft/s ²
CC9	Acceleration at 50 mph	4.92	ft/s ²

Table A3- 14 Lane Change Parameters

General Behavior	Freeway		Unit
	Free Lane Selection	Trailing Vehicle	
Maximum deceleration	-4	-3	ft/s ²
-1 ft/s ² per distance	200	200	ft
Accepted deceleration	-1	-0.5	ft/s ²
Waiting time before diffusion	N/A	60	s
Min. headway (front/rear)	N/A	0.5	ft

To slower lane if collision time above	N/A	0	s
Safety distance reduction factor	N/A	0.6	N/A
Maximum deceleration for cooperative braking	N/A	-3	ft/s ²
Overtake reduced speed areas	N/A	Leave box unchecked	N/A

Step 15.7: Set up the signal control at the metered ramps. Table A3-15 is the design criteria for metering rate and signal cycle of Federal Highway Administration. An example of fixed time signal is shown in Table A3-16 as the type of ramp metering for on-ramps. Then go to Step 15.8.

Table A3- 15 Ramp metering design criteria of the Federal Highway Administration

Flow Control Scheme	No. of Lanes	Cycle Length	Approximate Range of Metering Rates (veh/h)
One vehicle Per Green	1	4–4.5 sec.	240–900
Three Vehicles Per Green (Bulk)	1	6–6.5 sec.	240–1200
Dual-lane	2	6–6.5 sec.	400–1700

Table A3- 16 Signal Control Parameters

Signal Group	Type	Cycle (s)	Green Time (s)	Metering Rate
1	Fixed time	4	2	240–900

Step 15.8: Calibrate and validate microscopic model (more details are provided in Section 3.3.5). Table A3-17 shows an example of VISSIM calibration results, and Table A3-18 shows an example of validation results. Then go to Step 15.9.

Table A3- 17 VISSIM Calibration Final Parameter Values

Parameters		Value	Unit
CC0	Standstill Distance	4.99	ft
CC1	Headway Time	0.91	s
CC2	'Following' Variation	13.12	ft

CC3	Threshold for Entering 'Following'	-8	-
CC4	Negative 'Following' Threshold	-0.35	-
CC5	Positive 'Following' Threshold	0.35	-
CC6	Speed Dependency of Oscillation	11.44	-
CC7	Oscillation Acceleration	0.82	ft/s ²
CC8	Standstill Acceleration	11.48	ft/s ²
CC9	Acceleration at 50 mph	4.92	ft/s ²

Table A3- 18 VISSIM Validation Results

Traffic Volume					
LinkID	Real volume	Simulated volume	Difference	Criteria (Oregon)	Result
1	4791	4832	0.35	GEH<5	pass
2	5344	5431	1.40	GEH<5	pass
3	5344	5423	1.16	GEH<5	pass
4	5344	5425	1.22	GEH<5	pass
5	6130	6157	0.12	GEH<5	pass
6	6130	6154	0.09	GEH<5	pass
Travel Time					
Range	Real travel time (s)	Simulated travel time (s)	Difference	Criteria (<10%)	Result
Link 1-6	124.5	130	5.5	12.45	pass
Spot Speed					
Data collectionID	Real speed (mph)	Simulated speed (mph)	Difference	Criteria (10%real speed)	Result
1	59.08	64	4.92	5.908	pass
2	58	60.2	2.2	5.8	pass
3	58.73	63.1	4.37	5.873	pass
4	61.2	63.4	2.2	6.12	pass
5	56.08	56.6	0.52	5.608	pass
6	60.64	62.9	2.26	6.064	pass

Step 15.9: After using real site traffic volume, spot speed and travel time to calibration and validation the model, *Traffic Volume* and *truck percentage* (8.0% for all links) from the regional-level results of VISUM for each link are applied for two project-level analysis scenarios:

- Scenario 1 without any traffic control measure
- Scenario 2 with 4-sec cycle length ramp metering

Then, run VISSIM and export VISSIM outputs. Then go to Step 16.

Step 16: Import *Microscopic Simulation Link ID* in sheets 1 and 2 (Excel file; an example is shown in Tables A3-19 and A3-2, which are constructed in microscopic simulation software like VISSIM. The VISSIM model simulates traffic for one hour and finally produces second-by-second vehicle speed, queue length, and delay (as shown in Tables A3-21 and A3-22). Load *Microscopic Simulation Results* in sheets 1 and 2 (Excel file; examples are shown in Tables A3-21 and A3-22) under different scenarios, separately. Compare those imported results, and then go to step 17.

Table A3- 19 Microscopic Simulation Link ID (Sheet1)

GISLinkID	VissimLinkID
23540	1
23523	2
23523	3
26830	4
23876	5
23876	6
17830	12
16938	11

Table A3- 20 Microscopic Simulation Link ID (Sheet2)

GISLinkID	RoadType	LinkLength	LinkGrade
23540	4	0.477	0
23523	4	0.385	0
26830	4	0.316	0
23876	4	0.991	0
17830	4	0.193	0
16938	4	0.341	0

Table A3- 21 Microscopic Simulation Results (Sheet1)

VissimLinkID	Time (sim sec)	Car #	Car v (m/s)	Car a (m/s ²)	Truck #	Truck v (m/s)	Truck a (m/s ²)
1	1	0	0	0	0	0	0
2	1	1	22.6	0	0	0	0
3	1	0	0	0	0	0	0
4	1	0	0	0	0	0	0
5	1	3	29.7	-0.2	0	0	0
6	1	3	30.5	0.1	0	0	0
7	1	3	30	0	0	0	0
8	1	0	0	0	1	27.2	0.8
1	2	2	26.3	1.5	1	25.4	0
2	2	2	29	0	0	0	0
3	2	0	0	0	0	0	0
4	2	0	0	0	0	0	0
5	2	1	32.6	0	0	0	0
6	2	0	0	0	0	0	0
7	2	0	0	0	0	0	0
8	2	3	29.7	-0.2	0	0	0
1	3	3	30.5	0.1	0	0	0
2	3	3	30	0	0	0	0
3	3	0	0	0	0	0	0

Table A3- 22 Microscopic Simulation Results (Sheet2)

Link	Scenario 1			Scenario 2		
	Average Speed (mph)	Delay (s/veh)	Average Queue Length (vehs)	Average Speed (mph)	Delay (s/veh)	Average Queue Length (vehs)
1	63.72	1.8	0	63.79	1.7	0
2	59.21	1.5	0	60.07	1.4	0
3	59.41	3.2	3	59.61	2	0
4	46.01	13.6	31	59.65	2.5	2

Link	Scenario 1			Scenario 2		
	Average Speed (mph)	Delay (s/veh)	Average Queue Length (vehs)	Average Speed (mph)	Delay (s/veh)	Average Queue Length (vehs)
5	46.93	11.7	28	56.21	3.3	3
6	56.92	2.2	0	57.03	2.2	0
12	46.28	0.6	0	46.38	0.6	0
11	49.92	0.4	0	17.17	5.1	8

Note: veh(s) - vehicle(s)

Step 17: Select the **Emission Estimation Model** (only MOVES is currently available in the current version of AIR-SUSTAIN and will be added with more options in the future), then run MOVES (an example is shown in Table A3-23). After it is finished, go to Step 18.

Table A3- 23 An Example of Traffic Congestion Link Emissions by Different Scenarios

LinkID	S1_CO2 (kg)	S1_Energy (kJ)	S2_CO2 (kg)	S2_Energy (kJ)
23532	1406.47	19,409,200	1406.46	19,409,190
23540	1073.49	14,812,350	1056.59	14,579,600
23876	944.21	13,029,600	811.57	11,198,300
26830	1933.76	26681,300	1778.17	24,535,100
17830	31.95	441,704	31.92	440,866
16938	58.43	808,036	80.97	1,120,090

Note: S1 represents Scenario 1, and S2 represents Scenario 2.

Step 18: Update regional emission results by project level analysis emission results. The specification of variables and parameters in the program is shown in Table A3-24. If both target year and base year have been analyzed, then go to step 19; else go back to Step 2.

Step 19: Compare results between base year and target year. Then stop.

Table A3- 24 Variable and parameter coding type in AIR-SUSTAIN program

Name	Field		Description	Type
	TAZ		TAZ name, the format is TAZ_TAZ Number, i.e. TAZ_151	String
	TAZ_N		TAZ number	Integer
	TAZ_Order		The field to link TAZs in ArcGIS and TAZs in VISUM	Integer
	POP		Target year population	Integer
	HH		Target year household	Integer
	EMP		Target year employment	Integer
	HI		Target year high school enrollment	Integer
	UN		Target year university enrollment	Integer
	AREA_TYPE		1=CBD&Urban; 2= suburban; 3= rural	Integer
	GEOCODE_Base_1		Base year residential area (ft ²)	Double
	GEOCODE_Base_2		Base year employment area (ft ²)	Double
	GEOCODE_Base_3		Base year institutional area (ft ²)	Double
	GEOCODE_Base_4		Base year undeveloped area (ft ²)	Double
	GEOCODE_Base_5		Base year other area (ft ²)	Double
	GEOCODE_1		Target year residential area (ft ²)	Double
	GEOCODE_2		Target year employment area (ft ²)	Double

	GEOCODE_3		Target year institutional area (ft ²)	Double
	GEOCODE_4		Target year undeveloped area (ft ²)	Double
	GEOCODE_5		Target year other area (ft ²)	Double
Landuse_Target	GEOCODE		Land use type, 1=residential, 2=employment, 3=institutional, 4=undeveloped, 5=other	Integer
	Shape_Area		Area (ft ²)	Double
RoadNetwork	CO2_Equivalent_Updated		CO2 equivalent (kg)	Double
	Energy_Consumption_Updated		Energy consumption (kJ)	Double

Appendix B

Water Treatment Plant-Climate Change Adaption Model (WTP- CAM) User's Manual

Table of Contents

List of Tables	251
List of Figures.....	252
List of Abbreviations and Notations	253
B1.0 Program Overview.....	255
B1.1 WTP-CAM Setup	255
B1.2 WTP-CAM Workspace.....	256
B1.2.1 Main Menu Bar.....	256
B1.2.2 Tool Bars	258
B1.2.3 Status Bar	261
B1.2.4 Cursor Menu.....	261
B1.2.5 Processing Train Window	261
B.1.2.6 Property Editor	261
B1.3 Setting up a Processing Train	262
B1.3.1 Building a Physical Processing Train.....	262
B1.3.2 Editing Non-physical Settings.....	262
B1.4 Saving and Opening Projects	263
B1.5 Running WTP-CAM.....	263
B2.0 Understanding the Input Data.....	264
B.2.1. Introduction to the Example Processing Train	264
B 2.2. Inputs for Monte Carlo Simulation	264
B 2.2.1 Overview	264
B 2.2.2 Inputs for Monte Carlo Setting.....	268
B2.3 Customization of GAC Unit Process Model.....	272
B2.3.1 Overview	272
B2.3.2 Inputs for GAC Model Customization	273
B3.0 Understanding the Output Data	274
B3.1 Standard Output Tables for a One-time Run	274
B3.2 Tabular Outputs for Monte Carlo Simulation.....	280
B3.2.1 Samples/statistics of Raw Water Qualities	280
B3.2.2 Samples/Statistics of Effluent Water Quality.....	280
B3.2.3 Samples/Statistics of Adaptation Costs	281
B3.2.4 Samples/Statistics for Compliance/Non-compliance Realizations.....	282
B3.2.5 Running Log	282
B3.3.Graphic Outputs for Monte Carlo Simulation.....	283
B3.3.1. Sample Chart (to be developed)	283
B3.3.2. Frequency Chart (to be developed)	283
B3.3.3. Cumulative Frequency Chart (To be developed)	283
B4.0 Models and Algorithms in WTP-CAM.....	284

B4.1 Monte Carlo Methods	284
B4.1.1 Seasonal Multivariate Analysis.....	284
B4.1.2 Simulation of quarterly running average (TOC compliance).	287
B4.1.3 Adaptation of Unit Process	288
B4.2 Customization of Unit Process.....	289
B4.2.1 Customization of GAC Unit Process	292
B4.3 Economics.....	292
B4.3.1 Adaptation Costs for GAC Processing	292
B5.0 References.....	294
Attachment A: Confirmation Tests.....	296
A-1 Seasonal multivariate analysis.....	296
A-2 Customization of GAC model.....	298
Attachment B: Error and Warning Messages.....	303

List of Tables

Table B1- 1 List of Standard Toolbars	259
Table B1- 2 List of Unit Process Toolbars	260
Table B2- 1 Options for Monte Carlo Analysis.....	269
Table B4- 1 Illustration of calculating running annual average for finished water TOC	288
Table B4- 2 GAC Contactor Cost.....	293
Table B4- 3 GAC Reactivation Cost	293
Table A- 1 Comparison of the mean and standard deviation in summer.....	297
Table A- 2 Comparison of cross correlation matrix in summer	297
Table A- 3 Comparison of the mean and standard deviation in winter	298
Table A- 4 Comparison of cross correlation matrix in winter	298
Table A- 5 Parameters estimated for TOC breakthrough model	299
Table A- 6 Summary of field data sets and estimated parameters.....	301
Table A- 7 Comparison of sum of least square for customized GAC models.....	301
Table B- 1 Error message (to be developed)	303
Table B- 2 Warning message (to be developed).....	303

List of Figures

Figure B1- 1 WTP-CAM workspace.	256
Figure B1- 2 Three edit functions for unit process menu.	261
Figure B1- 3 The property editor.	261
Figure B1- 4 Setting dialogue box for Monte Carlo analysis.	263
Figure B2- 1 Schematic diagram TWP-CAM program flow in the example simulation.	265
Figure B2- 2 Schematic diagram for treatment unit process at the GCWW Richard Miller Treatment Plant.	265
Figure B2- 3 Original input data for the GCWW example processing train.	266
Figure B2- 4 Illustration diagram for Monte Carlo analysis.	267
Figure B2- 5 Monte Carlo inputs for the example processing train.	269
Figure B2- 6 Manual input window for influent water quality statistics.	270
Figure B2- 7 Dialogue window for name of data files.	271
Figure B2- 8 Example format of influent water quality data file.	271
Figure B2- 9 GAC unit process property window.	272
Figure B2- 10 Dialogue window for TOC breakthrough customization.	273
Figure B2- 11 Example format for TOC breakthrough data file.	273
Figure B3- 1 Standard output “Table 1” for the example processing train.	274
Figure B3- 2 Standard output “Table 2” for the example processing train.	275
Figure B3- 3 Standard output “Table 3” for the example processing train.	276
Figure B3- 4 Standard output “Table 4” for the example processing train.	276
Figure B3- 5 Standard output “Table 5” for the example processing train.	277
Figure B3- 6 Standard output “Table 6” for the example processing train.	277
Figure B3- 7 Standard output “Table 7” for the example processing train.	278
Figure B3- 8 Standard output “Table 8” for the example processing train.	278
Figure B3- 9 Standard output “Table 9” for the example processing train.	279
Figure B3- 10 Standard output “Table 10” for the example processing train.	279
Figure B3- 11 Sample outputs of raw water quality.	280
Figure B3- 12 Selected sample outputs of effluent water qualities at finished water.	281
Figure B3- 13 Sample outputs for adaptation costs.	281
Figure B3- 14 Sample outputs of raw water quality and adaptation cost for non-compliance events.	282
Figure B3- 15 Example format of the log file.	282
Figure B3- 16 Example sample chart for raw water TOC.	283
Figure B3- 17 Example frequency chart for raw water TOC.	283
Figure B3- 18 Example cumulative frequency chart for effluent TOC at finished water.	284
Figure B4 -1 Cost curve for annual cost of GAC unit process.	294

Attachments

Figure A- 1 Comparison of GAC models with RSSCT dataset 1.	299
Figure A- 2 Comparison of sum of error square for GAC models.	300
Figure A- 3 Comparison of GAC models with RSSCT dataset 2.	300
Figure A- 4 Validation of GAC model with field data.	302

List of Abbreviations and Notations

Abbreviations

AR(1)	autoregressive model of order one
Cl ₂	chlorine
CAM	climate change adaptation model
DBP	disinfection by-products
GAC	granular activated carbon
GCWW	Greater Cincinnati Water Works
HAAs	haloacetic acids (nine individual species and the total of five (HAA ₅), six (HAA ₆) and nine (HAA ₉) species)
ICR	information collection rule
ID	identification
MC	Monte Carlo
NH ₃	ammonia
O&M	operation and maintenance
PPI	Producers Price Index
RSSCT	rapid small-scale column test
TOC	total organic carbon
TTHM	sum of four individual species of trihalomethanes
USEPA	U.S. Environmental Protection Agency
UV	ultraviolet
UVA	ultraviolet absorbance at 254 nm
WTP	water treatment plant

Notations

θ	a vector of parameters to be estimated
θ_0	initial parameter vector
θ_1	corrected parameter vector
v	a variable between 0 and 1
ε_j	a (9×1) vector of standard normal deviates for season j
a	GAC model parameter, [-]
A	the Gauss-Newton coefficient matrix
A_j	(9×9) parameter matrix for season j
b	GAC model parameter, [-]
B_j	(9×9) parameter matrix for season j
c	GAC model parameter
d	GAC model parameter, [1/day]
D	a positive definite matrix, defined by $D = B_j B_j^T$
EBCT	empty bed contact time, [min]
$E[Y]$	mean of random variable Y
$f(t)$	TOC fraction remaining, defined by $f(t) = \frac{TOC_{eff}}{TOC_{in}}$, [-]
m_{x_i}	a mean of variable x_i
${}_j M_0$	a lag-zero covariance matrix of $(X_j - m_j)$ for season j
${}_j M_1$	a lag-one covariance matrix of $(X_j - m_j)$ for season j
n	sample size, [-]
$r_{x_i x_j}$	the lag-zero correlation between x_i and x_j , [-]
$r_{y_i x_j}$	the lag-one correlation between variables y_i and x_j , [-]
R	a right-hand-side vector of Gauss-Newton equation
S_{x_i}	standard deviation of variable x_i
S_{xx}	covariance matrix, defined by $S_{xx} = E[XX^T]$
t	GAC service time, [day]
t_k	field measurement of GAC service time, [day]
TOC_{eff}	effluent TOC concentrations at the GAC unit, [mg/L]
TOC_{in}	influent TOC concentrations at the GAC unit, [mg/L]
USRT	process design or operating variable
x_i'	log-normal distributed variable, defined by, $x_i' = \ln(x_i)$
X	defined by, $X = X_{j-1} - m_{j-1}$
X_j	a (9×1) vector of nine raw water quality parameters for season j
y	the capital, operational or maintenance cost, [US \$]
y_k	a field measurement of TOC fraction remaining, [-]
Y	defined by, $Y = X_j - m_j$
z	a parameter is either 0 or 1 for adjusting cost functions for a range of USRT values, [-]

The Water Treatment Plant-Climate Change Adaptation Model (WTP-CAM) program was developed from the climate adaptation models (CAMs) published in Li et al.(2012; 2014) and Clark et al.(2010). The computer program is developed on the basis of Water Treatment Plant (WTP) model that was proposed originally for the U.S. Environmental Protection Agency (USEPA) in 1992 (USEPA, 2005). WTP software exists in two versions. The Version WTP v2.2 is further improved from original 1992 WTP v.1.0. Appendix C contains a copy of the WTP v2.2 user manual.

This manual is intended to provide guidance to the WTP-CAM user with the new features:

- Utilizing the WTP-CAM program — navigating the user interface.
- Selecting inputs and interpreting outputs related to Monte Carlo analysis and adaptation.
- Understanding the algorithms applied in WTP-CAM relating multivariate analysis, customization of processing units, and cost analysis.

In addition to this introductory Section, this User's Manual contains four other Sections:

- Section 2 explains menu components and describes how to set up and run WTP-CAM.
- Section 3 describes how to input the required data for the new features. A model of a typical treatment plant is developed as an example; data input options are outlined.
- Section 4 provides guidance for interpretation of the output from the WTP-CAM based on the example developed in Section 3.
- Section 5 describes the new algorithms used in the WTP-CAM program.

The user manual also contains two appendices. Appendix A shows confirmation tests to verify the new algorithms introduced in WTP-CAM, including seasonal multivariate analysis, and Granular Activated Carbon (GAC) model customization. Appendix B provides tables of error and warning messages, including error or warning message identification (ID), their meanings, and recommended actions for error correction.

B1.0 Program Overview

B1.1 WTP-CAM Setup

WTP-CAM Version 1.0 is designed as a Windows-based program that can be run under the Windows 7 or newer operating system. It tested successfully on an Intel CPU 1.90 GHz computer with 2 GB memory. The disk space requirement is mainly used to save simulation results; 500 Mb minimal disk space is recommended. The program also allows users to use either free or professional version of the SQL database. The file formats and designations remain the same as those in the folder.

To run and use the WTP-CAM program, the user should set up a single folder in which to place three files:

- *WTP-CAM1.exe* — the main executable file
- *WTP-CAM User Manual* — this support document
- *WQ example input.txt* — a sample input file to illustrate the format of raw water quality parameters

When the executable file has been placed in a single directory, the user needs to double click on the *WTP-CAM.exe* icon to launch the program. To remove WTP-CAM from your computer, delete the file folder.

B1.2 WTP-CAM Workspace

The basic workspace for WTP-CAM consists of the following user interface elements: main Menu Bar, Cursor Menu, Tool Bars, Status Bars, Property Editor, and Processing Train window as shown in Figure B1-1.

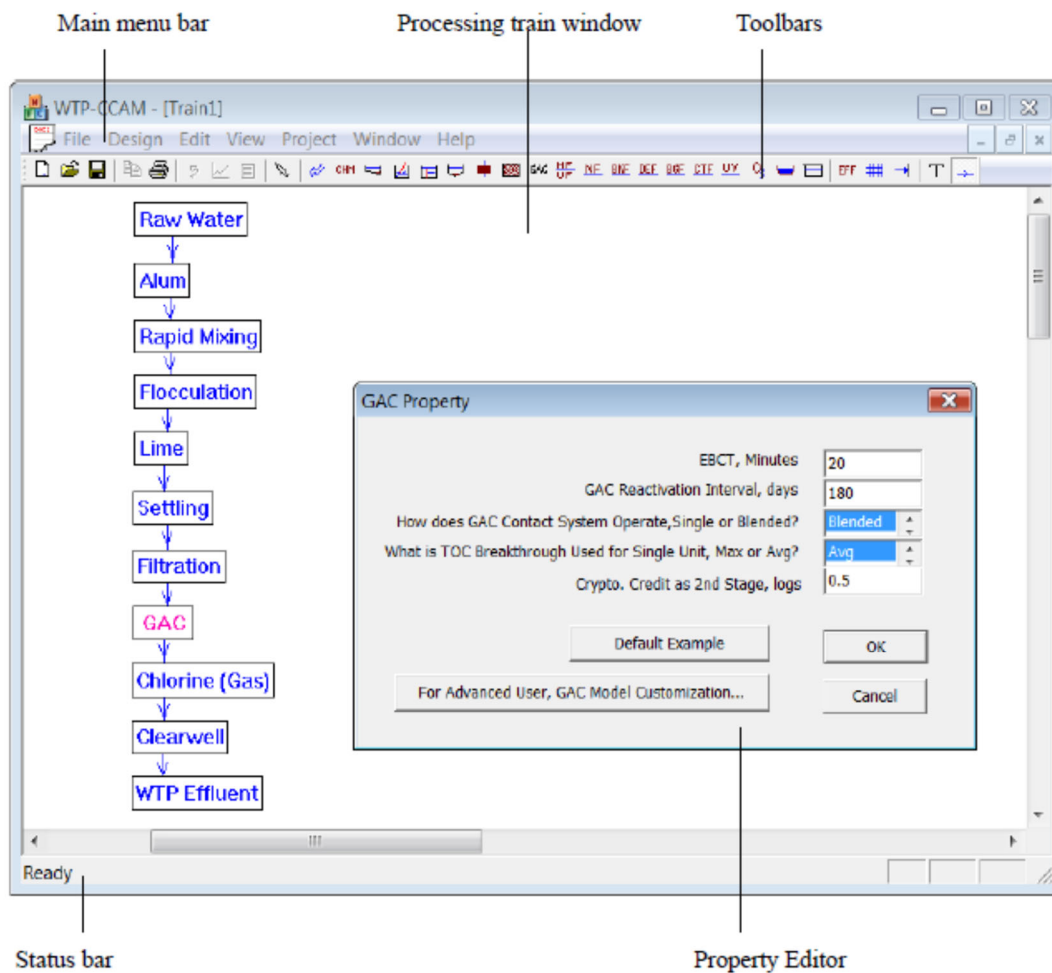


Figure B1- 1 WTP-CAM workspace.

B1.2.1 Main Menu Bar

The Menu Bar located across the top of the WTP-CAM workspace contains a collection of menus used to control the program, including File Menu, Design Menu, Edit Menu, View Menu, Project Menu, Window Menu, and Help Menu.

File Menu: Contains commands for opening and saving data files and for printing.

Command	Description
New	Creates a new WTP project
Open	Opens an existing project
Save	Saves the current project
Save As	Saves the current project under a different name
Print	Prints the current view
Print Preview	Previews a printout of the current view
Print Setup	Sets page margins, headers, and footers for printing
Exit	Exits WTP-CAM

Design Menu: Contains commands to select unit processes, chemical feeds, and sampling points.

Unit Processes	Chemical Feeds	Sampling Points
Raw Water	Alum	WTP Effluent
Pre-settling Basin	Ammonia Sulfate	Average Tap
Rapid Mix	Ammonia	End of System
Flocculation	Carbon Dioxide	
Settling Basin	Chlorine (Gas)	
Filtration	Chlorine Dioxide	
GAC	Iron	
MF/UF	Lime	
Nano-filtration	Ozone	
Slow Sand Filtration	Permanganate	
UV Disinfection	Sodium Hydroxide	
Ozone Chamber	Sodium Hypochlorite	
Contact Tank	Soda Ash	
Reservoir	Sulfur Dioxide	
Bank Filtration	Sulfuric Acid	
DE Filtration		
Bag Filtration		
Cartridge Filtration		

Edit Menu: Contains a control for copying.

Command	Description
Copy To	Copies the currently active view (processing train, graph, or table) to clipboard.

View Menu: Contains controls for the user interface and commands for reporting results in different formats.

Command	Description
Tool Bar	Toggles the tool bars on/off.
Status Bar	Toggles the status bars on/off.
Graph	Creates frequency/cumulative frequency chart of selected parameters.
Table	Creates a tabular display of selected parameters.
Options	Controls the display style of a graph, or table.

Window Menu: Contains commands for displaying open windows.

Command	Description
New Window	Open another window for the active document.
Cascade	Arrange windows so they overlap.
Window List	Lists all open windows; selected window currently with highlight.

Project Menu: Contains commands to define modeling conditions and to set up simulations for the current project being analyzed.

Command	Description
Monte Carlo Setting	Define conditions and inputs for Monte Carlo analysis.
Cost Analysis	Define the conditions for cost analysis.
Optimization Analysis	Define the conditions for unit process optimization analysis.
One Time Run	Simulate water treatment at a defined condition.
Multiple Runs	Make Monte Carlo simulations.

Help Menu: Contains commands for identifying problems and solutions during simulation.

Command	Description
Error Message	Identifies problems and suggested solutions during simulation.
About	Lists information about current version of WTP-CAM.

B1.2.2 Tool Bars

Toolbars provide shortcuts to commonly used operations. These operations are also available at the Main Menu Bar. The toolbars can be docked underneath the Main Menu bar or dragged to any location on the WTP-CAM workspace. The toolbars can be made visible or invisible by selecting *View >> Toolbar*. There are two types of toolbars:

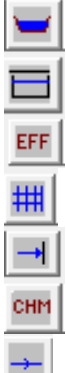
- Standard Toolbars: contain speed buttons for commonly used commands (see Table B1-1).

- Unit Processes Toolbars: contain buttons for working with processing train (see Table B1-2).

Table B1- 1 List of Standard Toolbars

Toolbar Icon	Equivalent command at the main menu bar
	File >> New
	File >> Open
	File >> Save
	File >> Print
	Edit >> Copy to
	Project >> MC Simulation
	View >> Graph
	View >> Table

Table B1- 2 List of Unit Process Toolbars

Toolbar Icon	Equivalent command at the main menu bar
	<p>Design >> Pointer (Deactivate selection)</p> <p>Design >> Raw Water</p> <p>Design >> Presettling Basin</p> <p>Design >> Rapid Mixing</p> <p>Design >> Flocculation</p> <p>Design >> Sedimentation</p> <p>Design >> Filtration</p> <p>Design >> Slow Sand Filter</p> <p>Design >> GAC</p> <p>Design >> Micro/Ultra Filter</p> <p>Design >> Nano-Filter</p> <p>Design >> Bank Filtration</p> <p>Design >> D.E. Filtration</p> <p>Design >> Bag Filtration</p> <p>Design >> Cartridge Filtration</p> <p>Design >> UV Disinfection</p> <p>Design >> Ozone Chamber</p>
Toolbar Icon	Equivalent command at the main menu bar
	<p>Design >> Reservoir</p> <p>Design >> Contact Tank</p> <p>Design >> Effluent</p> <p>Design >> Average Tap</p> <p>Design >> End of System</p> <p>Design >> Chemical Feed</p> <p>Design >> Connection</p>

B1.2.3 Status Bar

The Status Bar appears at the bottom of the WTP-CAM workspace to show information explaining the selected command in the Main Menu Bar or the Tool Bars.

B1.2.4 Cursor Menu

There are two status options for the Cursor Menu in the processing train window. When the mouse cursor does not point to any unit process in the processing train window, right clicking the mouse will show the same Design Menu in the Main Menu Bar (refer to the introduction to the Design Menu in Section B1.2.1). When the mouse cursor points to a unit process in the processing train window, right clicking the mouse leads to a new cursor menu with three commands (Figure B1-2) as following:

- Move – move the selected unit process box to any user desired location in the train window.
- Delete – delete the selected unit process from the processing train.
- Property – show the Property Editor for the selected unit process.



Figure B1- 2 Three edit functions for unit process menu.

B1.2.5 Processing Train Window

The Processing Train Window is the interface for users to build their own water treatment processing train and input parameters for unit processes or Monte Carlo analysis. Section B1.3 describes how to build a processing train in this window.

B.1.2.6 Property Editor

The Property Editor (Figure B1-3) is used to edit the properties of a unit process. It is invoked when a unit process in the Processing Train Window is selected and double-clicked or the property in the Cursor Menu is clicked. Following is an example Property Editor for flocculation.

The following points help explain how to use the Property Editor.

- The Editor usually consists of two columns (one for the property's name and the other for its value), an “OK” button, a “Cancel” button and a “WTP Example” button.
- The property value is initialized with zero or the first element in the dropdown list. Pressing the “WTP Example” button will provide user

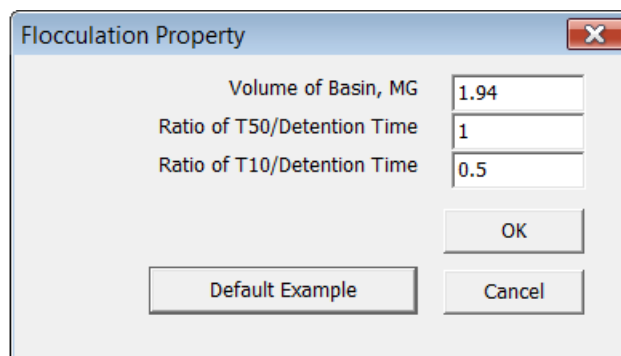


Figure B1-3 The property editor

example values for all properties in this opened Editor.

- Depending on the property, the value field can be entered either by typing in a value for a text edit box or by selecting from a list of choices in a dropdown list box.
- You can use both the mouse and the tab key on the keyboard to move between properties.
- To have WTP-CAM accept what you have entered, press the “OK” button; to cancel, press the “Cancel” button.
- The Editor window can be moved via the normal Windows procedures.

B1.3 Setting up a Processing Train

A processing train includes both physical objects that can appear on the Train Window, and non-physical settings that encompass design and operational information as well as simulation controls. The physical objects include water treatment unit processes, chemicals and connection lines. Non-physical settings cover the properties of unit processes and settings for Monte Carlo simulation, cost analysis, and optimization analysis.

B1.3.1 Building a Physical Processing Train

To add a unit process to a processing train, the first step is to select the object unit process from one of three methods (Design Menu, Cursor Menu or Toolbars), and then move the mouse to a desired location on the Train Window, and click to finalize.

To add a chemical to the train, select the “Chemical” first from either Design Menu/Cursor Menu, or the “Chemical” button in the Toolbars and then move the mouse to a desired location on the Train Window and click. A dialogue box will appear, select the desired chemical from the dropdown list and click “OK” button.

To add a connection line to the train, the first step is to select the “Connection” from either Design Menu/Cursor Menu, or the Connection button in the Toolbars. The second step is to move the mouse to the starting unit process and click; without releasing, continue to move the mouse to the ending unit process and then release.

An object in the processing train can be deleted or moved using the Cursor Menu. To delete or move an object, click on the object first, then click the right mouse key to invoke the Cursor Menu, finally click Delete or Move from the Cursor Menu. For moving an object, move the object to a desired location in the Train Window and click left mouse key to finish the moving action.

B1.3.2 Editing Non-physical Settings

The Property Editor (see Section B1.2.6) is used to edit the properties of objects that can appear in the Train Window. To edit one of these objects, select the object in the processing train, then click the Property in the Cursor Menu or double-click the selected object. The properties of objects usually consist of design and operational parameters for unit processes or chemical feeds. A detailed explanation of such parameters can be found in Chapter C3 of the WTP manual in Appendix C (U.S. EPA, 2005).

Settings for Monte Carlo analysis are illustrated in Figure B1-4, which includes control parameters for computer simulation, data source for raw water quality statistics and cross correlation matrix, and options available for the Monte Carlo simulation. Section 3 provides a detailed explanation of the settings for a Monte Carlo analysis.

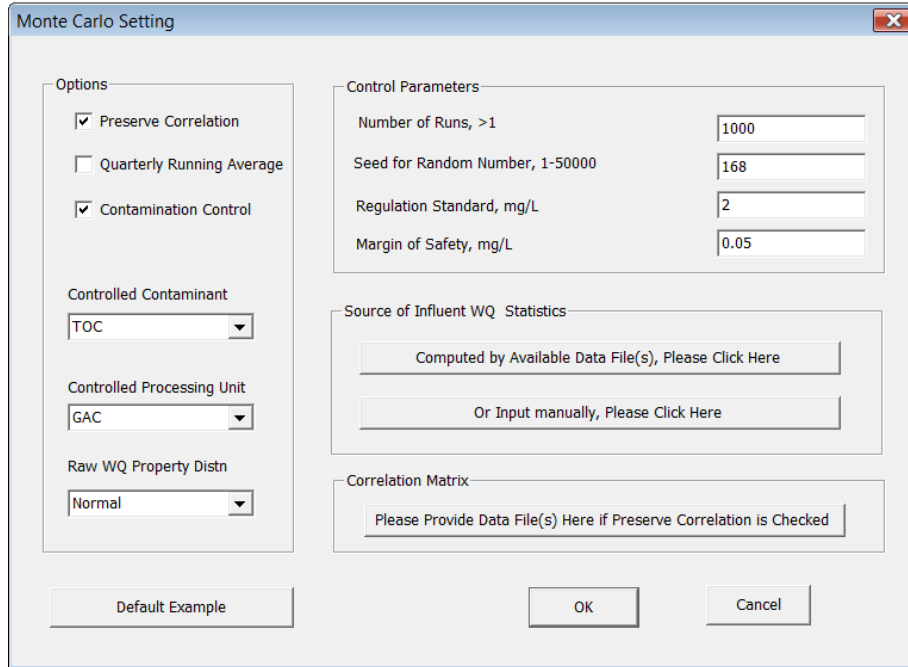


Figure B1-4 Setting dialogue box for Monte Carlo analysis.

B1.4 Saving and Opening Projects

Having completed the initial design and sequence of a processing train, it is a good idea to save the project to a file.

- From the File menu, select the Save As option.
- In the Save As dialog that appears, select a folder and file name under which to save this project. An extension of .wtp will be added to the file name.
- Click OK to save the project to file.

To open the project at some later time, select the Open command from the File menu.

B1.5 Running WTP-CAM

The WTP-CAM is designed to run under two modes:

- Single Case Run: make one-time run of the WTP analysis based on the deterministic influent water quality entered from the Property Editor of Raw Water without use of Monte Carlo setting.
- Monte Carlo Simulation: make multiple runs of the WTP analysis based on stochastic influent water quality simulated with Monte Carlo setting.

When design of a processing train is complete, the WTP-CAM can be run by selecting either

Project>>Single Case Run or

Project>>MC Simulation (i.e., Monte Carlo Simulation).

If the run is successful, a notice window will appear indicating end of simulation. The demonstrations and explanations of the outputs from WTP-CAM are described in Section 6.0 of the main report.

B2.0 Understanding the Input Data

As introduced in Section B1.0, input data for WTP-CAM can be categorized into original inputs and new inputs. The original inputs, including the design and operational parameters for unit processes and information for chemical feeds, are used to make a traditional single case simulation for a processing train and are introduced in detail in Chapter C3.0 of the original WTP manual (USEPA, 2005). This WTP-CAM manual will not replicate the description for the original inputs again. Instead, this manual focuses on definition and selection of the new inputs added for the new features such as Monte Carlo analysis or customization of the GAC unit process model. The description of the new inputs is illustrated through an example processing train at Greater Cincinnati Water Works (GCWW) Richard Miller Treatment Plant (“Miller plant”) for drinking water.

B.2.1. Introduction to the Example Processing Train

WTP-CAM arranges the unit process components of a treatment train in a sequential block diagram, as illustrated in Figure B2-1. In the Miller plant, the water treatment process is shown in Figure B2-2. The plant treats the raw water through coagulation, sedimentation, rapid sand filtration, followed by granular activated carbon (GAC) processing. The spent GAC is reactivated in two large on-site furnaces. After chlorination disinfection, the treated water is stored temporarily in a clearwell and then pumped into the distribution system. Figure B2-3 summarizes the original input data for the treatment train at the Miller plant.

B 2.2 Inputs for Monte Carlo Simulation

B 2.2.1 Overview

The ability to make Monte Carlo simulation is an important new feature not previously available in the original WTP model. To understand the inputs for Monte Carlo analysis, it is helpful to introduce the procedures involved in the analysis. Figure B2-4 outlines key steps of the Monte Carlo analysis and the application of the new inputs (in bold). It can be seen that there are three key options that govern the Monte Carlo analysis: Quarterly Running Average, Preserving Correlation and Contamination Control.

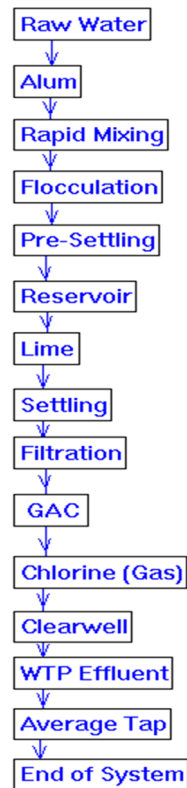


Figure B2-1 Schematic diagram WTP-CAM program flow in the example simulation.

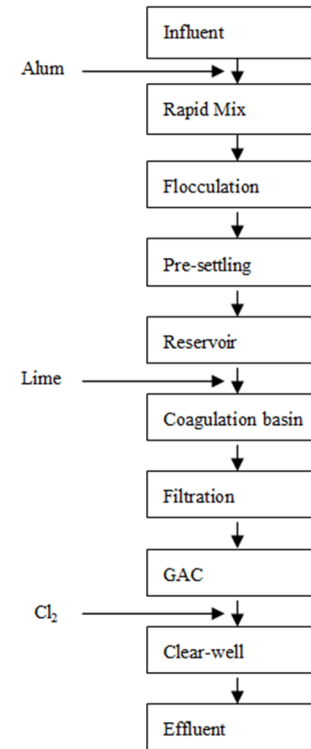


Figure B2-2 Schematic diagram for treatment unit process at the GCWW Richard Miller Treatment Plant.

Influent		
pH	7.8	
Influent Temperature	18.6	(Celsius)
Minimum Temperature	2.0	(Celsius)
Total Organic Carbon	2.6	(mg/L)
UV Absorbance at 254nm	0.096	(1/cm)
Bromide	0.069	(mg/L)
Alkalinity	72	(mg/L as CaCO3)
Calcium Hardness	77	(mg/L as CaCO3)
Total Hardness	141	(mg/L as CaCO3)
Ammonia	0.21	(mg/L as N)
Turbidity	151.0	(NTU)
Peak Flow	220.000	(MGD)
Plant Flow	120.600	(MGD)
Surface water by SWTR	TRUE	(TRUE/FALSE)
Source water Crypto. Concentration	0.000	(oocysts/Liter)
LT2 Rule watershed Control Prog. Credit?	FALSE	(TRUE/FALSE)
If GW System, Is Virus Disinfection Req'd?	FALSE	(TRUE/FALSE)
Virus Disinfection for GW, if Req'd	4.0	(logs)
Alum		
Alum Dose	1.1	(mg/L as Al2(SO4)3*14H2O)
Rapid Mix		
Volume of Basin	0.0084	(MG)
Ratio of T50/Detention Time	1.00	(ratio)
Ratio of T10/Detention Time	1.00	(ratio)
Flocculation		
Volume of Basin	1.9400	(MG)
Ratio of T50/Detention Time	1.00	(ratio)
Ratio of T10/Detention Time	0.50	(ratio)
Presed. Basin		
Volume of Basin	2.2300	(MG)
Ratio of T50/Detention Time	1.00	(ratio)
Ratio of T10/Detention Time	0.44	(ratio)
Eligible for LT2 Toolbox Crypto. Credit?	FALSE	(TRUE/FALSE)
LT2 Toolbox Crypto. Removal Credit	0.4	(logs)
Reservoir		
Volume of Basin	373.0000	(MG)
Ratio of T50/Detention Time	1.00	(ratio)
Ratio of T10/Detention Time	0.32	(ratio)
Lime		
Lime Dose	5.0	(mg/L as Ca(OH)2)
For pH adjustment (P) or Softening (S)	PH_ADJ.	(P or S)
Settling Basin		
Volume of Basin	26.0000	(MG)
Ratio of T50/Detention Time	1.00	(ratio)
Ratio of T10/Detention Time	0.42	(ratio)
Filtration		
Liquid Volume	2.4708	(MG)
Ratio of T50/Detention Time	1.00	(ratio)
Ratio of T10/Detention Time	0.12	(ratio)
Chlorinated Backwash Water?	FALSE	(TRUE/FALSE)
Filter Media (Anthracite/Sand or GAC)	A/S	(S or G)
Giardia Removal Credit - Conv. Filters	2.5	(logs)
Virus Removal Credit - Conv. Filters	2.0	(logs)
Crypto. Removal Credit - Conv. Filters	3.0	(logs)
Giardia Removal Credit - Direct Filters	2.0	(logs)
Virus Removal Credit - Direct Filters	1.0	(logs)
Crypto. Removal Credit - Direct Filters	3.0	(logs)
CFE Turb. Meets LT2 Toolbox Criteria?	FALSE	(TRUE/FALSE)
IFE Turb. Meets LT2 Toolbox Criteria?	FALSE	(TRUE/FALSE)
Crypto. Credit as 2nd Stage Filt.	0.5	(logs)
GAC		
Empty Bed Contact Time (at 'Plant Flow')	31	(minutes)
GAC Reactivation Interval	180	(days)
GAC Contacting System (Single/Blended)	Blended	(S or B)
TOC Breakthrough for Single Unit (Max/Avg)	Avg_TOC	(M or A)
Crypto. Removal Credit as 2nd Stage	0.5	(logs)
Chlorine (Gas)		
Chlorine Dose	3.0	(mg/L as Cl2)
Contact Tank		
Volume of Basin	28.3000	(MG)
Ratio of T50/Detention Time	1.00	(ratio)
Ratio of T10/Detention Time	0.20	(ratio)
WTP Effluent		
Average Tap		
Average Residence Time (For Average Flow)	1.0	(Days)
End of System		
Maximum Residence Time (For Average Flow)	3.0	(Days)

Figure B2-3 Original input data for the GCWW example processing train.

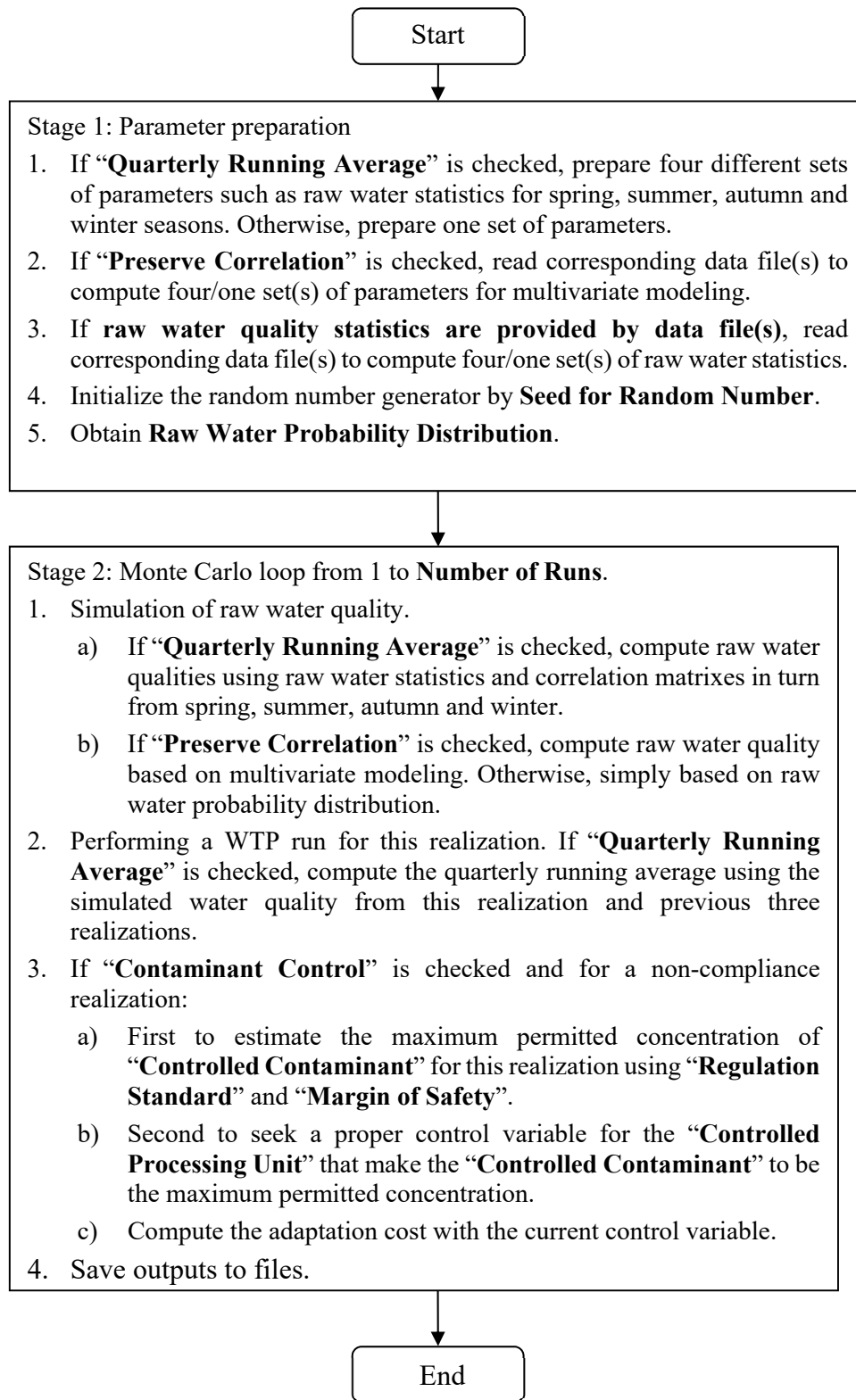


Figure B2-4 Illustration diagram for Monte Carlo analysis.

The simulation option for Quarterly Running Average is specially designed for regulation of contaminant total organic carbon (TOC). According to the USEPA disinfectant/disinfection byproduct (D/DBP) rule, an important compliance criterion for TOC treatment of surface water sources is that the treated water TOC level does not exceed 2.0 mg/L, calculated quarterly as a running annual average. WTP-CAM applies four seasons to represent the four quarters per year. As a result, this option affects the inputs of raw water quality (both statistics and correlation) and simulation procedure for pursuing the quarterly running average. More details for simulation related to Quarterly Running Average are introduced in Section B4.0.

The option for correlation is designed to preserve the joint correlation among raw water quality parameters when simulating stochastic raw water quality variables in each realization. In the presence of cross-correlation, concentrations of correlated reactants are possibly high or low simultaneously. As a result, cross correlated raw water quality parameters might exert a strong influence on DBP formation during water treatment and distribution. A multivariate seasonal autoregressive model of order one (Bras and Rodriguez-Iturbe, 1984) was applied in WTP-CAM. This seasonal model preserves all seasonal means and variance for all water quality parameters, all cross correlation among all water quality parameters, and lag-one correlations between adjacent seasons and between all water quality parameters. Section B5.0 describes the theoretical basis for the multivariate analysis applied.

Contamination option is designed to modify the design and operation of the current processing train when a non-compliance realization is simulated. For example, if a TOC violation is detected, the WTP-CAM program will modify operation by increasing the frequency of GAC regeneration in order to bring the TOC excursion within acceptable limits. The inputs for this option are controlled contaminant, regulation standard, margin of safety, and unit process to be controlled. So far, the option for contamination component has been developed only for TOC contaminant and GAC unit process. More details are available in Section B5.0.

B 2.2.2 Inputs for Monte Carlo Setting

The input parameters for Monte Carlo analysis may be divided into three groups: options, control parameters and source of influent water quality statistics/correlation. Figure B2-5 demonstrates these inputs for the example processing train shown in Figure B2-1.

Options: options are designed to govern the flow of Monte Carlo simulation. Table B2-1 provides the name of option, range of available values and description. Additional controlled contaminant and controlled unit processes will be added with further development of WTP-CAM.

Figure B2-5 Monte Carlo inputs for the example processing train.

Table B2- 1 Options for Monte Carlo Analysis

Control	Range of value	Description
Preserve Correlation	TRUE/FALSE	Multivariate analysis will be used to simulate stochastic raw water quality if TRUE (checked).
Quarterly Running Average	TRUE/FALSE	Simulation will be based on four seasons if TRUE.
System Adaptation	TRUE/FALSE	Loading adaptation program for the non-compliance realizations if TRUE.
Controlled Contaminant	TOC/None	Determining the contaminant to be controlled by adaptation.
Controlled Unit Process	GAC/None	Determining the unit process that can be adapted for controlled contaminant.
Raw Water Probability Distribution	Normal/Lognormal	Determining the probability distribution for all raw water quality parameters

Control parameters: four control parameters are used in the Monte Carlo simulation:

- Number of Runs – a user defined integer to specify the number of runs required.
- Seed for Random Number – a positive number to initialize the random number generator in the program. Monte Carlo simulation can be repeated using the same random number seed.
- Regulation standard – a value representing the compliance standard for the controlled contaminant selected in **Options**.
- Margin of Safety – refers to the difference between the compliance standard and the real controlled concentration that provides extra reliability for compliance. Margin of safety is usually within 1%–10% of the regulation standard.

Source of influent water quality statistics/correlation: influent water quality statistics are essential parameters to generate stochastic influent water quality parameters for each realization. There are two methods provided by WTP-CAM to obtain these parameters. One method is to input these parameters manually through clicking the manual input button. There will be four dialogue windows appearing one at a time for the four seasons if Quarterly Running Average is checked. Figure B2-6 illustrates an example of manual input window for the spring of the example processing train.

Parameter	Average	Standard Deviation
pH, -	7.7	0.17
Alkalinity, mg/L	55.5	18.2
Turbidity, NTU	43.4	38.0
Calcium Hardness, mg/L	63.5	23.3
Total Hardness, mg/L	110.4	18.4
TOC, mg/L	2.3	0.6
UVA, 1/cm	0.12	0.06
Bromide, mg/L	0.03	0.01
Ammonia, mg/L	0.29	0.41
Temperature, Celsius	12.4	0
Flow Rate, MGD	108.4	0

Figure B2-6 Manual input window for influent water quality statistics.

The other method is to compute the statistics using data file(s) provided by a user through clicking the button of “Computed by Available Data file.” Figure B2-7 demonstrates the input window for the name (including the extension name) of data files prepared by user. The following points are important:

- Location of file(s): the data file must reside in the same folder as WTP-CAM executive file.
- Format of data: as illustrated in Figure B2-8, the data file consists of 11 columns. The columns are pH, alkalinity, turbidity, calcium hardness, total hardness, TOC, UVA, bromide, ammonia, temperature, and inflow rate. The first two rows are used to indicate the title and unit for each column. There is no limit for the number of data points. Each column needs to be assigned a digit for correct reading of the input file. Empty columns are not allowed. If the value in a column is not available, fill the column with -100.

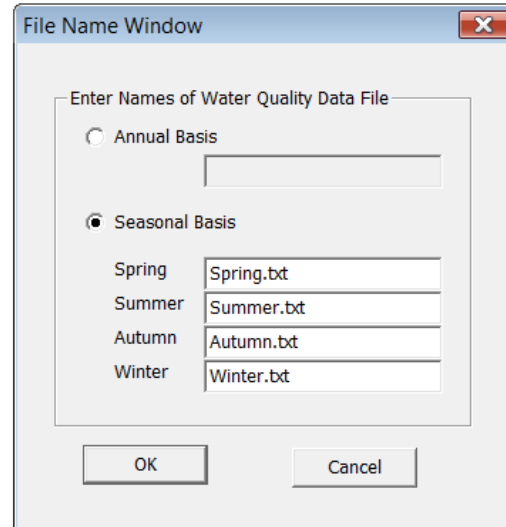


Figure B2-7 Dialogue window for name of data files.

If “Preserve Correlation” is checked, users are required to provide the raw water data file(s) for multivariate analysis through clicking the button in Correlation Matrix. The requirements for location of file(s), the format of file and the file name input window are the same as those for compute influent water quality statistics by file as described above.

pH	Alk	Turb	Ca-H	Tt_H	TOC	UVA	Bro	NH3	Temp	Qin
--	mg/l	NTU	mg/l	mg/l	mg/l	1/cm	mg/l	mg/l	Celsius	MGD
7.72	62.5	22.51	99.43	106.72	2.77	0.0924	0.028	0.253	14.4	108.4
7.57	68.2	56.74	57.08	111.41	4.91	0.2106	0.024	0.231	14.4	108.4
7.7	60.94	26.72	77.51	128.73	3.04	0.0768	0.039	0.199	14.4	108.4
7.25	19.12	19.96	53.73	62.22	1.82	0.0376	0.027	0.077	14.4	108.4
7.74	70.12	58.77	56.11	105.38	5.02	0.1991	0.028	0.091	14.4	108.4
7.55	36.65	64	70.74	75.75	2.82	0.061	0.028	0.291	14.4	108.4
7.83	53.49	26.97	54.36	103.91	3.7	0.1178	0.028	0.256	14.4	108.4
7.85	72.55	33.61	75.43	106.96	4.02	0.1536	0.028	0.065	14.4	108.4
7.7	84.91	24.4	53.93	136.28	4.25	0.2098	0.03	0.035	14.4	108.4
7.65	42.93	37.82	38.34	81.68	3.3	0.0848	0.026	0.375	14.4	108.4
7.78	89.18	91.96	36.55	96.79	5.7	0.267	0.023	0.351	14.4	108.4
7.71	49.82	39.61	28.41	80.11	4.21	0.1457	0.029	0.071	14.4	108.4
7.82	67.18	11.59	55.91	117.06	3.13	0.1153	0.026	0.064	14.4	108.4
7.98	73.69	26.57	113.48	124.85	3.79	0.0863	0.036	0.127	14.4	108.4
7.63	37.58	38.38	58.76	89.53	2.14	0.0655	0.026	0.232	14.4	108.4
7.81	49.56	12.52	58.76	97.8	2.95	0.081	0.028	0.158	14.4	108.4
7.74	68.48	27.88	31.01	103.98	3.82	0.2052	0.027	0.089	14.4	108.4
7.72	40.19	35.25	76.38	80.51	3.96	0.0561	0.033	0.376	14.4	108.4
7.97	89.01	4.31	77.95	128.13	3.53	0.0493	0.046	0.23	14.4	108.4
7.8	52.82	12.94	84.92	96.78	2.89	0.0748	0.027	0.083	14.4	108.4
7.82	56.56	36.99	73.16	94.35	4.41	0.0943	0.027	0.662	14.4	108.4

Figure B2-8 Example format of influent water quality data file.

B2.3 Customization of GAC Unit Process Model

B2.3.1 Overview

The performance of GAC for TOC removal has been studied using TOC breakthrough experiments in GAC columns under various conditions to examine different raw water sources, GAC size, pretreatment configuration, and bed depth/empty bed contact time (EBCT). In developing the WTP model, a classic logistic function was used to represent the TOC breakthrough curve for a single GAC contactor (USEPA, 2005), given by,

$$f(t) = \frac{TOC_{eff}}{TOC_{in}} = \frac{a}{1 + be^{-d \cdot t}} \quad (B2.1)$$

Where, $f(t)$ is TOC fraction remaining; TOC_{in} and TOC_{eff} are TOC influent and effluent concentrations at the GAC unit; t is GAC service time; a , b and d are model parameters estimated by statistical regression.

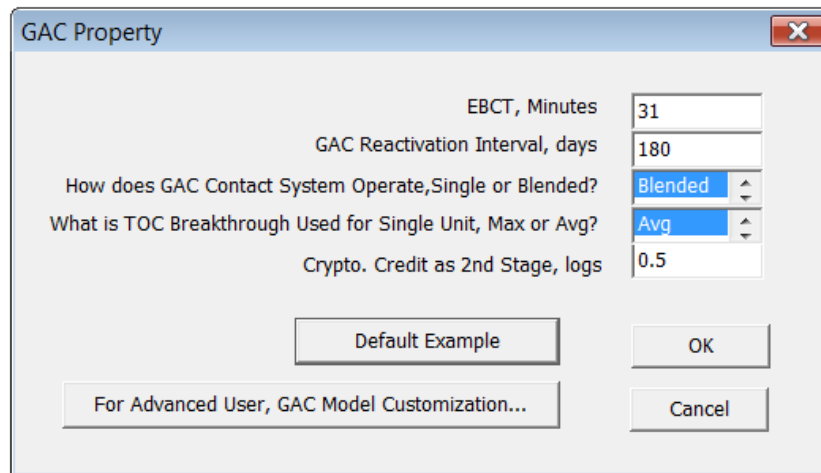


Figure B2-9 GAC unit process property window.

To improve the accuracy of GAC treatment modeling, WTP-CAM provides a new feature to customize parameters a , b and d using non-linear regression method if users can provide site-specific TOC treatment study data instead of the default statistical values. More details for the TOC breakthrough model and non-linear regression are introduced in Section B4.0.

B2.3.2 Inputs for GAC Model Customization

The GAC model customization is invoked by clicking the GAC model customization button located at the bottom of the GAC property window as shown in Figure B2-9. A dialogue window for TOC breakthrough customization will appear as shown in Figure B2-10. There are five edit boxes for the user's input.

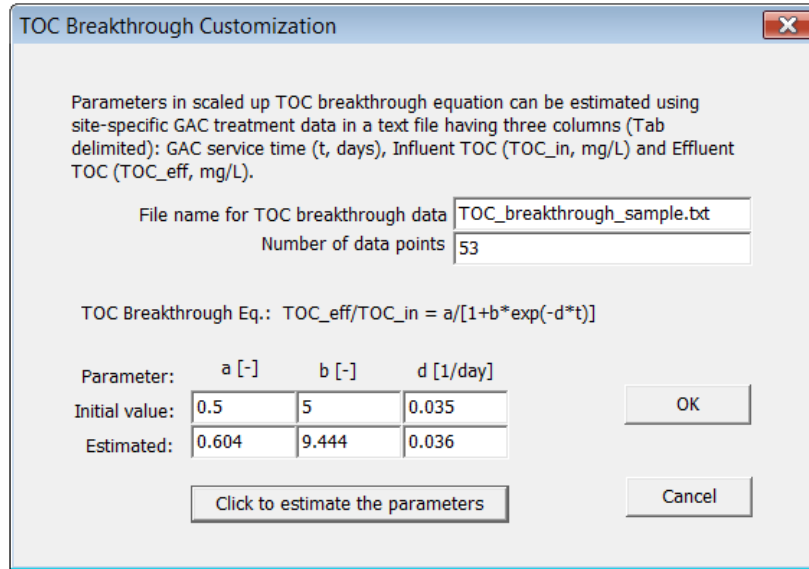


Figure B2-10 Dialogue window for TOC breakthrough customization.

- File name for TOC breakthrough data: provide the file name including the extension name in the edit box and keep the data file in the same folder as the WTP-CAM program. The format of data is illustrated in Figure B2-11. The data file consists of three columns: GAC service time, influent and effluent TOC concentration to the GAC processing unit. The first two rows are used to indicate the title and unit for each column. There is no limit on the number of data points. Empty columns are not allowed.
- Number of data points: number of valid data points in the data file.
- Initial value for the parameter *a*: a value between 0.6-0.9 (Roberts and Summers, 1982).
- Initial value for parameter *b*: a value between 3-30 (Based on USEPA [2005] and initial studies).
- Initial value for parameter *d*: a value between 0.01-0.1 (Based on USEPA [2005] and initial studies).

RunTime day	TOCin mg/l	TOCout mg/l
1.5	1.8452	0.1034
5	1.8452	0.1268
9	1.8452	0.084
13	1.8452	0.1103
17	1.8452	0.0812
21	1.8452	0.0772
25	1.8452	0.1372
29	1.8452	0.1223
33	1.8452	0.1867
.....		

Figure B2-11 Example format for TOC breakthrough data file.

B3.0 Understanding the Output Data

This Section provides a brief overview of the outputs generated by the WTP-CAM Model. Section B4.1 briefly describes the various output tables for a one-time run. Section B4.2 presents tabular outputs for Monte Carlo analysis. Section B4.3 introduces the graphic outputs based on Monte Carlo simulation. All outputs are based on the example processing train introduced in Section B3.0 for various inputs.

The output module for WTP-CAM is still in development. Therefore, some results in this Section are used for illustrative purposes to show program outputs expected in future.

B3.1 Standard Output Tables for a One-time Run

Based on the example treatment train shown in Figure B2-2, and input parameters summarized in Figure B2-3, the WTP-CAM will generate full standard outputs contained in 10 output tables and save temporarily in a text file named “WTP-CAM stdout.txt” in the working folder after “One Time Run” command. These 10 output tables are in fact replicated from the outputs of original WTP model. The Tables 1-9 in WTP-CAM outputs are associated with the (typical average) “Plant Flow” and “Influent Temperature” inputs. Outputs for “Table 10” are associated with worst-case disinfection input parameters of “Peak Flow” and “Minimum Temperature.” Figure B3-1 through B3-10 demonstrated the standard outputs by one-time run. For a detailed interpretation of these tables please refer to Chapter 4 of the WTP User Manual in U.S. EPA (2005).

Table 1 Water Quality Summary for Raw, Finished, and Distributed water At Plant Flow (120.6 MGD) and Influent Temperature (18.6 C)					
Parameter	Units	Raw water	Effluent	Avg. Tap	End of Sys
pH	(-)	7.8	8.1	8.2	8.2
Alkalinity	(mg/L as CaCO3)	72	74	74	74
TOC	(mg/L)	2.6	1.2	1.2	1.2
UV	(1/cm)	0.096	0.010	0.010	0.010
(T)SUVA	(1/cm)	3.7	0.9	0.9	0.9
Ca Hardness	(mg/L as CaCO3)	77	84	84	84
Mg Hardness	(mg/L as CaCO3)	64	64	64	64
Ammonia-N	(mg/L)	0.21	0.00	0.00	0.00
Bromide	(ug/L)	69	59	50	41
Free Cl2 Res.	(mg/L as Cl2)	0.0	1.0	0.6	0.4
Chloramine Res.	(mg/L as Cl2)	0.0	0.0	0.0	0.0
TTHMs	(ug/L)	0	14	26	37
HAA5	(ug/L)	0	5	8	10
HAA6	(ug/L)	0	6	10	13
HAA9	(ug/L)	0	6	12	17
TOX	(ug/L)	0	33	49	62
Bromate	(ug/L)	0	0	0	0
Chlorite	(mg/L)	0.0	0.0	0.0	0.0
TOC Removal	(percent)		55		
E.C. not required - raw TOC, raw SUVA, and/or finished TOC <= 2					
E.C. Step 1 TOC removal requirement ACHIEVED					
CT Ratios					
Virus	(-)	0.0	33.7	33.7	33.7
Giardia	(-)	0.0	4.2	4.2	4.2
Cryptosporidium*	(-)	1.0	1.0	1.0	1.0
*Crypto. Disinfection Calcs. Based on Proposed LT2 Rule					
Crypto. CT Ratio = 1 because other credits met full disinfection requirements					

Figure B3- 1 Standard output “Table 1” for the example processing train.

Table 2 Selected Input Parameters				
Parameter		Value	Units	
TEMPERATURES				
Average		18.6	(deg. C)	
Minimum		2.0	(deg. C)	
PLANT FLOW RATES				
Average		120.600	(mgd)	
Peak Hourly		220.000	(mgd)	
DISINFECTION INPUTS/CALCULATED VALUES				
Surface Water Plant?		TRUE		
Giardia: Total Disinfection Credit Required		3.0	(logs)	
Giardia: Credit Achieved (other than by CT)		2.5	(logs)	
Giardia: Inactivation Credit by CT Required		0.5	(logs)	
Virus: Total Disinfection Credit Required		4.0	(logs)	
Virus: Credit Achieved (other than by CT)		2.0	(logs)	
Virus: Inactivation Credit by CT Required		2.0	(logs)	
Crypto.: Total Disinfection Credit Required		3.0	(logs)	
Crypto.: Credit Achieved (other than by CT)		3.5	(logs)	
Crypto.: Inactivation Credit by CT Required		0.0	(logs)	
DISINFECT. CREDITS (not incl. CT): Giardia Virus Crypto				
(in order of appearance)				
Filtration		2.5	2.0	3.0
GAC	-2nd stage filt.	0.0	0.0	0.5
CHEMICAL DOSES				
(in order of appearance)				
Alum		1.1	(mg/L as Al ₂ (SO ₄) ₃ *14H ₂ O)	
Lime		5.0	(mg/L as Ca(OH) ₂)	
Chlorine (Gas)		3.0	(mg/L as Cl ₂)	
PROCESS HYDRAULIC PARAMETERS: T10/Tth T50/Tth VOL. (MG)				
(in order of appearance)				
Rapid Mix		1.0	1.0	0.0084
Flocculation		0.5	1.0	1.9400
Presed. Basin		0.4	1.0	2.2300
Reservoir		0.3	1.0	373.0000
Settling Basin		0.4	1.0	26.0000
Filtration		0.1	1.0	2.4708
Contact Tank		0.2	1.0	28.3000
GAC OPERATION INPUTS				
Empty Bed Contact Time		31.0	(minutes)	
Reactivation Frequency		180.0	(days)	
Sys. Config. ('s'= Single, 'B'= Blended)		B		

Figure B3- 2 Standard output "Table 2" for the example processing train.

Table 3 Predicted water Quality Profile At Plant Flow (120.6 MGD) and Influent Temperature (18.6 c)								
Location	pH (-)	TOC (mg/L)	UVA (1/cm)	(T)SUVA (L/mg-m)	Cl2 (mg/L)	NH2Cl (mg/L)	Residence Time Process (hrs)	Cum. (hrs)
Influent	7.8	2.6	0.096	3.7	0.0	0.0	0.00	0.00
Alum	7.7	2.6	0.096	3.7	0.0	0.0	0.00	0.00
Rapid Mix	7.7	2.6	0.084	3.3	0.0	0.0	0.00	0.00
Flocculation	7.7	2.6	0.084	3.3	0.0	0.0	0.39	0.39
Presed. Basin	7.7	2.6	0.084	3.3	0.0	0.0	0.00	0.39
Reservoir	7.7	2.6	0.084	3.3	0.0	0.0	74.23	74.62
Lime	9.0	2.6	0.084	3.3	0.0	0.0	0.00	74.62
Settling Basin	9.0	2.6	0.084	3.3	0.0	0.0	5.17	79.79
Filtration	9.0	2.6	0.084	3.3	0.0	0.0	0.49	80.28
GAC	9.0	1.2	0.015	1.3	0.0	0.0	0.52	80.80
Chlorine (Gas)	8.1	1.2	0.010	0.9	1.4	0.0	0.00	80.80
Contact Tank	8.1	1.2	0.010	0.9	1.0	0.0	5.63	86.43
WTP Effluent	8.1	1.2	0.010	0.9	1.0	0.0	0.00	86.43
Additional Point	8.2	1.2	0.010	0.9	0.8	0.0	12.00	98.43
Average Tap	8.2	1.2	0.010	0.9	0.6	0.0	24.00	110.43
Additional Point	8.2	1.2	0.010	0.9	0.5	0.0	48.00	134.43
End of System	8.2	1.2	0.010	0.9	0.4	0.0	72.00	158.43

TOC Removal (percent): 55
E.C. not required - raw TOC, raw SUVA, and/or finished TOC <= 2
E.C. Step 1 TOC removal requirement ACHIEVED

Figure B3- 3 Standard output “Table 3” for the example processing train.

Table 4 Predicted water Quality Profile At Plant Flow (120.6 MGD) and Influent Temperature (18.6 c)							
Location	pH (-)	Alk (mg/L)	Calcium Hardness (mg/L)	Magnesium Hardness (mg/L)	Solids (mg/L)	NH3-N (mg/L)	Bromide (ug/L)
Influent	7.8	72	77	64	0.0	0.2	69
Alum	7.7	71	77	64	0.0	0.2	69
Rapid Mix	7.7	71	77	64	0.0	0.2	69
Flocculation	7.7	71	77	64	0.0	0.2	69
Presed. Basin	7.7	71	77	64	211.9	0.2	69
Reservoir	7.7	71	77	64	211.9	0.2	69
Lime	9.0	78	84	64	211.9	0.2	69
Settling Basin	9.0	78	84	64	211.9	0.2	69
Filtration	9.0	78	84	64	211.9	0.2	69
GAC	9.0	78	84	64	211.9	0.2	69
Chlorine (Gas)	8.1	73	84	64	211.9	0.0	69
Contact Tank	8.1	74	84	64	211.9	0.0	59
WTP Effluent	8.1	74	84	64	211.9	0.0	59
Additional Point	8.2	74	84	64	211.9	0.0	53
Average Tap	8.2	74	84	64	211.9	0.0	50
Additional Point	8.2	74	84	64	211.9	0.0	45
End of System	8.2	74	84	64	211.9	0.0	41

Figure B3-4 Standard output “Table 4” for the example processing train.

Table 5 Predicted Trihalomethanes and other DBPs At Average Flow (120.6 MGD) and Temperature (18.6 C)								
Location	BrO3- (ug/L)	ClO2- (mg/L)	TOX (ug/L)	CHCl3 (ug/L)	BDCM (ug/L)	DBCM (ug/L)	CHBr3 (ug/L)	TTHMs (ug/L)
Influent	0	0.0	0	0	0	0	0	0
Alum	0	0.0	0	0	0	0	0	0
Rapid Mix	0	0.0	0	0	0	0	0	0
Flocculation	0	0.0	0	0	0	0	0	0
Presed. Basin	0	0.0	0	0	0	0	0	0
Reservoir	0	0.0	0	0	0	0	0	0
Lime	0	0.0	0	0	0	0	0	0
Settling Basin	0	0.0	0	0	0	0	0	0
Filtration	0	0.0	0	0	0	0	0	0
GAC	0	0.0	0	0	0	0	0	0
Chlorine (Gas)	0	0.0	0	0	0	0	0	0
Contact Tank	0	0.0	33	3	4	4	3	14
WTP Effluent	0	0.0	33	3	4	4	3	14
Additional Point	0	0.0	43	4	6	7	5	22
Average Tap	0	0.0	49	5	7	8	6	26
Additional Point	0	0.0	57	7	8	10	7	33
End of System	0	0.0	62	8	9	12	8	37

Figure B3- 5 Standard output “Table 5” for the example processing train.

Table 6 Predicted Haloacetic Acids - through HAA5 At Average Flow (120.6 MGD) and Temperature (18.6 C)						
Location	MCAA (ug/L)	DCAA (ug/L)	TCAA (ug/L)	MBAA (ug/L)	DBAA (ug/L)	HAA5 (ug/L)
Influent	0	0	0	0	0	0
Alum	0	0	0	0	0	0
Rapid Mix	0	0	0	0	0	0
Flocculation	0	0	0	0	0	0
Presed. Basin	0	0	0	0	0	0
Reservoir	0	0	0	0	0	0
Lime	0	0	0	0	0	0
Settling Basin	0	0	0	0	0	0
Filtration	0	0	0	0	0	0
GAC	0	0	0	0	0	0
Chlorine (Gas)	0	0	0	0	0	0
Contact Tank	1	2	1	0	1	5
WTP Effluent	1	2	1	0	1	5
Additional Point	1	2	1	0	2	7
Average Tap	1	3	1	1	2	8
Additional Point	1	3	1	1	3	9
End of System	1	4	2	1	3	10

Figure B3-6 Standard output “Table 6” for the example processing train.

Table 7 Predicted Haloacetic Acids (HAA6 through HAA9) At Average Flow (120.6 MGD) and Influent Temperature (18.6 c)						
Location	BCAA (ug/L)	BDCAA (ug/L)	DBCAA (ug/L)	TBAA (ug/L)	HAA6 (ug/L)	HAA9 (ug/L)
Influent	0	0	0	0	0	0
Alum	0	0	0	0	0	0
Rapid Mix	0	0	0	0	0	0
Flocculation	0	0	0	0	0	0
Presed. Basin	0	0	0	0	0	0
Reservoir	0	0	0	0	0	0
Lime	0	0	0	0	0	0
Settling Basin	0	0	0	0	0	0
Filtration	0	0	0	0	0	0
GAC	0	0	0	0	0	0
Chlorine (Gas)	0	0	0	0	0	0
Contact Tank	1	0	0	0	6	6
WTP Effluent	1	0	0	0	6	6
Additional Point	2	0	0	0	8	10
Average Tap	2	1	1	1	10	12
Additional Point	3	1	1	1	11	15
End of System	3	1	2	1	13	17

Figure B3- 7 Standard output “Table 7” for the example processing train.

Table 8 Predicted Disinfection Parameters - Residuals and CT Ratios At Plant Flow (120.6 MGD) and Influent Temperature (18.6 C)									
Location	Temp (C)	pH (-)	Cl2 (mg/L)	NH2Cl (mg/L)	Ozone (mg/L)	ClO2 (mg/L)	CT Ratios		
							Giardia	virus	Crypto
Influent	18.6	7.8	0.0	0.0	0.00	0.00	0.0	0.0	1.0
Alum	18.6	7.7	0.0	0.0	0.00	0.00	0.0	0.0	1.0
Rapid Mix	18.6	7.7	0.0	0.0	0.00	0.00	0.0	0.0	1.0
Flocculation	18.6	7.7	0.0	0.0	0.00	0.00	0.0	0.0	1.0
Presed. Basin	18.6	7.7	0.0	0.0	0.00	0.00	0.0	0.0	1.0
Reservoir	18.6	7.7	0.0	0.0	0.00	0.00	0.0	0.0	1.0
Lime	18.6	9.0	0.0	0.0	0.00	0.00	0.0	0.0	1.0
Settling Basin	18.6	9.0	0.0	0.0	0.00	0.00	0.0	0.0	1.0
Filtration	18.6	9.0	0.0	0.0	0.00	0.00	0.0	0.0	1.0
GAC	18.6	9.0	0.0	0.0	0.00	0.00	0.0	0.0	1.0
Chlorine (Gas)	18.6	8.1	1.4	0.0	0.00	0.00	0.0	0.0	1.0
Contact Tank	18.6	8.1	1.0	0.0	0.00	0.00	4.2	33.7	1.0
WTP Effluent	18.6	8.1	1.0	0.0	0.00	0.00	4.2	33.7	1.0
Additional Point	18.6	8.2	0.8	0.0	0.00	0.00	4.2	33.7	1.0
Average Tap	18.6	8.2	0.6	0.0	0.00	0.00	4.2	33.7	1.0
Additional Point	18.6	8.2	0.5	0.0	0.00	0.00	4.2	33.7	1.0
End of System	18.6	8.2	0.4	0.0	0.00	0.00	4.2	33.7	1.0

Crypto. CT Ratio = 1 because other credits met full disinfection requirements

Figure B3-8 Standard output “Table 8” for the example processing train.

Table 9 Predicted Disinfection Parameters - CT Values At Plant Flow (120.6 MGD) and Influent Temperature (18.6 C)				
Location	Cl2 <-----$(\text{mg/L} * \text{minutes})$----->	NH2Cl	ozone	ClO2
Influent	0.0	0.0	0.0	0.0
Alum	0.0	0.0	0.0	0.0
Rapid Mix	0.0	0.0	0.0	0.0
Flocculation	0.0	0.0	0.0	0.0
Presed. Basin	0.0	0.0	0.0	0.0
Reservoir	0.0	0.0	0.0	0.0
Lime	0.0	0.0	0.0	0.0
Settling Basin	0.0	0.0	0.0	0.0
Filtration	0.0	0.0	0.0	0.0
GAC	0.0	0.0	0.0	0.0
Chlorine (Gas)	0.0	0.0	0.0	0.0
Contact Tank	67.4	0.0	0.0	0.0
WTP Effluent	67.4	0.0	0.0	0.0
Additional Point	67.4	0.0	0.0	0.0
Average Tap	67.4	0.0	0.0	0.0
Additional Point	67.4	0.0	0.0	0.0
End of System	67.4	0.0	0.0	0.0

Figure B3- 9 Standard output “Table 9” for the example processing train.

Table 10 Predicted Disinfection Parameters At Peak Flow (220.0 MGD) and Minimum Temperature (2.0 C) for Surface Water Plant with Coagulation and Filtration									
Location	Temp (C)	pH (-)	Cl2 (mg/L)	NH2Cl (mg/L)	ozone (mg/L)	ClO2 (mg/L)	CT Ratios		
							Giardia	Virus	Crypto
Influent	2.0	7.8	0.0	0.0	0.00	0.00	0.0	0.0	1.0
Alum	2.0	7.7	0.0	0.0	0.00	0.00	0.0	0.0	1.0
Rapid Mix	2.0	7.7	0.0	0.0	0.00	0.00	0.0	0.0	1.0
Flocculation	2.0	7.7	0.0	0.0	0.00	0.00	0.0	0.0	1.0
Presed. Basin	2.0	7.7	0.0	0.0	0.00	0.00	0.0	0.0	1.0
Reservoir	2.0	7.7	0.0	0.0	0.00	0.00	0.0	0.0	1.0
Lime	2.0	9.1	0.0	0.0	0.00	0.00	0.0	0.0	1.0
Settling Basin	2.0	9.1	0.0	0.0	0.00	0.00	0.0	0.0	1.0
Filtration	2.0	9.1	0.0	0.0	0.00	0.00	0.0	0.0	1.0
GAC	2.0	9.1	0.0	0.0	0.00	0.00	0.0	0.0	1.0
Chlorine (Gas)	2.0	8.0	1.4	0.0	0.00	0.00	0.0	0.0	1.0
Contact Tank	2.0	8.0	1.0	0.0	0.00	0.00	0.8	6.5	1.0
WTP Effluent	2.0	8.0	1.0	0.0	0.00	0.00	0.8	6.5	1.0
Additional Point	2.0	8.0	0.9	0.0	0.00	0.00	0.8	6.5	1.0
Average Tap	2.0	8.1	0.8	0.0	0.00	0.00	0.8	6.5	1.0
Additional Point	2.0	8.1	0.6	0.0	0.00	0.00	0.8	6.5	1.0
End of system	2.0	8.1	0.5	0.0	0.00	0.00	0.8	6.5	1.0

Crypto. CT Ratio = 1 because other credits met full disinfection requirements

Figure B3-10 Standard output “Table 10” for the example processing train.

B3.2 Tabular Outputs for Monte Carlo Simulation

Tabular outputs are saved in text format with extension name “txt” in the working folder to allow viewing with any text editor. The tabular outputs will be managed through the main menu “View”-> “Table...” (To be developed). The tabular outputs for Monte Carlo simulations may be classified into five types as described in the following sections.

B3.2.1 Samples/statistics of Raw Water Qualities

The samples of influent water qualities plus inflow rate and temperature for all realizations can be collected as outputs to provide to users. At the bottom of results, the basic statistics, including sample number, mean, standard deviation, minimum and maximum, are also provided. Figure B3-11 illustrates a sample of influent water quality output.

Number --	Qin MGD	Alk mg/L	Bro mg/L	Ca-H mg/L	Tt-H mg/L	NH3 mg/L	Turb mg/L	PH --	Temp C	TOC mg/L	UVA 1/cm
1	120.6	55.52	0.035	49.4	100.8	0.061	12.0	7.60	18.6	3.06	0.061
2	120.6	63.23	0.033	44.4	107.3	0.124	19.5	7.80	18.6	3.76	0.109
3	120.6	61.30	0.033	71.0	104.9	0.191	28.5	7.57	18.6	4.74	0.110
4	120.6	30.96	0.027	62.6	83.5	0.141	26.8	7.72	18.6	1.99	0.095
5	120.6	82.32	0.035	54.8	117.0	0.171	21.1	7.77	18.6	4.99	0.147
6	120.6	59.12	0.031	95.9	108.1	0.063	15.9	7.93	18.6	2.77	0.061
7	120.6	100.52	0.026	89.0	120.5	0.268	281.7	7.87	18.6	5.81	0.406
8	120.6	45.33	0.036	45.6	94.3	0.291	32.3	7.39	18.6	3.14	0.100
~											
996	120.6	47.58	0.028	44.5	90.5	0.236	11.9	7.71	18.6	2.85	0.042
997	120.6	51.37	0.031	56.6	93.3	0.246	44.9	7.57	18.6	3.96	0.106
998	120.6	41.62	0.030	89.7	90.9	0.249	12.5	7.44	18.6	3.17	0.058
999	120.6	58.67	0.027	82.0	101.6	1.558	146.5	7.80	18.6	5.09	0.147
1000	120.6	40.39	0.031	72.4	94.3	0.351	18.1	7.60	18.6	2.14	0.041
~											
Samples	1000	1000	1000	1000	1000	1000	1000	1000	1000	1000	1000
Mean	120.6	58.18	0.030	62.6	98.9	0.359	43.7	7.71	18.6	3.83	0.113
St. dev	0.0	22.36	0.006	23.2	18.0	0.446	40.5	0.16	0.0	1.11	0.056
Min	120.6	15.48	0.014	23.8	49.5	0.003	2.1	7.14	18.6	1.36	0.024
Max	120.6	232.32	0.053	183.3	219.6	4.178	506.9	8.13	18.6	8.82	0.406

Figure B3-11 Sample outputs of raw water quality.

B3.2.2 Samples/Statistics of Effluent Water Quality

Similar to the sample outputs of raw water quality, the sample and basic statistics of effluent water qualities for all realizations can also be outputted. The difference is each unit process has effluent water. Therefore, a location has to be designated for the sample outputs. In addition, it may not be necessary to output all water quality parameters. Thus, an optional list will be provided to users to select output parameters (to be developed). Figure B3-12 demonstrates an example output for selected water quality parameters, pH, TOC, chlorine, TTHM (sum of four individual species of trihalomethanes) and HAA₅ (haloacetic acid, species five), at finished water.

Number --	pH --	TOC mg/L	Cl2 mg/L	TTHM ug/L	HAA5 ug/L
1	8.34	0.67	1.76	7.90	3.72
2	8.35	1.07	1.08	14.27	6.69
3	8.20	1.75	0.39	22.84	10.87
4	7.86	0.22	1.52	1.64	0.94
5	8.37	1.90	0.43	26.90	12.08
6	8.22	0.55	1.86	5.06	2.58
7	8.23	2.04	0.00	27.86	0.00
8	7.94	0.74	0.32	6.78	2.92
~					
996	8.08	0.55	0.77	4.31	2.06
997	8.10	1.21	0.34	13.63	6.40
998	7.94	0.75	0.55	7.00	3.45
999	8.12	1.97	0.00	8.20	5.52
1000	7.79	0.28	0.19	1.38	0.55
Samples	1000	1000	1000	1000	1000
Mean	8.14	1.12	0.66	10.93	4.08
St. Dev	0.21	0.57	0.67	9.82	3.82
Min	7.25	0.09	0.00	0.00	0.00
Max	8.70	2.05	2.27	41.41	15.62

Figure B3-12 Selected sample outputs of effluent water qualities at finished water.

B3.2.3 Samples/Statistics of Adaptation Costs

Similarly, the sample and basic statistics of adaptation variable and adaptation costs for all realizations can be outputted. Figure B3-13 demonstrates an example output for the adaptation variable, GAC reactivation period, and adaptation cost.

Number --	React days	cost M\$
1	180	13.622
2	180	13.622
3	93	17.511
4	180	13.622
5	82	18.760
6	180	13.622
7	56	22.663
8	180	13.622
~		
996	180	13.622
997	177	13.706
998	180	13.622
999	78	19.284
1000	180	13.622
Samples	1000	1000
Mean	146	15.480
St. Dev	46	3.142
Min	24	13.622
Max	180	32.481

Figure B3-13 Sample outputs for adaptation costs.

B3.2.4 Samples/Statistics for Compliance/Non-compliance Realizations

In certain sampling-based sensitivity analysis techniques used to identify important dynamic input variables, each vector of input variables is classified behaviorally into two sample sets: those that created simulation outputs above a threshold (regulated standard) as “non-compliance” sample set and those that created outputs below the threshold as “compliance” sample set. WTP-CAM provides similar outputs and their basic statistics for the compliance or the non-compliance sample set for selected parameters from optional list (to be developed). Figure B3-14 demonstrates an example for non-compliance samples to regulated TOC at finished water with selected parameters: the raw water quality parameters and the adaptation cost.

Number --	pH --	Alk mg/l	Turb NTU	Ca-H mg/l	Tt_H mg/l	TOC mg/l	UVA 1/cm	Bro mg/l	NH3 mg/l	Cost M\$
2	7.68	53.8	146.9	56.0	79.2	7.84	0.191	0.020	0.59	32.48
5	7.77	48.3	34.7	57.9	88.0	4.18	0.093	0.032	0.81	15.41
8	7.58	58.6	21.9	51.1	96.8	4.65	0.122	0.037	0.50	17.58
10	8.01	63.0	88.7	40.0	90.5	5.27	0.268	0.023	0.21	20.46
14	7.57	61.3	28.5	70.9	104.8	4.74	0.110	0.033	0.19	18.24
16	7.77	82.3	21.1	54.8	117.0	4.99	0.147	0.035	0.17	19.55
18	7.87	100.5	281.7	89.0	120.5	5.81	0.406	0.026	0.27	23.43
20	7.73	84.6	13.6	59.9	123.8	4.66	0.146	0.035	0.18	17.71
~										
~										
981	7.67	78.1	39.2	57.9	109.5	6.19	0.147	0.026	0.36	24.96
982	7.64	79.3	42.8	70.8	114.0	4.47	0.115	0.030	0.93	16.97
983	7.99	101.9	26.8	43.3	114.3	4.87	0.227	0.027	0.01	18.89
989	8.01	85.8	45.5	104.5	120.7	5.13	0.102	0.033	0.45	20.46
998	7.97	112.5	21.3	136.9	128.2	8.82	0.136	0.035	0.32	13.62
999	7.83	76.2	111.3	159.2	120.5	4.57	0.169	0.030	0.10	17.58
Samples	451	451	451	451	451	451	451	451	451	451
Mean	7.75	71.1	48.3	63.5	104.6	4.83	0.145	0.030	0.36	18.47
St. Dev	0.16	23.5	41.0	25.0	19.1	0.81	0.060	0.006	0.43	3.62
Min	7.28	27.8	5.3	25.9	66.9	3.85	0.047	0.017	0.01	13.62
Max	8.13	232.3	326.1	183.3	219.6	8.82	0.406	0.053	3.06	32.98

Figure B3-14 Sample outputs of raw water quality and adaptation cost for non-compliance events.

B3.2.5 Running Log

Running log (to be developed) will be generated automatically when WTP-CAM is executed. The log file provides the status of execution and messages of error or warning occurred, which will assist the user to diagnose problems. Appendix A provides further information concerning the error ID and warning ID. Figure B3-15 shows the format of the log file.

```

WTP-CCAM Version 1.0
Latest Update: August 12, 2010
Developed for USEPA by the University of Cincinnati
Name of project: Sample Processing Train
Date of running: Fri Aug 13 13:03:56 2010
-----
Reading input file... successfully
Monte Carlo simulation... successfully
Simulation is completed, thank you.
    
```

Figure B3-15 Example format of the log file.

B3.3. Graphic Outputs for Monte Carlo Simulation

The tabular results, after data processing, can be viewed using graphs. The graphs can be further printed or saved as a data file. The results of Monte Carlo analysis can be illustrated either with a sample versus realization chart, frequency chart, cumulative frequency chart or sensitivity chart for the sample-based data.

B3.3.1. Sample Chart (to be developed)

A sample chart is used to illustrate the changes of a sampled random variable with realization. The realization may represent the time sequence or spatial sequence depending on the circumstance studied. Figure B3-16 demonstrates a sample chart for raw water TOC. The realization may present daily, weekly, or monthly time horizon.

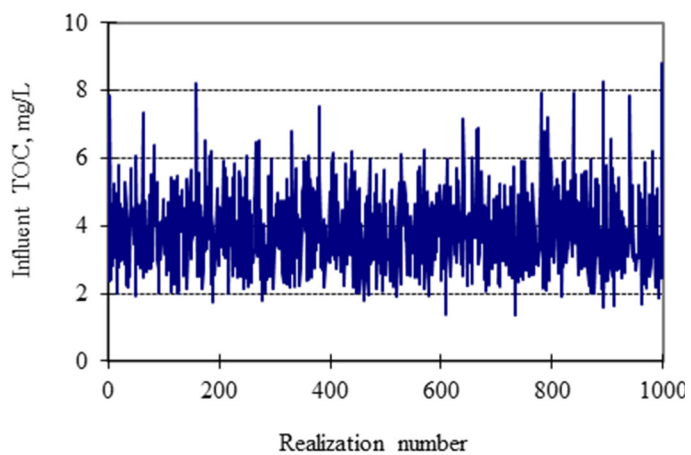


Figure B3-16 Example sample chart for raw water TOC.

B3.3.2. Frequency Chart (to be developed)

The frequency chart, a graphical display of tabular frequencies, is used to plot density of data and show the degree of uncertainty for a selected parameter. In other words, a frequency chart illustrates how often they occur in the range of the selected parameter values. Figure B3-17 shows an example frequency chart for raw water TOC.

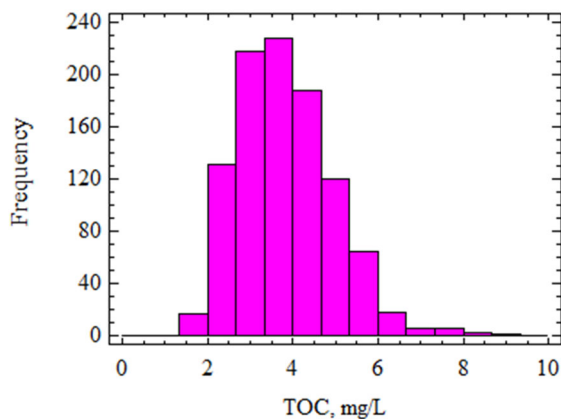


Figure B3-17 Example frequency chart for raw water TOC.

B3.3.3. Cumulative Frequency Chart (To be developed)

The cumulative frequency chart provides another way to explain the results from Monte Carlo simulation and is often preferred. This chart presents the probability that a value falls within, above or below a given range. Figure B3-18 illustrates an example cumulative frequency chart for effluent TOC at finished water. It can be seen that only 62% of the effluent TOC concentration is less than 2 mg/L, the regulation compliance. Conversely, the TOC compliance standard is violated in 38% of the samples.

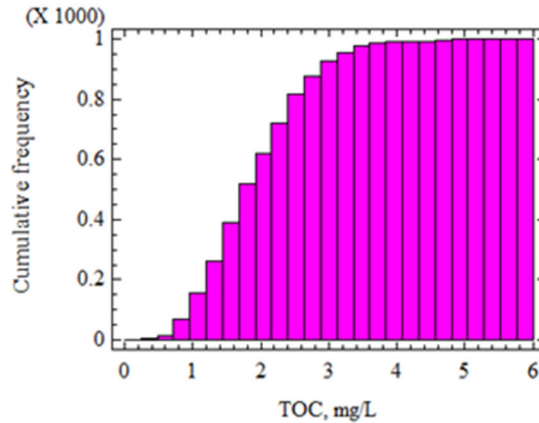


Figure B3-18 Example cumulative frequency chart for effluent TOC at finished water.

B4.0 Models and Algorithms in WTP-CAM

B4.1 Monte Carlo Methods

Monte Carlo analysis is a practical tool that is widely used to obtain sample solutions by repeating a simulation process for problems involving random variables with known probability distributions. Monte Carlo methods are useful for modeling phenomena with significant [uncertainty](#) in inputs such as climate change induced raw water qualities. Because Monte Carlo simulation considers random sampling of [probability distribution](#) functions as model inputs to produce hundreds or thousands of possible outcomes instead of a few discrete scenarios, the results provide probabilities of different outcomes occurring. Monte Carlo methods usually follow a particular procedure below:

- Define a domain of possible inputs.
- Generate inputs randomly from the domain using a specified probability distribution.
- Perform a [deterministic](#) computation using the inputs.
- Aggregate the results of the individual computations into the final result.

As briefly introduced in Section B3.1, the ability to conduct Monte Carlo simulation is an important new feature of WTP-CAM. Three key options govern the Monte Carlo analysis: Preserving Correlation, Quarterly Running Average and Contamination Control/Adaptation of Unit Process. Sections B4.1.1 to B4.1.3 provide descriptions of these controls.

B4.1.1 Seasonal Multivariate Analysis

The control for preserving correlation is designed to preserve the joint correlation among raw water quality parameters when simulating stochastic raw water quality inputs in each realization. A multivariate seasonal autoregressive model of order one, AR(1), (Bras and Rodriguez-Iturbe, 1984; Salas et al., 1980) was applied in WTP-CAM to simulate the raw water quality since this seasonal model preserves all seasonal means and variance for all water quality parameters, all cross correlation among all water quality parameters, and lag-one correlations

between adjacent seasons and between all water quality parameters. According to Bras and Rodriguez-Iturbe (1980), the lag-one multivariate seasonal autoregressive model is,

$$(X_j - m_j) = A_j(X_{j-1} - m_{j-1}) + B_j \varepsilon_j \quad (\text{B4.1})$$

Where, X_j is the (9×1) vector of nine raw water quality parameters for season j . m_j is the known vector of the means for the nine parameters for season j . ε_j is an (9×1) vector of standard normal deviates for season j . A_j and B_j are (9×9) parameter matrices for season j . A_j and B_j can be estimated by the covariance matrices (Bras and Rodriguez-Iturbe, 1984),

$$A_j = {}_jM_{1\ j-1} M_0^{-1} \quad (\text{B4.2})$$

$$B_j B_j^T = {}_jM_0 - {}_jM_{1\ j-1} M_0^{-1} {}_jM_1^T \quad (\text{B4.3})$$

where, ${}_jM_0$ is the lag-zero covariance matrix of $(X_j - m_j)$ for season j ; ${}_jM_1$ is the lag-one covariance matrix of $(X_j - m_j)$ for season j ; superscript (-1) refers 9 to the invertible matrix; superscript (T) refers to the transpose matrix.

Let $Y = X_j - m_j$ and $X = X_{j-1} - m_{j-1}$, Equation B4.1 becomes,

$$Y = A_j X + B_j \varepsilon_j \quad (\text{B4.1a})$$

The covariance matrices are defined by,

$${}_jM_0 = S_{yy} = E[YY^T] \quad (\text{B4.4})$$

$${}_jM_1 = S_{yx} = E[YX^T] \quad (\text{B4.5})$$

$${}_{j-1}M_0 = S_{xx} = E[XX^T] \quad (\text{B4.6})$$

Matrices S_{xx} , S_{yy} and S_{yx} can be represented in terms of variances, standard deviations and correlations as,

$$S_{xx} = \begin{pmatrix} S_{x_1}^2 & r_{x_1x_2} S_{x_1} S_{x_2} & \cdots & r_{x_1x_9} S_{x_1} S_{x_9} \\ r_{x_2x_1} S_{x_2} S_{x_1} & S_{x_2}^2 & \cdots & r_{x_2x_9} S_{x_2} S_{x_9} \\ \vdots & \vdots & \ddots & \vdots \\ r_{x_9x_1} S_{x_9} S_{x_1} & r_{x_9x_2} S_{x_9} S_{x_2} & \cdots & S_{x_9}^2 \end{pmatrix} \quad (\text{B4.7})$$

$$\mathbf{S}_{yy} = \begin{pmatrix} S_{y_1}^2 & r_{y_1 y_2} S_{y_1} S_{y_2} & \cdots & r_{y_1 y_9} S_{y_1} S_{y_9} \\ r_{y_2 y_1} S_{y_2} S_{y_1} & S_{y_2}^2 & \cdots & r_{y_2 y_9} S_{y_2} S_{y_9} \\ \vdots & \vdots & \ddots & \vdots \\ r_{y_9 y_1} S_{y_9} S_{y_1} & r_{y_9 y_2} S_{y_9} S_{y_2} & \cdots & S_{y_9}^2 \end{pmatrix} \quad (\text{B4.8})$$

$$\mathbf{S}_{yx} = \begin{pmatrix} r_{y_1 x_1} S_{x_1} S_{y_1} & r_{y_2 x_1} S_{x_1} S_{y_2} & \cdots & r_{y_9 x_1} S_{x_1} S_{y_9} \\ r_{y_1 x_2} S_{x_2} S_{y_1} & r_{y_2 x_2} S_{x_2} S_{y_2} & \cdots & r_{y_9 x_2} S_{x_2} S_{y_9} \\ \vdots & \vdots & \ddots & \vdots \\ r_{y_1 x_9} S_{x_9} S_{y_1} & r_{y_2 x_9} S_{x_9} S_{y_2} & \cdots & r_{y_9 x_9} S_{x_9} S_{y_9} \end{pmatrix} \quad (\text{B4.9})$$

where, S_{x_i} is the standard deviation of variable x_i , $r_{x_i x_j}$ is the lag-zero correlation between x_i and x_j , $r_{y_i x_j}$ is the lag-one correlation between variables y_i and x_j . The sample means, standard deviations and correlations are known parameters obtained from historical records.

Therefore, the matrix \mathbf{A}_j can be computed directly with Equation B4.2. Matrix \mathbf{B}_j can be obtained by decomposition of $\mathbf{B}_j \mathbf{B}_j^T$ through taking matrix \mathbf{B}_j as a lower triangular form,

$$\mathbf{B}_j = \begin{pmatrix} b_{11} & 0 & \cdots & 0 \\ b_{21} & b_{22} & \cdots & 0 \\ \vdots & \vdots & \ddots & \vdots \\ b_{91} & b_{92} & \cdots & b_{99} \end{pmatrix} \quad (\text{B4.10})$$

$$\text{Let } \mathbf{D} = \begin{pmatrix} d_{11} & d_{12} & \cdots & d_{19} \\ d_{21} & d_{22} & \cdots & d_{29} \\ \vdots & \vdots & \ddots & \vdots \\ d_{91} & d_{92} & \cdots & d_{99} \end{pmatrix} = \mathbf{B}_j \mathbf{B}_j^T \quad (\text{B4.11})$$

According to Salas et al.(1980), if \mathbf{D} is a positive definite matrix, a unique solution for \mathbf{B}_j can be obtained when \mathbf{B}_j is a lower triangular matrix. The non-zero elements of \mathbf{B}_j are calculated by,

$$\text{For } j=1, b_{ij} = d_{ij} / b_{jj} \quad i=1, \dots, 9 \quad (\text{B4.12})$$

$$\text{For } j=2, 3, \dots, 9 \text{ and } i=j, b_{ij} = \sqrt{d_{ij} - \sum_{k=1}^{j-1} b_{jk}^2} \quad (\text{B4.13})$$

$$\text{For } j=2, 3, \dots, 8 \text{ and } i=j+1, \dots, 9, b_{ij} = \left(d_{ij} - \sum_{k=1}^{j-1} b_{jk} b_{ik} \right) / b_{jj} \quad (\text{B4.14})$$

When matrices A_j and B_j are computed and vector ε_j is simulated, the normally distributed stochastic water quality parameters with preserved correlation, X_j , can be calculated with Equation B4.1.

If the elements of vector X and Y , x_i and y_i , are random variables following a two-parameter log-normal distribution, define the new variables, x'_i and y'_i , as following,

$$x'_i = \ln(x_i) \quad (\text{B4.15})$$

$$y'_i = \ln(y_i) \quad (\text{B4.16})$$

Thus, the transformed variables x'_i and y'_i are normally distributed with means $m_{x'_i}$ and $m_{y'_i}$, standard deviations $S_{x'_i}$ and $S_{y'_i}$, and the correlation coefficient among them given by $r_{x'_i y'_i}$.

The sample means, standard deviations and correlations of the transformed variables x'_i and y'_i can be also obtained from the transformed historical records through Equation B4.15 and B4.16.

The parameters of the transformed variables are then used to build the necessary auto-covariance and cross-covariance matrices using the equations B4.7 to B4.9. Matrices A_j and B_j can be obtained from the previous introduced Equations.

In order to get the original variables from results based on the transformed computation, the inverse transformation must be performed as following,

$$x_i = \exp(x'_i + m_{x'_i}) \quad (\text{B4.17})$$

$$y_i = \exp(y'_i + m_{y'_i}) \quad (\text{B4.18})$$

B4.1.2 Simulation of quarterly running average (TOC compliance).

The simulation of Quarterly Running Average is specially designed for regulation of contaminant TOC. According to the USEPA disinfectant/disinfection by-product (D/DBP) rule, an important compliance criterion for TOC treatment for surface water as source is that the treated water TOC concentration does not exceed 2.0 mg/L, calculated quarterly as a running annual average. WTP-CAM applies four seasons to represent the four quarters per year. Therefore, there are four running annual averages computed for each year. The running annual average is defined as the arithmetic average of TOC concentrations at current season and previous three seasons based on the USEPA D/DBP rule. Table B4-1 illustrates calculations of running annual average for TOC in finished water.

Since the means, variances and cross correlations of raw water parameters vary with seasonal changes in most circumstances, it is necessary to prepare four sets of input parameters for raw water qualities as shown in Figure 2-4. Therefore, there are four simulations each year, corresponding to the four seasons. The TOC concentration is recomputed each season with TOC values defined above.

Table B4- 1 Illustration of calculating running annual average for finished water TOC

Year	Season	TOC concentration	Running annual average
2009	Spring	1.3	--
	Summer	1.7	--
	Autumn	2.2	--
	Winter	1.7	1.7
2010	Spring	1.2	1.7
	Summer	1.4	1.6
	Autumn	2.4	1.7
	Winter	1.5	1.6

B4.1.3 Adaptation of Unit Process

Adaptation refers to necessary changes of design and/or operation of the current water treatment train when a non-compliance event is simulated. So far, the only adaptation module that has been developed is for TOC treatment in the GAC unit process. More contaminant controls and unit processes will be added with further development of WTP-CAM.

There are four parameters required from users: controlled contaminant, regulation standard, margin of safety, and unit process to be adapted. For example, if TOC is selected as the controlled contaminant, the regulation standard is 2.0 mg/L. In order to better ensure the compliance, a margin of safety may be applied to adaptation. Margin of safety refers to the difference between the compliance standard and the real controlled concentration that provides extra reliability for compliance. For instance, if margin of safety is 0.1mg/L, the controlled the TOC concentration will be $2.0 \text{ mg/L} - 0.1 \text{ mg/L} = 1.9 \text{ mg/L}$. In other words, the simulated running annual average of TOC concentration will be less than 1.9 mg/L after adaptation. The unit process to be adapted is where a change of a design or operation parameter happens. For example, if a noncompliance event happens for TOC in finished water and GAC unit process is available in the treatment train, an effective way to enhance TOC removal is to reduce the GAC service time in GAC contactors (see Section 5.2.1 for detail). WTP-CAM will seek a GAC service time so that the TOC concentration is right below the controlled concentration 1.9 mg/L.

The specific procedure of computation is as follows. The first step is to reduce current GAC service time by one day. The second step is to use the new service time to re-compute the TOC concentration for each of four seasons without change of other conditions in each season. The third step is to calculate the new running annual average of TOC. The final step is compare the new calculated TOC to the controlled concentration 1.9mg/L; if new TOC is less than 1.9 mg/L, the new service time is adopted; otherwise, go back to the first step and repeat computation again.

B4.2 Customization of Unit Process

Chapter 5 of original WTP model user manual (USEPA, 2005) in Appendix C provides a detail description of equations used to model various unit processes. The WTP Model primarily uses empirical correlations to predict central tendencies of natural organic material removal, disinfection, and DBP formation in a treatment plant. The algorithms were generally developed using multiple linear regression techniques. As a result, the empirical correlations usually consist of independent variables and empirical constants. These statistical models generally work well for providing the central tendencies. However, they may not provide sufficiently accurate predictions for a specific utility. As a new feature, therefore, WTP-CAM provides options to customize the empirical constants in regression equations using site-specific treatment study data. To date, only the GAC treatment unit process has modified to allow customization of the TOC breakthrough model. Customizations for other unit processes will be added with the development of WTP-CAM.

B4.2.1 Customization of GAC Unit Process

GAC treatment has been used as an alternative for reducing organic contamination in water supplies since early 1970's (Roberts and Summers, 1982). The performance of GAC for TOC removal has been studied using TOC breakthrough experiments in GAC columns under different conditions, such as GAC sources or pretreatment configurations. Roberts and Summers (1982) found that complete removal of TOC by GAC cannot be achieved under water treatment conditions. An immediate, partial breakthrough of TOC can be observed, even using a column filled with fresh GAC, which indicates that a portion of the influent TOC is not amenable to removal by GAC treatment. With increased service time, the effluent TOC concentration rises and eventually reaches a steady state value, which indicates that the GAC becomes saturated with organics. They also observed that the effluent TOC seldom reaches the influent concentration but is lower than the influent level. This constant steady-state removal usually is attributed to biodegradation (USEPA, 1996). During early stages of operation, the ratio of effluent to influent TOC concentration (called "fraction remaining") generally ranges from 0.1 to 0.5, depending on composition of the organic constituents and EBCT/bed depth. For steady-state removal, the fraction remaining varies from 0.6 to 0.9 with corresponding range of service times from 3,000 to 14,000 measured in bed volumes.

The TOC breakthrough curve in a single GAC contactor is often described mathematically by a logistic functions in Eq.2.1. The model parameters a , b and d are developed to reflect the impact of influent TOC and pH and EBCT. Based on statistical regression, these parameters can be estimated by (USEPA, 2005),

$$a = 0.682 \tag{B5.19}$$

$$b = 0.167pH^2 - 0.808pH + 19.086 \tag{B5.20}$$

$$d = TOC_m \{ pH [-0.0000058EBCT^2 + 0.000111EBCT + 0.00125] + 0.0001444EBCT^2 + 0.005486EBCT + 0.06005 \} \quad (B5.21)$$

To improve the accuracy of GAC treatment modeling, WTP-CAM provides a new feature to estimate parameters a , b and d using a non-linear regression method if site-specific TOC treatment study data are available instead of the statistical values estimated by Equations B5.19-B5.21.

It may be time-consuming and expensive to obtain site-specific data from a pilot-plant or full-scale study of GAC adsorption processes. Instead, the rapid small-scale column test (RSSCT) may be used to generate the data required (Crittenden et al. 1991; Zachman and Summers 2010). An RSSCT is a scaled-down version of a pilot or full-scale GAC column contactor. The RSSCT method use mass transfer models to scale down the full-scale contactor to a small column. Similarity of operation to that of large-scale contactors is assured by properly selecting the GAC size, hydraulic loading and EBCT of the small contactor (Crittenden et al. 1991; Zachman and Summers 2010). USEPA (1996, 2000) provides standardized guidelines for GAC treatment studies that help obtain quality assurance data of TOC breakthrough in a GAC column. The USEPA's information collection rule (ICR) treatment studies database also provide GAC treatment study data from 63 treatment studies nationwide (USEPA, 2000), including 44 RSSCT studies, 18 pilot studies and 1 full-scale study.

When $f(t)$ versus t dataset are obtained from GAC treatment studies, WTP-CAM applies a modified Gauss-Newton method to estimate model parameters a , b and d by fitting the non-linear regression function (Equation B2.1) through least square analysis based on Hartley (1961). The objective function is defined as,

$$\text{Min } Q(a, b, d) = \sum_{k=1}^n (y_k - f(t_k; a, b, d))^2 \quad (B5.22)$$

Where, $f(t; a, b, d) = \frac{a}{1 + be^{-d \cdot t}}$; a , b and d are the model parameters to be estimated; t_k and y_k are the known field values representing GAC service time and TOC fraction remaining; n is a known number of field samples.

As a widely used method, Gauss-Newton method seeks solutions through iteration. Therefore, an important step is to correct model parameters during iteration using equation,

$$\theta_1 = \theta_0 + vD \quad (B5.23)$$

Where, θ is a vector of parameters to be estimated, $\theta = \begin{pmatrix} a \\ b \\ d \end{pmatrix}$, θ_0 represent the initial parameter vector and θ_1 represent the corrected parameter vector; D is a correction vector to the initial

parameters as a solution from the Gauss-Newton equations, $\mathbf{D} = \begin{pmatrix} D_1 \\ D_2 \\ D_3 \end{pmatrix}$; ν is a value from 0 to 1

to minimize $Q(a,b,d)$ during each iteration.

The Gauss-Newton equation is given by,

$$\mathbf{AD} = \mathbf{R} \quad (\text{B5.24})$$

Where, \mathbf{A} is the Gauss-Newton coefficient matrix, defined by,

$$\mathbf{A} = \begin{pmatrix} 2 \sum_{k=1}^n \left(\frac{\partial f}{\partial a} \right)^2 & 2 \sum_{k=1}^n \frac{\partial f}{\partial a} \frac{\partial f}{\partial b} & 2 \sum_{k=1}^n \frac{\partial f}{\partial a} \frac{\partial f}{\partial d} \\ 2 \sum_{k=1}^n \frac{\partial f}{\partial b} \frac{\partial f}{\partial a} & 2 \sum_{k=1}^n \left(\frac{\partial f}{\partial b} \right)^2 & 2 \sum_{k=1}^n \frac{\partial f}{\partial b} \frac{\partial f}{\partial d} \\ 2 \sum_{k=1}^n \frac{\partial f}{\partial d} \frac{\partial f}{\partial a} & 2 \sum_{k=1}^n \frac{\partial f}{\partial d} \frac{\partial f}{\partial b} & 2 \sum_{k=1}^n \left(\frac{\partial f}{\partial d} \right)^2 \end{pmatrix} \quad (\text{Herein, } f = f(t; a, b, d)) \quad (\text{B5.25})$$

\mathbf{R} is a right-hand-side vector of Gauss-Newton equation, defined by,

$$\mathbf{R} = \begin{pmatrix} -\frac{\partial Q}{\partial a} \\ -\frac{\partial Q}{\partial b} \\ -\frac{\partial Q}{\partial d} \end{pmatrix} \quad (\text{Herein, } Q = Q(a, b, d)) \quad (\text{B5.26})$$

Vector \mathbf{D} can then be solved by,

$$\mathbf{D} = \mathbf{A}^{-1} \mathbf{R} \quad (\text{B5.27})$$

Where, \mathbf{A}^{-1} is inverse of matrix \mathbf{A} .

In order to find an approximate minimum of $Q(a,b,d)$, ν value is estimated by the parabola through $Q(\nu=0)$, $Q\left(\nu=\frac{1}{2}\right)$, and $Q(\nu=1)$, given by,

$$\nu = \frac{1}{2} + \frac{1}{4} \frac{[Q(\nu=0) - Q(\nu=1)]}{\left[Q(\nu=1) - 2Q\left(\nu=\frac{1}{2}\right) + Q(\nu=0) \right]} \quad (\text{B5.28})$$

Where, $Q(\nu=0)$, $Q(\nu=\frac{1}{2})$, and $Q(\nu=1)$ represent the $Q(a_1, b_1, d_1)$ values evaluated with $\nu=0$, $\nu=\frac{1}{2}$ and $\nu=1$ through Equation B5.23.

The specific procedure can be summarized by the following steps. Step 1 is to provide initial vector for θ_0 . Step 2 is to solve for the vector D using Equation B4.27. Step 3 is to solve for ν value with Equation 4.28. Step 4 is to check whether $Q(a_1, b_1, d_1)$ value meets the precision requirement. If the answer is “no”, the initial parameters are replaced by the values calculated with equation B4.23 and iterated from step 2.

B4.3 Economics

WTP-CAM provides an economic analysis to estimate the costs associated with adaptation made to design or operation of water treatment in order to provide a metric to assess impact of climate change. The total costs considered in WTP-CAM include capital, operational and management costs. To date, only the GAC treatment unit process has a cost analysis model. Cost models for other unit processes will be added with the development of WTP-CAM.

B4.3.1 Adaptation Costs for GAC Processing

The costs for GAC processing consist of four types of costs: initial GAC cost, annual GAC make-up cost, GAC contactor cost and GAC reactivation cost. The initial GAC cost is one-time charge for GAC required to fill the contactors, which is calculated by the product of the total volume of contactors, the density and unit cost of new GAC. The annual GAC make-up cost is yearly cost for GAC loss during reactivation, which is calculated by the product of GAC loss rate for reactivation, GAC reactivation rate and unit cost. The GAC contactor cost can be estimated with a general form of the cost models by Adams and Clark (1988),

$$y = a + b(USRT)^c d^z \tag{B4.29}$$

where, y is the capital, operational or maintenance cost; $USRT$ is the process design or operating variable, which is usually the total surface area of the GAC filter for contactors (total hearth area for GAC reactivation) or the total effective volume of the GAC unit for capital cost; a , b , c and d are empirical parameters determined from nonlinear regression analysis, and z is either 0 or 1 for adjusting the cost functions for a range of $USRT$ values. The model parameters can be found from Adams and Clark (1988), which was obtained based on the costs in 1983. For consistence of comparison, all costs were converted to 2009 currency using the Producers Price Index (US BLS, 2008). The contactor cost can be further categorized by the costs of capital, process energy, building energy, maintenance material and operation and maintenance (O&M) labor. The computational parameters for contactors are listed in Table B4-2.

Table B4- 2 GAC Contactor Cost

Type of Cost	Capital	Process energy	Building energy	Maintenance Material	O&M Labor
USRT	volume	area	area	area	area
a	93700	0	15150	540	1160
b	1999.1	12	350	23.6	0.3
c	0.712	1	0.916	0.753	1.068
d	0.958	1	1	1	1.152
z	1	1	1	1	1
Unit cost	Construction Cost 1.3y	0.08 \$/kwh (in 2009)	0.08 \$/kwh (in 2009)	--	9 \$/hr (in 1983)
Ratio of 2009 to 1983 cost	2009ENR/1983ENR R= R=2.16	--	--	2009PPI/1983 PPI = 2.56	2009 PPI/1983 PPI = 2.56

O&M, operation and maintenance; PPI, producers price index

The GAC reactivation cost can be estimated using a similar algorithm used to calculate GAC contactor cost based on Equation B4.29. However, the model parameters are different from those for contactor cost. Table B4-3 lists the parameters used to estimate GAC reactivation cost.

If the capital recovery analysis is assumed a return period of 20 years with an interest rate of 5%, a cost curve can be developed to illustrate the total annual cost of the GAC system varies with GAC service time (reactivation period). WTP-CAM takes the cost curve and uses the curve to estimate the adaptation cost through interpolations based on GAC service time.

Table B4- 3 GAC Reactivation Cost

Type of Cost	Capital	Process energy	Building energy	Maintenance Material	O&M Labor	Natural Gas
USRT	area	area	area	area	area	area
a	144000	354600	12250	0	2920	648400
b	198300.4	6387	312.1	4456.6	282	287714.9
c	0.434	0.755	0.649	0.401	0.7	0.899
d	1	1	1	1	1	1
z	1	1	1	1	1	1
Unit cost	Construction Cost 1.3y	0.08 \$/kwh (in 2009)	0.08 \$/kwh (in 2009)	--	9 \$/hr (in 1983)	\$0.0035 /scf (in 1983)
Ratio of 2009 to 1983 cost	2009ENR/1983ENR = R = 2.16	--	--	2009 PPI/1983PPI = 2.56	2009PPI/1983 PPI = 2.56	2009PPI/1983 PPI = 2.56

O&M, operation and maintenance; PPI, producers price index

Figure B4-1 demonstrate an example cost curve developed for GCWW's Miller plant. The Miller plant has 12 down flow gravity contactors and two multi-hearth furnaces for onsite reactivation. Each of the Miller plant contactors has a volume of 595 m³ and a surface area of 181 m². The overall GAC loss rate through the system is about eight percent. The carbon loading rate is 482 kg/day of GAC per square meter of hearth area.

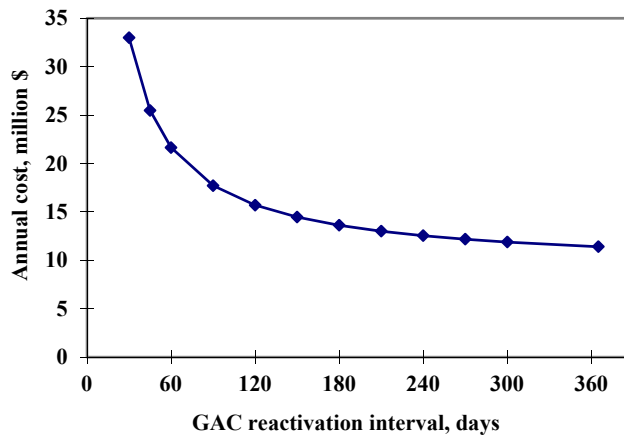


Figure B4-1 Cost curve for annual cost of GAC unit process.

B5.0 References

- Adams, J. Q., and Clark, R. M., (1988). Development of cost equations for GAC treatment systems. *Journal of Environmental Engineering*, 114 (3): 672-688.
- Bras, R.L. and Rodriguez-Iturbe, I., (1984). Random functions and hydrology. *Addison-Wesley Publishing Company*.
- Clark, R.M., (1987a). Modeling TOC Removal by GAC: The general logistic function. *J. AWWA*, 79 (1): 33-37
- Clark, R.M., (1987b). Evaluating the cost and performance of field-scale granular activated carbon systems. *Environmental Science and Technology*, 21 (6): 573-580.
- Clark, R. M. Yang, Y. J., Impellitteri, C. A., Haught, R. C., Schupp, D. A., Panguluri, S., and Krishnan, E. R., (2010). Chlorine fate and transport in distribution systems: Experimental and modeling studies. *J. AWWA*, 102:5

- Crittenden, J.C., Reddy, P.S., Arora, H., Trynoski, J., Hand, D.W., Perram, D.L., and Summers, R.S., (1991). Predicting GAC performance with rapid small-scale column tests. *J. AWWA*, 83 (1): 77-87.
- Hartley, H.O., (1961). The modified Gauss Newton method for the fitting of nonlinear regression functions by least squares. *Technometrics*, 3 (2): 269-280.
- Li, Z., Clark, R.M., Buchberger, S.G., Yang, Y.J., (2014). Evaluation of climate change impact on drinking water treatment plant operation. *J Environ Engrg.*, DOI:10.1061/EE.1943-7870.0000824
- Li, Z., Clark, R.M., Buchberger, S.G., Yang, Y.J., (2012). Evaluation of logistic model for GAC performance in water treatment. *J. AWWA*, DOI jawwa.2012.104.0120.
- Oulman, C.S., (1980). The logistic curve as a model for carbon bed design. *J. AWWA*. 75 (1): 51.
- Roberts, P.V. and Summers R.S., (1982). Granular activated carbon performance for organic carbon removal. *J. AWWA*, 74:113-118.
- Salas, J. D., Delleur, J. W., Yevjevich, V. and Lane, W. L., (1980). Applied modeling of hydrologic time series. *Water Resources Publications*, Littleton, Colorado, 484 pages.
- US BLS (Bureau of Labor Statistics), (2008). BLS Handbook of methods, Chapter 14 Producer Prices-Background. http://www.bls.gov/opub/hom/homch14_a.htm.
- U.S. Environmental Protection Agency (U.S. EPA), (2005). *Water treatment plant model version 2.2 user's manual*. Office of Ground Water and Drinking Water, U.S. Environmental Protection Agency, Cincinnati, Ohio.
- U.S. EPA, (2000). *ICR treatment study database, version 1.0*. Rep. No. EPA 815-C-00-003, Office of Water, Washington, D.C.
- U.S. EPA, (1996). *ICR manual for bench and pilot-scale treatment studies*. Rep. No. EPA 814-B-96-003, Office of Water, Washington, D.C.
- Zachman, B. A. and Summers, R.S., (2010). Modeling TOC breakthrough in granular activated carbon adsorbers. *J. Environmental Engineering* (ASCE). Pp 204-210. (February 2010)

Attachment A: Confirmation Tests

Confirmation tests are designed to verify that the algorithms applied in WTP-CAM are correctly coded and the modeling results with these algorithms are consistent to the corresponding evaluation criteria. The confirmation tests validate the following two algorithms in WTP-CAM: seasonal multivariate analysis, customization of GAC model.

A-1 Seasonal multivariate analysis

The algorithm of seasonal multivariate analysis is described in section B4.1.1. The purpose of incorporation of seasonal multivariate analysis is to preserve the means, variances, and cross correlations of the raw water quality parameters. For this purpose, the sample means, variances and cross correlations of raw water quality series from the Monte Carlo simulations are compared to the corresponding given means, variances and cross correlations of the inputted raw water quality parameters.

The comparisons are made in two seasons: summer and winter. The given means, standard deviations, and cross correlation matrix of raw water parameters are calculated from the input data files “summer_example_data.txt”, and “winter_example_data.txt”, which will be provided with this user manual as sample input files. There are 500 rows (sample size) in each of the input files. The sample means, standard deviation and cross correlation matrix of raw water quality are computed from 1000 Monte Carlo simulations.

Table A-1 compares the sample means and standard deviation in summer, it can be seen that the multivariate analysis algorithm well replicate the given mean since the maximum of the relative error between the simulated means and the given means is 6.3%. Reasonably good agreements are also achieved between the modeled standard deviation and given standard deviation as the maximum of relative error is 34.2%. Similar results are also obtained in winter as shown in Table A-3 since the maximum relative errors of means and standard deviations are 7.7% and 39.8%. The simulation of turbidity has much larger relative errors in sample mean and standard deviation than other water quality parameters owing to its large coefficient of variation (1.21 for summer and 1.34 for winter). Increase of number of Monte Carlo runs may reduce these relative errors.

Table A-2 compares the cross correlations between the given and modeled correlation matrix in summer. It can be observed that reasonably good agreements are achieved. Among the 36 pairs of correlation coefficients, the errors of 32 pairs are less than 0.1, errors of 3 pairs are greater than 0.1 but less than 0.2, and only 1 pair’s errors are greater than 0.2. Reasonably good agreements are also achieved for the comparisons in winter as shown in Table a.4. Among the 36 pairs of correlation coefficients, the errors of 30 pairs are less than 0.1, errors of the rest 6 pairs are greater than 0.1 but less than 0.2.

Table A- 1 Comparison of the mean and standard deviation in summer

Parameter Unit	pH --	Alkalinity mg/L	Turbidity NTU	Calcium hardness mg/L	Total hardness mg/L	TOC mg/L	UVA cm ⁻¹	Bromide mg/L	NH ₃ _N mg/L
μ_0	7.71	79.08	25.85	74.43	128.54	4.43	0.111	0.053	0.25
μ_m	7.71	79.96	27.48	75.01	129.05	4.42	0.110	0.054	0.25
Relative Error (%)	0.0	1.1	6.3	0.8	0.4	0.3	1.0	0.7	0.1
σ_0	0.24	22.19	31.17	27.92	24.96	0.91	0.056	0.022	0.128
σ_m	0.24	26.04	41.83	31.04	26.82	0.94	0.053	0.024	0.133
Relative Error (%)	0.0	17.3	34.2	11.2	7.5	3.5	4.8	9.4	4.0

Note: Subscript "0" representing given values from input data.
 Subscript "m" representing results from Monte Carlo analysis

Table A- 2 Comparison of cross correlation matrix in summer

Parameter	pH	Alkalinity	Turbidity	Calcium hardness	Total hardness	TOC	UVA	Bromide	NH ₃ _N
pH ₀	1	0.568	-0.145	0.104	0.432	0.367	0.203	0.102	-0.171
pH _m	1	0.473	-0.131	0.087	0.397	0.308	0.222	0.108	-0.187
Error		0.096	0.014	0.017	0.035	0.060	0.019	0.006	0.017
Alkalinity ₀		1	-0.114	0.136	0.798	0.737	0.515	0.304	-0.207
Alkalinity _m		1	-0.138	0.180	0.883	0.643	0.467	0.364	-0.300
Error			0.024	0.044	0.085	0.094	0.049	0.060	0.093
Turbidity ₀			1	-0.120	-0.256	0.131	0.387	-0.429	0.138
Turbidity _m			1	-0.110	-0.265	0.103	0.359	-0.362	0.154
Error				0.011	0.009	0.028	0.028	0.067	0.016
Ca hardness ₀				1	0.381	0.040	-0.155	0.296	-0.100
Ca hardness _m				1	0.419	0.019	-0.215	0.421	-0.134
Error					0.038	0.022	0.061	0.125	0.034
Total hardness ₀					1	0.496	0.296	0.565	-0.276
Total hardness _m					1	0.337	0.175	0.639	-0.334
Error						0.159	0.121	0.074	0.058
TOC ₀						1	0.698	0.128	0.020
TOC _m						1	0.654	-0.076	0.029
Error							0.044	0.204	0.009
UVA ₀							1	-0.335	-0.223
UVA _m							1	-0.335	-0.178
Error								0.000	0.045
Bromide ₀								1	-0.053
Bromide _m								1	-0.033
Error									0.020

Note: Subscript "0" representing given values from input data.
 Subscript "m" representing results from Monte Carlo analysis

The comparison results in the confirmation tests indicate that the multivariate analysis algorithm in the WTP-CAM works reasonably well and is confirmed for further application.

Table A- 3 Comparison of the mean and standard deviation in winter

Parameter Unit	pH --	Alkalinity mg/L	Turbidity NTU	Calcium hardness mg/L	Total hardness mg/L	TOC mg/L	UVA cm ⁻¹	Bromide mg/L	NH ₃ N mg/L
μ_0	7.78	64.14	39.64	72.19	121.14	4.06	0.089	0.071	0.23
μ_m	7.78	65.38	42.71	72.87	121.99	4.05	0.088	0.072	0.23
Relative Error (%)	0.0	1.9	7.7	1.0	0.7	0.3	1.2	1.7	0.1
σ_0	0.16	23.64	53.14	29.67	33.73	0.96	0.054	0.041	0.124
σ_m	0.16	28.56	74.28	33.19	36.65	0.99	0.051	0.046	0.129
Relative Error (%)	0.0	20.8	39.8	11.9	8.7	3.1	6.2	10.1	4.0

Note: Subscript "0" representing given values from input data.
Subscript "m" representing results from Monte Carlo analysis

Table A- 4 Comparison of cross correlation matrix in winter

Parameter	pH	Alkalinity	Turbidity	Calcium hardness	Total hardness	TOC	UVA	Bromide	NH ₃ N
pH ₀	1	0.562	-0.140	0.103	0.426	0.365	0.199	0.099	-0.171
pH _m	1	0.459	-0.128	0.086	0.390	0.305	0.219	0.106	-0.189
Absolute Error		0.103	0.013	0.016	0.036	0.060	0.020	0.006	0.018
Alkalinity ₀		1	-0.108	0.138	0.793	0.735	0.512	0.299	-0.205
Alkalinity _m		1	-0.125	0.184	0.885	0.627	0.451	0.365	-0.290
Absolute Error			0.017	0.046	0.093	0.109	0.061	0.066	0.086
Turbidity ₀			1	-0.119	-0.243	0.121	0.363	-0.377	0.133
Turbidity _m			1	-0.105	-0.240	0.096	0.343	-0.309	0.144
Absolute Error				0.014	0.003	0.025	0.020	0.068	0.012
Ca hardnss ₀				1	0.377	0.039	-0.151	0.286	-0.101
Ca hardnss _m				1	0.417	0.020	-0.208	0.415	-0.132
Absolute Error					0.040	0.019	0.057	0.129	0.031
Total hardness ₀					1	0.490	0.286	0.558	-0.272
Total hardness _m					1	0.332	0.168	0.630	-0.325
Absolute Error						0.158	0.117	0.072	0.052
TOC ₀						1	0.694	0.127	0.020
TOC _m						1	0.646	-0.072	0.027
Absolute Error							0.048	0.199	0.006
UVA ₀							1	-0.304	-0.215
UVA _m							1	-0.309	-0.174
Absolute Error								0.005	0.042
Bromide ₀								1	-0.054
Bromide _m								1	-0.038
Absolute Error									0.016

Note: Subscript "0" representing given values from input data.
Subscript "m" representing results from Monte Carlo analysis

A-2 Customization of GAC model

Section B4.2.1 introduces the algorithm of GAC model customization, which is used to provide users options to refine the empirical constants in GAC model using site-specific treatment study data so that better prediction can be obtained in a specific utility. There are two tasks in this confirmation tests for GAC model customization: one is to verify the improved performance of the customized GAC model over the original GAC model in the WTP model; the other is to validate the customized GAC model using field data from the GCWW's Richard Miller treatment plant.

To compare the performance between the customized GAC model and original model in the WTP model, two sets of RSSCT data from the Richard Miller Treatment Plant were used to

estimate the customized GAC model parameters in Equation B2.1 using the non-linear regression algorithm given by Equations B4.22-B4.28. The original GAC model parameters were calculated using Equations B4.19-B4.21 when pH is 7.8, EBCT is 20 minutes and inflow TOC concentration is 2.25 mg/L. Table A-5 summarized the model parameters for the two RSSCT datasets. Then, the customized and original models were used to simulate the GAC logistic curve and are compared to the corresponding RSSCT data sets. Obvious improvements can be observed with the customized GAC model over the original model as shown in Figures A-1 to A-2. Figure A-3 quantifies the improvements by comparison the sum of error squares given by Equation B5.22. It can be seen that the sum of error squares by the customized model is only 10.4% of that by the original model for RSSCT dataset 1 and 37.4% for the RSSCT dataset 2.

Table A- 5 Parameters estimated for TOC breakthrough model

Data source	GAC model	Parameter <i>a</i>	Parameter <i>b</i>	Parameter <i>d</i> [day ⁻¹]
RSSCT data 1	Customized	0.644	5.448	0.0314
	Original	0.682	22.94	0.0388
RSSCT data 2	Customized	0.604	9.445	0.0359
	Original	0.682	22.94	0.0388

Customized GAC model can be further validated with field data at the Miller plant. There are eight episodes identified from field measurements for one of 12 contactors at the Miller plant during January 2004 to May 2010. The TOC fraction remaining is obtained by calculation of the ratio of the contactor effluent TOC concentration over inflow TOC concentration. Each of the eight datasets were used to estimate the GAC model parameters the using the non-linear regression algorithm given by Equations B5.22-B5.28. Table A-6 summarizes the minimum and maximum TOC fraction remaining, GAC service period, and estimated parameters.

Figure A-4 exhibits the TOC breakthrough field measurements for the 8 datasets. TOC breakthrough field curves in Figures A-4a, A-4d, A-4e, and A-4h do not achieve steady state of a logistic curve. As a result, model parameters estimated with these datasets present great fluctuation as parameter *a* varies from 0.53 to 3.05 or parameter *d* changes from 0.016 to 0.046.

Obviously, GAC models with parameters estimated with these datasets are not amenable to represent the TOC breakthrough in the Miller plant because of the incomplete data. Thus, these incomplete datasets should be ignored. The averages of the parameters estimated from the rest four “complete” data sets are used for the customized GAC model, given by,

Figure A-1 Comparison of GAC models with RSSCT dataset 1

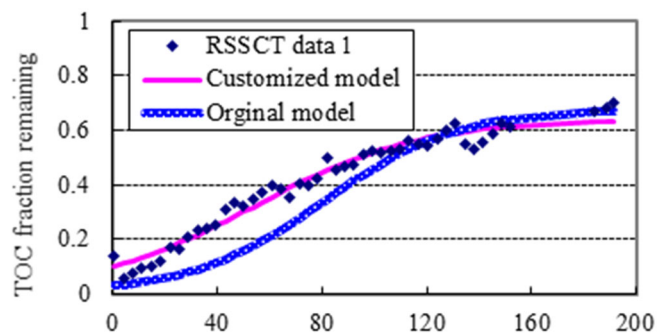


Figure A- 1 Comparison of GAC models with RSSCT dataset 1.

parameters estimated from the rest four “complete” data sets are used for the customized GAC model, given by,

$$f(t) = \frac{0.759}{1 + 8.124e^{-0.029 \cdot t}} \tag{A.1}$$

In addition to Equation A.1 (represented with “average-based” in Figure A-4), a customized GAC model using averages of parameters estimated with RSSCT data listed in Table A-5 is also validated against the field data (represented with “RSSCT-based” in Figure A-4), given by,

$$f(t) = \frac{0.624}{1 + 7.447e^{-0.034 \cdot t}} \tag{A.2}$$

For referen ce, customized GAC models with parameters estimated for individual datasets, as listed in Table A-6, are provided as well, represented with “self-based” in Figure A.4.

Table A-7 provides the sums of error square (defined by Equation 5.22) of “self-based,” “RSSCT-based” and “average-based” customized GAC model for all eight data sets. As expected, the self-based models provide the best fitting for individual datasets. Similar performances are achieved for both RSST-based and average-based models when GAC service time is less than 100 days (incomplete datasets). However, the average-based model presents a much better simulation

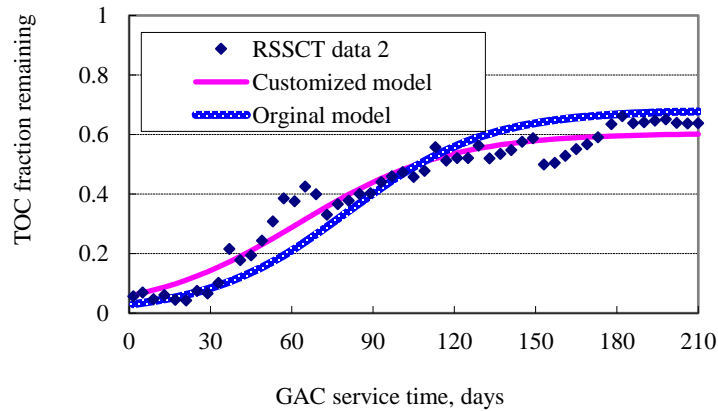


Figure A. 2 Comparison of GAC models with RSSCT dataset 2.

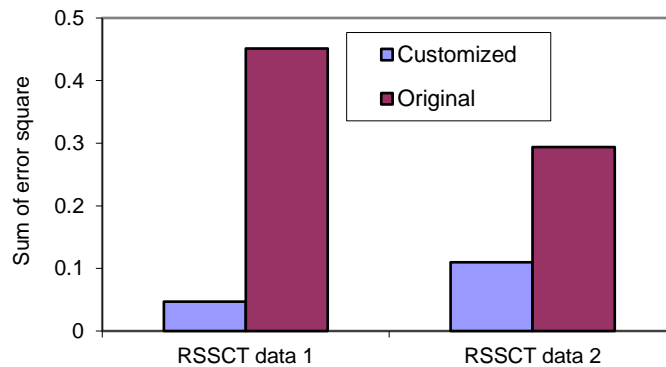


Figure A. 3 Comparison of sum of error square for GAC models.

Table A- 6 Summary of field data sets and estimated parameters

Data set #	Min. of observed $f(t)$	Max. of observed $f(t)$	GAC service period, day	Parameter a	Parameter b	Parameter d day ⁻¹	Comment
1	0.110	0.519	88	0.809	11.271	0.035	Incomplete
2	0.088	0.808	256	0.767	11.134	0.035	Complete
3	0.127	0.841	312	0.783	8.391	0.025	Complete
4	0.080	0.500	102	0.527	7.322	0.046	Incomplete
5	0.134	0.452	116	0.732	6.065	0.021	Incomplete
6	0.097	0.844	291	0.725	8.210	0.035	Complete
7	0.083	0.849	275	0.760	4.762	0.022	Complete
8	0.110	0.477	109	3.048	35.221	0.016	Incomplete
Average for "Complete" datasets	0.099	0.836	284	0.759	8.124	0.029	

Table A- 7 Comparison of sum of least square for customized GAC models

Data set #	1	2	3	4	5	6	7	8
Self-based GAC model ¹	0.019	0.036	0.036	0.040	0.021	0.082	0.072	0.029
RSSCT-based GAC model ²	0.037	0.434	0.417	0.052	0.054	0.300	0.232	0.107
Average-based GAC model ³	0.034	0.068	0.078	0.054	0.080	0.112	0.106	0.125

Note: ¹ Self-based GAC model refers to the model using parameters estimated for individual datasets given in Table A.6;

² RSSCT-based GAC model refers to the model using parameters estimated by RSSCT tests given by Equation A.2;

³ Average-based GAC model refers to the model using average of parameters based on "complete datasets" given by Equation A.1.

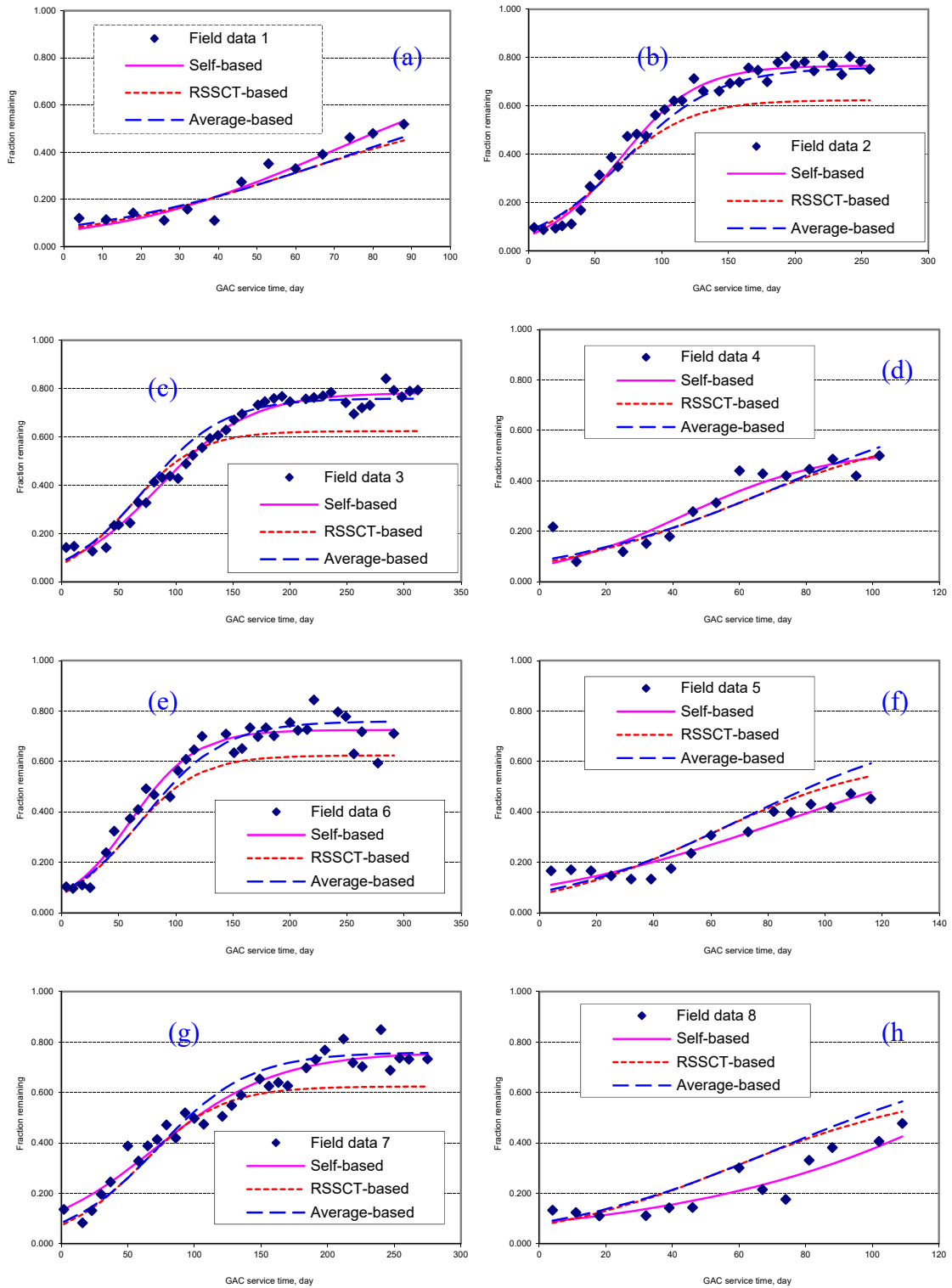


Figure A- 4 Validation of GAC model with field data.

Attachment B: Error and Warning Messages

WTP-CAM has two types of messages: error message and warning message. The error message is a fatal error and has to be corrected before the WTP-CAM can be executed successfully. The warning message is either caused by uncommon parameters user specified or used to provide user information for unusual running conditions of WTP-CAM. The warning messages do not affect execution of WTP-CAM. The error and warning message will be developed in subsequence refinement of WTP-CAM and summarized in Tables B-1 and B-2.

Table B- 1 Error message (to be developed)

ID	Explanation	Correction
1	Can't open file " <i>File name</i> "	Check the existence of file

Table B- 2 Warning message (to be developed)

ID	Explanation	Recommendation
1	User-defined parameter is out of range	Stay within recommend range

ISSUE SCIENCE



National Center for Environmental Assessment
Office of Research and Development
Washington, DC 20460

Official Business
Penalty for Private Use
\$300